Heart Rate Variability used to assess changing autonomic function in Transmissible Spongiform Encephalopathies.

A thesis submitted to the University of Manchester for the degree of Doctor of Philosophy in the Faculty of Medical and Human Sciences

2011

David George Glover

School of Medicine

Division of Cardiac and Endocrine Sciences

TABLE OF CONTENTS

LIST OF TABLES 5

TABLE OF FIGURES 6

LIST OF ABBREVIATIONS 8

ABSTRACT 9

REFERENCES 9

DECLARATION 10

COPYRIGHT STATEMENT 10

CHAPTER 1 INTRODUCTION: PRIONS, HEART AND BRAIN. 12

- Characterization of the disease associated marker 13
  - The Prion Theory 13
  - Alternative historical theories for TSE infection 14
  - Questions about the Prion Hypothesis 18
- Prion Strains 20
- Function of PrP 22
  - Evidence from transgenic mice studies and the GPI anchor 22
  - Interactions of PrP^{c} with other proteins 25
  - Synaptic function in relation to prions 26
  - Potential for a change in synaptic function in the diseased state 29
  - Signalling Functions of PrP^{C} 32
- Prion Pathogenesis 34
  - Different pathogenesis based upon different disease strains 34
  - Vagal route of entry for Prion to the CNS 36
  - Pseudorabies virus in relation to proposed prion infection 40
  - Possible polypeptides associated with prion pathogenesis 41
- Interaction of brain and heart 45
  - A wandering path from brainstem to heart 45
  - The Orienting Response 48
  - The Vagal Paradox 49
- Anatomical and functional evidence to support the Polyvagal Theory 52
  - From Reptiles to Mammals 57
  - The NA, DMNX and heart rate variability 59
- Characterizing the anatomy and function of distinct brainstem areas 62
  - Anatomy of the DMNX and NA 62
  - Function of DMNX and NA 63
- Intrinsic and thoracic cardiac ganglia 68
  - Intrathoracic Ganglia 71
  - Intracardiac Ganglia 72

CHAPTER 2 COMMON METHODS USED IN THIS THESIS 78

- Introduction 78
  - Electrodes 79
- Data Collection 83
- Limitations to data collection and Technical Caveats 89

CHAPTER 3 INVESTIGATION OF HEART RATE VARIABILITY IN SCRAPIE INFECTED SHEEP 95

- Introduction 95
- Methods 96
- Results 99
- Limitations and further work to investigate HRV changes in TSE diseases 109
- Discussion 113

CHAPTER 4 INVESTIGATION OF BSE INFECTED CATTLE USING HEART RATE VARIABILITY ASSESSMENTS 118

Introduction 118
Methods 122
Results 127
Limitations of this study 143
Discussion 148

CHAPTER 5 DEVELOPMENT OF METHODS USED TO INVESTIGATE HEART RATE VARIABILITY LINKED TO RESPIRATION 163

Introduction 163
Method 170
Representing circular statistical data. 181
Results 193
Limitations to this study 201
Discussion 206

CHAPTER 6 APPLICATIONS OF HEART RATE VARIABILITY LINKED TO RESPIRATION 211

Introduction 211
METHODS: Considerations involved in the application of HRV linked to respiration 215
Methods 1: Assessment of ability to distinguish R-wave distributions within a breath 215
Methods 2: Investigating the effects of heart rate on distribution of R-waves within each breath 216
Methods 3: Using the effect of anaesthesia on HRV during each breath cycle and comparing to prion disease 219
Results 220
Results 1: Assessment of ability to distinguish each R-wave within a breath 220
Results 2: Investigating the effects of heart rate on distribution of R-waves within each breath 230
Results 3: Investigating the effect of anaesthesia and sedation on the beat to beat variation of the heart during each breath cycle and comparisons to prion disease 240
Limitations 247
Discussion 248

CHAPTER 7 SUMMARY AND FURTHER WORK 259

Review of chapters and findings 259
Review of Chapter 1 259
Review of Chapter 2 260
Review of Chapter 3 261
Review of Chapter 4 262
Review of Chapter 5 263
Review of Chapter 6 264
Limitations 266
Methods of measuring HRV 266
HRV in a diseased state: Study of heart transplant patients to illustrate differences. . 267
Respiration linked to HRV 270
Application to different genotypes and other diseases. 273
Further Work 274
Discussion and Conclusions 275
References 277

APPENDIX **300**

Appendix 1.1 Batch output from written software to automatically calculate RMSSD **300**
Appendix 1.2 Power spectral values from sheep and simulator **301**
Appendix 1.3 Differences in windowing functions in power estimates **302**
Appendix 1.4 Bland Altman method of measuring agreement between measured and estimated breaths **303**
Appendix 1.5 Program listing, used to calculate circular statistics **305**
Appendix 1.6 Frequency response of 5 point filter of Methods section of chapter 5 ..... **336**
Appendix 1.7. Typical output from the program of appendix 1.5 ..... **337**
Appendix 1.8 Illustration of the changes in HRV over time in a vCJD patient. **342**
Appendix 1.9 Difference in mean vector length when using corrected breath estimates versus uncorrected estimate. **343**
Appendix 1.10 Figure to accompany figure 4.4 ..... **344**
Appendix 1.11 95% Confidence Intervals for figures 5.9,6.10 and 6.11 ..... **345**
Appendix 1.12 Tables of significance testing for data in figure 6.11 ..... **346**
Appendix 1.13. Published work related to this thesis **347**

Word Count 66,151

List of Tables

Table 1-1 The Vagal Paradox 51

Table 3- 1 The number of sheep in each group and their genotype and RAMALT biopsy result. 99

Table 4- 1 A table to display the tag numbers of the experimental animals analysed, their BSE status and PrPD in the spine. 128

Table 5- 1 Circular statistics illustrating the differences between controls and repeated measures from a vCJD patient. 196
Table 5- 2 Results of a Mardia-Watson-Wheeler test between R-wave distributions 200

Table 6- 1 Number of R-waves and breaths for control and patient data. 217
Table 6- 2 Summary statistics for the 5th R-wave in around 140 breaths from Controls and vCJD patients. 220
Table 6- 3 Mean vector angles and associated time estimates of R-wave events within a breath cycle 221
Table 6- 4 Statistics from all the 5th R-waves to compare with table 5-1. 222
Table 6- 5 Circular statistics for 6 R-waves from control data 224
Table 6- 6 Circular statistics for 6 R-waves from patient data. 224
Table 6- 7 Summary statistics for Cartwheel plots of figure 5.3. 228
Table 6- 8 To show significant differences between control and patient data 229
Table 6- 9 Values for model R-wave distributions for patients and controls. 230
Table 6- 10 Control and patient summary circular statistics for measured and model values. 233
Table 6- 11 Table of statistics for the distributions of the differences in R-wave position for measured and model values. 236
Table 6- 12 Table of correlation coefficients for MVL and MVA variables 238
Table 6- 13 Table of 95 % confidence intervals for correlation coefficients for MVL and MVA variables (dependent) against heart rate (independent) 239
Table 6- 14 Table of differences between correlation coefficients 239
Table 6- 15 Table of differences in R-wave distributions within a breath before and during anaesthesia 242
Table 6- 16 Table of differences in R-wave distributions within a breath before anaesthesia and vCJD patient 242
Table 6- 17 Table of differences in R-wave distributions within a breath during anaesthesia and vCJD patient 242
Table 6- 18 Table of differences in R-wave distributions within a breath for patient in figure 6.13 before and after sedation 246
Table 6- 19 Table of differences in R-wave distributions within a breath for patient in figure 6.13 before and during sedation. 246
Table 6- 20 Table of differences in R-wave distributions within a breath for patient in figure 6.14 before and after sedation 246
Table 6- 21 Table of differences in R-wave distributions within a breath for patient in figure 6.14 before and during sedation 246

Table of Figures

Figure 1. 1 All sail and no anchor. 23
Figure 1. 2 Role for prion in regulation of copper. 27
Figure 1. 3 Pathology of natural scrapie. 39
Figure 1. 4 Pathogenesis of PrPD in scrapie. 44
Figure 1. 5 Stimulation of DMNX and Aortic Depressor Nerve. 56
Figure 1. 6 Schematic of Neural connections from CNS to SA node via ganglionated complexes. 69

Figure 2. 1 Standard electrode and adapted electrode. 80
Figure 2. 2 Range of colours for constructed electrode to reduce cross contamination. .. 80
Figure 2. 3 Theoretical construction of Tachogram. 85
Figure 2. 4 Actual tachogram from a sheep. 86
Figure 2. 5 Summary of Methods used in this study. 87
Figure 2. 6 Illustration of the instantaneous rate 88
Figure 2. 7 The effect of artefacts on power spectrums 91

Figure 3. 1 Sheep in Cradle. 98
Figure 3. 2 Close up of electrode attached to thorax. 98
Figure 3. 3 Comparison of tachograms from control and infected sheep. 100
Figure 3. 4 HLF and HHF values for Experimental and Field animals. 102
Figure 3. 5 Heart rates and RMSSD for Experimental and Field animals. 103
Figure 3. 6 Boxplots to show significance of HLF and HHF grouped by biopsy result. 105
Figure 3. 7 Boxplots to show the lack of significance differences in heart rate and RMSSD grouped by biopsy. 106
Figure 3. 8 ROC curve to illustrate the performance of HLF index of HRV against rectal biopsy. 108
Figure 3. 9 Diagram to show putative inspiration events, indicated by change in amplitude of ECG. 111

Figure 4. 1 Cow in a crush with electrodes attached. 123
Figure 4. 2 Lorenz plot of a cow incubating BSE. 125
Figure 4. 3 Time domain HRV differences in BSE and scrapie. 130
Figure 4. 4 Frequency domain differences in HRV in BSE and scrapie. 131
Figure 4. 5 Time domain measures of cattle incubating BSE over 3 month periods. 133
Figure 4. 6 Spectral measures of HRV during BSE incubation over a 3 month periods. ... 134
Figure 4. 7 Time domain changes in HRV over 12 months in BSE by oral dose 136
Figure 4. 8 Change in time domain metrics for groups separated by spine result. 138
Figure 4. 9 Changes in Time domain metrics of HRV with respect to the identification of PrPD in spinal regions. 139
Figure 4. 10 Step change in time domain metrics of HRV. 140
Figure 4. 11 HRV showing distinction between field animals and controls and experimentally challenged animals 142
Figure 4. 12 Trends in HRV change over time in BSE infected cattle. 144
Figure 4. 13 Longitudinal changes in HRV in cattle incubating BSE. 145
Figure 4. 14 Difference in HRV change for 1 gram and 100 gram dosed animals. 146
Figure 4. 15 Action potential doublets. 158

Figure 5. 1 Interaction of vagus nerve and different areas of the brainstem. 164
Figure 5. 2 Decreasing RSA with increasing depth of anaesthesia. 166
Figure 5. 3 Schematic of Neural connections from CNS to SA node via ganglionated complexes. 168
Figure 5. 4 Relationship of lines of evidence used to assess breath event. 172
Figure 5. 5 Variation of ECG amplitude indicates breath event. 174
Figure 5. 6 Association between measured and estimated breath events. 176
Figure 5. 7 Construction of vector plot of R-wave distribution within a breath. 180
Figure 5. 8 Example of R wave dispersion within breaths I. 182
Figure 5. 9 Example of R wave dispersion within breaths II. 183
Figure 5. 10 Overlay of constituent breaths of figures 5.8 and 5.9. 184
Figure 5. 11 Summary "Cartwheel plot" 185
Figure 5. 12 Circular distributions compared to linear counterparts. 187
Figure 5. 13 Illustration of how breath estimates were deducted from Heartsim file. 191
Figure 5. 14 Distribution of R-waves for overlaid breaths 192
Figure 5. 15 Bland-Altman Plot of differences in estimated and measured breath events 194
Figure 5. 16 Relationship of measured to estimated breathing event 195
Figure 5. 17 Cartwheel plots. 196
Figure 5. 18 Concentration of R-waves within a breath. 198
Figure 5. 19 Variation of Mean Vector Length of R-waves within breaths. 199
Figure 5. 20 Difference in metrics used to assess HRV. 204
Figure 5. 21 Difference in range of measures obtained from different methods of calculating HRV. 205

Figure 6. 1 Distributions of constituent R-waves for controls and patients. 223
Figure 6. 2 Circular representations of the constituent R-waves contributing to the summary data presented in table 5-7. 225
Figure 6. 3 Summary of approximately 900 R-waves for each R-wave position for patient and control data. 227
Figure 6. 4 Plot of Circular Variance against R-wave position for control and vCJD patient data. 228
Figure 6. 5 Vector plot of model distributions of R-waves. 231
Figure 6. 6 Vector plot of model and measured distribution of R-waves. 232
Figure 6. 7 Differences between measured R-wave position and model R-wave position. 234
Figure 6. 8 Plot of differences between measured and model R-wave positions. 235
Figure 6. 9 The relationship between the MVL and MVA and heart rate. 237
Figure 6. 10 MVL for people before and during anaesthesia, compared to vCJD patients. 241
Figure 6. 11 Variation in MVL for controls, vCJD, sedated and anaesthetized people. 244
Figure 6. 12 Example of good sedation. 245
Figure 6. 13 Example of possible inadequate sedation 245

List of Abbreviations

ACh ..... Acetylcholine
ANS ..... Autonomic Nervous System
A-V ..... Atrioventricular
BSE ..... Bovine Spongiform Encephalopathy
CED ..... Cambridge Electronic Design
CNS ..... Central Nervous System
CWD ..... Chronic Wasting Disease
DMNX ..... Dorsal Motor Nucleus of the Vagus (X) Nerve
DNA ..... Deoxyribonucleic Acid
ECG ..... Electrocardiogram
ENS ..... Enteric Nervous System
EPSPs ..... Excitatory Post Synaptic Potentials
FDC ..... Follicular Dendritic Cells
FFT ..... Fast Fourier Transform
$GABA_A$ ..... Gamma Aminobutyric Acid
GFAP ..... Glial Fibrillary Acidic Protein
GI ..... Gastro Intestinal
GN ..... Ganglion Nodosum
GPI ..... Glycosylphosphatidylinositol
GSS ..... Gerstmann-Sträussler-Scheinker syndrome
H_2O_2 ..... Hydrogen Peroxide
hcrt-1 ..... Hypocretin 1
HF ..... High Frequency Spectral Band (0.05-1 Hz)
HHF ..... Human High Frequency Spectral band (0.15-0.5 Hz)
HLF ..... Human low Frequency Spectral Band (0.032-0.138 Hz)
HRV ..... Heart Rate Variability
I AHP ..... After Hyperpolarization Current
iCJD ..... iatrogenic Creutzfeldt-Jakob disease
IPSCs ..... Inhibitory Postsynaptic Currents
LF ..... Low Frequency Spectral Band (0.0-0.05 Hz)
LRS ..... Lymphoreticular System
LTP ..... Long Term Potentiation
mRNA ..... Messenger Ribonucleic Acid
NA ..... Nucleus Ambiguus
NA_{ex} ..... External formation of Nucleus Ambiguus
NMDA ..... *N*-methyl-D-aspartic acid)
NTS ..... Nucleus Tractus Solitarius
PAGP ..... Posterior Atrial Ganglionated Plexus
PNS ..... Peripheral Nervous System
PrP^C ..... Normal form of Prion Protein
PrP^D ..... Disease associated conformation of Prion Protein
PRV ..... Pseudo Rabies Virus
RAGP ..... Right Atrial Ganglionated Plexsus
RMSSD ..... Root Mean Square of Successive Differences
ROC ..... Receiver Operating Characteristic
RSA ..... Respiratory Sinus Arrhythmia
SA ..... Sino Atrial
sCJD ..... sporadic Creutzfeldt-Jakob disease
SIDS ..... Sudden Infant Death Syndrome
SPSS ..... Statistical Package for the Social Sciences
STI-1 ..... Stress Inducible Protein 1
TSE ..... Transmissible Spongiform Encephalopathie
UV ..... Ultra Violet
vCJD ..... variant Creutzfeldt-Jakob disease
VLA ..... Vetinary Laboratories Agency

The University of Manchester
David George Glover for the degree of Doctor of Philosophy
Thesis Title: Heart Rate Variability used to assess changing autonomic function in Transmissible Spongiform Encephalopathies.
October 2011

Abstract

The dorsal vagal nucleus (DMNX) and nucleus ambiguus (NA) are two anatomically distinct regions of the medulla oblongata of the brainstem involved with the control of the heart on a beat to beat basis. The vagus nerve has parasympathetic cell bodies located in the DMNX and NA. The presence of the disease associated prion (PrP^D) in the DMNX and NA is used in the post mortem diagnosis of transmissible spongiform encephalopathies (TSEs) in animals. It has been shown that PrP^D alters the neuronal discharge properties of infected tissue (Barrow, Holmgren et al. 1999;Collinge, Whittington et al. 1994). I wished to investigate whether a change in heart rate variability (HRV) influenced by the presence of PrP^D deposits in brainstem areas of animals and people incubating TSEs would be detectable.

Recordings from control and infected sheep, cattle and humans, consisting of three-hundred-second samples of electrocardiogram (ECG) were collected from species specific healthy controls and subjects incubating TSE disease. Data were digitised at a sampling frequency of 1kHz and were translated and analysed using standard software (CED Spike2 ; IBM SPSS). Artefacts and missed beats were corrected based upon screening by eye. ECG R-wave timings were obtained in order to determine variability in the R-R intervals. An instantaneous tachogram was constructed from which power spectra were calculated.

Power spectral analysis along with simpler time domain estimates of HRV, such as RMSSD, were employed to investigate differences between control and infected animals. In addition R wave variability within each breath was utilized to examine the vagal control of the heart in relation to breathing and thus investigate a change in function of the specific neurological areas of the brainstem used as diagnostic criteria for such diseases.

It was found there were significant differences ($p<0.05$) in the HRV of infected sheep, cattle and humans incubating TSE disease compared to control samples. Repeated non-invasive longitudinal tests may provide a means to screen animals and humans for the presence of disease associated prions and may give applications in the objective assessments of putative therapeutics in addition to identifying TSE disease at a preclinical stage.

References

Barrow, P. A., Holmgren, C. D., Tapper, A. J., & Jefferys, J. G. 1999, "Intrinsic physiological and morphological properties of principal cells of the hippocampus and neocortex in hamsters infected with scrapie", Neurobiol.Dis., vol. 6, no. 5, pp. 406-423.

Collinge, J., Whittington, M. A., Sidle, K. C., Smith, C. J., Palmer, M. S., Clarke, A. R., & Jefferys, J. G. 1994, "Prion protein is necessary for normal synaptic function", Nature, vol. 370, no. 6487, pp. 295-297.

Declaration

No portion of the work referred to in this thesis has been submitted in support of an application for another degree or qualification of this or any other university or institute of learning.

Copyright Statement

This thesis is dedicated to Chris for the encouragement along an academic pathway.

Thanks are given to my wife and family for their support.

Tsense Diagnostics and governmental agencies are acknowledged and thanked for their help in access to animals. Thanks are also given to vCJD patients and their families for their participation in this research.

About the author.

The author has a first degree in physiology and electronics. The author was initially involved in visual neuroscience research at Keele University for around ten years. Following this, the author was involved in sports physiology and sports psychology research at Staffordshire and Manchester Metropolitan Universities, writing computer programs for data capture and interpretation along with developing and interfacing novel transducers, stimulators and data capturing devices. A short period of screening and rehabilitating elite athletes in the private sector lead to a role as a clinical scientist at Derby Royal Infirmary in a “Gait Laboratory” investigating movement patterns in children with cerebral palsy and research into movement analysis in adults with Parkinson’s disease. Following this the author commenced his present position at Manchester Royal Infirmary as a research technician in Anaesthesia where, in addition to research in other areas of anaesthesia, he has been involved with two independent research topics involved with heart rate variability (HRV) along with four other research topics as a team member involved with HRV research.

Chapter 1 Introduction: Prions, heart and brain.

Transmissible Spongiform Encephalopathies (TSEs) which are also referred to as prion diseases, include kuru, variant Creutzfeldt–Jakob disease (vCJD), sporadic Creutzfeldt–Jakob disease (sCJD), iatrogenic Creutzfeldt–Jakob disease (iCJD) and Gerstmann– Sträussler–Scheinker disease (GSS) of humans as well as animal diseases such as scrapie in sheep, chronic wasting disease of deer (CWD) and bovine spongiform encephalopathy (BSE) in cattle. The diseases are almost always fatal, although one vCJD patient has survived over eight years post diagnosis (as of December 2010). A comprehensive understanding of prion diseases and their proposed infectious agents is useful in determining the risk of infection from various strains of TSEs to human and animal populations. In addition, an increased understanding and assessment of the problem of TSEs may help in the design of a treatment or cure for diseases of this type. This is highlighted by the threat of BSE to the human population and exemplifies the ability of TSEs to overcome the species barrier, where a disease of cattle, BSE, is thought to cause pathogenic disease in humans, vCJD (Asante, Linehan et al. 2002;Collinge 2001;Hill, Desbruslais et al. 1997).

More recent analysis of the epidemiology and risks involved in the transmission of BSE to the human population has been done (Ironside, Bishop et al. 2006). That work highlighted the possibility that vCJD may affect not only the methionine recessive genotype but also the heterozygous and valine homozygous genotypes. The proposed long incubation period of up to 40 years (Hilton 2006) in some individuals for this type of prion disease, coupled with the fact that there has now been 3 iatrogenic infections from blood transfusions (Wroe, Pal et al. 2006), raised concern about subclinical carriers of the disease donating blood to more susceptible genotypes. One of these iatrogenic infections was identified in a patient heterozygous at the PRNP codon 129, indicating that human to human transmission of prion diseases is not isolated to the methionine recessive genotype and suggests a lower barrier to transmission within species than between species (Peden, Head et al. 2004). This emphasizes the need to not only know those individuals who express the clinical signs of TSEs but also those that carry it.

Doubt about the infectious agent is being mooted in current research. Recent work has suggested there may be factors other than prions that cause the infection (Jeffrey, Gonzalez et al. 2006) or that prions need crucial cofactors (Caughey & Baron 2006;Fasano, Campana, & Zurzolo 2006). Even the prospect of silent prions lying dormant has been suggested; lying dormant in normal human brains that may seed the conversion cascade of normal cellular prion into the disease associated conformation (Yuan, Xiao et al. 2006). Around 30 years ago vCJD and BSE were unknown. The area of TSE diseases and prion research is still very active and will contribute to the knowledge of those diseases currently being studied and importantly may help in identification of diseases we do not yet know.

Characterization of the disease associated marker

The Prion Theory

In 1982, Stanley Prusiner used the term "Proteinacious Infectious Particle" or PRION to describe the biochemically purified scrapie agent which he equated to the prion protein PrP, which constituted the major component of the infectious preparation (Prusiner 1982).

Prion protein was thought to differ from all other infectious pathogens since it did not contain nucleic acid molecules that coded for the constituent protein. The principal component of the isolated scrapie agent was termed PrP. From this isolation the complementary DNA and gene were cloned and it was found to be encoded by the human gene, PRNP. In turn this lead to the identification of two types of PrP, the cellular isoform, PrP^{c} and the pathogenic protease resistant conformation, PrP^{Sc} (Prusiner.1982). It is thought that the normal cellular prion protein, PrP^{c}, is converted into an abnormal, protease-resistant isoform, PrP^{Sc}, by a post-translational process which involves a conformational change in the protein structure.

Various forms of this pathological isoform have been identified and may be denoted by different labels such as PrP^{cwd} , PrP^{vCJD} , PrP^{bse} depending on the disease under investigation. The nomenclature to designate the wild-type and mutant prion protein associated with the infectious disease, different prion isolates, and the normal and artificial prion proteins expressed in transgenic mice, are currently evolving. To denote the distinction between the naturally occurring shape and disease associated isoform of the prion, the term PrP^{D} will be used in this thesis to distinguish the disease associated pathological isoform from the naturally occurring conformer, PrP^{c}. Therefore, PrP^{c} designates the normal cellular isoform of prion found in humans and animals and PrP^{D} designates the pathogenic prion synthesized in any animal or human whether its synthesis is initiated by inoculation or infection with human or animal prions.

The presence of infectious prion (PrP^{D}) in regions of the medulla oblongata of the brainstem, specifically the dorsal vagal nucleus (DMNX) and nucleus ambiguus (NA), is used in post mortem diagnosis of Bovine Spongiform Encephalopathy (BSE). In addition, a range of human transmissible spongiform encephalopathies have a pathological hallmark of the accumulation of PrP^{D} in the central nervous system which included strongly stained regions of the DMNX in relation to variant Creutzfeldt Jakob Disease (vCJD) (Armstrong, Cairns et al. 2002;Armstrong, Lantos et al. 2003;Ironside 2000).

Alternative historical theories for TSE infection

Evidence for the existence and infectivity of TSEs was postulated as early as 1922 by McGowan. The term scrapie was applied to this disease due to the infected sheep scraping on fences. This disease had been evident since 1732, and became such a problem that there was a memorial to the House of Commons regarding its destructiveness from sheep breeders in 1755. It was considered “a disease of muscle caused by the parasite *Sarcosporidia*” (McGowan J 1922). In 1939, Cullié and Chelle demonstrated that scrapie was transmissible to sheep and goats by intraocular inoculation and later by intracerebral, oral, subcutaneous, intramuscular

and intravenous injection of brain extracts from scrapie incubating sheep (Cuillé & Chelle 1939). Gordon, in 1946, presented his observations when trying to develop a vaccination for louping-ill virus (an acute viral tick-transmitted disease primarily of sheep characterized by ataxia, muscular incoordination, tremors, posterior paralysis, coma, and death). After vaccinating with formalin (a solution of formaldehyde in water used to disinfect or preserve biological specimens) treated ovine lymphoid extracts, he found around 1500 sheep developed scrapie two years after vaccination. This highlighted that the infectious agent was resistant to formalin and also illustrated the lengthy incubation time for the disease (Gordon 1946). Alper, Haig and Clarke demonstrated that scrapie infectivity resisted inactivation by ultra violet (UV) and ionizing radiation and other evidence that was incompatible with the involvement of nucleic acid, lead them to postulate that the infectious agent may be a protein (Alper, Haig, & Clarke 1966). In addition, theories that suggested the infection for scrapie was related to a replicable change in the structure of commonly occurring unit membranes were being developed (Gibbons & Hunter 1967). Griffith then outlined the “protein only” hypothesis that suggested the infectious agent consisted of a modified form of a normal cellular protein and exhibited self-replication (Griffith 1967).

The development in the concept of prion infection evolved from the infectious agent first being thought of as a parasite (McGowan J.1922) and progressed to ideas of a “slow virus”(Leader & Hurvitz 1972;Sigurdsson 1954). The next postulates were then advanced since the “slow virus” postulated by Sigurdsson was able to withstand salt concentrations and UV radiation which destroys nucleic acid structure.

Various hypotheses on the structure of the prion are currently held. The most popular is the “Protein Only” hypothesis which suggests that the disease associated conformation of TSEs is able to reproduce itself independent of nucleic acid and initially the infectious agent is derived from a natural protein (prion , PrP^{c}) by a conformational change to form the disease associated isoform (PrP^{D}). (Cohen & Prusiner 1998). To accommodate both the protein only nature of this theory and to account for different strains of prion formed as a result of transfer in different hosts, the uniform theory of propagation was postulated (Weissmann 1999). This model assumed the disease causing isoform, designated the aproprion, was associated with

a small nucleic acid, the co-prion. This co-prion could confer the strain specific variations to the combined infectious agent, termed the holoprion (apoprion + co-prion = holoprion). The protein only component, the apoprion, is still able to mediate disease pathogenesis on its own. Coupling of these newly generated apoprions with a new nucleic acid co-prion from the host, could code for a different strain. The nucleic acid component not being essential for disease transmission, but would account for the strain varieties observed upon transfer to different hosts.

A number of other hypotheses have been presented and some are still under consideration as alternatives to the protein only model. The virus theory, suggested the disease pathogenesis may be described as a virus induced amyloidosis. The virus was suggested to replicate in the lymphoid tissue and then enter the brain where replication led to higher concentrations of the infectious agent which caused aggregation of nerve cell proteins into amyloid fibrils which caused cell death and loss of neuronal function (Diringer 1991).

The virino theory suggested a small amount of nucleic acid is involved with the infectious agent and this non translated nucleic acid is protected by a host derived protective coat. This is distinct from a virus, where the protective shield for the nucleic material is coded by the virus. This virino theory addressed the absence of an immune response in TSE diseases (Diener 1973). Another idea was based on the infectious agent, this time termed a viroid, that contained a nucleic acid of such a simple sequence that small sections of the polynucleotide retained the full informational sequence of the agent (Diener.1973).

The virus, viroid and virino hypotheses all fit into the concept of slow infections designated by Sigurdsson. They contrast to the protein only theory proposed by Prusiner which nominated the prion as the infectious agent devoid of nucleic material. Regardless of the exact mode of infection, TSE diseases are still causing death and contamination issues to humans and animals. As such, the protein only theory and the term prion can be used as an operational model whilst the history of TSEs is being written as the result of on-going research.

Further issues that relate to the protein only hypothesis of TSE transmission relate to the idea that PrP^D , the proposed infectious agent, is replicated by imparting its aberrant shape onto PrP^c . A prediction of the protein only hypothesis suggests that it should be possible to create infectivity of modified prion protein in vitro. Kurt Wüthrich has commented that continued failure to do this, calls the theory into question.

Although work by Castilla (Castilla, Saβ et al. 2005) and subsequent researchers (Deleault, Harris et al. 2007;Wang, Wang et al. 2010) goes a long way to accomplishing this goal by producing prion disease from a prion entirely generated in vitro and has inferred that a misfolded protein is an active component of the infectious agent it remains unclear whether another molecule besides the misfolded prion protein might be an essential element of the infectious agent (Soto 2010) . Also from the protein only postulate, it should be possible to abolish the structure of a prion by *in vitro* chemical treatment and then attempt to restore the original structure and function of the disease initiating prion. Experiments to achieve this have also failed to demonstrate the expected outcome.

Wüthrich has commented that accumulation of PrP^D may be considered as a build-up of garbage in cells and suggested that a better understanding of the normal prion protein and its function is needed to more fully understand prion diseases (reported in (Aguzzi & Heikenwalder 2003)commenting on (Wuthrich 2003). The accumulation of PrP^D , the garbage referred to above, in the cytosol of neurons is thought to bring about nerve cell death (Ma & Lindquist 2002;Ma, Wollmann, & Lindquist 2002).

It is suggested that PrP^c resides in the cell membrane and is transported there by the network of internal membranes, the endoplasmic reticulum(ER). However, a certain amount of PrP^c does not reach the cell membrane and re-enters the cytosol by "retrotranslocation" from the ER (the mechanism where a protein that has entered the ER gets back to the cytoplasm) in a similar manner that other mis-folded proteins are directed towards proteasomes for disposal. This PrP^c in the cytosol forming the basis for PrP^D expression.

Lindquist's group demonstrated that a prion protein specifically targeted to the cytosol caused rapid neural cell death in their experiments with mice. It was suggested that this prion protein did not acquire protease resistance as PrP^{D} but proteasome inhibition lead to the accumulation of slightly protease resistant prion protein in cultured cells. Lindquist postulated that mutations in prion protein associated with TSE diseases may lead to enhanced retrotranslocation which in conjunction with impaired proteasome function, may lead to the expression of a particular disease. In this case, the site of PrP mediated neuronal death begins in the cytosol, supporting the idea of a build-up of garbage.

This idea is contested by Harris' group who reported that cytosolic prion protein retains its "single peptide" which is normally removed after a protein enters the ER and cytosolic prion protein does not have the " glycosyl phosphatidyl-inositol (GPI) anchor" required to attach to membranes (Drisaldi, Stewart et al. 2003). Consequently it is suggested by Drisaldi et al that these proteins have never entered the ER and consequently could not have undergone retrotranslocation. The authors also state that proteasome inhibitors have strong effects on the levels of mRNA which may have contributed to differing results in previous work in this area.

Questions about the Prion Hypothesis

Currently there are increasing questions being raised that challenge the Prion Theory for TSE infectivity. Among the more recent evidence is the work where infectious prions inoculated into sheep, did not appear as expected in the Peyers patches, but were either digested by endogenous digestive chemicals or transported into the lymph nodes. It was also found that abnormal disease associated prions began accumulating in the Peyers patches 30 days after the initial inoculation (Jeffrey, Gonzalez et al.2006). This may suggest that some different infectious agent invaded the cells of the animal to provoke *de novo* accumulation of the diseases associated

PrP in the Peyers patches 30 days after the initial inoculation. The question may then be proposed as to where this infectious agent went during this 30 day period?

Further evidence of the existence of an infectious agent differing from PrP is given by the identification of damaged areas of brain where there were no prions (Jeffrey, Goodsir et al. 2004). An in depth critique of the prion hypothesis is given in the recent work that postulates that a 25 nm "virion" is the likely cause of TSEs (Manuelidis 2006). Here, it is suggested that the particle size may accommodate a viral genome of sufficient size to encode for an enzyme required for its replication and host PrP may act as a facilitator for infectious particles eventually acquiring pathological features. Here, PrP is thought to act as a viral receptor rather than infectious agent. Disassociation of prion protein and infectivity has also been demonstrated by treatment with hydrochloric acid where infectivity is always inactivated faster than PrP at differing concentrations and temperatures (Appel, Lucassen et al. 2006). It is also suggested that host responses similar to those found to other viral infections are also displayed in TSE disease incubation and are observed before PrP^{D} is evident (Lu, Baker, & Manuelidis 2004).

Furthermore, it is pointed out that the Prion Hypothesis does not accommodate any of Koch's postulates for an infectious agent. These may be summarized as: The agent must be present in every case of the disease; the agent must be isolated from the host with the disease and grown in pure culture; the specific disease must be reproduced when a pure culture of the agent is inoculated into a healthy susceptible host; the agent must be recoverable from the experimentally infected host (Manuelidis.2006).

Recent publications in relation to this topic review the work of Nazor, Castilla and Deleault and conclude that none of these reports provide conclusive evidence that the infectious agent for TSEs is composed of just protein and "robust" infection failed to be created *in vitro* from constituent building blocks. This work suggest that other molecules derived from the host, such as sulphated glycosaminoglycans and nucleic acids may be involved (Caughey & Baron.2006). In addition to prions, various co-factors are also being suggested due to *in vitro* experiments failing to generate robust infection (Fasano, Campana et al.2006). The possibility of disease associated prions

that may be “silent” in some host species awaiting the trigger from an infectious agent for disease expression to occur is also suggested (Yuan, Xiao et al.2006)

We must bear in mind that there is a possibility that prions may not be the primary causal agent of the disease and may be a secondary pathological marker for the family of diseases; correlation is not proof of causation.

Prion Strains

A surrogate marker for prion diseases is the presence of a proteinase resistant isoform (PrP^D) of the host prion protein (PrP^c). The proteinase resistant form may appear in a number of different subtypes, categorised by its glycosylation patterns. Both PrP^c and PrP^D may appear in unglycosylated, monoglycosylated or diglycosylated forms. These subtypes of prion are used to classify types of disease and the distinct glycosylation patterns of PrP^D correlate with a specific disease phenotype incubated in a particular host genotype. Hence, glycosylation of PrP^D may be considered a surrogate marker for strains of prion diseases. However, recent work has identified that some forms of CJD had both Type 1 and Type 2 glycosylation patterns, based from the banding patterns observed from western blot analysis of a range of neural tissues (Polymenidou, Stoeck et al. 2005). This leads to the possibility that more than one prion strain can be present in one disease phenotype and suggests a continuum of diseases may be expressed due to the diversity of strains and variable interactions with the genotype of the host. In the identification of CJD for example, the occurrence of new variant CJD may have been more akin to the discovery of yet another variety of the continuum of disease expression rather than a new disease, an idea that is supported by the increasing number of “atypical” cases of TSE diseases in a range of mammals. This in turn must then illustrate the potential for a future occurrence of another “new” variation of TSE disease. This emphasises the need for a better understanding of TSE diseases and their pathogenesis.

There is also diversity in strains of TSEs, some of which may be apparent as sporadic (as yet of undetermined origin) neurodegenerative diseases. In addition some strains may affect more than one species. For example the recent reoccurrence of scrapie has been suggested to be ovine BSE due to the difficulty in distinguishing scrapie and BSE in sheep (Aguzzi, Heikenwalder, & Polymenidou 2007). Indeed it may be noteworthy to recall that the florid plaques associated with the pathology of vCJD in humans were initially compared to those seen in mice with Icelandic scrapie (Ironside.2000). Here, the TSE from cows appeared in humans with similar traits to those of scrapie in mice. These facts illustrate that there may be a significant interaction of a strain of TSE disease with a particular host, consequently, different disease phenotypes may present as a result of the species and strain interaction.

It is suggested that if two strains co-infect a host, there is a possibility that one strain impedes the second strain in exercising its disease phenotype (Dickinson, Fraser et al. 1972;Manuelidis 1998). If this is the case, an infected animal may harbour two strains only one of which is pathogenic in that individual. If a host genotype, susceptible to the second strain, was then subjected to the same joint infection regime, the susceptible genotype may express a different disease phenotype than the original animal. Here a subclinical carrier for the previously silent infection may pass this on to a susceptible genotype in which it subsequently is expressed. The expression of infection may thus be interpreted as contracting only one strain, from a continuum, that is pathological for the particular host genotype. This theory would emphasise the diversity of strains of TSEs and their potential differing effect on a range of genotypes and highlight the prospect of subclinical carriers infecting susceptible genotypes.

The origins of certain TSEs are still unknown. Considerable debate surrounds the origin of sporadic CJD. Among the hypotheses proffered to address the aetiology of this disease are the random formation of PrP^{D} molecules from a somatic cell mutation or a change in the protein kinetics stabilizing PrP^{C} (Cohen 1999), the possible somatic mutation of PrP^{c} in neural tissue (Prusiner 1991) and a reduction in the ability to remove PrP^{D} with respect to increasing length of incubation time (Safar, Dearmond et al. 2005). Work by Deleault et al investigating the formation of native

prions from lipid molecules and a polyanion cofactor has suggested that native PrP^C may interact ,infrequently, with polyanions to create PrP^D (Deleault, Harris et al.2007). This method is suggested to be associated with the generation of the disease associated prions in sporadic forms of CJD (Lee & Caughey 2007). The origins of BSE may be via a similar polyanion interaction with native PrP^C molecules. Subsequent strains of TSEs, including the newly-arising atypical forms of BSE may be initiated by similar polyanion interactions with native PrP^C, which could also give rise to other unfamiliar prion diseases in the future. Suggestions that the H-type variant of BSE had a spontaneous origin support this theory (Gavier-Widen, Noremark et al. 2008).

Function of PrP

Evidence from transgenic mice studies and the GPI anchor

Prion protein is expressed in high levels in the brain and in many body tissues. However, work with PrP^c knockout mice (mice lacking PrP^c) has demonstrated that a natural role for PrP^c is somewhat of an enigma. These mice demonstrated changed sleeping patterns with little change in physiology and otherwise they functioned normally (Bueler, Fischer et al. 1992). The proposed functions of prion protein range from a universally vital role in cell survival to a more specific role as a metal ion binding protein which regulates the copper concentration in neuronal synaptic regions.

PrP^D was found to be harmless in its self by experiments where brain tissue devoid of PrP^D but having PrP is grafted onto brains of mice lacking normal prion protein and then subsequently exposed to infectious prions. The results of such experiments show that considerable amounts of PrP^D are formed but the mouse does not succumb to TSE disease. Therefore, this suggests that PrP deficient neurons are not affected by the infectious agent (Brandner, Isenmann et al. 1996)

Transgenic mice have been used in further studies to investigate the role of PrP^D in the pathogenesis of TSEs. During the construction of PrP^c, the molecule is involved in the cellular secretory pathway of the lumen of the endoplasmic reticulum. Following this a glycosylphosphatidylinositol (GPI) lipid anchor is added to the C terminus of the prion protein. This functions to tie the molecule to the outer cell membrane.

Transgenic mice were engineered to exhibit the lack of the single peptide responsible for GPI anchoring (GPI-negative mice) and so produced a non-anchoring soluble secreted form of PrP^c (Chesebro, Trifilo et al. 2005) Chesebro *et al* then infected these transgenic mice with three strains of scrapie and it was found that GPI negative transgenic mice never developed clinical signs of prion disease although their brains contained significant amounts of PrP^D deposits.

The inference from this study is that removing the GPI anchor abolishes the susceptibility to clinical disease but still allows the PrP^c molecule to support prion replication and hence the generation and accumulation of PrP^D in the brain (see figure1.1). Aguzzi (Aguzzi 2005), suggests that this idea concurs with accruing evidence that normal prion protein may function as a signalling molecule, with the abnormal PrP^D variant causing altered cell signalling that causes cell death.

Figure 1. 1 All sail and no anchor.

Diagram modified, From Aguzzi, A. 2005, "Cell biology. Prion toxicity: all sail and no anchor", *Science*, vol. 308, no. 5727, pp. 1420-1421. Reprinted with permission from AAAS.To illustrate the requirement for the PrP^D molecules to be attached to the cell membrane to induce a neurotoxic signal.

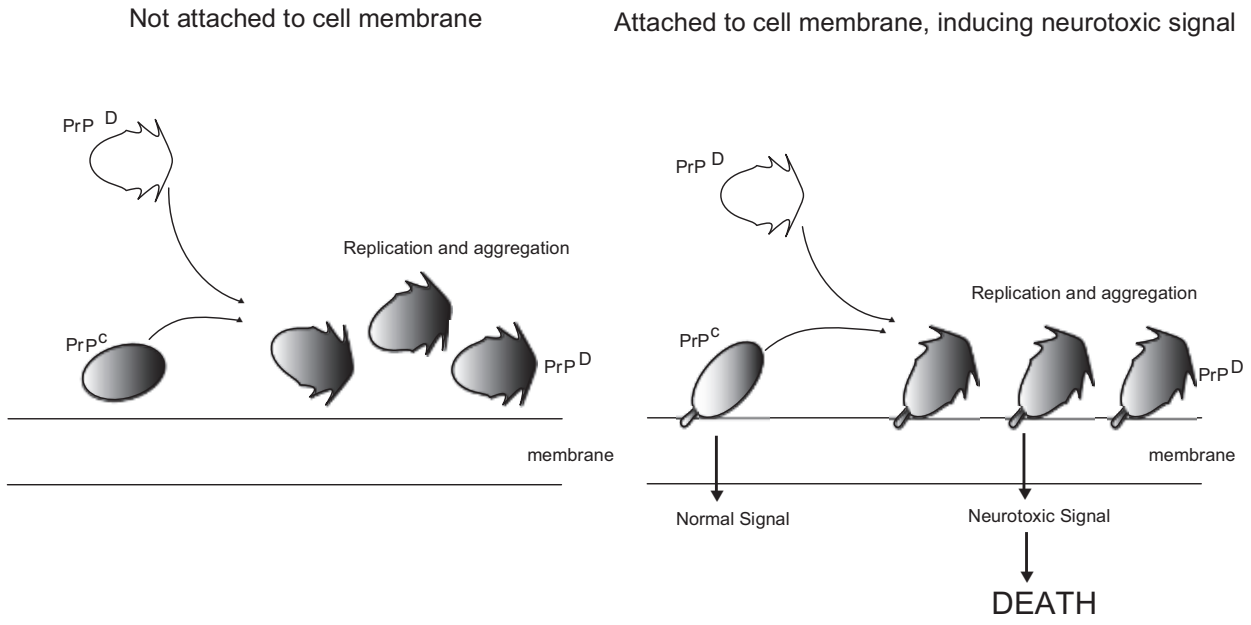

Some of the accruing evidence includes the work of Solforosi who indicated that cross linking of PrP^c on the surface of hippocampal neurons with antibodies causes these neurons to die (Solforosi, Criado et al. 2004). Mice lacking normal prion protein do not exhibit signs of prion disease and so loss or change in function of clustered PrP^c is not a cause of brain damage in TSEs. However clustering of PrP^c is a crucial step in the formation of PrP^D. The work of Chesebro *et al* gives evidence for a link between the cell surface topology of PrP^D and pathogenesis of TSEs. When PrP^c is disengaged from the membrane surface, PrP^D replication, accumulation and formation of brain plaques occurs but clinical disease is not evident. Consequently one interpretation of this evidence is that prion replication avails itself of membrane bound signal transducers to elicit brain damage and therefore membrane bound PrP^c would be required for the manifestation of clinical signs. Meier's work with transgenic mice that express a dimeric form of PrP^c do not accumulate PrP^D and do not develop or transmit TSEs. It is thought that this dimeric form competes and wins with endogenous PrP^c and delays prion pathogenesis (Meier, Genoud et al. 2003). In combination with the work of Chesebro , this indicates that the detachment of PrP^c from the membrane does not abolish its prion replication abilities. It may be that a soluble dimeric form requisitions PrP^D making it unavailable and thus inhibiting the disease. Infectious prions, therefore, may damage the brain by distorting signalling events at the membrane that PrP^c normally controls.

In non-neuronal cells, PrP^c is often found at the cell membranes allied to rafts of cholesterol (a combination of a lipid, steroid and alcohol and is an important constituent of cell membranes) rich molecules (Vey, Pilkuhn et al. 1996). One exception to this is in the stomach where PrP^c was observed in the secretion granules of epithelial cells (Fournier, Escaig-Haye et al. 1998). It is also found in the secretory mammary gland tissue where its expression is related to physiological state (Lasmezas 2003). This latter statement may have implications for the maternal transmission of TSEs as recently identified by Castilla and Bellworthy in mice and sheep respectively (Bellworthy, Dexter et al. 2005;Castilla, Brun et al. 2005).

Interactions of PrP^c with other proteins

PrP^c interacting proteins, such as synapsin I, are abundant not only in neural tissue but also in other tissues involved in exocytosis, such as tissues of the endocrine system. Another PrP^c interacting molecule is glial fibrillary acidic protein (GFAP), which is an astrocytic marker that is shown to accumulate at the same time with disease associated PrP^D during TSEs (Dormont, Delpech et al. 1981). Another interesting property of PrP^c is that it binds laminin, a molecule that promotes cell adhesion, neurite outgrowth and maintenance in primary neurons of rodents. As such the effects of laminin are mediated by PrP^c (Graner, Mercadante et al. 2000).

A further PrP^c ligand was identified as stress inducible protein 1 (STI-1) which is a heat shock protein (a protein which increases its expression when the cells which contain them are exposed to elevated temperatures) that resides in the cell membrane and cytoplasm. Both proteins are thought to interact in a specific and high affinity manner and PrP^c binds to cellular STI-1 *in vivo.* Furthermore, it was found that this binding of PrP^c and STI-1 induce neuroprotective signals that can rescue cells from apoptosis. (Zanata, Lopes et al. 2002) From this evidence it is clear that a disassociation between the diseased PrP^D and STI-1 molecule could abolish the protective effects of the conventional PrP^c and STI-1 binding and thus contribute to neuronal cell death.

It has been shown that the binding site of the laminin receptor precursor (37kDa, LRP) and its mature form, termed high affinity laminin receptor (67 kDa, LR), maps to amino acid 161-179 of the PrP^c molecule (Gauczynski, Peyrin et al. 2001). It is distinct from that of the STI-1 binding domain of amino acids 113-128 (Zanata, Lopes et al.2002). It is suggested by Zanata *et al*, that there may be the prospect of binding of both laminin and STI-1 to PrP^c. The binding of both ligands may have a contributory effect to the survival of neuronal cells. From this example, it is evident that the complexity of the potential cascade of a PrP^c macromolecular complex formed between the cell surface and extracellular proteins, may mediate signals that promote cell survival and differentiation. Again, this is another area that could be the target for the dysfunction of neuronal cells caused by the involvement of the mis folded PrP^D in diseased states.

Consequently the disruption in binding of STI-1 and laminin to the mis-shaped PrP^D, will have a direct effect on neuronal survival and have a direct consequence to the neurophysiological function of distinct brain regions infected with PrP^D. Reports show that heparan sulphates play a role in the life cycle of PrP^c molecules and in the pathogenesis of the disease state. Cell surface glycosaminoglycan molecules are components of heparan sulphates and play a role in the internalization of PrP^c. It is also possible that binding of laminin receptors and PrP^c is influenced by copper ions since the heparan sulphate proteoglycans binds to a PrP^c copper binding domain (Brown, Qin et al. 1997). Conversely PrP^c and STI-1 binding is not influenced by copper (Zanata, Lopes et al.2002) and the internalization of PrP^c may be involved in switching off signals triggered by the PrP^c -STI interaction. Sulphated glycans stimulate cell free conversion of PrP^c and are associated with amyloid plaque formation in PrP^D accumulation in TSE pathogenesis. Clearly, there are numerous areas for disruption in binding other molecules to prion proteins, caused by the replacement of PrP^c with PrP^D, that will have functional consequences for neurons. This in turn will disrupt the integrated, coordinated electrical communication properties of particular infected regions of the brain.

Synaptic function in relation to prions

The role of copper in the various associations and functions of PrP^c is still unclear. It may be of structural importance for the N terminus of PrP^c and may influence the binding of other proteins, such as those mentioned above. Further investigations on the role of copper have revealed that PrP^c shows cooperative copper binding (Kretzschmar, Tings et al. 2000). PrP^c found in brain homogenates reveals the highest concentration in synaptosomal fractions and mice devoid of PrP^c (Prnp 0/0) show a 50% reduction in synaptosomal copper concentrations. PrP^c was found in the presynaptic nerve terminal by several groups including Fournier (Fournier, Escaig-Haye et al. 1995), Sales (Sales, Rodolfo et al. 1998) and Herms (Herms, Tings et al. 1999). PrP^c has also been associated with synaptic vesicles (Pauly & Harris 1998;Shyng, Moulder et al. 1995). It is likely that PrP^c cycles between these two compartments as summarized by figure 1.2, postulated by Kretzschmar (Kretzschmar, Tings et al.2000).

Figure 1. 2 Role for prion in regulation of copper.

Figure adapted with kind permission of Springer Science and Business Media.
from Prion Diseases; Diagnosis and Pathogenesis Groschup, Martin H.; Kretzschmar, Hans (Eds.) Special edition of Archives of Virology, Suppl. 16 2000, IX, 290 p. 89 illus., Hardcover ISBN: 978-3-211-83530-2.
Kretzschmar (Kretzschmar, Tings et al.2000)

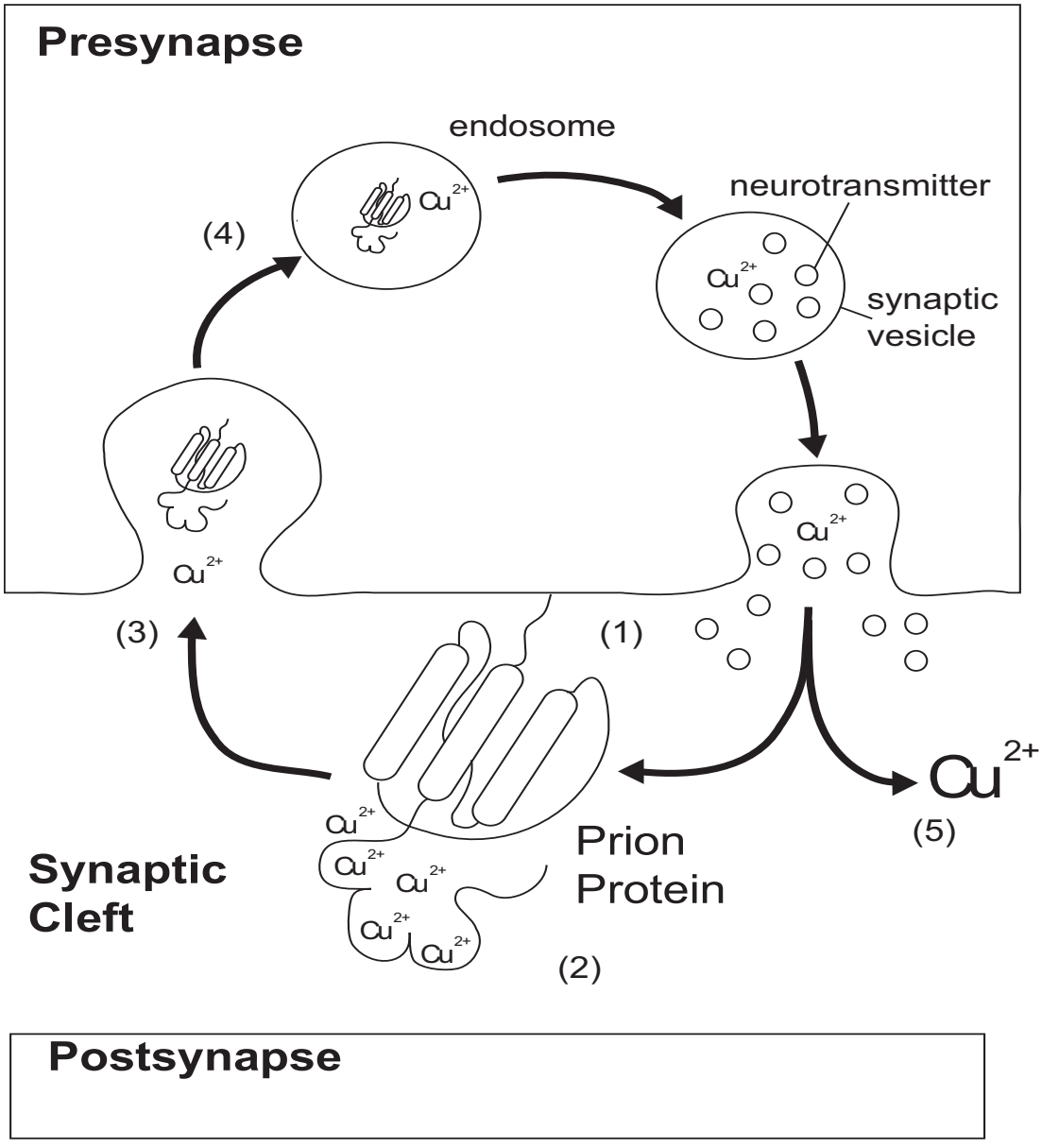

Figure adapted from Kretzschmar illustrating function of prion in binding copper.
(1) Prion protein attached to presynaptic plasma membrane.
(2) N terminal of prion binds free copper.
(3) Endocytic uptake of prion into presynapse.
(4) Prion bound copper is released possibly by changes in endosomal pH.
(5) Copper is released into synaptic cleft with synaptic vesicle release.

In this hypothetical model it is suggested that prion protein is attached to the presynaptic membrane where its N terminal domain may bind free copper in the synaptic cleft, due to synaptic vesicle release (Hartter & Barnea 1988;Kardos, Kovacs et al. 1989). An endocytic uptake of PrP^c into the presynapse (Pauly & Harris.1998;Shyng, Moulder et al.1995) is then postulated, where PrP^c bound copper is released. Hence PrP^c acts to keep the copper concentration in the presynaptic cytosol and the synaptic cleft constant despite losses due to synaptic vesicle release.

Research into the affinity of copper binding to PrP suggests that PrP may scavenge excess copper during neuronal activity and so protect the function of the synapse (Walter, Chattopadhyay, & Millhauser 2006b). Due to negative cooperativity, that is the PrP protein responds to copper over a wide concentration range, the "spikes" in copper concentration in the synapse may be matched during the synaptic process to the affinity of PrP. This "sponge like" behaviour of PrP for copper allows an antioxidant function that may be the key to long term preservation of neuronal function. In the diseased state, PrP^D may fail to "mop up" this excess copper and a perturbation in neural function could result.

Specific work on PrP^c and binding copper was done by Brown. (Brown, Qin et al.1997) It was reported here that the amino terminus of PrP^c contains an octapeptide (8 amino acids linked in a polypeptide chain, PHGGGWGQ) that is repeated four times and it is the best preserved region of mammalian PrP^c. It was shown that this amino terminal exhibits five or six sites that bind copper. This work also involved the use of two lines of Prnp 0/0 mice to evaluate the effects of copper in these lines versus wild type mice. The Prnp 0/0 mice demonstrated severe reduction in copper content of membrane enriched brain extracts and in synaptosomal and endosomal enriched cellular fractions. These mice also demonstrated altered electrophysiological properties in the presence of copper compared to wild type mice. Total X-ray fluorescence was used to test copper binding *in vitro* and it was found that wild type mice had 20.1 µg of copper per gram of membrane from brain homogenate compared to 1.3 µg of copper per gram for Prnp 0/0 mice. Little difference was found in other tissues from areas such as liver, kidney and muscle. It was concluded from this research that PrP^c is either a

principal copper binding protein in brain membrane fractions or that it controls activity of other membrane binding proteins. Brown (Brown, Qin et al.1997), stated that these copper binding proteins regulated via PrP^c either possess GPI anchors or are tethered to membranes through an interaction with PrP^c. Thus PrP^c may act as a buffer for excess copper and so regulate the copper content of the intracellular compartment.

Conformational changes to PrP^c when copper binds have been reported by Hornshaw. (Hornshaw, McDermott, & Candy 1995). As Hornshaw alludes to, cooperative binding may amplify the conformational shift in prion protein structure and consequently the misfolded PrP^D would not mimic the same transformation in shape following copper binding as the wild type PrP^c in diseased states. Copper binding to proteins may thus exert a deleterious effect on the normal function of such proteins. The work by Brown showed that prion protein is a cuproprotein like those implicated in the pathogenesis of Parkinson's disease and Alzheimer's disease. The common denominator of cuproproteins indicates that neurons are sensitive to changes in copper and physiological mechanisms may exist to regulate the distribution of this ion, such as that proposed by Walter(Walter, Chattopadhyay, & Millhauser 2006a).

Potential for a change in synaptic function in the diseased state

A role for prions in the recycling of the synaptic vesicles or a more direct role in synaptic activity is suggested by Herms (Herms, Tings et al.1999) This more direct role in synaptic activity is supported by electrophysiological work involving Prnp 0/0 mice, devoid of PrP^c. Collinge *et al* (Collinge, Whittington et al.1994) described a change in synaptic transmission (a change in long term potentiation, LTP) following repetitive stimulation in one particular Prnp 0/0 line generated by Bueler. (Bueler, Fischer et al.1992) These findings were replicated in the Prnp 0/0 mouse line generated by Manson (Manson, Clarke et al. 1994). Collinge also identified a change in the inhibitory postsynaptic currents (IPSCs) in hippocampal neurons of Prnp 0/0 mice. This prolonged rise time of $GABA_A$ receptor mediated IPSCs may have been due to changes in the $GABA_A$ receptor on the postsynaptic membrane. However other workers did not find this (Lledo, Tremblay et al. 1996). To clarify the question of

whether the increase in rise time seen in Prnp 0/0 mice was due to the loss of PrP^c expression in the presynapse or postsynapse, an additional transgenic line of mice was developed (tg20) which only expresses PrP^c at the presynapse (Fischer, Rulicke et al. 1996). In this line, rise times similar to the wild type were found and hence it was postulated that the loss of the presynaptic PrP^c expression at the inhibitory synapse is responsible for the prolongation of IPSCs in Prnp 0/0 mice.

Barrow also described another electrophysiological observation in scrapie infected hamsters (Barrow, Holmgren et al.1999). A disturbance of the late after hyperpolarisation current (I AHP) was observed. This current is involved in action potential repolarisation and hence affects the frequency of action potentials. The cause of the alterations in electrophysiological properties in PrP^c deficient mice are not yet fully understood but it is thought it relates to the decreased copper concentrations in synaptic membrane fractions of Prnp 0/0 mice. This decrease may be caused by deregulation of copper in the brains of Prnp 0/0 mice caused by the loss of PrP^c (Kretzschmar, Tings et al.2000). So, to associate these findings from Prnp 0/0 mice to the pathogenesis of TSEs it is useful to remember that the disease may result from a dominant negative effect of PrP^D leading to a progressive loss of function of PrP^c. To this extent, Prnp 0/0 mice may emulate this loss of function of PrP^c in a diseased state.

Consequently there is putative evidence that neurodegeneration caused by prion diseases may be pre-empted by a perturbation in neurophysiological function. One of the aims of this study is to investigate the change in electrophysiological function of specific areas of the brainstem, the histopathologically important NA and DMNX, to see if a change in their function could form the basis of a non-invasive live test for prion disease.

Synaptic transmission and short term plasticity were used to assess the differences in the expression of neurophysiological properties of two strains of PrP^c deficient mice and mice carrying a wild type transgene. It was found that the range of synaptic responses studied in sections of the hippocampus, *in vitro,* increased with the level of PrP^c expression. It was thought that the probability of transmitter release was unchanged in these situations (Carleton, Tremblay et al. 2001). In addition this group

found that with age, the absence of PrP^c is accompanied by an increased synaptic strength, assessed by comparing the slope of normalized input-output curves of excitatory postsynaptic potentials (EPSP). Increased strength was thought to happen by an increased recruitment of fibres before interactions at the synapse as opposed to increased probability of transmitter release at the synapse.

This latter observation would presume the existence of some mechanism by which older hippocampal fibres, depleted of PrP^c, may compensate for a smaller range in synaptic response to restore or maintain functionality of compromised neural networks (Turrigiano 1999). This study confirmed the synaptic location of PrP and its role in regulating synaptic transmission as found by other workers (Herms, Tings et al.1999). The data also support the idea of PrP^c being linked to the presynaptic vesicle protein synaptophysin (Fournier, Escaig-Haye et al.1995). Thus, there is strong evidence for a functional role of PrP^c in modulating synaptic transmission.

Additional evidence of the presynaptic location and function of prion protein is given in the work of Herms (Herms, Tings et al.1999). It was found that synaptic activity in response to hydrogen peroxide (H_2O_2) correlated with the amount of PrP^c expression in presynaptic neurons of the mouse cerebellum. H_2O_2 is known to decompose to hydroxyl radicals in the presence of iron or copper and alter synaptic activity. Consequently, evidence for the synaptic location and involvement in regulation of the presynaptic copper concentration for PrP^c was elucidated. Further investigations by these workers suggested that PrP^c is involved with the re-uptake of copper from the synaptic cleft since observations in Prnp 0/0 mice suggest copper is not taken up from the extracellular space and is not taken up into the presynaptic cytosol for reuse. Furthermore they postulated that the increase in concentration in the extracellular fluid in such mice may explain the change in $GABA_A$ receptors and change in long term potentiation reported by other workers such as Collinge. In addressing this functional role for PrP^c, Herms considered the conflicting results of Collinge, Lledo and others including their own previous work published in 1995 and concluded that slight differences in the extracellular copper concentration, temperature, brain sample thickness and location of cell recording within that sample may have contributed to the reported differences.

Other evidence for differences in observations by different groups on the location of PrP^c was given by Sales (Sales, Rodolfo et al.1998). It was suggested that PrP^c staining of cell bodies was not seen, which contrasts with the work of DeArmond (Dearmond, Mobley et al. 1987). Sales suggested the reason for this difference may be that the reagents used for the latter study were insensitive to PrP from hamster brains and that a more recent study by Taraboulos (Taraboulos, Jendroska et al. 1992), using the "histoblot" technique, supported the findings of their work. However one area that gave different observed PrP^c immunoreactivity between the study of Sales and Taraboulus was the basal ganglia. Sales noted a marked presence of PrP^c in the caudate, putamen and ventral pallidum. These reported differences in methodology represent caveats to a variety of histochemical analysis techniques and highlight the complexity and need for careful control in the identification of PrP^c at the cellular level. Possibly a complementary functional investigation of the changed neurophysiological function of normal versus abnormal prion may help comment on the overall effect of the pathogenesis of TSEs.

Signalling Functions of PrP^C

Further information on the role of PrP^c in the body comes from experiments on the signalling function of PrP^c. A cellular pathway through which PrP^c may influence synaptic function may be achieved by activation of the non-receptor, tyrosine kinase Fyn (Mouillet-Richard, Ermonval et al. 2000). This work involved the neuronal differentiation model 1C11. The 1C11 clone is a neuroectodermal progenitor with epithelial morphology that lacks neuron associated functions. Upon induction, the cells develop a neural like morphology and convert into serotonergic or noradrenergic cells. From this work it was observed that in order to trigger the PrP^c dependent tyrosine kinase Fyn activation in differentiating 1C11 cells, it depended upon the cells being fully differentiate serotonergic or noradrenergic progenies. Fyn is an intracellular protein and PrP^c is anchored to the outer membrane. Consequently, intermediate factors are likely to be involved in the PrP^c dependent signalling mechanism causing Fyn activation. It is also suggested that since the 37kDa laminin receptor binds PrP^c and that a GPI anchor relates PrP^c to the membrane, then a role as a cell surface signalling or cell adhesion molecule is possible for PrP^c. With the identification of PrP^c

as a signalling molecule there is an implication that extracellular signals may exist to trigger this membrane bound protein.

A signalling role during axonal growth has been suggested, with PrP^c localization at the surface of elongating retinal axons being reported by Sales (Sales, Hassig et al. 2002). This work highlights the importance of the interaction of PrP^c with the laminin receptor which binds laminin expressed on the surface of other cells. Laminin is regulated during development and contributes to axon growth and fibre tract formation by altering cell adhesion and presenting guidance cues dependent on structure and neuronal type (Dou & Levine 1995). Importantly, TSE infection is thought to spread along such fibre tracts (Beekes, McBride, & Baldauf 1998;Kimberlin, Hall, & Walker 1983). It is suggested that the transfer of these guidance cues may be achieved by PrP^c activation of Fyn (as alluded to by Mouillet-Richard, above). It was also noted that the relative abundance of PrP^c during neuronal development varied. If the results from this hamster study could be extrapolated to other mammalian species, it may suggest an abundance of PrP^c during brain development in childhood and adolescence which may have a bearing not only on the incidence of vCJD, but also on infection of BSE in young cows. In addition, this work identified regions such as the olfactory bulb and hippocampus as regions of high plasticity that were associated with high levels of PrP^c that remained high during adulthood. Consequently, the threat of prion infection could remain during adulthood. In contrast, the brainstem was seen to have little capacity for plasticity in adulthood and contained a lower level of PrP^c with little modulation of PrP^c during postnatal life.

The relationship of neuronal plasticity to PrP^c is also highlighted by the work of (Collinge, Whittington et al.1994). Here it was found that poor long term potentiation (LTP), which is associated with synaptic plasticity of memory and learning, is weakened in Prnp 0/0 mice. It was thought that the lack of PrP^c enhanced the N-methyl-D-aspartate (NMDA) receptor component of the excitatory post synaptic potentials (EPSPs) and this abnormal activation impaired LTP induction.

Prion Pathogenesis

Different pathogenesis based upon different disease strains

The dynamic process of prion pathogenesis may depend upon the strain of TSE infection. Aguzzi (Aguzzi, Heikenwalder, & Miele 2004) reported that prions are found in the lymph tissues in sheep scrapie and vCJD and less so in sCJD and BSE. He also states that it is well established that replication of the prion agent occurs in lymphoid tissues well before neuroinervation and subsequent detection in the CNS (Aguzzi, Heikenwalder et al.2004). This latter statement is supported by Glatzel, (Glatzel, Klein et al. 2000) who gave evidence for the role of the lymphoreticular system (LRS) in the spread of prions to the central nervous system.

The characteristic long incubation time for such diseases may be due to the multiplication of prions in reservoirs and it is suggested that parts of the peripheral nervous system or the LRS may be the location for such reservoirs (Glatzel, Klein et al.2000). Of particular interest are the intestinal Peyer's patches of the LRS which have been shown, in mice, to be the site of prion replication immediately after oral administration of infective agent (Kimberlin & Walker 1989). It is then postulated that certain components of the immune system such as follicular dendritic cells (FDC) are required for the spread of infection.

The transfer of infection from areas of the LRS to areas of the peripheral nervous system (PNS) may occur in unmyelinated nerve terminals associated with the mantle zone of the lymph follicles. This region may have processes belonging to FDC in close contact with nerve fibres of the PNS (Brown, Stewart et al. 2000). Axonal and non-axonal modes of transport may conceivably transport prions from the PNS to the central nervous system (CNS). Studies show that the rate of transport of PrP^{D} in the PNS was 1 to 2 mm per day (Kimberlin, Hall et al.1983) which does not correspond to fast axonal transport and so non axonal, retrograde transport via the glia or Schwan cells may be favoured.

A range of neural routes to transfer infectivity to the CNS is suggested from observations from the fact that direct intraneural injection of prions infects the CNS via the injected nerve. After intraperitoneal or oral infection, prions accumulate in lymphatic organs which are innervated mainly by fibres from the sympathetic nervous system (SNS). This would suggest a lymph-SNS-spinal cord-CNS pathway of infection. However, in more recent studies identification of a more direct route involving nerves of the parasympathetic nervous system (PNS), namely the vagus (cranial nerve X), have been shown (Beekes, McBride et al.1998). Glatzel reports that this more direct route seems to be highly significant when animals are challenged via the oral route (Glatzel, Klein et al.2000).

The pathogenesis of TSE diseases may depend on the particular strain of infection. Different strains may take a different route of infection. It may be possible that the target sites for this infection also play a part in the determination of the phenotype of the disease. For example, in the animal models involving intraperitoneal or intracerebral inoculation, the infection pathways may be different to those studies that mimic the “real world” postulate of infectivity by presenting oral challenge of infectious titre. Indeed, infectivity of one scrapie strain failed to produce pathology following intraperitoneal or intravenous inoculation but did demonstrate pathological signs following intracerebral inoculation (Blattler, Brandner et al. 1997).

Transfer of infectivity from the spleen to the central nervous system has been reported to be crucially dependent upon the expression of PrP in a “tissue compartment” interposed between the LRS and CNS (Blattler, Brandner et al.1997). Blattler further suggested that this compartment may comprise parts of the peripheral nervous system. Therefore, prion infectivity may well accumulate in areas of the LRS, specifically the Peyer’s patches of intestinal system, and then be directly transported via a PrP expressing tissue compartment, which may be the vagus, directly to the CNS, specifically the dorsal motor nucleus of the vagus nerve (DMNX).

From the work of Blattler, in mice it was observed that the only tissue outside the CNS in which scrapie prions had been detected was the LRS. It was not clear whether this may have been “spill-over”, infectivity generated in the CNS. One

postulate may be that there is a direct and relatively quick route of infection via the vagus to the CNS and due to centrifugal (down from brain) transport via peripheral nerves, secondary infectivity is promoted and replicated in areas of the LRS. Hence, there is a prospect of these reservoirs of infectivity facilitating the spread of PrP^D to many areas of the body. It may also be possible that the relatively small amounts of infectivity, initially seen in areas of the brainstem, may not be sufficient to be identified by current histochemical tests but may affect the neurophysiology, i.e. the functional activity of the brainstem neurons, in such a way as to be detectable.

New methods used to identify PrP^D have been recently developed which are many more times sensitive than previous tests. Such tests have been able to relate histological findings to biochemical investigations enabling the investigation of discrete areas of tissue (Krebs, Kohlmannsperger et al. 2006). In addition, continued refinement of the techniques used to identify the disease associated prion have been able to identify PrP^D in the muscle of scrapie infected hamsters (Thomzig, Schulz-Schaeffer et al. 2004) and autopsied muscles of humans with vCJD, CJD and iatrogenic CJD (Peden, Ritchie et al. 2006).

Vagal route of entry for Prion to the CNS

Evidence for the idea of multiple routes of infection comes from the work of Baldauf (Baldauf, Beekes, & Diringer 1997). The data from this study, using intraperitoneal infection in hamsters, suggested three points of entry into the spinal cord for scrapie infectivity. In addition, strong evidence for a direct route, by-passing the spinal cord, for infectivity to access the brain was seen. This alternative pathway to the brain was confirmed by data from hamsters which received an oral challenge. By assaying various tissue samples for scrapie infectivity for each animal, it was shown in many animals that accumulation of infective prion protein was seen in the lower spinal cord and in some brain areas with no pathological protein in the cervical spinal cord. Similar observations were seen in experiments with sheep (van Keulen, Schreuder et al. 2000) see figure 1.3.

Recent reports stated that the vagus of cows infected with BSE were found to be positive for the disease conformation of the prion protein (Yoshifumi Iwamaru, Yuka Okubo et al. 2005). Further observations from the work of Baldauf (Baldauf, Beekes et al.1997) were the lack of pathological prion in the spleens of some animals, leading to the conclusion that the spleen may play a role in the pathogenesis in some animals, but it may not be essential.

Further work on this proposed "alternative" direct route of infection was performed by Beekes, again with oral challenge of scrapie to hamsters (Beekes, McBride et al.1998). Results for this study presented evidence that in this animal model, initial infection of the brain occurred via the vagus nerve rather than by spread along the spinal cord. The first area of the brain to show prion deposition was the DMNX followed by the Nucleus Tractus Solitarii (NTS). Consequently, it is suggested that the spread of infectious prion to the brain may be facilitated by parasympathetic efferents and associated afferent fibres of the vagus.

Vagal efferents have nerve cell bodies in the DMNX and vagal afferents have nerve cell bodies in the ganglion nodosum (GN). However, afferent fibres terminate in the NTS where they synapse with interneurons which directly project to motor neurons in the DMNX. It is important to note that efferents and afferents of the vagal circuit innervate the heart and visceral organs of the digestive tract such as the stomach. Consequently a "fast vagal" route of infection from the stomach to DMNX may be provided by the vagus which may be the required "compartment" referred to by Blattler mentioned above. In addition if figures 1.3 and 1.4 are considered in conjunction with further evidence from van Keulen, it is suggested that the DMNX is stained positive for prion at around 10 months post inoculation. At this time in the same animal the GN was negative. This suggested an initial infection facilitated by the efferent vagal fibres and a later spread from the DMNX to cell bodies of the afferent branch of the vagus situated in the GN. Consequently there was putative evidence for a stomach-vagus-DMNX-NTS-GN chain of infectivity.

Examination of the DMNX of 10 scrapie infected sheep showed typical vacuolation and variable gliosis. In addition, herniation of membranes and organelles from seemingly healthy processes into neighbouring vacuoles and dendrites were seen (Ersdal, Simmons et al. 2003). Similar observations were identified by Jeffery(Jeffrey, Goodsir et al. 2009) and Dorban (Dorban, Defaweux et al. 2007) Consequently it may be possible that the abnormal PrP^{D} may cause herniation in the myelination of vagal fibres which would limit the transmission of neural control to and from target organs such as the heart, due to a breakdown in saltatory conduction as a result in this disruption of the myelination.

Figure 1. 3 Pathology of natural scrapie.
Figure adapted with kind permission of Springer Science and Business Media.
from Prion Diseases; Diagnosis and Pathogenesis Groschup, Martin H.; Kretzschmar, Hans (Eds.)
Special edition of Archives of Virology, Suppl. 16 2000, IX, 290 p. 89 illus.,
Hardcover ISBN: 978-3-211-83530-2.van Keulen 2000, Pathogenesis of natural scrapie in sheep

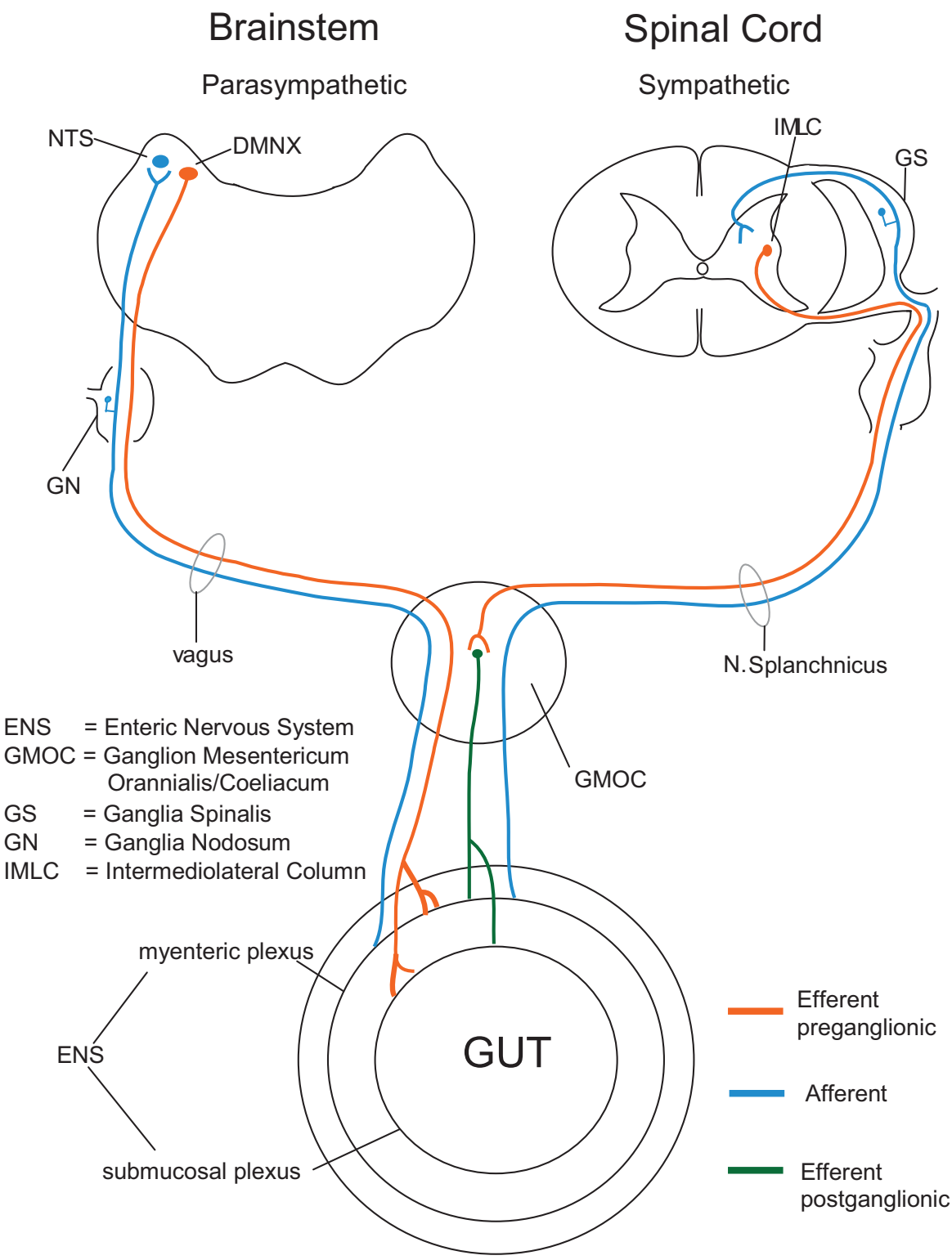

Pseudorabies virus in relation to proposed prion infection

Both Bauldauf and Beekes mentioned that the neuroanatomical sequence of target areas for TSE prions were reminiscent of the pathology of pseudorabies virus (PRV, a virus of the genus *Varicellovirus* that is the etiologic agent of pseudorabies and also called suid herpesvirus 1) as studied by Card and Standish (Card, Rinaman et al. 1993;Standish, Enquist, & Schwaber 1994). Although prions are not considered as viruses, the viral route of infection may also be a mode for brainstem infection for prions as recently illustrated by the spongiform neurodegeneration similar to that caused by prions induced by a retrovirus (Li, Cardona et al. 2010). Work using PRV to trace the innervation of the heart showed it was possible to trace the targets of the vagal motor neurons, which are interrupted by postganglionic neurons at the heart. The pseudorabies virus was used as a transynaptic tracer. PRV can be injected directly into the myocardium and traced from there to postganglionic neurons that innervate this area. Here, PRV is seen to replicate and then retrogradely crosses synapses to be transported to specific vagal preganglionic neurons. If prion was to follow a similar modality then this would highlight the importance of postganglionic complexes and also suggest a site for “reservoirs” of infectivity mentioned previously (Glatzel, Klein et al.2000).

The PRV work also suggests a potential difference in neuronal target sites dependent upon different strains. Experiments with PRV demonstrated that different distributions of vagal motor neurons were labelled by different viral strains. The more virulent strain labelled the DMNX and NA in contrast to two less virulent strains which targeted neurons of the NA and rarely those of the DMNX. This difference in labelling due to strain differences of the virus may also indicate a different functional consequence if TSE strains infect and damage different populations of neurons. Again, if this model may be applied to the passage of infective prion to similar areas of the brainstem then it may be possible that a less virulent strain of TSE may cause a different evolution with respect to time, neurophysiological and clinical signs. Consequently, one postulate may be the current incidence of vCJD may be due to one (virulent) strain of infectious TSE and other individuals may succumb to a lesser strain, later in time.

Work with PRV by Card illustrated a potential route of infection for TSEs (Card, Rinaman et al.1993). Card stated "the peripheral projections of the DMV (DMNX) neurons and the ability to infect them by injecting virus into the wall of the stomach provide an ideal system for evaluating the CNS response to infection." This statement highlights a potential route for prion infectivity, illustrated here with PRV, that suggests that the spread to the CNS following inoculation in the stomach may be accomplished by retrograde transport to the DMNX. This is supportive of the vagal route of infection postulated by Beekes as an alternative route of prion infection (see figure 1.3).

Possible polypeptides associated with prion pathogenesis

In support of the route of infection illustrated by the work with PRV, Mishra (Mishra, Basu et al. 2004) cited many workers, including Bons *et al*, Beekes and McBride, Foster *et al*, Nicotera, Haik *et al*, Aguzzi and Polymenidou, who reported accumulation of PrP^D in the Peyer's patches, lymphoid tissue of the gastro intestinal (GI) tract and peripheral and enteric nervous systems (an interdependent section of the autonomic nervous system pertaining to the small intestine) . PrP^D from the lumen of the intestine was believed to be involved with, among other cell types, dendritic cells of the intestine and M cells lining the mucosa as it was taken up into the lymphoid tissues of the gut and replicated. Mishra *et al* unexpectedly found, from *in vitro* studies, that ferritin was co transported with PrP^D. Ferritin is a prominent component of the PrP^D-protein complex formed when infected brain homogenate is treated with digestive enzymes. A receptor or transporter mediated pathway is thought to be used in the transport of the PrP^D – ferritin complex. Since ferritin has a similar homology across a wide range of species, there is thus potential that PrP^D associated proteins, such as ferritin, may facilitate PrP^D uptake in intestines of distant related species and therefore "lower the species barrier". This may allow the infected animal to become a carrier or confer increased susceptibility to a wider variety of prion strains.

Links between the vagus nerve and the intestines are expressed in research on ghrelin. Ghrelin is a 28 amino acid gastric peptide hormone that has been reported to coordinate multiple functions in the gastro intestinal (GI) system (Zhang, Lin et al. 2004). This coordination and regulation of the GI system is mediated by a vagus nerve (activity in cranial nerve X) dependent mechanism. Zhang *et al* also reported that ghrelin receptors were present in the DMNX of rats and that ghrelin promoted neurogenesis *in vitro* and *in vivo.* The dorsal vagal complex was found to respond to perturbation in the level of ghrelin, induced by vagotomy, by an increase in cell proliferation. This may, therefore, suggest a degree of neuronal plasticity in the DMNX. Thus, the DMNX could alter its neurogenesis and hence change its neurophysiological function dependent upon deficient vagal input. It is interesting to think that an intestinal protein such as ghrelin would have a neural link to the DMNX (via the vagus) with specific receptors situated in this brain region. The activation of these ghrelin receptors would promote neurogenesis to generate more neural activity so as to attempt to maintain functional loss caused by vagal mediated neuronal damage to areas of the DMNX. This work highlighted a vagal pathway for peptides from the gut to the brain and also raised the possibility of a degree of plasticity and recovery of function for regions in the DMNX. This deficient vagal input created in this experiment could also be achieved by the presence of PrP^{D} in the cell bodies of vagal fibres originating in the DMNX. Consequently a recovery of function in the output of vagal efferents, to the heart for example, may be seen in incubating subjects with TSE diseases, presenting a “see-saw” pattern in their output with respect to time.

Further research involving ghrelin illustrates a potential link to feeding in sheep. It was suggested that ghrelin secretion is modulated by cholinergic neurons of the vagus (Sugino, Yamaura et al. 2003). A similar relationship of ghrelin to parasympathetic preganglionic neurons of the rat and mouse has been observed (Zigman, Jones et al. 2006). This relationship between the stomach and neurons of the brainstem emphasises a neural pathway that may provide a route of infection for disease associated prion.

Additional evidence to support this “alternative” route of infection from stomach to brainstem via the vagus nerve fibres as intimated by Beekes, is presented in the work of van Keulen (van Keulen, Schreuder et al.2000). The pathogenesis of scrapie in sheep raised on land where scrapie had occurred at a high incidence for a number of years was investigated. It was found that at 5 months old, PrP^D was present in all lymphoid tissues, including Peyer’s patches and it was evident in the enteric nervous system (ENS) at the level of duodenum and ileum (see figure 1.4). At 10 months, PrP^D deposition was evident in the DMNX and by 17 months the entire nucleus of the DMNX stained positive in some animals and low grade vacuolation was also present in DMNX. In addition at 17 months old the NTS and NA were also stained indicating the presence of PrP^D. After 21 months PrP^D was widely distributed in the brain from the obex to the thalamic area and also infected the trigeminal ganglion and spinal ganglion of segments T7-T12. PrP^D was also seen in the grey matter of the spinal cord of segments T1-L3. In the late stages of the disease, around 26 months old, PrP^D was widely distributed in the brain and spinal cord encompassing all cervical, thoracic and lumbar segments and in the majority of spinal ganglia.

From such longitudinal studies of scrapie infection it is concluded that the ENS may act as a portal for entry of infectivity to neural tissues. Infectivity then spreads in a centripetal and retrograde manner through the parasympathetic efferent fibres to the DMNX at the same time as spread via sympathetic fibres to the spinal cord. PrP^D accumulation in sensory ganglia after infection of the CNS may be due to centrifugal and anterograde spread from the CNS through afferent fibres. This idea may equate to the “spill-over” of infectivity suggested by Blattler, mentioned above.

Figure 1. 4 Pathogenesis of PrP^D in scrapie.
Figure adapted with kind permission of Springer Science and Business Media.
from Prion Diseases; Diagnosis and Pathogenesis Groschup, Martin H.; Kretzschmar, Hans (Eds.)
Special edition of Archives of Virology, Suppl. 16 2000, IX, 290 p. 89 illus.,
Hardcover ISBN: 978-3-211-83530-2.
van Keulen 2000, Pathogenesis of natural scrapie in sheep

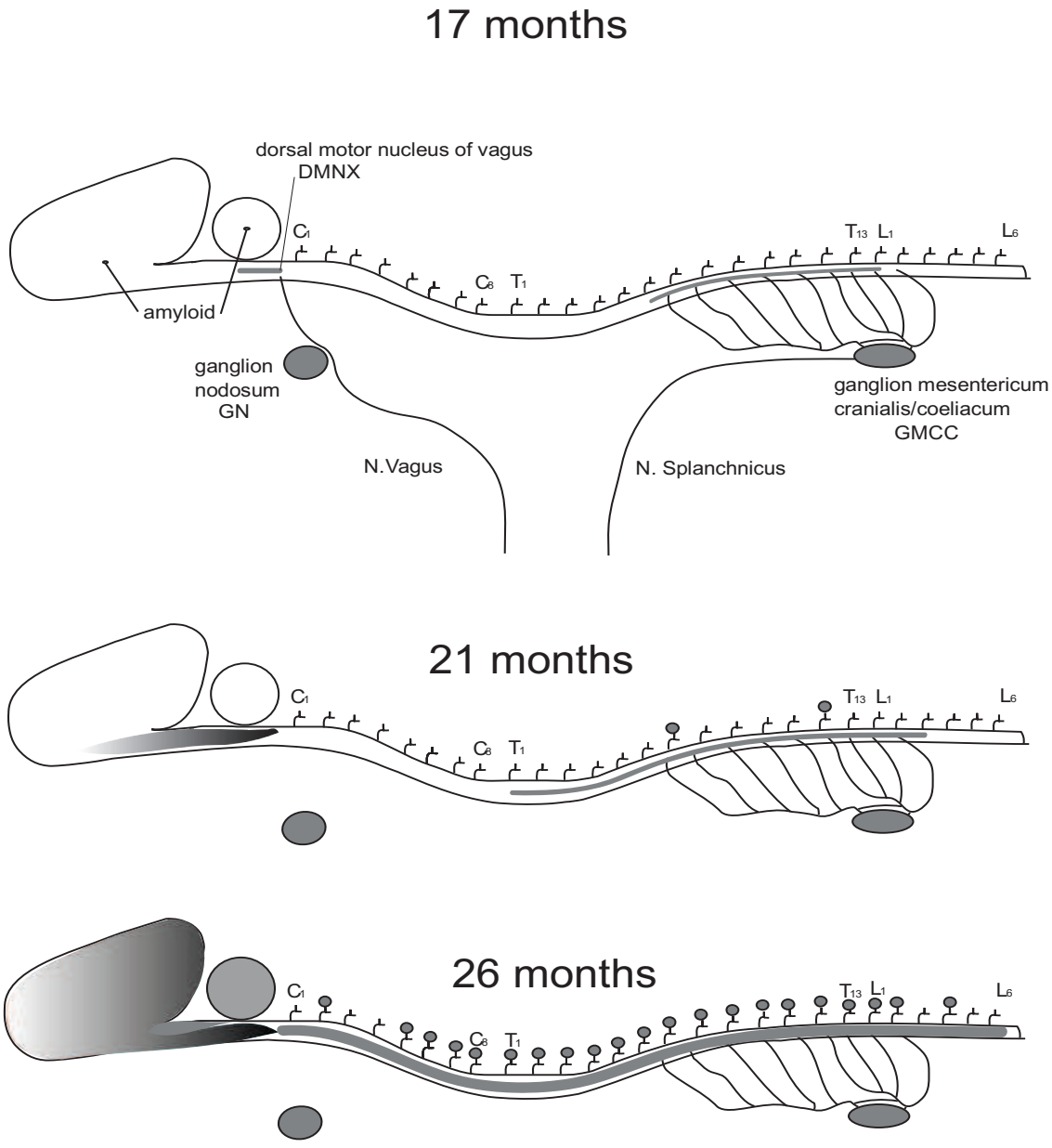

Schematic representation, adapted from van Keulen, indicating PrP^D accumulation (Grey shading) in the ENS, efferent nerve fibres and CNS. **Note DMNX is stained independently from spinal cord presumably via the vagus nerve at 17 and 21 months**

Interaction of brain and heart

A wandering path from brainstem to heart

The Dorsal Motor Nucleus (DMNX) and Nucleus Tractus Solatarii (NTS) of the brainstem are used as diagnostic regions in the diagnosis of TSEs. These regions of the brainstem are the locations of the cell bodies for the efferent and afferent parasympathetic nerve fibres that control the heart on a beat to beat basis and connect to the heart via the vagus nerve.

The vagus nerve (cranial nerve X) contains both afferent and efferent fibres forming an extensive "wandering" (vagus derived from the Latin *vagus* meaning wandering) network of neural communication. Among other alternative names for the vagus nerve is the pneumogastric nerve which emphasises the fact that the 10^{th} cranial nerve targets the lungs and stomach, especially relevant to the physiologically-coordinated function of the lungs and the postulated ingress of infectious agent in prion disease discussed here. In mammals, around 80% of the nerve fibres are afferent transmitting sensory information to the brainstem and the remaining 20% are efferent conveying information to target organs. Both myelinated and unmyelinated efferent cardiac nerve fibres have their nuclei in the medulla oblongata of the brainstem. The majority of myelinated, fast-conducting nerve fibres have their cell bodies in the nucleus ambiguus (NA) and cardiac motor efferents with slower, unmyelinated nerve fibres have their origin in the dorsal motor nucleus of cranial nerve X (DMNX). The nucleus tractus solitarii (NTS) provides a sensory centre for afferent information from a variety of target organs including coordinating the afferent information from the lungs, heart and stomach.

The efferent vagal control of the heart on a beat to beat basis is similarly complex. In addition to vagal innervation of the atria via the SA node, the ventricles have also been shown to have vagal innervation (Standish, Enquist et al.1994). As part of providing histological evidence for these neural connections, a new type of retrograde tracing technique using pseudorabies virus, instead of cholera toxin-conjugated horseradish peroxidase (CT-HRP), was required to overcome the barrier provided by intrinsic cardiac ganglion on the heart. Three strains that differed in their virulence

were used in the retrograde tracing studies and it was observed the most virulent strain labelled neurons of the DMNX and NA at the level of the obex, while the less virulent strains identified neurons of the NA and infrequently neurons of the DMNX. Secondly, it was noted that given a longer time following injection of the pseudorabies virus in the heart wall, the NTS was also identified by retrograde labelling. This latency in labelling suggests a possible interneuron connection between the NA/DMNX and NTS in cardiac vagal regulation of the heart (Standish, Enquist et al.1994). Prion infection could echo the pathway illustrated by the pseudorabies virus and affect those sites listed above.

Similar pseudorabies virus tracing has been performed on the vagal connection to the gut. It was found that injection of the stomach with the retrograde tracer, labelled neurons in the DMNX. This observation also highlights the path and a putative mechanism for the entry of disease associated causative agents whether or not they are prions or virus like particles as some workers point out (Manuelidis 2004;Manuelidis.2006;Manuelidis, Liu, & Mullins 2009;Manuelidis, Yu et al. 2007;Walker, Levine, & Jucker 2006).

The vagus nerve also communicates with the lungs and provides a means of matching the beat to beat change in the heart rate with the breathing frequency. The slight increase in heart rate during inspiration and decrease during expiration is termed respiratory sinus arrhythmia (RSA) and is mediated by cardioinhibitory parasympathetic neurons communicating from the brainstem to the heart by means of the vagus nerve. During the inspiratory phase of respiration, GABAergic and glycinergic spontaneous firing rates are reported to increase. Application of a nicotinic antagonist abolished the respiratory increase in GABAergic neurons and did not alter the increased rate seen in glycinergic neurons, consequently a functional role for acetylcholine is apparent in the coordination of RSA along with GABA and glycine (Neff, Wang et al. 2003).

Further work into the spontaneous GABAergic inhibitory post synaptic potentials in the control of cardiac vagal neurons has elicited that the presynaptic GABAergic input to these vagal neurons in the NA occurred at a lower frequency than those cardiac vagal neurons in the DMNX. When the NTS was electrically stimulated, neurons in both the NA and DMNX were evoked (Wang, Irnaten, & Mendelowitz 2001), emphasising the inter-relationship between the NTS, NA and DMNX. Also, this evoked activity was abolished by application of the $GABA_{(A)}$ antagonist bicuculline, therefore implicating a $GABA_{(A)}$ mediated pathway linking the NTS to both NA and DMNX.

The vagus nerve has been identified as being positive for disease associated prion protein (Prp^{D}) in cows incubating BSE (Masujin, Matthews et al. 2007). The DMNX is reported to be one of the first areas to be infected with Prp^{D} in similar transmissible spongiform encephalopathies (TSEs) (Ersdal, Simmons et al. 2004;Sigurdson, Spraker et al. 2001;Spraker, Zink et al. 2002;van Keulen, Bossers, & van Zijderveld 2008;van Keulen, Schreuder et al.2000). The NTS and NA are also reported to show the presence of disease associated prion in TSE disease (Ersdal, Ulvund et al. 2003;Nentwig, Oevermann et al. 2007). Prion has also been reported in heart muscle following prion disease infection (Jewell, Brown et al. 2006).

The complex dynamic neural interactions between the heart and brain were first noted by Bernard and Darwin in the nineteenth century. Claude Bernard in 1865 described the heart as a "...centre influenced by all sensory influences. They may be transmitted from the periphery through the spinal cord, from the organs through the sympathetic nervous system, or from the central nervous system itself" (Cournand 1979).

Charles Darwin emphasizes the findings of Bernard by stating that "especial notice" should be paid to a two way communication between the heart and brain, which Darwin refers to as "the two most important organs of the body". Darwin states on page 69 of "Expressions of the Emotions in Man and Animals"; "when the heart is affected it reacts on the brain; and the state of the brain again reacts through the pneumo-gastric [vagus] on the heart" (Darwin 1872). This quote, by referring to the

vagus as the pneumo-gastric nerve, also serves to remind us of the relationship of the vagus to the gut and lungs. The intimate association of the vagus with the gut may have a role to play in the infection for transmissible spongiform encephalopathies. It also suggests a neural feedback system between the heart and brain and in addition suggests why changing activity in the “pneumo-gastric nerve” [vagus] may relate to neural involvement of both the heart and lungs via this common pathway.

Although these observations and statements were made by adopting a psychophysiological approach, their effect on current neurophysiological and anatomical studies is clear. The dynamic interactive bi-directional relationship between the heart, lungs and brain was established and provided the topic for further investigation.

The Orienting Response

Further evidence for the neural regulation of the heart by the autonomic nervous system may be taken from research into the psychophysiological study of the bidirectional interactions between the brain and peripheral sensory processes that constitute psychological and physiological state (Sokolov 1963).

Contemporary studies of this orienting reflex, suggests there is a bradycardia which functionally influences the sensitivity of perception by allowing the processing of information about the external environment to occur. The time course of the responses and studies of clinical cases suggested that mediation of the cardiac orienting component is neural and specifically involves the brainstem and the thalamic portion of the reticular formation. (Graham & Clifton 1966;Lacey 1967;Sokolov.1963). In their review of the Sokolov and Lacey theories, Graham and Clifton state that the orientating reflex is not observed in human infants until after the first few months of life. From this evidence I note that this may also indicate that functional neuronal maturity is developed in the new-born infant during the first months of life and the lack of functional maturity in neural circuits may have relevance in Sudden Infant Death Syndrome (SIDS) during these first months of life.

Research utilizing atropine blockade demonstrated that the short duration slowing of the heart involved in this orienting response are mediated by cholinergic pathways of the vagus (Berntson, Cacioppo, & Quigley 1994). Various clinical populations with peripheral neuropathies report abnormal vagal function. Changes in heart rate, as a result of changing autonomic function, were observed with respect to changes in blood pressure and age (De Meersman 1993;Gribbin, Pickering et al. 1971;Weise & Heydenreich 1991;Wieling, van Brederode et al. 1982). Wieling and Weise used techniques based on the beat to beat variability of heart rate (RR interval analysis) to assess vagal tone in a diseased state (diabetes) and suggested that a change in such indices may be evident when the diabetic patient was first diagnosed as opposed to the more common observations of vagal dysfunction in patients who have endured diabetes for a length of time.

Further studies of individuals with unilateral brain damage indicate that heart rate responses are affected most in individuals with right side damage (Yokoyama, Jennings et al. 1987). This evidence relates to the neurophysiological and neuroanatomical investigations in animals and man, suggesting that the regulation of heart rate is mainly related to the right vagus affecting the sinoatrial node (SA node) (Mace & Levy 1983) with higher ipsilateral brain centres controlling heart rate (Williams & Warwick 1980). From these lines of evidence it may be concluded that the vagus, particularly the right hand branch, is able to convey neural signals which can have a direct and quickly acting beat to beat effect on the heart beat cycle.

The Vagal Paradox

Respiratory Sinus Arrhythmia (RSA) is the change in the beat to beat variability that is synchronized to the breathing cycle. Porges in his seminal work on the “Polyvagal Theory” (Porges 1995) indicated cases where heart rate increases and RSA decrease in relation to each other , such as in exercise (Billman & Dujardin 1990) and studies using atropine, as a neural blockade, to covary (negatively) both heart rate and RSA (Cacioppo, Berntson et al. 1994;Dellinger, Taylor, & Porges 1987;Porges 1986).

Physiological and anatomical evidence would suggest both chronotropic control of the heart (i.e. heart rate) and the degree of RSA are both controlled by vagal mechanisms (Jordan, Khalid et al. 1982;Katona & Jih 1975). Here, a direct linear relationship between change in the beat to beat interval, and parasympathetic activity is demonstrated.

So although there are occasions where certain measures of cardiac control, RSA and heart rate vary in conjunction with each other, there are occasions where the changes suggest independent sources for neural control of heart rate and RSA. This divergence in functional outcome for the control of the heart has been postulated as the result of the average heart rate representing tonic vagal influences (from neurons generating an extended sequence of activity or entering a state where action potentials are generated continuously) and the changing RSA as representing phasic vagal influences (from neurons generating one or more action potentials in a short time) (Berntson, Cacioppo, & Quigley 1993;Jennings & McKnight 1994;Malik & Camm 1993). Other explanations include the variations being due to changes in respiratory parameters and the methods used to quantify the changes in heart rate and RSA. Further explanations have taken a more holistic interpretation and suggested that the average heart rate is a product of complex and dynamic interactions of the sympathetic and parasympathetic systems in conjunctions with mechanical and biochemical constraints (Berntson, Cacioppo et al.1993), whereas RSA is considered to be a more purely vagal phenomenon. Similarly divergences have also been observed in anaesthesia where RSA may form a more useful indicator of depth of anaesthesia than heart rate (Donchin, Feld, & Porges 1985;Pomfrett 1995;Pomfrett, Sneyd et al. 1994).

Porges goes on to summarize that there may be a contradiction in the duality of the relationship of heart rate and RSA based on the assumption that there is one central source for cardiac vagal tone. He summarizes it as a Vagal Paradox in the table below:

Table 1-1 The Vagal Paradox

1 Increased vagal tone produces neurogenic bradycardia
2 Decreased vagal tone produces suppression of RSA
3 Bradycardia occurs during periods of suppressed RSA

(from Porges, A Polyvagal Theory, 1995)

On occasions RSA and heart rate seem to reflect the same physiological change but in other instances they seem to reflect separate processes. This line of reasoning led Porges to suggest that, in mammals, there are two anatomically based vagal response systems.

Porges suggests the proposed Polyvagal Theory is better understood if the neuroanatomy and neurophysiology related to the vagus are explored. The vagus nerve contains a variety of neural pathways, 80% of the experimentally evaluated 30,000 fibres were afferent fibres (Agostoni, De Daly et al. 1957;Chase & Ranson 1914). Cell bodies of the vagus are located in the left and right sides of the brainstem and these perform different functions in regulation, with the right side vagus being the dominant factor in chronogenic regulation of the heart. In addition to this, different vagi have different roles in the regulation of their target organs and may have opposing effects on the same target organ (Williams & Warwick.1980). Vagal tone then, may not be applied to either the vagus as a whole or indeed to the control of a specific organ but may be applied to a particular branch of a specific part of the vagus and caution on the assessment of vagal tone on the heart from interpretation of RSA alone is intimated (Grossman & Kollai 1993;Malik & Camm.1993).

Anatomical and functional evidence to support the Polyvagal Theory

Within the medulla of the brainstem, three neural structures are involved with the primary central regulation of the vagus. The dorsal motor nucleus (DMNX) and the nucleus ambiguus (NA) are areas of the medulla from which the vagal motor fibres originate, with DMNX located in the dorsomedial medulla and NA being more ventral (Kandell, Schwartz, & Jessell 2000;Williams & Warwick.1980). A third nucleus in the medulla, the nucleus tractus solitarius (NTS) is the site where many afferent pathways from peripheral organs terminate. Both the DMNX and NA have neural input from NTS along with input from central nucleus of the amygdala and hypothalamus (Hopkins 1987;Leslie, Reynolds, & Lawes 1992).

In mammals the main inhibitory motorneurons for the heart are located in the NA and motorneurons from the DMNX contribute non-myelinated axons to the cardiac vagal branch (Bennett, Ford et al. 1984;Bennett, Kidd et al. 1981). Myelinated vagal axons from neurons in the NA have a cardioinhibitory and bronchoconstrictor role and conduct in the B fibre range (McAllen & Spyer 1976;McAllen & Spyer 1978b). In contrast, the nonmyelinated fibres from neurons in the DMNX conduct in the slower C fibre range(Ford, Bennett et al. 1990). (There are also reports of cardioinhibitory neurons located in both the DMNX and NA of the rabbit and cat, with efferent axons conducting in the B fibre range (Ciriello & Calaresu 1980;Ciriello & Calaresu 1982;Jordan, Khalid et al.1982)).

The role of these nonmyelinated vagal fibres from neurons in the DMNX is not well understood at present, with conflicting responses to their stimulation seen in different animals. Heart rates of cats (Ford, Bennett et al.1990) and dogs (Donald, Samueloff, & Ferguson 1967) did not alter when these nonmyelinated fibres were stimulated. In contrast, the heart rate of rabbits slowed when these fibres were stimulated (Ford & McWilliam 1986;Woolley, McWilliam et al. 1987b). So their effect on HRV in different mammalian species is also not defined and raises the question of the organizational diversity of theses vagal nuclei in relation to function for different mammalian species.

Porges postulates that the function of these nonmyelinated fibres may be dependent on the outflow of the myelinated NA fibres. The contribution of these nonmyelinated fibres may change as the effect of the NA fibres on the SA node of the heart is changed. For example, when the "vagal brake" on the heart is released by decreased efferent activity from the NA fibres, the slower unmyelinated fibres from the DMNX may act as a lower frequency (longer time period) mediator of heart rate and HRV. Studies involving the rabbit have found that recruitment of nonmyelinated fibres of the vagus in conjunction to myelinated fibres increase the magnitude and duration of the evoked bradycardia in response to electrical stimulation (Ford & McWilliam.1986). This type of synergistic effect of myelinated and nonmyelinated vagal fibres may also play a role in the control of the heart. The complementary action of the DMNX to the NA is also suggested by domoic acid lesion studies in rats (Cheng, Zhang et al. 2004b).

I propose this idea may have direct relevance to malfunctioning vagal nuclei, as a result of incubating prion disease, leading to a change in beat to beat variability in the control of heart rate. In addition, if the gating of intrinsic cardiac ganglia (see Intrinsic and Thoracic Ganglia section, on page 60 of this thesis) is factored into the analysis then there is further atypical coordination that could result from damaged cardiac vagal efferent and afferent nerve fibres.

More evidence that relates to prion diseases possibly causing a change in the beat to beat variability in the control of heart rate (HRV) is the observation that degenerating fibres are present in the cardiac branch of the vagus following lesions to the DMNX (Calaresu & Cottle 1965). In the incubation of prion diseases, the build-up of prion protein may cause lesions in the DMNX, which is a diagnostic criterion, that could then cause cardiac vagal fibres to degenerate and hence malfunction. The resultant abnormal vagal output may be detected by HRV analysis. This advancing deterioration in vagal efferent and afferent traffic may give rise to a "See-Saw" response in the heart rate variability as the dynamic and integrated system of neural activity attempts to restore physiological homeostasis to the heart rate. This idea is supported by the recovery of function of areas of the brainstem in adult rats following

domoic acid lesions, with HRV returning to normal values 90 days after lesions (Cheng, Guo et al. 2002).

This neurophysiological and anatomical evidence suggests a clear structural difference between the two vagi which would support the functional dichotomy on which the “Polyvagal Theory” is based. Under certain circumstances, the control of the heart and degree of RSA (hence HRV) acts as if it is controlled by one “centre” and in other circumstances, behaves as at least two separate controllers are involved. Any model of functionality must account for this duality of control and changes in heart rate variability.

In addition to the central neurological control of the heart, Porges also states the “Polyvagal Theory” requires an expansive conceptualization of the ANS to include target organ afferent and efferent pathways. Furthermore his theory is derived from a series of neurological investigations that decompose and partition the beat to beat heart rate signal into constituent periodic components representing neurophysiological feedback loops that represent the sub second, beat to beat variability in the heart rate as the sum of several superimposed oscillations and slow trends that vary with metabolic demands. The two most reliably described oscillations occur at "fast" frequencies associated with breathing and a slower or "low" frequency change associated with the endogenous rhythm of blood pressure regulation via baroreceptors and vasomotor activity.(Porges 2006b). Consequently peripheral systemic factors are included in the evolution of the theory but only those that have a periodicity that would affect the "fast" and "slow bands" of oscillations on which the theory was developed.

From neuroanatomical and neurophysiological evidence, Porges’ Polyvagal Theory constructs various premises, the first of which is that the bradycardia associated with the orienting response is mediated by the DMNX and that suppression of the amplitude of RSA is mediated by NA. Porges states that suppression of heart rate variability is the same as reducing the amplitude of RSA. The degree of RSA may not be a total indicator of HRV since it may be possible to have very little RSA but have lower frequency changes in HRV. HRV being the sum of all spectral components not

just the high frequency band (>0.15 Hz) that represents RSA. The distinction of RSA as a subset of total HRV may be useful in interpreting subtle and dynamic variation in HRV and may give a better insight into the relationship of NA and DMNX on heart rate in diseased states where “normal” function is mitigated. For example if the normal NA efferent action is compromised, the slower acting DMNX efferents may alter the beat to beat fluctuations in heart rate as discussed above.

Further evidence is presented for the involvement for the DMNX in non-baroreceptor mediated bradycardia in rabbits. These animals exhibited different bradycardic conditioned responses following sinoaortic denervation. Here the afferent branch of the baroreceptor reflex was destroyed which did not stop bradycardia from occurring. It is argued that the induced conditioned bradycardia was mediated along DMNX pathways (Jarrell, Gentile et al. 1986).

The aortic depressor nerve communicates with both the DMNX and NA and when this was electrically stimulated in the rabbit, there was a bradycardia and increased RSA. Stimulation of the DMNX in isolation only gave bradycardia, with a 50% reduction in the extent of bradycardia elicited (McCabe, Yongue et al. 1984).

Figure 1. 5 Stimulation of DMNX and Aortic Depressor Nerve.

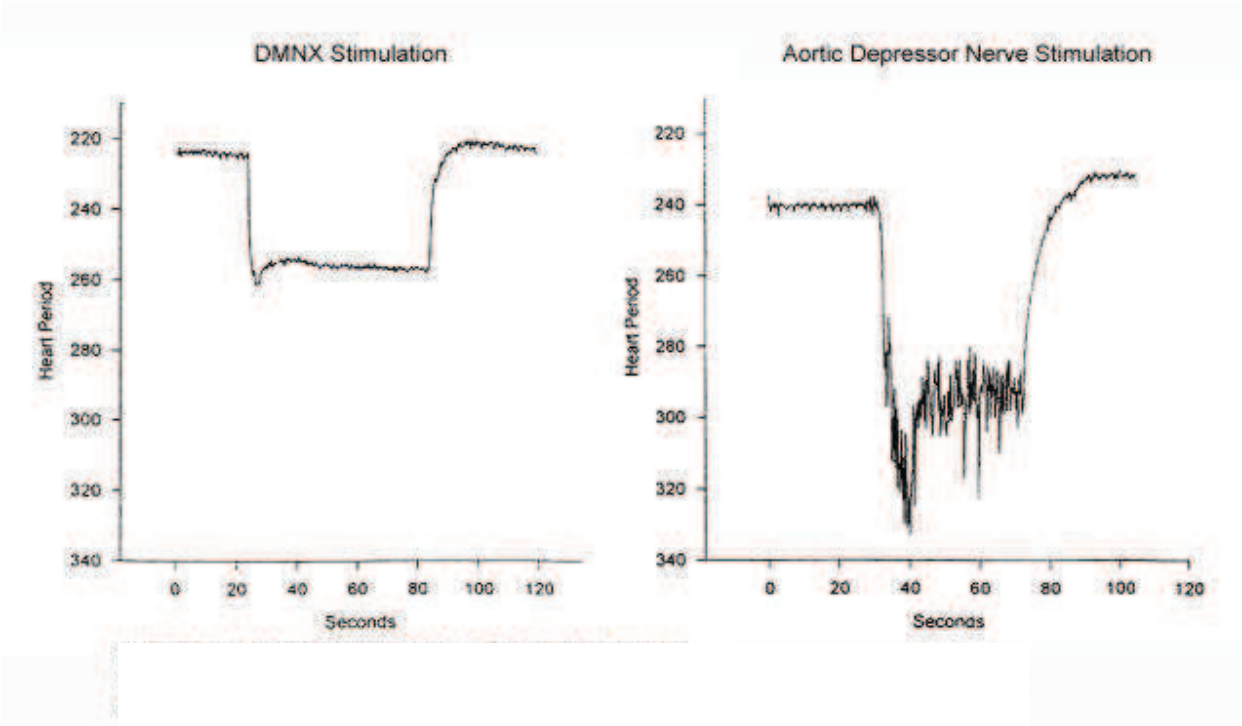

Figure 1.5, from Porges' Presidential Address to the Psychophysiology Society in 1994 (Porges.1995), representing the work of McCabe, illustrates the difference between electrical stimulation of the DMNX and the aortic depressor nerve stimulation to elicit bradycardia. There is a very obvious difference, not only in the magnitude of bradycardia, but also the manner in which that bradycardia was delivered. In the first of the figures (stimulation of the DMNX directly) there appears to be a more smoothly mediated increase in heart period hence slowing of the heart), with a relative smooth maintenance of the elicited bradycardia.

This contrasts markedly with the over shoot seen when both DMNX and NA were stimulated via aortic depressor nerve along with the large scale changes in heart period seen throughout the stimulation period. I postulate this could demonstrate a greater degree of deviation in the heart rate period when the NA and DMNX were stimulated together. There may be evidence here for an increased amount of HRV associated with the heart rate when both NA and DMNX are activated when compared with DMNX activation alone. Conversely there is a smaller deviation in heart period without the activation of neurons from the NA. Possibly a change in HRV would be evident if any abnormal or forced firing of these brainstem nuclei occurred. This may be the case in prion diseases where damage to one or both of the neural pathways could result in abnormal HRV.

So the NA plays a major role in baroreflex mediated changes in heart rate with contradicting evidence for the role of the DMNX in baroreflex mediated changes to heart rate. The weight of evidence from scientific investigation in many species, however, suggests that both the NA and DMNX are involved with the control and coordination of the heartbeat. This inconsistency in structure and function of the DMNX may be due to several reasons. Firstly, the method of stimulation or lesion generation may not be able to solely stimulate or lesion purely the DMNX due to its close proximity to NA. Secondly there may be species differences in the functions of these two areas of the medulla and some mammals may have neurons near or integrated with the DMNX that are part of a common cardiopulmonary oscillator (Richter & Spyer 1987). It is important to note that a change in activity in either or both vagal nuclei may give differing results depending upon the species being studied.

From Reptiles to Mammals

Porges gives more evidence to support his Polyvagal Theory by identifying evidence from the evolution of reptiles and mammals. He stated that in mammals, the DMNX maintains its reptilian functions of controlling digestion and slowing the heart and is regulated by hypothalamic communication (Hopkins.1987;Leslie, Reynolds et al.1992). He specifically uses the example of the vagal control of the heart to

highlight an apparent contradiction. In most reptiles there is no boundary between DMNX and NA and cardiac vagal efferent pathways appear only in the DMNX.

In mammals there is a distinction in the anatomy of the DMNX and NA and the cardiac vagal efferent pathways occur mainly in the NA. In mammals there are also direct neural connections between the amygdala and the NA, with the NA capable of regulating vocalization, facial expressions and coordinating breathing with sucking and swallowing. This evolutionary change in the structure and function of brainstem areas and corresponding change in the role of the vagus has led to the DMNX vagal general visceral efferents becoming part of the passive reflexive motor system and retaining the "vegetative" function of reptilian ancestors. The special vagal efferents from the NA are part of an active voluntary motor system involved with conscious functions such as communication and emotion, motion and attention. Thus, Porges has termed them as the DMNX being the "vegetative" vagus and the NA as the "smart" vagus.

Studies on rats has revealed the NA is made of a series of interconnected subdivisions (Bieger & Hopkins 1987). A respiratory rhythm was demonstrated in vagal fibres originating in one of these subdivisions, the external formation (NA_{ex}), that terminated in the bronchi (Haselton, Solomon et al. 1992) and the sinoatrial (SA) node of the heart (Spyer & Jordan 1987). Consequently, Porges suggests the resultant RSA may be thought of as having its origins, at least in part, in the NA. The results of cross correlation studies of the firing patterns of single units lead to the hypothesis that respiratory rhythm is dependent on the interaction between groups of neurons in both the NA and NTS (Richter & Spyer.1987). These areas are also the sites of motor neuronal activity that control cardiac, respiratory and laryngeal functions. This lead to the model of a cardio-respiratory control centre formed from the interaction of the NTS and NA, being distinct from the DMNX whose neurons were found to have no respiratory rhythm associated with them.

Further work has established that other brain structures are involved in the regulation of, if not the generation of, this cardio-pulmonary centre. Respiratory rhythms have been found in nuclei of the brainstem, midbrain and forebrain. Cross correlation

techniques were again used to identify these regions of the brain that demonstrated firing in time with the breath by breath rate. Regions that demonstrated this correlation with breathing were: periaqueductal grey where 62% of discharge from sampled neurons correlated with respiration, (Ni, Zhang, & Harper 1990); central nucleus of the amygdala contributed to inspiratory cycle (Frysinger & Harper 1986); hippocampus in humans, cells from which also demonstrated correlations with heart rate as well as breathing (Frysinger & Harper 1989); and anterior cingulate cortex which also demonstrated discharge properties of single neurons that were correlated with timing aspects of the respiratory and cardiac cycle (Frysinger & Harper.1986). In the light of this information, monitoring RSA as one component of HRV, may reflect the function and control of this complex integrated neuronal cardio-pulmonary oscillator. In relation to diseased states and malfunction of brainstem nuclei, RSA measures may yield a non-invasive measure of changing abnormal function.

The NA, DMNX and heart rate variability

There are other vagal and non-vagal effects that contribute to the rhythm and heart rate. The combined and synchronised effect on the SA node of the heart comprises influences from DMNX, NA, sympathetic nervous system and intrinsic rhythm generators of the heart. In considering aspects from Porges' Polyvagal Theory, "RSA is therefore, not a global measure of vagal tone nor is it a measure of total vagal control of the heart" (Porges.1995). RSA represents one aspect of HRV which indicates the complex and integrated functional consequences of a neuronal system consisting of vagal fibres originating in the NA and terminating on the SA node of the heart via intrinsic ganglionated complexes. To quantify the degree of RSA independent of slower oscillations and trends is therefore most important and will represent one spectral component of the total HRV.

Equally important in establishing neuronal interaction and function between areas of the brainstem and the heart, is the consideration of other spectral components of HRV, representing the effect of the DMNX, and these effects coupled with RSA. Possibly the dynamic interaction between RSA and other components of HRV could give greater information on the malfunction of the vagal control on the heart.

To support this theory, work on depth of anaesthesia demonstrated that inhalant anaesthetics dramatically reduce RSA but leave the overall heart rate little changed (Donchin, Feld et al.1985). This emphasises that the control of heart rate is not solely influenced by the NA since the drive from this centre is reduced, as indicated by the decrease in RSA during anaesthesia, but the heart rate is unaffected with both DMNX and NA being capable of influencing heart rate. Further work in analysing HRV with respect to anaesthesia demonstrated a shift in the power spectral analyses from respiratory frequencies to lower frequencies as anaesthesia increased (Blues & Pomfrett 1998;Pomfrett.1995). This may suggest a shift from a dominant NA influence on heart rate to more prominent role for the DMNX as the NA drive is reduced. The nonmyelinated fibres of the DMNX conduct with a slower velocity and so would exhibit a lower frequency control over the heart rate.

A further example of the utility of considering other aspects of HRV in conjunction with RSA is the evidence from research into high risk preterm babies (Porges 1992). Many of these infants show a depressed degree of RSA and bradycardia, which is often associated with apnea. This drop in available oxygen may be assumed to reflect the vestigial reptilian adaptive regulation of the heart by DMNX (Porges.1995). Perhaps the degree of the involvement of DMNX along with NA could be calculated by the relative shifts in the balance of low and high frequency indices of HRV, with this measure giving a better predictor of emerging dynamic physiological state.

There is a weight of evidence to support the interactive competition of the parasympathetic and sympathetic neuronal systems on individual organs (Berntson, Cacioppo, & Quigley 1991;Levy 1984;Vanhoutte & Levy 1979). There may also be competition between two branches of the vagus on the same target organ. For example, the two branches of the vagus on the heart are capable of affecting the cardiac cycle (Geis & Wurster 1980) and there may be competition at the SA node of the heart.

The continued drive from the NA to the SA of the heart (vagal brake) may be a protective mechanism to functionally limit the effects of the suppressed bradycardia

resultant from DMNX activity. This protection being functional achieved by the rate of acetylcholine (ACh) degradation on the SA nodal tissue which is thought to have a half-life of 2.7 s (Dexter, Levy, & Rudy 1989;Dexter, Saidel et al. 1989). In cases where this protective activity of neurogenic NA activity are removed, indicated by a decreased RSA measure, there may be a massive and acute pathological bradycardia which could be an explanation for the physiological stress induced in Sudden Infant Death Syndrome and may also be involved in sudden death following exercise in adult populations (Porges.1995).

The example above illustrates the functional interaction of the NA and the DMNX and suggests that measurement of RSA alone does not impart all the information available from HRV analysis and would not estimate the neural control of the heart from these two brainstem centres. Dual innervation of many organs, such as the heart, lungs, pancreas, liver, and stomach has been documented (Brown 1990). By investigating the control of bronchial asthma, the interaction of NA and DMNX may be researched further. In relation to asthma, NA efferents cause the bronchi to exhibit a cyclical change in relation to breathing (Porges.1995). It is proposed that the continuous stimulation of the bronchi by NA efferents may allow functional protection of the bronchi from a detrimental effect from the DMNX (In a similar fashion to the vagal brake on the heart, above). Without this protection, the bronchi would become vulnerable to the vagal surges from DMNX.
In an asthma attack, a monosynaptic reflex may be illustrated, with motor fibres originating from and afferent fibres terminating in the DMNX. There is also evidence that dendritic process from DMNX project into the NTS. This highlights an example of vagal afferent fibres that may communicate directly with DMNX neurons, forming an integrated reflex pathway (Neuhuber & Sandoz 1986).

Evidence from the investigation of both preterm babies and asthma attacks has suggested anatomical and functional relationships between DMNX and NA, which has led to notable changes in RSA. This leads to the idea that study of diseased and malfunctioning physiology, by means of investigating changes in HRV, may give an insight into the changing physiological state in the disease.

Characterizing the anatomy and function of distinct brainstem areas

Anatomy of the DMNX and NA

The DMNX and NA are two anatomically distinct regions of the brainstem and there is evidence to suggest that there are at least two populations of neurons which project to the cardiac vagal branches of many species such as rat, cat and dog (Bennett, Kidd et al.1981;Ciriello & Calaresu.1980;Ciriello & Calaresu.1982;Geis & Wurster.1980;Kalia & Mesulam 1980;Nosaka, Yasunaga, & Kawano 1979;Nosaka, Yasunaga, & Tamai 1982). Neurones with small myelinated axons conduct in the B fibre range, originating in the NA and have a respiratory related component to their on-going activity (Gilbey, Jordan et al. 1984;McAllen & Spyer.1978b). The other population of neurones have axons which conduct in the slower C fibre range and are located in the DMNX and do not have any respiratory related rhythm (Ford, Bennett et al.1990;Jones, Wang, & Jordan 1998). Efferent signals from the neurons in the NA are thought to convey a chronotropic action on the heart (McAllen & Spyer.1978b) and implicated heavily in respiratory sinus arrhythmia and the respiratory evoked reflex bradycardia (Richter & Spyer.1987;Spyer & Jordan.1987).

In addition, there is debate about the functional significance of the C fibres originating in the DMNX. It has been suggested that they may be involved in controlling blood flow to the heart (Feigl 1969) or have an inotropic action (Geis & Wurster.1980). Further work has been carried out where selective stimulation of vagal efferent C fibres can evoke bradycardia in rats, rabbits and cats. (Jones, Wang, & Jordan 1995;Nosaka, Yasunaga et al.1979;Woolley, McWilliam et al. 1987a).

Function of DMNX and NA

The baroreceptor reflex constitutes a major control mechanism for circulation and involves coordination between the sympathetic nervous system, somatic baroreceptors as well as the parasympathetic system (Julien, Chapuis et al. 2003;Ma, Abboud, & Chapleau 2002;Stauss 2002;Thrasher 2002). A focus on the parasympathetic involvement of the baroreceptor reflex demonstrates a pivotal role for the NA and DMNX in the reflex regulation of the heart to this reflex.

An association between the DMNX and neurogenic bradycardia has been demonstrated in studies involving chronic bilateral lesion of the NA in rats; it was shown that there was a reduction in, but not totally removal of, the baroreceptor reflex-mediated bradycardia while conscious (Machado & Brody 1988a;Machado & Brody 1988b). This supports two ideas. The first is that the DMNX is capable of mediating bradycardia with a latency associated with baroreceptor reflex. The second idea is that similar neuronal control is exerted by the NA since lesions of the cell bodies reduces the bradycardia suggesting that in an intact system it contributed to the control of heart rate.

Activation of baroreceptors in arteries evokes excitation in the vagal cardioinhibitory neurons of the external formation of the nucleus ambiguous NA(e) (Ciriello & de Oliveira 2003). Likewise, activation of neurons of the NA using hypocretin 1 (hcrt-1), a neuropeptide recently identified exclusively in the lateral and perifornical hypothalamic neurons, significantly potentiates the reflex decrease in heart rate elicited by activation of the arterial baroreflex. This work by Ciriello and de Oliveira presents data to suggest that hcrt-1 is changing the activity of vagal neurons of the NA to incoming baroreceptor inputs and that hrct-1 neurons of the hypothalamus and the NTS form part of a neuronal circuit involved in the control of the baroreceptor reflex at the level of the vagal efferent neuron (de Oliveira, Rosas-Arellano et al. 2003).

Suggestions of how hcrt-1 exerts its effects include direct action on the vagal cardiomotor neurons, or it may act by changing the release of neurotransmitters in the afferents of the NTS that pass on the baroreflex signals to the NA. Glutamate is used as a putative neurotransmitter in afferents of the NTS (Kodama & Kimura 2002;Siegel 2004;van den Pol 1999). Therefore, there is a possibility that hcrt-1 may act by increasing the release of glutamate from NTS axonal terminals within the NA and so potentiate the reflex vagal bradycardia (Ciriello & de Oliveira.2003). These lines of evidence underline the importance of the interaction of brainstem nuclei in the control of heart rate and give an insight on how damage to such areas caused by prion diseases could consequently affect HRV and cardiac reflexes in a complex and interlaced manner.

Extracellular recordings were made from cardiac vagal motorneurons conducting in the B fibre range of the NA of the rat. In response to brief arterial pressure changes, these neurons demonstrated that there was an increase in activity due to active cells firing faster and by recruitment of previously silent neurons (Rentero, Cividjian et al. 2002). This suggested that these neurons of the NA were barosensitive and that there may be a degree of functional redundancy associated with the integrated neural response to changes in arterial pressure. Patterns of spontaneous activity of these cardio vagal motorneurons were also investigated and it was found, from the small population investigated, that the fastest firing neurons showed a symmetrical distribution about its modal interval and the majority of the others showed a skewed, Poisson-like distribution indicating irregular firing. Superimposed on these firing rates were influences from the cardiac and respiratory cycles.

Bradycardias evoked by activation of arterial baroreceptors were partially or wholly blocked if they were stimulated during the inspiration phase of respiration (Davidson, Goldner, & McCloskey 1976;Gandevia, McCloskey, & Potter 1978). The study of such phenomenon suggests evidence for the neural coupling between brainstem nuclei and respiratory and cardiac control. In cats this attenuation of the bradycardia has been shown to be related to inspiration related inhibitory gating of the synaptic input to cardiac vagal preganglionic neurones (Gilbey, Jordan et al.1984). It has been shown that the bradycardia evoked by stimulating pulmonary C fibre afferents was not

influenced by the phase of respiratory cycle or degree of lung inflation (Daly & Kirkman 1989;Daly 1991). Daly suggested there may be two types of cardiac vagal preganglions, both with chronotropic actions on the heart. One that can be inhibited by pulmonary stretch afferents and the other population of neurons cannot. The degree of modulation of a cardioinhibitory reflex will depend on the proportion of the two populations of cardiac vagal motoneurons that are excited by lung inflation.

There is a possibility that non myelinated axons from the DMNX may mediate the bradycardia evoked by pulmonary C fibre stimulation and these neurones do not possess a central respiratory relationship (Daly.1991;Jones, Wang et al.1998). Jones suggested that the identification of such fibres in the cat did not completely account for the hypothesis proposed by Daly since the evoked changes on the heart from the pulmonary chemoreflex have a longer time course than the brief bursts of activity elicited in neurons of the DMNX. In conjunction with this observation, it has been observed that cardiac C fibre efferents alone are not potent enough to evoke dramatic changes in cardiac function, such as cardiac arrest (Jones, Wang et al.1995). These observations have led to an altered hypothesis being postulate by Jones. He suggests that cardiac projections from the NA and DMNX preganglionic neurons may converge on target neurons in the cardiac ganglia with the final integrated activity being translated into the homeostatic level of sinus arrhythmia and heart rate variability.

A small group of peripheral C fibre axons was found to have respiratory related modulation and some additionally had a cardiac related discharge and so giving an activity profile similar to preganglionic neurons with B fibre axons (Jones, Wang et al.1998). Research has revealed there was a small group of vagal preganglionic neurones located in the area between NA and DMNX which had slowly conducting axons (Nosaka, Yasunaga et al.1982). The possibility thus existed that Jones was recording from such neurons. An alternate idea may be taken from the research into vagal afferent (Duclaux, Mei, & Ranieri 1976) and efferent fibres (Chase & Ranson.1914) that suggests some fibres may be myelinated centrally and may lose their myelination peripherally, hence would present slower conduction velocities when recorded peripherally.

It was also observed that the respiratory association of the neurons of the rat NA were different to that seen in cats and dogs. In rats maximum activity always occurred during the central inspiratory phase rather than the expiratory phase. This was demonstrated by use of respiratory cycle triggered activity histograms and correlation with phrenic nerve activity. With this exception, the properties of the cardio vagal motorneurons of the rat NA agree well with findings from cat neuronal activity (McAllen & Spyer.1976;McAllen & Spyer 1978a;McAllen & Spyer.1978b) and fibre recordings in cats and dogs (Gilbey, Jordan et al.1984;Katona, Lipson, & Dauchot 1977;Katona, Poitras et al. 1970;Kunze 1972;Potter 1981). Evidence from the work of Mendelowitz and colleagues (Irnaten, Neff et al. 2001;Mendelowitz 1999;Mendelowitz 2000), using Bartha pseudorabies virus, found that the rat cardio vagal motorneurons are innervated by collateral axons from branches of Superior laryngeal neurons. Superior laryngeal neurons are most active during inspiration and Renetero suggested this may be the reason for this phasic change of firing during the respiration cycle in the rat that is distinct from other animals.

Research to investigate whether stimulation of pulmonary C fibres also activated respiratory modulated B fibre cardiac preganglionic neurons of the NA was undertaken (Wang, Jones et al. 2000). This work did demonstrate that stimulation of pulmonary C fibre afferents activated respiratory modulated B fibre axons and also suggested that part of this excitation was independent of inhibition of central respiratory drive from these C fibre afferents. Wang et al postulated that respiratory modulation may be inhibited by the activity of the stimulated pulmonary C fibre afferents on the inspiratory input synapses of these neurons.

Another idea presented was that an interaction between activity in non-respiratory modulated C fibres axons (as studied by (Jones, Wang et al.1998)) and respiratory modulated B fibre axons (as studied by (Wang, Jones et al.2000)) occur at the cardiac ganglion and, or, postganglionic nerve endings in the sinoatrial node (Cheng, Zhang et al. 2004a). This may serve to abolish the respiratory rhythm previously associated with vagal preganglionic neurons of the NA by the inhibitory action of the C fibre activity from the DMNX as the result of pulmonary afferent stimulation.

Work by Cheng utilizing domoic acid, an excitatory neurotoxin, to specifically disrupt neurons of the NA (Cheng, Zhang et al.2004b) has demonstrated that in the rat both DMNX and NA motor neurons are barosensitive with vagal cardioinhibitory neurons from the nucleus ambiguus (NA) demonstrating a powerful excitation to baroreflex stimulation. A 68% reduction in the numbers of neurons in the NA gave rise to an attenuation in barosensitivity of around 83%. Their results indicated that neurons in the NA and DMNX send axons that converge to the same cardiac ganglia but innervate distinct principal neurons within these cardiac ganglia. This suggests that both NA and DMNX could synergistically moderate heart rate activity, A-V conduction and myocardial contractility. The major control of the baroreflex bradycardia is from the NA but it is postulated that the DMNX may mediate the heart through some other cardiac reflex. It has been suggested that the DMNX may intervene in the pulmonary C fibre-evoked bradycardia.

One of the functional deductions from the work of Cheng is the fact that preganglionic motorneurons from the NA and DMNX may exercise control over distinct populations of cardiac ganglions. In addition, axons from these vagal efferents are routed via different nerves to innervate different populations of intrinsic cardiac cholinergic postganglionic neurons (Cheng, Zhang et al.2004a).

This would also mean the possibility exists for a degree of integrated complementary control for the vagal efferent activity from anatomically distinct parasympathetic nuclei at the cardiac ganglions. This idea, coupled with evidence of brainstem nuclei (specifically DMNX and NTS neurons) recovering function following brainstem lesions, would suggest a changing and integrated control of heart rate variability over a period of around 30 days as observed in a rat following domoic acid lesion to the brainstem nuclei (Cheng, Guo et al.2002).

Prion protein builds up in the DMNX and NA which causes lesion and subsequent loss of function in those nuclei in a similar manner to domoic acid lesions induced by the experiments of Cheng and colleagues. Following on from these lines of evidence, suggesting recovery of function of mammalian brainstem nuclei, it is worth

considering whether the incubation of prion diseases may cause a transient change in beat to beat control of the heart resultant from a change in the normal balance of DMNX and NA efferent output as brainstem nuclei regain their function.

Intrinsic and thoracic cardiac ganglia

The cardiac ganglia alluded to by Cheng above, include extracardiac intrathoracic neurons and intrinsic intracardiac neurons located on the heart itself. Their affects in conjunction with brainstem nuclei and the action of parasympathetic axonal efferent fibres need to be considered. These neurons are arranged in hierarchical control structures, with the neurons at the heart exerting beat by beat control over myocardial function (Armour 1994). Their interaction with higher brain structures is illustrated in figure 1.6.

Afferent and efferent intracardiac neurons form local circuits and extend throughout the atria and ventricles, displaying on-going activity in the beating heart. This activity may be modulated by inputs from intrathoracic ganglia and the central nervous system. Of particular interest is the interaction of the descending vagal drive from the medulla and the interaction with the intrinsic cardiac ganglia and resultant chronotropic regulation of the heart (Randall, Brown et al. 2003). The descending vagal efferent pathways are highlighted by red dots in figure 1.6. It can be seen that the activity from the DMNX and NA may be integrated and possibly gated at either or both of the intrinsic ganglionated plexus (RAGP and PAGP)

Figure 1. 6 Schematic of Neural connections from CNS to SA node via ganglionated complexes.

Used with permission, from Armour, J. A., Collier, K., Kember, G., & Ardell, J. L. 1998, "Differential selectivity of cardiac neurons in separate intrathoracic autonomic ganglia", *Am J Physiol*, vol. 274, no. 4 Pt 2, p. R939-R949. Figure 7. Comprising elements from Armour and Randall (Armour, Collier et al. 1998;Randall, Brown et al. 1998a;Randall, Brown et al.2003).

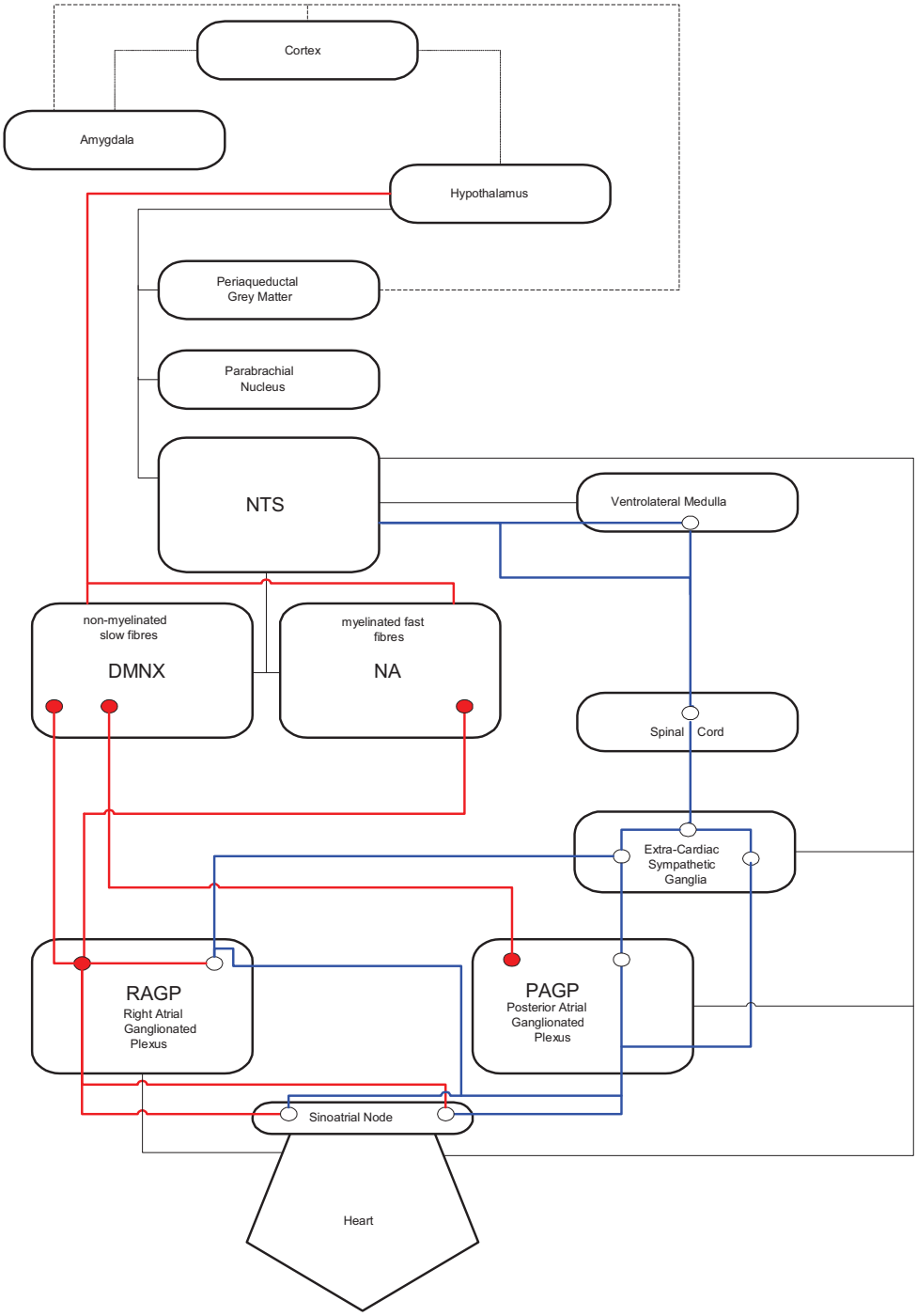

The “triumvirate” of brainstem nuclei (NTS, NA and DMNX) and their relationship to intrinsic ganglionated complexes (RAGP and PAGP) and subsequent action on the SA node is illustrated here. Parasympathetic efferent communication is indicated in red, sympathetic activity is indicated in blue. Black lines indicate efferent communication of the ANS with higher brain centres. Synergistic activity of the two branches of the ANS is indicated at the RAGP at the open circle.

Work by Thompson has given evidence for the potential involvement of local intracardiac control of the heart by investigating the functioning of the spinal cord and brainstem in conjunction with the nested feedback loops of intrathoracic and intracardiac neurones of the canine ganglionated plexus. (Thompson, Collier et al. 2000) The canine intrinsic cardiac ganglia cluster within fatty pads at discrete locations on the heart. This study involved taking simultaneous recordings from neurons in two separate locations of one fat pad during a control state and a state where substances (veratridine) known to activate sensory neuronal activity were applied to the epicardium of the heart. Their work illustrated that the activity of two populations of neurons at different regions within a single intrinsic cardiac plexus displayed intervals, of around ten seconds, of coupled behaviour every fifteen to thirty seconds.

These episodes of synchronicity described above, occurred during both the control periods and during the periods of topical application of substrate. These observations may be explained if these two population of neurons received common inputs or these two groups of neurons communicated with each other. To assess the mode of interaction, the activity of these two populations of neurons were cross correlated over five minutes and 15 from the 16 recorded neurons displayed synchronised bursting of activity. This coupled behaviour was not seen when intracardiac neuronal activity was compared with that of extracardiac intrathoracic neurons (Armour, Collier et al.1998). The interaction of intracardiac neurons and extracardiac intrathoracic neurons often generate low frequency rhythms that are out of phase and the suggested function of such activity is to stabilize overall coordination of cardiac function. Thus, there are indications that regional cardiac control of the heart is a result of integrative neuronal competition in the intrinsic ganglionated complexes located on the heart mediated by afferent neuronal feedback and extracardiac sensory input from intrathoracic neurons.

Intrathoracic Ganglia

Evidence for the contribution of intrathoracic ganglia to the control of the heart may be taken from the work of Armour (Armour, Collier et al.1998) The activity of neurons of the middle cervical or stellate ganglia were compared and contrasted to neurons of intrinsic cardiac ganglia in consequence to various cardiovascular changes. It was found that the spontaneous activity of 19% of intrathoracic neurons and 32% of intrinsic cardiac neurons were related to specific phases of cardiovascular perturbation. 14% of the identified extracardiac and 8% of the identified intrinsic cardiac neurons generated respiratory related activity. Other intrathoracic neurons generated sporadic activity. In addition, approximately 60% of extrinsic cardiac neurons and around 80% of intrinsic cardiac neurons displayed increased activity to epicardial mechanical stimulation. Activity generated by neurons in intrinsic cardiac ganglia did not show any short term relationship to activity in extracardiac ganglia.

Following experiments which involved decentralization (disconnection of intrathoracic nervous system from spinal cord and brainstem) it was suggested that intrinsic cardiac neurons received afferent inputs mainly from cardiac chemosensitive neuronal networks and the neurons of the middle cervical ganglia received afferent inputs mainly from cardiac mechanosensory neural networks.

Importantly, cardiac and respiratory related activity continued to be generated by sub populations of intrathoracic neurons after acute decentralization. Armour also summarized intrathoracic ganglia as containing afferent neurons, local circuit neurons, sympathetic efferent postganglionic neurons and parasympathetic efferent postganglionic neurons. It was concluded that different reflex controls of cardiac function may be established due to the activity of populations of neurons within different intrathoracic ganglia. Their redundancy of function and independent behaviour reduced the dependency on a single population of neurons and a single neuronal pathway in regulating the heart on a beat to beat basis.
Populations of neurons located in separate intrathoracic ganglia show little short term, in the order of milliseconds, interactions. Although sympathetic efferent preganglionic

neurons may input directly to both extrinsic and intrinsic subpopulations of neurons, these do not appear to be the main source of coordinated neuronal activity within intrathoracic ganglia. Armour et al suggested that most intrathoracic neurons function relatively independently when controlling cardiac function. They postulated that they act as a part of a subsystem of overlapping nested neural feedback loops. It was suggested that there exists various feedback loops characterised by the time of neural activation of the induced cardiac changes.

Short term feedback facilitated by intrinsic cardiac nervous system, medium term feedback by middle cervical and stellate ganglia and long term feedback occurs as the result of spinal cord and brain neural communication pathways. Functional redundancy of intrathoracic neurons is also suggested by the observation of functional selectivity of the behaviour of neurons when modulating cardiodynamics. Coordination of autonomic output from intrathoracic neurons is achieved to some degree by a sharing of inputs from higher centres in conjunction with neural communication between neurons in and between various peripheral ganglia. The independence of function of intrathoracic ganglia is endorsed by the 10-20 second bursting of neuronal activity of intrathoracic neurons when disconnected from central nervous system. This evidence supports the concept of a diversity of afferent feedback in the cardiac control cycle which creates a potential for the maintenance of coordinated efferent neuronal outflow while providing the flexibility required for the beat to beat regulation of efferent outflow to the heart.

Intracardiac Ganglia

The work of Armour et al above, by utilizing the decentralization technique, demonstrated the importance of input from the central nervous system. Some neurons of the intrinsic cardiac ganglia receive direct inputs from parasympathetic efferent preganglionic neurons (Armour & Hopkins 1984;Armour, Huang et al. 1994;Armour & Janes 1988). The subsequent loss of these direct connections with the change in function of the long feedback loops would be observed by a change in the coordinated regulation of the heart on a beat to beat basis. This surgical

decentralization may also be used as an analogy to the possible malfunction in neural function seen in affected brainstem neurons and the vagus nerve in TSE diseases.

Thus the work of Armour provided anatomical and neurophysiological evidence for a change in the beat to beat effects on heart rate caused by dysfunction in the nested neural feedback loops, altered by the breakdown of the normally coordinated neural communication to the heart, via the vagus, from the medullary areas of the brainstem.

The interaction of the sympathetic and parasympathetic nervous system also has a role to play in the regulation of the beat to beat variation of heart rate. It is thought that one site of interaction of these two branches of the autonomic nervous system is the autonomic neuroeffector junctions at the myocardium. The intracardiac ganglia have also been postulated to be a site for parasympathetic-sympathetic interaction. Reports have indicated that sympathetic terminals exist in intracardiac ganglia, so giving the prospect of both sympathetic and parasympathetic inputs converging on single intracardiac ganglia (Ellison & Hibbs 1976;Moravec, Moravec, & Forsgren 1990).

Research investigated the intracellular response of single intracardiac neurons to stimulation of both efferent limbs of the autonomic nervous system. The response of single intracardiac neurons, in vitro, to various patterns of stimulation delivered to the excised stumps of the vagus (parasympathetic) and cardiopulmonary nerve (sympathetic) were investigated in the pig (Smith 1999). In this study, none of the sampled neurons received inputs solely from cardiopulmonary nerves. Instead, extrinsic sympathetic inputs (to sampled neurons) converged on a subset (17%) of neurons that were vagally innervated.

Three types of intracardiac neurons were identified by Smith, based on their firing patterns to 60ms depolarizing test currents. 40% of those tested were found to be phasic, discharging one action potential at the start of the stimulus. 35% were accommodating, discharging multiple action potentials at a decreasing frequency as the stimulus continued and 27% were tonic, discharging multiple action potentials during the stimulus period with little change in the frequency of discharge throughout

the stimulus period. Of the 66% of neurons that responded to vagal stimulation, some did not depolarize sufficiently to reach the threshold to generate an action potential. Of these neurons incapable of generating an action potential to vagal stimulation, it was observed that multiple excitatory post synaptic potentials (EPSPs) were summed to generate an action potential. Therefore intracardiac neurons generating EPSPs must integrate synaptic inputs from multiple preganglionic axons.

Those neurons that gave an action potential in response to vagal stimulation may be the classical efferent parasympathetic neurons innervating the myocardium. Smith et al noted that these neurons did not represent the majority of intracardiac neurons sampled. If this sample was representative of the whole this would imply that vagal stimulation of intracardiac neurons involves integration of synaptic inputs from a range of postganglionic axons. The potential of intracardiac neuronal range and complexity of function is thus evident.

The postsynaptic effects of vagal stimulation are eliminated by using a nicotinic channel blocker (hexamethonium) or perfusion with a “Tyrode” solution containing reduced calcium and increased magnesium levels which block the release of neurotransmitter at nerve terminals. Utilizing these techniques, Smith’s work stated that the effects of nerve stimulation were mediated synaptically and the induced depolarisations were produced by acetylcholine (ACh) released from vagal preganglionic terminals acting at nicotinic postsynaptic receptors (Smith.1999).

The interaction of the sympathetic and parasympathetic systems at the level of these intracardiac ganglia was postulated by evidence obtained by observing the effects of stimulating the vagus and cardiopulmonary nerves in those neurons that are dually innervated. The duration of the action potential and afterhyperpolarization lengthened when the vagus and cardiopulmonary nerves were stimulated together, compared to stimulation of the vagus alone. This response was characterised as a type one response by Smith. Since there was no direct postsynaptic effect from stimulating the cardiopulmonary nerve, it is thought that the increase in duration of action potential and afterhyperpolarization is caused by a substance (another neurotransmitter or neuropeptide,) released from intraganglionic sympathetic terminals that may act

presynaptically on vagal terminals to increase the release of acetylcholine (ACh). The prolonged channel opening causing the increased action potential and afterhyperpolarization times, would result from higher ACh concentrations within the synaptic cleft (Smith.1999).

The majority of neurons that demonstrated an influence from cardiopulmonary nerve stimulation gave a type 2 response to concurrent stimulation of the vagus and cardiopulmonary nerve. Action potentials were generated as a result of costimulation and during vagal stimulation alone, evoked depolarisations could be blocked by hexamethonium and demonstrated similar amplitude and duration of mean EPSPs to those neurons only innervated by the vagus.

EPSPs produced by cardiopulmonary nerve stimulation with these type 2 responses were smaller in amplitude and duration than those produced in the same neurons by vagal stimulation. Nicotinic receptors were not involved in responses to cardiopulmonary nerve stimulation, as demonstrated by no change in the response to cardiopulmonary nerve stimulation of these neurons during exposure to hexamethonium. However, Timolol, a beta antagonist, blocked postsynaptic responses to cardiopulmonary nerve stimulation. When both hexamethonium and timolol were given together, no postsynaptic activity was seen when stimulation of the vagus and cardiopulmonary nerve were costimulated. This suggested that different synaptic inputs are activated by stimulation of these branches of the autonomic nervous system.

It was suggested by Smith that Ach released from vagal preganglionic terminals acting at nicotinic postsynaptic receptors, mediates the effects produced by vagal nerve stimulation. Smith also suggested it was likely that norepinephrine released from postganglionic sympathetic nerve terminals, acting at beta adrenergic receptors was involved in the effects of cardiopulmonary nerve stimulation.

It is thus possible that integration and mediation of function of the heart by both the sympathetic and parasympathetic branches of the autonomic nervous system can be established at the location of the intrinsic cardiac ganglia which may exert beat to beat changes on the cardiac cycle.

Other work has shown that application of nicotinic, muscarinic and β-adrenergic agonists to intracardiac ganglia of a dog heart *in vivo* produced an increase in the firing of intracardiac neurons and changed cardiac regulation (Huang, Smith, & Armour 1993b). Data from this work also confirms that *in situ* mammalian intracardiac neurons possess nicotinic, muscarinic and β-adrenergic receptors and are involved in cardiac regulation.

Smith also suggested that due to the lower membrane conductance of phasic neurons as deduced from his work, smaller currents would be required to depolarize the voltage gated channels responsible to generate an AP. This characteristic of phasic neurons may mean they are more excitable than the other accommodating or tonic neurons of intracardiac ganglia.

Smith reported that from his observations, extrinsic vagal inputs appeared to be directed to phasic and some accommodating neurons whereas extrinsic sympathetic input is directed to target phasic neurons of the intracardiac ganglia. Most tonic neurons received no extrinsic input. The firing properties of phasic and accommodating neurons were less able to respond to on-going high frequency synaptic input sufficient to depolarize the membrane to firing threshold. Consequently, phasic and accommodating neurons would act as a low pass filter to sustained high frequency synaptic input. It is also stated that the identification of sites of vagosympathetic convergence within the intrinsic ganglia allow the possibility of activity in one branch of the ANS to gate the activity in the other. For example, parasympathetic inputs may alter the activity of subsequent sympathetic inputs by "priming" the neuronal sensitivity to such vagal activity or vice versa. This interaction between the parasympathetic and sympathetic branches of the ANS are revealed in the paced breathing study where cardiac sympathetic outflow was found to mediate

RSA demonstrating that RSA is not mediated solely by vagal cardiac nerve activity (Taylor, Myers et al. 2001).

Research involving the ablation of specific atrial populations of intrinsic cardiac ganglia, the posterior atrial ganglionated plexus (PAGP), suggested that a major role for the constituent parasympathetic neurons was to inhibit sympathetic neurotransmitter release. PAGP ablation augments the HR increase by potentiating the action of sympathetic nervous system at the SA node (Randall, Brown et al. 1998b).

Leading on from this idea that there is potential for the parasympathetic activity to selectively modify sympathetic activity in addition to independent direct action, I suggest activities in certain brainstem nuclei may have the ability to “gate” the sympathetic action on the heart. This may also mean that damaged functional output of DMNX and NA, caused by prion invasion, may cause an abnormal disruption in descending neuronal vagal input to these complexes. Thus, a change in the gating of activity at the intrinsic ganglionated complexes that communicate to the SA node may consequently alter the cardiodynamics of the heart and affect HRV.

Chapter 2 Common Methods used in this thesis.

Introduction

Heart Rate Variability (HRV) is used as a non-invasive tool to investigate changing autonomic function. Certain analyses are reported to highlight cardiac parasympathetic activity in the study of diabetes; work by Ewing indicated a difference in HRV of diabetic patients suffering from neuropathy compared to healthy control subjects and also illustrated a difference in HRV of heart transplant patients having medically denervated hearts (Ewing, Neilson, & Travis 1984). In Parkinson's Disease (PD) and Lewey body dementia patients, where Lewey bodies appear in peripheral autonomic and enteric ganglia, autonomic dysfunction is reported in peripheral autonomic ganglia as a precursor to the neurodegeneration seen in the central nervous system (CNS) (Iwanaga, Wakabayashi et al. 1999;Kaufmann, Nahm et al. 2004). Specifically, HRV analysis was used to assess an early parasympathetic dysfunction in Parkinson's disease (Buob, Winter et al. 2010) that may occur before or at the same time as a sympathetic dysfunction of the autonomic nervous system (Shibata, Morita et al. 2009). Consequently the parasympathetic control of the heart on a beat to beat basis has been shown to be altered in early stages of Parkinson's Disease.

Questions about Parkinson's disease being a prion disorder have been mooted (Olanow & Prusiner 2009) consequently the comparisons to prion disease and how a disease can change cardiac function, specifically the parasympathetic mediated control of the heart, are apparent. Of particular interest to prion diseases is the vagus nerve and its parasympathetic control on the heart since branches of the vagus nerve, along with the enteric nervous system, have been postulated as a possible conduit for the infectious agent in prion diseases (Beekes, McBride et al.1998;Beekes & McBride 2007;Pomfrett, Glover, & Pollard 2007;van Keulen, Bossers et al.2008;van Keulen, Schreuder et al.2000).

In light of the above information I wished to investigate whether incubating TSEs changed heart rate variability (HRV) influenced by the presence of PrP^D deposits in brainstem areas as discussed in chapter 1, in a similar fashion to the changes reported in Parkinson's disease.

Electrodes

In order to accurately record a good quality ECG from sheep and cattle, specialized electrode pads were constructed. These were individually manufactured from polythene document wallets approximately 0.001 m thick that were cut into 0.1m diameter circles each with a hole approximately 0.02 m diameter cut in the middle of this circle. Standard 3M Silver/Silver Chloride monitoring electrodes with foam tape (3M ID: DH-9999-3816-9) were placed in these inner circles. Various colours were used to allow individual use for each animal and isolate each batch of electrodes to one of the testing pens (see figures 2.1 and 2.2). This was done to exclude cross contamination between control groups along with wiping the testing rig and equipment with “Chloros” solution (Sodium Hypochlorite solution from Martin Manufacturing Co. Ltd, Belfast) used to limit prion infection when moving between sheep of different groups. In addition protective clothing was changed between such groups.

Figure 2. 1 Standard electrode and adapted electrode.

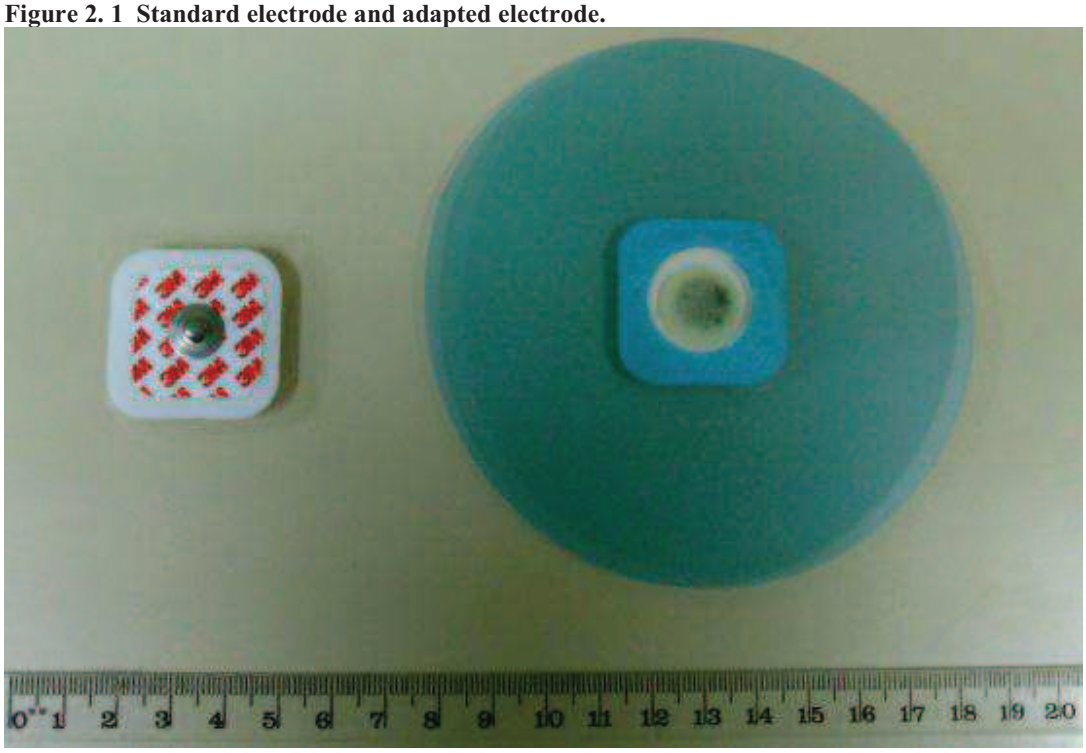

Figure 2. 2 Range of colours for constructed electrode to reduce cross contamination.

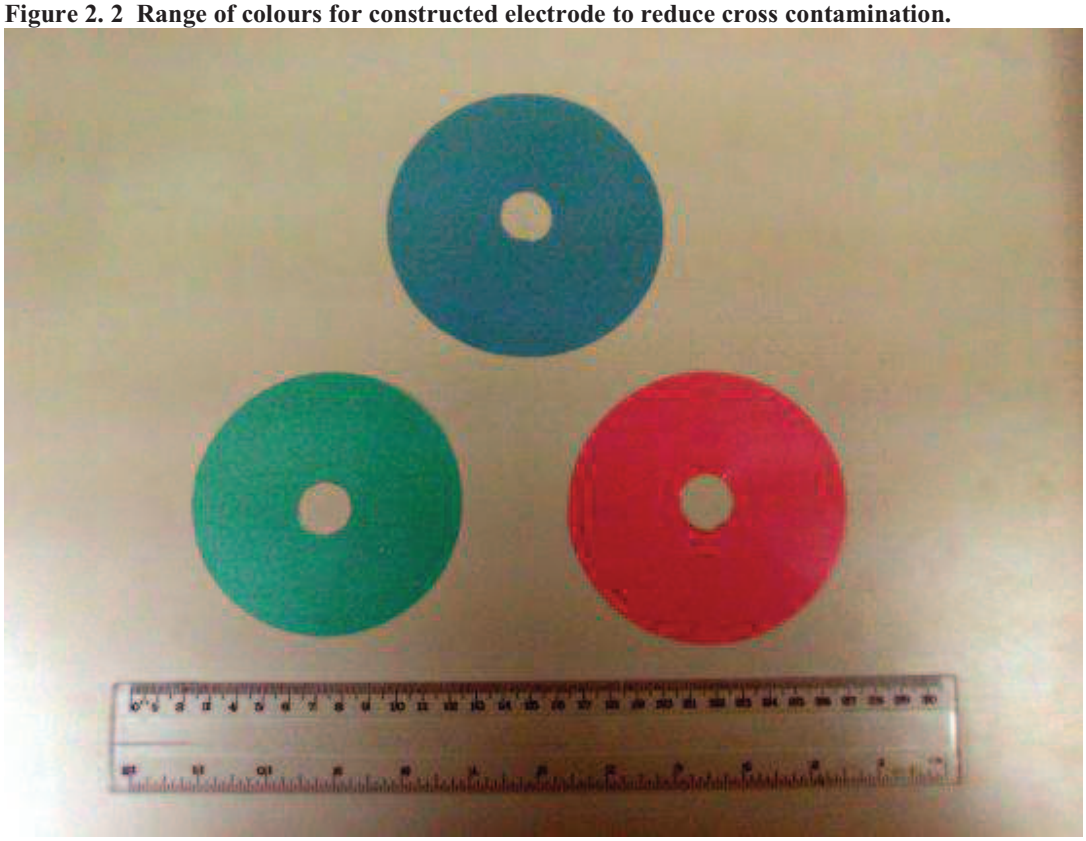

The contact surface of the constructed electrode was covered with a liberal amount of "Magnafloc" gel (Magnafloc LT20 Gel in 0.1 M sodium chloride solution. Magnafloc LT20 is a polyacrylamide gel approved under regulation 25(1)(a) of the Committee on Chemicals and materials for use in public water supplies and swimming pools for use as a flocculent, supplied by Ciba Specialty Chemicals, UK,Bradford,West Yorkshire).

A simple three connection bipolar ECG recording, giving a similar trace to a lead II configuration, was used since no interpretation of various ECG complexes would be required and it provided a quick, stable and accurate trace from which to detect the R-wave (the largest deviation in the ECG montage). Electrode position was adjusted to obtain the greatest difference between R-wave and baseline. No filtering was applied to the raw ECG since the accurate recording of the R-wave times was of paramount importance.

To record approximately 300 seconds of ECG data 3 devices were used in this thesis. Two "Depth of Anaesthesia" monitors were used along with a modified Variacardio TF4.

One of the "Depth of Anaesthesia" monitors was developed by Otter Controls Ltd, (Buxton, Derbyshire; (Blues & Pomfrett.1998;Pomfrett, Glover et al. 2004). This consisted of a programmable physiological amplifier (CED 1902) acquiring the ECG which was then digitized by a computer using a DAP800 12 bit card sampling at 1kHz. This was enclosed in a box which conformed to IP65 (IEC 60529 (ed2.1), clause 4.1) that facilitated the cleaning of the equipment with Chloros solution (Aguzzi & Collinge 1997;Defra 2007) which allowed the transfer of the equipment between pens and so prevented cross contamination between the experimental herds.

A second "Depth of Anaesthesia Monitor" was also used. This was called "Fathom", which is a commercially available depth of anaesthesia monitor based upon analysis of HRV during anaesthesia. This was available from Amtec Medical Ltd (County Antrim, BT41 1QS Antrim, 6 Technology Park, Belfast Road, Belfast, Northern Ireland.)

The TS1 recording device was adapted from a Variacardio TF4 (MIE Medical Research Ltd, 6 Wortley Moor Road, Leeds). The modifications to the TF4 were carried out by MIE to my specifications and a software program to export from the device and import into Spike 2 was written by MIE with advice and direction from myself. The modifications consisted of alterations to the transmission of the telemetric data to the computer for archiving. The ECG and R-R intervals were sampled at 1 kHz in this modified version compared to sampling rates of 500 Hz for ECG signals and 1 kHz for R-R intervals in the TF4 model. This was designed to give precise correlation between the raw ECG waveform and the R-wave times. This enabled accurate screening of missed or ectopic beats by comparing the two synchronous data streams. Further modifications to this device included the addition of a breath sensor based upon registering a change in current as the subjects exhaled breath changed the resistance of a thermistor positioned in proximity to the nose or mouth. This sensor was not used in this study, however.

The basic function of these devices was to accurately record the R wave times and archive these data to be later imported into Spike2. All devices used to collect ECG data recorded equivalent ECG data tested by common input to the systems and analysed with Spike2. All the devices used recorded the same R-wave times to the nearest millisecond.

Data Collection

For both types of “Depth of Anaesthesia” monitors, data were collected and archived in a common format (CED SON data Library provided by Cambridge Electronic Design) on the device and later transferred to a computer for analysis. This common pathway is illustrated in figure 2.5.

300 seconds of data without artefact were used to obtain spectral and time domain estimates of HRV. On occasions this required data collection to be in the range of 5 to 10 minutes for each animal. Each file was checked by eye to ensure there were no missed or ectopic beats since such errors were reported to affect the resultant estimate of HRV (Berntson & Stowell 1998). Spike 2 version 4.22 and version 6.02 software (CED, Cambridge Electronic Design) and an automated analysis program (BSEnsor v8, script file) was used to analyse the data files in batches.

To test the hypothesis that prion infection alters HRV, ECG data sampled at 1kHz was archived in a proprietary format to be imported to Spike 2 (Cambridge Electronic Design) for the analysis performed in this thesis. Following data capture R-waves were detected from the ECG waveform by an automated process based on a purpose-written script which performed peak detection based upon a signal change that was 3.5 times the standard deviation of the baseline between two cursors equally spaced in the data sample. The R-wave times were then put into an array and the R-wave events displayed on a new channel. These R-wave event markers were then screened by eye to look for missed R-waves and ectopic beats. Such abnormalities were corrected using automated and manual addition and removal of R-wave events from the event channel. However, analysing HRV data with the ectopic beats included has indicated that information about the dynamic cerebral autoregulatory response gained from observations from impulse like disturbances of blood pressure, associated with these ectopic beats, can be gained (Eames, Potter, & Panerai 2005). The use of the methods used to analyse HRV per breath used here may have utility in such analysis by analysing pulse pressures within the physiological epoch (breath) before the ectopic and contrasted with similar samples from the physiological epoch (breath) containing the ectopic beat. Ectopic beats may consequently have an effect

on HRV since they are reported to affect blood pressure which could alter the “set” point of regulation of the heart over a time scale of a few seconds correlating to very low frequency changes in HRV spectrum.

To facilitate this screening by eye, a separate channel illustrated the areas of the 300 second data file that contained abnormalities by showing a break in a continuous line. A channel of instantaneous heart rate was derived from the R-wave events by using the Spike2 command DrawMode. This error check channel was created by assessing “good” data as events that fell within the maximum and minimum acceptable instantaneous heart rates. The minimum rate was chosen to be 20 and the maximum was chosen to be 165. Figure 2.6 shows an example of how the instantaneous rate channel was created.

The instantaneous rate (IR) is related to the R-wave interval (t) by the following formula:

$$IR = \frac{1}{t} \times 60$$

The values chosen by the acceptable maximum and minimum rates equated to intervals of 3 seconds and 0.3636 seconds respectively. In reality these limits checked for a break in the ECG recording and noise being picked up as R-waves. Deviations from these limits were represented by large peaks or troughs in the instantaneous rate display and a break in the derived signal quality line.

For the TS1 device, data were digitised at a sampling frequency of 1 kHz and wireless transmission allowed the raw ECG to be imported into the TS1 software running on a conventional laptop computer (Dell Latitude P4 computer model PP01L). Using this software and hardware automated QRS wave detection was applied. The software was able to correct for missed beats and artefacts by the manual use of an in built proprietary routine. In addition to the filtered R-wave event times, the unfiltered R-wave event times and raw ECG were archived together for each recording epoch from each animal. The raw data, unfiltered and filtered R-wave

times were exported to a common file format (CED SON data Library) and then imported into and analysed using standard software (CED Spike2 ; SPSS). Artefacts and missed beats correction were again checked by eye by comparing the raw ECG with the filtered output from the TS1. Any corrections for missed or extra R-wave events were performed in Spike2.

An event series of ECG R-wave timings were obtained in order to determine variability in the R-R intervals and an instantaneous tachogram constructed from this event series. Using Spike 2 Software from Cambridge Electronic Design (CED), the tachogram was constructed by replacing each R-wave event marker by a raised cosine wave fragment of unit area (see figures 2.3, 2.4). This was done to investigate the frequency changes in the sequence of R-wave events. This technique used to construct a tachogram has been peer reviewed in publications investigating BSE in cows, scrapie in sheep and vCJD in humans and is reported to be equivalent to tachograms constructed from the interval of the time series (DeBoer, Karemaker, & Strackee 1984). An FFT was performed on filtered versions of this tachogram to indicate HF and LF components of HRV (see figure 2.4). The methods used here were adapted from previous work by our group to investigate BSE in cows (Pomfrett, Glover et al.2004) and vCJD in humans (L.A.M.Woolfson, D.G.Glover et al. 2003).

Figure 2. 3 Theoretical construction of Tachogram.
(Reproduced with permission from CED The Spike2 Script Language booklet)

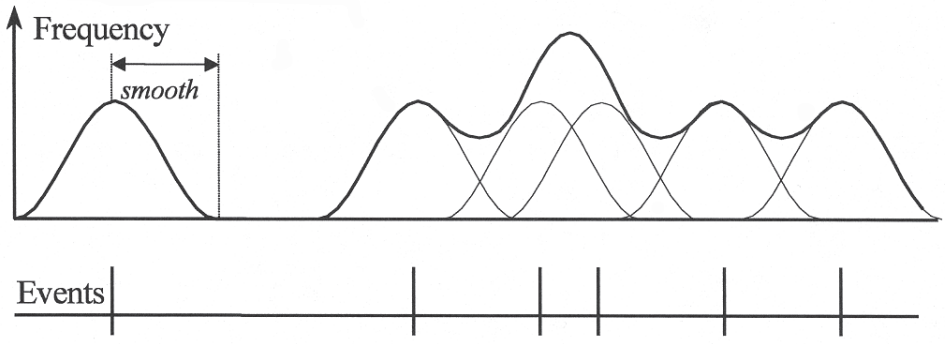

Construction of a Tachogram from R-wave event markers. An event at time t is spread over a range from t-smooth to t+smooth. This is performed to assess the slow frequency changes in the sequence of events.

Figure 2. 4 Actual tachogram from a sheep.

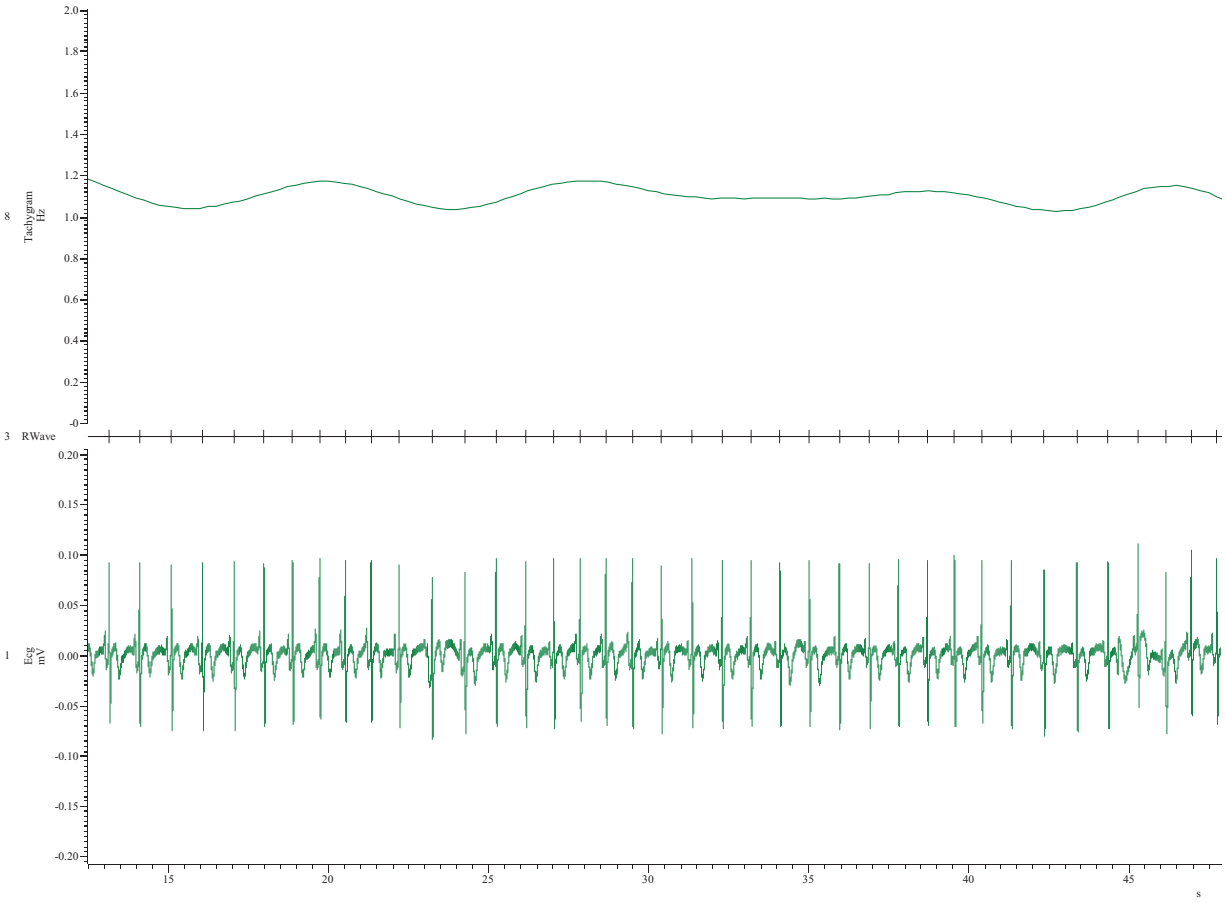

Figure 2. 5 Summary of Methods used in this study.

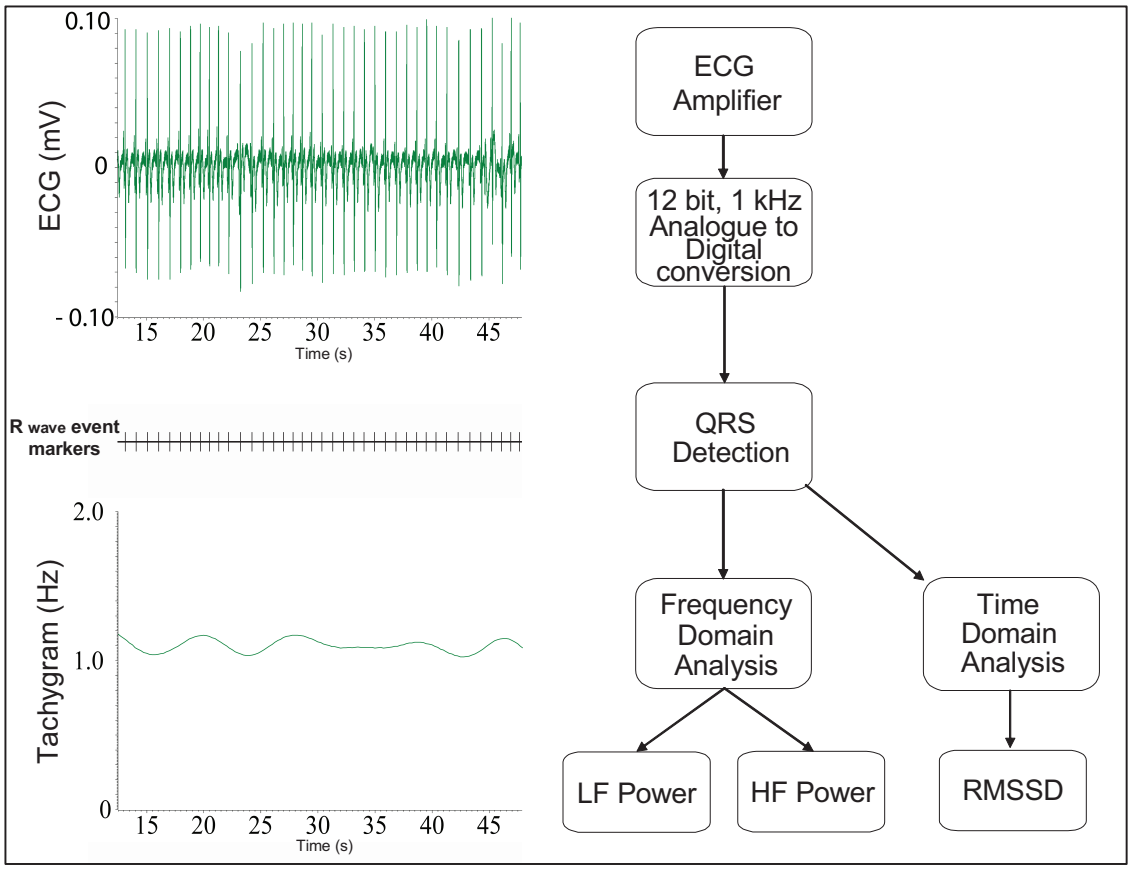

Off line analysis using "BSEnsor" v 8, automated software written by CED with contributions and specifications from myself, allowed batches of data to be analysed with resultant HF powers, LF powers, heart rate, and instantaneous heart rate along with other combination variables to be archived for each batch. The program was easily adapted to enable different frequency bands to be set to represent the HF and LF bands of interest. This program was modified to output the R-wave event time series for export into statistical packages such as SPSS v 11 and a routine was incorporated that calculated the RMSSD of the R-wave events (see appendix 1.1 for worked example). In addition time domain metrics of HRV were explored using CMETX software (John Allen 2002) on the exported R-wave event time series that explores the variation in the inter beat intervals (IBI) (Allen 2002;Allen, Chambers, & Towers 2007) .

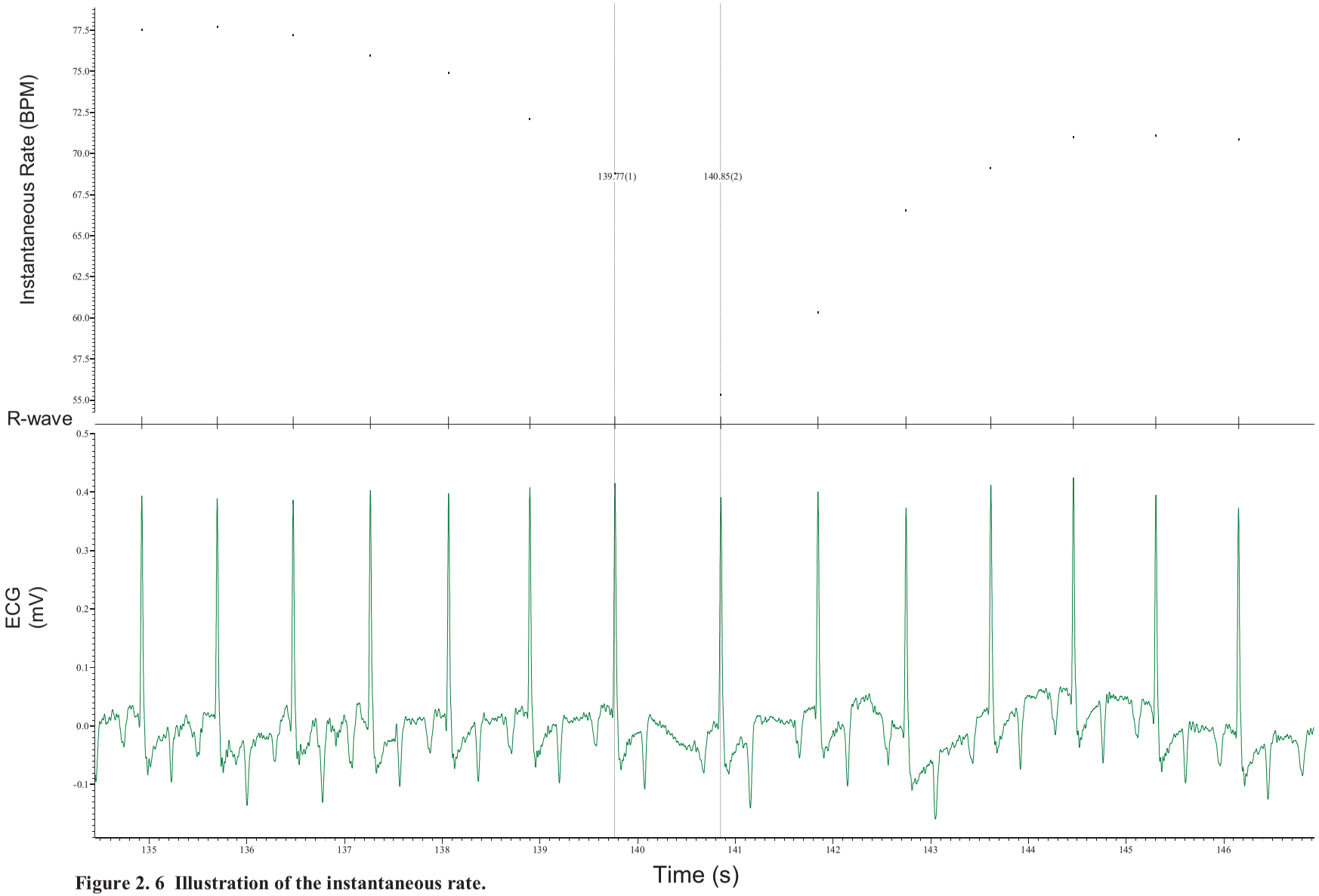

Figure 2. 6 Illustration of the instantaneous rate.
The interval between the cursors is 1.085 seconds which equates to a rate of 55.300 beats per minute.

From this basic series of R-wave events, various types of HRV analysis were performed. Data from sheep was analysed using power spectral analysis as described in Chapter 3. Data from cows, in addition, was analysed using a time domain metric (CMETX) which gave measures of CVI and CSI as described in chapter 4.

The development of a program to estimate breathing events from various parameters of the ECG trace was accomplished in chapter 5 and the algorithm tested against breathing events recorded with a Magtrak turbine (Ferraris Medical Ltd) used in conjunction with a face mask and filter (Intersurgical Mask 1515 and Intersurgical filter 1944: Intersurgical, Berkshire). Once this breath estimation was verified, some of chapter 5 and chapter 6 implemented it to investigate the relationship between the R-wave distributions within each breath. Circular statistics was employed in assessing the relationship to the beat to beat variability per breath since such statistics are suited to investigate physiological relationships where one event is related to another event in a cyclical manner. For example the heart beats within each breath are linked to the breath event and also to each beat within the breath. A heart beat is influenced by the preceding beat and influences the subsequent beat.

Limitations to data collection and Technical Caveats

Fourier analysis encompasses a range of mathematical techniques by which signals may be decomposed into a series of sine waves. This type of analysis is named after Jean Baptistie Joseph Fourier (1768-1830). He published a paper in 1807 that suggested any continuous periodic signal could be represented as the sum of properly chosen sinusoids (Brigham 1988).

The Fast Fourier transform (FFT) is an example of how to calculate the Discrete Fourier Transform (DFT) which is itself one example of this mathematical technique used with digitized signals to decompose a signal into sine waves. The DFT requires an input function that is discrete and the values have a finite duration that is greater than zero. These inputs are created by sampling a continuous function such as the constructed tachogram. Using the DFT implies that the finite segment that is analysed is one epoch or segment of an infinitely extended periodic signal. Multiple segments of data are used in the calculation of the FFT to

improve confidence in spectral estimates by reducing the variance of the DFT spectral estimate.

Various people have been involved with the concept of FFT including the German mathematician Karl Friedrich Gauss (1777-1855) who was using the technique around the 1840s. However, Cooley and Tukey were credited with bringing the FFT to the attention of the world in an effective algorithm that could be used on a computer (Cooley & Tukey 1965).

The continued development of the FFT and the advancement of computational power means that it is now a widely used signal processing tool. The FFT is now a practical and readily available procedure that may be applied effectively without detailed theoretical knowledge of the "complex" mathematics involved. The analysis package used here is based on the FFT algorithm incorporated in Spike 2 version 4.22 (CED software) and used with a personal desktop computer (Mesh Matrix A3500). The result of the analysis is scaled to RMS power so it may be converted to energy by multiplying by the time over which the transform was done. Consequently the bespoke program that was written to analyse the data, in one procedure, can provide a power spectrum from any selected waveform channel.

The tachogram constructed from the ECG waveform, on which the FFT is performed, is a very much simpler waveform than the raw ECG trace and more closely represents a sine wave, or at least a series of sine waves with similar amplitudes. The mathematics behind the FFT assumes the waveform the analysis is performed on repeats cyclically (see above in relation to the input function for the DFT).

In most cases there is a step or discontinuity in the data epoch if it is segmented in to "blocks" and each block spliced end to end. These steps may cause additional frequency components in the result. To limit the influence of these edge effects to the resultant power spectrum a solution is to taper the start and end of the blocks so they start and end smoothly. This is known as windowing and will cause smearing of the data and loss of power in the result.

Each "window" function has advantages and disadvantages with windows designed to have the smallest side lobes spreading the frequency peaks out more.

In an attempt the change the data by the least amount and give a more accurate representation of the spectral peaks the initial analysis was performed with no windowing function. (In appendix 1.3 HF and LF values obtained with different windowing functions are compared graphically).

Another critical area for data integrity is the consideration of missed and extra R-wave identification gained from the raw ECG trace. It has been suggested that even one missed or extra beat in a sample of 128 seconds may significantly alter the resultant computed spectral power(Berntson & Stowell.1998). The authors of this work found that the effect of the artefacts increased power in all frequency bands (0.15-0.4 Hz, 0.05-0.15 Hz, 0.008-0.05Hz, corresponding to high, mid and low frequency bands respectively) with missed beats causing a greater effect than additional erroneous R-wave detections. The resulting change in spectral powers obtained from FFT analysis on data sets with experimental artefacts are illustrated by figure 2.7, reproduced below.

Figure 2. 7 The effect of artefacts on power spectrums.
Reproduced with permission from Cambridge University Press; Figure 1 Berntson, G. G. & Stowell, J. R. 1998, "ECG artifacts and heart period variability: don't miss a beat!", *Psychophysiology*, vol. 35, no. 1, pp. 127-132.

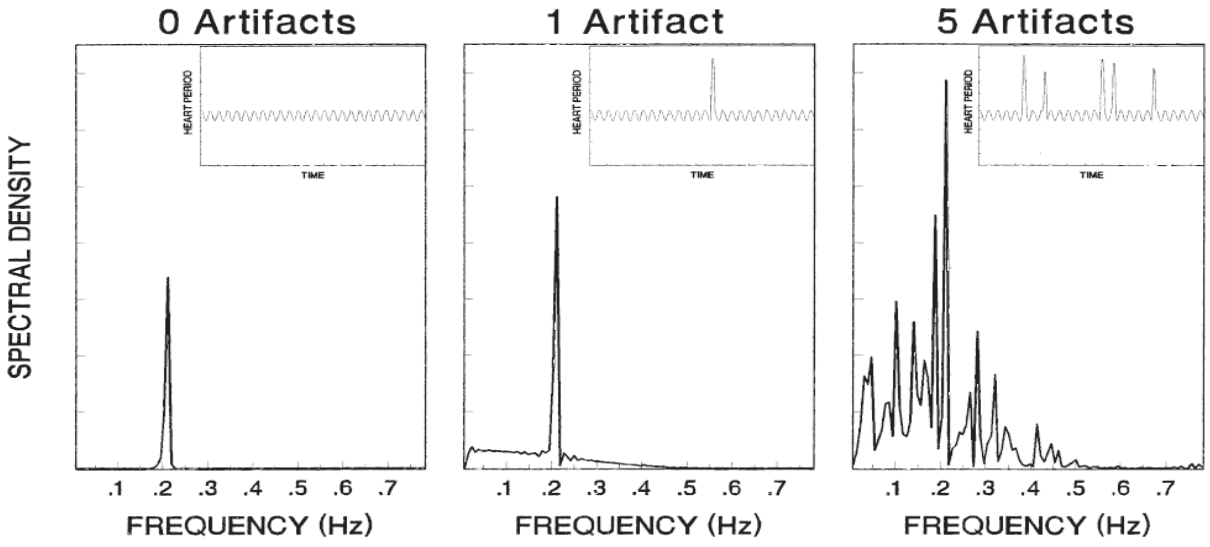

Here it can be seen that the introduction of the artefacts leads to a broadening and increase of spectral power. A slight lateral shift in the power spectra may have caused a reduction in power in one frequency band and a corresponding increase in another as a result of the introduction of an additional artefact. In addition Berntson and Stowell found that some patterns of artefacts may invalidate the

assumption of stationarity as discussed below although moderate deviations from the assumption of stationarity may not compromise analyses as suggested by Grossman et al. Berntson and Stowell also performed assessments for the effects of missed and extra beats on the time domain methods of analysis such as those used by Porges and Bohrer (1990) and found the artefacts caused similar effects in this assessment too.

Consequently the effects of such missed or additional R-wave detections are critical to the analyses performed on the data here. In an attempt to minimize the errors each 300 - 400 second data set was checked by eye to screen for such missed or extra beats following the automated R-wave pick off that was coded in the bespoke software program BSEnsor v8. Errors were corrected manually using purpose written routines to add or delete erroneous R-waves. For an animal with a heart rate of around 100 beats per minute, there may be around 500 R-wave events in 300 seconds of data. To screen and correct one such data set may take from a period of a few minutes up to an hour. This is a laborious but essential element to ensure accurate representation of the frequency variation in the beat to beat time series obtained from this analysis.

It is also prudent to consider the effect of such missed or erroneous R-waves may be much greater than the lack of a suitable windowing function or indeed violations of the principle of stationarity as discussed below.

Further considerations about data integrity and caveats for analysis concern the stationarity of those data on which spectral analysis is to be performed. For example if the heart rate transiently exhibited a step change during the period of analysis this may induce artificial frequency components in the resultant spectrum that were the result of this transient change in heart rate and not due to the autonomic change in HRV. In the written debate of Weber and Grossman on the subject of stationarity (Berntson, Bigger, Jr. et al. 1997;Grossman 1992;Grossman, van, & Wientjes 1990;Weber, Molenaar, & van der Molen 1992) Grossman argued that the lack of stationarity is very unlikely to compromise the calculation of RSA or the 0.1 Hz cardiac component to any great extent. Weber maintained that the time series on which an FFT is performed should be no more than “weakly stationary” and provides a relatively complicated algorithm based on a double window analysis technique performed on the time and frequency

domains leading to a two way analysis of variance which in turn yields a test for the stationarity of the data.

Both workers agreed that “very interesting things are likely to be happening during a non-steady state phase of a measurement period”. The question of the lack of stationarity in each frequency band also exists and we must bear in mind that it may be a change in the exhibited stationarity that is a sign of abnormal neuronal control as a result of incubating TSE diseases. It may be that in the diseased state there is a greater degree of stationarity, of the time series events, than in “healthy” controls. With the approach of testing data for stationarity and only analysing stationary data sets raises the issue that the results would be from highly selected segments of data and may not be a representative sample. Non-stationarity may be an inherent dynamic feature of the R-wave event time series and should not be removed since it may yield significant differences in the normal and TSE infected animal.

To limit erroneous effects of gross stationarity violations, the automated analysis program, BSEnsor, had a “screen” based upon maximal and minimal instantaneous heart rate values (see pages 80-82 of this thesis). Areas of data that were outside these limits were identified as bad data on channel 12 of the data file. This also had the benefit of focusing attention to missed or additional R-wave detection to make the correction of these errors easier. Only files without bad data were analysed and step changes in heart rate within the 300 second data file resulted in the file being excluded from the analysis. In addition, the epochs for data analysis were 300 seconds to minimize the possibility of non stationarity and the FFT was performed on the tachogram of R-wave events which was further filtered by band pass filters to remove slow trends and concentrate the FFT on low frequency and high frequency spectral components of HRV.

The epoch of 300 seconds was chosen to provide a standardized analysis duration that would allow comparisons between studies and comparisons between recordings within each study. HRV increases with the length of the analysed data epoch (Berntson, Bigger, Jr. et al.1997) but also will increase the chance that the assumptions of stationarity will be violated. It was found that the time period of 300 seconds and a sampling frequency of 1 KHz allowed an FFT of 512 bins and a frequency resolution of 0.004Hz over the range of 0-2 Hz which was considered

accurate enough to investigate the proposed frequency ranges involved in the analysis of HRV. The 300 second or 5 minute recording period is also recommended for clinical studies to investigate HF and LF components of HRV (Electrophysiology 1996).

In an attempt to quantify errors in my data capture and analysis routines, a heart rate simulator (HeartSim200 di) was used to create an ECG with very little natural HRV. Since this was an electronic simulation of an ECG rhythm designed to have little arrhythmia we would not expect much beat to beat variation in this trace since it was not programmed to output any. When the data capture and analysis routines were performed on this file the maximum powers reported in the power spectral estimates were at least 1000 x lower than the lowest real estimates of HRV from sheep. In some cases the powers were “0” (see appendix 1.2). What little powers that were calculated would represent the inherent “noise” in the system representing errors in mathematical calculations such as rounding errors. This gave confidence in the measurement system and that it was recording and analysing HRV that was little distorted by either errors in the mathematical calculations or by signal artefact from extraneous signals at higher frequencies that were reflected back into the power spectrum of interest.

The data collection and analysis were further verified following the analysis of one of our data sets by another laboratory using a moving polynomial approach (v hat) as described by McCabe (McCabe, Yongue et al.1984). Each group of workers compared the analysed results from the same sets of event time series and concluded the trends of various indices of HRV were similar for both groups with the test data lying outside the 95% confidence intervals for normal controls on most occasions from this longitudinal data set (Porges, S.W. personal communication). This exercise helps give validity to the methods used here by comparison with those used by Porges based on 30 years experience in HRV analysis.

Chapter 3 Investigation of heart rate variability in scrapie infected sheep

Introduction

I was invited to record HRV from scrapie-infected sheep and controls at the VLA International Research Centre, Lasswade. The animals were part of an on-going study investigating rectal biopsy as a means to identify the presence of scrapie in these sheep.

Studies of a large number of sheep with and without scrapie, show that PrP^{D} aggregates are consistently present in the recto-anal mucosa associated lymphoid tissue (RAMALT) of pre-clinically and clinically infected sheep (Gonzalez, Dagleish et al. 2006;Gonzalez, Jeffrey et al. 2005).

Following all local animal handling and welfare legislation and under the supervision of a government vet, I was given permission to record the electrocardiogram (ECG), non-invasively, from controls, naturally-infected field cases and orally-challenged infected sheep. Epochs of at least three-hundred-seconds from control and scrapie-infected sheep were collected and archived for off line analysis.

Methods

As previously stated, the electrode modifications and cleaning of the recording equipment before moving between groups was carried out. In addition protective clothing was also changed before moving to the next group of sheep.

Data were collected using a modified Variacardio TF4 which is called a TS1, as previously described in chapter 2.

The sheep were placed on their backs in a commercially available treatment cradle previously used to inspect and maintain hoof health (See figure 3.1). The electrode gel complex was attached to the recording leads from the data recording telemetric headstage (labelled Transmitter in figure 3.1) via “press studs” on the leads, typical of conventional ECG recording devices.

The sheep were shaved around their thorax to remove body hair and the contact surface of the constructed electrode was covered with a liberal amount of “Magnafloc” gel.

The closely shaved skin of the animal was dampened down with normal saline and the electrodes were placed either side of the animal’s heart to obtain a useable trace (See figure 3.2). The gel allowed repeated repositioning of the electrode around the thorax to obtain the best trace for this purpose. This took around 30 - 90 seconds for each animal and allowed time for the animal to settle in the cradle. It was noted that some animals tolerated the inverted position better than others with the majority becoming still after a 10-30 seconds in the cradle.

The resultant power spectral analysis on the filtered tachograms (described in chapter 2) was easily recalculated to produce different spectral bands. The ones that were used here were : LF 0.0-0.15 Hz; HF 0.15-1.0 Hz; HLF 0.032-0.138 Hz and HHF 0.15-0.5 Hz. The heart rate along with other derivatives of these data were calculated and archived for each data file from each animal.

In addition the R-wave event series was analysed using time domain measures to gain the root mean square of successive differences (RMSSD) which was calculated by finding the square root, of the mean of the squared differences between adjacent RR intervals (Bloomfield, Zweibel et al. 1998;Electrophysiology.1996) (see Appendix 1.1 for worked example).

Boxplots were used to graphically illustrate groups of data from sheep. Boxplots display differences between groups of data without making any assumption about the constituent distribution and may be considered to be nonparametric. The spacings between the different parts of the box help indicate the degree of dispersion and skewness in the data. The box is defined by the first and third quartile and the "whiskers" illustrate the range. The median is illustrated as the line between these two bounds. Outliers are show as values that are between 1.5 and 3 times the interquartile range (see figure 3.4 for an example).

To address the problem of multiple significant testing for nonparametric data, a Kruskal-Wallis test followed by Mann-Whitney tests using Bonferroni correction (Bland & Altman 1995) was used. The Kruskal-Wallis test identifies if there is a statistically significant difference between the groups based upon their ranked means. To investigate the difference, if one exists, between the groups a Mann-Whitney test with Bonferroni correction was used.

Figure 3. 1 Sheep in Cradle.

Figure 3. 2 Close up of electrode attached to thorax.

Results

Data were collected from 26 animals, one of which showed clinical signs at the time of measurement and so was excluded from this analysis (group 4 below). The remaining 25 animals were from the following groups.

Group 1	Control Animals, orally challenged with scrapie free brain homogenate	3 Sheep
Group 2	Orally challenged with scrapie agent, no clinical signs, rectal biopsy negative.	4 Sheep
Group 3	Orally challenged with scrapie agent, no clinical signs, rectal biopsy positive.	6 Sheep
Group 4	Orally challenged with scrapie agent showing clinical signs.	1 Sheep
Group 5	Naturally exposed, resistant genotype, biopsy negative.	9 Sheep
Group 6	Naturally exposed, no clinical signs mixed genotype, biopsy negative.	3 Sheep

	Negative Biopsy	Positive Biopsy
Unexposed	2 ARQ/ARQ (grp 1) 1 VRQ/VRQ (grp 1)	-
Oral exposure	4 ARQ/ARQ (grp 2)	3 ARQ/ARQ (grp 3) 3 VRQ/VRQ(grp 3)
Natural exposure	9 ARR/ARR (grp 5) 2 ARQ/ARR (grp 6) 1 ARQ/ARQ (grp 6)	-

Table 3- 1 The number of sheep in each group and their genotype and RAMALT biopsy result.

From table 3-1, groups 1, 2 and 3 constituted “Experimental animals” that were kept in isolation pens under strict regulations to minimise potential cross contamination of the groups with scrapie agent. Groups 5 and 6 represent “field animals” that were not orally challenged but allowed to feed and inhabit fields where naturally scrapie infected sheep had previously been farmed. The box plots in figures 3.4 and 3.5 represent these groups of animals that form the “Experimental” and “Field” animals.

A typical example of a control animal from group 5 (top panel figure 3.3) shown against a scrapie infected animal from group 3 (lower trace figure 3.3) is shown. The R-wave events are shown on the bottom of each panel along with the tachogram that has been filtered to show the LF and HF components of this

waveform. A difference in these two files may be seen by eye, with the control animal demonstrating more power in both the HF and LF bands in the power spectrum. This is illustrated here by the greater undulations in the representations of the power spectrums, with the infected animal showing “flat lines” by comparison.

Figure 3. 3 Comparison of tachograms from control and infected sheep.

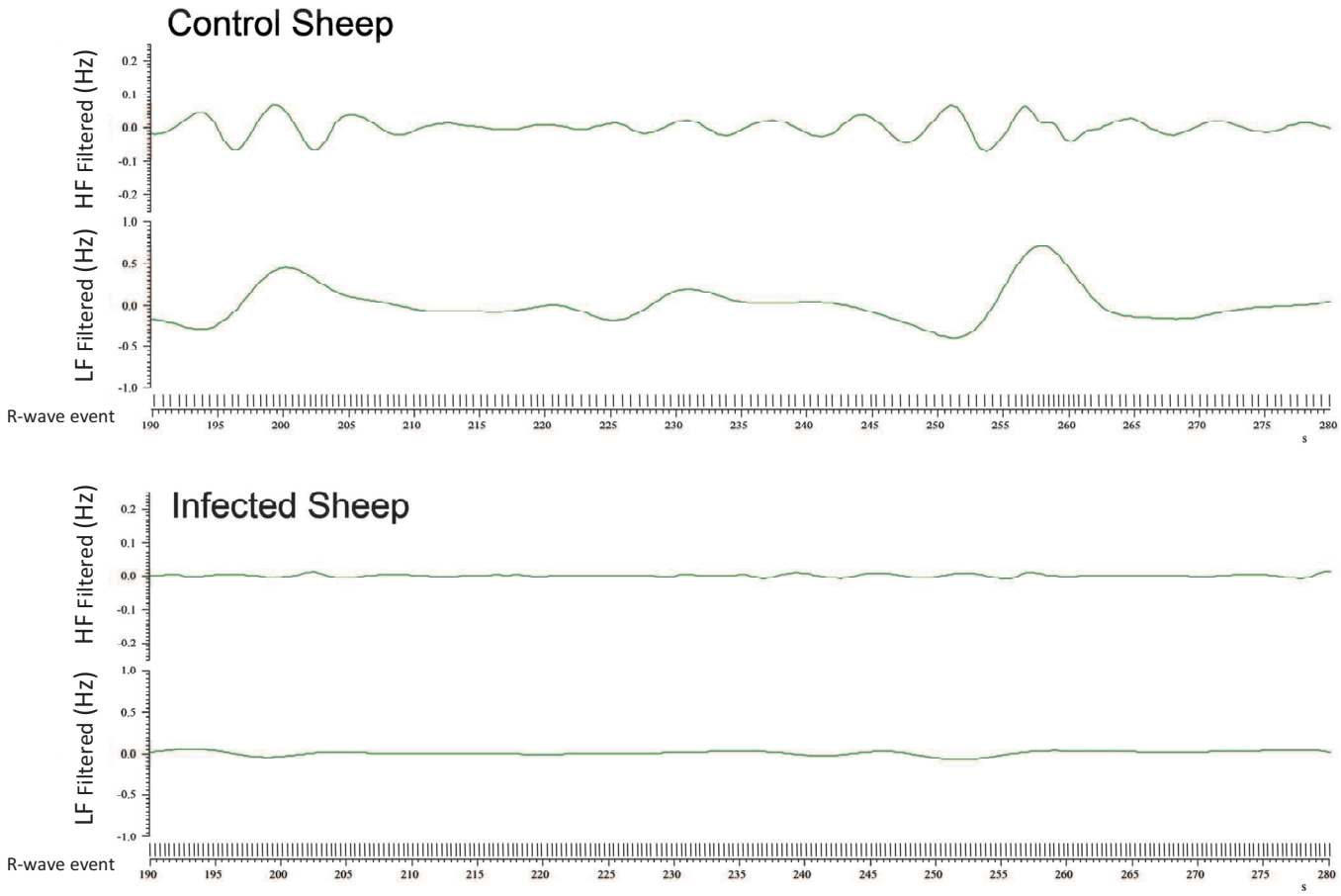

A box plot showing median and upper and lower quartiles for each sheep group against each variable were plotted in SPSS v11.5. It was found that the variable that seemed to show the greatest differences between the groups was HLF (see figure 3.4). This distribution of the HLF values was tested for normality by using a Kolmogorov-Smirnov test with Lilliefors Significance Correction.

It was found that the data did not fit a normal distribution and so nonparametric tests were used to investigate the differences in HLF values between the groups. These statistical tests were performed to compare the values of the animals that had a positive biopsy result (group 3) against all the other groups. Group 4 was excluded from the analysis since it was a group of one and showed clinical signs unlike all the other animals.

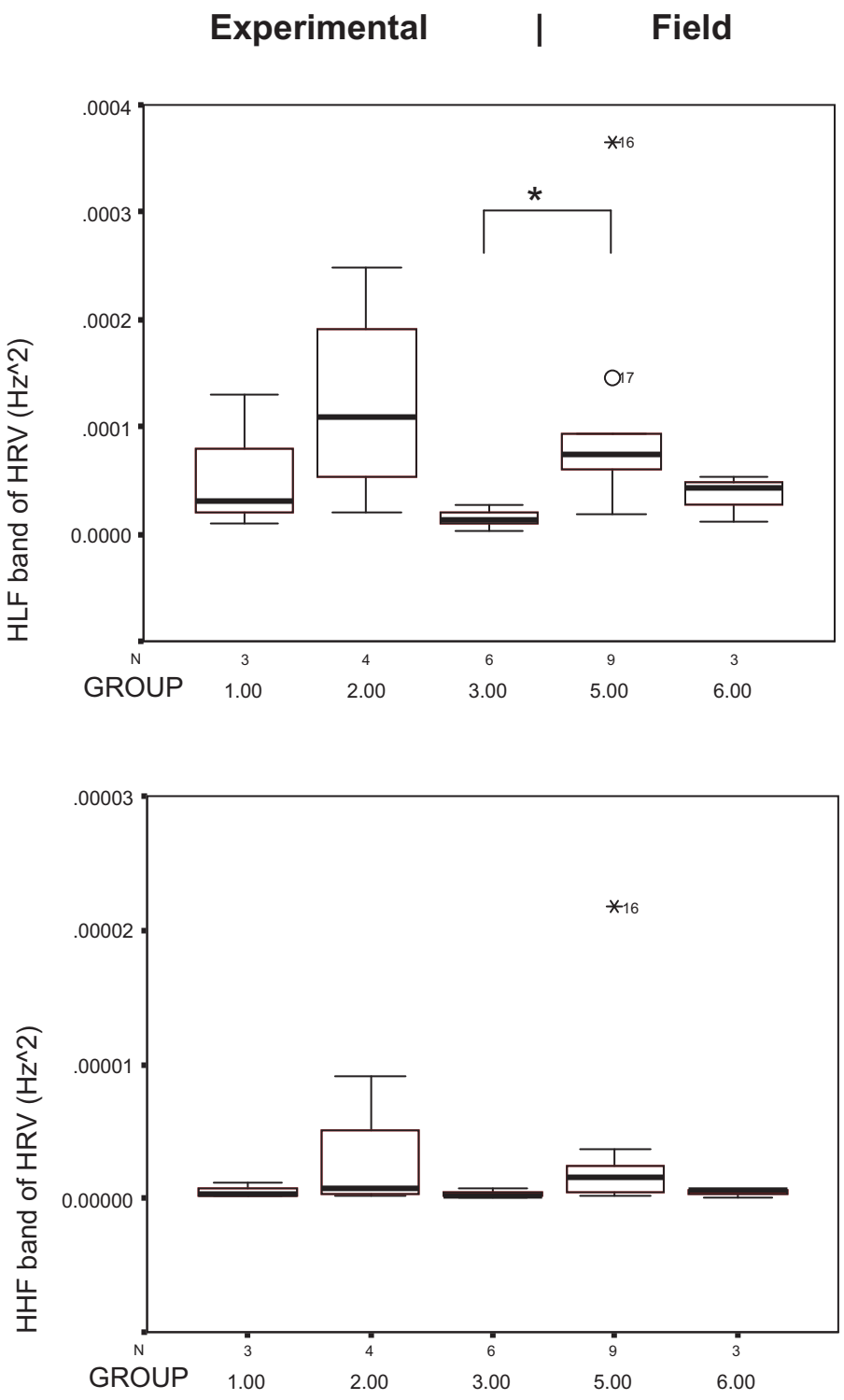

Figure 3. 4 HLF and HHF values for Experimental and Field animals.
Box plots (median, upper and lower quartiles and range) to show significance of HLF and HHF for 5 groups. Significant differences, as assessed by Mann-Whitney test with Bonferroni correction following a Kruskal-Wallis test, are indicated by * with $p<0.05$

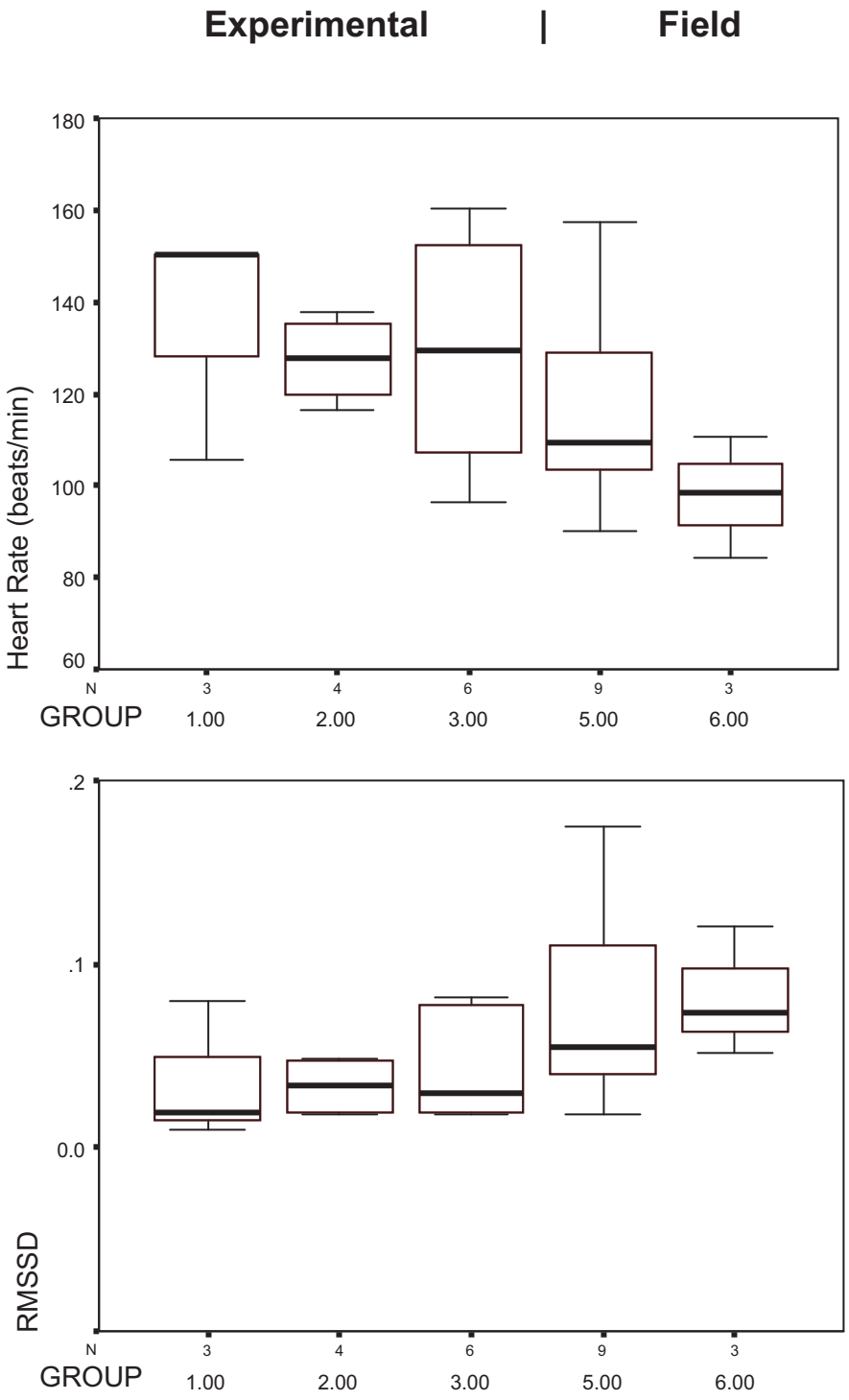

Figure 3. 5 Heart rates and RMSSD for Experimental and Field animals.

Boxplots to show significance of heart rate and RMSSD for 5 groups.
By comparison with fig 3.4, HLF is distinct from heart rate and RMSSD, between field and experimentally infected animals since no significant difference in RMSSD or heart rate is seen between group 3 and any other group. (note: the lack of a top range bar for group 1 heart rate illustrates that 2 of the measures were at the level indicated by the median line and the group only had 3 data points).

From figure 3.4 it can be seen that there is a significant difference ($p<0.05$, using the Mann-Whitney test with Bonferroni correction) in HLF values between the field animals that were of a resistant genotype (group 5, scrapie free) and animals that were orally challenged with scrapie, showing no clinical signs but rectal biopsy positive (groups 3). This would indicate that this index of HRV was able to detect scrapie infection between experimentally infected sheep and non-infected field cases.

It may also be noted, from figure 3.5, that the heart rate and RMSSD do not show this significant difference and so emphasise the fact that the HLF variable is distinct from heart rate and RMSSD. The HHF band of HRV also did not show any significant differences between the groups.

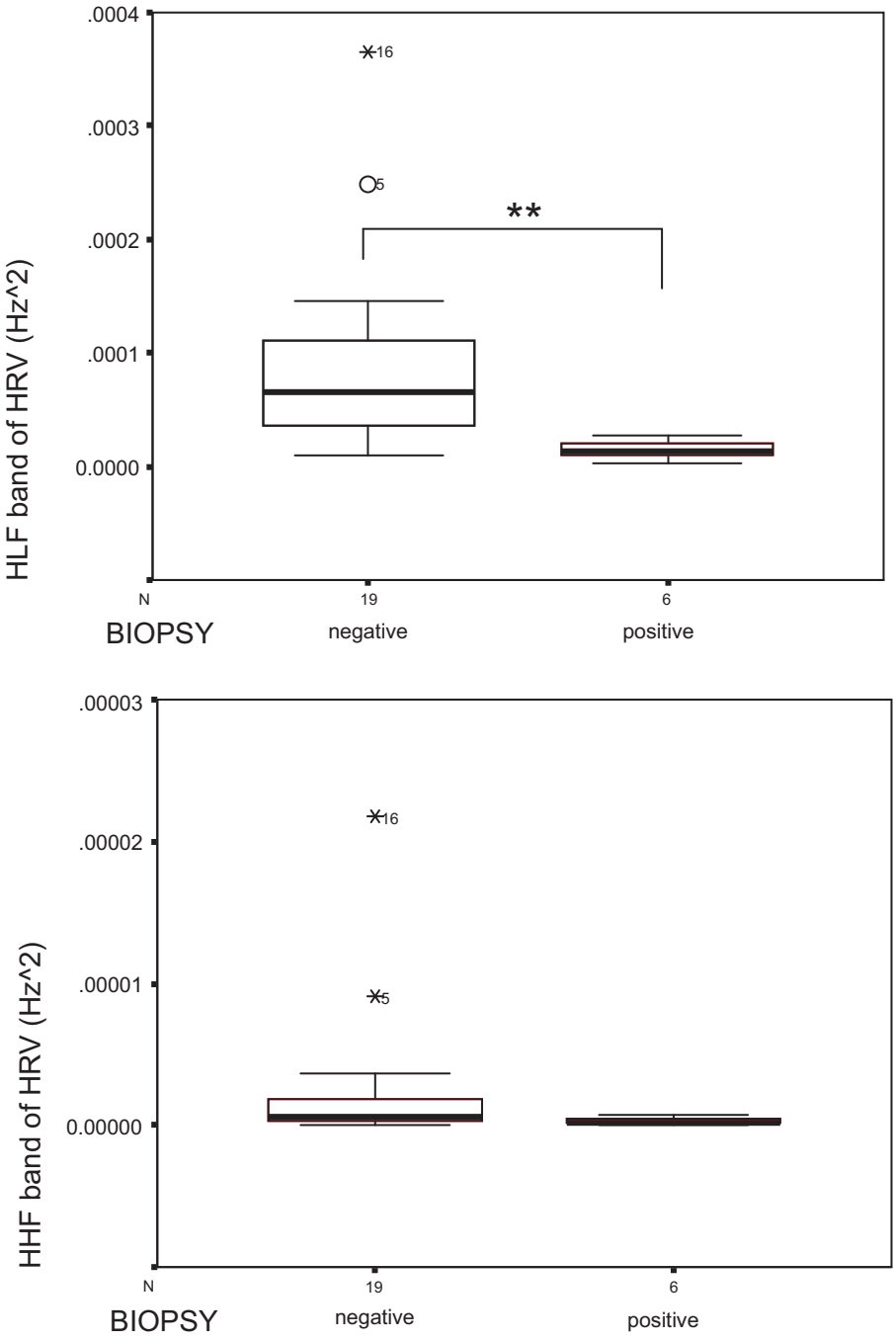

Figure 3. 6 Boxplots to show significance of HLF and HHF grouped by biopsy result.
HLF signifies a difference ($p<0.005$) in animals that were negative and positive for rectal biopsy. This difference is not seen in HHF band of HRV. Significant differences, as assessed by Mann-Whitney tests are indicated by ** with $p<0.005$

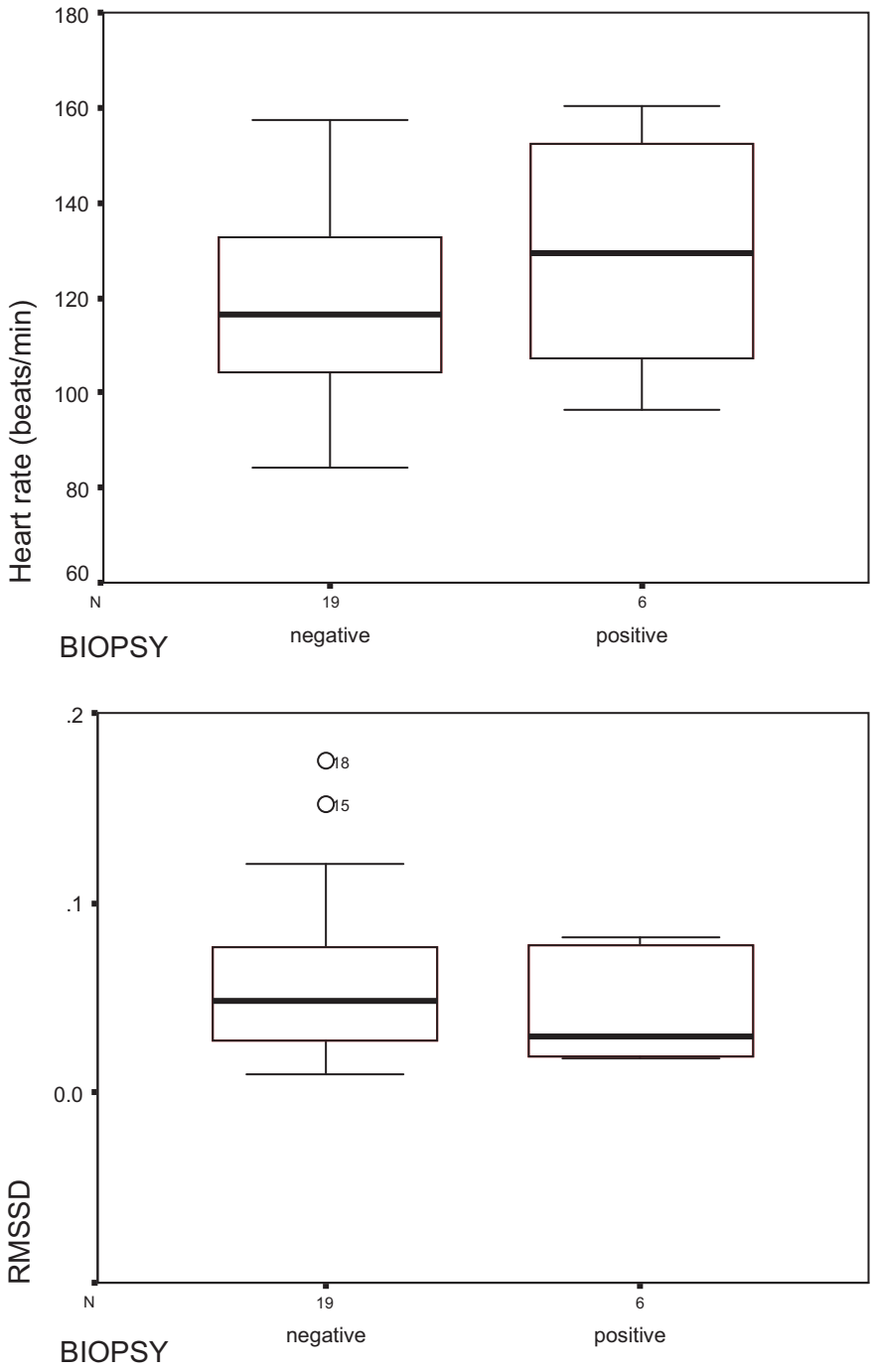

Figure 3. 7 Boxplots to show the lack of significance differences in heart rate and RMSSD grouped by biopsy.

Again HLF is distinct from RMSSD and heart rate values, in animals that were negative and positive for rectal biopsy.

Following this investigation of the data, comparisons with the rectal biopsy results were explored with a positive result showing the presence of PrP^D (Gonzalez, Dagleish et al.2006;Wadsworth, Joiner et al. 2006). In figures 3.6 and 3,7, it may be seen that HLF is able to distinguish a significant difference ($p<0.004$, using the Mann-Whitney test) between the animals that showed a negative rectal biopsy, which include groups 1,2, 5 and 6 from those with a positive biopsy in group 3. These groups now contain 19 animals for the negative biopsy group and 6 for the positive biopsy group.

Figure 3.8 shows a Receiver Operating Characteristic (ROC) curve that illustrates how HLF performs against the biopsy result for these sheep. Sensitivity on the Y-axis indicates the probability that a positive is correctly classified and on the X-axis, 1-specificity equals the probability of a false positive. The associated table in the figure displays the area under the curve which represents the probability that the value of HLF for a randomly chosen positive will exceed the result for a randomly chosen negative case. The indicated significance value suggests that this is not a chance observation.

This graph suggest that for 100% sensitivity, based on HLF indicating the presence of scrapie, there may be 25% false positives. This test would be a live repeatable test and would be easily repeated at a later stage in the disease pathology and this may help in the utility of such a methodology in distinguishing diseased animals from controls. In addition, we must remember that rectal biopsy may not be the “gold standard” in identifying diseased animals from healthy ones. Since it is based on the presence of PrP^D and doubts are being raised about the association of prions as the causative agent, doubts about the rectal biopsy results may be postulated. Could it be that the HRV index of HLF is a better predictor of Scrapie than rectal biopsy? Could the time course of the disease affect either of these results?

Figure 3. 8 ROC curve to illustrate the performance of HLF index of HRV against rectal biopsy.

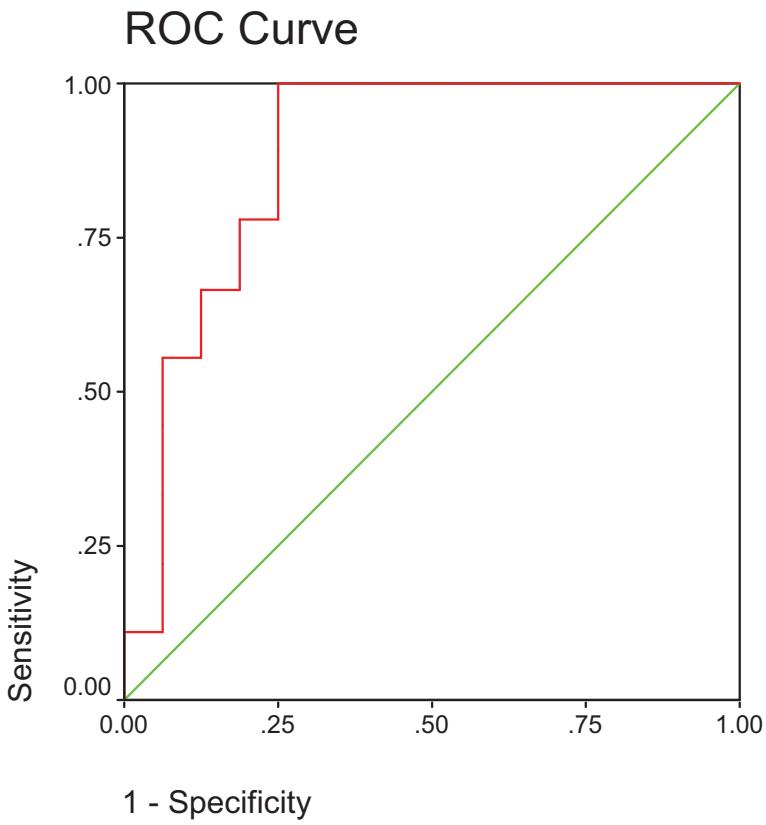

Area Under the Curve

Test Result Variable(s): HLF

Area	Std. Error[a]	Asymptotic Sig.[b]	Asymptotic 95% Confidence Interval	
			Lower Bound	Upper Bound
.882	.069	.002	.748	1.016

a. Under the nonparametric assumption

b. Null hypothesis: true area = 0.5

Limitations and further work to investigate HRV changes in TSE diseases

Caution should be exercised in interpretation of statistics from such small numbers of animals, but it may indicate that the HLF band as opposed to the HHF band, would be a better discriminator for the groups at this stage of the disease pathogenesis.

Due to the small size of group 6 this difference may have been due to individual differences in HRV of each animal. One of the animals was of susceptible genotype and, although negative in Ramalt at the time of testing, may have been incubating scrapie and so may have consequently distorted the HLF values of the group.

The lack of difference in the values of HLF between animals in group 1 (scrapie free controls) and group 3 (orally challenged and rectal biopsy positive) may be, again, due to the small number of animals in the "experimental" control group. However it may be observed from the box plot in figure 3.4, all of the animals in group 3 had HLF values below the median of those animals in group 1 and displayed a very much more condensed range.

If an individual animal's general physiology is considered in relation to this observation, it may be the case that individuals would express a range of values in this index of HRV during normal non infected state. These data represent one measurement on one day. A better method to deduce differences in this measure of HRV may be to do longitudinal repeated measures on each animal and look for significant changes in its baseline measures over time. This may give a more sensitive insight into changes of HRV with respect to TSE disease incubation in individual animals. The intra-variability of measures of HRV are reported to be less than inter-variability measures (Gavin Sandercock 2008;Jira, Zavodna et al. 2010;Sandercock, Bromley, & Brodie 2005). Future work would be required to investigate these facts in animals incubating TSE diseases. It may be that there are greater magnitudes in the change in HRV for individual animals incubating disease and so, in the diseased state, could give greater intra-variability than inter-variability between control populations and in the diseased physiology of animals incubating TSE diseases.

Other limitations in relation to this study will include the possibility that the Bonferroni correction method, used to address the problem of multiple testing, may be too conservative and miss significant differences when they are there.

A number of other methods to estimate HRV are currently used, including FFT analysis, autoregressive modelling and a moving polynomial technique. All methods have caveats and the potential to generate aberrant results due to violations of data integrity. No consensus has emerged on an optimal approach and since the methods used here attain significant differences it may be prudent to continue using these standardised and practiced methods in future studies. The possibility of refinement in the technique and the complementary addition of other techniques should also be investigated. Of particular importance would be the characterization of breathing frequency of the subjects and investigation of techniques that may be used to estimate a respiration event from the change in amplitude of the ECG recording (shown below).

Figure 3. 9 Diagram to show putative inspiration events, indicated by change in amplitude of ECG.

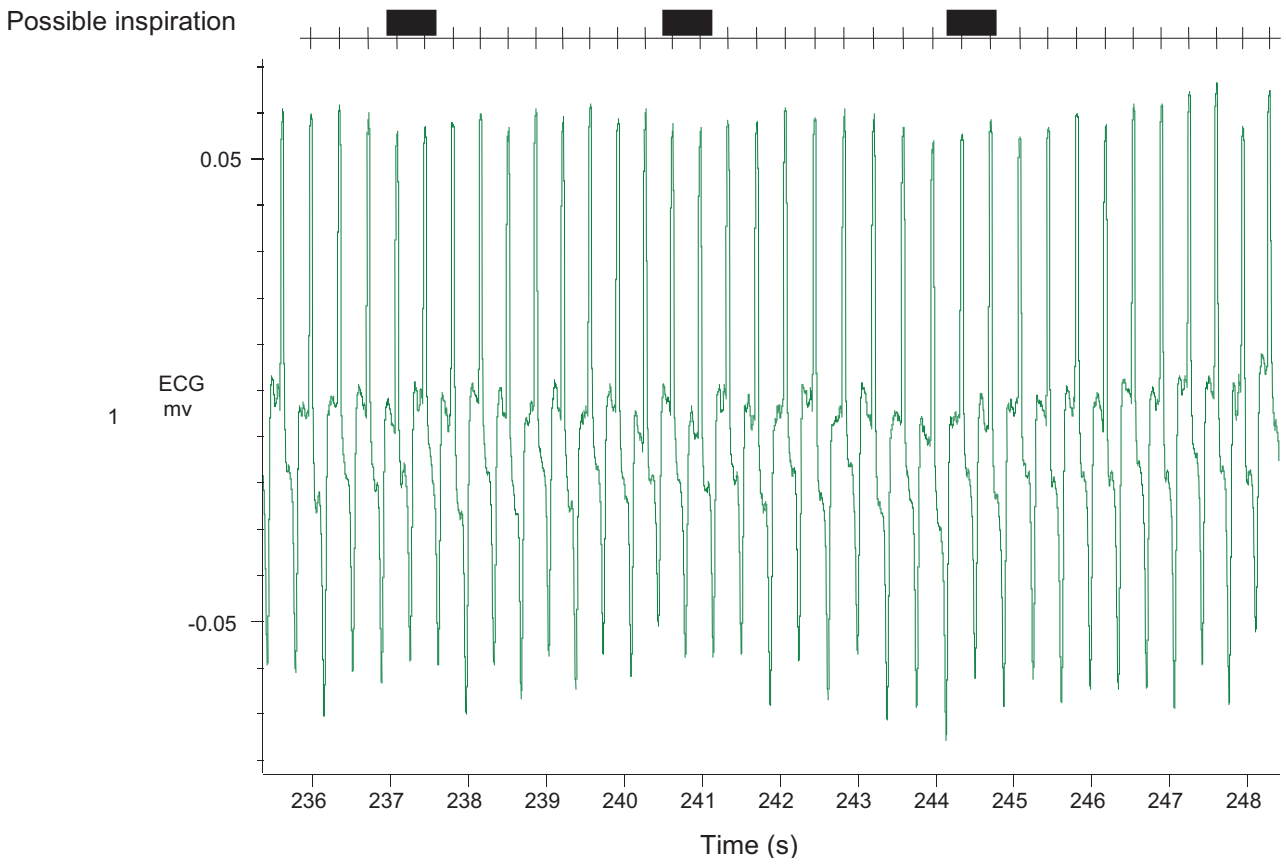

An automated program running within Spike2 could identify the maximum and minimum ECG amplitudes that would correspond to the change in recorded amplitude of the ECG signal as the thorax expands and contracts. This method has been used by Moody (Moody, Mark et al. 1985), Noh (Noh, Park et al. 2007) and Cysarz (Cysarz, Zerm et al. 2008). These events would then indicate inspiration and expiration for each breath cycle. This data could then be used to give a precise indicator of RSA using circular statistical techniques (Batschelet 1981;Pomfrett.1995;Wang, Pomfrett, & Healy 1993) that would relate HRV to each breath cycle. A number of such cycles could be studied to compare the degree of coupling of RSA to the heart beat cycle in control and infected populations. It has been stated that RSA may contaminate the conventional LF range of 0.05-0.15 Hz if the breathing frequency is below about 10 breaths per minute (Berntson, Bigger, Jr. et al.1997). It is apparent that the frequency band discussed here, HLF 0.032-0.138 Hz, may equally be subject to such contamination and consequently it would be useful to dissect the precise component of RSA from this range and it may yield more information in relation to the pathogenesis of this and similar diseases.

The breathing events may be more conveniently measured from human populations than animals “in the field” since the positioning of any breath sensors is less prone to damage and the cooperation of the human populace is, generally, greater than that of animals. Once the process of obtaining the breath events from the change in ECG amplitude has been programmed it could be validated using data from human controls where the calculated breath events from the software could be correlated to the actual breath events obtained by a suitable transducer. The ability to accurately represent the true RSA of each subject would give the opportunity to better estimate the degree of decoupling of RSA from the heart beat cycle than spectral estimates based on FFT analysis due to some of the caveats mentioned above. RSA calculated in this way would provide another index of HRV and may mean an earlier divergence from normality is observed in the diseased population and may aid both the diagnosis and also increase the efficacy of any putative treatments being developed for TSE diseases.

It would also be interesting to study other TSE diseases in different animal and human populations to see if there is a characteristic signature change in HRV that could estimate the specific disease or estimate the rate of disease pathogenesis. For example, do the HRV indices exhibit a similar transition with respect to time in Scrapie, BSE and vCJD? Would there be differences that may determine the stage of the disease that the individual is at? Could this longitudinal change be monitored by these and other HRV indexes?

If the analysis of HRV was useful in distinguishing TSE infected subjects from controls, the utility of its application, in isolation and in conjunction with other tests, to screen for humans and animals incubating such diseases may be explored.

From the initial study described here on scrapie infected sheep, it is evident that indices of HRV are able to significantly distinguish sheep with the disease associated marker from those free of the marker before any of the animals showed clinical signs of the disease. This highlights the potential for such methods in helping identify diseased animals and their consequential elimination from the food chain. It may also give rise to the possibility to screen human populations and reduce human susceptibility to iatrogenic TSE diseases resultant from blood transfusions and surgical procedures.

Discussion

The dorsal vagal nucleus (DMNX) and nucleus ambiguus (NA) are two anatomically distinct regions of the medulla oblongata of the brainstem involved with the control of the heart on a beat to beat basis. The vagus nerve has parasympathetic cell bodies located in the DMNX and NA. The presence of disease associated prion (PrP^D) in DMNX and NA are used in the post mortem diagnosis of transmissible spongiform encephalopathies (TSEs) in animals.

It has been shown that PrP^D alters the neuronal discharge properties of infected tissue (Barrow, Holmgren et al.1999;Collinge, Whittington et al.1994). Collinge from his work with PrP null mice, that is mice that are genetically modified to have no prion, reported a pair of intracellular action potentials recorded as the result of a train of stimuli on hippocampal slices from such mice. Similarly, Barrow recorded similar action potential doublets following a series of stimulations in hippocampal slices of scrapie-infected hamster. Taken together, this suggests that the presence of PrP^D is functionally equivalent to having no PRP, consequently abnormal synaptic function would result in the diseased state. The reduced amplitudes of medium and late afterhyperpolarizations observed in scrapie infected hamster are suggested to be involved in the production of these double action potentials, It is also reported that these changes in afterhyperpolarization appeared before the onset of overt neurological symptoms and histopathological change.

These lines of evidence, coupled with the work of Carleton and Jeffery who suggests strong evidence for a functional role for PrP^C in modulating synaptic transmission, suggest that abnormal prion will disrupt the normal synaptic flow of neural information used to regulate target organs, such as the heart. before clinical signs of the disease (Carleton, Tremblay et al.2001;Jeffrey, Halliday et al. 2000).

The presence of PrP^D in rectal mucosa has been demonstrated to be a marker of TSE disease in animals and humans (Gonzalez, Dagleish et al.2006;Jeffrey, McGovern et al. 2000;Spraker, Gidlewski et al. 2006;Wadsworth, Joiner et al.2006). From the results of this initial investigation described above (see figure 3.6) it can be seen that animals with PrP^D positive biopsy, demonstrate a different beat to beat control in their autonomic control of the heart compared to the control

non-infected animals. To my knowledge this is the first time that heart rate variability has been used on sheep to distinguish preclinical infected animals from controls.

From the results obtained from this study it is apparent that some of the orally infected sheep (group2) were negative for PrP^D by rectal biopsy testing. When the results for the HLF between the groups are examined it may be seen that this group only contained four animals and this group displays a wide range in values of HLF, indicated by the quartile bars in the boxplots. Individual differences in the amount of infectivity in the oral challenge these animals received along with individual genotype and strain interactions may explain why these animals were not positive for PrP^D. In addition individual differences in disease pathology may have meant that these animals were at a different stage of infection compared to those animals in group 3, for example. This highlights the possibility of a dynamic change in autonomic neural regulation of the heart in a diseased state. From work with transplant patients and animal ablation studies the time course for such changes in autonomic control of the heart on a beat to beat basis may be over months (Bernardi, Bianchini et al. 1995;Fallen, Kamath et al. 1988;Koskinen, Virolainen et al. 1996;Pozza, Kleinmann et al. 2006;Smith, Ellenbogen et al. 1990). This may give rise to a see-saw response in various indices of HRV seen in incubating subjects over a similar time frame. It is also reported that a similar see-saw in clinical signs of cattle incubating BSE is observed (Wells, Konold et al. 2007), emphasising the dynamic nature of TSE disease.

Consequently, a more robust testing regime based on HRV analysis should include repeated longitudinal analysis of HRV, using each individual as their own control and emphasis put on significant changes in autonomic beat to beat regulation of the heart as controlled by the diagnostic brainstem regions of the DMNX, NA and NTS. The data was initially analysed by separating the experimentally-infected and naturally-infected field animals into groups as shown in figures 3.4 and 3.5. This was done to investigate any effects due to different disease pathogenesis due to different routes of infection as discussed in the introduction and figures 1.3 and 1.4. The naturally-exposed sheep may have had a different method of infection than the orally challenged, experimental group.

The enteric nervous system (ENS) as shown in figure 1.3 connects the gut to the NTS and DMNX via efferent and afferent vagal fibres. Card suggests a neural connection from stomach to the DMNX (Card, Rinaman et al.1993). In addition the ENS connects with the rectal mucosa via efferent and afferent vagal fibres. This provides a neural conduit to and from the DMNX and NTS respectively. Consequently, prion translocation may occur from the rectal mucosa to the DMNX or indeed from the DMNX to the rectal mucosa. This provides two possibilities for the origin of PrP^D in the rectal mucosa. The first is that it originated from passage from the gut to the rectum and then infects mucosal tissue. Secondly, PrP^D deposits originating in the brainstem areas may travel via a neural route to the rectal mucosa, having previously been deposited in the brainstem by a vagal route from gut to brain.

If the second of these methods for PrP^D deposition in the rectal mucosa is viable then it may be that a perturbation in HRV indices, HLF possibly, may be observed before the rectal mucosa biopsy was positive. For those animals orally infected, there was a significant difference ($p<0.05$, using Mann-Whitney test with Bonferroni correction) between those having a positive rectal biopsy result (group 3) and those with a negative result (group 5) although the small number of experimental controls (group 1) did not differ significantly from either of these groups. The difference between these groups (group 3 and group 5) indicate that HLF may give a similar indication as rectal biopsy, for the presence of scrapie in pre-clinical animals.

In addition, the first variable to change may not be HLF. It may be that dysfunction in different neural pathways earlier in the disease gives a different signature of disruption in the neural control of the heart and different indices of HRV would better show this change in function due to TSE incubation. Some of the neural tissue that would be putative sites to cause a disruption to normal HRV are indicated by the red dots on figure 1.6. These sites include the intrinsic cardiac ganglia. The range of sites for potential disruption in the integrated and normal control of beat to beat variability of the heart cycle illustrate the potential for differences in HRV that may be evident in individual animals within an infected group. This underlines the importance for longitudinal monitoring of HRV in the early diagnosis of TSE diseases for individuals.

For this study, with relatively small numbers, it is surprising that such a clear difference between the groups is observed when segregated based upon their rectal biopsy results (see figure 3.6). All of the experimental animals had a mix of breeds (Suffolk and Cheviot) and genotypes (ARQ/ARQ, VRQ/VRQ and ARQ/VRQ) within them but no significant differences based upon these criteria were seen in the calculated HRV indices. The naturally exposed field animals were the same breed but different genotypes. The resistant genotype was designated ARR/ARR and the others were ARQ/ARQ. The differences reported here in infected animals not showing clinical signs, suggest they are independent of breed and genotype and relate directly to the presence or not of PrP^{D} in the rectal biopsy.

The HLF component of the analysis can distinguish between sheep with scrapie from those scrapie free sheep that do not have PrP^{D}. All sheep tested and analysed did not show any clinical signs for scrapie, consequently assessment of HRV indices in incubating animals is able to identify the disease before clinical signs are evident. For the biopsy groups HHF was not able to distinguish positive from negative animals, although HLF was.

Non myelinated vagal fibres from the DMNX and faster myelinated vagal fibres from the nucleus ambiguus (NA) are involved in the control of heart rate variability (HRV). Cardiac vagal tone may be considered to be the sum of low frequency (HLF) variation in HRV from influences from vagal efferents from the DMNX, plus high frequency (HHF) variations, influenced by the respiratory frequency, from the efferent output from the NA (Porges 2006a).

These facts coupled with the neuroanatomical finding of van Keulen may give further support to the use of HRV in early diagnosis of HRV. van Keulen suggested that the initial site of infection for the disease agent in scrapie was via the vagus nerve, with an initial build-up of PrP^{D} in the DMNX, followed by the NTS and then the NA (van Keulen, Schreuder et al.2000). Correspondingly a functional change in the brainstem areas of the DMNX and later the NA may be seen in a perturbation in the HLF and HHF bands of HRV respectively.

RMSSD has been suggested to reflect the high frequency changes in HRV in the respiratory frequency range. It has also been reported that levels of RMSSD between subjects correlate with HHF spectral estimates of HRV (Berntson, Lozano, & Chen 2005). Consequently both HHF and RMSSD may be considered to represent estimates of the activity of the NA. From these observations in sheep with scrapie it may be suggested that the difference in low frequency values in HRV, and not in higher frequency values, may implicate a malfunctioning DMNX but normal functioning NA.

I present here, empirical evidence for such a theory, with those animals positive in rectal biopsy being distinguished from animals of mixed provenance that are negative in RAMALT biopsy by the HLF component of HRV. The HHF band is not able, at this preclinical stage of disease, to differentiate between the groups. This may suggest that a neurophysiological malfunction has occurred in the DMNX but the function of the NA is intact. This would agree with the neuroanatomical observations of van Keulen. Whilst there is a need to record data from many more animals to attain more reliable indicators of this theory, the proof of principle is demonstrated.

The relatively simple and non-invasive assessment has a role in public health issues at many levels and may have utility in other current neurological diseases and in addition it may help to characterise any new diseases we have not yet discovered.

Chapter 4 Investigation of BSE infected Cattle using heart rate variability assessments

Introduction

Prion diseases affect a wide range of mammals and are classed as transmissible spongiform encephalopathies (TSEs) due to their infectious nature and the spongiform or sponge like appearance observed in neural tissues of infected organisms. Bovine Spongiform Encephalopathy (BSE) is a transmissible spongiform encephalopathy of cattle that has etiological links to vCJD in humans (Hill, Desbruslais et al.1997;Scott, Will et al. 1999).

Two atypical forms of BSE have so far been reported: L-Type or BASE (bovine amyloidotic spongiform encephalopathy), with a lower molecular size of the unclycosylated isoform of PrP^D (without any sugar side chains) compared to PrP^D from "classic" BSE; H-Type BSE which demonstrates higher molecular sizes of the unclycosylated isoform of PrP^D compared to "classical" BSE. Investigations into the transmission of L-Type BSE into different mouse lines demonstrated atypical disease phenotypes in human and bovine PrP transgenic mice but gave a "classic" BSE phenotype in mice expressing ovine PrP (Beringue, Andreoletti et al. 2007). This highlights the interaction of both the strain of TSE and host genotype in the final expression of the disease phenotype.

Further implications from this work demonstrated that the transfer of L-Type BSE agent to certain mouse populations (tga20 mouse lines with 6–7 times the normal PrPC level) did not produce any overt clinical symptoms; this disease was subclinical and therefore masked in this genotype. Yet when this agent was transferred to a different mouse line (tgHu transgenic mouse line with human PrP) it did result in early accumulation of PrP^D in brain regions compared to classical BSE and other phenotype traits similar to atypical BSE (Beringue, Andreoletti et al.2007). Thus, it may be possible that a different strain of BSE, here BSE-L, may be more virulent to certain genotypes of the human population than "classic" BSE. Secondly, it again highlights the possibility of subclinical carriers, in a different host genotype, being able to infect susceptible genotypes.

Past work investigating the species barrier, involving the transfer of hamster TSEs to mice, found that the recipient species did not display overt signs of disease. However, upon histopathological investigation there were neuronal signs of the disease and high levels of infectious agent. These subclinical mice were also found to be able to infect other mice despite not showing any clinical signs of the disease (Hill, Joiner et al. 2000). Here, the initial hamster prions had caused mouse prion to become infectious to mice following passage via a mouse line. This raises concerns about an asymptomatic carrier state that, if extrapolated to the human population, may raise awareness to the risk of future iatrogenic infection. Consequently, current and future novel strains of such TSE diseases may pose further risk to human populations. Hence, research is vital to not only identify more accurately the disease pathogenesis and causative agents of the present prion diseases but also to prepare for those diseases we, as yet, do not know.

TSEs in farm animals have historically been reported using tests designed and developed to be used for surveillance, to assess changes in the level of TSE diseases within a population over time. These tests predated the identification of atypical BSE strains and so may have failed to identify these and other strains of BSE. They were designed to be an epidemiological tool and not a test for preclinical or clinical infection in animals. Initially the diagnosis was based on the visualization of vacuolation of a precise histological section of the medulla oblongata region of the brainstem (Wells, Hancock et al. 1989). Subsequently the identification of the disease associated confirmation of the prion was achieved by immunohistochemical (IHC) analysis of fixed brain tissue (Wells, Spencer, & Haritani 1994). The “Rapid tests” (ELISA or Western blot based) approved by the European Union (EUROPEAN COMMISSION 1999;EUROPEAN COMMISSION 2002) use antibodies to detect the disease associated conformation of the native prion protein. This raises two questions on the efficacy of the tests.

The first is the specificity of the antibody for the disease associated conformation of the prion. Potentially, a different antibody may not recognise and identify a different strain of BSE that may have a different disease associated conformation of the protein. Arsac suggests the sensitivity of such tests depends on the selection of antibody used and they found that one antibody was able to identify both typical and “unusual” BSE types with differing sensitivities (Arsac, Biacabe et

al. 2007). This reasoning has been further supported by Swedish workers investigating a H-type variant of BSE using Western Blot techniques (Gavier-Widen, Noremark et al.2008) who found that the choice of antibody also affected the ratios of PrP^D glyco-types. This coupled with the statement that differences in the reagents used, such as water (USDA 2005), during the performance of the tests highlight the potential for erroneous results. Recent work has also confirmed the existence of more than one strain of BSE with differing affinities for the antibody used in the tests and different sensitivities to PK digestion at different pH values (Jacobs, Langeveld et al. 2007). This work concludes the use of 2 different pH values and three antibodies during the testing procedures would provide the ability to identify and discriminate the BSE strains currently identified and may help in the identification of other variants. It must be remembered the testing regimes previously used did not benefit from these additional refinements and consequently there is a probability that some cases of BSE have been omitted from the historic epidemiological analysis for the disease.

Secondly, PrP^D may not be the infectious agent hence the test may be directly assessing a surrogate marker for the disease, as supported by recent and on-going research and theories (Aguzzi, Heikenwalder et al.2007;Barron, Campbell et al. 2007;Baskakov 2007;Bastian, Sanders et al. 2007;Collinge & Clarke 2007;Jeffrey, Gonzalez et al.2006;Liberski & Brown 2007;Manuelidis.2004;Manuelidis.2006;Manuelidis, Yu et al.2007). In addition there is also the possibility that PK sensitive particles may be able to cause TSE disease and would have been nullified by the PK digestion phase of the testing regime (Nazor, Kuhn et al. 2005;Safar, Wille et al. 1998)

Debate in relation to the infectious agent of TSEs and the sensitivity and specificity of historic tests indicates that improvements in the testing regime are needed. To assist in the current assessment and the early identification of infection of TSEs, HRV analysis may form a suitable adjunct. Analysis of repeated longitudinal measure of HRV data from cattle has demonstrated significant differences between infected cattle and controls. In addition the utility of using HRV analysis in the identification of subclinical scrapie infection in sheep has also been established. HRV analysis is an antemortem test and readily allows repeated measures to be recorded and analysed as the disease progresses. Repeated measures and subsequent analysis has the advantage of reinforcing the diagnosis

and provides data to assess changing HRV in relation to disease pathogenesis. This will allow us to build on the knowledge of neural dysfunction as TSE diseases progress and will lead to an early preclinical indication of the disease. This early identification would increase the opportunity for the application of putative therapies in relation to human disease or allow the removal of infected animals from herds and reduce the chance of horizontal transmission of TSEs in farmed animals and, as recently reported, in humans (Riverol, Palma et al.).

The cattle studied in the independent work of Masujin (Masujin, Matthews et al.2007) and Pomfrett (Pomfrett, Glover et al.2004) were part of a government established research project termed SE1736 (Defra.2007). Some of these animals were also the same animals that had repeated longitudinal measures of their ECG recorded before they demonstrated clinical signs and were culled for histopathological examination (personal communication with Dr D. Mathews VLA). The sub group of animals that were subjected to detailed pathological examination by Masujin and others form the subject group for this detailed analysis using metrics of HRV. Different metrics of HRV, based on time domain analysis as compared to the frequency domain metrics used previously, are reported here.

Methods

In order to investigate perturbations in HRV in cattle incubating BSE, data was obtained from cattle purposefully infected with 1 gram or 100 grams of infectious material. These animals were part of a Veterinary Laboratories Agency (VLA) directed governmental study based at the ADAS Drayton site (Defra.2007). Data was also collected contemporaneously from control animals held at the same facility. The initial numbers of animals in each group and related methods were as described previously (Pomfrett, Glover et al.2004) and summarized here.

The control group consisted of 48 animals, the 1 gram group contained 43 animals and the 100 gram group had 42 animals in it. The animals were orally challenged once with either 1g or 100g of infectious brainstem homogenate made from a pool of positive and symptomatic field cattle brainstems, or in the case of the controls, received no brainstem homogenate. The homogenate was not assessed for strain diversity (reported communication Pomfrett and VLA staff) and so there is a possibility that more than one strain was inoculated in some of the animals. The animals were kept in isolated herds with stringent controls in place to eliminate cross contamination between the three groups.

The recording of data from these animals commenced in January 2001. This was 29 months after the oral challenge of infectious material. We were invited to record the ECG from these animals after the experiment and associated protocol was initiated. Our investigations had to follow the protocol already running for the SE1736 experiment. This involved a sequential kill to provide a range of infected tissues at different stages in the disease pathogenesis which was to be the subject for subsequent analysis after euthanasia. We had no control over the selection of the animals that were sequentially killed which contributed to our partial data set. Data was also not collected during the 2001 foot and mouth crisis due to limited movement of the equipment to and within the facility at DVLA. We endeavoured to collect data once a month from each animal.

In an analogous method to the data collection used to study sheep (Chapter 2 and Chapter 3) data was obtained using similar electrode and gel combinations but captured using a “Depth of Anaesthesia” monitor developed by Otter Controls Ltd, as described previously in chapter 2.

Data were collected by VLA staff due to access restrictions to the governmental institution. Once collected data were sent to Manchester University to be archived, checked for quality and analysed. I analysed all the data presented in this chapter in relation to these cattle and liaised with staff at VLA in relation to data collection and use and repair of the data collection equipment.

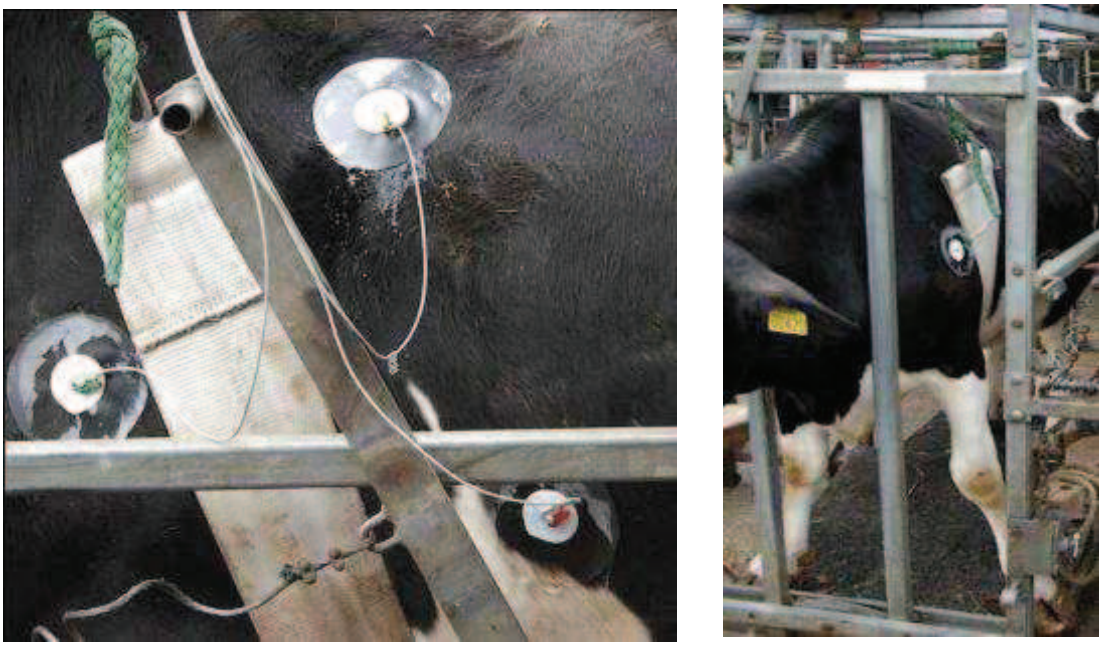

Figure 4. 1 Cow in a crush with electrodes attached.
Typical cow in a crush with electrodes attached via gel pad arrangement as described in chapter 2.

BSEnsor v8, a script running in Spike2 software was modified by myself to output raw inter beat intervals (IBI) that were derived from the same section of the data file from which the frequency domain measures of HRV were calculated. This ensured the same data series was used in the calculation of time and frequency domain metrics by using this IBI series as the input file for the CMETX program.

CMETX (written by John Allen) is a command-line based utility that will calculate several metrics of cardiac chronotropy given a simple inter beat interval (IBI) series as an input. The inter beat interval input is in the form of an ASCII file that contains one IBI per row. CMETX runs in a DOS environment under any version of Windows (Details of its development and use are in (Allen.2002;Allen, Chambers et al.2007). The software has recently been used in peer reviewed publications in the area of psychological research and human development (Gustafson, Allen et al. 2011;Lutz, Greischar et al. 2009;Weinberg, Klonsky, & Hajcak 2009). This software provided metrics of cardiac vagal index (CVI) and cardiac sympathetic index (CSI) amongst others that were based on work of Toichi (Toichi, Sugiura et al. 1997).

CVI and CSI are constructed from Lorenz plots which analyse the R-R fluctuations of the data sampled as indicated in figure 4.2. In order to obtain the values of L and T, the axes were rotated clockwise by 45^{0} so the line L was parallel to the x-axis (Allen.2002). The values of L and T were estimated as four times the standard deviation of the points along the respective axes.

CVI is designated as $\log_{10}(LxT)$ where L is derived from the length of the longitudinal axis parallel to the line $I_n = I_{n+1}$ where I_n represents the nth item in the RR sequence and I_{n+1} represents the next item in the RR sequence. CSI is given by L/T (Toichi, Sugiura et al.1997). It was found that the measures of T were sensitive to both parasympathetic and sympathetic blockade to some extent, in contrast to the CVI metric which was not affected during administration of propranolol (sympathetic blockade) but diminished by atropine (parasympathetic blockade). CSI was found to be attenuated during sympathetic blockade. These responses were found to be posture sensitive with CSI not reflecting sympathetic activity in the supine position (Allen, Chambers et al.2007;Toichi, Sugiura et al.1997).

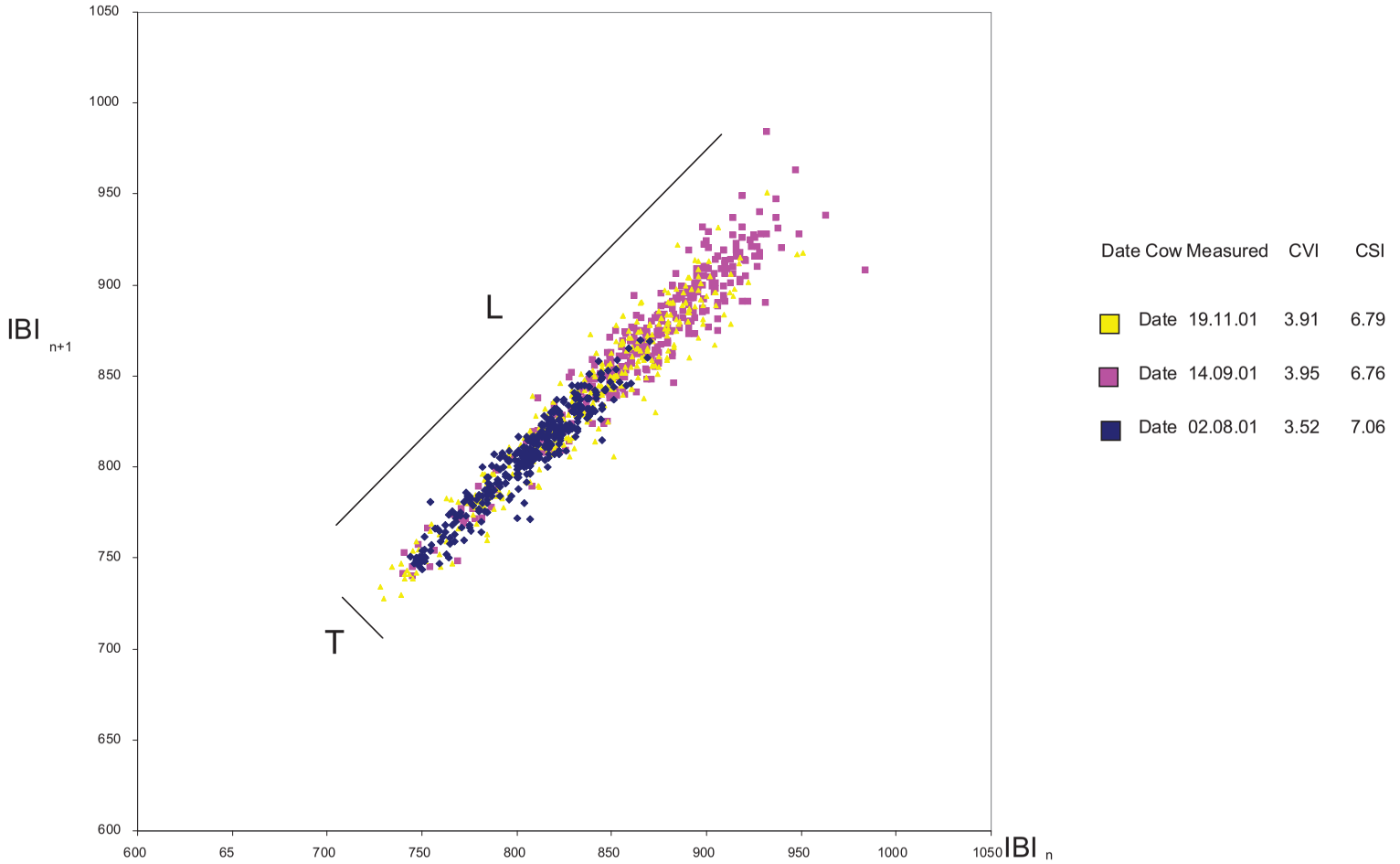

A Lorenz plot as described by Toichi et al (1997). Each inter beat interval (IBI) is plotted on the x-axis and the subsequent interval is plotted on the y-axis. Variations in the direction of the line "T" (orthogonal to the line L) represent a large beat to beat variability. L is affected only by parasympathetic blockade whereas T is affected by both sympathetic and parasympathetic blockade

Figure 4. 2 Lorenz plot of a cow incubating BSE.

The aims of this study were to investigate if a difference between the HRV of cattle incubating BSE and control cattle could be seen.

Using the CVI and CSI (Toichi, Sugiura et al.1997) metrics of HRV, calculated using CMETX (Allen.2002) the 3 groups of cattle were longitudinally analysed over a 12 month period corresponding to 29-41 months post inoculation (PI).

In addition the utility of this method was applied to investigate the idea that field animals (animals that were suspected of having BSE based upon clinical signs and due for euthanasia) could be distinguished from controls and to explore differences between the experimental animals of this chapter, if they existed.

Data were investigated by inspection of box plots derived from SPSS v 11.5. These display groups of data graphically and illustrate the group's lower quartile, median, upper quartile along with the lowest and largest observation for that group. The data was tested for normality and not all of the groups' data were normally distributed. Consequently, the nonparametric data sets were compared using the Kruskal-Wallis test for differences between groups followed by a Mann-Whitney test with Bonferroni correction as described in chapter 2.

Results

For this analysis, animals were chosen from those listed in tables 3 and 4 in the work of Masujin. Animals were selected based upon their "BSE status" which were derived from IHC examination and identification of disease associated prion in midbrain, rostral medulla and medulla obex. In addition the animals analysed here were also designated as either positive or negative in either C1-2, C2-3 or T9-10 regions of the spinal cord. ECG data collection from these animals was initiated at 29 months following the oral challenge, consequently we did not have data for those killed at 27 months after challenge and not all of the animals sacrificed at 30 months appeared in our data archive. Animal no 161 was excluded since the data obtained was incomplete and animals 140 and 174 were excluded from this analysis since despite having a positive BSE status, this was not confirmed by the standard brainstem investigation for the presence of PrP^D. It was noted that for all the animals included in this analysis, a positive result for PrP^D in the spinal cord indicated that both regions of the spinal cord were identified as positive. This gave reassurance for the classification of a negative result in either spinal region as being negative overall. The animals used in this analysis to investigate changing autonomic performance during TSE incubation are summarized in table 4-1. These infected animals were compared to a sample of contemporaneous controls that were also part of the SE1736 study.

TAG	BSE Status	Spine (either)	Group
115	+	+	100
120	+	+	100
143	+	+	100
146	+	+	100
173	+	+	100
313	+	+	1
257	+	+	1
194	-	-	100
132	-	-	100
165	-	-	100
178	-	-	100
180	-	-	100
193	-	-	100
196	-	-	100
203	-	-	100
224	-	-	1
247	-	-	1
248	-	-	1
259	-	-	1
271	-	-	1
312	-	-	1
214	-	-	1
234	-	-	1
236	-	-	1
263	-	-	1
266	-	-	1
300	-	-	1

Table 4- 1 A table to display the tag numbers of the experimental animals analysed, their BSE status and PrPD in the spine.

CVI was able to distinguish ($p<0.05$) the 1g and 100g dosed animals from contemporaneous controls in cattle over a twelve month period when the repeated measures for each animal were pooled into the three groups (figure 4.3). Significant differences ($p<0.05$) in these groups were also identified by spectral assessment of HRV in both the HLF (0.032-0.138 Hz) and HHF (0.15-0.5 Hz) bands (figure 4.4). Interestingly, over this period of investigation, for cattle of the challenged groups, the HLF values were significantly higher than controls. This contrasts with the relationship in scrapie-infected sheep where infected animals showed significantly lower values than controls (see figures 4.4 and appendix 1.10) (Glover, Pollard et al. 2007).

For the cows forming the experimental study groups for this research there was a significant difference in CVI between controls and 1g and controls and 100g groups of the infected animals when looked at over the entire year. The challenged animals demonstrated higher median values in this metric compared to controls. The CSI values only indicated a difference, compared to controls over the year, for the 1g group. The CSI values for the 100g group were not significantly different from controls during this period (Figure 4.3).

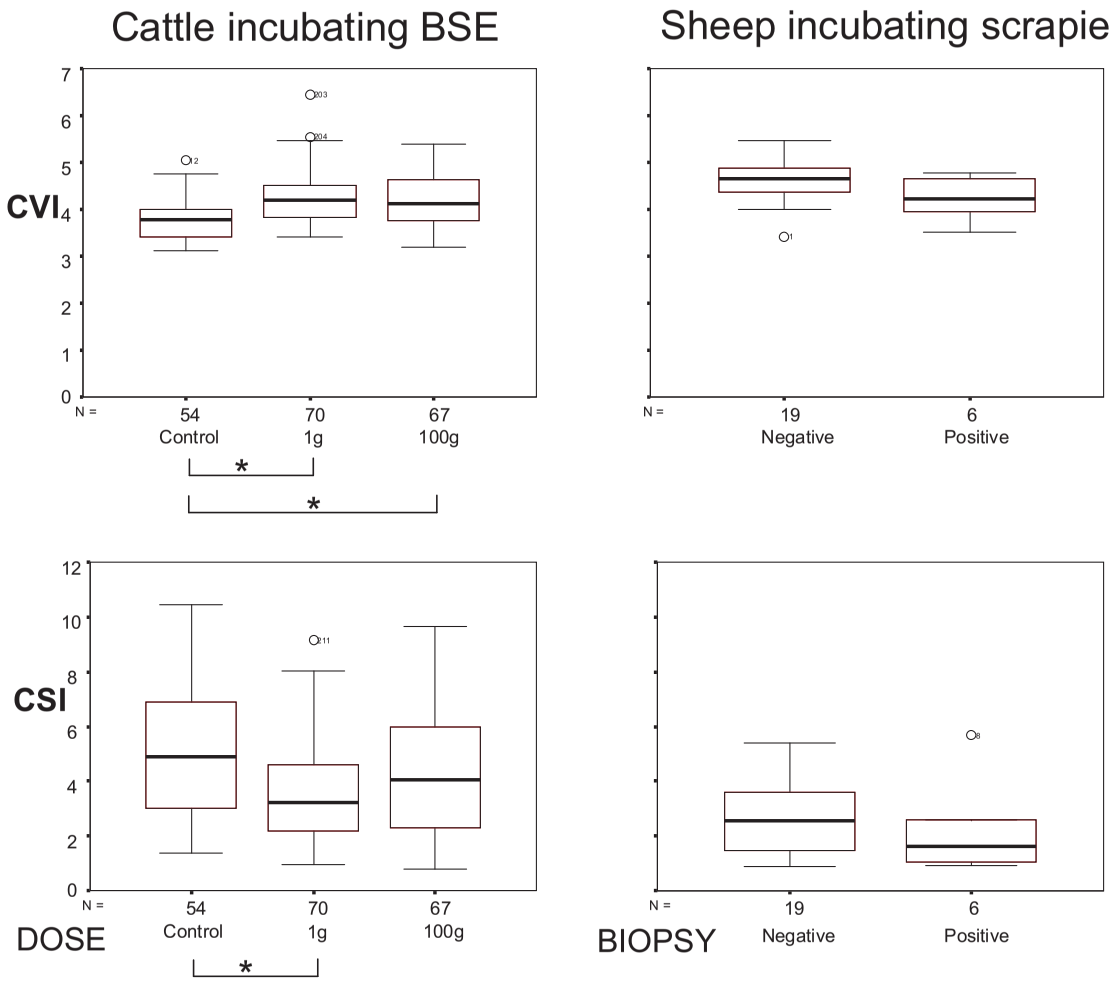

Illustrating the differences in time domain analysis of HRV during BSE and scrapie incubation (Significant differences, as assessed by Mann-Whitney test with Bonferroni correction following a Kruskal-Wallis test, are indicated by * with $p<0.05$)

Figure 4. 3 Time domain HRV differences in BSE and scrapie.

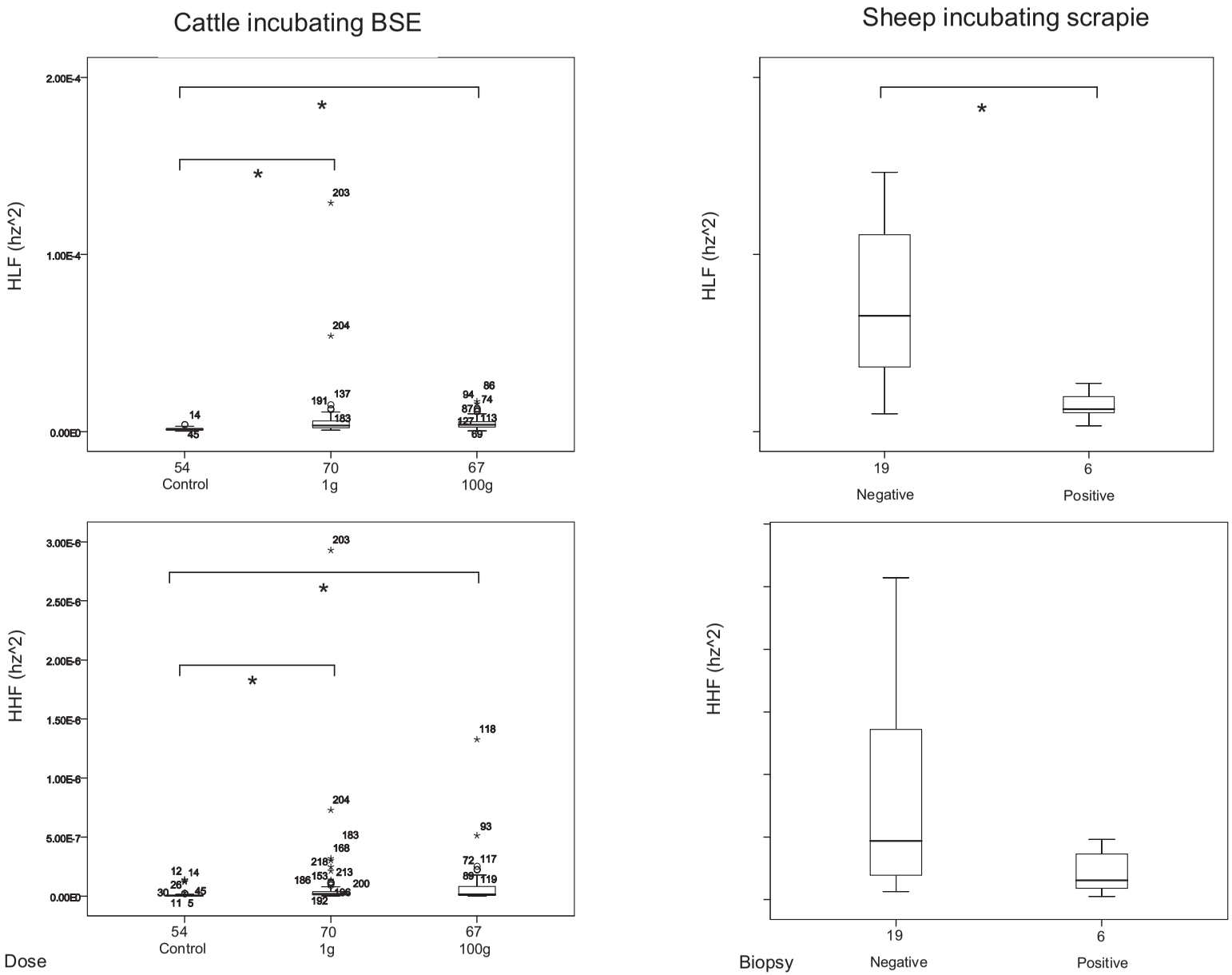

Illustrating the differences in spectral estimates of HRV during BSE and scrapie. Vertical scale is same for both sheep and cattle. Significant differences, as assessed by Mann-Whitney test with Bonferroni correction following a Kruskal-Wallis test, are indicated by * with $p<0.05$ (Appendix 1.10 shows the cattle data on expanded y-axis)

Figure 4. 4 Frequency domain differences in HRV in BSE and scrapie.

Figure 4.5 shows the variation of CVI, CSI and Figure 4.6 shows the variation of two spectral estimates of HRV, shown per quarter (3 month epoch) of the year of interest. It can be seen that the HLF values for cattle incubating BSE, either challenged with 1g or 100g of infectious material, for any of the 4 epochs are always significantly higher than controls (Figure 4.6). These cattle were measured much earlier in the incubation of TSE disease than the stage of incubation the sheep were measured at. The differences in the HRV metrics observed here between the cattle and sheep may be due to a difference in disease pathogenesis with respect to time. Some of the sheep displayed clinical signs 1-2 months after the measures were taken in contrast to some of the cattle not showing clinical signs of BSE for a further 12 months after the initial measurements.

CVI for the 1 gram group was different than controls during measures taken in the first 6 months of the year but not in the last 6 months. Similarly CVI for the 100g animals showed an increase, compared to controls, for the first 6 months of the year. CVI between the 1g group and the 100g group were not different (See figure 4.5).

CSI values for the 1g group demonstrated a significant difference compared to control values in the first 3 months of the year. There was then no significant difference in this metric over the three remaining quarters between controls and the 1g challenged animals. CSI values for the 100 g group showed a significant decrease compared to controls in the 2nd quarter of the year (See figure 4.5).

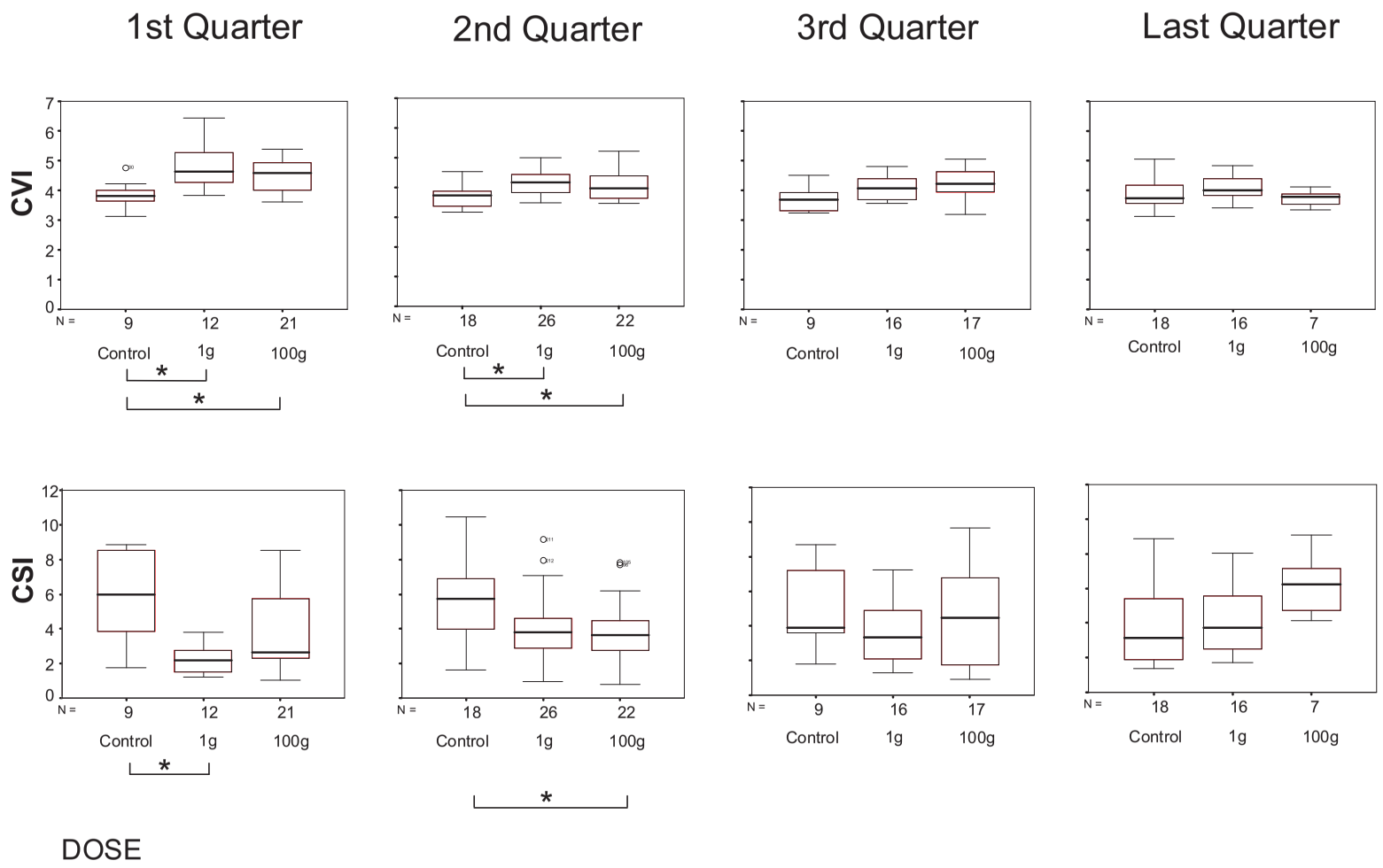

To show change in time domain measures of HRV of cattle incubating BSE. Significant differences, as assessed by Mann-Whitney test with Bonferroni correction following a Kruskal-Wallis test, are indicated by * with $p<0.05$

Figure 4. 5 Time domain measures of cattle incubating BSE over 3 month periods.

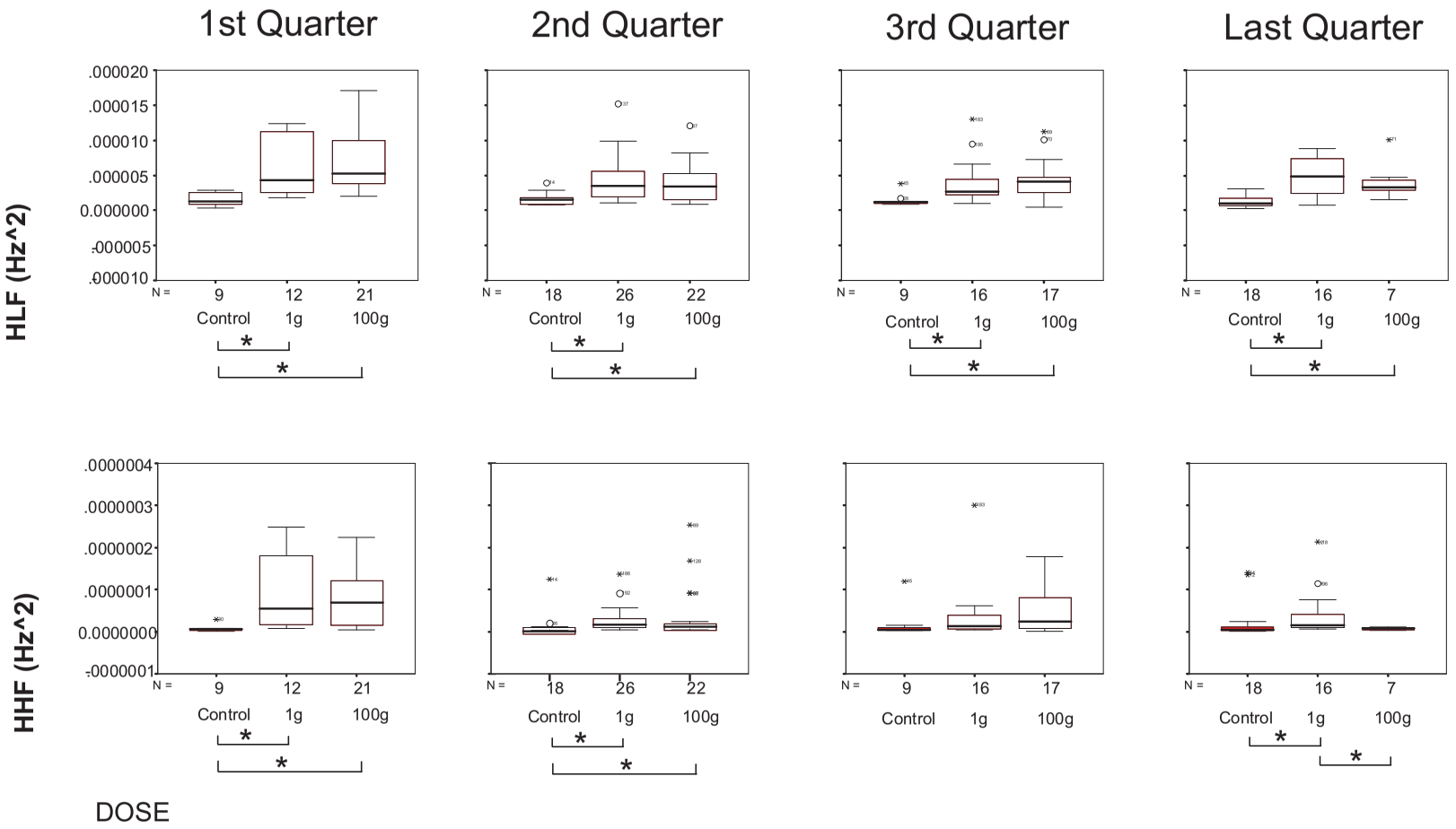

To show change in spectral measures of HRV in cattle incubating BSE. Significant differences, as assessed by Mann-Whitney test with Bonferroni correction following a Kruskal-Wallis test, are indicated by * with $p<0.05$

Figure 4. 6 Spectral measures of HRV during BSE incubation over a 3 month periods.

Figure 4.7 illustrates the changes in CVI and CSI metrics for the challenged groups over 4 epochs, each of 3 months, of the year of study. By comparing the changes in CVI and CSI in figure 4.7, it may be seen that the 1g and 100 g groups of animals show a different profile. The 1 g group showed a step wise change in CVI that was not seen in the 100g animals. Following the first three months, there was a stepped decrease in CVI in the 1g group. These changes remained significantly different from the values in the first quarter of the year for the subsequent quarters of the year (see figure 4.7).

When the 100 gram group are examined in a similar fashion, the “step” change deviation in CVI seen in the 1g group is not apparent (see figure 4.7). There is no significant change in the CSI values of the 100g animals during the 4 quarters of the year (CSI values for the 1 gram animals did show significant change during the year). The 100g animals only show a significant decrease in the CVI values between the 1st and last quarter.

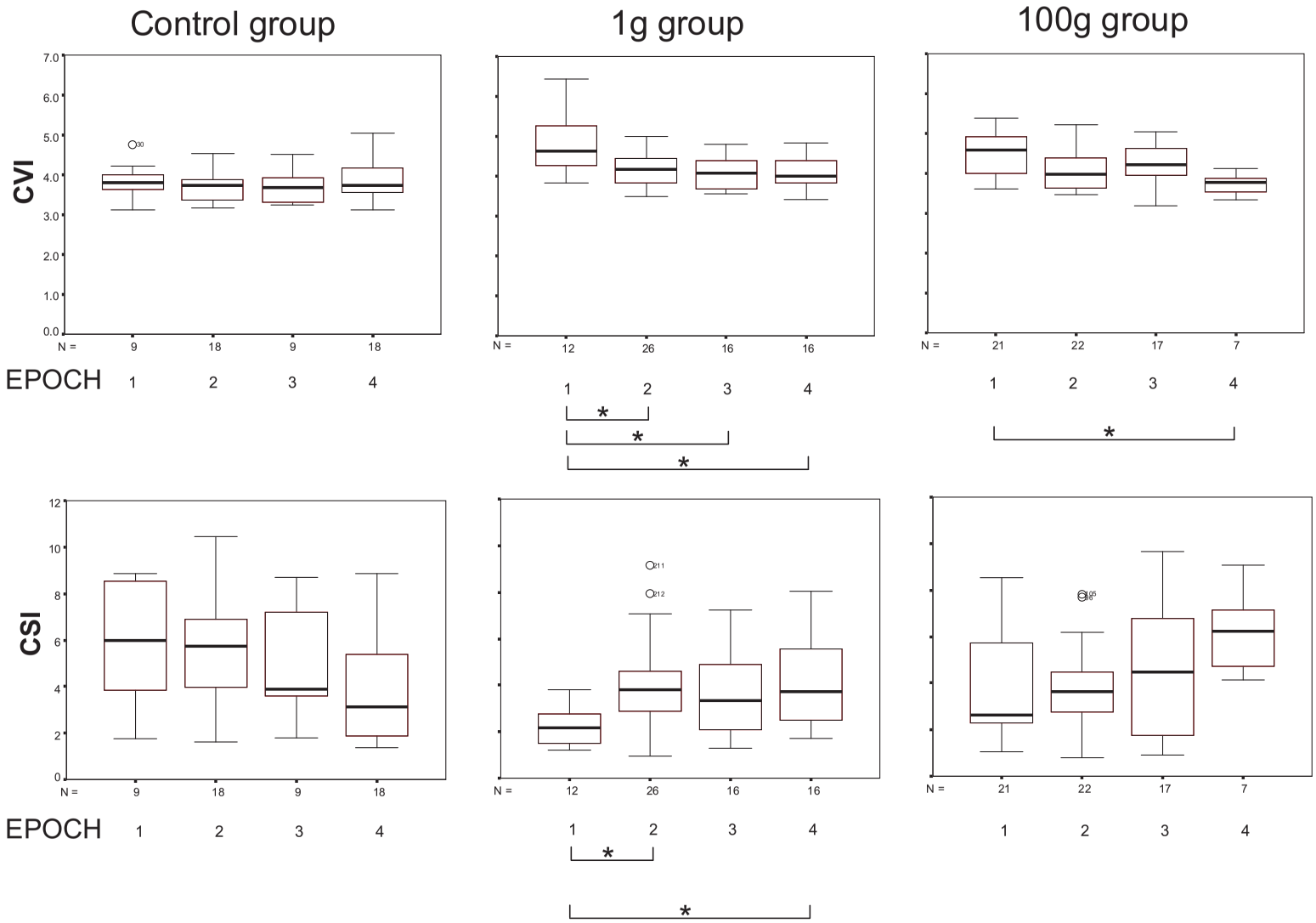

Time domain metrics for each group over the 4 epochs (3 months) of the study Significant differences, as assessed by Mann-Whitney test with Bonferroni correction following a Kruskal-Wallis test, are indicated by * with $p<0.05$. (No significant difference between the heart rates of the groups was found)

Figure 4. 7 Time domain changes in HRV over 12 months in BSE by oral dose.

Changes in HRV may also demonstrate a relationship to the peripheral identification of PrP^D in tissues. When the metrics of HRV are analysed based upon the results of tissue screening done by Masujin (Masujin, Matthews et al.2007) and separated into those animals from the 100g group that were positive in the spine for PrP^D and compared to those tested that were negative, a distinction may be seen.

Over the 12 month period it may be seen that the CSI of the 1 gram animals that were not identified as having PrP^D in the spine (group 1) was the only group that did have a significantly different CSI value compared to controls, although CVI was significantly higher than the control group (See fig 4.8).

It may also be observed that CVI values for all the challenged animals, apart from the small number in group 2, were significantly higher than controls despite some of the 100 g animals (group 3) and some of the 1g animals (group 1) being classed as BSE negative in the Masujin paper based on IHC examination of midbrain, rostral medulla and medulla-obex sections (Masujin, Matthews et al.2007).

If the trends in CVI and CSI are explored over a 12 month period between the spine positive and negative groups (see figure 4.9) it may be seen that a change in the CVI values are observed in the spine negative 100g group (group 3). This group demonstrated a “step” decrease in CVI from the first to second quarter of the year. This step drop remains significantly different to the first quarter in the third and last quarter. Interestingly this trend is not observed in the CVI values of the spine positive animals.

If the animals are grouped together based upon their spine result (i.e. amalgamating groups 1 and 3 to form a spine negative group and groups 2 and 4 to form a spine positive group) the step decrease in the negative animal’s CVI values are accompanied by a step increase in their CSI values for the 2nd and 4th quarters of the year (see figure 4.10). By contrast there is no significant change in the CVI or CSI of the spine positive group during the 12 months of study (Figure 4.10).

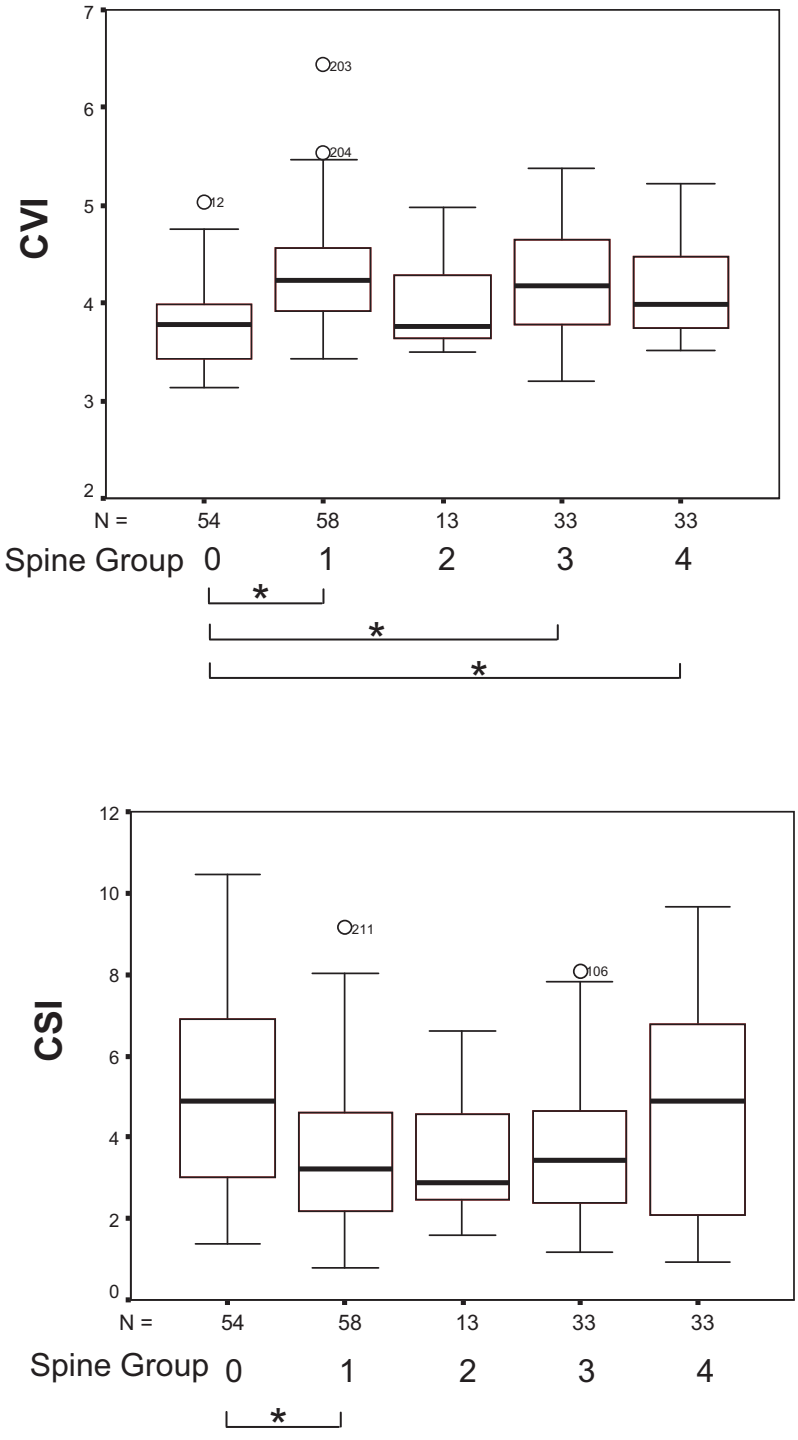

Spine Group		
0	= Controls	
1	= 1g, spine	– ve
2	= 1g, spine	+ ve
3	= 100g, spine	– ve
4	= 100g, spine	+ ve

Figure 4. 8 Change in time domain metrics for groups separated by spine result.
Significant differences, as assessed by Mann-Whitney test with Bonferroni correction following a Kruskal-Wallis test, are indicated by * with $p<0.05$

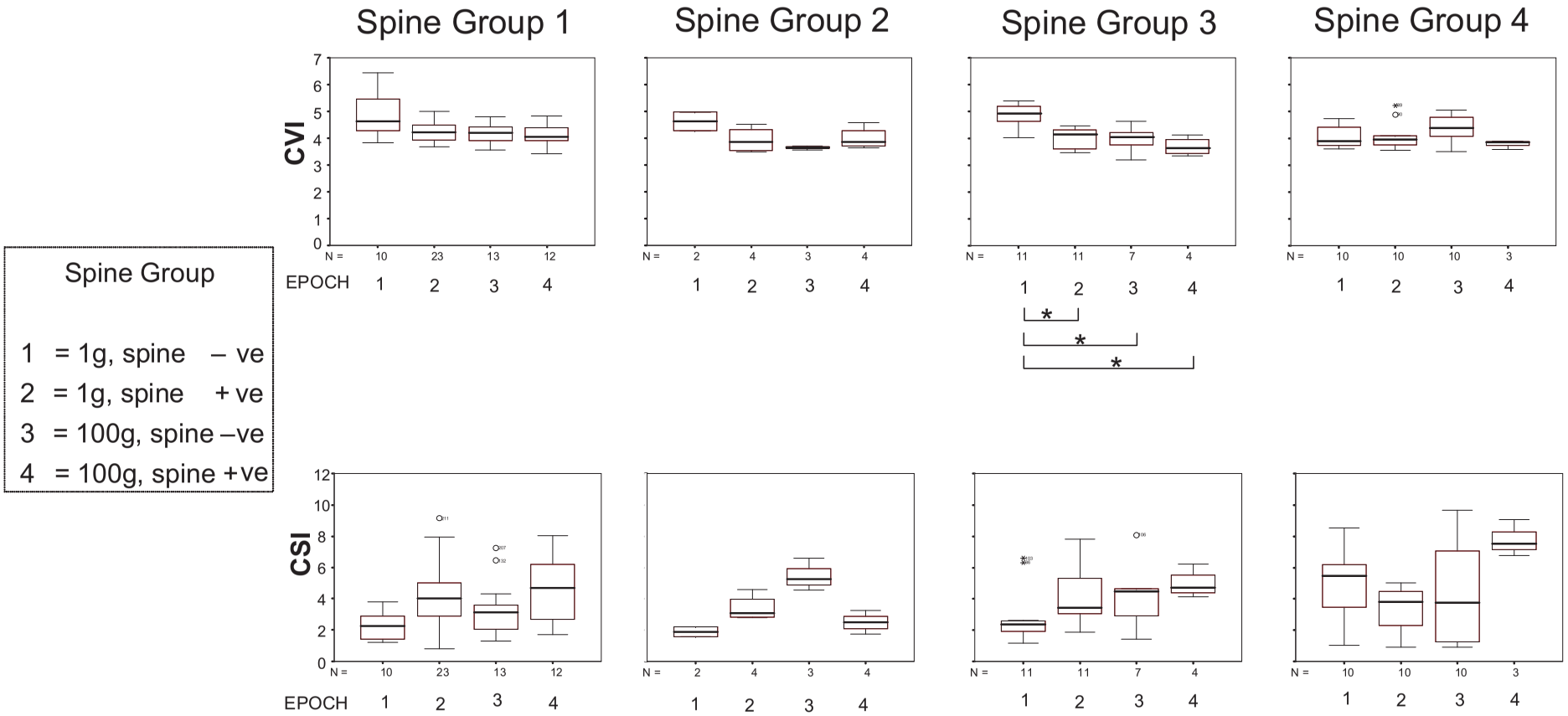

Figure 4. 9 Changes in Time domain metrics of HRV with respect to the identification of PrP^D in spinal regions.
Significant differences, as assessed by Mann-Whitney test with Bonferroni correction following a Kruskal-Wallis test, are indicated by * with $p<0.05$

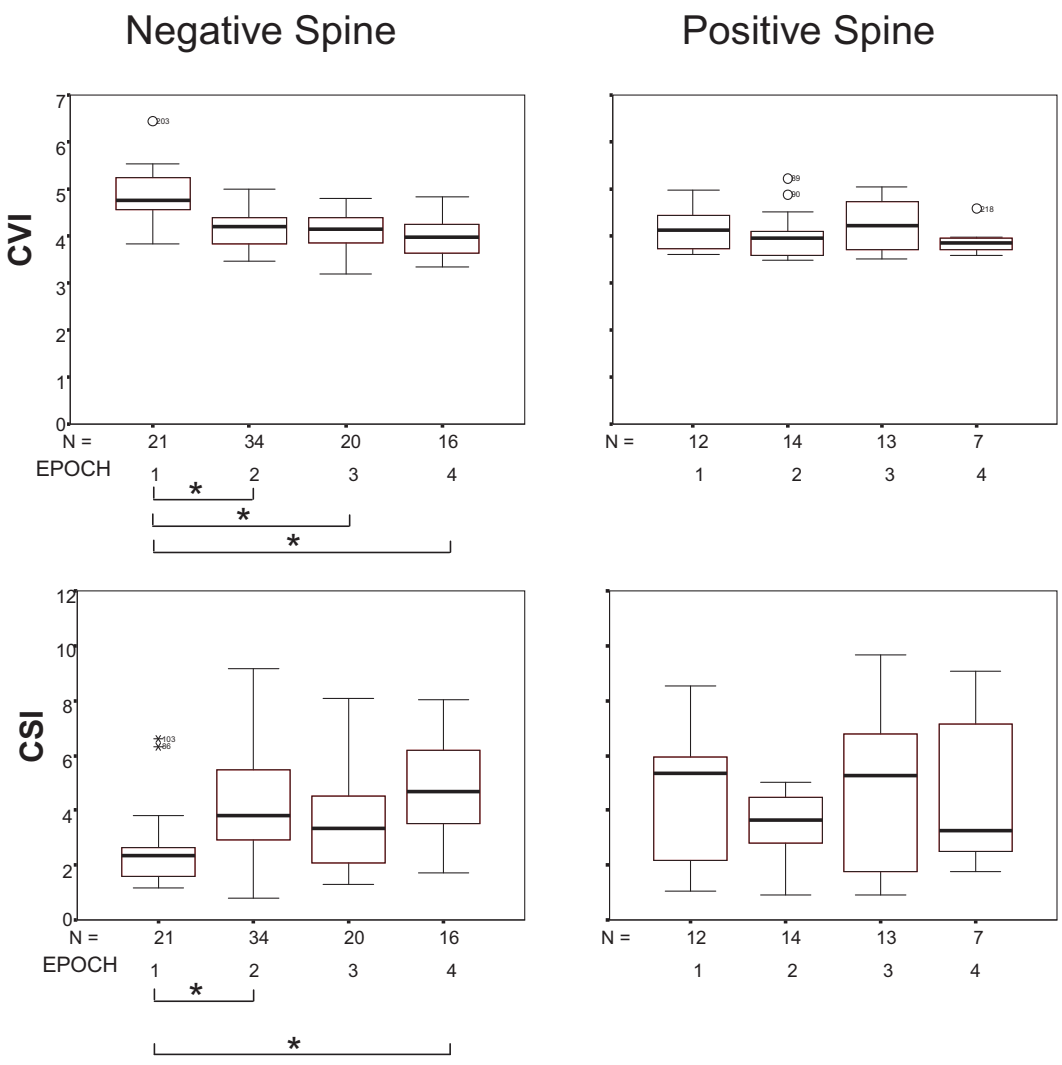

Indicating a step change in CVI and CSI seen in spine negative but not spine positive animals. (HRV is suggested to be able to distinguish disease pathogenesis) Significant differences, as assessed by Mann-Whitney test with Bonferroni correction following a Kruskal-Wallis test, are indicated by * with $p<0.05$

Figure 4. 10 Step change in time domain metrics of HRV.

When the same metrics of HRV are used to investigate the differences between the experimental animals used in this chapter and "field" animals that acquired BSE "naturally" from infection in the "field" (opposed to purposeful oral challenge of the experimental cattle) it was found that CVI and CSI were able to distinguish experimental and field cases from controls. CVI was also able to differentiate experimental cattle from field animals (see figure 4.11).

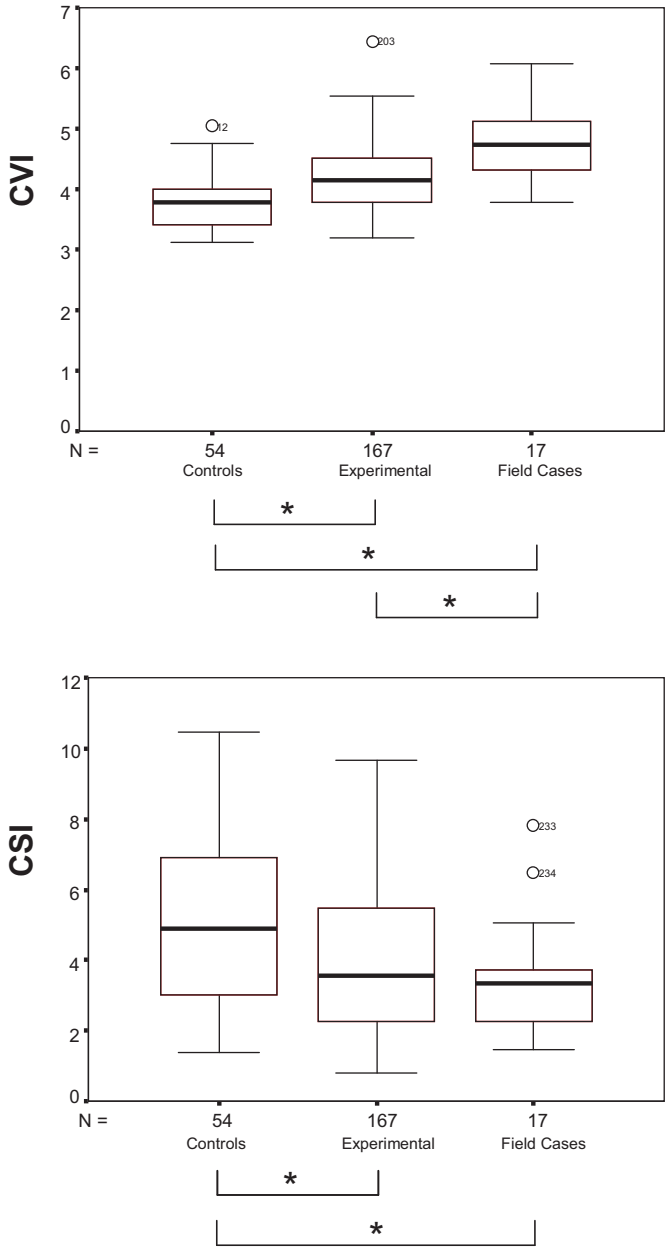

Indication that HRV metrics are able to distinguish field cases from controls and experimentally challenged animals. Significant differences, as assessed by Mann-Whitney test with Bonferroni correction following a Kruskal-Wallis test, are indicated by * with $p<0.05$

Figure 4. 11 HRV showing distinction between field animals and controls and experimentally challenged animals.

Limitations of this study

This study was an opportunistic study based upon the re-analysis of archived data previously collected as part of a Department of Environment, Food and Rural Affairs experiment. The cattle selected for re-analysis were dictated by those subjects that were included in the work of Masujin (Masujin, Matthews et al.2007) which presented histopathological data for these animals. As a consequence detailed measures of individuals animals blood pressure, respiration and temperature were not made. However all the animals were frequently and routinely monitored by trained observers for gross changes in the vital signs and assessed for common diseases of cattle, before, during and after data collection. These observers were those individuals who obtained the data from the cattle and reported changes in behaviour or physiological signs along with any extraneous environmental variables, e.g. noise or gross changes in temperature during recording HRV data. For all the animal's data include here, no reports of deviations from the norm were reported. For cows the average heart rate is between 60-80 beats per minute and respiratory frequency is 15-25 breaths per minute.

Work on the intra and intervariability of the heart rate of cows has been reported and little change was observed over many thousands of measures. Similar methods to obtain HRV data were used to collect data for this chapter as those employed by Janzekovic (Janzekovic, Vindis et al. 2011). To address these limitations of individual variability the control group of cattle endured the same posture, temperature and environmental constraints as the animals in the 100g and 1g groups. It was assumed that differences in measures of HRV between the dosed groups and controls was related to the oral challenge and prion infection in areas of the brainstem.

The use of the control group from which comparisons to the orally challenged groups were made, was an attempt to limit these confounding variations in individual parameters. In addition, in animals incubating TSE disease individual variability in HRV measures may be more or less than individual variability of healthy animals. It may be that a certain times in the incubation of the disease, specific measures of HRV show a similar trend in all the animals of a certain group (similar to the "spike" reported in the work of Pomfrett (Pomfrett, Glover et

al.2004)). At other times in the disease incubation, individual animals may show particular episodes of abnormal change. This is illustrated in figure 4.12. Analysis of HRV changes in cattle, orally challenged with 100 grams of infectious material on the same day, demonstrate two broad patterns. Figure 4.12 illustrates these two groups of cattle. Cattle may be split, by eye, into those cattle that exhibit a wide range of change in HRV metrics with repeated measures (Tag 202, 160,143) and a second group consists of cattle that do not demonstrate these large deviations in HRV (Tag 189, 173, 125, 118). These patterns in HRV perturbation may be due to different disease pathogenesis with prion protein causing differing functional change in neurological areas concerned with the regulation of the heart on a beat to beat basis.

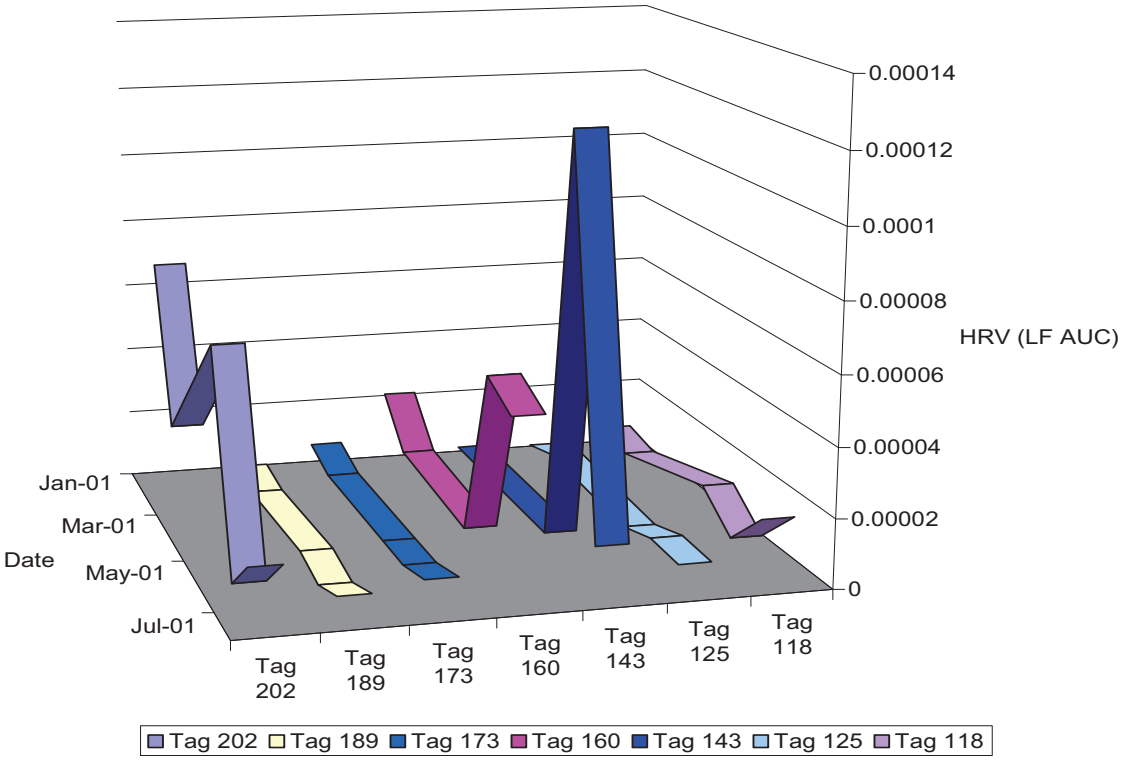

Figure 4. 12 Trends in HRV change over time in BSE infected cattle.
Illustration of 2 trends in HRV change over time. Tag denotes the unique animal identifier via ear tag numbering.

Figure 4.12 illustrates that changes in HRV are a property of individuals, shown here for animals in the 100 gram group but equal diversity in individuals in the 1 gram group and controls may be seen. It is unknown if prion infection is causing these differences in intra-variability shown here. Consequently investigations into the intra and inter variability of diseased animals in comparison to controls would present a suitable extension to this study.

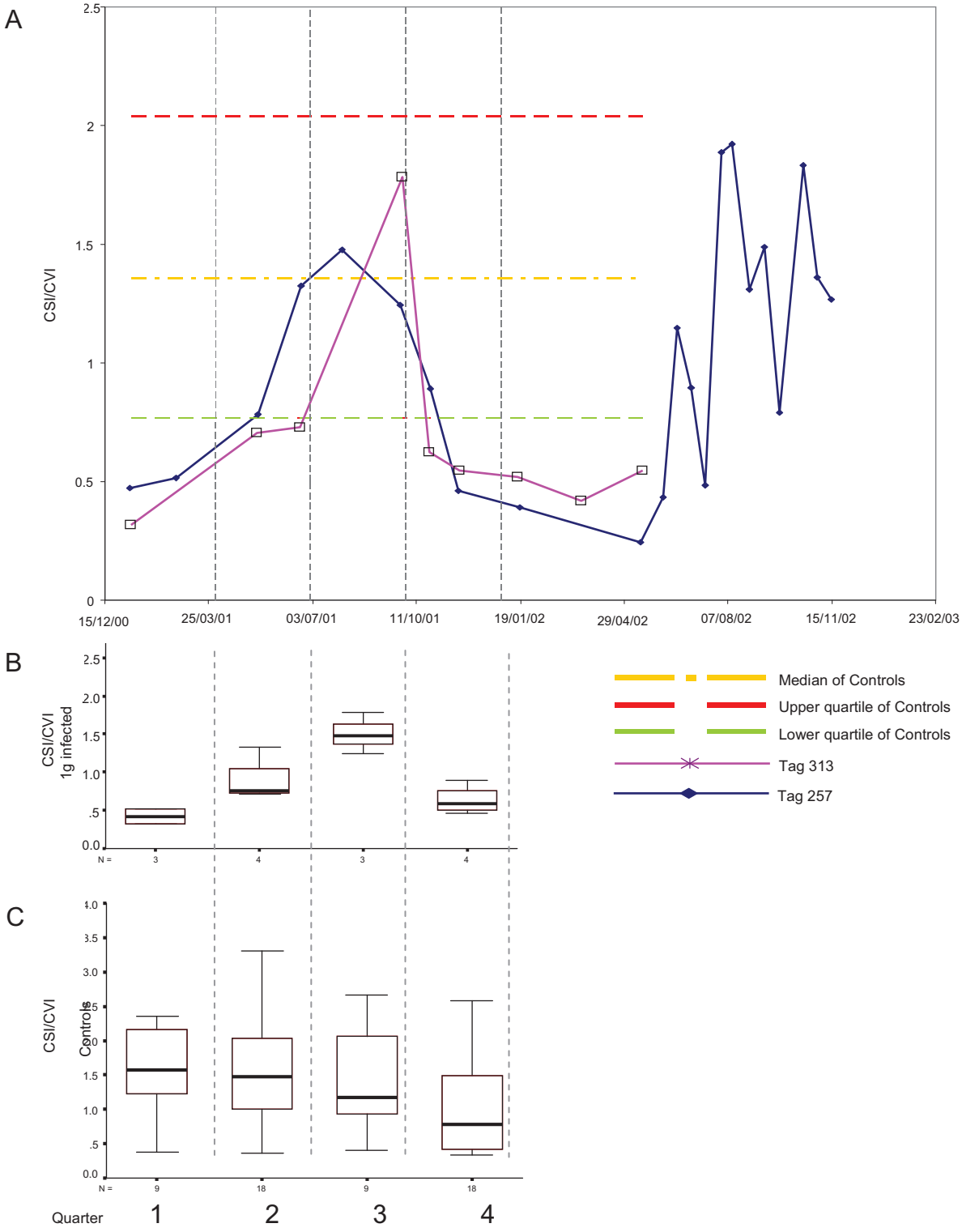

Figure 4. 13 Longitudinal changes in HRV in cattle incubating BSE.

Two infected animal's longitudinal values of HRV changes (CSI/CVI) with respect to time compared to control animals over the same four quarters of a year. No significant differences were seen in the values of CSI/CVI for the control animals (shown in lower panel) over the four quarters.

Significant differences in HRV measures over a 12 month period are shown in fig 4.7 for 1g dosed animals.

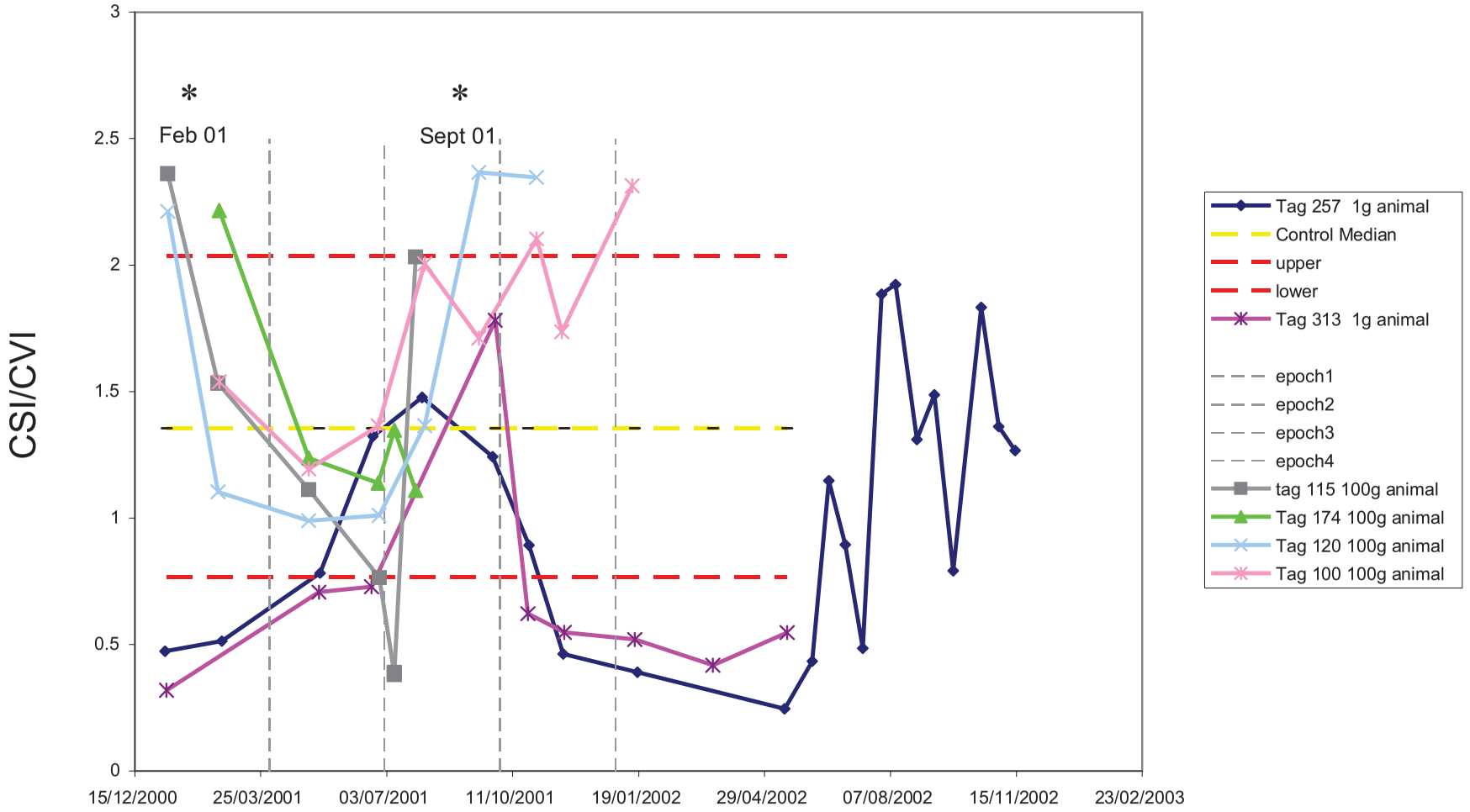

Figure 4. 14 Difference in HRV change for 1 gram and 100 gram dosed animals.
100g animals and 1g animals showing different stages of perturbation in HRV metric.
Significant differences in HRV measures over a 12 month period are shown in fig 4.7 for 1g and 100g dosed animals.

Further evidence to illustrate the prospect of transient changes in measures of HRV in animals incubating TSE disease are illustrated in figures 4.13 and 4.14. These figures show common patterns in the change in HRV measures for the 1 gram animals (fig 4.13) and different common patterns for the 100 gram animals (fig 4.14).

Caution in the interpretation of the results from this chapter is warranted since repeated measures are used in the analysis and not all animals were represented in all epochs due to the “random cull” that was part of the protocol.

While not all the animals in all the groups may echo these patterns of change of HRV, it is likely that the significant differences between groups of animals reported in the results of this chapter are representative of the different patterns of change illustrated in fig 4.14. While the prospect of not all the animals in one particular group demonstrating the same change in HRV at the same time (unlikely due to individual physiological differences) may be considered a limitation to this study, it also represents a novel finding in relation to the pathogenesis of BSE in cattle. It identifies the fact that patterns of HRV change in infected animals may be different depending on the amount of infectious agent they receive. It also illustrates that HRV may change with respect to time during preclinical disease incubation and does not follow a simple two stage process representing before and after infection. Rather the change in HRV illustrates sequences of normal HRV parameters mixed with periods of abnormal HRV measures.

In light of these limiting factors it has been suggested in this thesis that an ideal method to investigate changes in HRV in animals would be to use repeated longitudinal measures of specific metrics of HRV gathered from individual animals. The longitudinal measures should include a series of measures before purposeful infection with TSE disease. In this way an individual's "baseline" measure of HRV change could be gathered, to which future changes could be compared. This would help create a profile of changes in HRV with respect to time as a result of prion infection in individual animals. Limitation of cost and access to large numbers of bovine or ovine animals prevented this stage of the investigation.

Discussion

CVI and CSI are increasingly being used to investigate HRV changes and their effectiveness is reported (Allen, Chambers et al.2007). The other metrics used to assess HRV in the frequency domain are subject to problems concerning stationarity and the application of complicated mathematical algorithms. In the analysis of this data it was noted that the frequency domain measures displayed many more outliers than the equivalent time domain metrics. These outliers may have been the result of an error in mathematical computation due to a violation of the stationarity recommendations. In addition measures of the parasympathetic component of HRV rely on investigating RSA which must have an associated respiratory component. In a malfunctioning diseased system this coupling of breathing with arrhythmia may be the very relationship that breaks down during TSE disease pathogenesis. Consequently the paradigms used to measure RSA may be, in some stages of the disease, invalid in these particular circumstances.

For example the frequency range often used for humans to monitor RSA, and hence estimate parasympathetic effect, is 0.15-0.5 Hz. This would rely on a breathing frequency in the range of 9-30 breaths per minute to allow the derived components of FFT analysis to represent the arrhythmia due to respiration. This is based upon human adults and may not correlate with healthy cattle, sheep or any species incubating TSEs with compromised neurological function. The frequency band correlating with RSA in these cases may vary over such a wider range and some measures of RSA, such as HF band (0.15-0.5Hz) may not account for this changing respiration range for all individuals and populations. In addition, in a diseased state the average breathing rate, on which estimates of RSA are based, may vary significantly within the sampling period due to compromised neural control for this autonomic reflex. Measures of RSA may average out this deviation from the normal respiratory pattern and not give a true representation of the breath to breath variations of RSA.

Although these metrics may not be widely accepted, investigations using blockade studies suggest that CVI and CSI metrics may give a better representation of *changing* regulatory activity of the autonomic nervous system than spectral analysis (Toichi, Sugiura et al.1997). From this work it is also suggested that the

stability of these metrics may be due to a lack of affect from “physiological noise” (signal artefacts caused from other physiological processes that alter the results of the spectral assessment of HF and LF values from spectral methods of analysis). Slight changes, rather than the degree of activity, in the autonomic system are reported to be described by CVI and CSI and pictorially represented by Lorenz plots (Toichi, Sugiura et al.1997) like those in figure 4.2. Various ways to calculate RSA may be employed but many rely on a mean breathing frequency for their derivation. This coupled with the average magnitude of RSA over a sample period representing vagal tone may give rise to the metric of RSA not being able to detect changes in the breath to breath variations in HRV. Possible CVI and CSI metrics may be more sensitive to perturbations in activity in either branch of the ANS. By using a longitudinal observation of theses indices of autonomic function a change in an individual’s performance may be more easily seen. It has also been established that CVI differs from measures of RSA, from various methods, and this may be due to it not being marred by respiratory band constraints (Allen, Chambers et al.2007).

A recent publication examining peripheral nervous tissue in BSE infected cattle has identified PrP^{D} in the peripheral nervous system, which is reported to appear after or at the same time as PrP^{D} deposition in the central nervous system. Furthermore, the vagus nerves of similar animals was found to not only contain PrP^{D} but also was proven to be infectious (Masujin, Matthews et al.2007). This supports the idea of a vagal route of entry to the central nervous system for TSE infection, an idea first proposed in sheep with scrapie (van Keulen, Schreuder et al.2000) then suggested in cattle with BSE (Arnold, Ryan et al. 2007;Pomfrett, Glover et al.2004) and recently hypothesised to other TSE diseases where the utility of using HRV analysis to investigate infection was mooted (Pomfrett, Glover et al.2007).

A perturbation in certain frequency domain indices of HRV has been reported in cattle with BSE and a dose response relationship was suggested by comparison with control animals (Pomfrett, Glover et al.2004). The use of HRV analysis in the frequency domain was used to identify subclinical sheep incubating scrapie, the identification of the infected animals was provided by a positive rectal biopsy result (Glover, Pollard et al.2007). In the work investigating preclinical scrapie in sheep

spectral analysis in the 0.038-0.15 HZ band was found to distinguish those animals that were negative in rectal biopsy from those positive animals.

Analysis of data in the time domain in addition to the frequency domain is reported here. The time domain metrics were calculated using the inter beat interval (IBI) from the ECG R-wave intervals and processed using CMETX (Allen.2002). Certain metrics calculated with his program were interpreted with caution since the variables used to calculate them were designed and optimized for use on human subjects and not diseases animals. Consequently RSA estimates were not used since breathing frequency used in the calculation may not be appropriate for cattle or sheep incubating TSE diseases. The neuroanatomical functional link that is responsible for RSA, may be the site of malfunction of neurons caused by incubating TSE diseases.

CVI and CSI for the control animals did not alter significantly between the 4 epochs making up the 12 month period. The step changes in CVI and in CSI reported here for the 1 gram and 100 gram dosed animals are deviations towards control values (see figure 4.7). This questions the previous values of these metrics in the challenged groups, before we gained access and measurements were taken. What was the relationship between the infected animals and controls in the months before we were able to obtain data from these animals? Could it be that we may have been able to observe an earlier and greater deviation from normality apparent in the neurological malfunction in diseased animals incubating TSE diseases?

Further support for this idea of increased disturbance in neurophysiological function appearing before clinical signs is given by work investigating spiroplasma (small wall-less bacteria) and the association to spongiform encephalopathies in ruminants (Bastian, Sanders et al.2007). Sheep infected with spiroplasma did not show clinical signs during 16.5 months of observations following the inoculation but subsequent histological investigation revealed spongiform change in the brainstem of these animals. It was reported here that those observations correlated well with the histology from subclinical scrapie infected sheep at half way through their incubation period. It would therefore be likely that a disturbed neurological function in relation to these brainstem areas would have been evident due to the vacuolation in the neural tissue.

The utility of using HRV analysis to indicate disease pathogenesis is given by figure 4.11. Here CVI indicates significant differences, not only between control and experimental animals, but also between control and field cases in addition to a significant difference between experimental and field animals. The field animals were cases that were clearly symptomatic and had been sent for euthanasia; one animal that had to be immediately euthanized after measurements were taken due to the severity of the symptoms. Consequently, these field animals may have been at a more advanced stage of disease pathogenesis than the experimental animals that did not show clinical signs. The difference in the group data in figure 4.11 is likely to reflect this differing stage of disease pathogenesis.

If individual animal's longitudinal results are investigated within the experimental groups, an illustration of the disease pathogenesis per individual animal may be gleaned. Figure 4.13 shows a combined metric of CSI/CVI that demonstrates the change in CVI and CSI values over time for 2 animals. The combination of CSI and CVI may give a representation of the function and balance between the two arms of the autonomic nervous system, since it is postulated that CVI represents the change in activity in the parasympathetic nervous branch and that CSI represents changes in the sympathetic nervous system (Allen.2002;Allen, Chambers et al.2007;Toichi, Sugiura et al.1997). In this respect it may be similar to the standard spectral estimate of LF/HF ratio used to assess changing autonomic function in many investigation in relation to HRV (Balocchi, Cantini et al. 2006;Chen, Chen et al. 2006;Choi, Hong et al. 2006;Electrophysiology.1996;Hanss, Bein et al. 2006;Malliani, Lombardi, & Pagani 1994;Malliani, Pagani et al. 1991;Pagani, Lombardi et al. 1986;Sollers, III, Buchanan et al. 2007).

Figure 4.13 shows spine PrP^{D} positive animals (tag 257 and tag 313) that were orally challenged with 1g of infected brainstem homogenate. From these longitudinal measures a pattern in the change in CSI/CVI may be seen. These two animals were spine positive from the 1g challenged group, and demonstrate a deviation in this value when compared to controls (illustrated in figure 4.13 by the upper and lower quartile ranges in the top panel, A). The peak seen in epoch 3 of this figure is due to reduced values of CSI/CVI in the first, second and final

quarters of the year of investigation. This may be due to either a reduction in sympathetic activity, an increase in vagal activity or a combination of both as is suggested from figure 4.9, spine group 2. Figure 4.13 illustrates the see-saw nature in the activity of the ANS during TSE disease incubation and gives support for the idea of changing neural response during disease pathogenesis. For one of the animals, tag 257, recordings were taken over a longer time scale and this profile then shows a distinct change in the smooth mediated peak seen in the previous 12 months. Extreme deviations in the values of HRV are seen here and this again emphasises the fact that there are phases in neural performance of the ANS as the disease progresses. It is possible these phases may be useful in assessing an individual's signature change in HRV, suggestive of a particular stage in TSE pathogenesis.

By comparison with the 2 animals shown in figure 4.13, figure 4.14 also shows 3 animals from the spine positive but 100g animal group. It is as if the first data taken from these animals (marked by * February 2001) corresponded to the "peaks" of the traces for tags 313 and 257 (marked by *September 2001). The 100g animals demonstrate the decrease in CSI/CVI and then enter into a second phase where extremes are seen.

The time difference between the 1g and 100g animals, if this is the case, would suggest that the 100g animals were approximately 7 months ahead of the 1g group of animals in the disease incubation. HRV was previously reported to be able to indicate a dose response relationship in animals orally challenged with 1g or 100g of brainstem homogenate (Pomfrett, Glover et al.2004). In addition, these findings of a dose response difference in individual animal's ANS function, supports the findings of Arnold. In this work, PrP^{D} was invariably found in the brainstem, the earliest signs were reported to be at 30 and 44 months following oral challenge for the 100g and 1g dosed animals respectively, with a low probability of finding PrP^{D} in any tissues examined at more than 12 months before clinical onset. From their statistical model, it is suggested that the 100g group lead the 1g group by 7.9 months since PrP^{D} may be detected before clinical onset, by IHC in 50% of animals tested, at 9.6 months PI for the 100g animals and 1.7 months for the 1g animals (Arnold, Ryan et al.2007).

The empirical neurophysiological data presented here helps support the model proposed by Arnold. However, significant perturbation in HRV measures may also be observed over 12 months before clinical onset of the disease.

Another factor to consider is that animals from either the 1g or the 100g groups may contain individuals of mixed provenance and may be at differing stages of disease pathogenesis. This is indicated by some of the 100g group not having PrP^D identified in the spine and some that did. Similar diversity is seen in the 1g group. This suggests that analysing the animals based upon the dose of oral challenge received may weaken the findings that could relate to individual animals.

From this investigation of changing HRV metrics during TSE incubation, it was found that significant differences between groups of cattle were apparent over a 12 month period of investigation, corresponding to 29-41 months following purposeful oral challenge. In addition to this, differences were found within these groups with specific metrics of HRV demonstrating a see-saw change with respect to time during disease incubation. These changes in HRV measures were able to distinguish infected from control animals and also identify the 100g dosed animals from the 1g dosed animals. Finally these same metrics of HRV were able to predict those infected animals that were spine positive for PrP^D from those animals that were spine negative at the time of autopsy based upon analysis of HRV measures taken months before. This type of analysis may help to give insight into the disease pathogenesis of TSEs and provide an early screen for such diseases.

When individual animals were investigated by repeated longitudinal measures of HRV it was seen that there was variation in HRV within the groups: not all animals displaying the same deviation in HRV measures at the same point in time. This may be due to individual differences in each animal's physiology and an interaction between the strain and specific host. There may have been more than one strain in the inoculum and each animal may have subtle differences in how the infectious agent infects its body. It is also likely that the disease pathogenesis was different in individuals within the group, echoed by the histological findings of Arnold and Masujin (Arnold, Ryan et al.2007;Masujin, Matthews et al.2007).

The variation within individuals from the same group may also be explained if the intrinsic cardiac ganglia are considered with respect to HRV. It is suggested that at least 2 intracardiac ganglia interact to mediate the parasympathetic action controlling the heart in many mammalian species including humans, sheep and cows (Davies, Francis, & King 1952;Gray, Johnson et al. 2004;Johnson, Gray et al. 2004). Interactions of the parasympathetic and sympathetic nervous systems are also thought to occur in these intrinsic cardiac ganglia (Randall, Brown et al.1998a;Smith.1999;Zhong, Bai et al. 2007). The intrinsic cardiac ganglia are not simple relay stations for the descending efferent vagal communication but may act in an integrative and synergistic capacity to facilitate the control of the heart on a beat to beat basis and lead to modulation of the HF and LF frequency bands in HRV analysis (Zhong, Bai et al.2007). These intrinsic ganglia are reported to vary with age and species (Pauza, Pauziene et al. 2002) and may vary significantly between individuals of a species (Pauza personal communication September 2007). Consequently the degree of HRV deviation from control values may be different, with respect to time, for individuals within a group based on their individual neurophysiology.

Collinge speculates that different cellular populations of PrP^{D} within a host may offer different environments in which infectivity may be expressed. It is suggested in this work that the time delay reported between lymphoid accumulation of PrP^{D} and development of neural disease may be due to the appearance and interaction of a neuroinvasive strain of the infectious agent (Collinge & Clarke.2007). It may also be postulated therefore, that this compartmentalization may also be extrapolated to different parts of the nervous system and indeed different aggregations of cell bodies within the nervous system. This may give support for the observed stepped and changing responses of neurophysiological function observed in this investigation, obtained by monitoring the changing function in specific brainstem regions that correspond to those areas responsible for the control of HRV.

However, Collinge uses PrP^{D} to illustrate this compartmentalization of prion disease pathogenesis and not his postulated toxic counterpart, PrP^{L} (PrP^{L} either being an intermediate or a side product of the conversion of PrP^{c} to PrP^{D}). PrP^{L} was suggested to account for the decoupling of the level of PrP^{D} and the extent of disease pathology (Collinge & Clarke.2007). This underlines the fact that PrP^{D}

may only be a surrogate marker for the disease and not the infectious agent. It may be that PrP^{L} is the entity that makes the "foot prints in the snow", the foot prints being the PrP^{D} molecules, that many investigators have been studying and basing their opinions of infection on. Hence the identification of PrP^{D} molecules may reflect where the infectious agent has been and may not be the best marker for infectivity.

PrP^{L} may build to toxic levels before a specific type of PrP^{D} is identified. PrP^{L} may cause neurological malfunction before PrP^{D} is detected and may thus explain why an observed malfunction in parts of the ANS responsible for controlling the heart on a beat to beat basis, may be seen before PrP^{D} is detected. This idea may also account for the animals classed as BSE negative, despite being orally challenged with infectious material. From HRV analyses, some of these cattle were identified as significantly different from control animals (groups 3 in the analysed groups here, see figure 4.9, first quarter).

Arnold reports that PrP^{D} is unlikely to be detected in sub-clinical cattle at more than 12 months before clinical signs were evident. (Arnold, Ryan et al.2007). From figure 4.11, HRV analysis was able to distinguish subclinical animals from clinical field cases as well as being able to discriminate both these groups from control cattle. Consequently this technique may be tracking the change in neural dysfunction caused by PrP^{L}, the progression of which is distinct from PrP^{D}. The effect of PrP^{L} in the branches of the autonomic nervous system may not be a single irreversible perturbation in function. Rather, there may be a changing and integrated effect on neurological function in both branches of the ANS, as the disease progresses causing a see-saw change in the balance of the two branches of the ANS.

Of particular importance in the changing neural function during TSE pathogenesis may be the pathology of dendritic spines. These appear as a variety of shapes including small (0.001-1 μm^3) mushroom or doorknob shaped protrusions and form the postsynaptic part of many excitatory neurons. Abnormalities in spine shapes and distributions are commonly detected in many brain dysfunctions (Nimchinsky, Sabatini, & Svoboda 2002) and have been described in scrapie models (Jeffrey, Halliday et al.2000) and in humans with CJD (Landis, Williams, & Masters 1981). It is also thought that the initial damage to the dendrites, caused by TSE

incubation, is at the synaptic spine and is preceded by dendritic varicosities at these sites (Fuhrmann, Mitteregger et al. 2007). Such damage may well be a mechanism affecting processing of information in the vagal complex of the medulla and hence HRV measures. Loss of synapses and spines may lead to eventual neuronal apoptosis due to extensive reduced excitatory input to pyramidal neurons throughout the dendritic trees (Jeffrey, Halliday et al.2000).

Other important observations of changing neural function during TSE incubation include studies on long term potentiation (LTP) of synaptic transmission. LTP may be described as the persistent change in a postsynaptic potential following a high frequency stimulation of a synapse, a change that may last from 30 minutes to days or weeks and may include modification to postsynaptic receptors and dendritic spines (Malenka & Bear 2004). Neurons that demonstrate LTP thus have an enhanced response to stimuli compared to those neurons not demonstrating LTP.

This enhancement is achieved by improving the cell's postsynaptic sensitivity to signals arriving from the presynaptic cell membrane. The postsynaptic sensitivity is achieved by increasing the activity of existing receptors and by increasing the number of receptors on the postsynaptic cell surface (Malenka & Bear.2004).

It has been reported that certain neurons lose their ability to maintain LTP during TSE pathogenesis (a postsynaptic effect). This was observed at 40% of the total incubation period (100 days PI) of a TSE disease when presynaptic functions showed no change, assessed by observations in response to paired pulse facilitation and post tetanic potentiation both of which are associated with presynaptic calcium concentrations (Johnston, Fraser et al. 1998) These authors provided evidence that the attenuation of LTP is likely to be a result of either a loss of presynaptic efferents or to be a postsynaptic functional decrement related to loss of dendritic spines. Furthermore, they reported that a change in LTP is observed before any detectable significant spine loss, again emphasising the earliest signs of TSE infection would be echoed in a change in neurophysiological function.

Much of the work researching LTP was focused on brain slices of the hippocampus. However it has been suggested that LTP is a general function of synapses and it has been observed in both autonomic ganglia (Brown & McAfee

1982) and in the nucleus tractus solitarii of mammals (Brooks & Glaum 1995). Both of these regions are involved in the control of heart rate variability.

It has also been established that LTP may be induced from the postsynaptic synapse by tetanic stimulation of a single pathway to that synapse. Alternatively, when weak stimulation (insufficient to generate a postsynaptic depolarization on its own) is applied to many pathways to a synapse, each weak stimulation may act cooperatively to induce LTP. In this latter case weak stimuli may converge on an area of postsynaptic membrane and the collective weak stimulations may depolarize the postsynaptic membrane enough to induce LTP (Golding, Staff, & Spruston 2002;Lee 1983). This highlights the fact of not only spatial summation of inputs, that is potentials from different multiple presynaptic cells adding to evoke an action potential, but also the arrival of these weak stimulations with respect to time, temporal summation, may influence LTP . Consequently, synaptic malfunction resultant from TSE infection could well result in a reduction of LTP due to errors in both spatial and temporal summation of inputs.

This line of reasoning taken together with the interconnection of the brainstem nuclei with the extrinsic and intrinsic cardiac ganglia give sites where a change in HRV may be elicited during TSE disease incubation due to synaptic functional change. With reference to figure 1.6 and Chapter 1, Intrinsic and Extrinsic Cardiac Ganglia, and the work of Brooks on the NTS in rats (Brooks & Glaum.1995) it could be the case that an inhibitory interneuron in the NTS, or an intrinsic cardiac ganglia for that matter, may be stimulated by the coordinated timing of different inputs to drive the interneuron. In the diseased state, the timing of these inputs may be disrupted and the inhibitory interneuron would not be driven and hence the inhibition may be lost, leading to an increase in activity in the ANS controlling the heart on a beat to beat basis and thus lead to a perturbation in HRV.

A further example of how this change in synaptic function can alter the neurophysiological timing of neuronal signals is given by the work of Collinge from his work with PrP null mice (mice lacking prion protein). It was reported that a pair of intracellular action potentials were recorded as the result of a train of stimuli on slices of brain tissue (Collinge, Whittington et al.1994). Similarly, Barrow recorded

these action potential doublets following a series of stimulations in brain slices from scrapie infected hamsters.

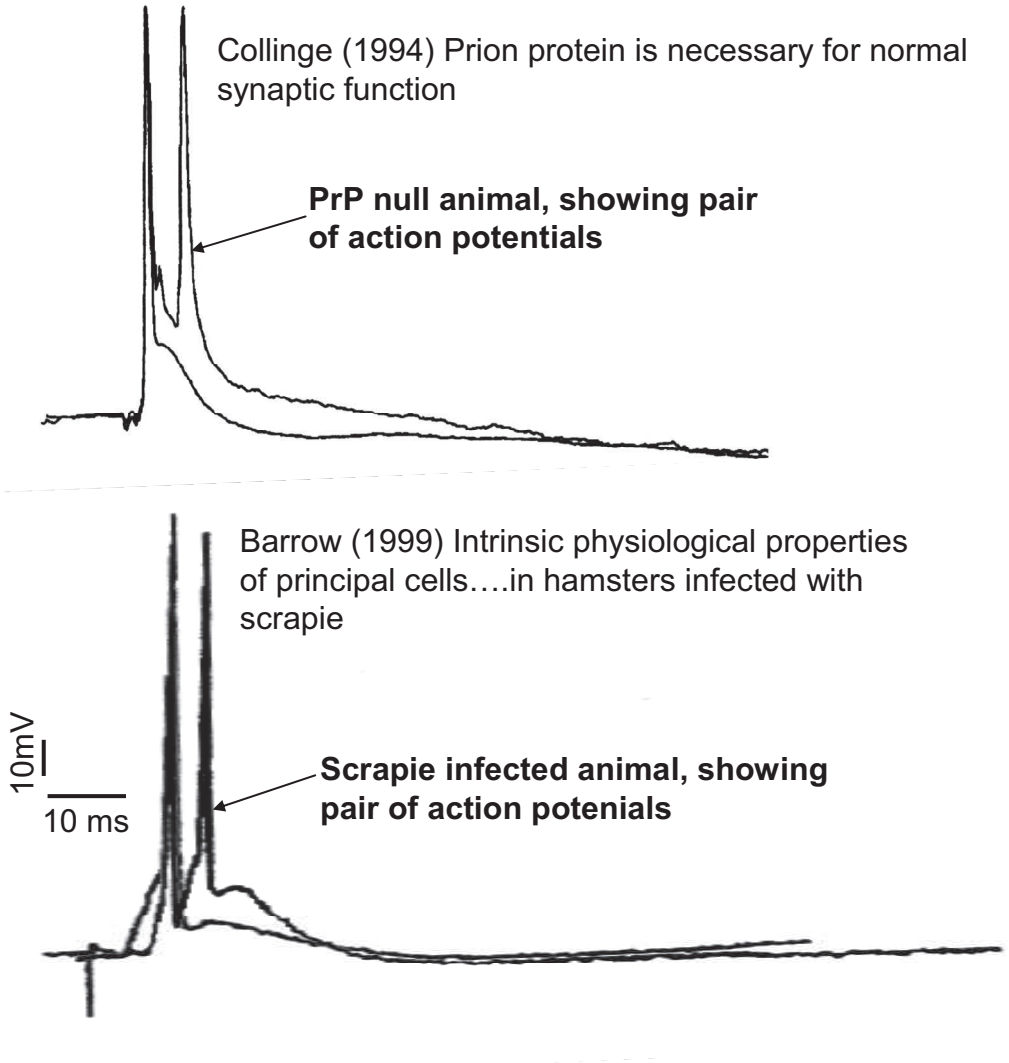

Figure 4. 15 Action potential doublets.

Based on the work of Collinge 1994 and Barrow 1999. To show action potential doublets in scrapie infected hamsters and mice lacking PrP.
Reprinted by permission from Macmillan Publishers Ltd: Collinge, J., Whittington, M. A., Sidle, K. C., Smith, C. J., Palmer, M. S., Clarke, A. R., & Jefferys, J. G. 1994, "Prion protein is necessary for normal synaptic function", Nature, vol. 370, no. 6487, pp. 295-297.
Reprinted and adapted from Barrow, P. A., Holmgren, C. D., Tapper, A. J., & Jefferys, J. G. 1999, "Intrinsic physiological and morphological properties of principal cells of the hippocampus and neocortex in hamsters infected with scrapie", Neurobiol.Dis., vol. 6, no. 5, pp. 406-423.with permission from Elsevier.

These findings considered together, suggest that the presence of PrP^D is functionally equivalent to having no PrP^c. The action potential doublets may then have an effect on the temporal and spatial summation at integrating axon hillocks. Consequently, abnormal synaptic function would result in the diseased state and this may lead to a change in the coordinated output of the ANS to the heart that may be observed as a disruption in normal HRV parameters.

The reduced amplitudes of medium and late afterhyperpolarizations observed in scrapie-infected hamster were suggested to be involved in the production of these double action potentials. It is also reported that these changes in afterhyperpolarization appeared before the onset of overt neurological symptoms and histopathological change (Barrow, Holmgren et al.1999).

These lines of evidence coupled with the work of Kretzschmar, Carleton and Encalada (Carleton, Tremblay et al.2001;Encalada, Moya et al. 2008;Kretzschmar, Tings et al.2000) who presents evidence for a functional role for PrPc in modulating synaptic transmission suggests that abnormal PrP will disrupt the normal synaptic flow of neural information used to regulate target organs, such as the heart, before clinical signs of the disease.

In studies of scrapie in mice, it was observed that dendritic dysfunction and synaptic loss preceded neuronal cell death (Jamieson, Jeffrey et al. 2001;Jeffrey, Halliday et al.2000). Significant decrease in the number of synapses in brain regions in these experiments were observed before clinical signs were expressed (34% of incubation period) and even before a decrease in spine numbers (50% incubation period).

It has also been reported that electrophysiological changes may occur in neurons in some animal models of the disease before PrP aggregates are seen and neuronal pathological change may be independent of neuronal PrP expression (Jeffrey, Goodsir et al. 1997;Jeffrey, Goodsir et al.2004). It is also stated that synaptic change and dysfunction is an early step in pathogenesis of prion diseases and may be correlated to behavioural changes that constitute clinical signs of TSE diseases (Cunningham, Deacon et al. 2003).

Consequently there is evidence to indicate that a change in neurological function may be observed before clinical signs of the disease or before PrP^{D} aggregates are detectable. This gives support to the observed aberrant function of the brainstem nuclei and other neural tissue involved in the control of the heart on a beat to beat basis.

The results presented here would also suggest that the agent responsible for BSE in these cattle, that may or may not be PrP^{D}, causes a disturbance in brainstem function in the regulation of the heart in infected animals before clinical signs and

importantly in animals that have not been confirmed as BSE positive by IHC although purposely orally fed with either 100g or 1g of infectious material.

The work by Masujin was undertaken to increase the understanding of BSE disease pathogenesis in cattle. The authors stated that, contrary to previous belief, there is a build-up of PrP^D in the peripheral nervous system and adrenals that coincides with, or follows, the appearance of PrP^D in the CNS and the build-up of PrP^D in the PNS is “the rule rather than the exception” in the clinical stages of the disease.

In scrapie, neuronal malfunction and cell death have been described to occur before prion protein accumulation (Jamieson, Jeffrey et al.2001), synapse loss associated with abnormal PrP is reported to precede neuronal degeneration (Jeffrey, Halliday et al.2000) and neuronal lesions have been observed in neurones that are independent of PrP expression (Jeffrey, Goodsir et al.2004). The utility of using HRV analysis to identify preclinical scrapie infected animals (Glover, Pollard et al.2007) and BSE in cattle (Pomfrett, Glover et al.2004) has been indicated.

A difference between sheep and cattle incubating TSE disease (figure 4.4) may be due to a different signature in HRV as a result of different disease pathogenesis of scrapie and BSE or that these groups of animals were at a different stage in the HRV perturbation caused by incubating TSEs. In addition, CVI and CSI for sheep were not significantly different on the one occasion that measurements were taken (figure 4.3). Studies on the pathogenesis of scrapie and BSE in sheep have revealed very similar patterns of disease progression with respect to time and neural tissues that are infected. (van Keulen, Vromans et al. 2007;van Keulen, Bossers et al.2008;van Keulen, Schreuder et al.2000). The main difference in the pathogenesis of scrapie in sheep and BSE in cattle being the reduced involvement of the lymphoreticular tissues in cattle (BSE is limited to the GALT, gut associated lymphoid tissue) although neural routes of infection via the parasympathetic efferent fibres are reported to be similar (van Keulen, Bossers et al.2008). There still remains the possibility that the difference between sheep and cows incubating TSEs identified here is due to the stage of incubation individual animals were at when tested. Hence there is a likelihood that a change in neural function in central

nervous system areas, such as the brainstem, may appear before PrP^D deposits are detected.

The disassociation between the presence of PrP^D and infection may be due to some of the caveats to the testing methods used for PrP^D described in this and previous chapters. The current tests being developed are more sensitive in the detection of PrP^D in many tissues and indeed the work of Masujin has found numerous new sites of the peripheral nervous system to contain PrP^D. It may be anticipated with future tests that PrP^D is detected in many more areas of the infected animals and thus help confirm the BSE status as positive and help identify the route of entry for the infectious agent.

There is evidence that this technique of monitoring HRV from incubating animals may be able to not only identify infected from control animals but also to indicate a high dose group from a low dose group as frequency domain analysis suggested in previous studies (Pomfrett, Glover et al.2004). It is suggested that the 1g animals are at an earlier stage of disease incubation than the 100g animals based upon a model of the disease pathogenesis (Arnold, Ryan et al.2007). Therefore the difference in HRV measures, with respect to time, for these groups observed here may give information in relation to a particular stage of disease pathogenesis following oral inoculation of infectious agent. It is stated that the initial tissue to be detected as positive for PrP^D was the medulla-obex section (Arnold, Ryan et al.2007), which is the area where the nuclei that control the heart on a beat to beat basis are located. Consequently malfunction in these areas caused by either neuronal loss or synaptic change will manifest as a perturbation in HRV. Repeated measures of HRV may prove a useful diagnostic tool for the screening for TSE diseases and help understand the pathogenesis of the infectious agent.

HRV may be considered to be the result of a series of nested feedback loops coordinated efferent activity involving both sympathetic and parasympathetic branches of the ANS (see figure 1.6). The involvement of the NTS, NA and DMNX in relation to baroreflex sensitivity have been discussed in Chapter 1 (pages 62-66). These areas are also involved in the short term and long term regulation of blood pressure. While inference of changes on heart rate are implied by changes of HRV measures it is also possible that prion infection in the diagnostic areas of the brainstem may change sympathetic activity in addition to vagal activity with

consequential changes in blood pressure and baroreflex sensitivity. These changes in baroreflex mediation of blood pressure are also associated with RSA (Berger, Saul, & Cohen 1989;Saul, Berger et al. 1989b;Taylor, Myers et al.2001;Taylor & Eckberg 1996) . This illustrates the intimate relationship between parasympathetic and sympathetic branches of the ANS and suggests that prion infection in areas of the brain responsible for their coordination may result in abnormal control of these functions.

Chapter 5 Development of Methods used to Investigate heart rate variability linked to respiration

Introduction

Heart rate variability (HRV) is described as a beat to beat change in consecutive cardiac cycles often measured by the change in RR interval. Measures of HRV may be used to assess the neural activity between the brain, heart and lungs. It has been shown that respiratory sinus arrhythmia (RSA) is correlated with changing activity in specific areas of the brainstem (Pomfrett & Alkire 1999). These depressions in brainstem activity, indicated by the highlighted areas in figure 5.2 below, implicate the right nucleus tractus solitarii (NTS) of the medulla oblongata. The NTS is the primary site for the integration of the cardiorespiratory reflex and its output transmitted, via other brainstem nuclei and the vagus nerve, to ganglia at and near the heart. Hence, perturbation in the activity in this area would manifest as a change in the association of heart rate and breathing on a beat to beat basis and therefore would change measures of RSA.

Breathing is an autonomic rhythmic and centrally regulated mechanical process and its main purpose is to supply oxygen to all the cells of the body and so is intimately linked to the cardiovascular system.

In humans the medullary respiratory centre consists of at least two neural groups. One, whose activity relates to inspiration and another that relates to expiration. A central rhythmic generator is situated in the medulla maintaining alternate activity of these inspiratory and expiratory neurons. This rhythmic activity is present in cats after destruction of afferent pathways caused by brainstem sectioning (Comroe 1954;Tang 1953) see figure 5.1.

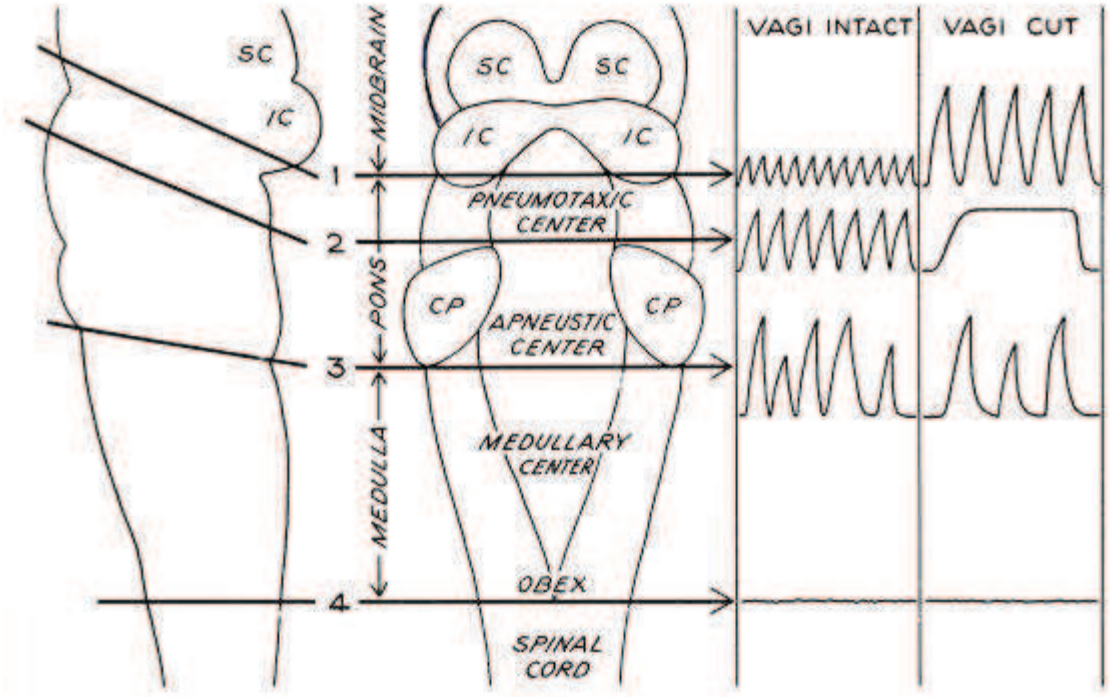

Figure 5. 1 Interaction of vagus nerve and different areas of the brainstem.
To show the interaction of the vagus and different brainstem areas on breathing patterns. Sections below the medulla result in no respiratory effort. Severe apneustic respiration is seen following brainstem section at level 2 and lesion of the vagus. (SC = superior colliculus, IC= inferior colliculus, CP=cerebellar peduncles) Reproduced by permission from Comroe, J. H., Jr. 1954, "Respiration", Annu.Rev Physiol, vol. 16, pp. 135-154.

Other neural sites for the maintenance for this generation of respiratory rhythm are suggested to be the pons (pneumotaxic centre) and some neurons anterior to the medulla (apneustic centre) which cause prolonged inspiration as a result of absent rhythmic drive from the pneumotaxic centre and reflex vagal inhibition from stretch receptors in the lung. Individual cell recordings have suggested that the rhythm generator is located in a group of neurons in the NTS. This central rhythm generator also activates neurons in the rostral nucleus retroambigualis (NRA) (Randall 1978). In turn the NRA projects directly to the NA and acts as a pool of premotor interneurons each producing motor actions in response to changes in eupneic breathing (normal “resting” breathing). Different combinations of these premotor neurons resulting in the final effect (Subramanian & Holstege 2009).

The effects of vagal stimulation on respiratory neurons of the NTS have also been studied and it was found that vagal stimulation inhibited inspiratory neurons of the NTS (Subramanian, Chow, & Balnave 2007). These lines of evidence point to a link of vagal activity and coordinated neural output from the NTS to achieve respiration. The importance of the vagus and areas of the brainstem in coordinating respiration have been further emphasised in studies of vagotomy and lesions in different areas of the brainstem (Figure 5.1).

Vagal reflexes in the modulation of breathing are evoked from the activation of several different types of receptors, including stretch receptors located in the lung and chemoreceptors located in the aortic wall. Vagal fibres from the lung, entering into the NTS as cranial vagal fibres, serve to augment the excitability of the respiratory centre in conjunction with the main effect from afferent cardiac fibres (Liljestrand 1958). The effects of the vagus in relation to respiration have been shown to have a moderating effect in the pattern of respiration and limit apneustic breathing (as indicated in figure 5.1) thus helping to regulate the respiratory pattern (Tang.1953).

Evidence from the Hering-Breuer reflex summarizes the relationship of vagal coordination of respiration. Activation of pulmonary stretch afferents inhibit the central inspiratory drive and activate expiration, facilitated by the vagus nerve. Inhibitory information from the lung afferents is also relayed to cardiac vagal motor neurons in the NA and DMNX. Motor fibres from these centres relay neural information to the heart, controlling its activation on a beat to beat basis. Increasing pulmonary stretch receptor activity results in inhibition of cardiac vagal motor neurons (release of the vagal brake on heart rate) thus increasing heart rate as respiration changes phase. This is the fundamental process involved in RSA.

The medulla oblongata is a diagnostic area for many prion diseases (Ironside.2000;Wells, Hancock et al.1989), demonstrating accumulation of disease associated prion protein. The presence of prion in brain tissue has been associated with a change in neurological function (Chiesa, Piccardo et al. 2008;Collinge, Whittington et al.1994;Jeffrey, Halliday et al.2000;Kretzschmar, Tings et al.2000). The change in neurological function in individual neurons, or pools of neurons, associated with the control of the heart on a beat to beat basis

would alter HRV and also disrupt the normal coordination between breathing and the control of the heart beat on a beat by beat basis.

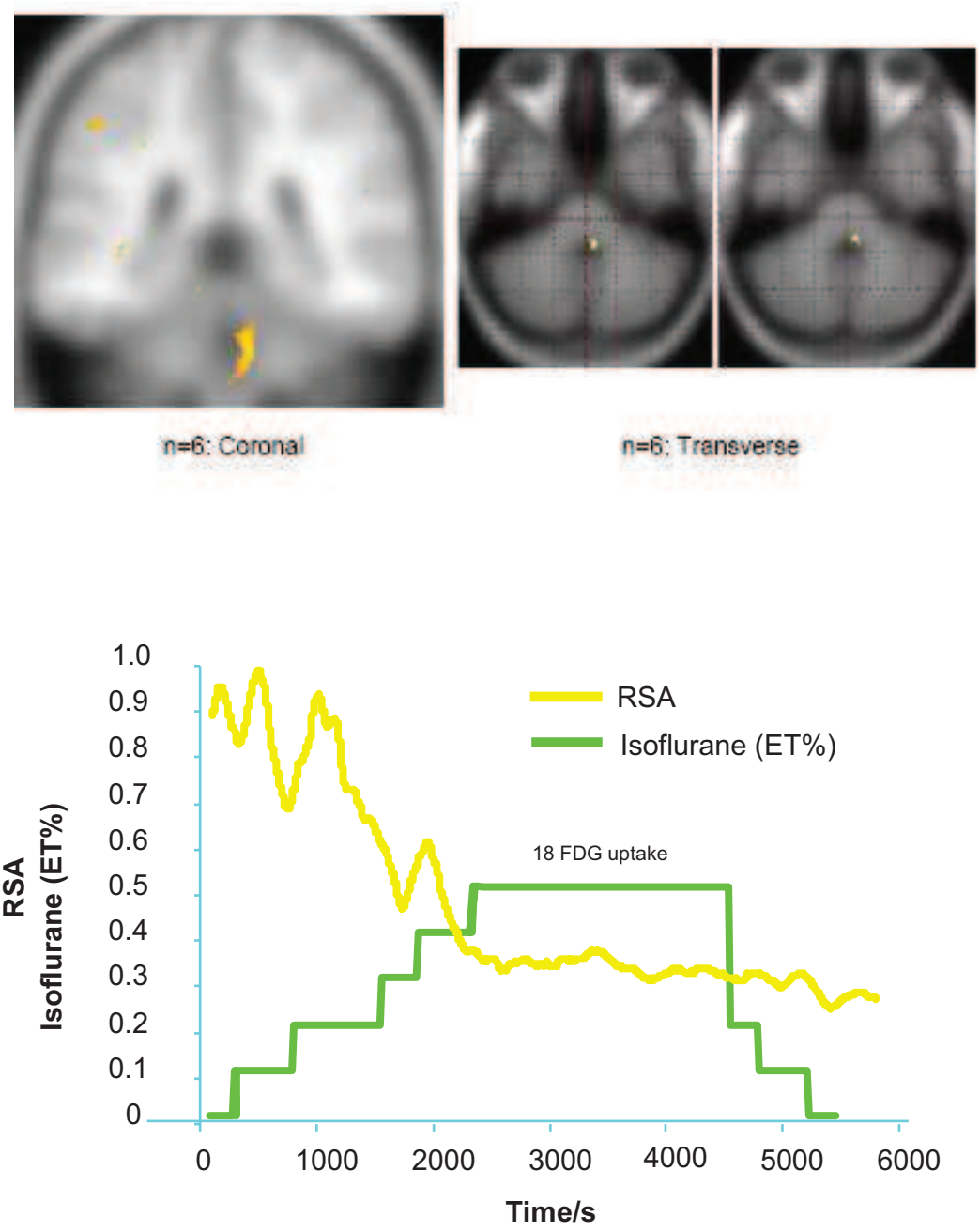

Figure 5. 2 Decreasing RSA with increasing depth of anaesthesia.

From Pomfrett and Alkire illustrating decreasing RSA with increasing depth of anaesthesia and associated areas of brainstem affected. Image obtained using 18 Fluorodeoxyglucose (18 FDG) uptake and subsequent Positron Emission Tomography (PET) (Pomfrett & Alkire 1999).

The proposed integration of the parasympathetic and sympathetic branches of the autonomic nervous system, along with the integrative centres of the NTS, NA and DMNX are illustrated in the diagram below (Figure 5.3, modified from chapter 1). The oblongs represent specific areas of the brain and neural structures relating to the control of the heart on a beat to beat basis. The intimate functional relationship of specific groups of brainstem nuclei (NTS, NA, DMNX) are illustrated. In addition the potential “gating” effect of the sympathetic and efferent neural signals from the NTS can be seen to act in the areas of the intrinsic cardiac ganglia (RAGP and PAGP). The gating effect may result in the flow of neural information being allowed or denied to pass onwards depending upon the state of the gate, which in turn may be set by other neural inputs.

The potential for a change in function in these areas as a result of prion infection can be seen to have influence on feed-back and feed-forward neural relationships, resulting in changing heart rate variability due to deviant neural impulses arriving at the SA node on the heart. This, coupled with the function of the NTS to coordinate inspiration and expiration with the heart on a beat to beat basis, gives further sites for a potential alteration of the synchronised neural flow resulting in the optimized control of the heart on a beat to beat basis.

Figure 5. 3 Schematic of Neural connections from CNS to SA node via ganglionated complexes. Used with permission, from Armour, J. A., Collier, K., Kember, G., & Ardell, J. L. 1998, "Differential selectivity of cardiac neurons in separate intrathoracic autonomic ganglia", Am J Physiol, vol. 274, no. 4 Pt 2, p. R939-R949. Figure 7. Comprising elements from Armour and Randall (Armour, Collier et al.1998;Randall, Brown et al.1998a;Randall, Brown et al.2003).

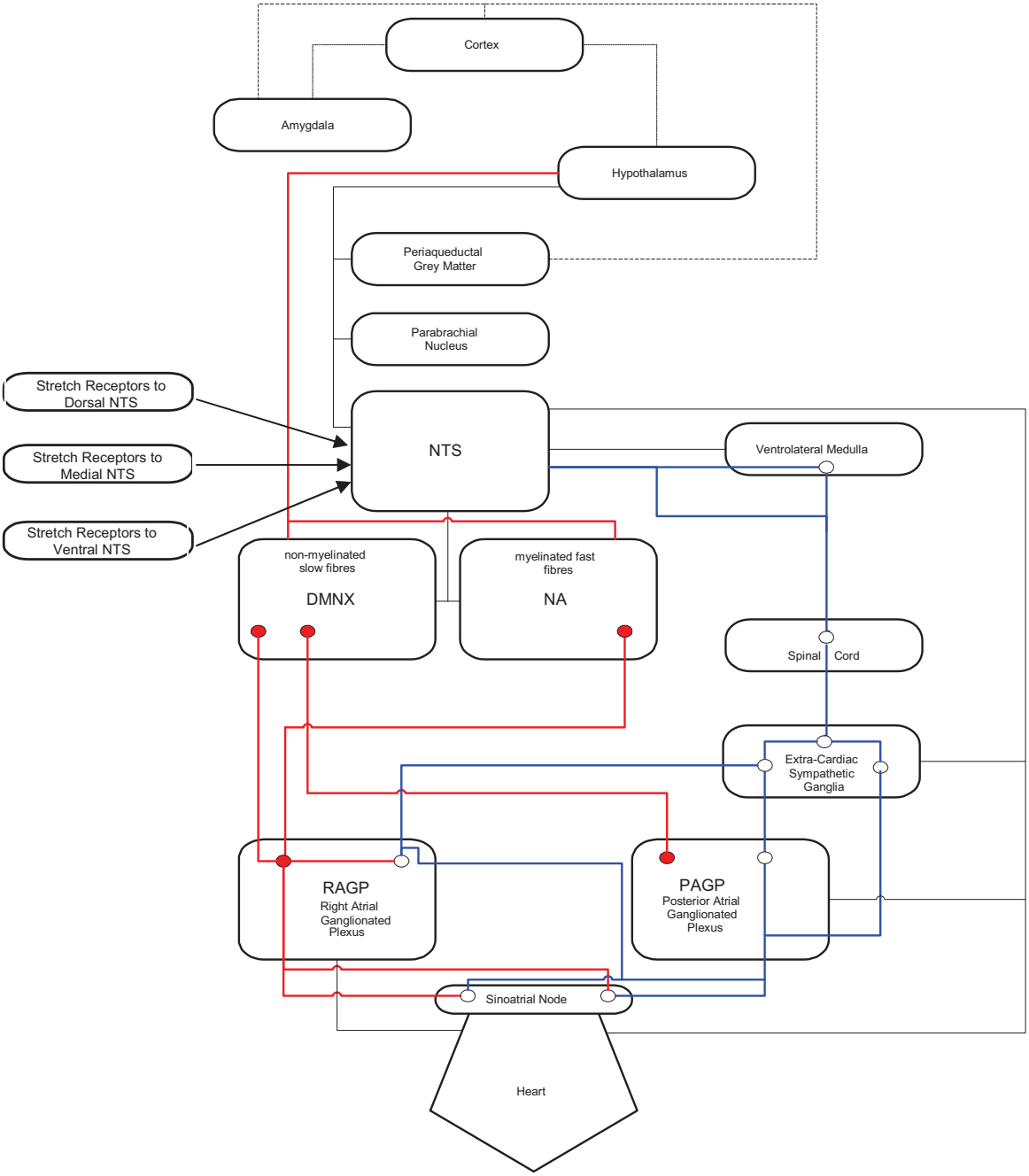

The “triumvirate” of brainstem nuclei (NTS, NA and DMNX) and their relationship to intrinsic ganglionated complexes (RAGP and PAGP) and subsequent action on the SA node is illustrated here. Parasympathetic efferent communication is indicated in red, sympathetic activity is indicated in blue. Black lines indicate efferent communication of the ANS with higher brain centres. Synergistic activity of the two branches of the ANS is indicated at the RAGP at the open circle. Comprising elements from Armour, Randall and Berger et al (Armour, Collier et al.1998;Berger & Averill 1983;Randall, Brown et al.1998a;Randall, Brown et al.2003).

To investigate the perturbation in neurological function as a result from prion infection, focus was put on the link between cardiac and respiratory events. To analyse this relationship independently of power spectral or simple time domain measures, circular statistics were used to relate each R-wave to a breath epoch. Each derived R-wave's interval, from the start of the preceding breath event, was plotted on a circle whose circumference represented the duration of the breath. The association between the breath and the first, second, third etc., R-waves in each breath was then explored to examine the relationship of the neurological control of the cardiorespiratory reflex.

The link between respiratory events and heart beats has also been explored during anaesthesia by Galletly (Galletly & Larsen 1997;Galletly & Larsen 2001). Although the application of circular statistics to investigate the relationship of each R-wave to the subsequent breath event was not made, patterns in cardioventilatory coupling (CVC) were observed in anaesthetised humans.

It was difficult to obtain reliable breath event markers from vCJD patients due to ataxia, dysphagia and myoclonus being impairments caused by the disease (Todd, Morrow et al. 2005). Similarly, in animals incubating prion diseases, transducers to record breath events, either thoracic belts or nasal thermistors were not tolerated and were difficult to operate reliably.

To more accurately assess the relationship between RR interval changes and respiratory events, some sort of breath estimate would be needed. This contrasts with the respiratory frequency zones used in power spectral analysis typically 0.15 to 0.5 Hz in humans. This represents a broad band of respiratory events and may smear any relationship between HRV and individual breathing events. By looking at each breath and the subsequent change in RR intervals, more information about the control of RSA may be observed.

Consequently attempts to estimate a breath were computed from the raw high resolution ECG trace. An average event time for respiration was calculated by combining information from the HF filtered tachogram of the RR time series (see earlier chapter 2), the change in the magnitude of ECG (the development and reliability of this technique are described in (Cysarz, Zerm et al.2008;Moody, Mark

et al.1985;Moody, Mark et al. 1986;Noh, Park et al.2007) and a cubic spline derived conversion of the RR time series.

Method

Following a favourable ethical opinion from the relevant ethical committee (granted by the North West MREC, reference MREC 01/8/92), 300 seconds of ECG data were digitised at a sampling frequency of 1 kHz using a commercially available monitor with a high resolution analogue to digital convertor (Fathom, Depth of anaesthesia monitor Amtec Ltd and TS1, modified version of Variacardio TF4 by Advanced Medical Diagnostics Group.

A simple three connection bipolar ECG recording, giving a similar trace to a lead II configuration, was used since no interpretation of various ECG complexes would be required and it provided a quick, stable and accurate trace from which to detect the R-wave (the largest deviation in the ECG montage). Electrode position was adjusted to obtain the greatest difference between R-wave and baseline. No filtering was applied to the raw ECG since the accurate recording of the R-wave times was of paramount importance.

Once collected, the data were archived and analysed via a hard drive on a conventional PC, exceeding the specified standards for the software to operate and using standard software (Spike2 v6.02, CED; Oriana2, Kovach Computing Services). Using this software and hardware, automated QRS wave detection was applied. Artefacts and missed beats correction were performed in Spike2 and were checked by eye by comparing the raw ECG with the output from the automated R-wave detection program. Any corrections for missed or extra R-wave events were made using purpose written scripts in Spike2. An event series of ECG R-wave timings were obtained in order to determine variability in the R-R intervals and an instantaneous tachogram constructed from this event series, again using Spike 2 Software V 6.02 from Cambridge Electronic Design (CED) (As described previously in chapter 2).

In addition, I designed and implemented a computer program, again in Spike2 script language, that estimated breath events during the 300 second recording window by averaging estimates gained from: analysis of the breathing frequency

(HF) filtered tachogram (Channel 3 in figure 5.4); analysis of changing magnitude of the recorded ECG due to the movement of the thorax (Channel 4 in figure 5.4); an assessment of breath events derived from the cubic spline interpolated time series of the R to R intervals (Channel 5 in figure 5.4) (Noh, Park et al.2007;Schafer & Kratky 2008).

Figure 5. 4 Relationship of lines of evidence used to assess breath event.
Graph of relationship of cubic spline of RR time series, filtered tachogram and change in amplitude of R-waves relating to a breath on control humans.

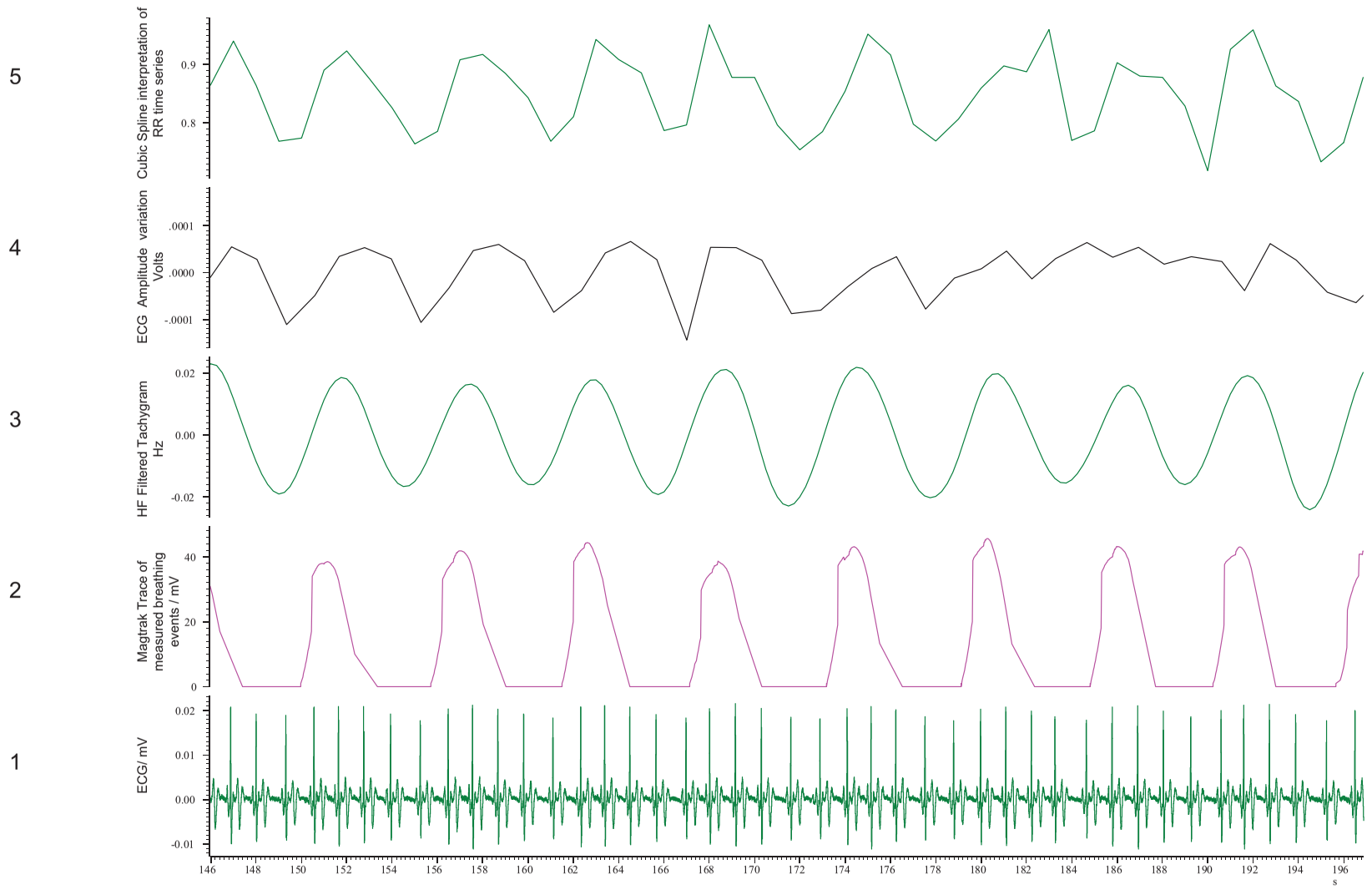

The first stage in the development of the program employed to estimate the breath events was to investigate the variation in the slow frequency changes of the ECG. This consisted of using the extrapolated event series of ECG R-wave timings from which an instantaneous tachogram was constructed using Spike 2 Software V 6.02 from Cambridge Electronic Design. The tachogram was constructed by replacing each R-wave event marker by a cosine wave fragment of unit area (see figure 2.3 chapter 2). This was done to investigate the frequency changes in the sequence of R-wave events and hence the periodicity of the ECG. This tachogram was then filtered to exclude frequencies outside the 0.15 to 0.5 Hz range. This is the range for HRV that represents the power associated with breathing following FFT analysis of the tachogram. Thus, this filtered version of the tachogram would represent the frequency changes in the RR time series associated with breathing. This is shown in figure 5.4 as channel 3.

Secondly, breath events were estimated from the variation in the amplitude of the ECG corresponding to changing thoracic impedance as the chest wall and recording electrodes moves away from and closer to the heart in time with breathing (Channel 4 in figure 5.4). From the high resolution ECG waveform channel, any DC component of the signal was removed using Spike 2 and the script language to process data following collection. This was achieved by using a script command which replaced the value of the original waveform at a time, say t, with a value representing the original value minus the average value calculated from the waveform data from time *t-0.1s* to *t+0.1s*. This process reduced the channel offset to zero without altering the channel scale and so allowing the difference in amplitude of the R-wave peaks to be identified and compared to the breathing events (figure 5.5).

Figure 5. 5 Variation of ECG amplitude indicates breath event.

Spike output illustrating how the variation in the amplitude of the DC filtered ECG trace varies with breath events, here represented by the Magtrak output on channel 2.

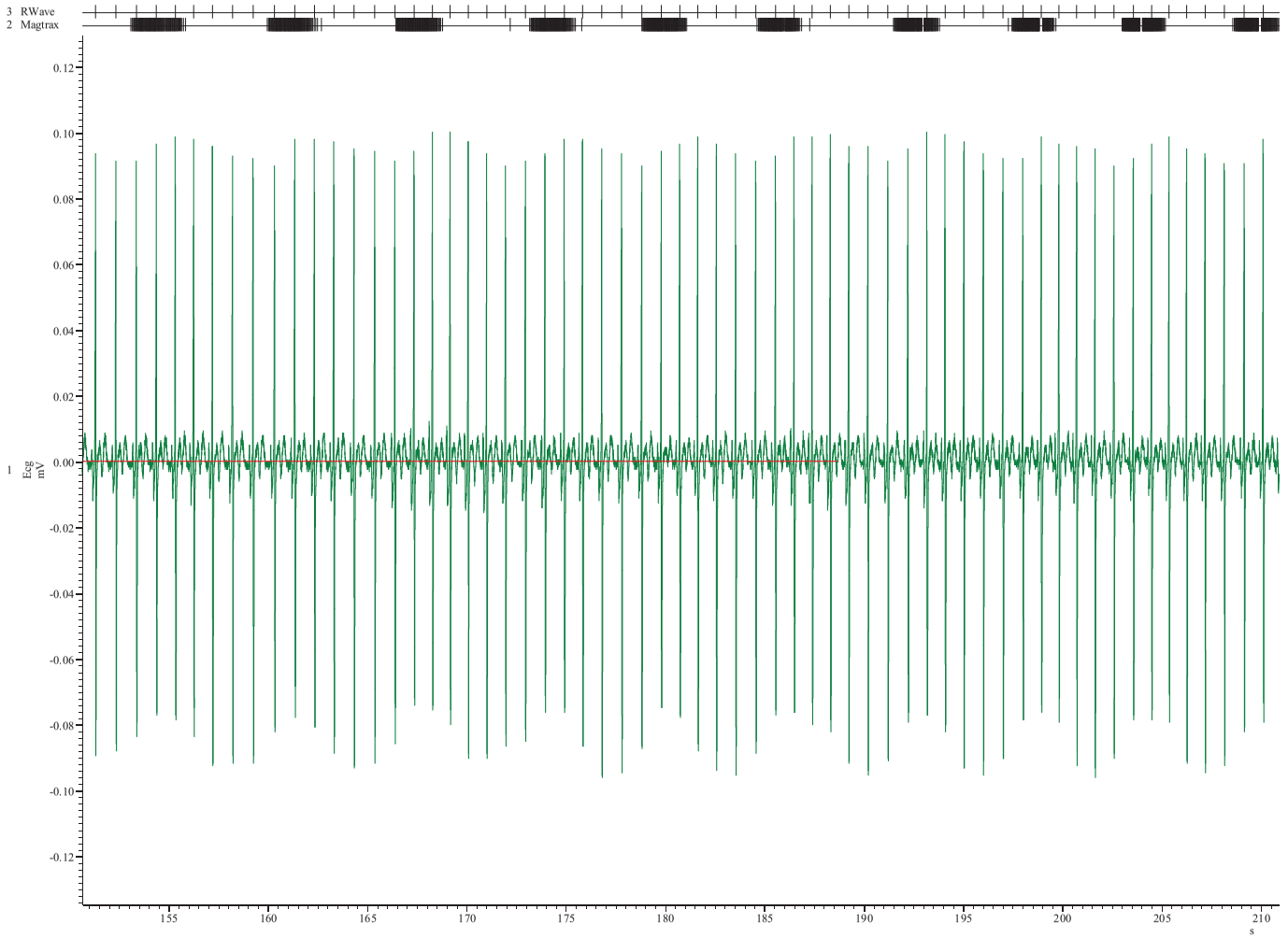

A further method of estimating the breathing rate from the ECG trace is to use a cubic spline smoothing transformation of the RR time series (Noh, Park et al.2007;Schafer & Kratky.2008) produced here following automated identification of R-waves from the ECG and checking by eye for artefacts. The cubic spline was again performed using a Spike2 script function which mathematically interpolates data resulting in a smoothing of the time series. This is shown as channel 5 in figure 5.4.

Following the construction of the three traces derived to estimate breathing events, the turning points in the waveforms were calculated in the analysis program and compared to breathing events measured by a Magtrak turbine (Ferraris Medical Ltd) used in conjunction with a face mask and filter (Intersurgical Mask 1515 and Intersurgical filter 1944: Intersurgical, Berkshire). The Magtrak transducer measures a breath event by emitting a series of electrical pulses in response to a vane rotating as a consequence of the passage of gas flow across a slotted cylinder, in a similar fashion to a Wrights respirometer. These breath events are then interpreted from the series of electrical pulses shown in figure 5.5. The start of each series of electrical pulses corresponding to each breath is taken as the breath event, the start of inspiration.

Figure 5. 6 Association between measured and estimated breath events.
Illustration of the association between measured, estimated and averaged breath events.

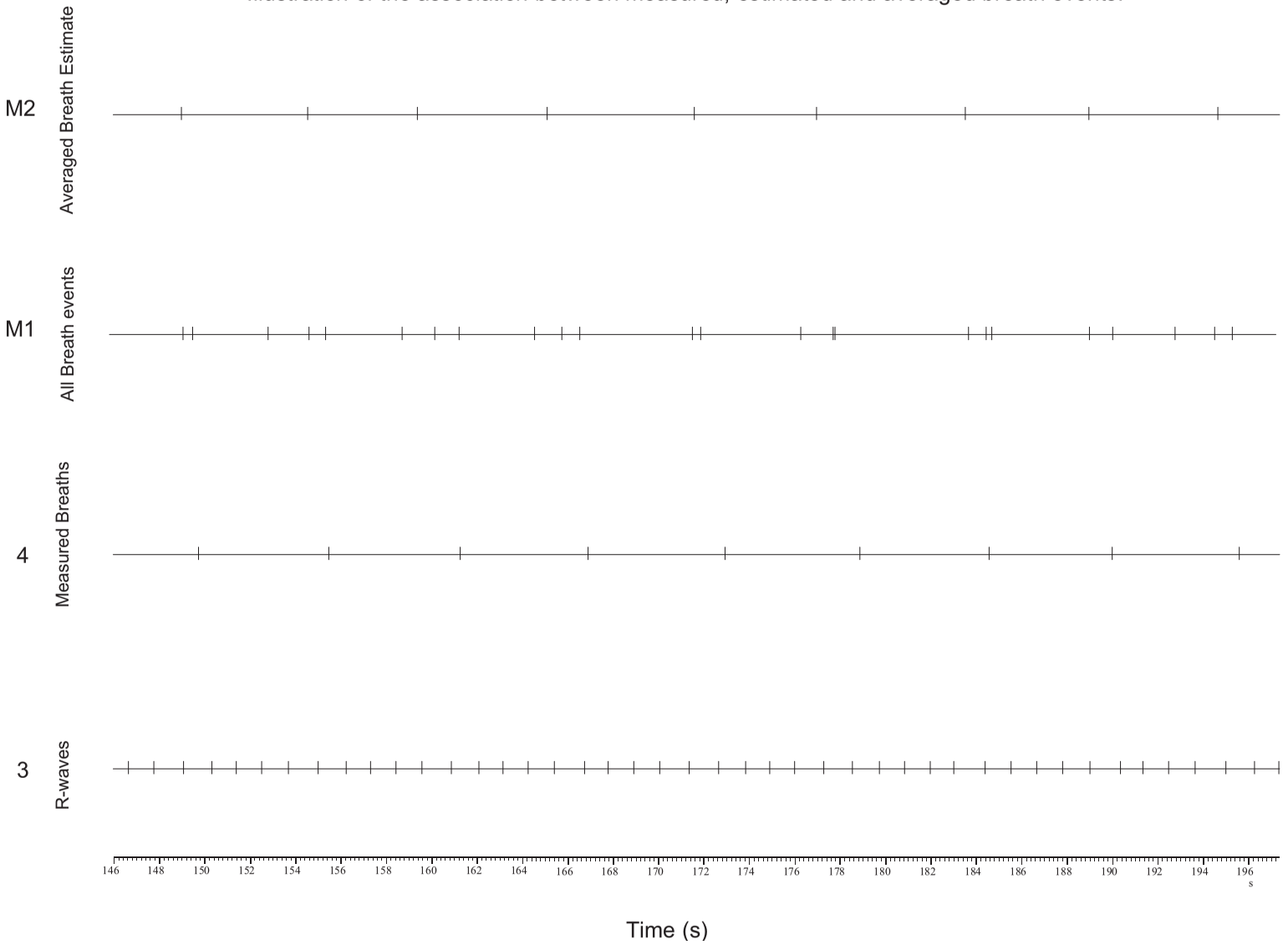

Figure 5.6 shows the three derived estimates displayed on channel M1. At some measured breath events there may not have been an event estimated by all three of the methods. For example in figure 5.6 there were only 2 estimates available from the three methods for the measured breath event at time 150 seconds. This shows that not all three methods were equally affective at determining the breath event on all occasions. The three estimated events were then averaged to form one event which approximated to the breathing event recorded from the Magtrak (Shown in figure 5.6 as channel M2).

The average breath estimate channel still contained values that were not physiological and to help make the estimates more applicable to the real world values, smoothing of these averaged events was performed in 2 stages. Events from the average breaths (channel M2) were copied to a new channel if they were physiologically valid, e.g. occurring within 3 seconds of each other and thus representing a breathing rate of more than 20 breaths per minute (channel SmoothAVG in the program listing in appendix 1.5).

The second stage consisted of taking the average breaths from channel SmoothAVG , putting the event times into an array to which a Finite Infinite Response (FIR) filter with 5 coefficients was applied thus producing a second filtered channel (FiltAVG in the program listing in appendix 1.5). The FIR filters defined in the Spike2 script language, use future as well as past data to generate each output point. It is suited to this application since information in relation to the previous and next breathing events are considered in this smoothing algorithm (the frequency response of this filter is shown in appendix 1.6). The physiological processes determining each breath are also linked in a cyclical fashion with each breath being affected by the previous breath and constrained by physiological feedback and feed forward neurological loops. With 5 coefficients, this meant that 2 events before the data point and two events after the data point were used to find the average of this series of 5 breathing events. The next breath event in the array would then be subject to this procedure, being the centre data point in the smoothing algorithm.

There is a problem at the start and end of the array where some coefficients have no associated data element. The solution to this problem is to take these missing points as copies of the first and last points as implemented in the script command

(ArrFilt, Spike2 Script Language version 6). The result of applying this function to the array is to produce a five point smoothing of data, replacing each point by the mean of itself and the two points before it and the two points after it.

Whilst it is understood such ECG derived respiration (EDR) events will have errors associated with them, it was considered that breaths estimated in this fashion may provide utility in the investigation in the link between respiration and the change of the heart beat on the sub second time scale. Since the proposed method of analysis would rely on breath by breath investigations, one or two erroneous breath events may not affect the trend derived from 5 minutes of data containing around 40-50 breaths. Although the estimated and recorded breath events showed good agreement by eye, a measure of how well the constructed algorithm estimated the event compared to the recorded event would be required to validate the method used to estimate breath events.

As stated by Bland and Altman, new methods of measurement need to be validated against current methods of measurement. A true measure of a particular physiological quantity may not exist. The best measured approximation to its true value can be used, but this may also be subject to errors. Consequently it is suggested that the degree of agreement between the new and traditional measurements are assessed and it is stated that it is inappropriate to use correlation coefficients (Bland & Altman 1986).

In considering the problem of assessing how good the agreement of measured versus estimated breath events is, it was considered appropriate to use the technique described in the above quoted paper by Bland and Altman. This method finds the bias, estimated by calculating the mean difference between two measures ($\bar{d}$) and the standard deviation of the differences (s) to summarise the agreement between the two methods of measurement. A graphical representation displaying average value of the breath event (abscissa) against the difference in estimated times (ordinate) helps summarize these differences.

The estimated breath events were then used with the corresponding R-wave events in a commercial package (Oriana2) and in a bespoke Spike 2 script to calculate indices of circular statistics (Batschelet 1981) such as mean vector length, circular variance, concentration and mean vector angle. Investigations into the link between respiration event and the time to the first, second, third... R-wave after each breath were also performed to investigate respiratory cardiac coupling. In this way estimates of RSA and the changing association of beat to beat heart rate and breathing could be assessed to test the hypothesis in a direct fashion.

The R-wave times from each breath are extracted and the first, second, third etc. R-wave times are plotted on a circle whose circumference of 360 degrees represents the breath epoch as illustrated in figure 5.7.

Figure 5. 7 Construction of vector plot of R-wave distribution within a breath.

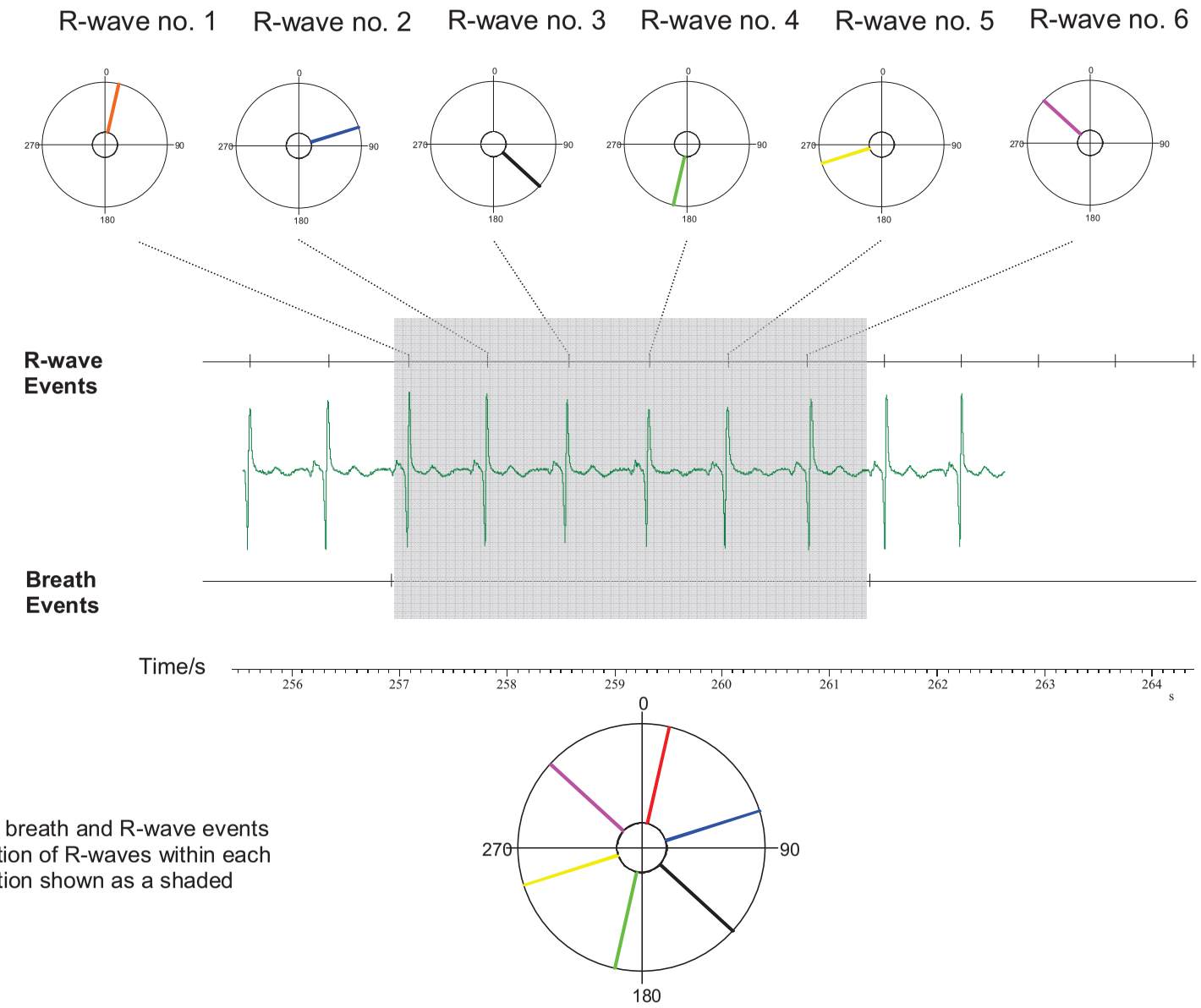

Translation of linear breath and R-wave events to a circular distribution of R-waves within each breath (Breath duration shown as a shaded area).

Representing circular statistical data.

From the circular statistical analysis, two types of diagram were produced by importing the R-wave times, translated to an angle where 360 degrees represented the duration of that particular breath, into Oriana (Kovack Computing), a software package used to perform circular statistical analysis. These two types of circular plot represented:

1. The distribution of the R-waves within each breath figures 5.8, 5.9 and 5.10 (visualised as a series of "over-head transparencies" overlaid on top of each other with each layer representing the distribution of the first 6 R-waves within each breath. For illustrative purposes, six breaths are used in this example).

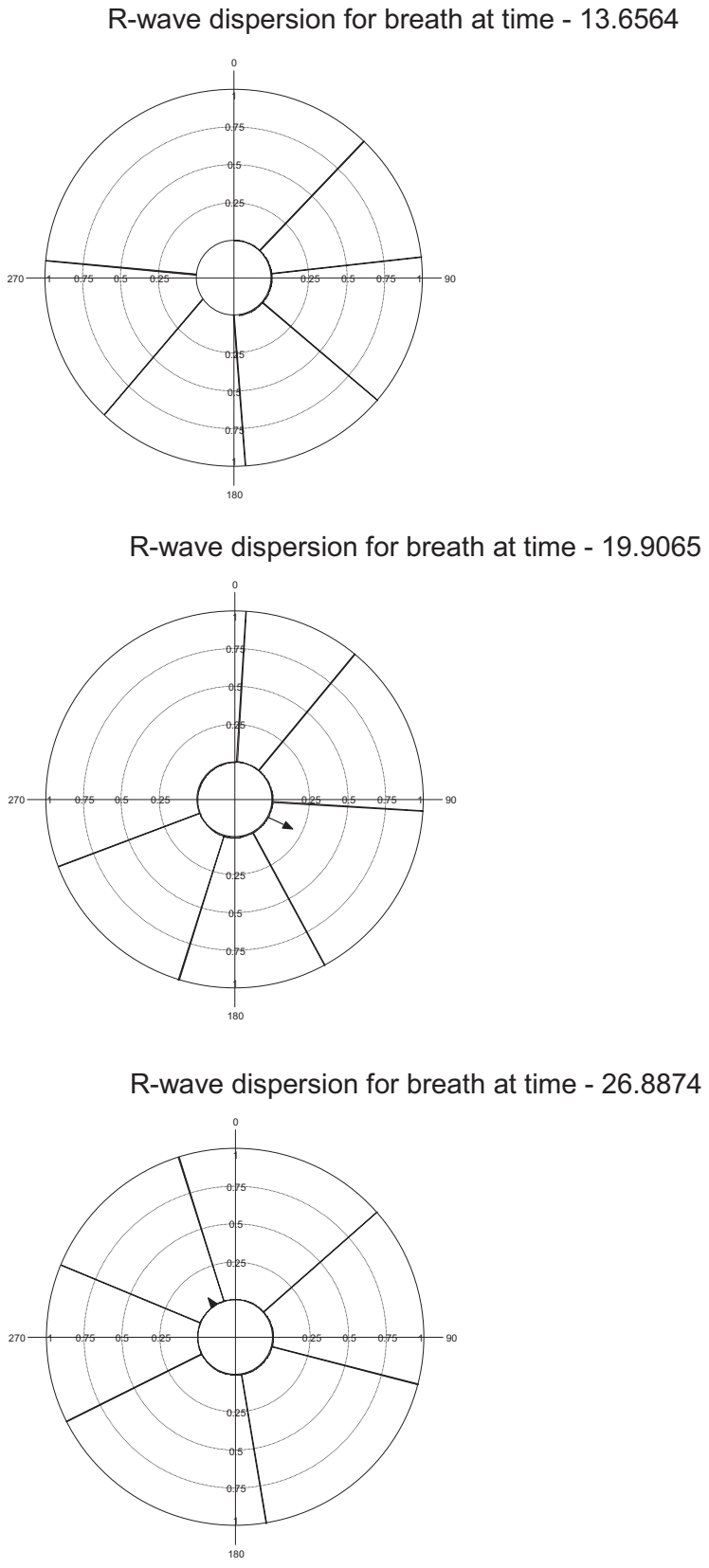

Figure 5. 8 Example of R wave dispersion within breaths I.

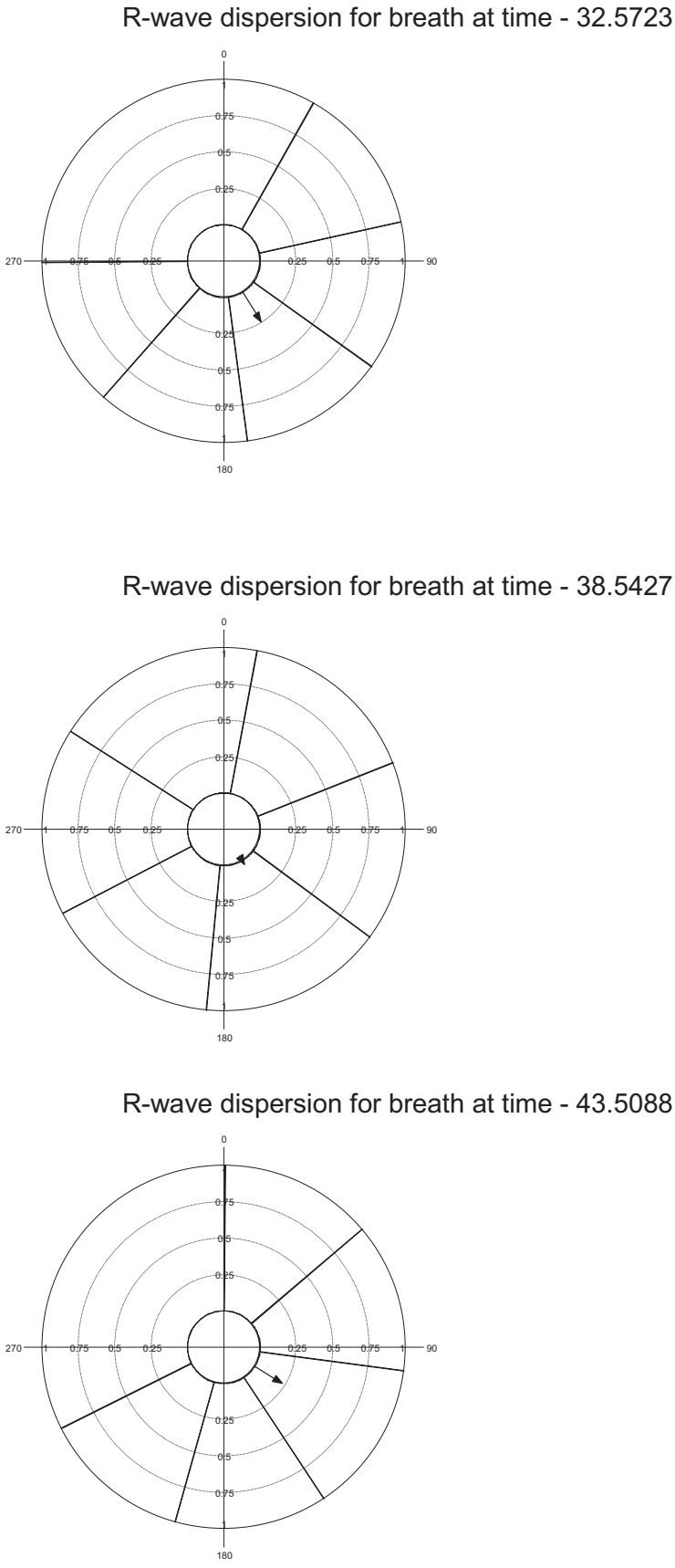

Figure 5. 9 Example of R wave dispersion within breaths II.

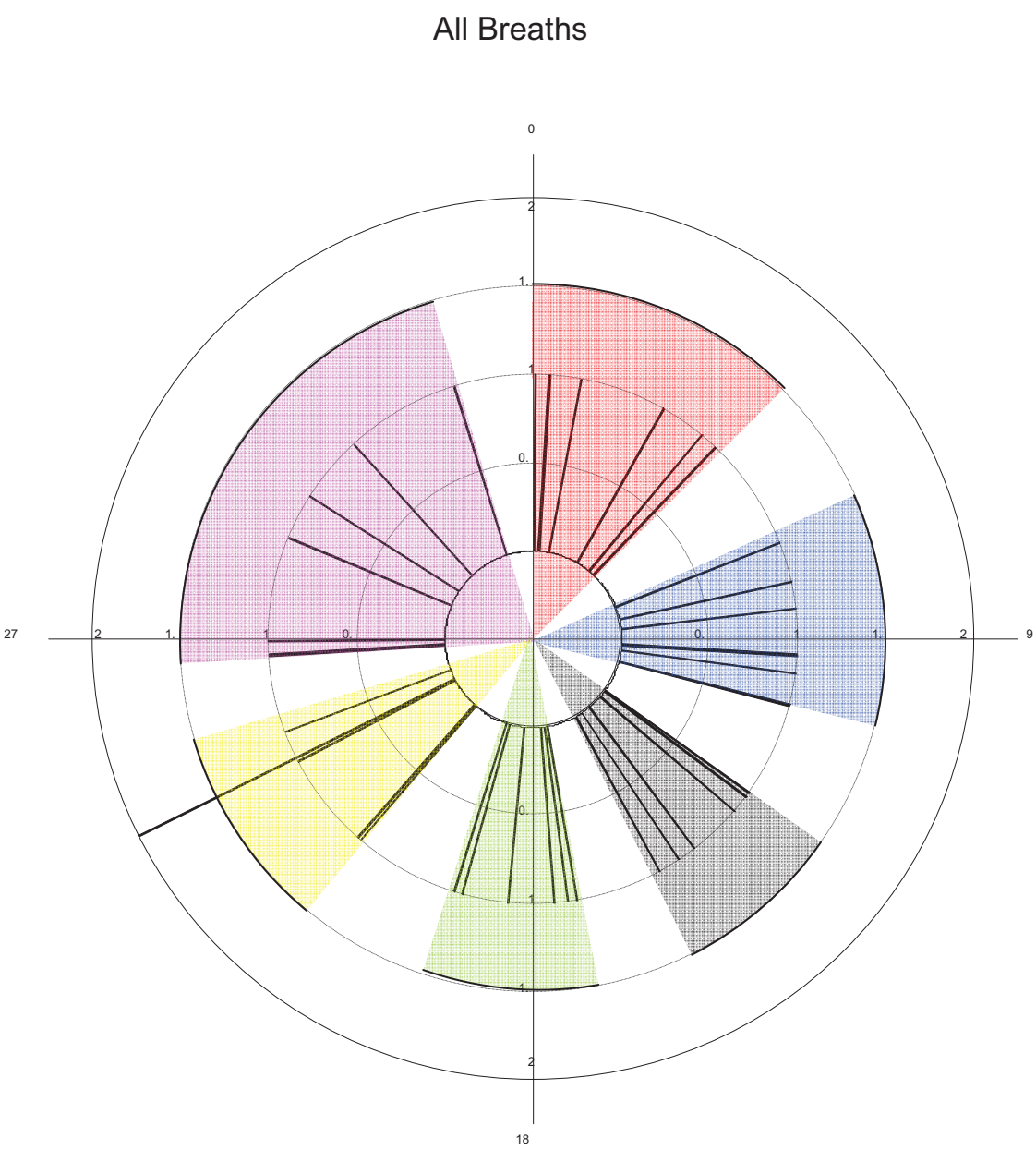

Figure 5. 10 Overlay of constituent breaths of figures 5.8 and 5.9.

R-waves derived from 6 breaths overlaid to illustrate how the derived resultant vectors constitute the “Cartwheel plot” of figure 5.11. The amplitude of the rings represent the number of vectors in each bin. Here the bin width is set to 1 to illustrate the construction of the plot.

And

2. A summary plot (Cartwheel plot) where the “spokes” of the wheel represented the resultant mean vectors of the summation of the individual beats associated with the first, second third etc., heart beat with in each breath. The black arrowed line represents the resultant mean vector angle and length for all the data in the file.

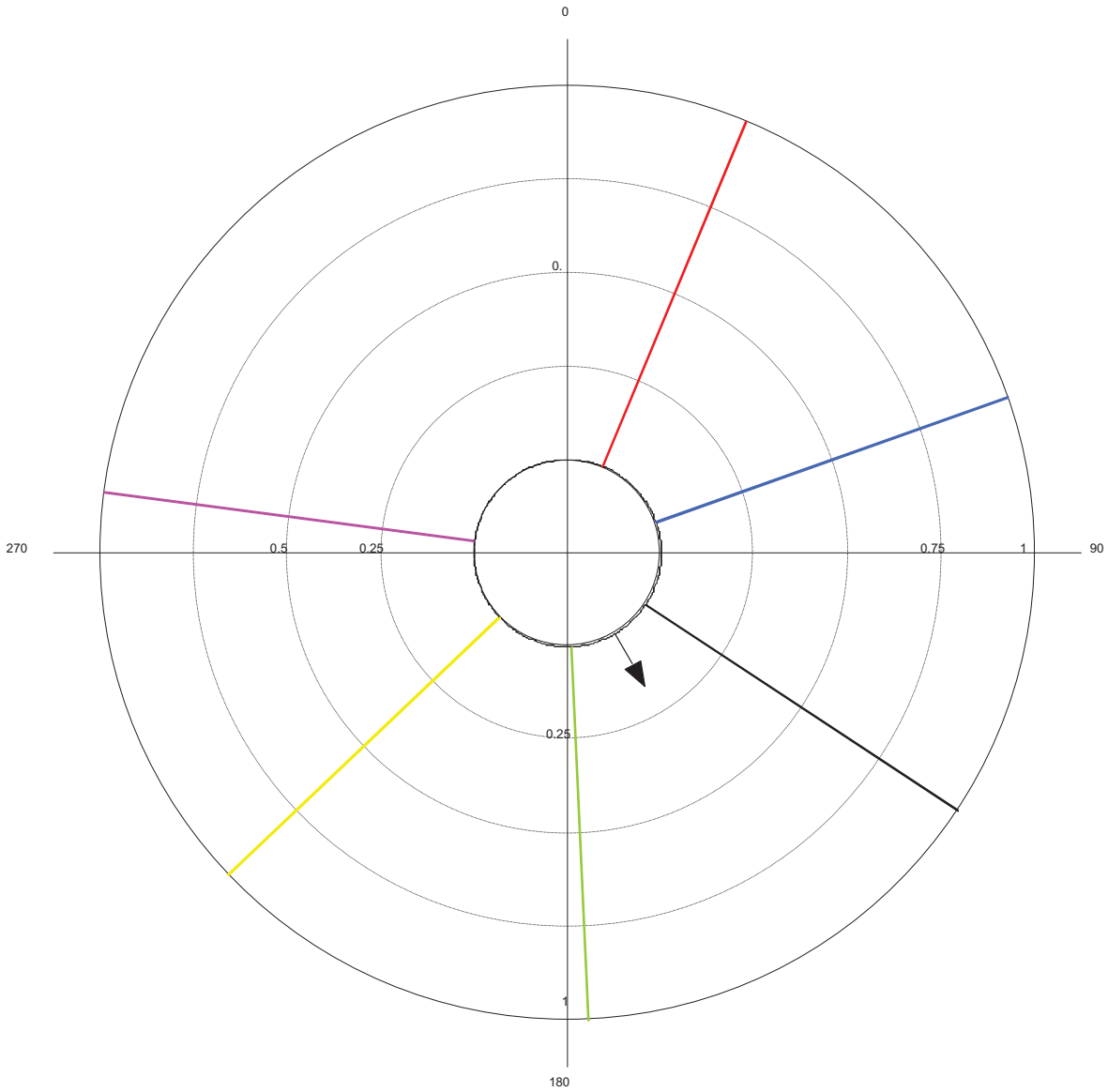

Figure 5. 11 Summary “Cartwheel plot” .

made from the resultant vectors derived from R-waves of figure 5.10. The coloured lines represent the summary vectors for the same coloured areas of figure 5.10

From these cartwheel plots a resultant mean angle and vector length could be calculated to provide a summary of the clustering of the R-waves to each breath within the 300 second sampling epoch. Typically around 50 breaths for each sample were analysed.

In addition resultant mean vector angles and lengths could be calculated for individual R-waves within the breath epoch based from the type 1 angular plots shown in figures 5.8, 5.9 and 5.10.

The mean vector length gave an approximation to the clustering of R-waves to the breath. A high value of MVL indicated that R-waves were more clustered to the breath event and hence the breath had a greater influence on the R-wave distribution than a data set with a lower value of MVL.

The value of concentration (k) represents the extent the von Mises distribution (a circular equivalent to its linear counterpart of the normal distribution) deviates from a perfect circle representing a uniform distribution (see figure 5.12). If k = 0 then the distribution is uniform and as k increases the distribution is concentrated more about the mean (Batschelet.1981).

Circular variance and circular standard deviation are comparable to their linear equivalents although variance (V) is calculated from the length of the mean vector (r) by using the formula V = 1 – r; and the standard deviation (S) is calculated as $S = \sqrt{(-2\ln(r))}$ (Oriana V2 User manual(Batschelet.1981).

Figure 5. 12 Circular distributions compared to linear counterparts.

Uniform and von Mises probability distribution and their linear counterparts

Probability plot of Uniform Distribution

Probability plot of von Mises Distribution

Circular Representation

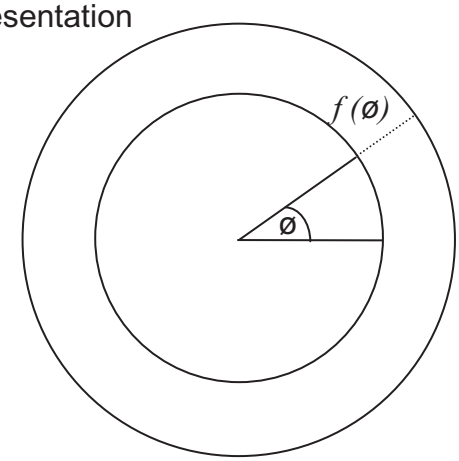

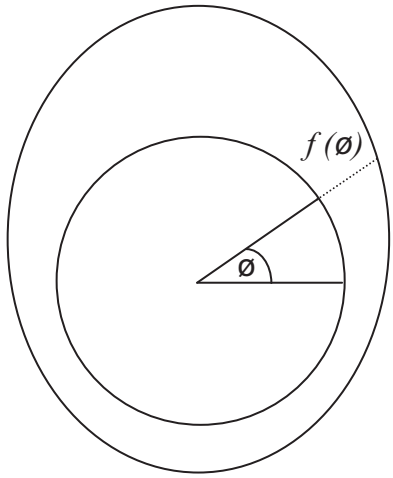

The probability density is constant over the circumference of the unit circle (no sector is preferred to any other sector.

Probability density is given by the equation:

$$f(\phi) = \frac{\exp[k\cos(\phi - \theta_1)]}{2\pi I_0(k)}$$

where ø is angle as shown above, θ is the mean angle assumed to be zero in this example, k is the parameter of concentration and I_0 is a modified Bessel function of order 0. If k = 0 then the function represents a Uniform distribution. As k increases, the more the distribution is concentrated around the mean direction.

Linear Representation

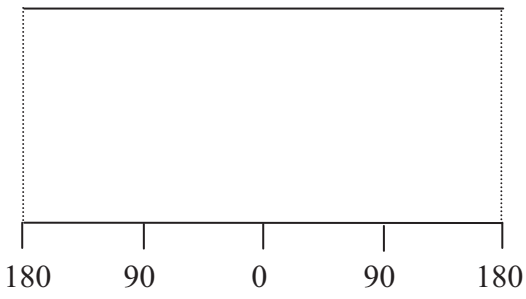

k = 0

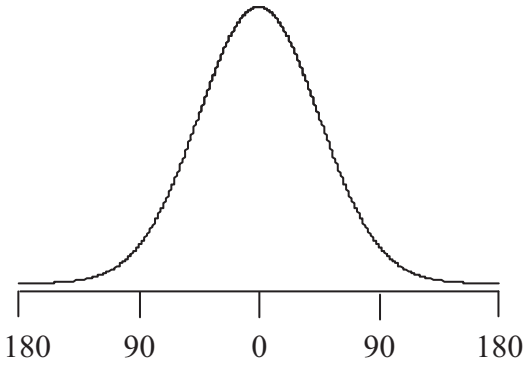

k = 2

Circular statistics are used in many publication in areas such as sciences (Aradottir, Robertson, & Moore 1997;Bowers, Morton, & Mould 2000;Gao, Chia et al. 2006) psychology and criminology (Brunsdon & Corcoran 2006) and political and social research (Gill & Hangartner 2010). The basis for these circular statistical measures is the calculation of the mean vector length and mean vector angle which are calculated by vector addition. The first step is to transform the R-wave times forming each vector (representing the occurrence of the R-wave after the breath event) to unit vectors where the x coordinate of the vector corresponds to the cosine of the angle and the y coordinate corresponds to the sine of the angle.

$$r_i = \begin{pmatrix} cos\alpha_i \\ sin\alpha_i \end{pmatrix}$$

The vectors r_i are then vector averaged for all the R-waves by

$$\bar{r} = \frac{1}{N}\sum_i r_i$$

This gives $\bar{r}$, the mean resultant vector. This mean resultant vector is transformed using the four quadrant inverse tangent rule to give μ, the mean vector angle. (This, along with the calculation of mean vector length is performed in the program listing as shown in appendix 1.5). The length of the resultant mean vector is derived by using Pythagoras' theorem as:

$$r = \frac{1}{n}\sqrt{\left(\sum_{i=1}^{n} \cos \alpha_i\right)^2 + \left(\sum_{i=1}^{n} \sin \alpha_i\right)^2}$$

Consequently, both the mean vector angle and mean vector length are derived from the angular position of the constituent vectors, hence depend critically on the angle (representative of the time of the R-wave after the breath event).

Concentration is related to the length of the mean vector and measures the spread of angular distributions. The summary r statistic can be subject to significance testing using the Rayleigh test which indicates the presence of a preferred

direction in the grouped data and this is also based on the mean vector angle, μ and concentration parameter k.

The Rayleigh test calculates the probability of the null hypothesis that the data are distributed in a uniform manner. The Z value is calculated simply as $Z = nr^2$, where n is the number of observations and r is the length of the mean vector. A longer mean vector (and the resulting larger value of Z) means greater concentration of the data around the mean, and thus less likelihood of the data being uniformly distributed. A probability less than a chosen significance level (usually 0.05) indicates that the data are not distributed uniformly and that they show evidence of a preferred direction.

The Mardia-Watson-Wheeler test also referred to as the Uniform Scores Test, is a non-parametric multisample test for determining whether two or more distributions are identical. If the distributions of the samples are identical then the uniform scores for the samples should be evenly interspersed around the circle, and their resultant vector lengths, r, should be short and similar. Any significant difference between the vector lengths will lead to a large W test statistic and rejection of the null hypothesis of identical distributions.

From the publications listed above, there is a trend in how circular statistical data is presented. Data is presented to summarize properties of angular data such as central tendency and spread of the data. Since many of the parameters of circular distribution are derived from the mean vector angle, the 95% confidence intervals are often quoted and or plotted on graphs of the mean vector angles but the concentration values are plotted as unitless discrete points (see (Bowers, Morton et al.2000;Haskey 1988). However, Batschelet illustrates how confidence intervals for the parameter of concentration may be obtained from charts using the calculated mean vector length of the sample (pages 89-92 (Batschelet.1981)).

Use of an ECG simulator to test the program

In order to further validate the algorithm used here to estimate breath events and calculate circular statistics related to the dispersion of the R-wave intervals within each breath cycle, an electronic simulation of an ECG was analysed. This came from a HeartSim 2000 (Laerdal-EKG-L-SIM2000) and provided a “standard” ECG trace without any arrhythmias programmed. This gave a simulated ECG with little or no variability in the appearance of the R-waves. The breaths for this file were estimated by running the data through the purpose written script but the thresholds for picking off the breath estimates were lowered to allow estimations to be made. The periodicity of these derived breath estimates were similar to those obtained from human subjects.

Figure 5.13 below illustrates the ECG from the Heartsim and illustrates how the breath estimates for this file were obtained. The Heartsim data is distinct from an electronically generated rhythmic series of pulses such as that generated from a signal generator, since it contains a small change in the amplitude of the ECG along with very small changes in the R-R intervals of the waveform. This allowed an estimation of breathing events from these two facts, as shown in the figure.

This is the same file used to assess the power spectral estimates in appendix 1.2 and consequently the reduced amplitudes of the tachograms required the thresholds for picking off the breath estimates to be lowered to allow estimations of breath events to be made.

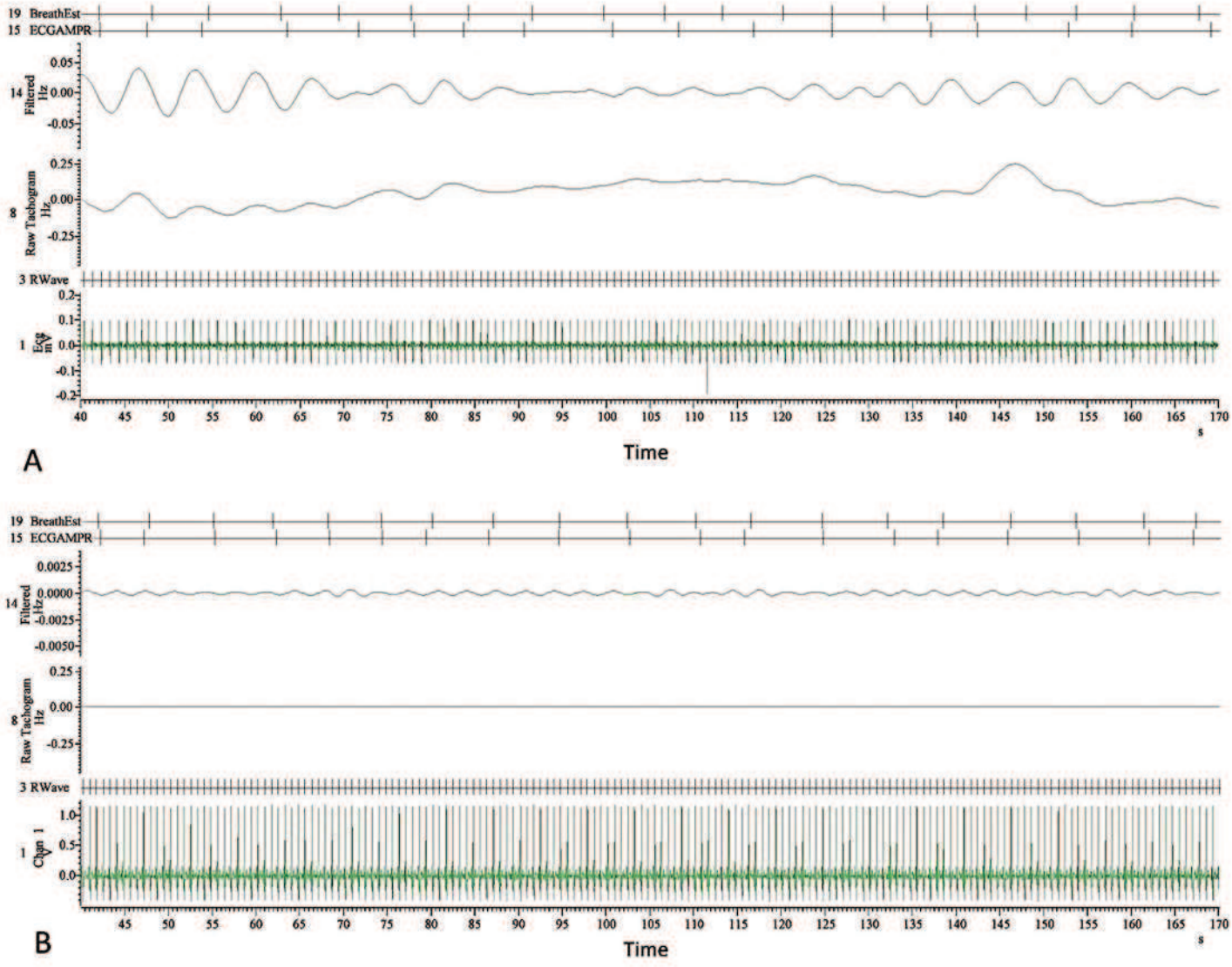

Figure 5. 13 Illustration of how breath estimates were deducted from Heartsim file.
A: data from a control to compare the breath estimation process.
B: data from the Heartsim showing breath estimates derived from changing amplitude of ECG trace (channel 15) and modified by information from channel 14 which represents a breathing frequency filtered tachogram. Note the reduced amplitudes of channels 8 and 14 in B, compared to those in A.

The purpose written computer program firstly estimated the breath events as described above and then extracted the first R-wave from each breath and calculated the resultant mean vector from all the first R-waves for all the breaths in the data file. This process was then repeated for the nth R-wave in each breath cycle where n ranges from 1 to 6. These plots indicate the dispersion of the nth R-wave for all breaths as shown in figure 5.14. The resultant mean vector (shown in the circular histogram plots below as an arrowed black line) for all the first, second, third etc., R-waves in each breath cycle is shown.

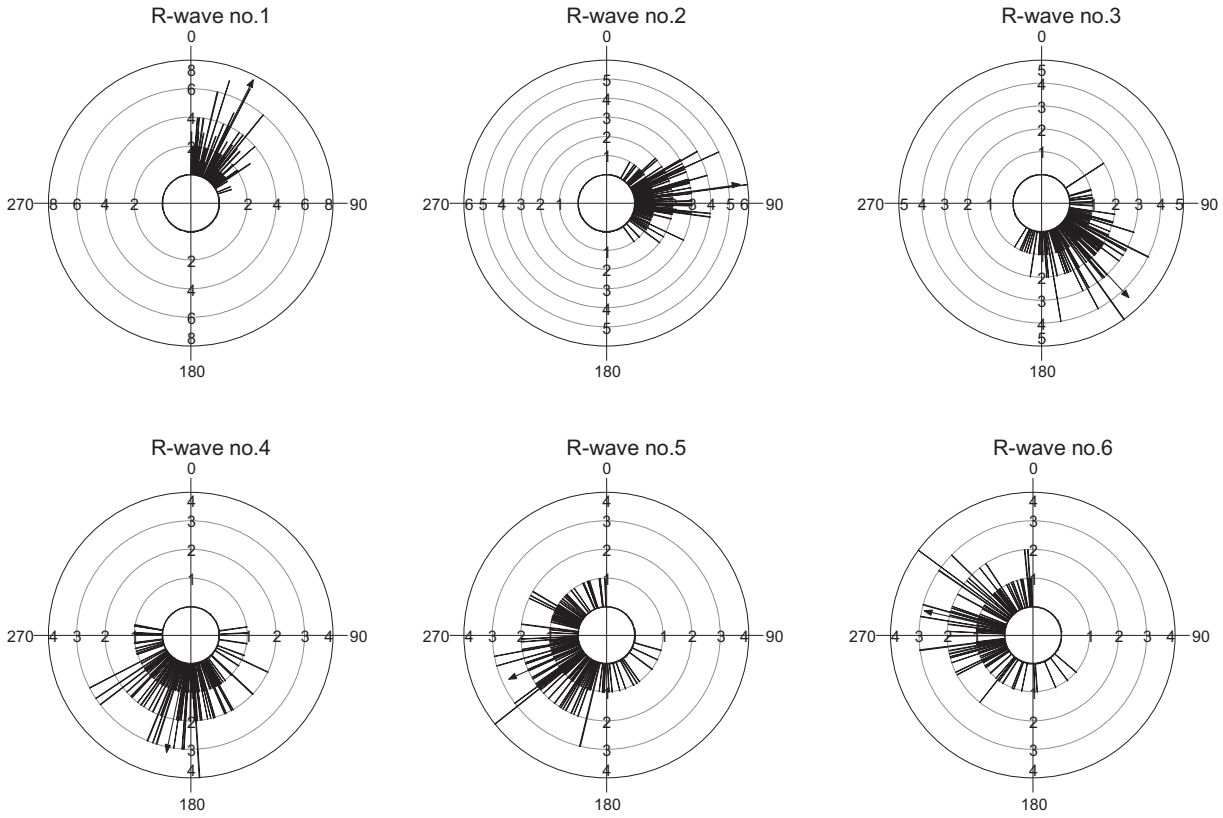

Figure 5. 14 Distribution of R-waves for overlaid breaths
Circular histogram plots showing the dispersion of the nth R-wave (n from 1 to 6) within each breath cycle for all breaths in a 300 second recording from a control subject. The rings represent the number of vectors in each bin. A bin is represented by the radial black lines.

The resultant mean vectors from these circular histogram plots were then plotted on a second “cartwheel” histogram (an example is shown in figure 5.11), representing the associations between each R-wave in the breath cycle, averaged for the whole data sampling period, containing approximately 50 breaths for each subject.

Results

Shown below is the data used to evaluate the agreement between measured and estimated breathing events (figure 5.15).

When the derived breath estimating algorithm was used to estimate breath events and compared to measured breath events, it was found that the estimated breaths displayed a mean difference of -0.51727 with 95% confidence interval of -0.61937 seconds to -0.41517 seconds by comparison with 905 measured breath events from 15 human subjects (see appendix 1.4). The typical association of estimated and measured breaths is shown in figure 5.16. The breath estimates were calculated using the algorithm on the same files that contained measured breath events and the Bland-Altman test for agreement between measurements (Bland & Altman 1986) was used to assess the level of agreement.

Figure 5. 15 Bland-Altman Plot of differences in estimated and measured breath events

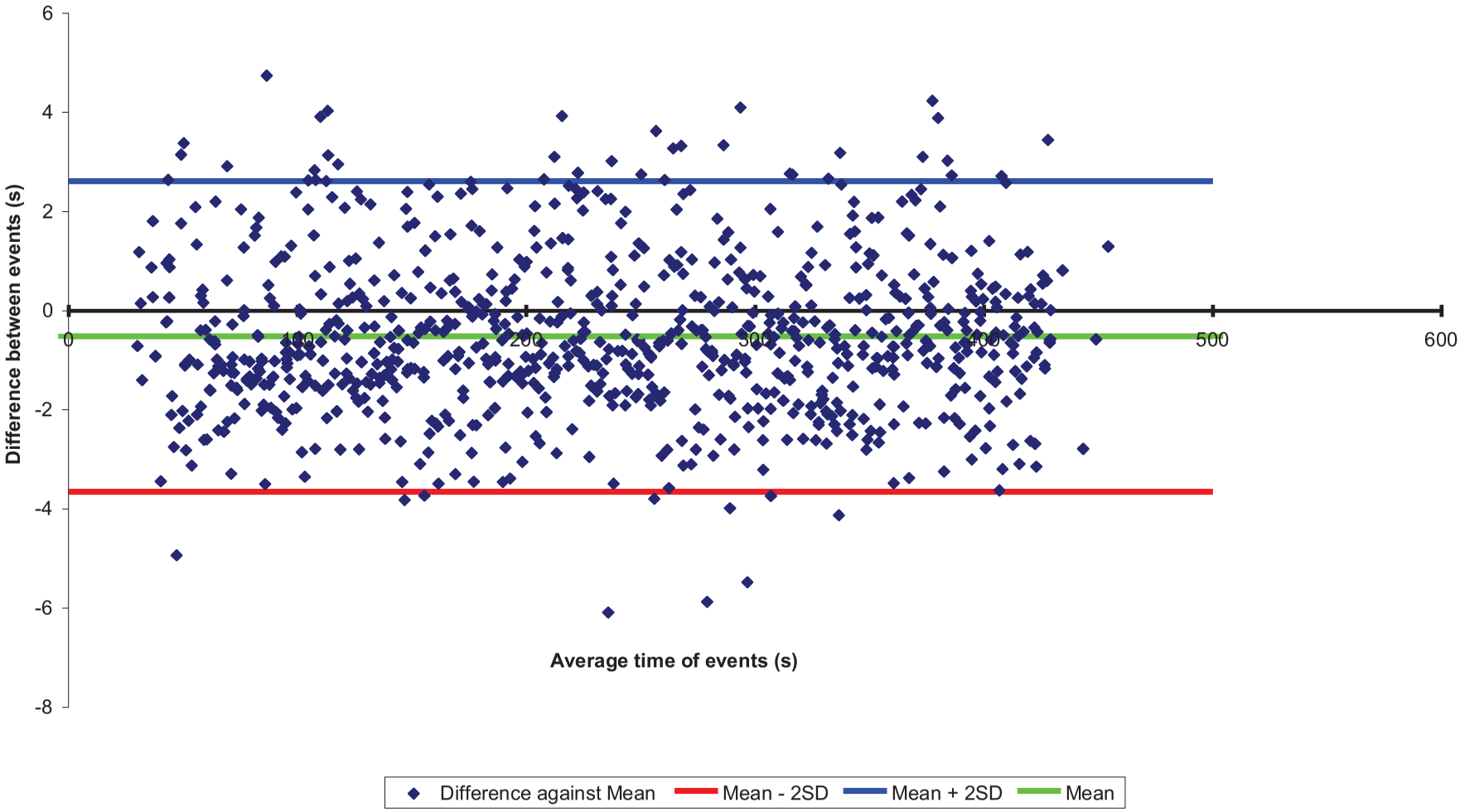

Figure 5. 16 Relationship of measured to estimated breathing event
Graph illustrating typical relationship of the estimated breath event against the measured breath event. Time between cursor 1 (estimated) and cursor 2 (measured) is 0.53683 s.

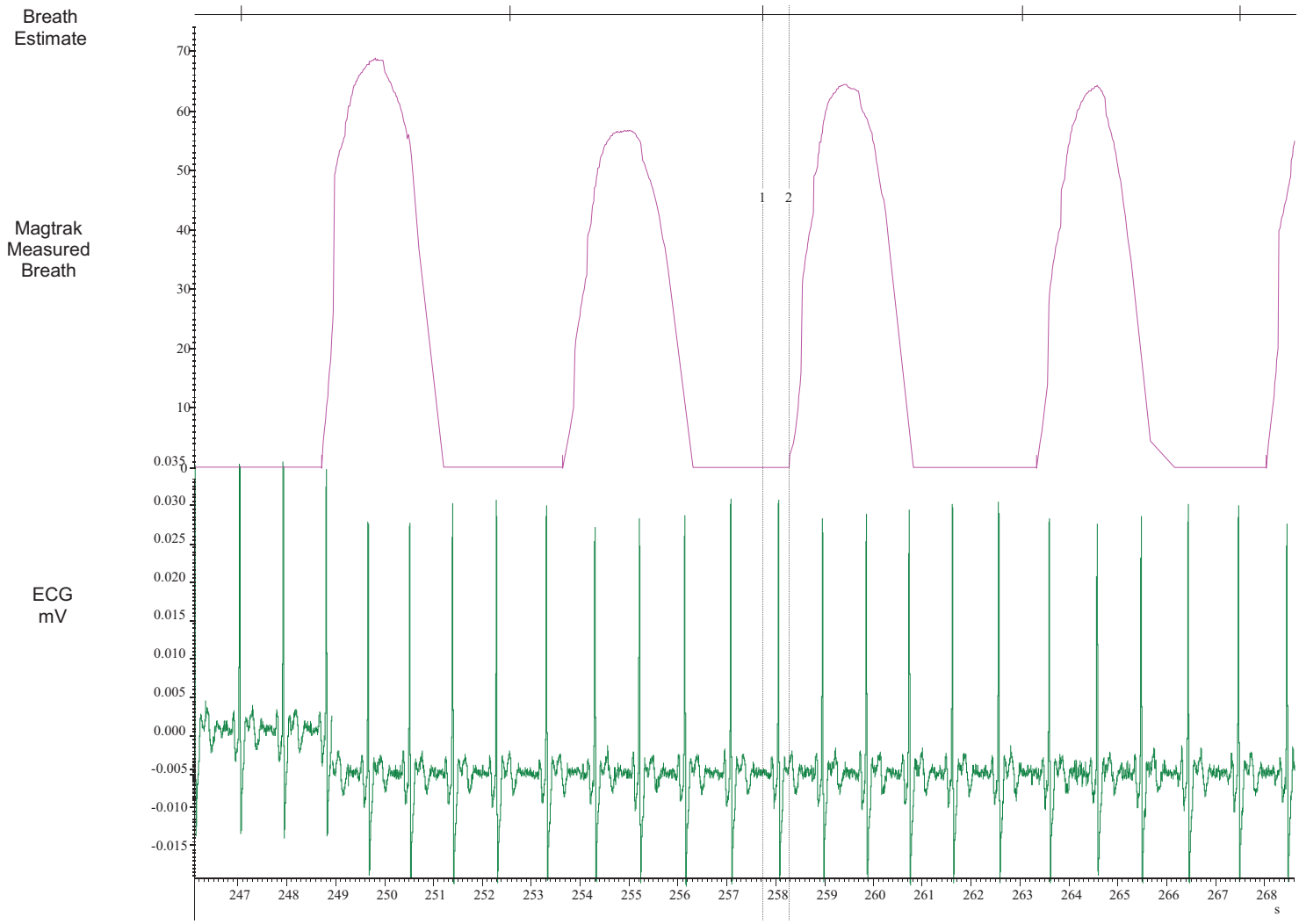

Typical summary plots are shown in figure 5.17. These give estimates of circular dispersion for the first, second, third etc. R-wave in each breath. The length of the mean vector, shown as an arrowed line in the figure, will range from 0 to 1 with a larger value of r suggesting that the observations are clustered more around a mean value than a lower r value.

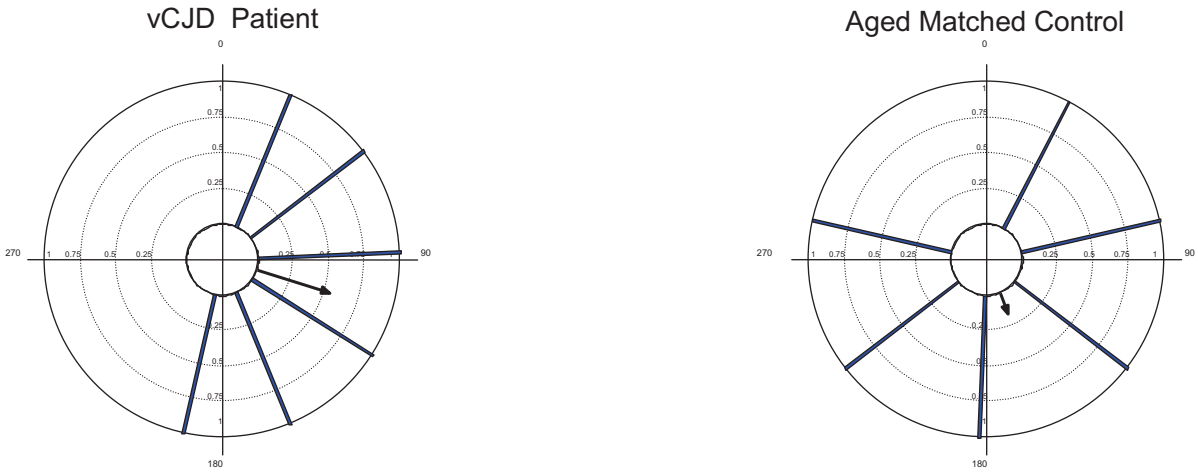

Figure 5. 17 Cartwheel plots.
"Cartwheel" summary plot illustrating the difference in dispersion of the R-waves within each breath for a vCJD patient and the control data used to construct figure 5.11

The summary variables shown in table 5-1 below were calculated by importing the data from the bespoke Spike2 script into the Oriana software package.

	Case2vCJD December	Case2vCJD January	Case2vCJD March	HeartSim Simulator	Control Aged 21	Control Aged 33	Control Aged 45
Mean Vector (μ)	132.892°	128.439°	107.35°	134.894°	158.79°	207.286°	177.258°
Length of Mean Vector (r)	0.31	0.38	0.54	0.31	0.16	0.10	0.17
Median	132.553°	107.378°	124.789°	134.796°	155.925°	144.853°	136.833°
Concentration	0.14	0.40	1.01	0.20	0.00	0.00	0.00
Circular Variance	0.69	0.63	0.46	0.69	0.84	0.90	0.83
Circular Standard Deviation	87.635°	80.219°	63.947°	88.102°	109.01°	122.133°	108.631°

Table 5- 1 Circular statistics illustrating the differences between controls and repeated measures from a vCJD patient.
(based on analysis of summary plots shown in figure 5.11 for 3 measures from one vCJD patient and 3 controls.)

From table 5-1 it can be seen, as expected, the HeartSim data when analysed in the same fashion as the human data, demonstrated little variation in the distribution of R-waves. What is surprising is that in the latter two data files from the vCJD patient, these values of variance were lower than the values from the simulator, perhaps demonstrating the degree of decrement in autonomic function in the patient. The file from the simulator was based upon a human ECG which was electronically manipulated by the manufacturers to provide a base ECG on to which various arrhythmias could be programmed to use for training purposes.

When the circular statistics for each R-wave within the breath epoch are investigated, the concentration values for the vCJD patient are higher than the values from the controls and the HeartSim for the first to fourth R-wave in each breath (see figure 5.18). The concentration values for the vCJD patient then drop below the values obtained from the HeartSim. This illustrates that the values from the vCJD patient display a greater range in the concentration of R-waves within each breath cycle compared to either the controls or data from the HeartSim. The graph also illustrates the greater divergence in concentration values for the vCJD patient compared to controls and HeartSim for the first 3 R-waves of each breath. This suggests the first 3 R-waves of each breath are more grouped for the vCJD patient than controls and implies the R-waves demonstrate less variability than controls for this time period.

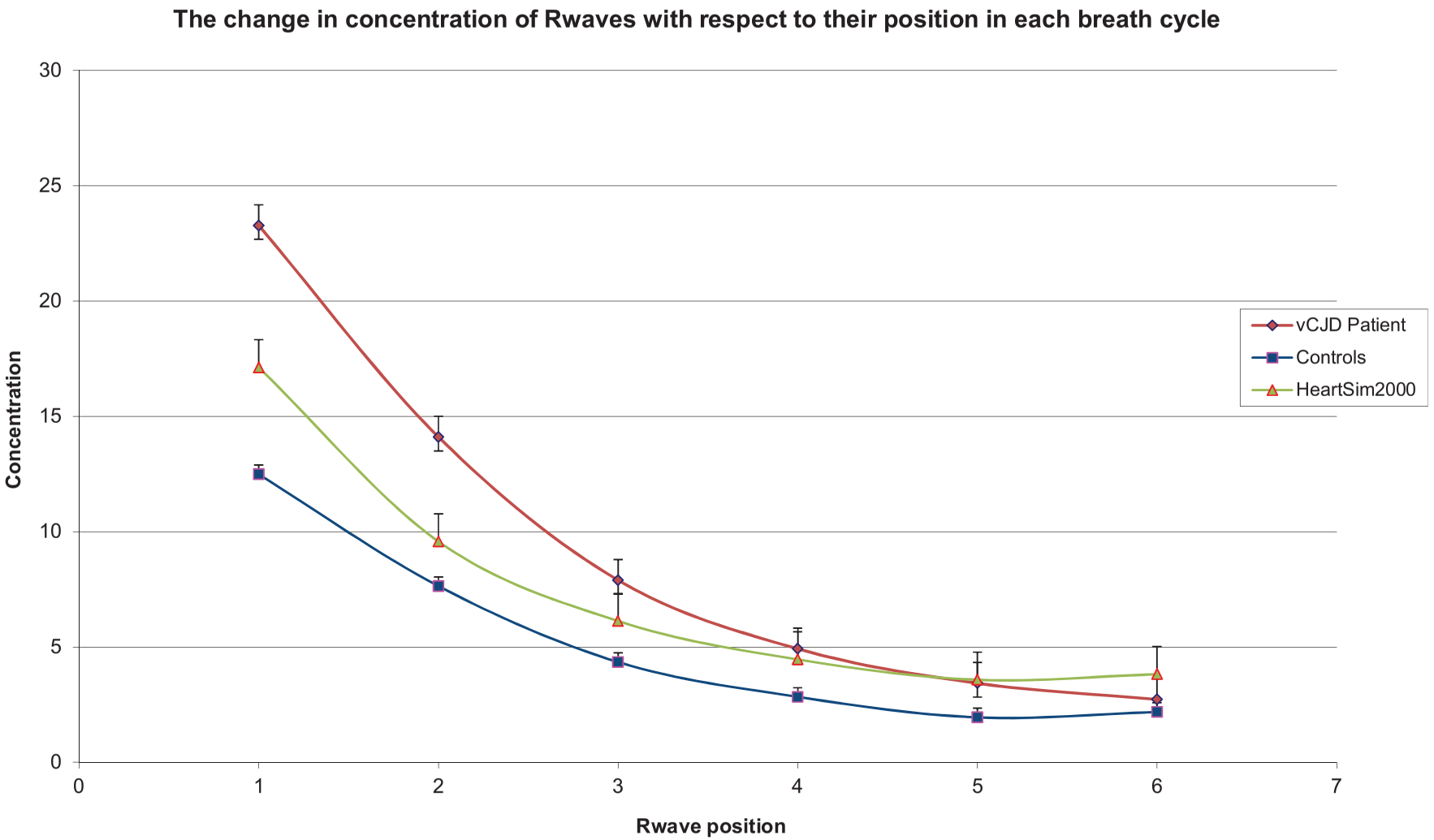

Figure 5. 18 Concentration of R-waves within a breath.

Concentration values are plotted with 98% confidence intervals obtained using charts in Batschelet 1981(Batschelet.1981)

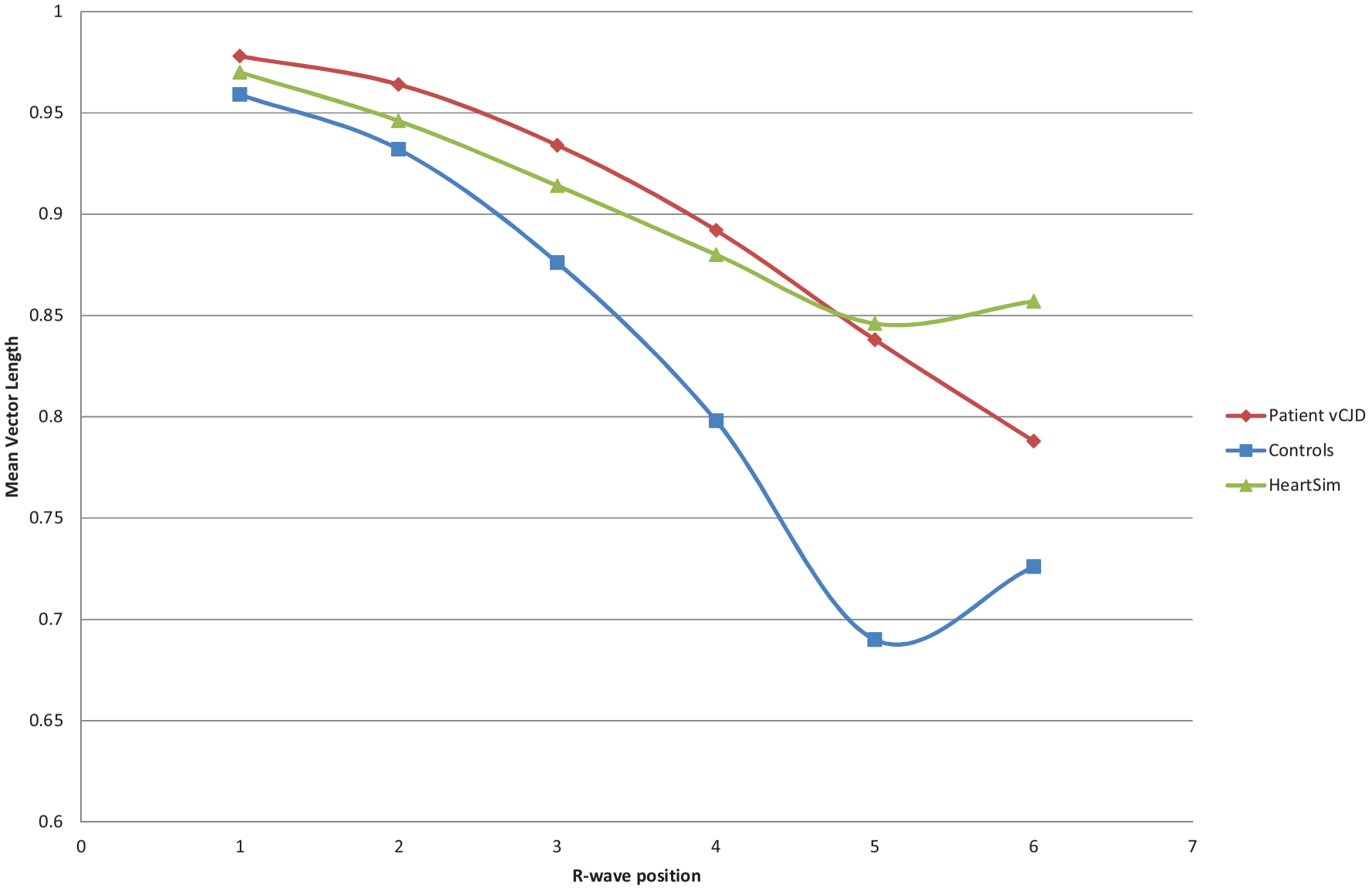

Figure 5. 19 Variation of Mean Vector Length of R-waves within breaths.
Tables of the 95% confidence intervals of the constituent Mean Vectors for these data are given in appendix 1.11.
Significant differences between these data points are given in table 5-2.

Figure 5.19 illustrates the difference in MVL for R-waves within breaths for patients and controls along with the heartsim machine. The Rayleigh test cave significant values for the sample points (see page 187). Table 5-2 shows the results of a Mardia-Watson-Wheeler test (page 187) for significant differences in these values.

	Patient v Control		Control V Heartsim		Patient v Heartsim	
R-wave position	W statistic	p value	W statistic	p value	W statistic	p value
R1	9.033	0.001 *	53.434	2.49E-12 *	60.886	0 *
R2	36.012	1.15E-08 *	23.362	8.45E-06 *	6.563	0.038
R3	73.828	0 *	39.156	3.14E-09 *	7.281	0.027
R4	89.816	0 *	48.609	2.78E-11 *	8.029	0.018
R5	93.057	0 *	51.61	6.12E-12 *	9.388	0.009 *
R6	57.011	0 *	41.456	9.98E-10 *	13.942	9.4E-04 *

Table 5- 2 Results of a Mardia-Watson-Wheeler test between R-wave distributions
The table shows * indicating significant differences ($p<0.05$) following Bonferroni correction between the MVL of patients and controls and controls and patient compared to Heartsim data (A "0" in the table represents a value less than 1.0E-12).

Limitations to this study

Whilst the technique used in this chapter to assess HRV does not benefit from decades of refinement and review as does power spectral and time domain estimates of HRV, the significant differences found using this method of assessing the breath by breath variation in HRV demonstrates the proof of principle.

The rationale for using breath by breath assessment of HRV was involved in trying to address some of the problems inherent in power spectral estimates. Changes in power spectral estimates of HRV are reported to be more applicable to the underlying physiology (Berger, Saul et al.1989). Vagal and sympathetic efferent activity is modulated by respiration and RSA may be considered to involve both branches of the ANS following investigations using transfer function analysis, positional change and selective autonomic blockade (Berger, Saul et al.1989;Saul, Berger et al.1989b;Taylor, Myers et al.2001).

Berger (Berger, Saul et al.1989) reports the work of Sayers (Sayers 1973) and Akselrod (Akselrod, Gordon et al. 1981) who divided the spectral estimates of HRV into bands. HRV regulation occurring at around the 0.1Hz band represents arterial baroreceptor modulation and frequencies above 0.15 Hz represent RSA. Their work also confirmed the role of vagal modulation in the control of RSA and indicated the importance of the sympathetic and angiotensin systems in the lower frequency oscillations of HRV.

It is reported that healthy individuals do not breathe at one set frequency or depth and some breaths may occur below 9 breaths per minute (0.15 Hz) or above 20 breaths per minute (0.33 Hz) (Grossman & Wientjes 1986). These breathing cycles would be outside the typical frequency window of RSA used in spectral estimation of HRV and confound conventional estimates. In attempt to limit these issues paced or controlled breathing has been postulated. However, this also has limitations in extracting information about the underlying physiology involved in the regulations of HRV, with the mental effort involved in the voluntary control of breathing reported to alter the interpretation of the autonomic control of HRV linked to respiration (Berntson, Bigger, Jr. et al.1997).

By using the variable duration of a breath cycle, represented by the circumference of the circle the R-waves are placed on , to investigate changes in HRV may help address some of these issues by focusing on all aspects of the ANS activity with respect to the respiratory cycle. This will include parasympathetic and sympathetic activity occurring in synchrony with respiration to give estimates of HRV constrained by the periodicity of each breath cycle. By overlaying the variability of each R-wave within each breath cycle (visualised as a series of OHP (overhead projector) transparent sheets, each having the R-wave variability per breath on it) a picture of the R-wave variability per breath averaged over a set time can be established. The circumference of the circle for each breath is variable and represents the duration of the breath cycle.

The estimates of breathing cycles used here are not ideal. It would be better to measure the start of each breathing cycle using a transducer of some type to better monitor this physiological trigger used to sub-divide the spectrum of HRV. To some degree the wide limits of agreement found in the estimation process used here (see appendix 1.4) may be influenced by the non-regular breathing frequency and different depths of breathing described above. Further refinement to the method used to estimate breathing events is required or the use of transducers to measure the breathing events directly could be used. As described previously this is difficult in the diseased human and animal populations.

Further consideration to the measured inspiration event compared to the neural initiation of the event may also be needed. From the empirical evidence presented here it was found the mean difference between the measured versus the estimated breath event was the estimated breath occurred 0.52 seconds before the measured breath event with a 95% confidence interval of 0.62-0.42s before the measured breath. This delay between neural activity in the ANS and the start of inspiration is also highlighted in the work of Saul (Saul, Berger et al.1989b). By taking into account this deviation in the start of inspiration it is likely that a different subset of HRV is being assessed compared to assessments made with the unadjusted inspiration marker (see figure in Appendix 1.9 and sections of the discussion).

When we look at the R-R variability within each breath, it can be seen that the time between successive R-waves is sub second. This would imply a frequency band in spectral estimates of HRV >1Hz. Power spectral estimations do not normally investigate this high a frequency band. The technique developed here would focus on this R-R variability within a breath. Consequently it is likely different results would be obtained when power spectral estimates of HRV are compared to HRV measures derived from circular statistical analysis of R-R variability within each breath. Circular statistics is not widely used but using the physiological relevant epoch of breath duration on which to base the division of HRV may have utility and be more discriminating when comparing the diseased human with controls.

Figure 5.20 (below), illustrates the differences in assessments using power spectral analysis and the concentration of R-waves within breath epochs. The second set of histograms indicates that using circular statistics to obtain estimates of the associations of the R-waves within each breath cycle may be better able to demonstrate the sequential change in HRV, shown here as an increasing concentration or a decreasing variability. The same trend of reduced arrhythmia (lower power in the respiratory band of the FFT) is shown in the upper set of histograms. However, when using concentration to investigate the changing autonomic control of the heart, there is a greater range shown for the vCJD patients compared to controls. This association is reversed if power spectral analysis is used (shown as the range in the boxplots of figure 5.21). This may be related to the fact that with power spectral analysis there is no distinct breathing event, a wide range of breathing frequencies (0.15-0.5 Hz) are used. With the circular statistical method the changing beat to beat variability is calculated for each breath and so may give a better representation of the sub second R-R variability linked to respiration.

The "zero" concentration values for the controls in figure 5.20 represent the degree that the distribution of R-waves deviates from a circle. Conversely the higher values for concentration for the patients represent the R-waves follow a von Mises distribution (illustrated in figure 5.12).

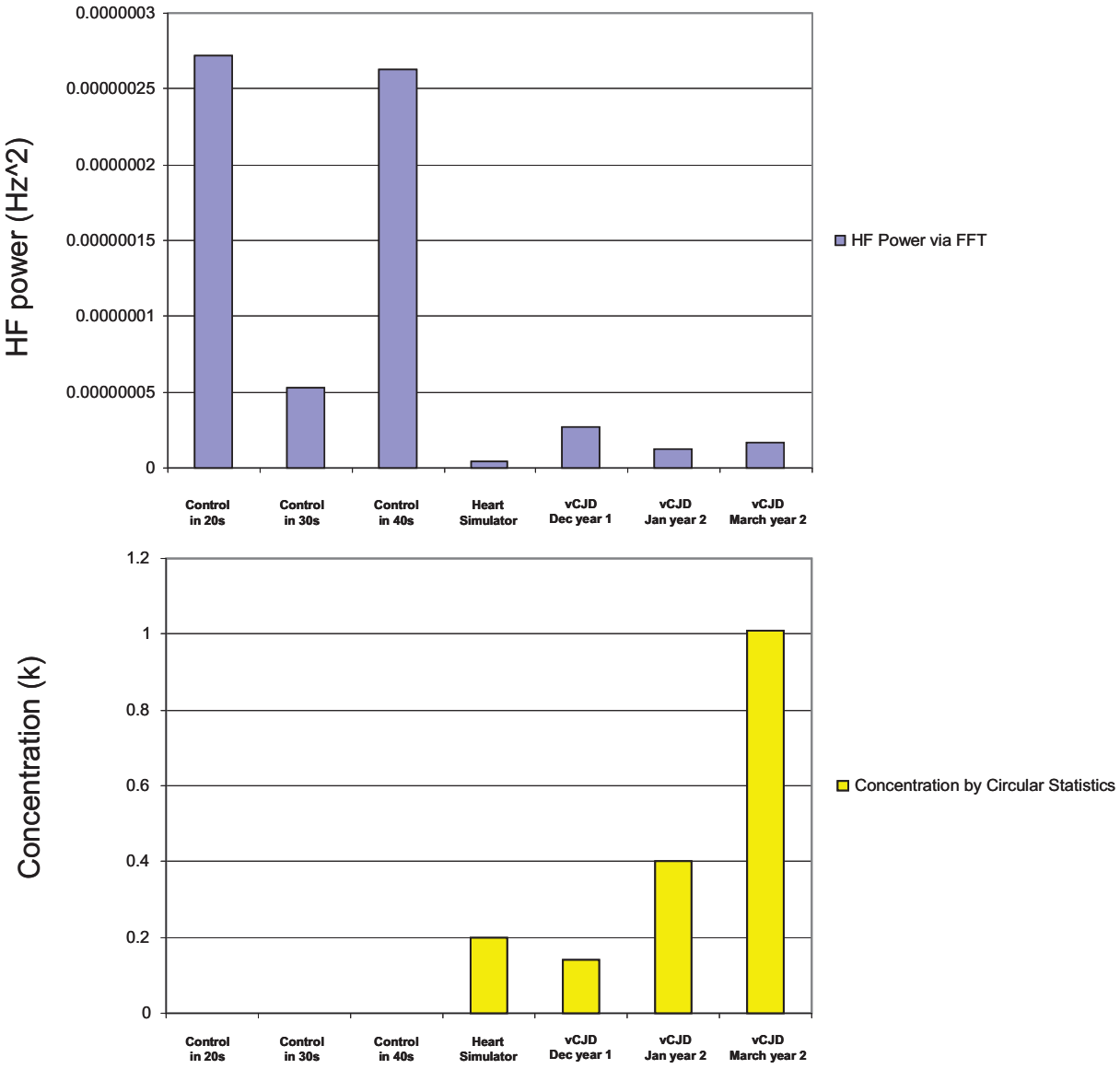

Figure 5. 20 Difference in metrics used to assess HRV.
Histograms indicating differences in metrics used to assess HRV.

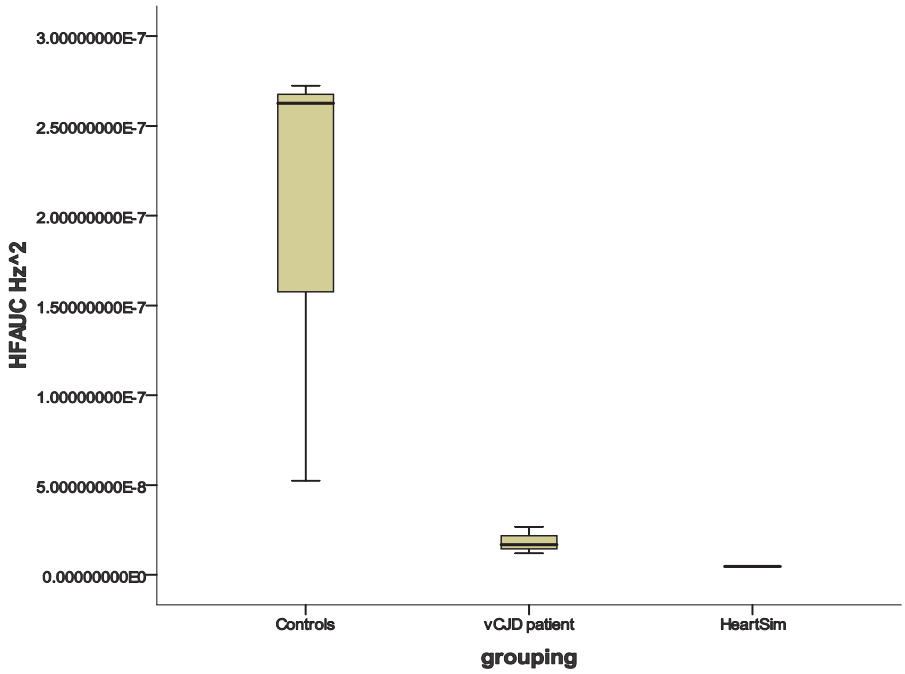

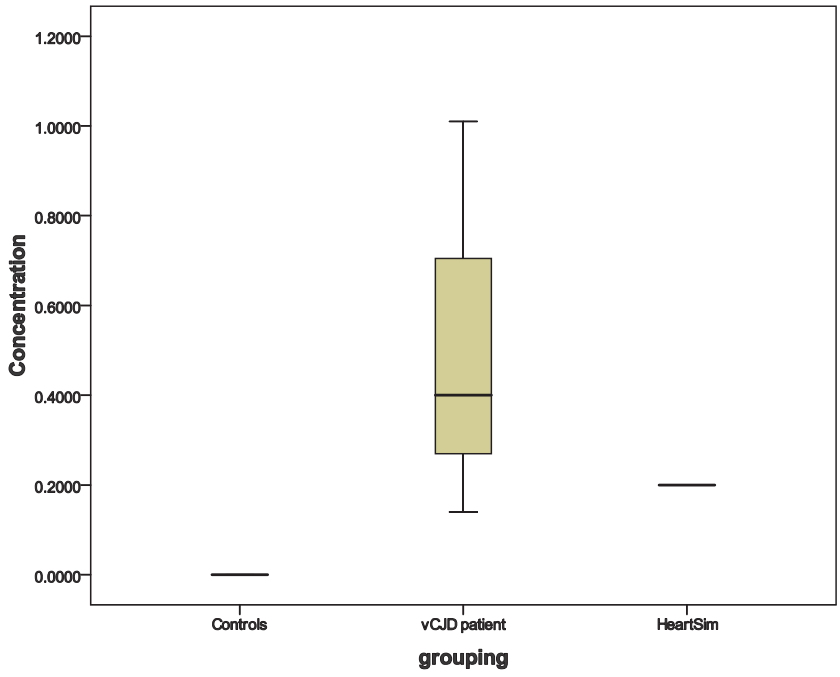

Figure 5. 21 Difference in range of measures obtained from different methods of calculating HRV.

Boxplots illustrating the ranges of measures using two metrics of HRV.

Discussion

The markers shown in figure 5.16 are estimates of breath events that differ from the measured breath events. However, with further thought about the problem, I was trying to assess the neurological control of breathing and its relationship to the neurological control of heart rate. By using a transducer such as the Magtrak and a face mask as used here, there is an offset with respect to time, in the breath event by the time taken for the neural conduction of breathing initiation and the time taken for the muscles involved in the inspiration to contract and finally the diaphragm to move and cause a change in airflow. This sequence will take a finite, but small time. Hence, a difference in the estimated breath event derived from neural information and that derived from mechanical external transducers would be expected.

In studies of the sequence of respiratory muscle activation it is suggested that in awake humans there is a delay between the onset of muscle activation and inspiratory event. From experiments this delay was found to be around 90ms (Strohl, Hensley et al. 1980). In addition to this delay, further offsets from neural initiation of inspiration and the time taken for the inspiratory effort to be measured is indicated by the sequence of activation in other muscle groups associated with normal breathing in humans. Upper airway muscles are stimulated preceding the activation of the diaphragm muscles. It is also reported that these upper airway muscles take around 400ms to reach their peak activity which is well before peak activity of the diaphragm muscles (Patrick, Strohl et al. 1982). Taken together these lines of evidence suggest a delay of around 500ms or half a second from neural initiation of a breath to the inspiration event occurring. To further support the idea of a delay between vagal firing and lung inflation, work by Kollai illustrates that vagal firing occurred between activity in the phrenic nerve with the vagal volley ending approximately 300 ms before the start of phrenic nerve activity (Berne, Levy et al. 1998;Kollai & Koizumi 1979).

Investigations on cardiac coupling during anaesthesia have revealed a peak incidence for the R-wave preceding the breath event (RI-1) and this was found to be 0.5 seconds. The position of this R-wave was found to be the least variable compared to the six R-waves assessed following the breath event (Galletly & Larsen.1997). The authors state that they measured the start of ventilatory timing by a valve in the breathing circuit (absorption system) hence measured the time to airflow change and not the start of neural initiation of the breath. The arrangement and activation of this valve was also stated as causing a small delay in the measured event, although in later publications using the same technique, these authors state the delay is unlikely to affect the conclusions of their study.

However, it may be that the RI-1 R-wave was not the preceding R-wave of the breath but the first R-wave of the current breath cycle. (The neural initiation of the breath actually occurring some 0.5s before). With these observations in mind the results of Galletly et al support the results of this study, namely the first R-wave within each breath was the least variable. If the breath estimates derived here were offset by 0.5 second the R-waves were found to show less association (see Appendix 1.9).

Appendix 1.9 illustrates the difference in a measure from a vCJD patient compared to that measure with breath events altered by 0.5 seconds. The mean vector lengths obtained by using the estimated breath event versus the estimated event time plus 0.5 seconds are shown. In all cases, the mean vector length for all R-wave positions was less when the breath estimate was adjusted. Significant differences ($p<0.05$) between the 3rd, 4th and 5th R-waves are reported from a Mardia-Watson-Wheeler test. This suggests that the R-waves were less clustered around a mean value when the estimate was adjusted and therefore less related to the breath event.

Hence the association of this R-wave to the breath event is critical especially when the quoted times for R-wave occurrence in relation to this breath event are in the hundreds of milliseconds (ms) and the consequences in having an error in the order of 500ms may alter the conclusions. The delay in neural inspiratory activation and the measured airflow change may be important.

RSA is considered to be the beat to beat change in the heart rate modulated by afferent information from lung inflation mediated, often on a sub-second time scale, by changing activities of the vagus nerve. Cardioventilatory coupling (CVC) is considered to be distinct from RSA and is considered to be the modulation of inspiratory timing by afferent haemodynamic information taking place over many seconds. The result of CVC is said to be a temporal synchronisation of heart beats and ventilation.

Whether the observed physiologically-optimized association seen here is the result of each breath being triggered by the heart beat in the preceding breath cycle, as suggested by Galletly is debatable. The time course for the synchronisation of RR intervals to breathing is often on the sub-second time scale and the proposed method for the control of the CVC is postulated to be from changing afferent arterial receptors reflecting haemodynamic change being feedback and integrated by higher brain centres and consequently delivered to the heart independently of the vagus nerve is not compatible with this time scale (arguments supported by Eckberg (Eckberg 2009). CVC therefore, may be considered as a separate phenomenon with a periodicity of 3-5 seconds mediated by the sympathetic branch of the ANS on the SA node (Saul, Berger et al. 1989a) and the size of its effect may depend on the breathing rate (Eckberg 2003). However the observations by Galletly *et al* do suggest a strong concentration of certain R-waves within each breath cycle similarly to the results presented here.

With reference to the diagram formulated from ideas by Armour and others (1983-2003, figure 1.6), the beat to beat associations to ventilatory frequency are likely to be the result of complex, integrated and variable neural communication from both the parasympathetic and sympathetic branches of the ANS as suggested in the work of Taylor (Taylor, Myers et al.2001).

In addition, afferent information from pulmonary stretch receptors have monosynaptic relays to various areas of the NTS (Berger & Averill.1983). This arrangement and integration of neural information allows the sub-second responses that may alter the duration of R-wave intervals in response to changing lung inflation.

The cardiac ganglionated complexes may well be sites which gate the efferent outflow that physiologically optimizes the beat to beat variability and respiratory event to maximise blood passing by the alveoli air sacs to optimise gaseous exchange. This rapid sub-second change in beat to beat variability being under the control of the parasympathetic branch of the ANS and specifically being mediated by the vagus nerve. Consequently, breathing events are inextricably linked to the quick change in beat to beat variability of the heart controlled, principally by the vagus nerve acting on the SA node. Again, the distribution of the heart beats within each breath epoch being governed by the effect of the neural outflow from the intrinsic cardiac ganglia, targeted on the SA node of the heart. It is the presence of these nested neural control loops that may be the site for disruption in beat to beat variability caused by the presence of pathological prion.

This association of R-wave occurrence to breathing events suggests there is a progressive decrease in the variability of the R-waves within each breath in incubating vCJD patients compared to controls. It is suggested that these observations may be due to perturbation in the function of prion infected neurons in the medulla of the infected patient. Recently, it has been shown that components of the auditory evoked potential are disrupted in cattle incubating BSE and it is concluded that brainstem nuclei responsible for the evoked potential are affected by the presence of disease associated prion (Arai *et al.* 2009). Similarly, the abnormally folded prion associated with the disease in humans, located in the brainstem nuclei responsible for the control of the heart on a beat to beat basis, may cause mis-timing in the coordinated control cascade of impulses from the brain to the heart. This would result in perturbation in the physiologically-optimized heart beat and breath coordination. The results from incubating human subjects shown here suggest there is reduced variation in the dispersion of R-waves within each breath cycle compared to controls. This loss of variation reflects the lack of coordinated control in optimizing the heart beat with each breath. This fact is emphasised when the degree of variance is compared to the

“Heartsim” analysed data which represents an artificial heart rate electronically manipulated that has little HRV and consequently little variation in the beat to beat measures within the breath epochs (table 5-1).

In conclusion, this method of analysis may give further insight into the disruption in function of the neurological control of the heart. More conventional metrics of HRV, such as high frequency (HF) power investigations, also demonstrate this progressive decrement in function associated with disease progression for this subject. This trend is echoed in the values for mean vector length and circular variance calculated here. This provides support for the methods used here and basing the analysis on the direct relationship between breath and R-wave distribution may help identify which brainstem nuclei, at which time point in the disease pathogenesis, become infected if recordings could be made early in the disease progression. Putative results from cattle incubating BSE (Pomfrett *et al*. 2004) and sheep incubating scrapie (Glover *et al*. 2007) suggest that measures of HRV are able to identify the diseases in preclinical animals. Consequently this and other HRV analysis may provide a useful screen for transmissible spongiform encephalopathy (TSE) in animals and humans.

Applications for this non-invasive repeated measures method of assessing the development of prion pathogenesis may have utility in giving objective assessment for any putative treatments for prion disease and help manage similar illness. Although the numbers of measures analysed here are limited due to the rarity of vCJD, testing the method on historic data from cows incubating BSE will give support for such analysis. Other applications for this assessment of the decoupling of R-wave with breath event may have utility in assessing the depth of anaesthesia or sedation in “routine” procedures in the hospital environment.

Chapter 6 Applications of heart rate variability linked to respiration

Introduction

Victims of variant Creutzfeldt Jakob disease (vCJD) are few in number. An initial study to investigate heart rate variability (HRV) perturbations in patients was a pilot study for which the recruitment of subjects was expected to be difficult. The recruitment was limited by the number of people alive with the disease at the time of the study (less than 200 in total worldwide had been diagnosed with vCJD at the time of data collection) and their, or their relatives, choice to take part in this research.

I reanalysed historical data for this chapter using a purpose-written program to interrogate the relationship between heart rate variability and breath events. This analysis was not foreseen at the time of the design of the initial study. Consequently, a power calculation based on the data structure used here (specifically breath by breath measures of HRV) was not previously performed.

Heart rate variability is related to heart rate but the relationship may be significantly correlated on occasions (Madanmohan, Prakash, & Bhavanani 2005) or changes in the beat to beat variation of the heart beat may precede changes in the heart rate (Hon & Lee 1963). Since the assessment of HRV using the breath by breath methods developed in chapter 5 is novel, further validation of the expected results would be gained from assessing the relationship between heart rate and the specific metric of HRV that assesses the beat to beat variation of R-waves within each breath cycle. This would emphasise that the heart rate is distinct from the beat to beat variation of R-waves within each breath cycle developed in chapter 5 and the derived HRV is not merely an artefact of changing heart rates.

Following on from the concept that the distribution of the R-waves within each breath cycle could give a measure of HRV, the prospect of the change in distribution being to do with the average heart rate was considered. It is known that when the heart rate increases there can also be an associated increase in breathing rate, thus the length of the breath cycle may be reduced at the same

time the interval between R-waves is also reduced. This may result in a similar distribution of R-waves for a fast beating heart with increased breathing frequency as a slower beating heart and a slower breathing rate, within certain physiological limits.

This association may thus account for changes in heart rate in the analysis of changes in HRV in relation to breathing since the interpretation of HRV is based on a breath by breath cycle. An analogy between the speed of a car (the heart rate) and the revolutions of the engine (HRV) helps illustrate the link between heart rate and HRV. The relationship between the engine speed and engine revolutions, although linked, may change depending on the gear selected between engine and transmission. It is possible for the engine to produce considerably more revolutions for a given speed depending on the gearing. Similarly, HRV may have different magnitudes for a given heart rate.

Research has also demonstrated a change in breath by breath measures of HRV during anaesthesia (Pomfrett, Barrie, & Healy 1993). The areas of the brainstem involved in controlling HRV are those areas that anaesthetic agents act on. The nucleus tractus solitarii (NTS) and nucleus ambiguous (NA) are areas of the brainstem involved in the regulation of the heart on a beat to beat basis. It has been suggested that anaesthetic agents may perturb inhibitory glycine and GABAergic synapses in the NTS and NA (Pomfrett 1999) and GABAergic receptors have been shown to mediate vagal inhibition in the NTS of rats (Wang, Jordan, & Ramage 2010).

Thus, there are putative sites where anaesthesia alters the coordinated neural output of these brainstem nuclei and consequently affect the regulation of the heart on a beat to beat basis consequently altering metrics of HRV. Furthermore, the functional link between the NTS and limbic system may also be affected by the action of anaesthesia on the endogenous peptides located in the hypothalamus which have been reported to affect the control of cardiac rhythm mediated by the vagus nerve (Pokrovsky & Osadchiy 1995).

Regulatory peptides have also been suggested to produce an effect on parasympathetic intrinsic cardiac ganglia located on the heart (Pokrovskii, Osadchii, & Kurzanov 1992) and may serve to condition the local neural

environment to the flow of descending neural information. Prions and neuropeptides both being proteins, have a potential to change their conformation. This change in shape of the protein has consequences on its function. The region of influence for mis-shaped prions may also be at these intrinsic cardiac ganglia, in addition to the central influences in the NA and NTS.

The link between anaesthesia and brainstem nuclei has further been highlighted by images from positron emission tomography (PET) of the human brain during anaesthesia. These images demonstrate an association between the right NTS and concentration of anaesthetic agent (Pomfrett & Alkire.1999) and consequently suggest the anatomical location for the change in functional synapses causing a change in beat to beat regulation of the heart, resultant from anaesthesia. PrP^{c} has been demonstrated as a requirement for the proper function of hippocampal neurons due to its relationship to GABA mediated neurotransmission (Rangel, Madroal et al. 2009). Early research into prion and synaptic function suggested that $GABA_{(A)}$ mediated synaptic function was impaired in PrP null mice (Collinge, Whittington et al.1994).

It has been suggested that the presence of PrP^{D} may interact directly with GABA mediated neural transmission in scrapie infected hamsters (Lu, Sturman, & Bolton 1995). It is likely that the GABA system in other brain regions would be affected by the presence of disease associated prion.

GABA receptors in the NTS that mediate vagal inhibition, shown to be affected by anaesthesia (Wang, Jordan et al.2010), could also be the sites of disruption in the homeostatic neural coordination of the heart seen in prion disease (Glover, Pollard et al.2007;Pomfrett, Glover et al.2004;Woolfson, Glover et al. 2003). Thus the presence of prion has the potential to affect GABA mediated synapses similarly to the action of anaesthetic agents. The extent and signature of the effects may be different. However, both have the potential to disturb the normal function of such synapses that could result in a perturbation in the neural output with a consequent change in the action on the target organs. Specifically, the GABA-mediated synaptic coordination of neurons of the NTS, affected by anaesthesia, could also be the sites of change in the control of the heart on a beat to beat basis observed as a result of prion infection.

A recent publication has demonstrated that an observed cardiac dysfunction in the early stages of Parkinson's disease is due to the parasympathetic branch of the ANS and not the sympathetic branch (Buob, Winter et al.2010). This echoes the ideas expressed here in that early dysfunction in cardiac regulation, due to change in parasympathetic activity, may be a clue to burgeoning gross neurological disease. Other research has also described a change in parasympathetic functions that appears concurrent with sympathetic denervation (Shibata, Morita et al.2009). This difference in the findings of Buob and Shibata may be due to Parkinson's disease patients being studied at different stages of the disease progression. The difference in balance between the two branches of the autonomic nervous system showing different relationships at different times of the diseases course. This would echo the observations and suggestions made in this thesis of changing autonomic balance in prion diseases. Suggestions about prion and Parkinson's disease have also been mooted. It was stated that the accumulation of the aggregated mutant proteins responsible for the disease (one of which is α-synuclein) are first seen in the dorsal motor nucleus of the lower brainstem and frequently detected in plexi of the autonomic nervous system associated with the gastrointestinal tract in preclinical cases of Parkinson's disease (Olanow & Prusiner.2009). Consequently, parallels between cardiac dysfunction in vCJD and Parkinson's disease can be drawn and early changes to the control of the heart on a beat to beat basis may be a common but subtle observation in the progression of both of these neurological diseases.

The aims of this chapter are to validate the algorithm developed in chapter 5. By inspection of the results comparing changes in HRV between vCJD patients and healthy controls, R-wave variability between successive R-waves in a breath are compared for differences. The effect of heart rate on this measure of HRV is investigated and the algorithm is applied to patients undergoing anaesthesia to see if the changes in HRV are as reported in the literature.

METHODS: Considerations involved in the application of HRV linked to respiration

Methods 1: Assessment of ability to distinguish R-wave distributions within a breath

Using the data from chapter 5, derived from R-waves within each breath epoch, and looking at the change in the angular direction of the resultant vector from circular statistical analysis, it was noted that the 5th R-wave in the breath cycle was at the point in the breath cycle that demonstrated a turning point in the pattern of mean vector length (figure 5.19).

The mean angular vector for each of the R-waves equates to the time the R-wave occurs from the start of the breath event. The circle, in the circular statistical analysis, represents the duration of the breath cycle. An average breath cycle from these data suggests this to be around six seconds (50 breaths in a 300 second sampling window equates to an average breath duration of 300/50=6 seconds). Consequently, using the data from the summary circular statistics performed on data from chapter 5 (shown in table 6-2) we can calculate that for the 5th R-wave having a mean vector angle of 246 degrees for control data and a mean vector angle of 183 degrees for patients, the 5th R-wave in controls occurs at around 4.10 seconds after the breath and for patients this value is 3.06 seconds. (given by equations 1 and 2 below)

For controls time of 246/360 x 6000 ms = 4100 ms Equation 1

For patients time of 183/360 x 6000 ms = 3055 ms Equation 2

The next stage of the investigation would be to use a greater number of breath epochs to see if the distinction still held up. Since the number of vCJD patients involved in the initial study was small (n=4), all of the data was included and a similar number of data files from controls was also analysed in the same manner.

Around 900 breath epochs from 17 vCJD measures from 4 patients and 900 breath epochs from 19 measures from 19 controls were analysed to see if the association in the distribution of R-waves within the breath epoch still demonstrated the differences previously seen. The 300 second samples of ECG, from both controls and vCJD patients, contained around 50 breath cycles in each 300 second sample. Consequently 17 samples each of 300 seconds gave 850 breath cycles to analyse (17 x 50 =850). Similarly around 950 breath cycles from control subjects were used (19 x 50 =950).
The controls for this investigation were screened for abnormal blood pressure and BMI and did not take any medication thought to affect heart rate variability. These assessments were overviewed by a small team of health care professional which was a mix of clinical scientists, nurses and consultant anaesthetists. The mean heart rate for the controls was 67.9 beats per minute and that of vCJD patients was 84.2 beats per minute.

Methods 2: Investigating the effects of heart rate on distribution of R-waves within each breath

A question still remained as to extent the distribution of the R-wave events was linked to heart rate. The average R-wave events in each breath for controls and patients were calculated (see table 6-1) and found to be 6.5 and 7.8 for controls and patients respectively. Thus, increased heart rate resulted in around one extra R-wave event in each breath cycle for the patient data compared to control data.

Table 6- 1 Number of R-waves and breaths for control and patient data.

	Control (17 measures)		Patient (19 measures)
R-wave count	326.9		381.4
Breath count	50.3		48.9
R-waves per breath	6.5		7.8

Thus there are approximately 7 and 8 R-waves within each breath cycle for controls and patients respectively. This average was derived from around 900 breath cycles from 17 patient and 19 control files of 300 seconds of ECG.

Further differences between the control and patient data become apparent if the measured distributions of R-waves for each group are compared to a model distribution for each group derived from the average number of beats per breath cycle. Separate models of R-wave distributions were constructed for patient and control data. The duration of the breath represented the circumference of the circle for the model. The standard positions of 7 and 8 R-waves for patients and controls was calculated by allowing for a typical offset of 20 degrees, to represent the average delay of the first R-wave following the breath and then dividing the remaining angular space of the circumference (360-20 degrees) into equal segments (for controls this was 340/7=48.5 degrees and for patients 340/8=42.5 degrees). The rest of the circle, corresponding to the remaining breath epoch, then had a R-wave placed at these standard angular intervals as listed in the table below (table 6-9).

To investigate the extent the distribution of R-waves within each breath cycle was associated to the heart rate (HR), the mean vector length (MVL) and mean vector angle (MVA) were inspected. A scatter plot of MVL and MVA for controls and patients was plotted to illustrate the relationship between these indices of HRV and HR. A one sample Kolmogorov-Smirnov test, to test for normality, was performed on the values of MVL and MVA using SPSS v 16, followed by the

calculation of the correlation coefficients. These correlation coefficients were then compared using the " Fishers Z transformation " method as detailed in Gardner (Gardner & Altman 1989). This transformation results in the calculation of the 95% confidence intervals for the correlation coefficients. A statistical test between the correlation coefficients was also performed (Preacher 2002).

Example of the method of Z transformation of the correlation coefficient to obtain 95% confidence intervals.

If the correlation coefficient is r= 0.638, Z is given by:

$$Z = \frac{1}{2}\log_e \frac{1+r}{1-r}$$

$$Z = \frac{1}{2}\log_e \frac{1+0.638}{1-0.638}$$

$$Z = 0.5081$$

$z_1 = 0.5081 - \frac{1.96}{\sqrt{17}}$ and $z_2 = 0.5081 + \frac{1.96}{\sqrt{17}}$

$z_1 = 0.0327$ and $z_2 = 0.9835$

The values of z_1 and z_2 need to be transformed back to the original scale to give the confidence interval for the correlation coefficient. This is given by:

$\frac{e^{2z1}-1}{e^{2z1}+1}$ to $\frac{e^{2z2}-1}{e^{2z2}+1}$

0.0327 to 0.7546

So the correlation coefficient for r is given by
r = 0.638 with a 95% confidence interval of 0.0327 to 0.7546.

Methods 3: Using the effect of anaesthesia on HRV during each breath cycle and comparing to prion disease

To investigate the theory that a change in the control of the heart on a beat to beat basis may be observed in anaesthesia as well as prion diseases, the same analysis techniques used previously in this chapter were performed on data from patients undergoing anaesthesia. Data was analysed by comparing the distribution of R-waves within each breath cycle before and during anaesthesia.

Around 400 breaths from 10 patients were analysed using the same technique of applying the purpose written script to 300 seconds of ECG data previously described in chapter 4. This historic data was obtained as part of another study carried out in 2000 to 2002 to investigate Delta Sleep Inducing Peptide (DSIP) (Pomfrett, Dolling et al. 2009) and data was obtained following written informed consent and approval of the protocol by the Central Manchester local ethics committee. The data chosen for the analysis performed in this chapter was from control subjects of the DSIP trial to exclude any effects from the administered pharmacology that was part of the investigation. All files were from female ASA 1 or ASA 2 patients undergoing minor elective surgery and received routine anaesthesia for surgery. The ASA (American Society of Anesthesiologists) scale is a classification system used to assess individual's physical fitness before surgery. It has six categories ranging from ASA 1 to ASA 6, with ASA 1 representing normal healthy patients with no organic, physiologic, or psychiatric disturbance. Healthy with good exercise tolerance. ASA 2 patients are classed as having mild systemic disease but no functional limitations and have well-controlled disease of one body system for example, controlled hypertension or diabetes without systemic effects.

Similarly, data for patients undergoing procedural sedation for endoscopic investigations was obtained as part of a previous study. Sedation was achieved by administration of midazolam. Data was recorded for a baseline measure before the procedure for at least five minutes, during the procedure and for at least five minutes following the procedure in recovery. Data was collected in accordance with a protocol approved by the central Manchester local research ethics committee.

Results

Results 1: Assessment of ability to distinguish each R-wave within a breath

Summary statistics for 5th R-wave	Control	Patient
Number of Observations	141	144
Mean Vector (μ)	246.013°	183.283°
Length of Mean Vector (r)	0.69	0.838
Median	240.921°	185.13°
Concentration	1.945	3.427
Circular Variance	0.31	0.162
Circular Standard Deviation	49.375°	34.014°
Standard Error of Mean	4.165°	2.817°
95% Confidence Interval (-/+) for μ	237.847°	177.761°
	254.179°	188.805°
99% Confidence Interval (-/+) for μ	235.281°	176.026°
	256.744°	190.54°

Table 6- 2 Summary statistics for the 5th R-wave in around 140 breaths from Controls and vCJD patients.
This is from the same data tabulated in table 5-1. It represents data from 3 controls compared against 3 measures from one vCJD patient over time.

Some statisticians suggest it may be more useful to quote the confidence intervals (CI) for the mean after data has been collected rather than calculate the power of the study (Swinscow & Campbell 2002). In addition any results of a power calculation would be confounded by the difficulty in recruitment of vCJD patients and the number of these patients alive at any one time. Consequently the sample size would be dictated by the availability of vCJD subjects. By considering the confidence intervals (CI), we may say that, with a 99% chance of being correct, that the CI range includes the population mean. For this data the values of the mean vector angle for the 5th R-wave and ranges are given by:

Control mean is 246.013 with 99% CI of the mean is 235.281°to 256.744°

Patient mean is 183.283 with 99% CI of the mean is 176.026°to 190.54°

By observation of the values in table 6-2, derived from around 140 constituent R-waves, it may be seen that the 5th R-wave for controls shows less concentration and shows greater circular variance than the data from vCJD patients. It may also be seen that the mean vector angle for the 5th R-wave differs by around 60 degrees.

Table 6-3 shows the differences between the mean vector angles for the first 6 R-waves within a breath (obtained from analysis of the data in chapter 5, tabulated in table 5-1, analysed in the same manner as the analysis for the 5th R-wave). These values are based upon the mean values from all the data. The mean vector angle equates to the mean position of the R-wave in an average breath cycle.

R-wave position	R1	R2	R3	R4	R5	R6
Patient Mean Vector (μ) (degrees)	21.12	61.663	102.196	142.774	183.283	223.233
Estimated time after breath of R-wave (s)	0.352	1.028	1.703	2.379	3.055	3.721
Control Mean Vector (μ) (degrees)	26.744	81.944	137.164	191.807	246.013	282.692
Estimated time after breath of R-wave (s)	0.446	1.366	2.286	3.197	4.100	4.711

Table 6- 3 Mean vector angles and associated time estimates of R-wave events within a breath cycle.

By inspection of the values in table 6-3, we can see that each R-wave is separated by at least 0.5 second from R-waves on either side of it. Hence a difference of 30 degrees in the mean vector angle equates to a time difference of 0.5s (30/360 x breath epoch, 6s). Thus using 30 degree displacement in the mean vector angle of the 5th R-wave suggests that it should not be confused with adjacent R-waves.

Table 6-4 illustrates a difference in the position of the 5th R-wave within each breath cycle exists between more vCJD patient data compared to controls (using around 900 breaths from controls and patients).

Table 6- 4 Statistics from all the 5th R-waves to compare with table 5-1.

Variable	Angles	Angles
Subgroup	Control	patient
Number of Observations (breath epochs)	890	870
Mean Vector (μ)	236.773°	197.342°
Length of Mean Vector (r)	0.720	0.766
Median	234.468°	195.368°
Concentration	2.141	2.499
Circular Variance	0.280	0.234
Circular Standard Deviation	46.393°	41.872°
Standard Error of Mean	1.547°	1.404°
95% Confidence Interval (-/+) for μ	233.740°	194.589°
	239.805°	200.095°
99% Confidence Interval (-/+) for μ	232.788°	193.724°
	240.757°	200.96°
Kuiper's Test (von Mises, V)	1.807	1.425
Kuiper's Test (p)	< 0.05	> 0.15

This table shows greater clustering of R-waves for patient data for the 5th R-wave. The 5th R-wave from control data demonstrates a greater variance and less concentration around its mean position. The trend for these data is the same as that seen when around 140 breath cycles for each group were averaged.

A Kuiper's test for a von Mises distribution compares the measured data to a theoretical distribution equating to a normal linear distribution (von Mises distribution for circular statistics is the equivalent of a normal distribution in linear statistics). The large value of V and significant p value for the control data suggests that the null hypothesis is rejected. Hence, the test distribution does not fit a von Mises distribution. Conversely this statistic also suggests the R-waves for patients do fit a von Mises distribution. There is a statistically different distribution in the 5th R-wave within a breath between controls and vCJD patients. This is illustrated in figure 6.1.

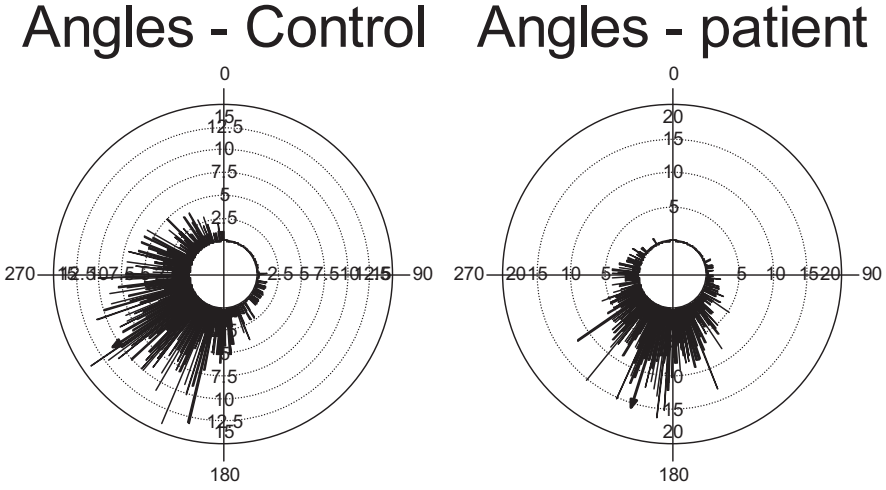

Figure 6. 1 Distributions of constituent R-waves for controls and patients. Scale denotes number of R-waves. Arrowed lines denote mean vector angle and length. The number of R-waves within each bin is represented by the amplitude of each ring.

Figure 6.1 illustrates the distribution of around 900 R-waves that contribute to the mean vector length and angle data in table 6-2. Note the difference in shape of the circular distributions for controls and patients (not a von Mises distribution and a von Mises distribution for controls and patients respectively. von Mises distributions are depicted in figure 5.12).

When all of the R-wave positions are compared in a similar fashion, the results are summarized in table 6-5 and 6-6 and graphically displayed in figure 6.2. Figure 6.3 represents the summary distributions of these R-waves along with the summary statistics for the cart wheel plots of figure 6.3, shown in table 6-7. The change in circular variance between successive R-waves for control and vCJD patient data is shown in figure 6.4.

Controls						
Mean HR 67.875						
R-wave position	1	2	3	4	5	6
Number of Observations	899	899	899	899	890	779
Mean Vector (μ)	26.273°	80.075°	133.350°	185.664°	236.773°	278.328°
Length of Mean Vector (r)	0.961	0.931	0.876	0.801	0.720	0.733
Median	25.605°	78.85°	131.675°	183.814°	234.468°	278.412°
Concentration	12.631	7.562	4.341	2.869	2.143	2.226
Circular Variance	0.040	0.069	0.124	0.199	0.282	0.267
Circular Standard Deviation	16.462°	21.609°	29.458°	38.213°	46.393°	45.198°
Standard Error of Mean	0.549°	0.723°	0.980°	1.261°	1.547°	1.607°
95% Confidence Interval (-/+) for μ	25.197°	78.663°	131.429°	183.192°	233.740°	275.177°
	27.349°	81.486°	135.271°	188.135°	239.805°	281.479°
99% Confidence Interval (-/+) for μ	24.859°	78.219°	130.826°	182.415°	232.788°	274.187°
	27.687°	81.932°	135.874°	188.912°	240.757°	282.469°
Kuiper's Test (von Mises, V)	3.404	1.704	1.528	1.767	1.807	1.895
Kuiper's Test (p)	< 0.01	0.10 > p > 0.05	> 0.15	< 0.05	< 0.05	< 0.025

Table 6- 5 Circular statistics for 6 R-waves from control data

vCJD Patients						
Mean HR 84.206						
R-wave position	1	2	3	4	5	6
Number of Observations	873	873	873	873	870	861
Mean Vector (μ)	21.261°	65.499°	109.551°	153.516°	197.342°	240.661°
Length of Mean Vector (r)	0.971	0.946	0.900	0.836	0.766	0.694
Median	19.802°	62.878°	107.847°	151.889°	195.368°	238.977°
Concentration	17.671	9.601	5.279	3.389	2.499	1.971
Circular Variance	0.029	0.054	0.100	0.164	0.234	0.306
Circular Standard Deviation	13.832°	19.018°	26.336°	34.262°	41.872°	48.956°
Standard Error of Mean	0.468°	0.643°	0.89°	1.152°	1.404°	1.669°
95% Confidence Interval (-/+) for μ	20.342°	64.238°	107.807°	151.258°	194.589°	237.389°
	22.178°	66.76°	111.296°	155.774°	200.095°	243.934°
99% Confidence Interval (-/+) for μ	20.054°	63.842°	107.259°	150.548°	193.724°	236.361°
	22.466°	67.156°	111.844°	156.483°	200.96°	244.962°
Kuiper's Test (von Mises, V)	3.769	2.752	2.025	1.505	1.425	1.338
Kuiper's Test (p)	< 0.01	< 0.01	< 0.01	> 0.15	> 0.15	> 0.15

Table 6- 6 Circular statistics for 6 R-waves from patient data.

Figure 6. 2 Circular representations of the constituent R-waves contributing to the summary data presented in table 6-7.

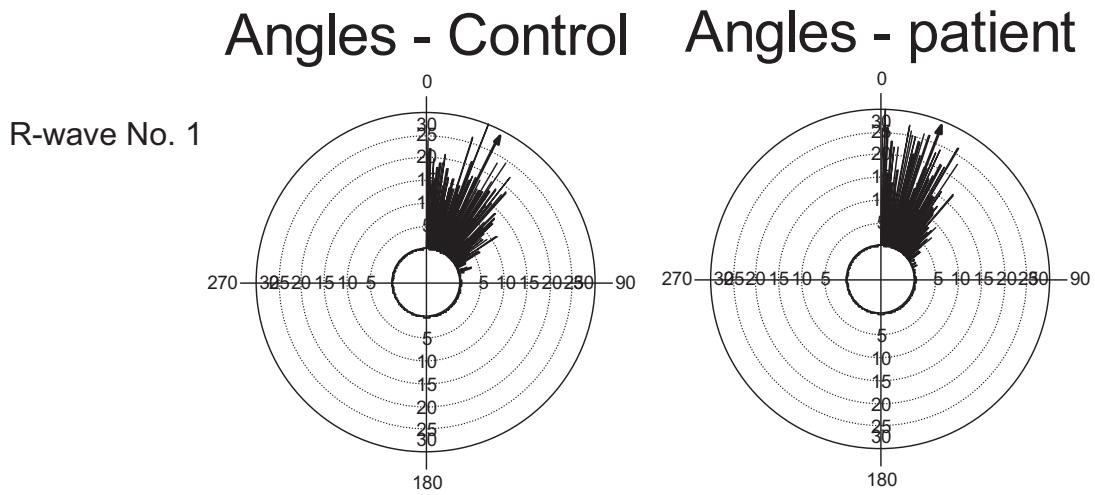

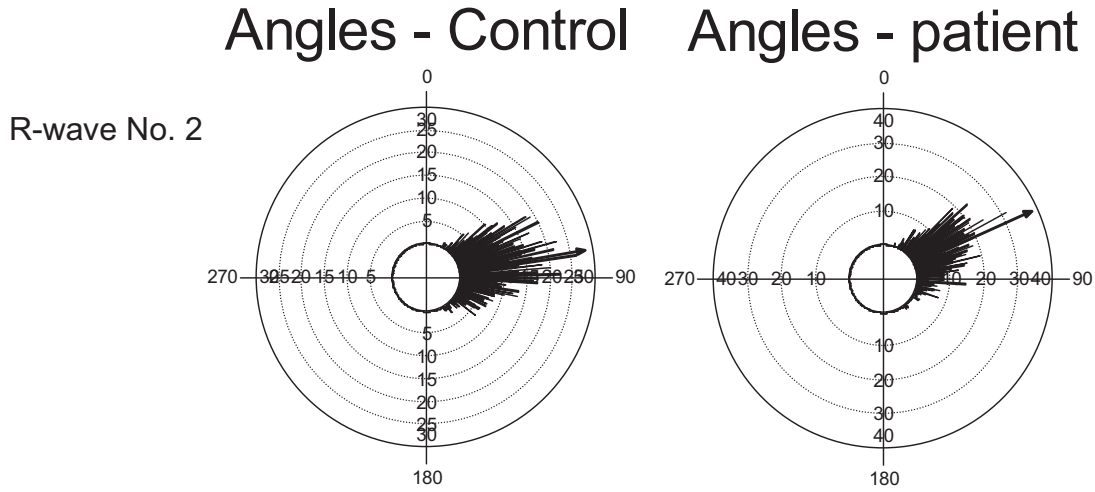

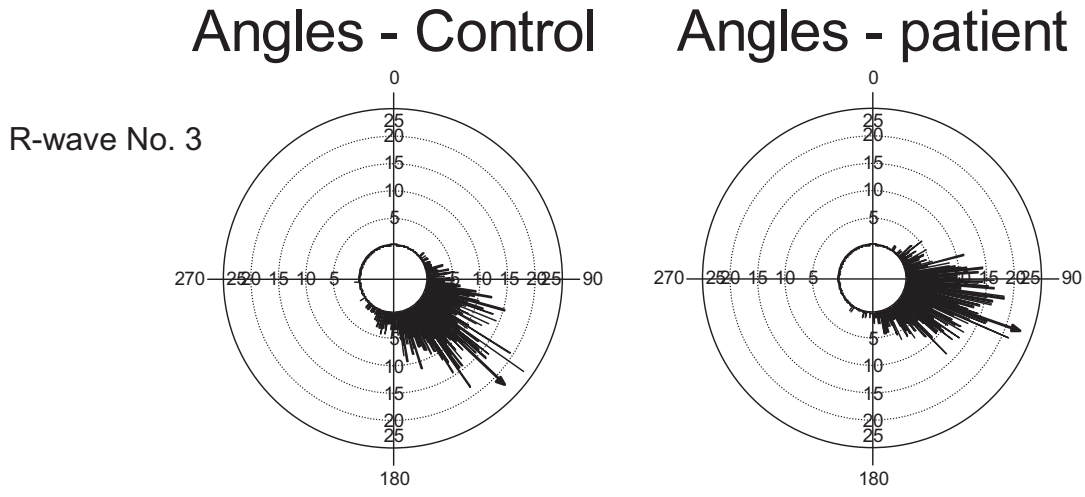

Figure 6.2 continued.

R-wave No. 4

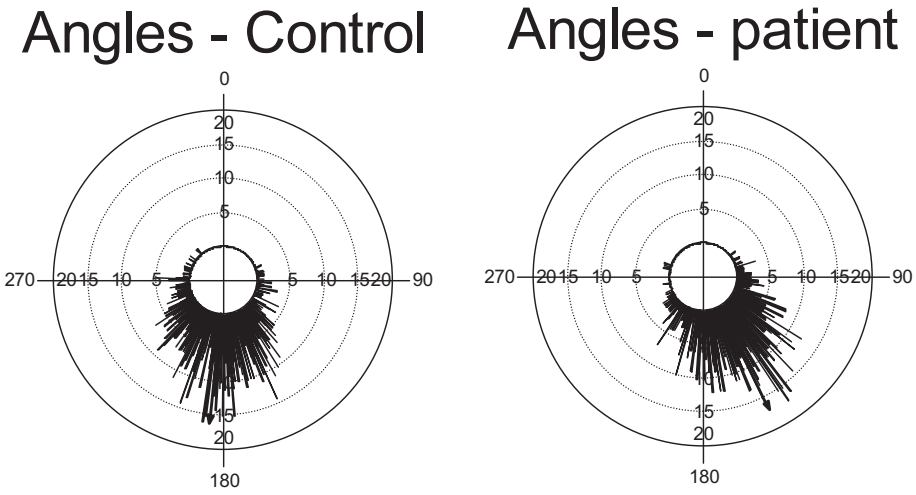

R-wave No. 5

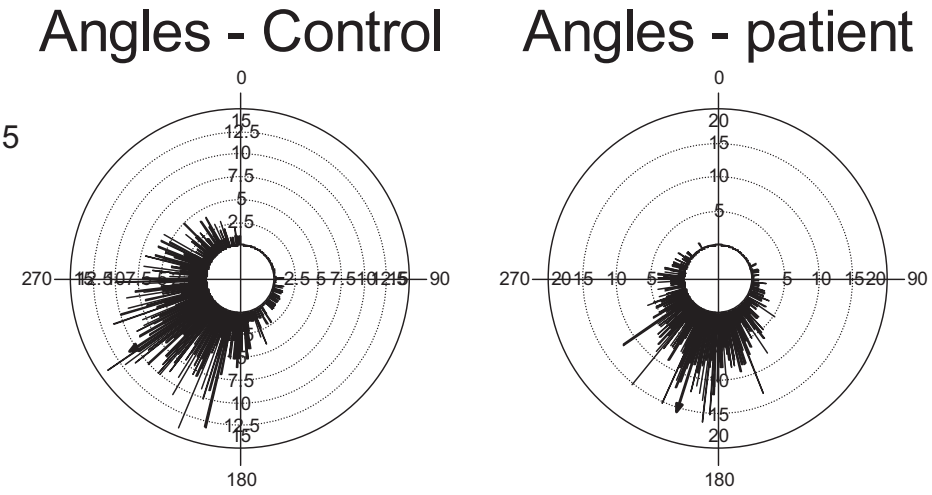

R-wave No. 6

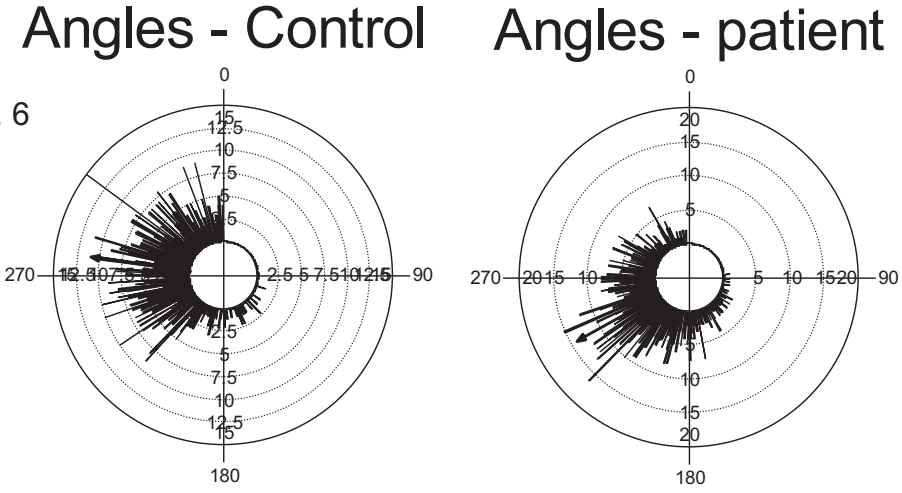

Figure 6. 3 Summary of approximately 900 R-waves for each R-wave position for patient and control data.
The raw distributions of these R-waves are shown in figure 6.2 and the data is tabulated in tables 6-5 and 6-6.
The summary indicates the difference in the distributions of all the R-waves indicated by the arrowed lines which have different direction and length (summarized in table 6-7)

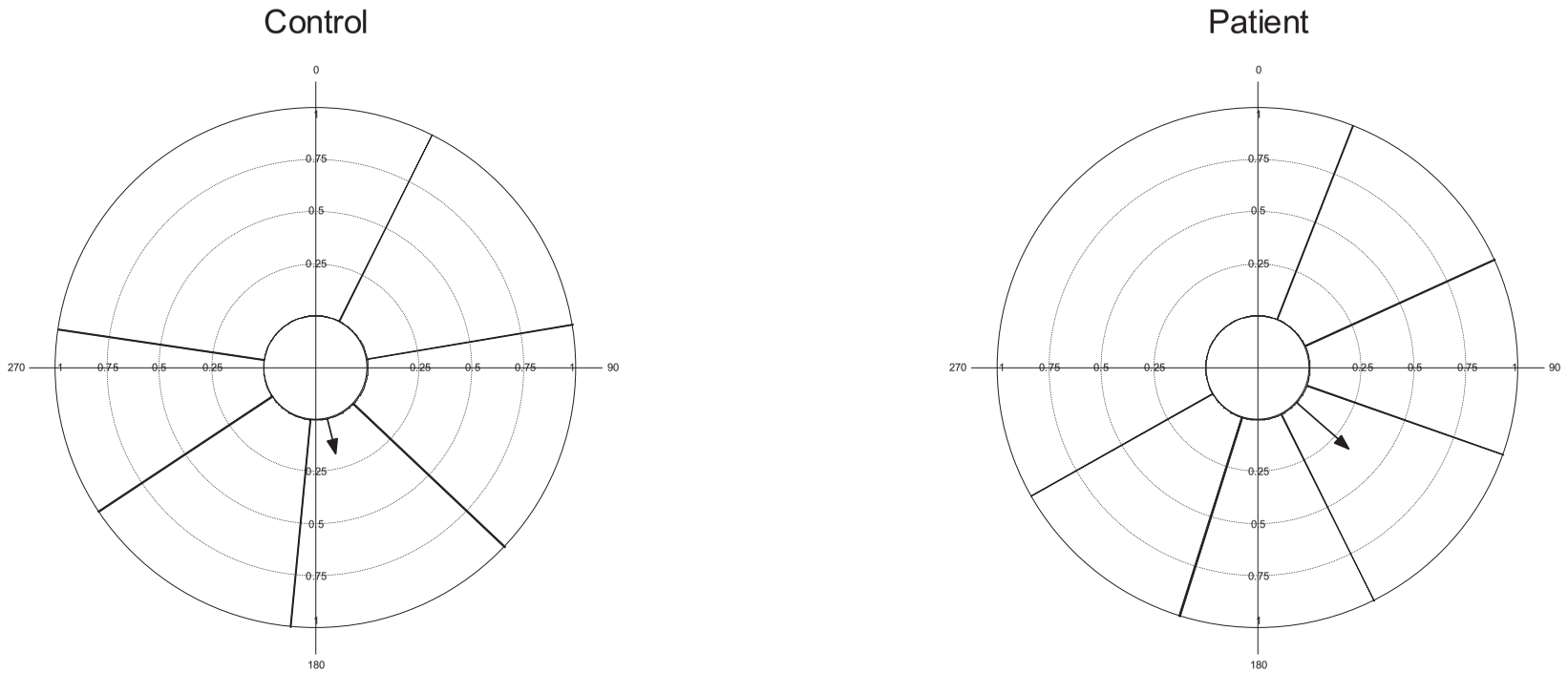

Variable	Control	Patient
Number of Observations	6	6
Mean Vector (μ)	167.226°	131.682°
Length of Mean Vector (r)	0.174	0.333
Median	185.66°	131.535°
Concentration	0	0.233
Circular Variance	0.826	0.667
Circular Standard Deviation	107.225°	84.999°

Table 6- 7 Summary statistics for Cartwheel plots of figure 6.3.

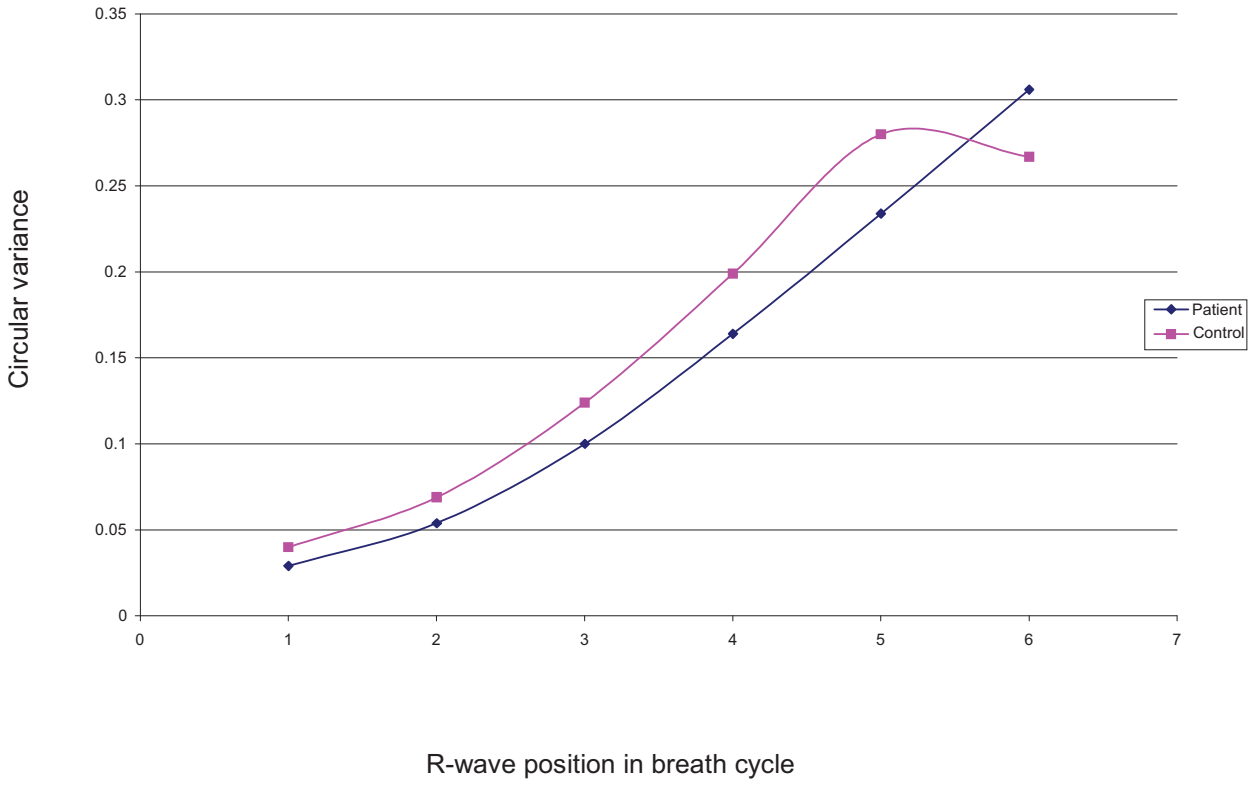

Figure 6. 4 Plot of Circular Variance against R-wave position for control and vCJD patient data.

Circular variance is given by 1-r, where r is the mean vector length. Table 6-8 gives the results of the Mardia-Watson-Wheeler tests for differences in the distributions of the R-waves for controls and patients for the data in figure 6.4. Significant differences between patient and control data were found for all R-wave positions (based on around 900 R waves at each R wave position). A zero indicates a p value less than 1.0E-12.

This distinction in R wave distributions between controls and vCJD patients is supported by the discrete 99% CI of the mean vector in tables 6-5 and 6-6.

R-Wave Position	W statistic	P value
R1	31.601	1.37E-07
R2	111.657	0
R3	179.123	0
R4	182.409	0
R5	179.767	0
R6	137.153	0

Table 6- 8 To show significant differences between control and patient data

Results 2: Investigating the effects of heart rate on distribution of R-waves within each breath

The investigation of the effects of heart rate on this measure of HRV described in the methods section resulted in the following models of R-wave distributions for controls and patients.

Table 6- 9 Values for model R-wave distributions for patients and controls.

R-Wave Position in breath cycle	Model Control R-waves (Deg)	Model Patient R-waves (Deg)
R1	20	20
R2	68.5	62.5
R3	117	105
R4	165.5	147.5
R5	214	190
R6	262.5	232.5

The circular representation of the model R-wave distributions are shown in figure 6.5 and compared to the measured R-wave distribution within each breath in figure 6.6. It may be seen that the model distribution is a better fit to the measured distribution from patient data than control data. The model data is derived from a simple mathematical progression for the R-waves. From table 6-10 and figure 6.6 the variation in the R-wave incidence within each breath is less and closer to the model distribution for patient data than for control data. This suggested the simple invariant model represented the patient's data better than the control data.

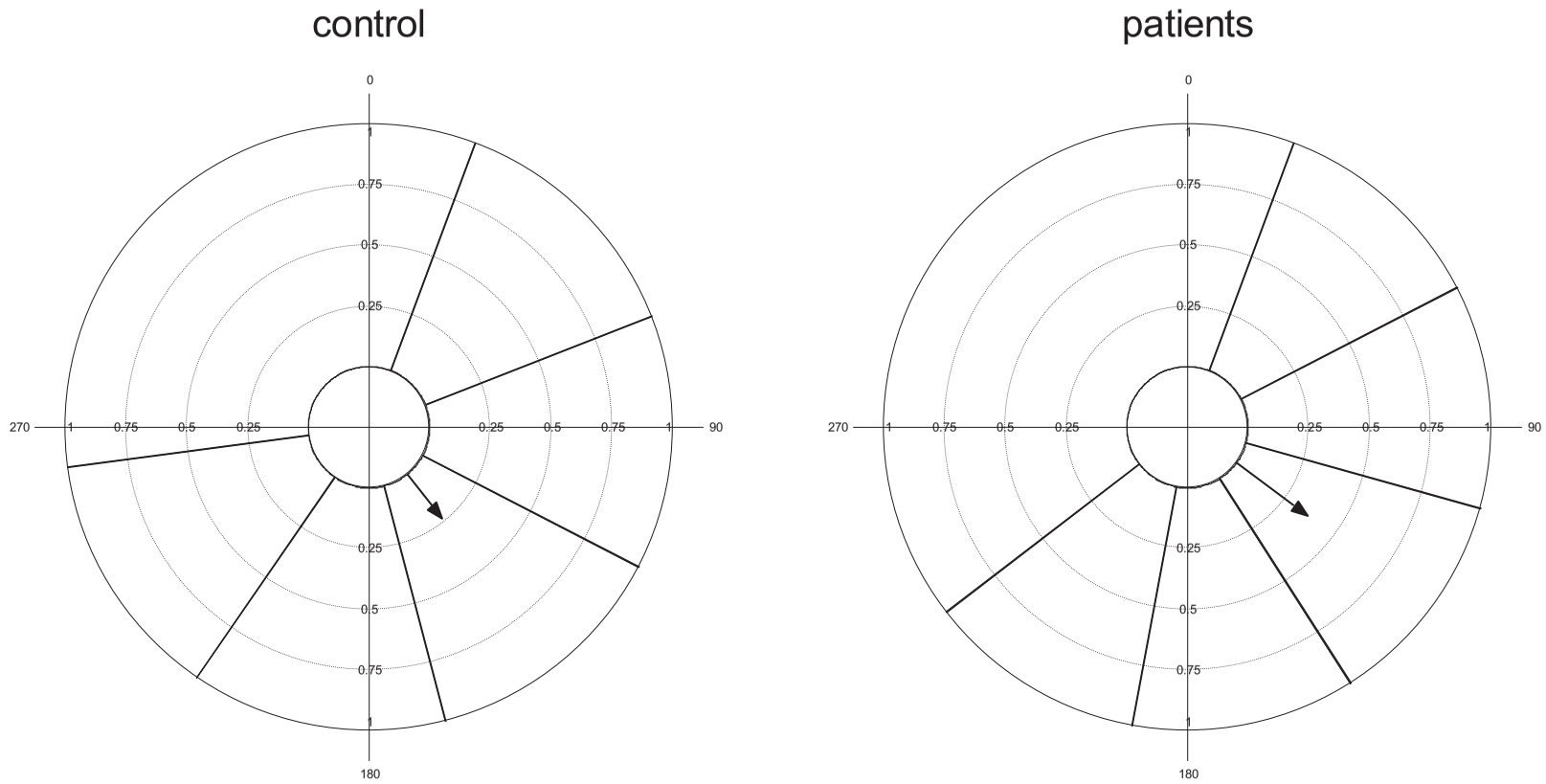

Figure 6. 5 Vector plot of model distributions of R-waves.

Vector plot of model distributions of R-waves within a breath epoch for controls and patients based on average number of heart beats per breath (first 6 R-waves shown in each model

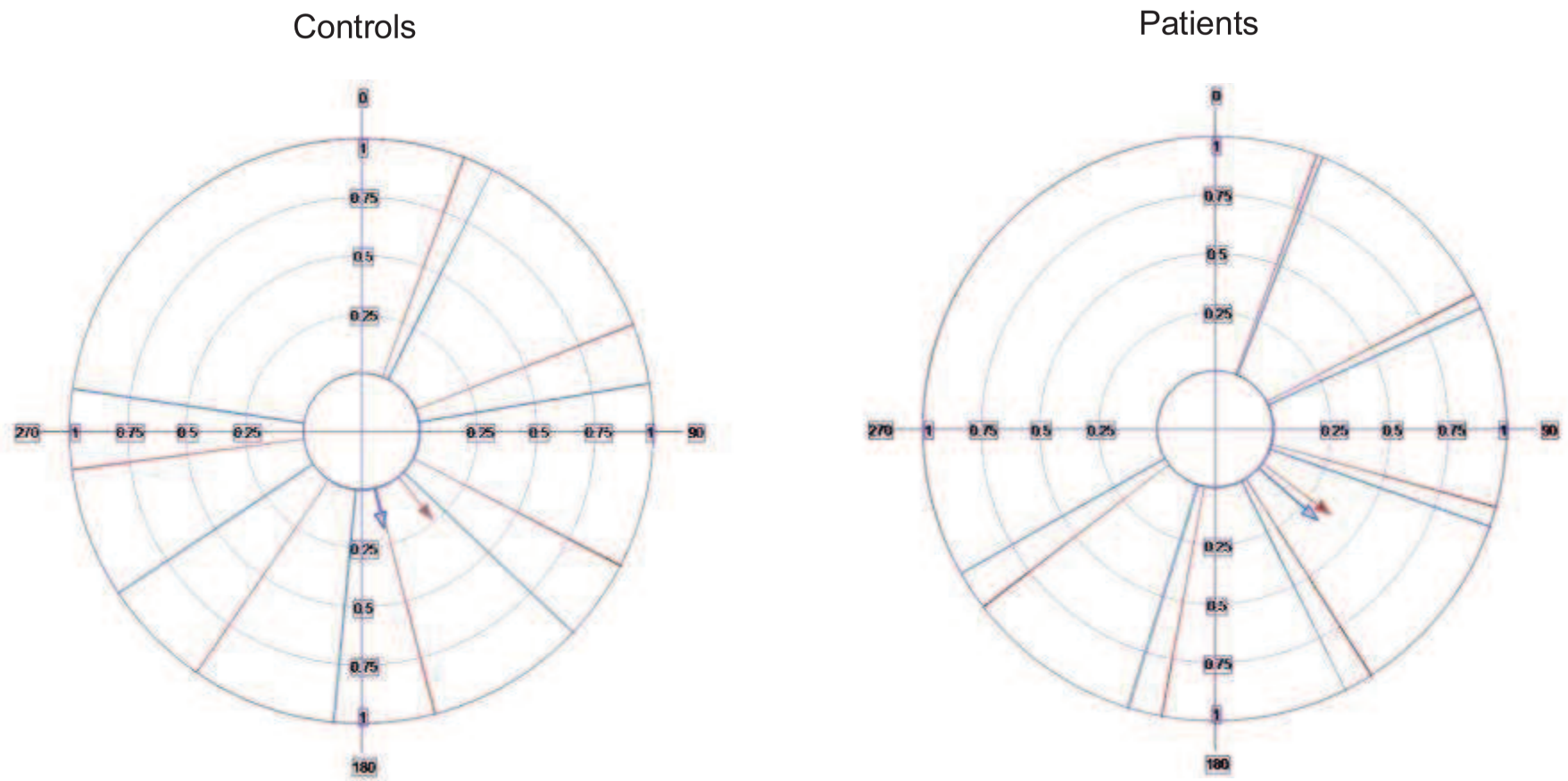

Figure 6. 6 Vector plot of model and measured distribution of R-waves.

Vector plot of model distributions of R-waves (RED) overlaid with measured distribution of R-waves (BLUE) within a breath epoch for controls and patients. Summary circular statistics for these distributions are in Table 6-10

Circular Statistics for Model data		
Variable	control	patients
Number of Observations	6	6
Data Grouped?	No	No
Mean Vector (μ)	**141.25°**	**126.25°**
Length of Mean Vector (r)	**0.23**	**0.365**
Median	141.25°	126.25°
Concentration	**0**	**0.358**
Circular Variance	**0.77**	**0.635**
Circular Standard Deviation	98.254°	81.366°
Standard Error of Mean	*****	64.707°
95% Confidence Interval (-/+) for μ	*****	359.399°
	*****	253.101°
99% Confidence Interval (-/+) for μ	*****	319.553°
	*****	292.947°
Circular Statistics for Measured data		
Variable	Control	Patient
Number of Observations	6	6
Data Grouped?	No	No
Mean Vector (μ)	**167.226°**	**131.682°**
Length of Mean Vector (r)	**0.174**	**0.333**
Median	185.66°	131.535°
Concentration	**0**	**0.233**
Circular Variance	**0.826**	**0.667**
Circular Standard Deviation	107.225°	84.999°
Standard Error of Mean	*****	83.938°
95% Confidence Interval (-/+) for μ	*****	327.13°
	*****	296.235°
99% Confidence Interval (-/+) for μ	*****	275.441°
	*****	347.924°

***** indicates that a result could not be calculated

Table 6- 10 Control and patient summary circular statistics for measured and model values.
From data in figure 6.6

The differences in the R-wave positions for the model and measured distributions are shown in figure 6.8. The differences are shown as boxplots in figure 6.7. The control data displays a greater median value for the differences and a larger range in the differences than for the patient data set. Conversely, the patient data displays a smaller median difference between measured and model incidence and a smaller range of differences. This helps to illustrate the simple mathematical model fits the measured values for the R-wave distributions for patients.
The relationship between the mean vector length (MVL) and mean vector angle (MVA) and heart rate are shown in figure 6.9. (MVL and MVA variables (dependent) against heart rate (independent)) Correlation coefficients were calculated in SPSS and are tabulated in table 6-12. Tables 6-13 and 6-14 show the relationship between these correlation coefficients.

Figure 6. 7 Differences between measured R-wave position and model R-wave position.

Boxplot to show differences between measured R-wave position and model R-wave position for controls and patients. Note there is less deviation from the model R-wave positions in patients compared to controls.

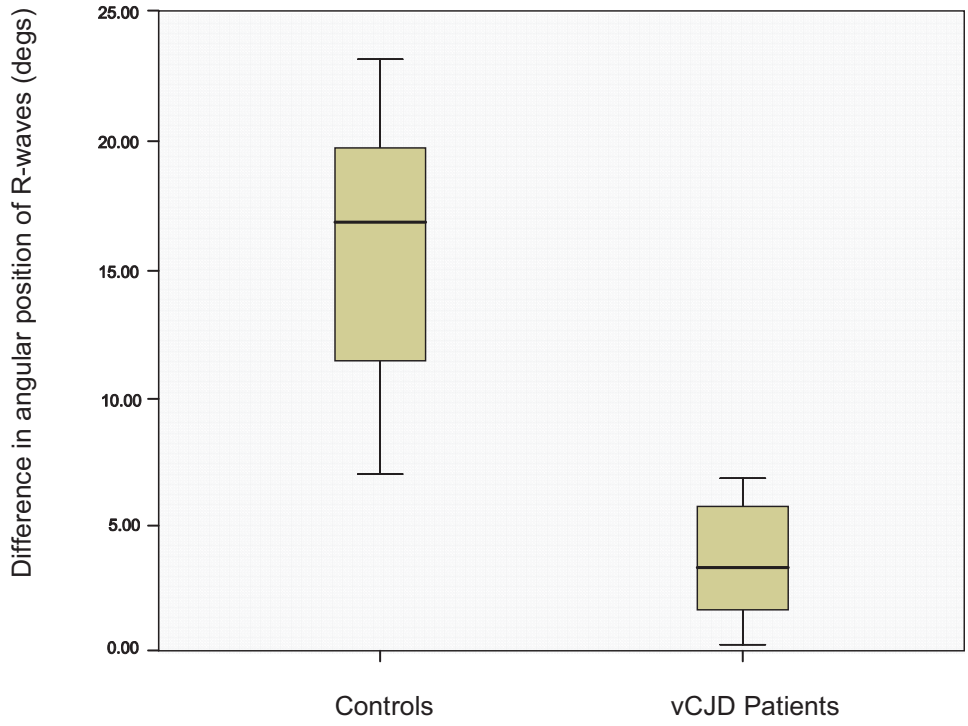

The spacings between the different parts of the box in the boxplot help indicate the degree of dispersion and skewness in the data. The box is defined by the first and third quartile and the "whiskers" illustrate the range. The median is illustrated as the line between these two bounds.

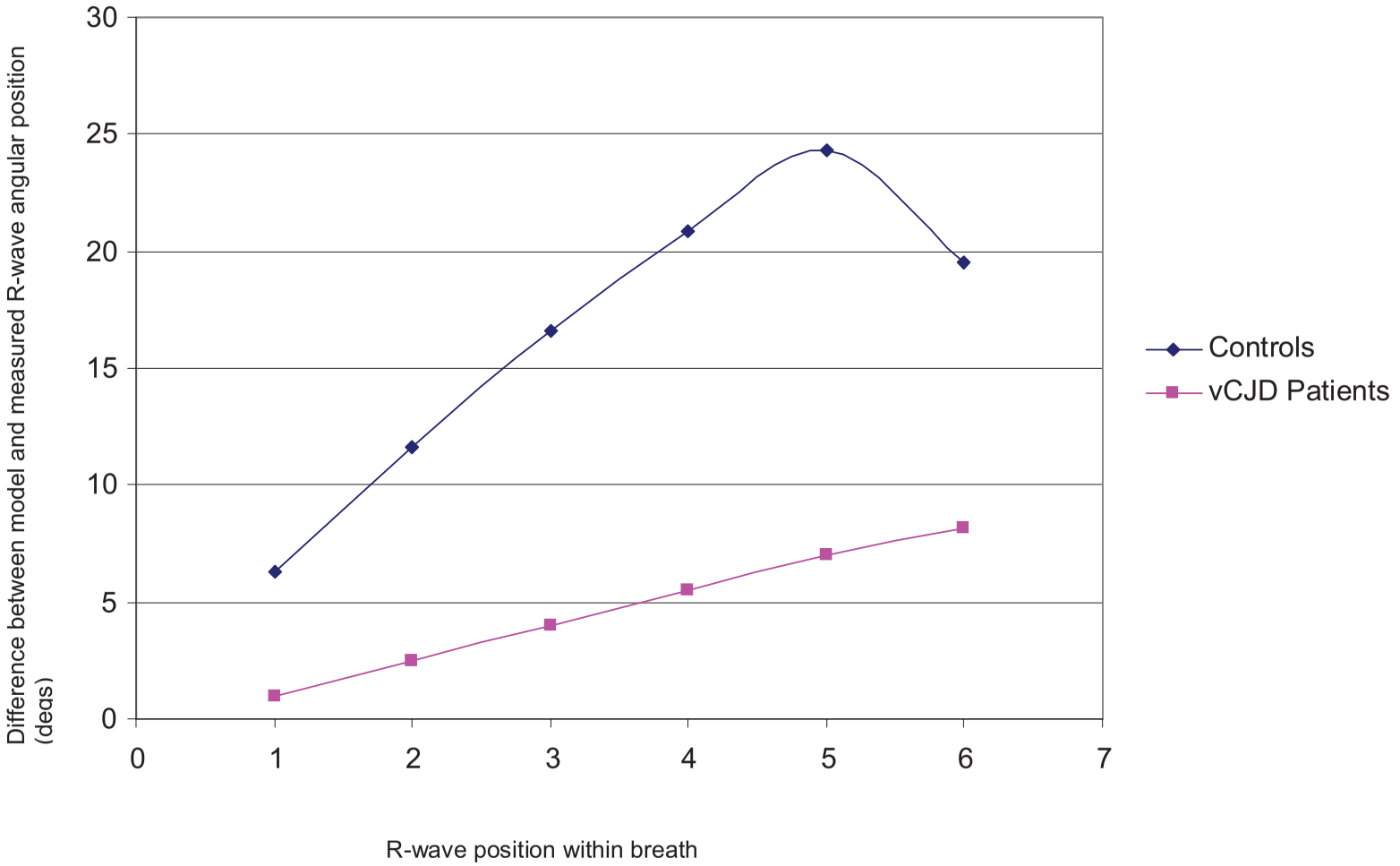

Figure 6. 8 Plot of differences between measured and model R-wave positions.
Note controls have greater and increased rate of change (higher value and steeper incline) in deviations than do patients.

Table 6- 11 Table of statistics for the distributions of the differences in R-wave position for measured and model values.

Descriptive Statistics

	N	Range	Minimum	Maximum	Mean		Std. Deviation	Variance	Skewness		Kurtosis	
	Statistic	Statistic	Statistic	Statistic	Statistic	Std. Error	Statistic	Statistic	Statistic	Std. Error	Statistic	Std. Error
Control Difference	6	18.01	6.28	24.29	16.5308	2.69117	6.59199	43.454	-.648	.845	-.436	1.741
Patient Difference	6	7.23	.98	8.21	4.7008	1.11688	2.73577	7.484	-.097	.845	-1.315	1.741

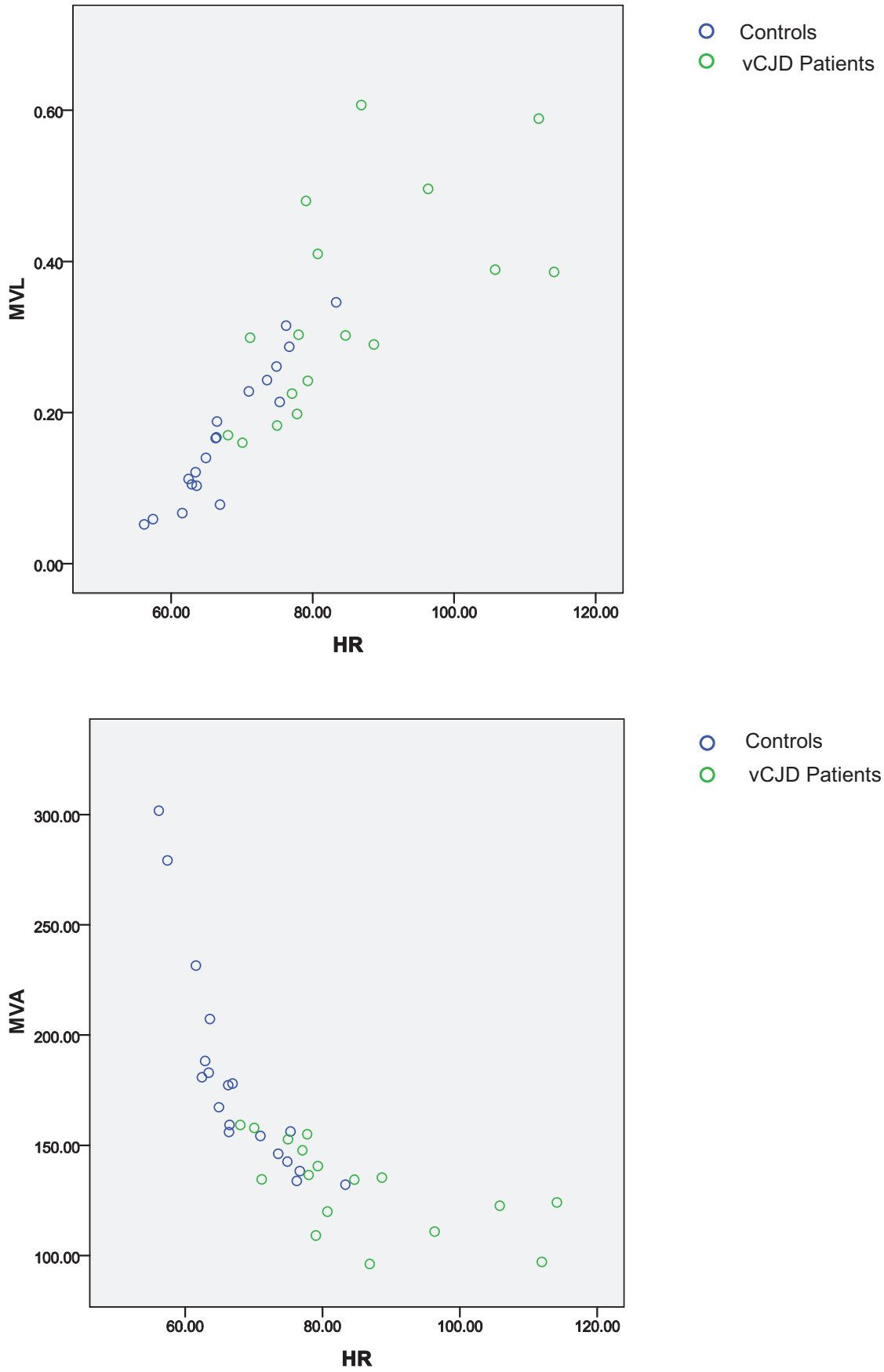

Figure 6. 9 The relationship between the MVL and MVA and heart rate.

Table 6- 12 Table of correlation coefficients for MVL and MVA variables (dependent) against heart rate (independent)

Controls

Correlations

		HR	MVL	MVA
HR	Pearson Correlation	1.000	.948**	-.838**
	Sig. (2-tailed)		.000	.000
	N	19	19	19
MVL	Pearson Correlation	.948**	1.000	-.812**
	Sig. (2-tailed)	.000		.000
	N	19	19	19
MVA	Pearson Correlation	-.838**	-.812**	1.000
	Sig. (2-tailed)	.000	.000	
	N	19	19	19

**. Correlation is significant at the 0.01 level (2-tailed).

Patients

Correlations

		HR	MVL	MVA
HR	Pearson Correlation	1.000	.638**	-.643**
	Sig. (2-tailed)		.006	.005
	N	17	17	17
MVL	Pearson Correlation	.638**	1.000	-.993**
	Sig. (2-tailed)	.006		.000
	N	17	17	17
MVA	Pearson Correlation	-.643**	-.993**	1.000
	Sig. (2-tailed)	.005	.000	
	N	17	17	17

**. Correlation is significant at the 0.01 level (2-tailed)

N represents the number of data files analysed for controls and vCJD patients.

Table 6- 13 Table of 95 % confidence intervals for correlation coefficients for MVL and MVA variables (dependent) against heart rate (independent)

MVL is mean vector length, MVA is mean vector angle and HR is heart rate.

Description of Correlation	Correlation Coefficient	Lower interval	Upper interval
Control HR vs MVL	0.948	0.877	0.979
Control HR vs MVA	0.838	0.644	0.931
Control MVL vs MVA	0.812	0.594	0.919
Patient HR vs MVL	0.638	0.033	0.755
Patient HR vs MVA	0.643	0.280	0.845
Patient MVL vs MVA	0.993	0.982	0.997

Table 6- 14 Table of differences between correlation coefficients

MVL is mean vector length, MVA is mean vector angle and HR is heart rate.

Description of Correlation	Patient Correlation Coefficient	Control Correlation Coefficient	Z Statistic	P value
HR vs MVL	0.638	0.948	-2.888	0.003
HR vs MVA	0.643	0.838	-1.233	0.218
MVL vs MVA	0.993	0.812	-4.626	0.000

Results 3: Investigating the effect of anaesthesia and sedation on the beat to beat variation of the heart during each breath cycle and comparisons to prion disease

In a similar fashion to previous analysis of HRV variables performed in this chapter, R-wave distributions within each breath were compared before and during anaesthesia and these associations compared to R-wave distributions from patients with vCJD.

Figure 6.10 illustrates the difference in MVL for 6 R-waves within a breath cycle for Controls, anaesthetised patients and vCJD patients.

From table 6-15, the Mardia-Watson-Wheeler test on the distributions of the R-waves within a breath suggests there are significant differences identified in the first 6 R-waves of a breath between people before and during anaesthesia. The mean vector length (MVL) of the anaesthetised patients is less than their MVL before (controls) for all R-wave positions.

This reduction in MVL during anaesthesia has previously been reported (Blues & Pomfrett.1998;Pomfrett.1995;Pomfrett, Sneyd et al.1994) although the relationship between successive R-waves within the breath to the start of the breath was not investigated. This agreement in the trend in HRV during anaesthesia helps validate the developed and applied algorithm.

Tables 6-6 and 6-7 indicate the distribution of R-waves are significantly different when vCJD patients are compared to people before anaesthesia(table 6-6). Only the first R-wave position in a breath does not show a significant difference. vCJD patients also have a significantly different distribution in all the R-waves within a breath compared to people undergoing anaesthesia, table 6-7. (A zero in the tables indicates a p value less than 1.0E-12)

Figure 6. 10 MVL for people before and during anaesthesia, compared to vCJD patients.

(approximately 400 breaths for humans (10 individuals) before and during anaesthesia and 800 breaths from vCJD patients (17 repeated measures from 4 individuals))
Tables of the 95% confidence intervals of the constituent Mean Vectors for these data are given in appendix 1.11.
Significant differences between these data points are given in table 6-15, 6-16 and 6-17.

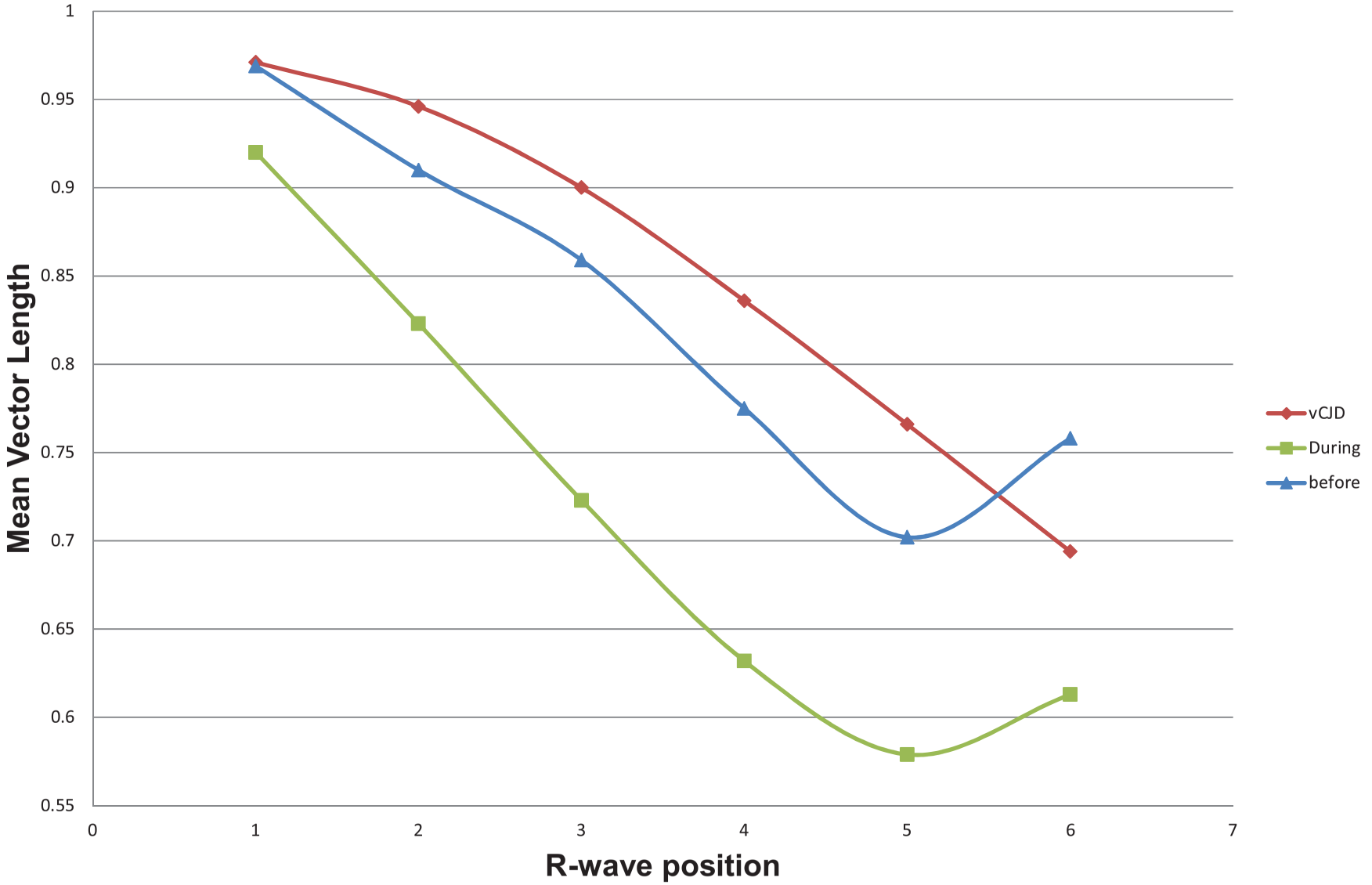

Table 6- 15 Table of differences in R-wave distributions within a breath before and during anaesthesia

R-wave position	W statistic	p value
R1	12.472	0.002 *
R2	46.824	6.80E-11 *
R3	63.883	0 *
R4	67.299	0 *
R5	85.862	0 *
R6	116.634	0 *

Table 6- 16 Table of differences in R-wave distributions within a breath before anaesthesia and vCJD patient

R-wave position	W statistic	p value
R1	2.079	0.354
R2	12.132	0.002 *
R3	24.785	4.15E-6 *
R4	41.176	1.14E-09 *
R5	63.858	0 *
R6	79.297	0 *

Table 6- 17 Table of differences in R-wave distributions within a breath during anaesthesia and vCJD patient

R-wave position	W statistic	p value
R1	14.062	8.84E-04 *
R2	55.979	0 *
R3	79.956	0 *
R4	87.321	0 *
R5	86.914	0 *
R6	70.880	0 *

*** in the tables indicates a significant difference following Bonferroni correction**

Data from patients undergoing anaesthesia and sedation were compared to control subjects and people with vCJD. This comparison relied upon assessing HRV within each breath cycle. Figure 6.11 illustrates the variability in successive R-waves within each breath. Between 100 and 800 breaths were used to gain estimates for the variability in the R-waves.

Similar analysis from people undergoing sedation are able to suggest the effectiveness of sedation during a procedure. Figures 6.12 and 6.13 represent this. Significant differences (following Bonferroni correction) are indicated in the tables (tables 6-18 to 6-21) by *. Data for figure 6.13 representing inadequate sedation was from a patient reported to be non-compliant to the procedure and the procedure was stopped due to the inability to sedate the patient.

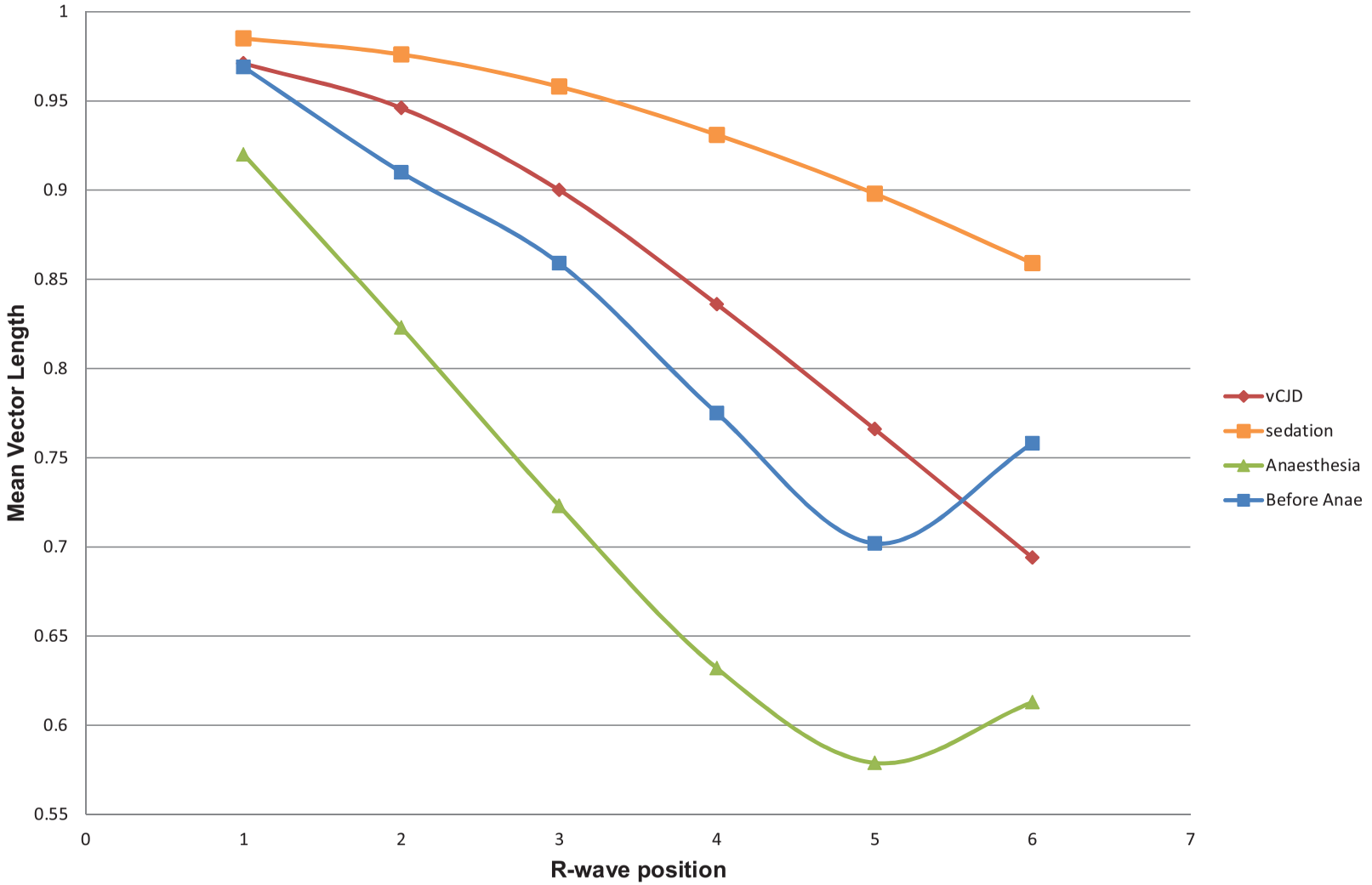

Figure 6. 11 Variation in MVL for controls, vCJD, sedated and anaesthetized people.
Variation in R-wave distributions in controls, anaesthetised, sedated and vCJD patients. These measures are from 400 breaths for anaesthetised humans and 800 breaths from vCJD patients and 100 breaths from sedation. The Mardia-Watson-Wheeler multisample test (with Bonferroni correction) states there are significant differences in the distributions of R waves (for all 6 R-wave positions) between sedation compared to anaesthesia. Similarly significant differences exist between R3, R4, R5 and R6 of sedation MVL compared to vCJD MVL and significant differences exist between R3, R4 and R5 of sedation MVL and MVL before anaesthesia.
Tables of the 95% confidence intervals of the constituent Mean Vectors for these data are given in appendix 1.11.
Significant differences between these data points are given in table 6-15, 6-16 and 6-17 and appendix 1.12.

Figure 6. 12 Example of good sedation.

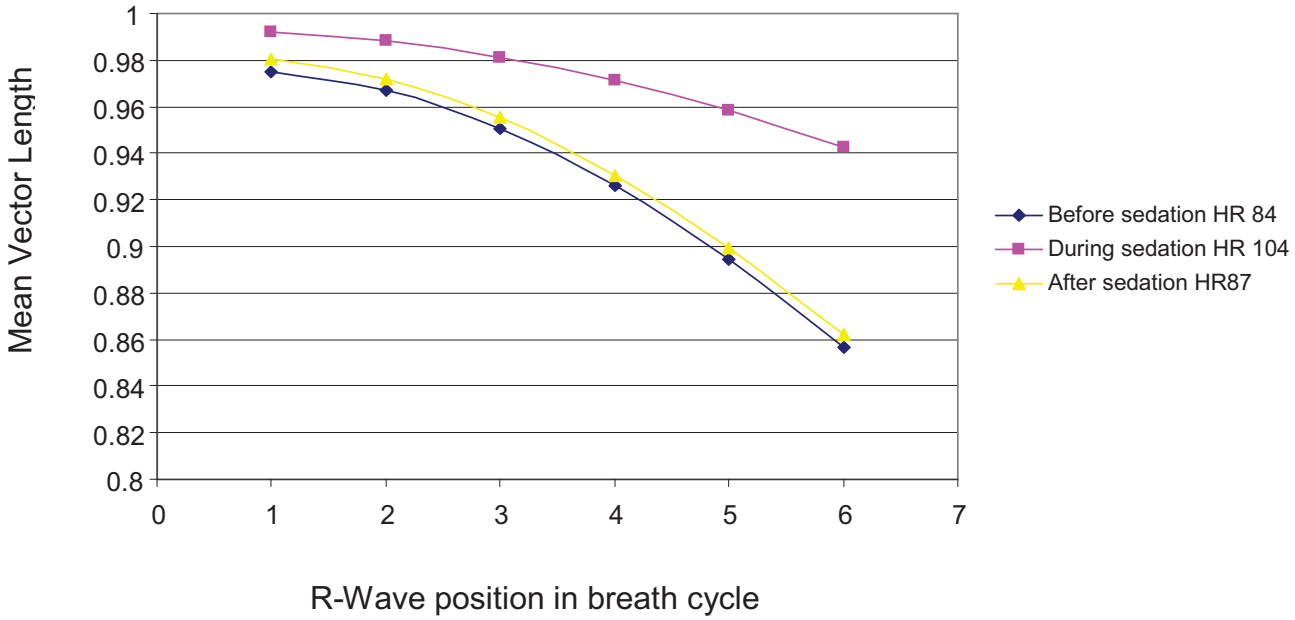

Figure 6. 13 Example of possible inadequate sedation

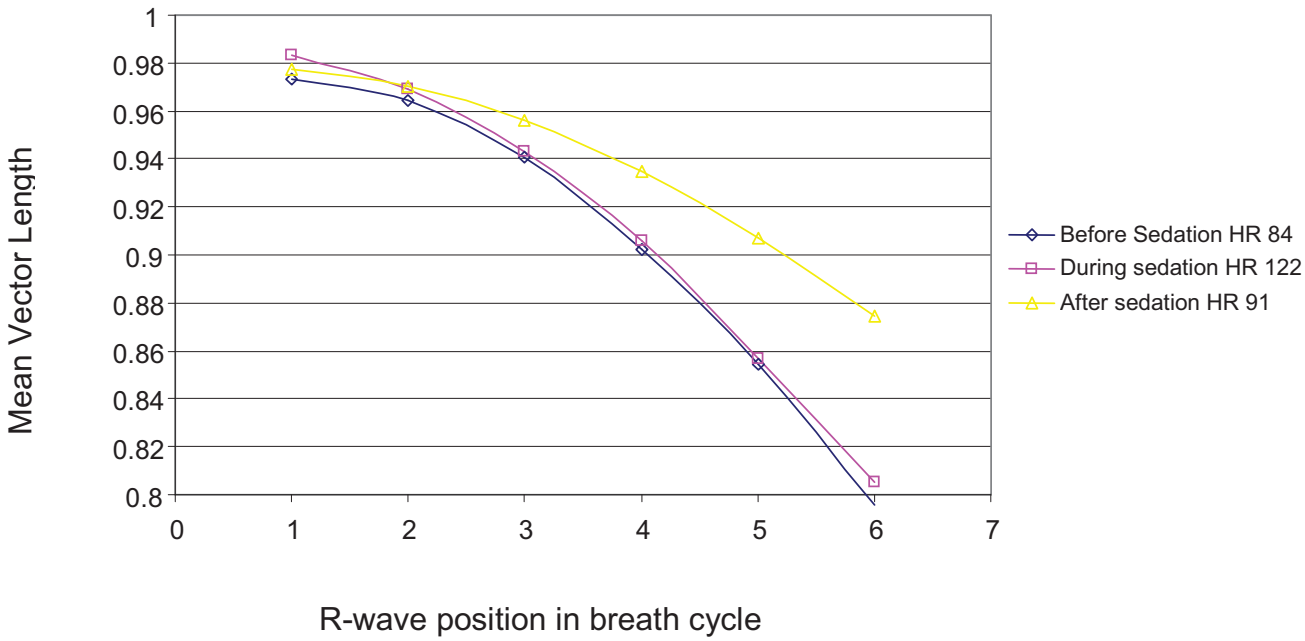

Table 6- 18 Table of differences in R-wave distributions within a breath for patient in figure 6.13 before and after sedation

R-wave position	W statistic	p value
R1	1.646	0.439
R2	1.397	0.497
R3	4.095	0.129
R4	4.262	0.119
R5	5.255	0.072
R6	5.228	0.073

Table 6- 19 Table of differences in R-wave distributions within a breath for patient in figure 6.13 before and during sedation.

R-wave position	W statistic	p value
R1	11.261	0.004 *
R2	35.375	2.08E-08 *
R3	60.836	0 *
R4	69.239	0 *
R5	71.449	0 *
R6	72.083	0 *

Table 6- 20 Table of differences in R-wave distributions within a breath for patient in figure 6.14 before and after sedation

R-wave position	W statistic	p value
R1	0.883	0.643
R2	0.002	0.999
R3	1.584	0.453
R4	3.684	0.158
R5	5.584	0.045
R6	7.013	0.030

Table 6- 21 Table of differences in R-wave distributions within a breath for patient in figure 6.14 before and during sedation

R-wave position	W statistic	p value
R1	3.29	0.193
R2	0.930	0.628
R3	1.330	0.514
R4	1.223	0.543
R5	4.004	0.135
R6	5.906	0.052

*** in the table indicates a significant difference following Bonferroni correction**

Limitations

In relation to the comparisons of vCJD data with data from other groups used in this study, the vCJD patient data contained repeated measures from only 4 individuals. These 4 vCJD patients were at different times in the stage of disease incubation. The time of death from the last data measured, ranged from 2 weeks to eight years. There is evidence from previous chapters that there may be a decrement in HRV measures with respect to time, for vCJD patients incubating the disease. Evidence from cattle suggests a perturbation in measures of HRV may be apparent in pre-clinical animals incubating BSE. For these reasons the repeated measures for all the vCJD patients were included in the analysis so as not to use extremes of data. HRV has better intravariability than intervariability (Jira, Zavodna et al.2010;Kobayashi 2007) but this information comes from studies of healthy individuals. Given the evidence of changing HRV in animals and humans incubating TSE diseases this relationship may not hold true for diseased subjects. Further studies in clinical populations are required (Sandercock, Bromley et al.2005).

The control data for part of this analysis came from 10 individuals undergoing minor elective surgery with no gross changes from normal values of blood pressure nor BMI. These individuals were then the same subjects that were anaesthetised. The control data and data from anaesthetised subjects consequently had the same confounding physiological co-variates (such as blood pressure and BMI. Blood pressure would have been monitored and controlled during anaesthesia to be maintained at the normal value for that individual). The vCJD patients were not monitored constantly for changes in blood pressure but were screened before and after data collection for changes in their blood pressure. No gross changes were noted. Patients undergoing anaesthesia were ventilated using a respiratory pump. It is noted that this may have influence on the calculation of HRV per breath since the "natural" breathing rate is obscured (see discussion in relation to the work of Blues and Pomfrett 1998).

Although significant differences between the groups was found the numbers of individuals in the various groups was small. For vCJD patients this was a function of the small number of patients diagnosed with the disease and difficulty recruiting subjects. Future work in this area could include investigations of sCJD patients

and comparisons to the data collected and analysed for this study. In addition other physiological co-variates could be more tightly controlled in this future study.

Discussion

From figure 6.6 which overlays the measured and model distributions of R-waves within each breath, the measured distribution (shown in blue) from vCJD patients fit the model R-wave events (shown in red) better than the controls. This is indicated by the relatively small departure between the red and blue lines for the patient distribution of R-waves and by the similar length and direction of the resultant mean vectors for both model and measured distributions, shown as arrows in the diagrams. In addition to the observations stated, analysis of the distribution of the 800-900 R-waves that make up each R-wave estimate for each R-wave position, demonstrates that the circular variance is greater for controls than for patient's R-waves for the first 5 R-wave events in each breath (see tables 6-5 and 6-6).

The 6^{th} R-wave for the controls differs in that there is a significantly different increase in MVL to a value higher than that of the vCJD patients 6^{th} R-wave as shown in figure 6.9 and table 6-16. This "kick" in the graph of the MVL from control R-waves may be the result of greater neural control at this point in the breath cycle, increasing the link between the breath cycle and R-wave event, hence increasing the clustering of R-waves around a mean value, which is not seen in the patient data.

The degree that the measured R-wave distribution matches the model one is illustrated by the percentage change seen in the Mean Vector Length (MVL) and Mean Vector Angle (MVA) of the summary cartwheel plots.

From table 6-10;
Control MVL change of 0.056 in 0.230 = 24% change
Patient MVL change of 0.032 in 0.365 = 9% change
Control MVA change of 26 deg from 141 deg = 18% change
Patient MVA change of 5 deg from 126 deg = 4% change

Thus there is a greater change in both MVL and MVA between the measured and model distribution for controls than there is for the patient data sets. In this way, the patient's distribution of R-waves within the breath demonstrates little variation from the model containing a prescribed pattern of R-waves. This is reminiscent of the observations from chapter 4 when longitudinal vCJD data was compared to data from a heart simulator. In this instance the variation in metrics of HRV were comparable to the simulator, again demonstrating a mechanistic pattern to the heart beat in relation to each breath, without the normal speeding and slowing of heart rate within the breath cycle thus demonstrating changed respiratory sinus arrhythmia compared to controls.

By examination of the differences between the measured and estimated R-wave events, distinctions between controls and patients can be seen. The box plot in figure 6.7 shows the range of differences is larger in the control group and also the median difference is greater for controls. The associated values of skewness and kurtosis are given in table 6-11 along with the variances for the two groups. The differences for the patients show a distribution that has greater kurtosis with less variance. This suggests the measured and calculated positions of the R-waves are similar for patient data, with smaller deviations from the model values.

From the plot of the differences in R-wave positions shown in figure 6.8, it can be seen that the control values show a greater and increased rate of change for the differences between the measured and model R-wave values compared to similar patient data. Consequently the first few R-waves within the breath cycle display a smaller variation from the simple model values with the latter R-waves showing a greater variation from the model values. Although this trend is seen in the vCJD patient data, the extent of the deviation from the model values are greatly reduced. It may be that in the control data sets, the increased variation from the simplistic model data observed is the result of complex integrated neurological control using feedback and feed forward communication to alter the heart beat to the breathing event, as seen in respiratory sinus arrhythmia. This variation within the breath is greatly reduced in vCJD patients possibly due to an alteration in the synchrony of neurological control resultant from prion infection and altered synaptic function in areas of the brainstem specifically involved in the regulation of the heart on a beat to beat basis.

Different types of coupling are described by Archie (Archie, Jr. 1981). They are mathematical, functional, algebraic and physiological coupling. The author highlights problems with one component containing all or parts of the other component of interest. Heart rate was measured as beats per minute and MVL and MVA were calculated via a separate route using beat positions per breath. This method of deriving the components of interest helped minimise algebraic coupling and provides support for functional and physiological coupling between HR and HRV per breath derived here.

When correlation analysis of HR and metrics of HRV analysis of circular statistical analysis based on a breath by breath basis obtained from summary cartwheel plots derived from around 900 breaths were investigated, it was found that there were significant correlations, however, this is not proof of causation. In chapter 2 when HRV in scrapie incubating sheep were investigated, certain metrics of HRV were shown to be independent of HR (figures 2.12, 2.13).

There is a significant difference between the relationship of HR and MVL and MVL and MVA between controls and vCJD patients as shown in table 6-14. Consequently the results shown suggest that there is less physiological coupling between heart rate and R-wave distribution within each breath in patients compared to controls. This may be due to aberrant function in the neurological homeostasis controlling the most efficient heart beat timings to breathing frequency, caused by perturbation in function by the presence of disease associated prion.

There was a trend for metrics of HRV to be more strongly associated to heart rate for control data than patient data (as seen in the scatter plots of figure 6.9). Statistics (MVL and MVA) from the summary cartwheel plots of the whole 300 second data epoch were compared to the average heart rate over this period for controls and patients. These associations are summarized in tables 6-12, 6-13 and 6-14.

Correlations may be described as weak (r=0.40-0.59) moderate (r=0.6-0.79) and strong (0.80-1) (Swinscow & Campbell.2002).

In controls, there was a strong correlation between HR and MVL (0.948) and MVA (0.838). These significant correlations suggest that approximately 90% (r squared=0.948 x0.948) of the variability of MVL is explained by HR and similarly about 70% (r squared= -0.838 x -0.838) of the variability in MVA is explained by HR. These values contrast with data from vCJD patients where 41% of MVL and MVA (0.638 x 0.638 and -0.643 x -0.643 respectively) are associated with HR.

These associations suggest a different pattern in the distribution of R-waves within the breath cycle for controls and patients. There is less association in the R-wave position and variation per breath cycle and HR in patients than in controls (significant differences between the correlation coefficients are given in table 6-14). Around 60% of the change in MVL and MVA with respect to each breath is not associated with HR. This may suggest less physiological control in the relationship to heart beat and breathing in patients compared to controls. This could be the result of aberrant neural coordination of the heart beat within the breath cycle seen in vCJD patients as a result of prion infected synapses mis-firing. The normal increase in heart rate when individuals breath in and associated slowing of heart beat when exhaling (RSA) is absent in the patient group.

Figure 6.10 illustrates the significant differences in the distribution of R-waves between controls, the same controls undergoing anaesthesia and vCJD patients. Of interest is the inflection seen between the 5^{th} and 6^{th} R-waves, in the control data and data for those individuals undergoing anaesthesia . The kick represents an increase in the MVL, indicating a greater clustering of R-waves around each mean position for the 5th and 6th R-waves for controls and these people undergoing anaesthesia. This suggests some entrainment towards a secondary regulatory mechanism which could well be the re-application of the vagal brake previously having been released to facilitate the increase of heart rate occurring in step with respiration events, associated with RSA. This switch is not seen in vCJD patient data possibly indicating abnormal neurological function.

By observation of the graph of MVL, figure 6.10, for people undergoing anaesthesia it may be seen for all R-waves the values of MVL are lower during anaesthesia than before anaesthesia. This means the R-waves are less associated to the respiration event during anaesthesia than before it.

For vCJD patients the converse is true, the MVL is higher for all R-wave positions suggesting there are reduced influences on the variation of the appearance of R-waves in patients. The variability in their occurrence is more related to the respiratory event. This could be due to abnormal neural control mitigated by prion infection in specific brainstem and peripheral areas.

The suggestion of aberrant neurological control, affecting HRV, as seen in vCJD patients, is echoed in studies of HRV following heart transplant surgery. It was reported that following such surgery, where the normal neural control of the heart was abolished, there still remained a small degree of RSA associated with myogenic properties of the heart and wall compression (Bernardi, Keller et al. 1989). The vCJD patients may be in an interim state with malfunctioning and reduced neurological complexity controlling the heart on a beat to beat basis, where the main effect on the beat variance within each breath is the myogenic properties of the heart and wall compression along with a change in pleural cavity pressure as the lungs inflate and deflate.

Some of the sites of action of the anaesthetic agent are located in the brainstem, NTS and NA, and specifically affect the GABA receptor system. Disease associated prion is thought to alter $GABA_{(A)}$ mediation of neural transmission. It is possible that the lack of variability in R-wave position seen in vCJD patients is the result of induced aberrant function of $GABA_{(A)}$ mediated synaptic communication and synchronisation of the heart beat to breath event.

This physiological observation may be of use in identifying subclinical carriers (human or animal) of prion disease since these particular areas of the brainstem are the first to be affected by prion invasion (van Keulen, Schreuder et al.2000) and the vagus may be a conduit for the initial infection of the central nervous system (Pomfrett, Glover et al.2007).

Figure 6.12 shows that during sedation the MVL increases suggesting the R-waves are more clustered to the breath event. This trend is restored to values of MVL seen before sedation took place. In the lower panel of figure 6.13, a similar series of analysed data are presented to illustrate ineffectual sedation. This patient was a chronic alcoholic and the procedure had to be abandoned due to noncompliance of the patient. These two graphs may therefore illustrate the

required swing in MVL to achieve sedative levels that allow the progression of the procedure compared to inappropriate sedative levels suggested in figure 6.13.

Sedation and anaesthesia demonstrate a perturbation in the distribution of R-waves within each breath compared to controls (see figure 6.11). During anaesthesia R-waves are less associated to the start of the breath indicated by the reduction in MVL for all R-waves. In sedation the R-waves show a greater coupling to respiration, shown by an increase in MVL for all R-waves. vCJD patients also demonstrate this increased coupling to respiration when compared to controls.

The nucleus tractus solitarii (NTS) of the medulla receives afferent sensory information from stretch receptors in the lungs, which then drives respiratory-linked vagal inhibition of the heart via efferent fibres originating in the nucleus ambiguus (NA) of the medulla. The GABA system mediates neural communication in the NTS. It has also been shown that GABA signalling in the nucleus tractus solitarius sets the level of activity in dorsal motor nucleus of the vagus (Herman, Cruz et al. 2009). This work involving efferents to the gut in the DMNX is suggestive of similar GABA mediated communications to the NA from the NTS involved in the coordination of breathing and heart beat and GABAergic receptors have been shown to mediate vagal inhibition in the NTS of rats (Wang, Jordan et al.2010).

In Chapter 1, the link between prion and the proper function of neurons has been suggested, due to its relationship to GABA mediated neurotransmission (Rangel, Madroal et al.2009). GABA mediated synaptic function is altered by the presence of prion (Collinge, Whittington et al.1994;Lu, Sturman et al.1995). It is likely that the GABA system in other brain regions would be affected by the presence of disease associated prion.

Consequently, GABA receptors in the NTS that mediate vagal inhibition, shown to be affected by anaesthesia (Wang, Jordan et al.2010), could also be the sites of disruption in the homeostatic neural coordination of the heart seen in prion disease (Glover, Pollard et al.2007;Pomfrett, Glover et al.2004;Woolfson, Glover et al.2003). Thus the presence of prion has the potential to affect GABA mediated synapses as does the action of anaesthetic and sedative agents.

A change in the synaptic function in this region due to atypical GABA activity may manifest as abnormal vagal communication to the heart and so the normal increase in heart beat at the start of respiration followed by the slowing of the heart beat is not seen. For each breath this would mean less variability for the R-waves within the breath.

So why is there a difference between the HRV during anaesthesia and sedation? Why is the trend in HRV change observed in vCJD patients similar to sedated patients? The recordings from anaesthetised patients were ventilated and this may have presented an artificial "set point" for the respiratory linked HRV compared to free breathing individuals. This conflict in ventilated respiratory frequency and "natural" respiratory frequency has been seen in infants undergoing surgery. From spectral analysis of the HRV, two peaks in the HF band were seen indicating the ventilation of the pump and the "natural" ventilatory frequency. Thus it appeared as if the natural rhythm was fighting the applied ventilation frequency of the pump. (Pomfrett, personal communication relating to the work of (Blues & Pomfrett.1998) Finally, anaesthetic agents may act on different populations of neurons than do sedative agents.

Anaesthetic agents can inhibit excitatory receptors or potentiate inhibitory receptors. The anaesthetic state comprises many components including immobilization, amnesia and unconsciousness. Specific components of anaesthesia can be produced by specific actions at different sites in the CNS. It is reported that inhalation anaesthetics produce immobilization by action on the spinal cord (Antognini & Schwartz 1993;Rampil 1994). However, sites for amnesia and unconsciousness must clearly be different from the spinal cord since any affects here would not result in central effects such as unconsciousness. Neural sites in the CNS would be the targets for the action of amnesia and unconsciousness effects. Inhalation anaesthetic can produce hyperpolarisation of neurons (Nicoll & Madison 1982) such motorneurons may play a part in the pacemaker and pattern generation of neural communication. Synaptic communication in these sets of neurons will be affected since hyperpolarisation will reduce the probability that an action potential will be generated as a result of neurotransmitter release.

GABA receptors are proteins located on membranes which can be divided into two major groups. $GABA_{(A)}$ receptors are made from five subunits forming a ligand gated ion channel (Inotropic receptor). Sixteen subunits have been identified which are classed into seven subunit families as follows:- six α, three β, three γ, and single δ, ε, π, and θ subunits. A pentamer of these subunits makes up the ionic channel through which chloride ions can pass and so alters the membrane potentials, inhibiting the firing of new action potentials. Consequently these receptors are involved in neural inhibition. $GABA_{(B)}$ receptors are G protein-coupled receptors (metabotropic receptors) and are in two groups dependent on receptor subtypes ($GABA_{(B1)}$ and $GABA_{(B2)}$). They stimulate the opening of K^+ channels, hyperpolarizing the neuron which in turn prevents neurotransmitter release. Consequently these are also inhibitory receptors.

Among the many postulated targets for anaesthetic agents are chloride channels that are gated by inhibitory $GABA_{(A)}$ receptors (Krasowski & Harrison 1999). The action of anaesthetics on the $GABA_{(A)}$ receptor are mediated by binding of the anaesthetic to specific sites on the $GABA_{(A)}$ protein based from evidence that mutations in the GABA receptor can eliminate the effects of the anaesthetic (Krasowski & Harrison.1999;Mihic, Ye et al. 1997). Reduced responses to noxious stimuli from the administration of propofol or etomidate are reported to be related to the β3 subunit on the $GABA_{(A)}$ receptor (Jurd, Arras et al. 2003) and the sedative effects of these anaesthetics are related to β2 subunit on the same receptor type (Reynolds, Rosahl et al. 2003). This illustrates that different effects of anaesthetics and sedatives are the result of different actions of the $GABA_{(A)}$ receptor subtypes.

In addition to these GABA receptors, anaesthetics act on other ligand-gated receptors and affect the release of neurotransmitters. Several anaesthetic agents potentiate the action of glycine on the glycine-gated chloride channels in the inhibitory neural pathways in the spinal cord and brainstem (GoodMan & Gilmore 2010). The protein complex syntaxin and the syntaxin-binding proteins SNAP-25 and synaptobrevin are required for the effects of some anaesthetics to be shown. This protein complex is involved in synaptic neurotransmitter release (van, Saifee et al. 1999) and may be implicated in the amnesic effect of anaesthesia causing presynaptic inhibition in neurons of the hippocampus (GoodMan & Gilmore.2010).

The sedative used in the procedure reported here was midazolam, a benzodiazepine often used in colonoscopies. The sites of action of this drug, compared to anaesthetics, are less widespread and the level of neural depression is less than for anaesthetics. Awareness usually persists even when high doses are administered and sufficient relaxation for surgery can't be achieved, thus making the drug unsuitable to replace anaesthesia. These facts illustrate the difference between sedation and anaesthesia.

The effects of midazolam are mainly exerted by action on the $GABA_{(A)}$ system in contrast to the varied targets of anaesthetics. Research into receptors have shown that the congregation of a γ subunit with α and β subunits is required to make $GABA_A$ receptors sensitive to benzodiazepine (Burt 2003). Midazolam modulates GABA binding and GABA alters the binding of midazolam (GoodMan & Gilmore.2010). At the doses used in colonoscopy procedures it is reported that midazolam may slightly depress alveolar ventilation as a result of decreased drive related to oxygen mediated chemoreceptors (hpoxic) and not the respiratory drive associated with carbon dioxide chemoreceptors (hypercapnic). Minor cardiovascular effects are reported where midazolam may increase heart rate slightly and decrease blood pressure.

It is suggested that both anaesthesia and sedation exert their effects via $GABA_{(A)}$ receptor systems. Different subunits of the $GABA_{(A)}$ receptor system are proposed to be responsible for the sedative and anaesthetic effects for some anaesthetic agents. Sedative effects are the result of action on the $GABA_{(A)}$ -β2 subunit and the loss of consciousness involves the $GABA_{(A)}$ -β3 subunit (Jurd, Arras et al.2003;Nelson, Guo et al. 2002;Reynolds, Rosahl et al.2003). It is thus possible that anaesthesia and sedation as studied here exert their effects via different population of $GABA_{(A)}$ receptors. The GABA receptor system has also been implicated in prion diseases such as vCJD. Prion infection has reported to demonstrate a different distribution in GABA receptors in the brain (Lu, Sturman et al.1995). The lack of function of normal cellular prion causes a decrease in $GABA_{(A)}$-mediated inhibitory postsynaptic currents (Collinge, Whittington et al.1994).

The precise action and effects of prion on the GABA system have still to be elucidated. However, the GABA system is suitably complex to demonstrate heterogeneity in its functional association with anaesthetics, sedatives and possibly prions. The effects induced by sedation show a similar decrease in the variability of R-waves per breath as the effect of prion infection in vCJD patients demonstrates. Anaesthesia causes the R-waves within the breath to be more variable with respect to the breath event. Consequently the difference seen during anaesthesia may be a result of an increased number, type and method of neuronal change compared to the changes observed in sedation and prion incubation.

Neural transmissions involving the GABA system are not confined solely to the CNS. Intrinsic cardiac neurons have been shown to utilize nicotinic, muscarinic and beta-adrenergic receptors to regulate the heart (Huang, Smith et al.1993b). It has also been shown that in hearts without neural communication to the brain, GABA alters neuronal and cardio-regulatory effects following hexamethonium application (a ganglionic blocker, acting as a nicotinic receptor antagonist). This suggests that synapse other than nicotinic ones were involved in GABA induced responses in these intrinsic cardiac ganglia. Consequently, amino acids such as GABA can change the neuronal activity in intrinsic cardiac ganglia with a resultant change in cardiac regulation (Huang, Smith, & Armour 1993a) illustrating a possible peripheral effect of GABA and hence a peripheral target for the effects of prion during disease incubation.

In conclusion, the application of the developed technique of assessing HRV per breath shows significant differences between controls and patients with vCJD. The methods used in this chapter are able to identify variations between individual R-wave distributions for control and vCJD patients. Heart rate has been shown to have differing effects on the calculated measures of HRV for controls and vCJD patients. Patients HRV measures have a significantly different association to heart rate than do controls.

By investigating anaesthesia and sedation and comparing these results with people incubating TSE disease, the association of GABA-mediated neuronal control and the presences of disease associated prion may present an opportunity to investigate the neurological functional change seen in prion infection.

Pharmacological intervention using a battery of agonists and antagonists may present different responses in animals or people with prion infection compared to control subjects. HRV monitoring may provide objective evidence for an abnormal response to the particular pharmacological intervention and help discern the presence or, degree of, prion infection. Repeated measures over time may also help to investigate, from a neuronal functional perspective, the pathogenesis of the disease.

Chapter 7 Summary, Limitations and Further work

Review of chapters and findings

Review of Chapter 1

Chapter 1 provides a review of the literature to provide information to describe the infectious particle and a review of the theories for TSE infection. Functions of prion are discussed and focus is placed upon a functional change in synaptic communication during disease incubation. This leads to discussion about the neuroanatomical reasons why the presence of prion in the disease classifying regions of the brain may alter heart rate variability. The relationship of the NA, DMNX and NTS are discussed in relation to the control of the heart on a beat to beat basis. In addition intrinsic and intrathoracic cardiac ganglia are discussed in relation to potential sites for integrating the parasympathetic and sympathetic branches of the ANS.

From the information in chapter 1, one putative route for the neural transport, via the vagus nerve, of disease associated prion from the gut to these brain centres could be:-
From innervations of the stomach (Powley & Phillips 2002) and the afferent sensory pathways via the nodose ganglia to the NTS (Browning & Mendelowitz 2003) with a degree of plasticity in the neuronal circuits associated with the vagus nerve and the interconnections between the NTS and DMNX being possible. These interconnections having GABAergic mediated inputs (Travagli, Hermann et al. 2003). Other infectious pathways are possible and need not be mutually exclusive. For example the DMNX has shown to be positive for PrP^{D} before the nodose ganglia reflected infectivity suggesting an efferent retrograde mode of infection from gut to DMNX (van Keulen, Schreuder et al.2000)

Review of Chapter 2

Electrophysiological studies on the effects of aberrant prion on neural function have illustrated that the lack of natural prion, analogous to the presence of non-functioning disease associated prion, causes impaired $GABA_{(A)}$ mediated synaptic inhibition and it is postulated that this dysfunction in neural communication may lead to synaptic and neuronal loss seen in prion diseases (Collinge, Whittington et al.1994). Similar work with scrapie-infected hamsters has shown aberrant postsynaptic function of neurons (Barrow, Holmgren et al.1999). A functional role for prion in modulating synaptic transmission has been suggested (Carleton, Tremblay et al.2001). Consequently these lines of evidence help to construct the hypothesis that disease associated prion in the diagnostic brainstem regions of the medulla will disrupt the normal synaptic flow of neural information used to regulate target organs such as the heart causing a perturbation in the beat to beat control which manifests as a change in HRV.

Chapter 2 summarizes the common methods used to collect data for subsequent analysis of HRV in other chapters. The construction of adapted ECG electrodes is described to facilitate good quality recordings from sheep and cattle along with the description of the gel used to locate these electrodes on the animal. The data capturing devices are described and the common software used to analyse the data are listed. Some of the technical caveats to collecting and analysing heart rate variability data are discussed and measures taken to minimize the effects of these in the results are described. To test the data capture and analysis routines a heartbeat simulator was used which had particularly low variability encoded in to the rhythm. This machine's original function was to provide a "real" ECG rhythm onto which specific clinical arrhythmias could be programmed. This was used to simulate cardiac dysfunction of a manikin used for cardiac resuscitation training. The results of the simulator are included in appendix 1.2.

Review of Chapter 3

Evidence from chapter 3 of this thesis and published research by this author (Glover, Pollard et al.2007) provides examples of how HRV analysis can identify scrapie infected sheep from controls at the pre-clinical stage. In addition it was observed that these deviations in HRV were concurrent with positive rectal biopsy analysis indicating prion protein in the enteric nervous system before overt clinical signs of the disease (the enteric nervous system often classified as part of the ANS (Gershon 2003)). A particular frequency band (0.032-0.138 Hz) previously demonstrated to have utility by our group in HRV analysis (Pomfrett, Dolling et al.2009) was found to show significant differences ($p<0.05$) between rectal biopsy prion positive sheep and rectal biopsy negative sheep.

This difference was not seen in higher frequency bands of HRV variability, RMSSD time domain measures of HRV nor heart rate. This observation highlights the fact that different metrics of HRV may give different results and a discussion was started in the limitations section of this chapter concerning better methods to subdivide the spectrum of HRV to focus on particular physiological subsets of the variability. The limitations section of this chapter also addresses the caution required in interpretation of these results from a small number of sheep with mixed genotype. However the proof of the principle in using HRV to investigate prion infection is demonstrated.

Review of Chapter 4

Work with cows incubating BSE has shown a relationship between the amount of infectious inoculum the animals were challenged with and HRV at certain time points after the oral challenge (Pomfrett, Glover et al.2004).

In this thesis (chapter 4), HRV analysis of cows from the same study but using a different method of HRV analysis based on the work of Toichi and Allen (Allen, Chambers et al.2007;Toichi, Sugiura et al.1997), was performed.

Chapter 4 illustrated a difference in HRV between sheep incubating scrapie and cattle incubating BSE. This analysis was also able to separate 1 gram dosed cattle from 100gram dosed cattle by comparison to controls (figures 4.5, 4.7). Significant differences in the HRV of cattle based upon histopathological examination of their spine in relation to the presence of prion were shown (figures 4.8, 4.9 and 4.10) and this method was extended to show significant differences in control cattle, orally challenged cattle and "field" animals showing clinical signs of BSE.

The use of HRV investigations illustrated the changing pathogenesis of the disease during incubation, as postulated in the work into the spread of prion protein in neural tissues of the animal with respect to time (Beekes, McBride et al.1998;Beekes & McBride.2007;Pomfrett, Glover et al.2007;van Keulen, Bossers et al.2008;van Keulen, Schreuder et al.2000). As prion protein affects more neural compartments as the disease progresses, a change in the neural output from these areas would occur. This change in neural communication to target organs such as the heart would appear as a change in HRV. Both sympathetic communication, mediated via the spinal cord and parasympathetic activity mediated via the vagus nerve are integrated at the intrinsic cardiac ganglia. A change in this dynamic balance due to transient perturbations in either or both of the branches of the ANS would change HRV.

In this opportunistic study, the practicalities of measuring a cow's individual physiological co-variates were limited. To this extent the control group had the same treatment as the animals in the other two groups to hopefully minimize the effects of changes in temperature, position when monitoring and blood pressure.

The experiment was designed so the only difference between these groups of cattle would be the amount of oral challenge they received (0 gram, 1 gram or 100 gram). Other limitations to this study involved the changing metrics of HRV in individuals during disease incubation and the departure from the normal intra and inter variability considerations of HRV measures observed in healthy populations (Jira, Zavodna et al.2010;Kobayashi.2007).

Review of Chapter 5

Chapter 5 presents the rationale for the development of a different technique to assess heart rate variability per breath. It discusses RSA and the associated neuroanatomical sites responsible for the control of RSA and the particular effects on the respiration cycle modulated by the vagus nerve. Prion infection in these neural structures is postulated to cause a resultant change in HRV measures per breath compared to controls. To investigate this prospective change, circular statistics were employed to examine the relationship of the R-wave variability within breath cycles.

Difficulty in obtaining breathing events directly from vCJD patients was described and a method to estimate breathing events from analysis of the ECG trace was developed via a purpose written computer program written by myself and include in the appendix (Appendix 1.5). The program then was developed to archive the R-wave times occurring with each respiratory cycle (Figure 5.7 illustrates the translation of the linear events into their circular representation). Breath estimates were compared to breaths measured from control subjects and the Bland-Altman method to measure the level of agreement between estimating and measuring breath events was used. Data from the program was input to commercially available software (Oriana) to perform circular statistical analysis.

The change in R-wave distribution per breath was compared to data from a heart rate simulator and controls to indicate the range and magnitude of the deviations from control and artificially generated data. Changes in the R-wave distributions with respect to their position in the breath cycle were found between controls and vCJD patients. Significant differences were found in the mean vector length (MVL) of R-wave distributions within a breath cycle between vCJD patients and controls,

controls and heart simulator data and for some R-wave positions between vCJD patient data and heart simulation data (Table 5-2, figure 5.19).

Limitations to the technique were discussed including the problem associated with estimating the start of the respiration cycle and how this may differ between the neurological initiation of the event and the time taken to measure a change in airflow in the respiratory tract. It is reported that a change in the vagal and sympathetic efferent activity occurs 0.5 seconds before the onset of inspiration (Saul, Berger et al.1989a). This time difference would have substantial effects on the sub second relationship between R-waves within a breath cycle.

Review of Chapter 6

In chapter 6 the application of the technique developed in chapter 5 was considered. Assessment of the ability to distinguish R-wave distributions within a breath between controls and vCJD patients were investigated. Significant differences ($p<0.05$) in R-wave distributions between controls and vCJD patients were reported following a Mardia-Watson-Wheeler test (table 6-8), a finding supported by the non-overlapping confidence intervals for the mean vector angle listed in tables 6-5 and 6-6.

The effect of heart rate on the distributions of R-waves within a breath was considered and it was reported that there was a significantly different ($p<0.05$) correlation between heart rate and mean vector length (MVL) for controls and vCJD patients (table 6-14).

Based upon the fact that the areas of the brainstem involved in anaesthesia are the same as those used for a diagnostic test for prion diseases and are those areas that control the heart on a beat to beat basis, HRV measures using the technique developed in chapter 5 were used to investigate changes in HRV in patients undergoing general anaesthesia. In addition patients undergoing procedural sedation were also investigated to investigate if similar HRV changes were seen in these two pharmacological interventions.

Significant differences ($p<0.05$) in the R-wave distributions per breath were reported before and during anaesthesia (table 6.15), during anaesthesia compared to vCJD patients distributions (table 6-17) and some R-wave positions showed significant differences between vCJD patients compared to controls before anaesthesia (table 6-16, only the first R-wave in the breath was not significantly different in its distribution). Significant differences ($p<0.05$) were reported in the R-wave distributions of people undergoing sedation compared to people undergoing anaesthesia (figure 6.11). The utility of this method of assessing HRV was indicated by a significant change ($p<0.05$) in R-wave distributions per breath induced by adequate sedation which contrasted with the lack of a significant change during a procedure abandoned due to inadequate sedation of the patient (Figures 6.12 and 6.13, tables 6-18 to 6-21)

Comparisons with changing HRV per breath in vCJD patients, healthy controls and patients undergoing sedation or anaesthesia have led to the postulation of a link between prions and the GABA system, potentially the $GABA_{(A)}$ beta 2 receptor.

Limitations

Methods of measuring HRV

Different methods of HRV analysis may give different assessments of the degree of change in autonomic function of a system since each method may represent different interactions between branches or pathways of the autonomic nervous system.

The response of the ANS is a dynamic system tailored to individual physiological requirements at a particular time. Problems in relation to what HRV analysis may tell us about the function of the ANS are highlighted in the opinions of Parati and Rienzo versus Taylor and Studinger (Parati, Mancia et al. 2006). One of the main issues is of the implied absolute measures of autonomic tone and the limitations of an accurate method of measurement.

Analysis of the beat to beat variations gives an approximation to the coordinated activity of the ANS in the control of the heart during the period of sampling. As such, results represent a "snap-shot" of the dynamic state of the autonomic integration within the physiological system. In addition, all measurements are fundamentally relative. For example take measuring a length of string. One may use a ruler and read off a value from the scale provided. However this is relative to which "yardstick" (ruler) is used. Similarly measures of HRV will be related to which method of analysis is used. Inappropriate quantification may lead to improper interpretation of heart rate variability and its underlying physiological correlates.

Consequently, the most powerful analysis of HRV will compare any values obtained from individual measures with ranges of normality, derived during similar standardised conditions. Further insight and utility from HRV analysis is gained if the diseased or non-functioning range of a particular HRV analysis methodology is defined. For example the work of Ewing (Ewing, Neilson et al.1984) used diabetic patients compared to healthy controls and also comparisons to heart transplant patients having medically denervated hearts to illustrate the trend in reduced parasympathetic activity displayed by diabetic patients. Similarly, the analysis of HRV data performed in chapter 5 of this thesis compared data from control human

subjects and patients with vCJD and both measures were referenced to data from an electronically simulated ECG displaying little or no HRV. As well as acting as a point of reference in the comparisons of the results, the inclusion of data with no HRV helped validate the purpose written algorithm used to analyse the data. The analysis of the data from the simulator gave very small measures of HRV and helped indicate the downward trend in longitudinal measures from a vCJD patient.

HRV may be most sensitive in identifying a change in longitudinal studies and looking for a change in an individual's range of autonomic function. This would minimise the errors in an individual's HRV having a different baseline value than the normal population. Having a bespoke baseline from which deviation could be assessed would make any deviation from the day to day variability easier to see. However from these studies it is likely that the degree of day to day variability is small in comparison to the extremes of HRV seen in the diseased state. But utilizing the longitudinal study method would yield an analysis that could more easily and sooner identify a significant change in the metric measured.

HRV in a diseased state: Study of heart transplant patients to illustrate potential for differences.

Interpretation of the results of HRV analysis is further complicated when HRV is applied to a progressive detrimental disease of the autonomic system where different functions of the system may be seen with respect to disease pathology. This decrement in function may also prescent a "see-saw" pattern in coordinated branches of the autonomic system with respect to time, as seen in the investigations of cattle incubating BSE in chapter 4 and the latter stages of the disease shown in figures 4.13 and 4.14. This change in measures of HRV over time observed in subjects incubating TSE diseases is also indicated in appendix 1.8. (Significant differences ($p<0.05$) are seen between measurements taken 12 months apart from this individual represented in appendix 1.8). One possible reason for the change in function over time is the activation and use of different pathways in the autonomic system. This potential for recovery of function is illustrated by the resurgence of utility in the ANS following ablation as a result of transplant surgery.

Heart transplants in dogs have provided evidence for neural re-innervation (Sakamoto, Schuessler et al. 2009) but re-innervation is less well accepted in human transplants. However, the techniques employed to explore re-innervation in the human use indirect techniques such as pharmacological intervention and autonomic reflex responses to exercise. It has been suggested that such changes in the beat to beat rate of the heart may be due to an increased and progressive sensitivity of the donor heart to adrenalin (Koskinen, Virolainen et al.1996).

Reports of re-innervation in human heart transplant patients using power spectral assessments of HRV have been suggested. Power spectral analysis of the transplanted heart was found to be similar to a normally innervated heart and the observed respiratory peak corresponding to respiratory frequency was abolished following the administration of atropine (Fallen, Kamath et al.1988). More evidence for parasympathetic and sympathetic re-innervation has also been reported (Gallego-Page, Segovia et al. 2004) using HRV, histological techniques and imaging studies using radioactive sources (scintigraphy).

The time after transplantation is reported to have an effect on re-innervation. It has been reported that HRV increases with the length of time after the operation. Significant changes in sympathetically mediated HRV are seen in patients having had a heart transplant after 3 years from the transplant compared to patients having had a transplant within 3 years (Halpert, Goldberg et al. 1996;Koskinen, Virolainen et al.1996). Time after transplantation has also been shown to be a factor in the parasympathetic re-innervation of the heart (Uberfuhr, Frey et al. 1997).

Further support for a sympathetic re-innervation in human heart transplants is seen in studies of children. HRV changes are seen following 4 years after transplantation in children and demonstrate a growing sympathetic influence on the heart with respect to time after transplantation (Pozza, Kleinmann et al.2006). It is suggested that sympathetic re-innervation to the sinus node and left ventricle occur at different times after transplantation (Lovric, Avbelj et al. 2004).

Evidence for re-innervation by both branches of the ANS is also found (Tio, Reyners et al. 1997;Uberfuhr, Frey et al.1997) although it is reported that signs of parasympathetic re-innervation are more common (Tio, Reyners et al.1997). Evidence involving analysis of HRV in patients after transplant has suggested both branches of the ANS may re-innervate the heart many years after surgery. These lines of evidence suggest a remodelling or resurrection of function of neural connections controlling the heart. One possibility into the uncertainty of re-innervation may be the oversight of intrinsic cardiac ganglia located on the heart. Different surgical techniques or variation within the technique could result in complete, partial or absent cardiac ganglionated complexes following transplantation. This would cause different rates of recovery in the local independent function of the intrinsic cardiac ganglia in the control of the heart with respect to time after transplantation. In this respect the intrinsic ganglia could be viewed as a separate “brain” in an analogous fashion as the ideas postulated in Gershon’s thoughts on the enteric nervous system being a “second brain” (Gershon.2003).

This recovery of function may be seen as a “see saw” in the regulation of the heart after transplant occurs. The "see saw" nature in HRV may be revealed as a predominance of parasympathetic or sympathetic variability over time, accounting for the diverse reports on the re-innervation of the branches of the ANS.
To this end adaptations to the surgery involved in transplants to reduce damage to the cardiac ganglia has been suggested to improve the recovery of patients after surgery and achieve better electrical stability of the heart (Singh, Johnson et al. 1996). If the cardiac ganglia were kept as functional units some HRV may be possible from “pre-programed” activity pathways.

Similarly changes in the activity of cardiac ganglia may be seen due to prion causing aberrant function in either the descending neural efferent information, changing afferent communication to integrative centres within the medulla, influences at the interneurons of the cardiac intrinsic ganglia or, most likely, a mixture of perturbation in the interactivity of all these sites due to prion infection causing neuronal mis-firing and or neuronal apoptosis (for a diagram summarizing the interconnections and neuronal pathways for the regulation of the heart see figure 1.6 chapter 1). These areas of neuronal mal-function may be represented as "see saw" changes in metrics of HRV as reported in this thesis.

This pathway has been highlighted by research into depth of anaesthesia and retrograde virus studies. The areas of the brainstem involved in regulation of heart on beat to beat basis are those areas where prion deposits are seen in prion diseases. Prions cause disruption in neural signalling so it is likely that aberrant neural communication from these infected areas would result in a functional change at the target organ, the heart in this case.

Respiration linked to HRV

At rest, changes in parasympathetic nervous activity represent the major part in the generation of HRV(Electrophysiology.1996). Quick cholinergic communication of neural impulses coupled with muscarinic receptor signalling at the SA node is reported to account for the modulation in the RR interval, contrasting with the slower noradrenergic and beta receptor signalling of the sympathetic system (Chapleau & Sabharwal 2010;Electrophysiology.1996;Laude, Baudrie, & Elghozi 2008;Thireau, Zhang et al. 2008).

Debate about the relationship of vagal tone to RSA has been discussed. It has been reported that the cardiac vagal tone is disassociated from RSA when the respiration rate is changed (Grossman & Taylor 2007), this relationship was stronger if respiration rate was controlled for. This idea is countered by suggestions that strong correlations of RSA and respiration are not suggestive of an effect of respiration on vagal tone (Denver, Reed, & Porges 2007). It is suggested that RSA represents phasic control of the heart affected by the integration of neural events (Berntson, Cacioppo, & Grossman 2007) involving sympathetic and parasympathetic interactions and is not simply a measure of vagal activity. This latter idea is supported by the dynamic change in HRV linked to each breath seen in prion disease pathogenesis. This change in HRV shows a recovery of function at certain stages of the disease, emphasising the dynamic nature of the regulation of the heart on a beat to beat basis.

As the control of HRV is a dynamic process, at one time slice, RSA may be intimately and exclusively related to parasympathetic activity and at others may

become disassociated from it due to changing physiological states, such as hormonal and blood pressure effects feeding back to the control of the electrical activity of the heart.

In this thesis I proffer the idea that intrinsic cardiac ganglia are mediators in the determination of the integrated coordinated effects of branches from the parasympathetic and sympathetic arms of the ANS. Inclusion of this level of neural structure may well answer, to some degree, the conflicting observations of Grosman and Porges and support the thoughts of Berntson of a dynamic regulation of HRV.

Further to the discussion in the relationship to RSA and parasympathetic activity, questions remain about the method of assessing RSA. Time domain methods such as RMSSD and PNN50 are confounded by the fact that the magnitude of the heart rate deviations on a beat to beat basis increases at lower respiratory frequencies and high tidal volumes. Similarly frequency domain methods of assessing RSA may have limited utility in circumstances where the depth and frequency of respiration change during the sampling period. For long sampling intervals this is more likely. The power spectrum in humans, as a result of the FFT method of assessing RSA, may be represented in 3 bands, VLF less than 0.04 Hz, LF0.04-0.15 Hz and HF 0.15-0.54Hz (Electrophysiology.1996). The latter HF band represents fluctuations in RR interval associated with the breathing cycle. The specific frequency involved in any one sample and therefore any one assessment, vary between individuals and between species.

Power spectral measure of HRV assessment assume a regular breathing frequency and depth with ANS frequency components above 0.15 Hz and below 1 Hz. This is not the case , so such estimates may be confounded. Similarly paced breathing has been criticised for altering ANS activity from the natural free breathing measures due to mental volitional control of breathing affecting the estimates of HRV. Volitional control of breathing would require other physiological processes outside of the autonomic control of respiration.

In addition, the pattern in a breathing cycle may vary even during a relatively short period such as the five minute epochs used in this thesis. Consequently the proposed frequency band used in FFT analysis smears the breath by breath

variations in the respiratory cycle and the RR variability associated with respiration is also compromised. This may contribute to the contention about the link to RSA and vagal tone discussed by Porges and Berntson above. Consequently, respiration should be monitored, if not recorded, to ensure the associated power falls within the specific frequency band (0.15 Hz represents one breath every 6.666 seconds and 0.5 Hz represents one breath every 2 seconds). If an individual is breathing at a rate of one breath every 8-10 seconds or if a few of the breaths occur at these rates, then the power represented in the FFT band will not wholly represent the activity of the parasympathetic and sympathetic nervous system on the heart. This would infer less of an association between RSA and vagal tone for example in this instance as a result of an inaccurate technique for assessing this dynamic system.

Consequently the method to investigate HRV adopted and developed in chapters 5 and its application in chapter 6 for using the RR distribution within a breath, may have extended utility to more specifically examine the link between vagal activity and its effects on the synchronicity of breathing events, in conjunction with the sympathetic contributions of the ANS. Overlaying many breaths gives an estimate of the HRV per breath where “noise” from other cardiac neuronal activity, not directly linked to beat to beat variability, is "random" by comparison and so when averaged the most predominant associations become apparent i.e. vagal mediated beat to beat variability within each breath.

Since prion infection has been shown to affect areas of the brainstem including the DMNX, NTS, reticular formation, NA and the vagus (as described earlier in this thesis), disruption in the normal neural function of these areas is probable. By examination of the effects of the functional interdependency involving these areas of brainstem in the coordination of breathing and heart rate, the application of HRV studies is able to interrogate specific parts of the neurology affected by prion infection. As prion infection proceeds to more neural structures, a changing and abnormal coordination between breathing and the beat to beat regulation of the heart would be seen. Such neural pathogenesis may account for the see saw nature observed in data from incubating subjects.

It is possible such investigations are able to identify changes in HRV per breath before clinical signs of the disease appear. This may have benefit for putative

therapies and may help reduce the risk of iatrogenic infection in the human population from the use of prion contaminated medical instruments and products.

Application to different genotypes and other diseases.

Prions are reported to affect synaptic transmission (Brown 2001;Jeffrey, Halliday et al.2000;Kretzschmar, Tings et al.2000;Mallucci 2009;Moreno & Mallucci 2010) and the possibility is raised that aberrant function may arise before clinical signs of infection (Jeffrey, Halliday et al.2000) since the clinical signs are an outward manifestations of changing neural communication and coordination, it is likely the investigations monitoring the changing neurology will show a change before clinical signs. Prion disease is still an enigma. A continuum of disease phenotypes are becoming evident and much of what we have recorded about the epidemiology of the diseases was based on histopathological tests that are in the process of being refined to now be able to identify new strains of prion disease and disease in different genotypes that was not previously possible. The very search for the elusive prion may be a search for foot prints in the snow and we are looking at the imprint of the disease-causing particle and not directly at the cause of the disease.

Whether this is true or not, using HRV to assess the potential for disease incubation is independent of the cause of the disease and initial results show that such analysis may be able to indicate the presence of prion disease before clinical signs are evident.

Recent reports of vCJD having been identified in different genotypes of the population (Kaski, Mead et al. 2009) raises questions about the future expression of this one version of prion disease (Will 2010). Furthermore, there is the prospect of a “new” new variant of CJD appearing in the future in a similar fashion as did nvCJD (now called vCJD) in the 1990s.

Further Work

In an ideal experiment designed to investigate changes in HRV during prion disease incubation, samples of HRV data should be obtained preferably daily and monitored for any deviations from control values previously assessed. Following a signature change in HRV the experimental animals should be euthanized and histologically examined for the presence of prion in associated neural tissue. A map of prion protein spread and associated change in HRV could be constructed from large samples and this would give functional physiological evidence for a proposed pathway for the disease associated prion in the diseased state. This ideal experiment would also help validate the utility of monitoring HRV to assess the presence of prion protein and may help in the differential diagnosis of prion diseases versus other neurological disease. Within this ideal experiment other physiological variables could also be monitored to assess the inter-relationship with changes in HRV. Accurate and reliable breath estimation could also be included to present more accurate calculations of the respiration cycle and consequently better relate each R-wave to its particular breath cycle.

This ideal study could be further developed to investigate the changes in HRV observed here during anaesthesia and sedation. The use of animals may allow local topical administration of specific anaesthetics and sedative agents to particular neurological tissues and direct neurophysiological recordings could be made. This would help identify the particular neural pathways involved and help associate changes in HRV to the underlying neurological processes.

Discussion and Conclusions

The methods and techniques developed in this research, in addition to screening for new prion diseases in the future, may also have application in the study of disease such as Parkinson's and Alzheimer's disease. Comparisons with the trends in changing HRV per breath in vCJD patients, healthy controls and patients undergoing sedation or anaesthesia have led to the postulation of a link between prions and the GABA system, potentially the $GABA_{(A)}$ beta 2 receptor. This may lead to further areas of research that may address therapeutic treatments for prion disease.

vCJD is termed “invariably fatal” (Knight 2006). However one victim survived more than 9 years after initial diagnosis. When a cancer patient survives longer than 5 years after the diagnosis, they are considered cancer-free. If the same regulation was applied to vCJD, the disease would not be invariably fatal.

The prospect of a different genotype taking longer to express clinical signs of the disease have also been raised. The length of time to express the disease may well be longer than the individual’s life. This should not mean that it should be ignored since iatrogenic infection from these carriers could still threaten individuals of a susceptible genotype. A non-invasive repeatable ante mortem assessment may have utility in the longitudinal tracking of suspected individuals as an adjunct to other putative tests.

Further applications for the monitoring HRV have been indicated by the work on sedation and anaesthesia. As indicated in figures 6.13 and 6.14 the efficacy of a sedative may be assessed from the changing effect the drug has on HRV measures. In non-standard patients, for example the chronic alcoholic in figure 6.14, an assessment of sedative effect may suggest an increase in the amount given and thus provide adequate sedation of the patient as intended.

Monitoring autonomic function using HRV has many applications. The nature of the autonomic system is that it is not under voluntary control and so we do not readily know when it is compromised or malfunctioning. Left untreated or undiscovered this malfunction can lead to further pathogenesis and health

problems. Consequently monitoring autonomic function may have utility not only in prion diseases but in general health care applications.

The overall aim of this thesis was to investigate if a change in HRV measures was detectable when animals and humans incubating TSE diseases were compared to controls. In conclusion this thesis has reported evidence for significant differences in HRV measures between sheep with scrapie, cattle with BSE and humans with vCJD and species specific controls. The use of different methods of HRV estimation were used to address questions about different techniques having different relevance to the underlying physiological processes controlling the heart on a beat to beat basis. In further attempting to answer these questions a new technique was developed to assess changing HRV per breath.

This technique was developed to assess the effects of all the changing ANS activity apparent within a breath cycle and to reduce the effects of autonomic events outside this physiologically relevant and variable epoch.

Using this putative technique significant differences were found between vCJD patients and controls. In addition this technique also reported significant reduction the clustering of R-waves related to the breath cycle during anaesthesia, which was also supported by other workers. The technique was also able to distinguish between sedation and anaesthesia and by comparison with deviations seen in vCJD patients particular GABA subunit types were implicated as target sites for the abnormal neurological function resulting from prion infection. The proof of principle of investigating HRV as an indicator for TSE infection has been shown. However further work and validation is necessary to develop the technique to more accurately describe the changes in autonomic nervous control of the heart on a beat to beat basis as the result of prion infection in TSE diseases.

References

1. Agostoni, E., De Daly, M. B., Murray, J. G., & Chinnock, J. 1957, "Functional and histological studies of the vagus nerve and its branches to the heart, lungs and abdominal viscera in the cat", *J Physiol*, vol. 135, no. 1, pp. 182-205.
2. Aguzzi, A. 2005, "Cell biology. Prion toxicity: all sail and no anchor", *Science*, vol. 308, no. 5727, pp. 1420-1421.
3. Aguzzi, A. & Heikenwalder, M. 2003, "Prion diseases: Cannibals and garbage piles", *Nature*, vol. 423, no. 6936, pp. 127-129.
4. Aguzzi, A., Heikenwalder, M., & Miele, G. 2004, "Progress and problems in the biology, diagnostics, and therapeutics of prion diseases", *J.Clin.Invest*, vol. 114, no. 2, pp. 153-160.
5. Aguzzi, A., Heikenwalder, M., & Polymenidou, M. 2007, "Insights into prion strains and neurotoxicity", *Nat Rev Mol Cell Biol*, vol. 8, no. 7, pp. 552-561.
6. Aguzzi, A. & Collinge, J. 1997, "Post-exposure prophylaxis after accidental prion inoculation", *The Lancet*, vol. 350, no. 9090, pp. 1519-1520.
7. Akselrod, S., Gordon, D., Ubel, F. A., Shannon, D. C., Berger, A. C., & Cohen, R. J. 1981, "Power spectrum analysis of heart rate fluctuation: a quantitative probe of beat-to-beat cardiovascular control", *Science*, vol. 213, no. 4504, pp. 220-222.
8. Allen, J. J. B. 2002, "Calculating metrics of cardiac chronotropy: A pragmatic overview", *Psychophysiology*, vol. 39, S18..
9. Allen, J. J. B., Chambers, A. S., & Towers, D. N. 2007, "The many metrics of cardiac chronotropy: A pragmatic primer and a brief comparison of metrics", *Biological Psychology*, vol. 74, no. 2, pp. 243-262.
10. Alper, T. A., Haig, D. A., & Clarke, M. C. 1966, "The exceptionally small size of the scrapie agent", *Biochem.Biophys.Res.Commun.*, vol. 22, pp. 278-284.
11. Antognini, J. F. & Schwartz, K. 1993, "Exaggerated anesthetic requirements in the preferentially anesthetized brain", *Anesthesiology*, vol. 79, no. 6, pp. 1244-1249.
12. Appel, T. R., Lucassen, R., Groschup, M. H., Joncic, M., Beekes, M., & Riesner, D. 2006, "Acid inactivation of prions: efficient at elevated temperature or high acid concentration", *J Gen.Virol.*, vol. 87, no. Pt 5, pp. 1385-1394.
13. Aradottir, s. L., Robertson, A., & Moore, E. 1997, "Circular statistical analysis of birch colonization and the directional growth response of birch and black cottonwood in south Iceland", *Agricultural and Forest Meteorology*, vol. 84, no. 1-2, pp. 179-186.
14. Archie, J. P., Jr. 1981, "Mathematic coupling of data: a common source of error", *Ann Surg.*, vol. 193, no. 3, pp. 296-303.
15. Armour, J. A. 1994, "Peripheral Autonomic Neuronal Interactions in cardiac regulation," in *Neurocariology*, pp. 219-244.
16. Armour, J. A., Collier, K., Kember, G., & Ardell, J. L. 1998, "Differential selectivity of cardiac neurons in separate intrathoracic autonomic ganglia", *Am J Physiol*, vol. 274, no. 4 Pt 2, p. R939-R949.
17. Armour, J. A. & Hopkins, D. A. 1984, "Anatomy of the Extrinsic Efferent Autonomic Nerves and Ganglia Innervating the Mammalian Heart," in *Nervous Control of Cardiac Function*, W. C. Randall, ed., Oxford University Press, New York, pp. 20-45.
18. Armour, J. A., Huang, M. H., Pelleg, A., & Sylven, C. 1994, "Responsiveness of in situ canine nodose ganglion afferent neurones to epicardial mechanical or chemical stimuli", *Cardiovasc.Res.*, vol. 28, no. 8, pp. 1218-1225.
19. Armour, J. A. & Janes, R. D. 1988, "Neuronal activity recorded extracellularly from in situ canine mediastinal ganglia", *Can.J Physiol Pharmacol.*, vol. 66, no. 2, pp. 119-127.
20. Armstrong, R. A., Cairns, N. J., Ironside, J. W., & Lantos, P. L. 2002, "The spatial patterns of prion protein deposits in cases of variant Creutzfeldt-Jakob disease", *Acta Neuropathol.(Berl)*, vol. 104, no. 6, pp. 665-669.

21. Armstrong, R. A., Lantos, P. L., Ironside, J. W., & Cairns, N. J. 2003, "Differences in the density and spatial distribution of florid and diffuse plaques in variant Creutzfeldt-Jakob disease (vCJD)", *Clin.Neuropathol.*, vol. 22, no. 5, pp. 209-214.
22. Arnold, M. E., Ryan, J. B., Konold, T., Simmons, M. M., Spencer, Y. I., Wear, A., Chaplin, M., Stack, M., Czub, S., Mueller, R., Webb, P. R., Davis, A., Spiropoulos, J., Holdaway, J., Hawkins, S. A., Austin, A. R., & Wells, G. A. 2007, "Estimating the temporal relationship between PrPSc detection and incubation period in experimental bovine spongiform encephalopathy of cattle", *Journal of General Virology*, vol. 88, no. Pt 11, pp. 3198-3208.
23. Arsac, J. N., Biacabe, A. G., Nicollo, J., Bencsik, A., & Baron, T. 2007, "Biochemical identification of bovine spongiform encephalopathies in cattle", *Acta Neuropathol (Berl)*.
24. Asante, E. A., Linehan, J. M., Desbruslais, M., Joiner, S., Gowland, I., Wood, A. L., Welch, J., Hill, A. F., Lloyd, S. E., Wadsworth, J. D., & Collinge, J. 2002, "BSE prions propagate as either variant CJD-like or sporadic CJD-like prion strains in transgenic mice expressing human prion protein", *EMBO J.*, vol. 21, no. 23, pp. 6358-6366.
25. Baldauf, E., Beekes, M., & Diringer, H. 1997, "Evidence for an alternative direct route of access for the scrapie agent to the brain bypassing the spinal cord", *J.Gen.Virol.*, vol. 78 (Pt 5), pp. 1187-1197.
26. Balocchi, R., Cantini, F., Varanini, M., Raimondi, G., Legramante, J. M., & Macerata, A. 2006, "Revisiting the potential of time-domain indexes in short-term HRV analysis", *Biomed.Tech.(Berl)*, vol. 51, no. 4, pp. 190-193.
27. Barron, R. M., Campbell, S. L., King, D., Bellon, A., Chapman, K. E., Williamson, R. A., & Manson, J. C. 2007, "High titres of TSE infectivity associated with extremely low levels of PrPSc in vivo", *Journal of Biological Chemistry* p. M704329200.
28. Barrow, P. A., Holmgren, C. D., Tapper, A. J., & Jefferys, J. G. 1999, "Intrinsic physiological and morphological properties of principal cells of the hippocampus and neocortex in hamsters infected with scrapie", *Neurobiol.Dis.*, vol. 6, no. 5, pp. 406-423.
29. Baskakov, I. V. 2007, "The reconstitution of mammalian prion infectivity de novo", *FEBS Journal*, vol. 274, no. 3, pp. 576-587.
30. Bastian, F. O., Sanders, D. E., Forbes, W. A., Hagius, S. D., Walker, J. V., Henk, W. G., Enright, F. M., & Elzer, P. H. 2007, "Spiroplasma spp. from transmissible spongiform encephalopathy brains or ticks induce spongiform encephalopathy in ruminants", *J Med Microbiol*, vol. 56, no. Pt 9, pp. 1235-1242.
31. Batschelet, E. 1981, *Circular Statistics in Biology* Academic Press inc, London.
32. Beekes, M., McBride, P. A., & Baldauf, E. 1998, "Cerebral targeting indicates vagal spread of infection in hamsters fed with scrapie", *J.Gen.Virol.*, vol. 79 (Pt 3), pp. 601-607.
33. Beekes, M. & McBride, P. A. 2007, "The spread of prions through the body in naturally acquired transmissible spongiform encephalopathies", *FEBS Journal*, vol. 274, no. 3, pp. 588-605.
34. Bellworthy, S. J., Dexter, G., Stack, M., Chaplin, M., Hawkins, S. A., Simmons, M. M., Jeffrey, M., Martin, S., Gonzalez, L., & Hill, P. 2005, "Natural transmission of BSE between sheep within an experimental flock", *Vet.Rec.*, vol. 157, no. 7, p. 206.
35. Bennett, J. A., Ford, T. W., Kidd, C., & McWilliam, P. N. "J Physiol. 1984; 351(Suppl): 27P.".
36. Bennett, J. A., Kidd, C., Latif, A. B., & McWilliam, P. N. 1981, "A horseradish peroxidase study of vagal motoneurones with axons in cardiac and pulmonary branches of the cat and dog", *Q.J.Exp.Physiol*, vol. 66, no. 2, pp. 145-154.
37. Berger, A. J. & Averill, D. B. 1983, "Projection of single pulmonary stretch receptors to solitary tract region", *J Neurophysiol.*, vol. 49, no. 3, pp. 819-830.
38. Berger, R. D., Saul, J. P., & Cohen, R. J. 1989, "Transfer function analysis of autonomic regulation. I. Canine atrial rate response", *Am.J Physiol*, vol. 256, no. 1 Pt 2, p. H142-H152.

39. Beringue, V., Andreoletti, O., Le Dur, A., Essalmani, R., Vilotte, J. L., Lacroux, C., Reine, F., Herzog, L., Biacabe, A. G., Baron, T., Caramelli, M., Casalone, C., & Laude, H. 2007, "A Bovine Prion Acquires an Epidemic Bovine Spongiform Encephalopathy Strain-Like Phenotype on Interspecies Transmission", *Journal of Neuroscience*, vol. 27, no. 26, pp. 6965-6971.
40. Bernardi, L., Keller, F., Sanders, M., Reddy, P. S., Griffith, B., Meno, F., & Pinsky, M. R. 1989, "Respiratory sinus arrhythmia in the denervated human heart", *Journal of Applied Physiology*, vol. 67, no. 4, pp. 1447-1455.
41. Bernardi, L., Bianchini, B., Spadacini, G., Leuzzi, S., Valle, F., Marchesi, E., Passino, C., Calciati, A., Vigano, M., Rinaldi, M., Martinelli, L., Finardi, G., & Sleight, P. 1995, "Demonstrable Cardiac Reinnervation After Human Heart Transplantation by Carotid Baroreflex Modulation of RR Interval", *Circulation*, vol. 92, no. 10, pp. 2895-2903.
42. Berne, R. M., Levy, M. N., Koeppen, B. M., & Stanton, B. A. 1998, *Physiology*, 4th edition edn.
43. Berntson, G. G., Bigger, J. T., Jr., Eckberg, D. L., Grossman, P., Kaufmann, P. G., Malik, M., Nagaraja, H. N., Porges, S. W., Saul, J. P., Stone, P. H., & van der Molen, M. W. 1997, "Heart rate variability: origins, methods, and interpretive caveats", *Psychophysiology*, vol. 34, no. 6, pp. 623-648.
44. Berntson, G. G., Cacioppo, J. T., & Quigley, K. S. 1991, "Autonomic determinism: the modes of autonomic control, the doctrine of autonomic space, and the laws of autonomic constraint", *Psychol.Rev.*, vol. 98, no. 4, pp. 459-487.
45. Berntson, G. G., Cacioppo, J. T., & Quigley, K. S. 1993, "Respiratory sinus arrhythmia: autonomic origins, physiological mechanisms, and psychophysiological implications", *Psychophysiology*, vol. 30, no. 2, pp. 183-196.
46. Berntson, G. G., Cacioppo, J. T., & Quigley, K. S. 1994, "Autonomic cardiac control. I. Estimation and validation from pharmacological blockades", *Psychophysiology*, vol. 31, no. 6, pp. 572-585.
47. Berntson, G. G., Lozano, D. L., & Chen, Y. J. 2005, "Filter properties of root mean square successive difference (RMSSD) for heart rate", *Psychophysiology*, vol. 42, no. 2, pp. 246-252.
48. Berntson, G. G. & Stowell, J. R. 1998, "ECG artifacts and heart period variability: don't miss a beat!", *Psychophysiology*, vol. 35, no. 1, pp. 127-132.
49. Berntson, G. G., Cacioppo, J. T., & Grossman, P. 2007, "Whither vagal tone", *Biological Psychology*, vol. 74, no. 2, pp. 295-300.
50. Bieger, D. & Hopkins, D. A. 1987, "Viscerotopic representation of the upper alimentary tract in the medulla oblongata in the rat: the nucleus ambiguus", *J.Comp Neurol.*, vol. 262, no. 4, pp. 546-562.
51. Billman, G. E. & Dujardin, J. P. 1990, "Dynamic changes in cardiac vagal tone as measured by time-series analysis", *Am J Physiol*, vol. 258, no. 3 Pt 2, p. H896-H902.
52. Bland, J. M. & Altman, D. G. 1986, "Statistical methods for assessing agreement between two methods of clinical measurement", *Lancet*, vol. 1, no. 8476, pp. 307-310.
53. Bland, J. M. & Altman, D. G. 1995, "Multiple significance tests: the Bonferroni method", *BMJ*, vol. 310, no. 6973, p. 170.
54. Blattler, T., Brandner, S., Raeber, A. J., Klein, M. A., Voigtlander, T., Weissmann, C., & Aguzzi, A. 1997, "PrP-expressing tissue required for transfer of scrapie infectivity from spleen to brain", *Nature*, vol. 389, no. 6646, pp. 69-73.
55. Bloomfield, D. M., Zweibel, S., Bigger, J. T., Jr., & Steinman, R. C. 1998, "R-R variability detects increases in vagal modulation with phenylephrine infusion", *Am.J.Physiol*, vol. 274, no. 5 Pt 2, p. H1761-H1766.
56. Blues, C. M. & Pomfrett, C. J. 1998, "Respiratory sinus arrhythmia and clinical signs of anaesthesia in children", *British Journal of Anaesthesia*, vol. 81, no. 3, pp. 333-337.
57. Bowers, J. A., Morton, I. D., & Mould, G. I. 2000, "Directional statistics of the wind and waves", *Applied Ocean Research*, vol. 22, no. 1, pp. 13-30.

58. Brandner, S., Isenmann, S., Raeber, A., Fischer, M., Sailer, A., Kobayashi, Y., Marino, S., Weissmann, C., & Aguzzi, A. 1996, "Normal host prion protein necessary for scrapie-induced neurotoxicity", *Nature*, vol. 379, no. 6563, pp. 339-343.
59. Brigham, E. O. 1988, *The Fast Fourier Transform* Prentice Hall, New Jersey.
60. Brooks, P. A. & Glaum, S. R. 1995, "GABAB receptors modulate a tetanus-induced sustained potentiation of monosynaptic inhibitory transmission in the rat nucleus tractus solitarii in vitro", *Journal of the Autonomic Nervous System*, vol. 54, no. 1, pp. 16-26.
61. Brown, D. R., Qin, K., Herms, J. W., Madlung, A., Manson, J., Strome, R., Fraser, P. E., Kruck, T., von, B. A., Schulz-Schaeffer, W., Giese, A., Westaway, D., & Kretzschmar, H. 1997, "The cellular prion protein binds copper in vivo", *Nature*, vol. 390, no. 6661, pp. 684-687.
62. Brown, D. R. 2001, "Prion and prejudice: normal protein and the synapse", *Trends in Neurosciences*, vol. 24, no. 2, pp. 85-90.
63. Brown, J. W. 1990, "Prenatal development of the human nucleus ambiguus during the embryonic and early fetal periods", *Am.J Anat.*, vol. 189, no. 3, pp. 267-283.
64. Brown, K. L., Stewart, K., Ritchie, D., Fraser, H., Morrison, W. I., & Bruce, M. E. 2000, "Follicular dendritic cells in scrapie pathogenesis", *Arch.Virol.Suppl* no. 16, pp. 13-21.
65. Brown, T. H. & McAfee, D. A. 1982, "Long-term synaptic potentiation in the superior cervical ganglion", *Science*, vol. 215, no. 4538, pp. 1411-1413.
66. Browning, K. N. & Mendelowitz, D. 2003, "Musings on the wanderer: what's new in our understanding of vago-vagal reflexes?: II. Integration of afferent signaling from the viscera by the nodose ganglia", *Am J Physiol Gastrointest.Liver Physiol*, vol. 284, no. 1, pp. G8-14.
67. Brunsdon, C. & Corcoran, J. 2006, "Using circular statistics to analyse time patterns in crime incidence", *Computers, Environment and Urban Systems*, vol. 30, no. 3, pp. 300-319.
68. Bueler, H., Fischer, M., Lang, Y., Bluethmann, H., Lipp, H. P., Dearmond, S. J., Prusiner, S. B., Aguet, M., & Weissmann, C. 1992, "Normal development and behaviour of mice lacking the neuronal cell-surface PrP protein", *Nature*, vol. 356, no. 6370, pp. 577-582.
69. Buob, A., Winter, H., Kindermann, M., Becker, G., Moller, J. C., Oertel, W. H., & Bohm, M. 2010, "Parasympathetic but not sympathetic cardiac dysfunction at early stages of Parkinson's disease", *Clin Res Cardiol.*
70. Burt, D. R. 2003, "Reducing GABA receptors", *Life Sci*, vol. 73, no. 14, pp. 1741-1758.
71. Cacioppo, J. T., Berntson, G. G., Binkley, P. F., Quigley, K. S., Uchino, B. N., & Fieldstone, A. 1994, "Autonomic cardiac control. II. Noninvasive indices and basal response as revealed by autonomic blockades", *Psychophysiology*, vol. 31, no. 6, pp. 586-598.
72. Calaresu, F. R. & Cottle, M. K. 1965, "Origin of cardiomotor fibres in the dorsal nucleus of the vagus in the cat: A histological study", *J.Physiol*, vol. 176, pp. 252-260.
73. Card, J. P., Rinaman, L., Lynn, R. B., Lee, B. H., Meade, R. P., Miselis, R. R., & Enquist, L. W. 1993, "Pseudorabies virus infection of the rat central nervous system: ultrastructural characterization of viral replication, transport, and pathogenesis", *Journal of Neuroscience*, vol. 13, no. 6, pp. 2515-2539.
74. Carleton, A., Tremblay, P., Vincent, J. D., & Lledo, P. M. 2001, "Dose-dependent, prion protein (PrP)-mediated facilitation of excitatory synaptic transmission in the mouse hippocampus", *Pflugers Arch.*, vol. 442, no. 2, pp. 223-229.
75. Castilla, J., Brun, A., az-San, S. F., Salguero, F. J., Gutierrez-Adan, A., Pintado, B., Ramirez, M. A., Del, R. L., & Torres, J. M. 2005, "Vertical transmission of bovine spongiform encephalopathy prions evaluated in a transgenic mouse model", *The Journal of Virology*, vol. 79, no. 13, pp. 8665-8668.

76. Castilla, J., Saβ, P., Hetz, C., & Soto, C. In Vitro Generation of Infectious Scrapie Prions. Cell 121[2], 195-206. 22-4-2005.
Ref Type: Abstract
77. Caughey, B. & Baron, G. S. 2006, "Prions and their partners in crime", *Nature*, vol. 443, no. 7113, pp. 803-810.
78. Chapleau, M. W. & Sabharwal, R. 2010, "Methods of assessing vagus nerve activity and reflexes", *Heart Fail.Rev*.
79. Chase, M. R. & Ranson, S. W. 1914, "The structure of the roots, trunk and branches of the vagus nerve", *The Journal of Comparative Neurology*, vol. 24, no. 1, pp. 31-60.
80. Chen, K. Y., Chen, C. L., Yang, C. C., & Kuo, T. B. 2006, "Cardiac Autonomic Dysregulation in Patients with Acute Hepatitis", *Am.J Med.Sci.*, vol. 332, no. 4, pp. 164-167.
81. Cheng, Z., Guo, S. Z., Lipton, A. J., & Gozal, D. 2002, "Domoic acid lesions in nucleus of the solitary tract: time-dependent recovery of hypoxic ventilatory response and peripheral afferent axonal plasticity", *J Neurosci.*, vol. 22, no. 8, pp. 3215-3226.
82. Cheng, Z., Zhang, H., Guo, S. Z., Wurster, R., & Gozal, D. 2004a, "Differential control over postganglionic neurons in rat cardiac ganglia by NA and DmnX neurons: anatomical evidence", *Am.J.Physiol Regul.Integr.Comp Physiol*, vol. 286, no. 4, p. R625-R633.
83. Cheng, Z., Zhang, H., Yu, J., Wurster, R. D., & Gozal, D. 2004b, "Attenuation of baroreflex sensitivity after domoic acid lesion of the nucleus ambiguus of rats", *J.Appl.Physiol*, vol. 96, no. 3, pp. 1137-1145.
84. Chesebro, B., Trifilo, M., Race, R., Meade-White, K., Teng, C., LaCasse, R., Raymond, L., Favara, C., Baron, G., Priola, S., Caughey, B., Masliah, E., & Oldstone, M. 2005, "Anchorless prion protein results in infectious amyloid disease without clinical scrapie", *Science*, vol. 308, no. 5727, pp. 1435-1439.
85. Chiesa, R., Piccardo, P., Biasini, E., Ghetti, B., & Harris, D. A. 2008, "Aggregated, Wild-Type Prion Protein Causes Neurological Dysfunction and Synaptic Abnormalities", *Journal of Neuroscience*, vol. 28, no. 49, pp. 13258-13267.
86. Choi, J. B., Hong, S., Nelesen, R., Bardwell, W. A., Natarajan, L., Schubert, C., & Dimsdale, J. E. 2006, "Age and ethnicity differences in short-term heart-rate variability", *Psychosom.Med*, vol. 68, no. 3, pp. 421-426.
87. Ciriello, J. & Calaresu, F. R. 1980, "Distribution of vagal cardioinhibitory neurons in the medulla of the cat", *Am.J.Physiol*, vol. 238, no. 1, p. R57-R64.
88. Ciriello, J. & Calaresu, F. R. 1982, "Medullary origin of vagal preganglionic axons to the heart of the cat", *J.Auton.Nerv.Syst.*, vol. 5, no. 1, pp. 9-22.
89. Ciriello, J. & de Oliveira, C. V. 2003, "Cardiac effects of hypocretin-1 in nucleus ambiguus", *Am J Physiol Regul.Integr.Comp Physiol*, vol. 284, no. 6, p. R1611-R1620.
90. Cohen, F. E. 1999, "Protein misfolding and prion diseases", *J Mol Biol*, vol. 293, no. 2, pp. 313-320.
91. Cohen, F. E. & Prusiner, S. B. 1998, "Pathologic conformations of prion proteins", *Annu.Rev.Biochem.*, vol. 67, pp. 793-819.
92. Collinge, J. 2001, "Prion diseases of humans and animals: their causes and molecular basis", *Annu.Rev.Neurosci.*, vol. 24, pp. 519-550.
93. Collinge, J., Whittington, M. A., Sidle, K. C., Smith, C. J., Palmer, M. S., Clarke, A. R., & Jefferys, J. G. 1994, "Prion protein is necessary for normal synaptic function", *Nature*, vol. 370, no. 6487, pp. 295-297.
94. Collinge, J. & Clarke, A. R. 2007, "A General Model of Prion Strains and Their Pathogenicity", *Science*, vol. 318, no. 5852, pp. 930-936.
95. Comroe, J. H. 1954, "Respiration", *Annu.Rev Physiol*, vol. 16, pp. 135-154.
96. Cooley, J. W. & Tukey, J. W. 1965, "An Algorithm for the Machine Calculation of Complex Fourier Series", *Mathematics of Computation*, vol. 19, no. 90, pp. 297-301.

97. Cournand, A. 1979, "Claude Bernard's Contributions to Cardiac Physiology," in *Claude Bernard and the Internal Environment*, E. D. Robin, ed., Marcel Decker, Inc, New York, pp. 97-121.
98. Cuillé, J. & Chelle, P. L. 1939, "Experimental transmission of trembling to the goat", *C.R.Seances Acad.Sci*, vol. 208, pp. 1058-1060.
99. Cunningham, C., Deacon, R., Wells, H., Boche, D., Waters, S., Diniz, C. P., Scott, H., Rawlins, J. N., & Perry, V. H. 2003, "Synaptic changes characterize early behavioural signs in the ME7 model of murine prion disease", *Eur J Neurosci.*, vol. 17, no. 10, pp. 2147-2155.
100. Cysarz, D., Zerm, R., Bettermann, H., Fruhwirth, M., Moser, M., & Kroz, M. 2008, "Comparison of Respiratory Rates Derived from Heart Rate Variability, ECG Amplitude, and Nasal/Oral Airflow", *Ann.Biomed.Eng*.
101. Daly, M. B. & Kirkman, E. 1989, "Differential modulation by pulmonary stretch afferents of some reflex cardioinhibitory responses in the cat", *J Physiol*, vol. 417, pp. 323-341.
102. Daly, M. D. 1991, "Some reflex cardioinhibitory responses in the cat and their modulation by central inspiratory neuronal activity", *J Physiol*, vol. 439, pp. 559-577.
103. Darwin, C. 1872, *The Expression of the Emotions in Man and Animals.*
104. Davidson, N. S., Goldner, S., & McCloskey, D. I. 1976, "Respiratory modulation of barareceptor and chemoreceptor reflexes affecting heart rate and cardiac vagal efferent nerve activity", *J Physiol*, vol. 259, no. 2, pp. 523-530.
105. Davies, F., Francis, E., & King, T. 1952, "Neurological studies of the cardiac ventricles of mammals", *J Anat*, vol. 86, no. 2, pp. 130-143.
106. De Meersman, R. E. 1993, "Aging as a modulator of respiratory sinus arrhythmia", *J.Gerontol.*, vol. 48, no. 2, p. B74-B78.
107. de Oliveira, C. V., Rosas-Arellano, M. P., Solano-Flores, L. P., & Ciriello, J. 2003, "Cardiovascular effects of hypocretin-1 in nucleus of the solitary tract", *Am.J Physiol Heart Circ.Physiol*, vol. 284, no. 4, p. H1369-H1377.
108. Dearmond, S. J., Mobley, W. C., DeMott, D. L., Barry, R. A., Beckstead, J. H., & Prusiner, S. B. 1987, "Changes in the localization of brain prion proteins during scrapie infection", *Neurology*, vol. 37, no. 8, pp. 1271-1280.
109. DeBoer, R. W., Karemaker, J. M., & Strackee, J. 1984, "Comparing Spectra of a Series of Point Events Particularly for Heart Rate Variability Data", *Biomedical Engineering, IEEE Transactions on*, vol. BME-31, no. 4, pp. 384-387.
110. Defra, S. D. M. S. a. F. T. Experimental production of bovine tissues for validation of BSE diagnostic tests (SE1736). http://64.233.183.104/search?q=cache:QXgpWOF60z0J:randd.defra.gov.uk/Document.aspx%3FDocument%3DSE1736_6093_FRP.doc+chloros+DEFRA&hl=en&ct=clnk&cd=3&gl=uk . 2007.
Ref Type: Electronic Citation
111. Deleault, N. R., Harris, B. T., Rees, J. R., & Supattapone, S. 2007, "Formation of native prions from minimal components in vitro", *Proceedings of the National Academy of Sciences* p. 0702662104.
112. Dellinger, J. A., Taylor, H. L., & Porges, S. W. 1987, "Atropine sulfate effects on aviator performance and on respiratory-heart period interactions", *Aviat.Space Environ.Med*, vol. 58, no. 4, pp. 333-338.
113. Denver, J. W., Reed, S. F., & Porges, S. W. 2007, "Methodological issues in the quantification of respiratory sinus arrhythmia", *Biological Psychology*, vol. 74, no. 2, pp. 286-294.
114. Dexter, F., Levy, M. N., & Rudy, Y. 1989, "Mathematical model of the changes in heart rate elicited by vagal stimulation", *Circ.Res.*, vol. 65, no. 5, pp. 1330-1339.
115. Dexter, F., Saidel, G. M., Levy, M. N., & Rudy, Y. 1989, "Mathematical model of dependence of heart rate on tissue concentration of acetylcholine", *Am.J Physiol*, vol. 256, no. 2 Pt 2, p. H520-H526.

116. Dickinson, A. G., Fraser, H., Meikle, V. M., & Outram, G. W. 1972, "Competition between different scrapie agents in mice", *Nat New Biol*, vol. 237, no. 77, pp. 244-245.
117. Diener, T. O. 1973, "Similarities between the scrapie agent and the agent of the potato spindle tuber disease", *Ann.Clin.Res.*, vol. 5, no. 5, pp. 268-278.
118. Diringer, H. 1991, "Virus-induced amyloidoses", *Behring Inst.Mitt.* no. 89, pp. 146-152.
119. Donald, D. E., Samueloff, S. L., & Ferguson, D. 1967, "Mechanisms of tachycardia caused by atropine in conscious dogs", *Am J Physiol*, vol. 212, no. 4, pp. 901-910.
120. Donchin, Y., Feld, J. M., & Porges, S. W. 1985, "Respiratory sinus arrhythmia during recovery from isoflurane-nitrous oxide anesthesia", *Anesth.Analg.*, vol. 64, no. 8, pp. 811-815.
121. Dorban, G., Defaweux, V., Demonceau, C., Flandroy, S., Van Lerberghe, P. B., Falisse-Poirrier, N., Piret, J., Heinen, E., & Antoine, N. 2007, "Interaction between dendritic cells and nerve fibres in lymphoid organs after oral scrapie exposure", *Virchows Arch*.
122. Dormont, D., Delpech, B., Delpech, A., Courcel, M. N., Viret, J., Markovits, P., & Court, L. 1981, "[Hyperproduction of glial fibrillary acidic protein (GFA) during development of experimental scrapie in mice]", *C.R.Seances Acad.Sci III*, vol. 293, no. 1, pp. 53-56.
123. Dou, C. L. & Levine, J. M. 1995, "Differential effects of glycosaminoglycans on neurite growth on laminin and L1 substrates", *Journal of Neuroscience*, vol. 15, no. 12, pp. 8053-8066.
124. Drisaldi, B., Stewart, R. S., Adles, C., Stewart, L. R., Quaglio, E., Biasini, E., Fioriti, L., Chiesa, R., & Harris, D. A. 2003, "Mutant PrP is delayed in its exit from the endoplasmic reticulum, but neither wild-type nor mutant PrP undergoes retrotranslocation prior to proteasomal degradation", *Journal of Biological Chemistry*, vol. 278, no. 24, pp. 21732-21743.
125. Duclaux, R., Mei, N., & Ranieri, F. 1976, "Conduction velocity along the afferent vagal dendrites: a new type of fibre", *J Physiol*, vol. 260, no. 2, pp. 487-495.
126. Eames, P. J., Potter, J. F., & Panerai, R. B. 2005, "Assessment of cerebral autoregulation from ectopic heartbeats", *Clin Sci (Lond)*, vol. 109, no. 1, pp. 109-115.
127. Eckberg, D. L. 2003, "The human respiratory gate", *J Physiol*, vol. 548, no. Pt 2, pp. 339-352.
128. Eckberg, D. L. 2009, "Point:Counterpoint: Respiratory sinus arrhythmia is due to a central mechanism vs. respiratory sinus arrhythmia is due to the baroreflex mechanism", *Journal of Applied Physiology*, vol. 106, no. 5, pp. 1740-1742.
129. Electrophysiology, T. F. o. t. E. S. o. C. t. N. A. S. o. P. 1996, "Heart Rate Variability : Standards of Measurement, Physiological Interpretation, and Clinical Use", *Circulation*, vol. 93, no. 5, pp. 1043-1065.
130. Ellison, J. P. & Hibbs, R. G. 1976, "An ultrastructural study of mammalian cardiac ganglia", *J Mol.Cell Cardiol.*, vol. 8, no. 2, pp. 89-101.
131. Encalada, S. E., Moya, K. L., Lehmann, S., & Zahn, R. 2008, "The role of the prion protein in the molecular basis for synaptic plasticity and nervous system development", *J Mol Neurosci*, vol. 34, no. 1, pp. 9-15.
132. Ersdal, C., Simmons, M. M., Gonzalez, L., Goodsir, C. M., Martin, S., & Jeffrey, M. 2004, "Relationships between ultrastructural scrapie pathology and patterns of abnormal prion protein accumulation", *Acta Neuropathol.(Berl)*, vol. 107, no. 5, pp. 428-438.
133. Ersdal, C., Simmons, M. M., Goodsir, C., Martin, S., & Jeffrey, M. 2003, "Sub-cellular pathology of scrapie: coated pits are increased in PrP codon 136 alanine homozygous scrapie-affected sheep", *Acta Neuropathol.(Berl)*, vol. 106, no. 1, pp. 17-28.
134. Ersdal, C., Ulvund, M. J., Benestad, S. L., & Tranulis, M. A. 2003, "Accumulation of Pathogenic Prion Protein (PrPSc) in Nervous and Lymphoid Tissues of Sheep with Subclinical Scrapie", *Veterinary Pathology Online*, vol. 40, no. 2, pp. 164-174.
135. EUROPEAN COMMISSION. The evaluation of tests for the diagnosis of transmisible spongiform encephalopathoies in bovines.

http://ec.europa.eu/food/food/biosafety/bse/bse12_en.pdf . 1999.
Ref Type: Electronic Citation
136. EUROPEAN COMMISSION. The evaluation of 5 rapid tests for the diagnosis of transmisible spongiform encephalopathoies in bovines. http://ec.europa.eu/food/food/biosafety/bse/bse42_en.pdf . 27-3-2002.
Ref Type: Electronic Citation
137. Ewing, D. J., Neilson, J. M., & Travis, P. 1984, "New method for assessing cardiac parasympathetic activity using 24 hour electrocardiograms", *Br Heart J*, vol. 52, no. 4, pp. 396-402.
138. Fallen, E. L., Kamath, M. V., Ghista, D. N., & Fitchett, D. 1988, "Spectral analysis of heart rate variability following human heart transplantation: evidence for functional reinnervation", *J Auton.Nerv.Syst.*, vol. 23, no. 3, pp. 199-206.
139. Fasano, C., Campana, V., & Zurzolo, C. 2006, "Prions: protein only or something more? Overview of potential prion cofactors", *J Mol.Neurosci.*, vol. 29, no. 3, pp. 195-214.
140. Feigl, E. O. 1969, "Parasympathetic control of coronary blood flow in dogs", *Circ.Res.*, vol. 25, no. 5, pp. 509-519.
141. Fischer, M., Rulicke, T., Raeber, A., Sailer, A., Moser, M., Oesch, B., Brandner, S., Aguzzi, A., & Weissmann, C. 1996, "Prion protein (PrP) with amino-proximal deletions restoring susceptibility of PrP knockout mice to scrapie", *EMBO J.*, vol. 15, no. 6, pp. 1255-1264.
142. Ford, T. W., Bennett, J. A., Kidd, C., & McWilliam, P. N. 1990, "Neurones in the dorsal motor vagal nucleus of the cat with non-myelinated axons projecting to the heart and lungs", *Exp.Physiol*, vol. 75, no. 4, pp. 459-473.
143. Ford, T. W. & McWilliam, P. N. 1986, "The effects of electrical stimulation of myelinated and non-myelinated vagal fibres on heart rate in the rabbit", *J.Physiol*, vol. 380, pp. 341-347.
144. Fournier, J. G., Escaig-Haye, F., Billette, d., V, & Robain, O. 1995, "Ultrastructural localization of cellular prion protein (PrPc) in synaptic boutons of normal hamster hippocampus", *C.R.Acad.Sci.III*, vol. 318, no. 3, pp. 339-344.
145. Fournier, J. G., Escaig-Haye, F., Billette, d., V, Robain, O., Lasmezas, C. I., Deslys, J. P., Dormont, D., & Brown, P. 1998, "Distribution and submicroscopic immunogold localization of cellular prion protein (PrPc) in extracerebral tissues", *Cell Tissue Res.*, vol. 292, no. 1, pp. 77-84.
146. Frysinger, R. C. & Harper, R. M. 1986, "Cardiac and respiratory relationships with neural discharge in the anterior cingulate cortex during sleep-walking states", *Exp.Neurol.*, vol. 94, no. 2, pp. 247-263.
147. Frysinger, R. C. & Harper, R. M. 1989, "Cardiac and respiratory correlations with unit discharge in human amygdala and hippocampus", *Electroencephalogr.Clin.Neurophysiol.*, vol. 72, no. 6, pp. 463-470.
148. Fuhrmann, M., Mitteregger, G., Kretzschmar, H., & Herms, J. 2007, "Dendritic Pathology in Prion Disease Starts at the Synaptic Spine", *Journal of Neuroscience*, vol. 27, no. 23, pp. 6224-6233.
149. Gallego-Page, J. C., Segovia, J., onso-Pulpon, L., onso-Rodriguez, M., Salas, C., & Ortiz-Berrocal, J. 2004, "Re-innervation after heart transplantation: a multidisciplinary study", *J Heart Lung Transplant.*, vol. 23, no. 6, pp. 674-682.
150. Galletly, D. C. & Larsen, P. D. 1997, "Cardioventilatory coupling during anaesthesia", *Br J Anaesth.*, vol. 79, no. 1, pp. 35-40.
151. Galletly, D. C. & Larsen, P. D. 2001, "Inspiratory timing during anaesthesia: a model of cardioventilatory coupling", *Br J Anaesth.*, vol. 86, no. 6, pp. 777-788.
152. Gandevia, S. C., McCloskey, D. I., & Potter, E. K. 1978, "Reflex bradycardia occurring in response to diving, nasopharyngeal stimulation and ocular pressure, and its modification by respiration and swallowing", *J Physiol*, vol. 276, pp. 383-394.

153. Gao, F., Chia, K. S., Krantz, I., Nordin, P., & Machin, D. 2006, "On the application of the von Mises distribution and angular regression methods to investigate the seasonality of disease onset", *Statistics in Medicine*, vol. 25, no. 9, pp. 1593-1618.
154. Gardner, M. & Altman, D. 1989, *Statistics with Confidence* British Medical Journal, London.
155. Gauczynski, S., Peyrin, J. M., Haik, S., Leucht, C., Hundt, C., Rieger, R., Krasemann, S., Deslys, J. P., Dormont, D., Lasmezas, C. I., & Weiss, S. 2001, "The 37-kDa/67-kDa laminin receptor acts as the cell-surface receptor for the cellular prion protein", *EMBO J.*, vol. 20, no. 21, pp. 5863-5875.
156. Gavier-Widen, D., Noremark, M., Langeveld, J. P. M., Stack, M., Biacabe, A. G., Vulin, J., Chaplin, M., Richt, J. A., Jacobs, J., Acin, C., Monleon, E., Renstrom, L., Klingeborn, B., & Baron, T. G. M. 2008, "Bovine spongiform encephalopathy in Sweden: an H-type variant", *Journal of Veterinary Diagnostic Investigation*, vol. 20, no. 1, pp. 2-10.
157. Gavin Sandercock, e. a. Association between RR interval and high-frequency heart rate variability acquired during short-term, resting recordings with free and paced breathing. Physiological Measurement 29[7], 795. 2008.
Ref Type: Abstract
158. Geis, G. S. & Wurster, R. D. 1980, "Cardiac responses during stimulation of the dorsal motor nucleus and nucleus ambiguus in the cat", *Circ.Res.*, vol. 46, no. 5, pp. 606-611.
159. Gershon, M. D. 2003, *The Second Brain*, third edn.
160. Gibbons, R. A. & Hunter, G. D. 1967, "Nature of the scrapie agent", *Nature*, vol. 215, no. 105, pp. 1041-1043.
161. Gilbey, M. P., Jordan, D., Richter, D. W., & Spyer, K. M. 1984, "Synaptic mechanisms involved in the inspiratory modulation of vagal cardio-inhibitory neurones in the cat", *J Physiol*, vol. 356, pp. 65-78.
162. Gill, J. & Hangartner, D. 2010, "Circular Data in Political Science and How to Handle It", *Political Analysis*, vol. 18, no. 3, pp. 316-336.
163. Glatzel, M., Klein, M. A., Brandner, S., & Aguzzi, A. 2000, "Prions: from neurografts to neuroinvasion", *Arch.Virol.Suppl* no. 16, pp. 3-12.
164. Glover, D. G., Pollard, B. J., Gonzalez, L., Siso, S., Kennedy, D., & Jeffrey, M. 2007, "A non-invasive screen for infectivity in transmissible spongiform encephalopathies", *Gut*, vol. 56, no. 9, pp. 1329-1331.
165. Golding, N. L., Staff, N. P., & Spruston, N. 2002, "Dendritic spikes as a mechanism for cooperative long-term potentiation", *Nature*, vol. 418, no. 6895, pp. 326-331.
166. Gonzalez, L., Dagleish, M. P., Bellworthy, S. J., Siso, S., Stack, M. J., Chaplin, M. J., Davis, L. A., Hawkins, S. A., Hughes, J., & Jeffrey, M. 2006, "Postmortem diagnosis of preclinical and clinical scrapie in sheep by the detection of disease-associated PrP in their rectal mucosa", *Vet.Rec.*, vol. 158, no. 10, pp. 325-331.
167. Gonzalez, L., Jeffrey, M., Siso, S., Martin, S., Bellworthy, S. J., Stack, M. J., Chaplin, M. J., Davis, L., Dagleish, M. P., & Reid, H. W. 2005, "Diagnosis of preclinical scrapie in samples of rectal mucosa", *The Veterinary Record*, vol. 156, no. 26, pp. 846-847.
168. GoodMan & Gilmore 2010, *The Pharmacological Basis of Therapeutics* McGraw-Hill.
169. Gordon, W. S. 1946, "Louping ill, tick-borne fever and scrapie.", *Vet.Rec.*, vol. 58, no. 47, pp. 516-525.
170. Graham, F. K. & Clifton, R. K. 1966, "Heart-rate change as a component of the orienting response", *Psychol.Bull.*, vol. 65, no. 5, pp. 305-320.
171. Graner, E., Mercadante, A. F., Zanata, S. M., Forlenza, O. V., Cabral, A. L., Veiga, S. S., Juliano, M. A., Roesler, R., Walz, R., Minetti, A., Izquierdo, I., Martins, V. R., & Brentani, R. R. 2000, "Cellular prion protein binds laminin and mediates neuritogenesis", *Brain Res.Mol.Brain Res.*, vol. 76, no. 1, pp. 85-92.
172. Gray, A. L., Johnson, T. A., Ardell, J. L., & Massari, V. J. 2004, "Parasympathetic control of the heart. II. A novel interganglionic intrinsic cardiac circuit mediates neural control of heart rate", *J.Appl.Physiol*, vol. 96, no. 6, pp. 2273-2278.

173. Gribbin, B., Pickering, T. G., Sleight, P., & Peto, R. 1971, "Effect of age and high blood pressure on baroreflex sensitivity in man", *Circ.Res*, vol. 29, no. 4, pp. 424-431.
174. Griffith, J. S. 1967, " Self-replication and scrapie.", *Nature*, vol. 215, pp. 1043-1044.
175. Grossman, P. 1992, "Breathing rhythms of the heart in a world of no steady state: a comment on Weber, Molenaar, and van der Molen", *Psychophysiology*, vol. 29, no. 1, pp. 66-72.
176. Grossman, P. & Kollai, M. 1993, "Respiratory sinus arrhythmia, cardiac vagal tone, and respiration: within- and between-individual relations", *Psychophysiology*, vol. 30, no. 5, pp. 486-495.
177. Grossman, P., van, B. J., & Wientjes, C. 1990, "A comparison of three quantification methods for estimation of respiratory sinus arrhythmia", *Psychophysiology*, vol. 27, no. 6, pp. 702-714.
178. Grossman, P. & Wientjes, K. 1986, " Respiratory sinus arrhythmia and parasympathetic cardiac control: Some basic issues concerning quantification, applications and implications.," in *Cardiorespiratory and cardiosomatic psychophysiology In P.Grossman, K. H. L.Janssen, & D.Vaitl, (Eds.), .*, Plenum Press., New York, pp. 117-138.
179. Grossman, P. & Taylor, E. W. 2007, "Toward understanding respiratory sinus arrhythmia: Relations to cardiac vagal tone, evolution and biobehavioral functions", *Biological Psychology*, vol. 74, no. 2, pp. 263-285.
180. Gustafson, K. M., Allen, J. J. B., Yeh, H. w., & May, L. E. 2011, "Characterization of the fetal diaphragmatic magnetomyogram and the effect of breathing movements on cardiac metrics of rate and variability", *Early Human Development*, vol. 87, no. 7, pp. 467-475.
181. Halpert, I., Goldberg, A. D., Levine, A. B., Levine, T. B., Kornberg, R., Kelly, C., & Lesch, M. 1996, "Reinnervation of the transplanted human heart as evidenced from heart rate variability studies", *Am J Cardiol.*, vol. 77, no. 2, pp. 180-183.
182. Hanss, R., Bein, B., Francksen, H., Scherkl, W., Bauer, M., Doerges, V., Steinfath, M., Scholz, J., & Tonner, P. H. 2006, "Heart rate variability-guided prophylactic treatment of severe hypotension after subarachnoid block for elective cesarean delivery", *Anesthesiology*, vol. 104, no. 4, pp. 635-643.
183. Hartter, D. E. & Barnea, A. 1988, "Evidence for release of copper in the brain: depolarization-induced release of newly taken-up 67copper", *Synapse*, vol. 2, no. 4, pp. 412-415.
184. Haselton, J. R., Solomon, I. C., Motekaitis, A. M., & Kaufman, M. P. 1992, "Bronchomotor vagal preganglionic cell bodies in the dog: an anatomic and functional study", *J.Appl.Physiol*, vol. 73, no. 3, pp. 1122-1129.
185. Haskey, J. C. 1988, "The relative orientation of addresses of spouses before their marriage:an analysis of circular data", *Journal of Applied Statistics*, vol. 15, no. 2, pp. 183-195.
186. Herman, M. A., Cruz, M. T., Sahibzada, N., Verbalis, J., & Gillis, R. A. 2009, "GABA signaling in the nucleus tractus solitarius sets the level of activity in dorsal motor nucleus of the vagus cholinergic neurons in the vagovagal circuit", *AJP - Gastrointestinal and Liver Physiology*, vol. 296, no. 1, p. G101-G111.
187. Herms, J., Tings, T., Gall, S., Madlung, A., Giese, A., Siebert, H., Schurmann, P., Windl, O., Brose, N., & Kretzschmar, H. 1999, "Evidence of presynaptic location and function of the prion protein", *Journal of Neuroscience*, vol. 19, no. 20, pp. 8866-8875.
188. Hill, A. F., Desbruslais, M., Joiner, S., Sidle, K. C., Gowland, I., Collinge, J., Doey, L. J., & Lantos, P. 1997, "The same prion strain causes vCJD and BSE", *Nature*, vol. 389, no. 6650, pp. 448-50, 526.
189. Hill, A. F., Joiner, S., Linehan, J., Desbruslais, M., Lantos, P. L., & Collinge, J. 2000, "Species-barrier-independent prion replication in apparently resistant species", *Proc.Natl.Acad Sci U.S.A*, vol. 97, no. 18, pp. 10248-10253.

190. Hilton, D. A. 2006, "Pathogenesis and prevalence of variant Creutzfeldt-Jakob disease", *J Pathol.*, vol. 208, no. 2, pp. 134-141.
191. Hon, E. & Lee, S. 1963, "Electronic Evaluation of the Fetal Heart Rate. VIII. Patterns Preceeding Fetal Death, Further Observations", *Am.J Obstet.Gynecol.*, vol. 87, pp. 814-826.
192. Hopkins, D. A. 1987, "The dorsal motor nucleus of the vagus nerve and the nucleus ambiguus: structure and connections," in *Cardiogenic Reflexes* , R. Hainsworth, P. N. McWilliam, & D. A. S. G. Mary, eds., Oxford University Press, USA September, pp. 185-203.
193. Hornshaw, M. P., McDermott, J. R., & Candy, J. M. 1995, "Copper binding to the N-terminal tandem repeat regions of mammalian and avian prion protein", *Biochem.Biophys.Res.Commun.*, vol. 207, no. 2, pp. 621-629.
194. Huang, M. H., Smith, F. M., & Armour, J. A. 1993a, "Amino acids modify activity of canine intrinsic cardiac neurons involved in cardiac regulation", *Am J Physiol*, vol. 264, no. 4 Pt 2, p. H1275-H1282.
195. Huang, M. H., Smith, F. M., & Armour, J. A. 1993b, "Modulation of in situ canine intrinsic cardiac neuronal activity by nicotinic, muscarinic, and beta-adrenergic agonists", *Am.J Physiol*, vol. 265, no. 3 Pt 2, p. R659-R669.
196. Irnaten, M., Neff, R. A., Wang, J., Loewy, A. D., Mettenleiter, T. C., & Mendelowitz, D. 2001, "Activity of cardiorespiratory networks revealed by transsynaptic virus expressing GFP", *J Neurophysiol.*, vol. 85, no. 1, pp. 435-438.
197. Ironside, J. W. 2000, "Pathology of variant Creutzfeldt-Jakob disease", *Arch.Virol.Suppl* no. 16, pp. 143-151.
198. Ironside, J. W., Bishop, M. T., Connolly, K., Hegazy, D., Lowrie, S., Le, G. M., Ritchie, D. L., McCardle, L. M., & Hilton, D. A. 2006, "Variant Creutzfeldt-Jakob disease: prion protein genotype analysis of positive appendix tissue samples from a retrospective prevalence study", *BMJ*, vol. 332, no. 7551, pp. 1186-1188.
199. Iwanaga, K., Wakabayashi, K., Yoshimoto, M., Tomita, I., Satoh, H., Takashima, H., Satoh, A., Seto, M., Tsujihata, M., & Takahashi, H. 1999, "Lewy body-type degeneration in cardiac plexus in Parkinson's and incidental Lewy body diseases", *Neurology*, vol. 52, no. 6, pp. 1269-1271.
200. Jacobs, J. G., Langeveld, J. P. M., Biacabe, A. G., Acutis, P. L., Polak, M. P., Gavier-Widen, D., Buschmann, A., Caramelli, M., Casalone, C., Mazza, M., Groschup, M., Erkens, J. H. F., Davidse, A., van Zijderveld, F. G., & Baron, T. 2007, "Molecular discrimination of atypical bovine spongiform encephalopathies from a wide geographical region in Europe", *Journal of Clinical Microbiology* p. JCM.
201. Jamieson, E., Jeffrey, M., Ironside, J. W., & Fraser, J. R. 2001, "Apoptosis and dendritic dysfunction precede prion protein accumulation in 87V scrapie", *Neuroreport*, vol. 12, no. 10, pp. 2147-2153.
202. Janzekovic, M., Vindis, P., Stajnko, D., & Brus, M. **Polar Sport Tester for Cattle Heart Rate Measurements.** http://www.intechopen.com/source/pdfs/12347/InTech-Polar_sport_tester_for_cattle_heart_rate_measurements.pdf . 20-6-2011.
Ref Type: Electronic Citation
203. Jarrell, T. W., Gentile, C. G., McCabe, P. M., & Schneiderman, N. 1986, "Sinoaortic denervation does not prevent differential Pavlovian conditioning of bradycardia in rabbits", *Brain Research*, vol. 381, no. 2, pp. 251-258.
204. Jeffrey, M., Gonzalez, L., Espenes, A., Press, C. M., Martin, S., Chaplin, M., Davis, L., Landsverk, T., MacAldowie, C., Eaton, S., & McGovern, G. 2006, "Transportation of prion protein across the intestinal mucosa of scrapie-susceptible and scrapie-resistant sheep", *J Pathol.*, vol. 209, no. 1, pp. 4-14.
205. Jeffrey, M., Goodsir, C. M., Bruce, M. E., McBride, P. A., & Fraser, J. R. 1997, "In vivo toxicity of prion protein in murine scrapie: ultrastructural and immunogold studies", *Neuropathol.Appl.Neurobiol.*, vol. 23, no. 2, pp. 93-101.

206. Jeffrey, M., Goodsir, C. M., Race, R. E., & Chesebro, B. 2004, "Scrapie-specific neuronal lesions are independent of neuronal PrP expression", *Ann.Neurol.*, vol. 55, no. 6, pp. 781-792.
207. Jeffrey, M., Halliday, W. G., Bell, J., Johnston, A. R., MacLeod, N. K., Ingham, C., Sayers, A. R., Brown, D. A., & Fraser, J. R. 2000, "Synapse loss associated with abnormal PrP precedes neuronal degeneration in the scrapie-infected murine hippocampus", *Neuropathol.Appl.Neurobiol.*, vol. 26, no. 1, pp. 41-54.
208. Jeffrey, M., McGovern, G., Martin, S., Goodsir, C. M., & Brown, K. L. 2000, "Cellular and sub-cellular localisation of PrP in the lymphoreticular system of mice and sheep", *Arch.Virol.Suppl* no. 16, pp. 23-38.
209. Jeffrey, M., Goodsir, C., McGovern, G., Barmada, S. J., Medrano, A. Z., & Harris, D. A. 2009, "Prion Protein with an Insertional Mutation Accumulates on Axonal and Dendritic Plasmalemma and Is Associated with Distinctive Ultrastructural Changes", *American Journal of Pathology* p. ajpath.
210. Jennings, J. R. & McKnight, J. D. 1994, "Inferring vagal tone from heart rate variability", *Psychosom.Med*, vol. 56, no. 3, pp. 194-196.
211. Jewell, J. E., Brown, J., Kreeger, T., & Williams, E. S. 2006, "Prion protein in cardiac muscle of elk (Cervus elaphus nelsoni) and white-tailed deer (Odocoileus virginianus) infected with chronic wasting disease", *Journal of General Virology*, vol. 87, no. 11, pp. 3443-3450.
212. Jira, M., Zavodna, E., Novakova, Z., Fiser, B., & Honzikova, N. 2010, "Reproducibility of blood pressure and inter-beat interval variability in man", *Physiol Res*, vol. 59 Suppl 1, p. S113-S121.
213. John Allen. CMetX (John Allen) A command-line based utility to calculate several metrics of cardiac chronotropy. 2002.
Ref Type: Internet Communication
214. Johnson, T. A., Gray, A. L., Lauenstein, J. M., Newton, S. S., & Massari, V. J. 2004, "Parasympathetic control of the heart. I. An interventriculo-septal ganglion is the major source of the vagal intracardiac innervation of the ventricles", *J Appl.Physiol*, vol. 96, no. 6, pp. 2265-2272.
215. Johnston, A. R., Fraser, J. R., Jeffrey, M., & MacLeod, N. 1998, "Synaptic plasticity in the CA1 area of the hippocampus of scrapie-infected mice", *Neurobiol.Dis*, vol. 5, no. 3, pp. 188-195.
216. Jones, J. F., Wang, Y., & Jordan, D. 1995, "Heart rate responses to selective stimulation of cardiac vagal C fibres in anaesthetized cats, rats and rabbits", *J Physiol*, vol. 489 (Pt 1), pp. 203-214.
217. Jones, J. F., Wang, Y., & Jordan, D. 1998, "Activity of C fibre cardiac vagal efferents in anaesthetized cats and rats", *J Physiol*, vol. 507 (Pt 3), pp. 869-880.
218. Jordan, D., Khalid, M. E., Schneiderman, N., & Spyer, K. M. 1982, "The location and properties of preganglionic vagal cardiomotor neurones in the rabbit", *Pflugers Arch.*, vol. 395, no. 3, pp. 244-250.
219. Julien, C., Chapuis, B., Cheng, Y., & Barres, C. 2003, "Dynamic interactions between arterial pressure and sympathetic nerve activity: role of arterial baroreceptors", *Am J Physiol Regul.Integr.Comp Physiol*, vol. 285, no. 4, p. R834-R841.
220. Jurd, R., Arras, M., Lambert, S., Drexler, B., Siegwart, R., Crestani, F., Zaugg, M., Vogt, K. E., Ledermann, B., Antkowiak, B., & Rudolph, U. 2003, "General anesthetic actions in vivo strongly attenuated by a point mutation in the GABA(A) receptor beta3 subunit", *FASEB J*, vol. 17, no. 2, pp. 250-252.
221. Kalia, M. & Mesulam, M. M. 1980, "Brain stem projections of sensory and motor components of the vagus complex in the cat: I. The cervical vagus and nodose ganglion", *J.Comp Neurol.*, vol. 193, no. 2, pp. 435-465.
222. Kandell, E. R., Schwartz, J. H., & Jessell, T. M. 2000, *Principles of Neural Science*, 4th edn.

223. Kardos, J., Kovacs, I., Hajos, F., Kalman, M., & Simonyi, M. 1989, "Nerve endings from rat brain tissue release copper upon depolarization. A possible role in regulating neuronal excitability", *Neurosci.Lett.*, vol. 103, no. 2, pp. 139-144.
224. Kaski, D., Mead, S., Hyare, H., Cooper, S., Jampana, R., Overell, J., Knight, R., Collinge, J., & Rudge, P. 2009, "Variant CJD in an individual heterozygous for PRNP codon 129", *Lancet*, vol. 374, no. 9707, p. 2128.
225. Katona, P. G. & Jih, F. 1975, "Respiratory sinus arrhythmia: noninvasive measure of parasympathetic cardiac control", *J Appl.Physiol*, vol. 39, no. 5, pp. 801-805.
226. Katona, P. G., Lipson, D., & Dauchot, P. J. 1977, "Opposing central and peripheral effects of atropine on parasympathetic cardiac control", *Am.J Physiol*, vol. 232, no. 2, p. H146-H151.
227. Katona, P. G., Poitras, J. W., Barnett, G. O., & Terry, B. S. 1970, "Cardiac vagal efferent activity and heart period in the carotid sinus reflex", *Am.J Physiol*, vol. 218, no. 4, pp. 1030-1037.
228. Kaufmann, H., Nahm, K., Purohit, D., & Wolfe, D. 2004, "Autonomic failure as the initial presentation of Parkinson disease and dementia with Lewy bodies", *Neurology*, vol. 63, no. 6, pp. 1093-1095.
229. Kimberlin, R. H., Hall, S. M., & Walker, C. A. 1983, "Pathogenesis of mouse scrapie. Evidence for direct neural spread of infection to the CNS after injection of sciatic nerve", *J.Neurol.Sci.*, vol. 61, no. 3, pp. 315-325.
230. Kimberlin, R. H. & Walker, C. A. 1989, "Pathogenesis of scrapie in mice after intragastric infection", *Virus Res.*, vol. 12, no. 3, pp. 213-220.
231. Knight, R. S. G. Potential treatments for Creutzfeld-Jakob disease. NCJDSU . 2006. Ref Type: Electronic Citation
232. Kobayashi, H. 2007, "Inter- and intra-individual variations of heart rate variability in Japanese males", *J Physiol Anthropol.*, vol. 26, no. 2, pp. 173-177.
233. Kodama, T. & Kimura, M. 2002, "Arousal effects of orexin-A correlate with GLU release from the locus coeruleus in rats", *Peptides*, vol. 23, no. 9, pp. 1673-1681.
234. Kollai, M. & Koizumi, K. 1979, "Reciprocal and non-reciprocal action of the vagal and sympathetic nerves innervating the heart", *J Auton.Nerv.Syst.*, vol. 1, no. 1, pp. 33-52.
235. Koskinen, P. E. K. K., Virolainen, J. U. H. A., Koskinen, P. K., Hayry, P. E. K. K., & Kupari, M. A. R. K. 1996, "Evolution of heart rate variability in cardiac transplant recipients: a clinical study", *Journal of Internal Medicine*, vol. 239, no. 5, pp. 443-449.
236. Krasowski, M. D. & Harrison, N. L. 1999, "General anaesthetic actions on ligand-gated ion channels", *Cell Mol Life Sci*, vol. 55, no. 10, pp. 1278-1303.
237. Krebs, B., Kohlmannsperger, V., Nolting, S., Schmalzbauer, R., & Kretzschmar, H. A. 2006, "A Method to Perform Western Blots of Microscopic Areas of Histological Sections", *J Histochem.Cytochem.*
238. Kretzschmar, H. A., Tings, T., Madlung, A., Giese, A., & Herms, J. 2000, "Function of PrP(C) as a copper-binding protein at the synapse", *Arch.Virol.Suppl* no. 16, pp. 239-249.
239. Kunze, D. L. 1972, "Reflex discharge patterns of cardiac vagal efferent fibres", *J Physiol*, vol. 222, no. 1, pp. 1-15.
240. L.A.M.Woolfson, D.G.Glover, B.J.Pollard, & Chris J.D.Pomfrett "Symptomatic vCJD alters heart rate variability", in *Trinity College Dublin (2003) J Physiol 551P, C47 Communications*.
241. Lacey, J. L. 1967, "Somatic response patterning and stress: Some revisions of activation theory.," in *Psychological Stress: Issues in Research*, M. H. Appley & R. Trumbull, eds., pp. 14-37.
242. Landis, D. M., Williams, R. S., & Masters, C. L. 1981, "Golgi and electronmicroscopic studies of spongiform encephalopathy", *Neurology*, vol. 31, no. 5, pp. 538-549.
243. Lasmezas, C. I. 2003, "Putative functions of PrP(C)", *Br.Med.Bull.*, vol. 66, pp. 61-70.

244. Laude, D., Baudrie, V., & Elghozi, J. L. 2008, "Effects of atropine on the time and frequency domain estimates of blood pressure and heart rate variability in mice", *Clin Exp.Pharmacol Physiol*, vol. 35, no. 4, pp. 454-457.
245. Leader, R. W. & Hurvitz, A. I. 1972, "Interspecies patterns of slow virus diseases", *Annu.Rev.Med.*, vol. 23, pp. 191-200.
246. Lee, K. S. 1983, "Cooperativity among afferents for the induction of long-term potentiation in the CA1 region of the hippocampus", *Journal of Neuroscience*, vol. 3, pp. 1369-1372.
247. Lee, K. S. & Caughey, B. 2007, "A simplified recipe for prions", *Proceedings of the National Academy of Sciences* p. 0703910104.
248. Leslie, R. A., Reynolds, D. J. M., & Lawes, I. N. C. 1992, "Central Connections of the Nuclei of the Vagus Nerve," in *Neuroanatomy and Physiology of Abdominal Vagal Afferents*, S. Ritter, R. C. Ritter, & C. D. Barnes, eds., CRC Press Inc (27 Jul 1992), pp. 81-98.
249. Levy, M. N. 1984, "Cardiac sympathetic-parasympathetic interactions", *Fed.Proc.*, vol. 43, no. 11, pp. 2598-2602.
250. Li, Y., Cardona, S. M., Traister, R. S., & Lynch, W. P. 2010, "Retrovirus-induced spongiform neurodegeneration is mediated by unique CNS viral targeting and expression of Env alone", *The Journal of Virology* p. JVI.
251. Liberski, P. P. & Brown, P. 2007, "Disease-specific particles without prion protein in prion diseases - phenomenon or epiphenomenon?", *Neuropathol.Appl.Neurobiol.*, vol. 33, no. 4, pp. 395-397.
252. Liljestrand, A. N. 1958, "Neural control of respiration", *Physiol Rev*, vol. 38, no. 4, pp. 691-708.
253. Lledo, P. M., Tremblay, P., Dearmond, S. J., Prusiner, S. B., & Nicoll, R. A. 1996, "Mice deficient for prion protein exhibit normal neuronal excitability and synaptic transmission in the hippocampus", *Proc.Natl.Acad.Sci.U.S A*, vol. 93, no. 6, pp. 2403-2407.
254. Lovric, S. S., Avbelj, V., Trobec, R., Zorman, D., Rakovec, P., Hojker, S., Gersak, B., & Milcinski, M. 2004, "Sympathetic reinnervation after heart transplantation, assessed by iodine-123 metaiodobenzylguanidine imaging, and heart rate variability", *Eur J Cardiothorac.Surg*, vol. 26, no. 4, pp. 736-741.
255. Lu, P., Sturman, J. A., & Bolton, D. C. 1995, "Altered GABA distribution in hamster brain is an early molecular consequence of infection by scrapie prions", *Brain Research*, vol. 681, no. 1-2, pp. 235-241.
256. Lu, Z. Y., Baker, C. A., & Manuelidis, L. 2004, "New molecular markers of early and progressive CJD brain infection", *J Cell Biochem.*, vol. 93, no. 4, pp. 644-652.
257. Lutz, A., Greischar, L. L., Perlman, D. M., & Davidson, R. J. 2009, "BOLD signal in insula is differentially related to cardiac function during compassion meditation in experts vs. novices", *Neuroimage.*, vol. 47, no. 3, pp. 1038-1046.
258. Ma, J. & Lindquist, S. 2002, "Conversion of PrP to a self-perpetuating PrPSc-like conformation in the cytosol", *Science*, vol. 298, no. 5599, pp. 1785-1788.
259. Ma, J., Wollmann, R., & Lindquist, S. 2002, "Neurotoxicity and neurodegeneration when PrP accumulates in the cytosol", *Science*, vol. 298, no. 5599, pp. 1781-1785.
260. Ma, X., Abboud, F. M., & Chapleau, M. W. 2002, "Analysis of afferent, central, and efferent components of the baroreceptor reflex in mice", *Am J Physiol Regul.Integr.Comp Physiol*, vol. 283, no. 5, p. R1033-R1040.
261. Mace, S. E. & Levy, M. N. 1983, "Neural control of heart rate: a comparison between puppies and adult animals", *Pediatr.Res.*, vol. 17, no. 6, pp. 491-495.
262. Machado, B. H. & Brody, M. J. 1988a, "Effect of nucleus ambiguus lesion on the development of neurogenic hypertension", *Hypertension*, vol. 11, no. 2 Pt 2, p. I135-I138.
263. Machado, B. H. & Brody, M. J. 1988b, "Role of the nucleus ambiguus in the regulation of heart rate and arterial pressure", *Hypertension*, vol. 11, no. 6 Pt 2, pp. 602-607.

264. Madanmohan, Prakash, E. S., & Bhavanani, A. B. 2005, "Correlation between short-term heart rate variability indices and heart rate, blood pressure indices, pressor reactivity to isometric handgrip in healthy young male subjects", *Indian J Physiol Pharmacol.*, vol. 49, no. 2, pp. 132-138.
265. Malenka, R. C. & Bear, M. F. 2004, "LTP and LTD: an embarrassment of riches", *Neuron*, vol. 44, no. 1, pp. 5-21.
266. Malik, M. & Camm, A. J. 1993, "Components of heart rate variability--what they really mean and what we really measure", *Am J Cardiol.*, vol. 72, no. 11, pp. 821-822.
267. Malliani, A., Lombardi, F., & Pagani, M. 1994, "Power spectrum analysis of heart rate variability: a tool to explore neural regulatory mechanisms", *Br Heart J*, vol. 71, no. 1, pp. 1-2.
268. Malliani, A., Pagani, M., Lombardi, F., & Cerutti, S. 1991, "Cardiovascular neural regulation explored in the frequency domain", *Circulation*, vol. 84, no. 2, pp. 482-492.
269. Mallucci, G. R. 2009, "Prion neurodegeneration: Starts and stops at the synapse", *Prion*, vol. 3, no. 4.
270. Manson, J. C., Clarke, A. R., McBride, P. A., McConnell, I., & Hope, J. 1994, "PrP gene dosage determines the timing but not the final intensity or distribution of lesions in scrapie pathology", *Neurodegeneration.*, vol. 3, no. 4, pp. 331-340.
271. Manuelidis, L. 1998, "Vaccination with an attenuated Creutzfeldt-Jakob disease strain prevents expression of a virulent agent", *Proc.Natl.Acad Sci U.S.A*, vol. 95, no. 5, pp. 2520-2525.
272. Manuelidis, L. 2004, "A virus behind the mask of prions?", *Folia Neuropathol.*, vol. 42 Suppl B, pp. 10-23.
273. Manuelidis, L. 2006, "A 25 nm virion is the likely cause of transmissible spongiform encephalopathies", *J Cell Biochem.*
274. Manuelidis, L., Liu, Y., & Mullins, B. 2009, "Strain-specific viral properties of variant Creutzfeldt-Jakob disease (vCJD) are encoded by the agent and not by host prion protein", *J Cell Biochem*, vol. 106, no. 2, pp. 220-231.
275. Manuelidis, L., Yu, Z. X., Banquero, N., & Mullins, B. 2007, "Cells infected with scrapie and Creutzfeldt-Jakob disease agents produce intracellular 25-nm virus-like particles", *Proceedings of the National Academy of Sciences* p. 0610999104.
276. Masujin, K., Matthews, D., Wells, G. A. H., Mohri, S., & Yokoyama, T. 2007, "Prions in the peripheral nerves of bovine spongiform encephalopathy-affected cattle", *Journal of General Virology*, vol. 88, no. 6, pp. 1850-1858.
277. McAllen, R. M. & Spyer, K. M. 1976, "The location of cardiac vagal preganglionic motoneurones in the medulla of the cat", *J.Physiol*, vol. 258, no. 1, pp. 187-204.
278. McAllen, R. M. & Spyer, K. M. 1978a, "The baroreceptor input to cardiac vagal motoneurones", *J.Physiol*, vol. 282, pp. 365-374.
279. McAllen, R. M. & Spyer, K. M. 1978b, "Two types of vagal preganglionic motoneurones projecting to the heart and lungs", *J.Physiol*, vol. 282, pp. 353-364.
280. McCabe, P. M., Yongue, B. G., Porges, S. W., & Ackles, P. K. 1984, "Changes in heart period, heart period variability, and a spectral analysis estimate of respiratory sinus arrhythmias during aortic nerve stimulation in rabbits", *Psychophysiology*, vol. 21, no. 2, pp. 149-158.
281. McGowan J, P. 1922, "Scrapie in sheep", *Scott.J.Agric.*, vol. 5: pp. 365-375.
282. Meier, P., Genoud, N., Prinz, M., Maissen, M., Rulicke, T., Zurbriggen, A., Raeber, A. J., & Aguzzi, A. 2003, "Soluble dimeric prion protein binds PrP(Sc) in vivo and antagonizes prion disease", *Cell*, vol. 113, no. 1, pp. 49-60.
283. Mendelowitz, D. 1999, "Advances in Parasympathetic Control of Heart Rate and Cardiac Function", *News Physiol Sci.*, vol. 14, pp. 155-161.
284. Mendelowitz, D. 2000, "Superior laryngeal neurons directly excite cardiac vagal neurons within the nucleus ambiguus", *Brain Res.Bull.*, vol. 51, no. 2, pp. 135-138.
285. Mihic, S. J., Ye, Q., Wick, M. J., Koltchine, V. V., Krasowski, M. D., Finn, S. E., Mascia, M. P., Valenzuela, C. F., Hanson, K. K., Greenblatt, E. P., Harris, R. A., & Harrison, N. L.

1997, "Sites of alcohol and volatile anaesthetic action on GABA(A) and glycine receptors", *Nature*, vol. 389, no. 6649, pp. 385-389.
286. Mishra, R. S., Basu, S., Gu, Y., Luo, X., Zou, W. Q., Mishra, R., Li, R., Chen, S. G., Gambetti, P., Fujioka, H., & Singh, N. 2004, "Protease-resistant human prion protein and ferritin are cotransported across Caco-2 epithelial cells: implications for species barrier in prion uptake from the intestine", *Journal of Neuroscience*, vol. 24, no. 50, pp. 11280-11290.
287. Moody, G., Mark, R., Bump, M., Weinstein, J., Berman, A., Mietus, J., & Goldberger, A. L. Clinical Validation of the ECG-Derived Respiration (EDR) Technique. Computers in Cardiology 13, 507-510. 1986. Washington, DC: IEEE Computer Society Press.
Ref Type: Electronic Citation
288. Moody, G., Mark, R., Zoccola, A., & Mantero, S. Derivation of Respiratory Signals from Multi-lead ECGs. Computers in Cardiology 12, 113-116. 1985.
Ref Type: Journal (Full)
289. Moravec, M., Moravec, J., & Forsgren, S. 1990, "Catecholaminergic and peptidergic nerve components of intramural ganglia in the rat heart. An immunohistochemical study", *Cell Tissue Res.*, vol. 262, no. 2, pp. 315-327.
290. Moreno, J. A. & Mallucci, G. R. 2010, "Dysfunction and recovery of synapses in prion disease: implications for neurodegeneration", *Biochem Soc Trans*, vol. 38, no. 2, pp. 482-487.
291. Mouillet-Richard, S., Ermonval, M., Chebassier, C., Laplanche, J. L., Lehmann, S., Launay, J. M., & Kellermann, O. 2000, "Signal transduction through prion protein", *Science*, vol. 289, no. 5486, pp. 1925-1928.
292. Nazor, K. E., Kuhn, F., Seward, T., Green, M., Zwald, D., Purro, M., Schmid, J., Biffiger, K., Power, A. M., Oesch, B., Raeber, A. J., & Telling, G. C. 2005, "Immunodetection of disease-associated mutant PrP, which accelerates disease in GSS transgenic mice", *EMBO J.*, vol. 24, no. 13, pp. 2472-2480.
293. Neff, R. A., Wang, J., Baxi, S., Evans, C., & Mendelowitz, D. 2003, "Respiratory Sinus Arrhythmia: Endogenous Activation of Nicotinic Receptors Mediates Respiratory Modulation of Brainstem Cardioinhibitory Parasympathetic Neurons", *Circulation Research*, vol. 93, no. 6, pp. 565-572.
294. Nelson, L. E., Guo, T. Z., Lu, J., Saper, C. B., Franks, N. P., & Maze, M. 2002, "The sedative component of anesthesia is mediated by GABA(A) receptors in an endogenous sleep pathway", *Nat Neurosci*, vol. 5, no. 10, pp. 979-984.
295. Nentwig, A., Oevermann, A., Heim, D., Botteron, C., Zellweger, K., Dr+Âgem++ller, C., Zurbriggen, A., & Seuberlich, T. 2007, "Diversity in Neuroanatomical Distribution of Abnormal Prion Protein in Atypical Scrapie", *PLoS Pathog*, vol. 3, no. 6, p. e82.
296. Neuhuber, W. L. & Sandoz, P. A. 1986, "Vagal primary afferent terminals in the dorsal motor nucleus of the rat: Are they making monosynaptic contacts on preganglionic efferent neurons?,", *Neuroscience Letters*, vol. 69, no. 2, pp. 126-130.
297. Ni, H. F., Zhang, J. X., & Harper, R. M. 1990, "Respiratory-related discharge of periaqueductal gray neurons during sleep-waking states", *Brain Res.*, vol. 511, no. 2, pp. 319-325.
298. Nicoll, R. A. & Madison, D. V. 1982, "General anesthetics hyperpolarize neurons in the vertebrate central nervous system", *Science*, vol. 217, no. 4564, pp. 1055-1057.
299. Nimchinsky, E. A., Sabatini, B. L., & Svoboda, K. 2002, "Structure and function of dendritic spines", *Annu.Rev Physiol*, vol. 64, pp. 313-353.
300. Noh, Y. S., Park, S. J., Park, S. B., & Yoon, H. R. 2007, "A novel approach to classify significant ECG data based on heart instantaneous frequency and ECG-derived respiration using conductive textiles", *Conf.Proc IEEE Eng Med Biol Soc.*, vol. 2007, pp. 1503-1506.
301. Nosaka, S., Yasunaga, K., & Kawano, M. 1979, "Vagus cardioinhibitory fibers in rats", *Pflugers Arch.*, vol. 379, no. 3, pp. 281-285.

302. Nosaka, S., Yasunaga, K., & Tamai, S. 1982, "Vagal cardiac preganglionic neurons: distribution, cell types, and reflex discharges", *Am.J Physiol*, vol. 243, no. 1, p. R92-R98.
303. Olanow, C. W. & Prusiner, S. B. 2009, "Is Parkinson's disease a prion disorder?", *Proceedings of the National Academy of Sciences*.
304. Pagani, M., Lombardi, F., Guzzetti, S., Rimoldi, O., Furlan, R., Pizzinelli, P., Sandrone, G., Malfatto, G., Dell'Orto, S., Piccaluga, E., & . 1986, "Power spectral analysis of heart rate and arterial pressure variabilities as a marker of sympatho-vagal interaction in man and conscious dog", *Circulation Research*, vol. 59, no. 2, pp. 178-193.
305. Parati, G., Mancia, G., Rienzo, M. D., Castiglioni, P., Taylor, J. A., & Studinger, P. 2006, "Point:Counterpoint: Cardiovascular variability is/is not an index of autonomic control of circulation", *Journal of Applied Physiology*, vol. 101, no. 2, pp. 676-682.
306. Patrick, G. B., Strohl, K. P., Rubin, S. B., & Altose, M. D. 1982, "Upper airway and diaphragm muscle responses to chemical stimulation and loading", *Journal of Applied Physiology*, vol. 53, no. 5, pp. 1133-1137.
307. Pauly, P. C. & Harris, D. A. 1998, "Copper stimulates endocytosis of the prion protein", *Journal of Biological Chemistry*, vol. 273, no. 50, pp. 33107-33110.
308. Pauza, D. H., Pauziene, N., Pakeltyte, G., & Stropus, R. 2002, "Comparative quantitative study of the intrinsic cardiac ganglia and neurons in the rat, guinea pig, dog and human as revealed by histochemical staining for acetylcholinesterase", *Ann Anat*, vol. 184, no. 2, pp. 125-136.
309. Peden, A. H., Head, M. W., Ritchie, D. L., Bell, J. E., & Ironside, J. W. 2004, "Preclinical vCJD after blood transfusion in a PRNP codon 129 heterozygous patient", *Lancet*, vol. 364, no. 9433, pp. 527-529.
310. Peden, A. H., Ritchie, D. L., Head, M. W., & Ironside, J. W. 2006, "Detection and Localization of PrPSc in the Skeletal Muscle of Patients with Variant, Iatrogenic, and Sporadic Forms of Creutzfeldt-Jakob Disease", *Am.J Pathol.*, vol. 168, no. 3, pp. 927-935.
311. Pokrovskii, V. M., Osadchii, O. E., & Kurzanov, A. N. 1992, "[Somatostatin as a modulator of vagal effects on heart rhythm]", *Biull.Eksp.Biol Med*, vol. 114, no. 7, pp. 15-17.
312. Pokrovsky, V. M. & Osadchiy, O. E. 1995, "Regulatory peptides as modulators of vagal influence on cardiac rhythm", *Can J Physiol Pharmacol*, vol. 73, no. 9, pp. 1235-1245.
313. Polymenidou, M., Stoeck, K., Glatzel, M., Vey, M., Bellon, A., & Aguzzi, A. 2005, "Coexistence of multiple PrP(Sc) types in individuals with Creutzfeldt-Jakob disease", *Lancet Neurol.*, vol. 4, no. 12, pp. 805-814.
314. Pomfrett, C. J. 1995, "R-R intervals and the depth of anaesthesia," in *Recent Advances in Anaesthesia and Analgesia*, volume 19 edn, pp. 89-105.
315. Pomfrett, C. J. 1999, "Heart rate variability, BIS and 'depth of anaesthesia'", *Br J Anaesth.*, vol. 82, no. 5, pp. 659-662.
316. Pomfrett, C. J. & Alkire, M. T. "Respiratory sinus arrhythmia as an index of anaesthetic depth in man:evidence from functional imaging studies", p. 180.
317. Pomfrett, C. J., Dolling, S., Anders, N. R., Glover, D. G., Bryan, A., & Pollard, B. J. 2009, "Delta sleep-inducing peptide alters bispectral index, the electroencephalogram and heart rate variability when used as an adjunct to isoflurane anaesthesia", *Eur J Anaesthesiol.*, vol. 26, no. 2, pp. 128-134.
318. Pomfrett, C. J., Glover, D. G., Bollen, B. G., & Pollard, B. J. 2004, "Perturbation of heart rate variability in cattle fed BSE-infected material", *Vet.Rec.*, vol. 154, no. 22, pp. 687-691.
319. Pomfrett, C. J., Glover, D. G., & Pollard, B. J. 2007, "The vagus nerve as a conduit for neuroinvasion, a diagnostic tool, and a therapeutic pathway for transmissible spongiform encephalopathies, including variant Creutzfeld Jacob disease", *Med Hypotheses*, vol. 68, no. 6, pp. 1252-1257.

320. Pomfrett, C. J., Sneyd, J. R., Barrie, J. R., & Healy, T. E. 1994, "Respiratory sinus arrhythmia: comparison with EEG indices during isoflurane anaesthesia at 0.65 and 1.2 MAC", *British Journal of Anaesthesia*, vol. 72, no. 4, pp. 397-402.
321. Pomfrett, C. J. D., Barrie, J. R., & Healy, T. E. 1993, "Respiratory Sinus Arrhythmia: An Index of light anaesthesia", *British Journal of Anaesthesia*, vol. 71, no. 2, pp. 212-217.
322. Porges, S. W. 1986, "Respiratory Sinus Arrhythmia: Physiological Basis, Quantitative Methods and Clinical Implications," in *Cardiorespiratory and Cardiosomatic Psychophysiology*, P. Grossman, K. Janssen, & D. Vaitl, eds., Plenum Pub Corp 01 October, 1986, pp. 101-115.
323. Porges, S. W. 1995, "Orienting in a defensive world: mammalian modifications of our evolutionary heritage. A Polyvagal Theory", *Psychophysiology*, vol. 32, no. 4, pp. 301-318.
324. Porges, S. W. 2006b, "The polyvagal perspective", *Biol.Psychol.*
325. Porges, S. W. 2006a, "The polyvagal perspective", *Biol.Psychol.*
326. Porges, S. W. 1992, "Vagal Tone: A Physiologic Marker of Stress Vulnerability", *Pediatrics*, vol. 90, no. 3, pp. 498-504.
327. Potter, E. K. 1981, "Inspiratory inhibition of vagal responses to baroreceptor and chemoreceptor stimuli in the dog", *J Physiol*, vol. 316, pp. 177-190.
328. Powley, T. L. & Phillips, R. J. 2002, "Musings on the wanderer: what's new in our understanding of vago-vagal reflexes? I. Morphology and topography of vagal afferents innervating the GI tract", *Am J Physiol Gastrointest.Liver Physiol*, vol. 283, no. 6, p. G1217-G1225.
329. Pozza, R. D., Kleinmann, A., Bechtold, S., Fuchs, A., & Netz, H. 2006, "Reinnervation after heart transplantation in children: Results of short-time heart rate variability testing", *Pediatr.Transplant.see ref list for HF changes*, vol. 10, no. 4, pp. 429-433.
330. Preacher, K. J. Calculation for the test of the difference between two independent correlation coefficients. 2002.
Ref Type: Computer Program
331. Prusiner, S. B. 1982, "Novel proteinaceous infectious particles cause scrapie", *Science*, vol. 216, no. 4542, pp. 136-144.
332. Prusiner, S. B. 1991, "Molecular biology and transgenetics of prion diseases", *Crit Rev Biochem Mol Biol*, vol. 26, no. 5-6, pp. 397-438.
333. Rampil, I. J. 1994, "Anesthetic potency is not altered after hypothermic spinal cord transection in rats", *Anesthesiology*, vol. 80, no. 3, pp. 606-610.
334. Randall, D. C. 1978, "Exchange of Gases," in *Animal Physiology*, First edn, pp. 469-509.
335. Randall, D. C., Brown, D. R., Li, S. G., Olmstead, M. E., Kilgore, J. M., Sprinkle, A. G., Randall, W. C., & Ardell, J. L. 1998b, "Ablation of posterior atrial ganglionated plexus potentiates sympathetic tachycardia to behavioral stress", *Am.J.Physiol*, vol. 275, no. 3 Pt 2, p. R779-R787.
336. Randall, D. C., Brown, D. R., Li, S. G., Olmstead, M. E., Kilgore, J. M., Sprinkle, A. G., Randall, W. C., & Ardell, J. L. 1998a, "Ablation of posterior atrial ganglionated plexus potentiates sympathetic tachycardia to behavioral stress", *Am J Physiol*, vol. 275, no. 3 Pt 2, p. R779-R787.
337. Randall, D. C., Brown, D. R., McGuirt, A. S., Thompson, G. W., Armour, J. A., & Ardell, J. L. 2003, "Interactions within the intrinsic cardiac nervous system contribute to chronotropic regulation", *Am.J.Physiol Regul.Integr.Comp Physiol*, vol. 285, no. 5, p. R1066-R1075.
338. Rangel, A., Madroal, N., Mass, A. G., Gavn, R., Llorens, F., Sumoy, L., Torres, J. M., gado-Garc, J. M., & R, J. A. D. 2009, "Regulation of GABAA and Glutamate Receptor Expression, Synaptic Facilitation and Long-Term Potentiation in the Hippocampus of Prion Mutant Mice", *PLoS ONE*, vol. 4, no. 10, p. e7592.

339. Rentero, N., Cividjian, A., Trevaks, D., Pequignot, J. M., Quintin, L., & McAllen, R. M. 2002, "Activity patterns of cardiac vagal motoneurons in rat nucleus ambiguus", *Am J Physiol Regul.Integr.Comp Physiol*, vol. 283, no. 6, p. R1327-R1334.
340. Reynolds, D. S., Rosahl, T. W., Cirone, J., O'Meara, G. F., Haythornthwaite, A., Newman, R. J., Myers, J., Sur, C., Howell, O., Rutter, A. R., Atack, J., Macaulay, A. J., Hadingham, K. L., Hutson, P. H., Belelli, D., Lambert, J. J., Dawson, G. R., McKernan, R., Whiting, P. J., & Wafford, K. A. 2003, "Sedation and Anesthesia Mediated by Distinct GABAA Receptor Isoforms", *Journal of Neuroscience*, vol. 23, no. 24, pp. 8608-8617.
341. Richter, D. W. & Spyer, K. M. 1987, "Cardiorespiratory Control," in *Central Regulation of Autonomic Function*, A. D. Loewy & K. M. Spyer, eds., Oxford University Press, Oxford, pp. 189-207.
342. Riverol, M., Palma, J. A., Ala+¦+í, M. +., Guerrero-M+írquez, C., Luquin, M. a. R., & R+íbano, A. "Variant CreutzfeldtΓÇôJakob disease occurring in mother and son", *Journal of Neurology, Neurosurgery & Psychiatry*.
343. Safar, J., Wille, H., Itri, V., Groth, D., Serban, H., Torchia, M., Cohen, F. E., & Prusiner, S. B. 1998, "Eight prion strains have PrP(Sc) molecules with different conformations", *Nat.Med.*, vol. 4, no. 10, pp. 1157-1165.
344. Safar, J. G., Dearmond, S. J., Kociuba, K., Deering, C., Didorenko, S., Bouzamondo-Bernstein, E., Prusiner, S. B., & Tremblay, P. 2005, "Prion clearance in bigenic mice", *Journal of General Virology*, vol. 86, no. Pt 10, pp. 2913-2923.
345. Sakamoto, S. i., Schuessler, R. B., Lee, A. M., Aziz, A., Lall, S. C., & Damiano, J. 2009, "Vagal denervation and reinnervation after ablation of ganglionated plexi", *The Journal of Thoracic and Cardiovascular Surgery*, vol. In Press, Corrected Proof.
346. Sales, N., Hassig, R., Rodolfo, K., Di, G. L., Traiffort, E., Ruat, M., Fretier, P., & Moya, K. L. 2002, "Developmental expression of the cellular prion protein in elongating axons", *Eur.J.Neurosci.*, vol. 15, no. 7, pp. 1163-1177.
347. Sales, N., Rodolfo, K., Hassig, R., Faucheux, B., Di, G. L., & Moya, K. L. 1998, "Cellular prion protein localization in rodent and primate brain", *Eur.J.Neurosci.*, vol. 10, no. 7, pp. 2464-2471.
348. Sandercock, G. R. H., Bromley, P. D., & Brodie, D. A. 2005, "The reliability of short-term measurements of heart rate variability", *International Journal of Cardiology*, vol. 103, no. 3, pp. 238-247.
349. Saul, J. P., Berger, R. D., Chen, M. H., & Cohen, R. J. 1989a, "Transfer function analysis of autonomic regulation. II. Respiratory sinus arrhythmia", *Am J Physiol*, vol. 256, no. 1 Pt 2, p. H153-H161.
350. Saul, J. P., Berger, R. D., Chen, M. H., & Cohen, R. J. 1989b, "Transfer function analysis of autonomic regulation. II. Respiratory sinus arrhythmia", *Am.J Physiol*, vol. 256, no. 1 Pt 2, p. H153-H161.
351. Sayers, B. M. 1973, "Analysis of heart rate variability", *Ergonomics*, vol. 16, no. 1, pp. 17-32.
352. Schafer, A. & Kratky, K. W. 2008, "Estimation of Breathing Rate from Respiratory Sinus Arrhythmia: Comparison of Various Methods", *Ann Biomed.Eng*.
353. Scott, M. R., Will, R., Ironside, J., Nguyen, H. O., Tremblay, P., Dearmond, S. J., & Prusiner, S. B. 1999, "Compelling transgenetic evidence for transmission of bovine spongiform encephalopathy prions to humans", *Proc.Natl.Acad Sci U.S.A*, vol. 96, no. 26, pp. 15137-15142.
354. Shibata, M., Morita, Y., Shimizu, T., Takahashi, K., & Suzuki, N. 2009, "Cardiac parasympathetic dysfunction concurrent with cardiac sympathetic denervation in Parkinson's disease", *Journal of the Neurological Sciences*, vol. 276, no. 1-2, pp. 79-83.
355. Shyng, S. L., Moulder, K. L., Lesko, A., & Harris, D. A. 1995, "The N-terminal domain of a glycolipid-anchored prion protein is essential for its endocytosis via clathrin-coated pits", *Journal of Biological Chemistry*, vol. 270, no. 24, pp. 14793-14800.

356. Siegel, J. M. 2004, "Hypocretin (orexin): role in normal behavior and neuropathology", *Annu.Rev.Psychol.*, vol. 55, pp. 125-148.
357. Sigurdson, C. J., Spraker, T. R., Miller, M. W., Oesch, B., & Hoover, E. A. 2001, "PrP(CWD) in the myenteric plexus, vagosympathetic trunk and endocrine glands of deer with chronic wasting disease", *J Gen.Virol.*, vol. 82, no. Pt 10, pp. 2327-2334.
358. Sigurdsson, B. 1954, "Observations on three slow infections of sheep.", *British Veterinary Journal*, vol. 110, pp. 225-270.
359. Singh, S., Johnson, P. I., Lee, R. E., Orfei, E., Lonchyna, V. A., Sullivan, H. J., Montoya, A., Tran, H., Wehrmacher, W. H., & Wurster, R. D. 1996, "Topography of cardiac ganglia in the adult human heart", *The Journal of Thoracic and Cardiovascular Surgery*, vol. 112, no. 4, pp. 943-953.
360. Smith, F. M. 1999, "Extrinsic inputs to intrinsic neurons in the porcine heart in vitro", *Am J Physiol*, vol. 276, no. 2 Pt 2, p. R455-R467.
361. Smith, M. L., Ellenbogen, K. A., Eckberg, D. L., Sheehan, H. M., & Thames, M. D. 1990, "Subnormal parasympathetic activity after cardiac transplantation", *Am J Cardiol.*, vol. 66, no. 17, pp. 1243-1246.
362. Sokolov, E. N. 1963, *Perception and the Conditioned Reflex*.
363. Solforosi, L., Criado, J. R., McGavern, D. B., Wirz, S., Sanchez-Alavez, M., Sugama, S., DeGiorgio, L. A., Volpe, B. T., Wiseman, E., Abalos, G., Masliah, E., Gilden, D., Oldstone, M. B., Conti, B., & Williamson, R. A. 2004, "Cross-linking cellular prion protein triggers neuronal apoptosis in vivo", *Science*, vol. 303, no. 5663, pp. 1514-1516.
364. Sollers, J. J., III, Buchanan, T. W., Mowrer, S. M., Hill, L. K., & Thayer, J. F. 2007, "Comparison of the ratio of the standard deviation of the R-R interval and the root mean squared successive differences (SD/rMSSD) to the low frequency-to-high frequency (LF/HF) ratio in a patient population and normal healthy controls", *Biomed.Sci Instrum.*, vol. 43, pp. 158-163.
365. Soto, C. 2010, "Prion hypothesis: the end of the controversy?", *Trends Biochem Sci*.
366. Spraker, T. R., Gidlewski, T. L., Balachandran, A., VerCauteren, K. C., Creekmore, L., & Munger, R. D. 2006, "Detection of PrP(CWD) in postmortem rectal lymphoid tissues in Rocky Mountain elk (Cervus elaphus nelsoni) infected with chronic wasting disease", *J Vet Diagn Invest*, vol. 18, no. 6, pp. 553-557.
367. Spraker, T. R., Zink, R. R., Cummings, B. A., Sigurdson, C. J., Miller, M. W., & O'Rourke, K. I. 2002, "Distribution of protease-resistant prion protein and spongiform encephalopathy in free-ranging mule deer (Odocoileus hemionus) with chronic wasting disease", *Vet.Pathol.*, vol. 39, no. 5, pp. 546-556.
368. Spyer, K. M. & Jordan, D. 1987, "Electrophysiology of the nucleus ambiguus," in *Cardiogenic Reflexes*, R. Hainsworth, P. N. McWilliam, & D. A. S. G. Mary, eds., pp. 237-249.
369. Standish, A., Enquist, L. W., & Schwaber, J. S. 1994, "Innervation of the heart and its central medullary origin defined by viral tracing", *Science*, vol. 263, no. 5144, pp. 232-234.
370. Stauss, H. M. 2002, "Baroreceptor reflex function", *Am J Physiol Regul.Integr.Comp Physiol*, vol. 283, no. 2, p. R284-R286.
371. Strohl, K. P., Hensley, M. J., Hallett, M., Saunders, N. A., & Ingram, R. H., Jr. 1980, "Activation of upper airway muscles before onset of inspiration in normal humans", *Journal of Applied Physiology*, vol. 49, no. 4, pp. 638-642.
372. Subramanian, H. H., Chow, C. M., & Balnave, R. J. 2007, "Identification of different types of respiratory neurones in the dorsal brainstem nucleus tractus solitarius of the rat", *Brain Res*, vol. 1141, pp. 119-132.
373. Subramanian, H. H. & Holstege, G. 2009, "The nucleus retroambiguus control of respiration", *J Neurosci*, vol. 29, no. 12, pp. 3824-3832.
374. Sugino, T., Yamaura, J., Yamagishi, M., Kurose, Y., Kojima, M., Kangawa, K., Hasegawa, Y., & Terashima, Y. 2003, "Involvement of cholinergic neurons in the

regulation of the ghrelin secretory response to feeding in sheep", *Biochem.Biophys.Res Commun.*, vol. 304, no. 2, pp. 308-312.
375. Swinscow, T. D. V. & Campbell, M. J. 2002, *Statisticsw At Square One*, 10th edn, BMJ Books.
376. Tang, P. 1953, "Localization of the pneumotaxic center in the cat", *Am J Physiol*, vol. 172, no. 3, pp. 645-652.
377. Taraboulos, A., Jendroska, K., Serban, D., Yang, S. L., Dearmond, S. J., & Prusiner, S. B. 1992, "Regional mapping of prion proteins in brain", *Proc.Natl.Acad.Sci.U.S A*, vol. 89, no. 16, pp. 7620-7624.
378. Taylor, J. A., Myers, C. W., Halliwill, J. R., Seidel, H., & Eckberg, D. L. 2001, "Sympathetic restraint of respiratory sinus arrhythmia: implications for vagal-cardiac tone assessment in humans", *Am.J Physiol Heart Circ.Physiol*, vol. 280, no. 6, p. H2804-H2814.
379. Taylor, J. A. & Eckberg, D. L. 1996, "Fundamental Relations Between Short-term RR Interval and Arterial Pressure Oscillations in Humans", *Circulation*, vol. 93, no. 8, pp. 1527-1532.
380. Thireau, J., Zhang, B. L., Poisson, D., & Babuty, D. 2008, "Heart rate variability in mice: a theoretical and practical guide", *Experimental Physiology*, vol. 93, no. 1, pp. 83-94.
381. Thompson, G. W., Collier, K., Ardell, J. L., Kember, G., & Armour, J. A. 2000, "Functional interdependence of neurons in a single canine intrinsic cardiac ganglionated plexus", *J Physiol*, vol. 528, no. Pt 3, pp. 561-571.
382. Thomzig, A., Schulz-Schaeffer, W., Kratzel, C., Mai, J., & Beekes, M. 2004, "Preclinical deposition of pathological prion protein PrPSc in muscles of hamsters orally exposed to scrapie", *J.Clin.Invest*, vol. 113, no. 10, pp. 1465-1472.
383. Thrasher, T. N. 2002, "Unloading arterial baroreceptors causes neurogenic hypertension", *Am J Physiol Regul.Integr.Comp Physiol*, vol. 282, no. 4, p. R1044-R1053.
384. Tio, R. A., Reyners, A. K., van Veldhuisen, D. J., van den Berg, M. P., Brouwer, R. M., Haaksma, J., Smit, A. J., & Crijns, H. J. 1997, "Evidence for differential sympathetic and parasympathetic reinnervation after heart transplantation in humans", *J Auton.Nerv.Syst.*, vol. 67, no. 3, pp. 176-183.
385. Todd, N. V., Morrow, J., Doh-ura, K., Dealler, S., O'Hare, S., Farling, P., Duddy, M., & Rainov, N. G. 2005, "Cerebroventricular infusion of pentosan polysulphate in human variant Creutzfeldt-Jakob disease", *Journal of Infection*, vol. 50, no. 5, pp. 394-396.
386. Toichi, M., Sugiura, T., Murai, T., & Sengoku, A. 1997, "A new method of assessing cardiac autonomic function and its comparison with spectral analysis and coefficient of variation of R-R interval", *J Auton.Nerv.Syst.*, vol. 62, no. 1-2, pp. 79-84.
387. Travagli, R. A., Hermann, G. E., Browning, K. N., & Rogers, R. C. 2003, "Musings on the wanderer: what's new in our understanding of vago-vagal reflexes? III. Activity-dependent plasticity in vago-vagal reflexes controlling the stomach", *Am J Physiol Gastrointest.Liver Physiol*, vol. 284, no. 2, p. G180-G187.
388. Turrigiano, G. G. 1999, "Homeostatic plasticity in neuronal networks: the more things change, the more they stay the same", *Trends Neurosci.*, vol. 22, no. 5, pp. 221-227.
389. Uberfuhr, P., Frey, A. W., Fuchs, A., Paniara, C., Roskamm, H., Schwaiger, M., & Reichart, B. 1997, "Signs of vagal reinnervation 4 years after heart transplantation in spectra of heart rate variability", *Eur J Cardiothorac.Surg*, vol. 12, no. 6, pp. 907-912.
390. USDA. Media Conference by USDA June 24. USDA . 2005.
Ref Type: Internet Communication
391. van den Pol, A. N. 1999, "Hypothalamic Hypocretin (Orexin): Robust Innervation of the Spinal Cord", *Journal of Neuroscience*, vol. 19, no. 8, pp. 3171-3182.
392. van Keulen, L., Vromans, M., Dolstra, C., Bossers, A., & van Zijderveld, F. 2007, "Pathogenesis of bovine spongiform encephalopathy in sheep", *Archives of Virology*.

393. van Keulen, L. J., Bossers, A., & van Zijderveld, F. 2008, "TSE pathogenesis in cattle and sheep", *Vet Res*, vol. 39, no. 4, p. 24.
394. van Keulen, L. J., Schreuder, B. E., Vromans, M. E., Langeveld, J. P., & Smits, M. A. 2000, "Pathogenesis of natural scrapie in sheep", *Arch.Virol.Suppl* no. 16, pp. 57-71.
395. van, S. B., Saifee, O., Shebester, L., Roberson, R., Nonet, M. L., & Crowder, C. M. 1999, "A neomorphic syntaxin mutation blocks volatile-anesthetic action in Caenorhabditis elegans", *Proc Natl Acad Sci U S A*, vol. 96, no. 5, pp. 2479-2484.
396. Vanhoutte, P. M. & Levy, M. N. 1979, "Cholinergic Inhibition of Adrenergic Neurotransmission in the Cardiovascular System," in *Integrative functions of the Autonomic Nervous System*, C. M. Brooks, K. Koizumi, & A. Sato, eds., University of Tokyo Press, Tokyo, pp. 159-176.
397. Vey, M., Pilkuhn, S., Wille, H., Nixon, R., Dearmond, S. J., Smart, E. J., Anderson, R. G., Taraboulos, A., & Prusiner, S. B. 1996, "Subcellular colocalization of the cellular and scrapie prion proteins in caveolae-like membranous domains", *Proc.Natl.Acad.Sci U.S A*, vol. 93, no. 25, pp. 14945-14949.
398. Wadsworth, J. D., Joiner, S., Fox, K., Linehan, J. M., Desbruslais, M., Brandner, S., Asante, E. A., & Collinge, J. 2006, "Prion infectivity in vCJD rectum", *Gut*.
399. Walker, L., Levine, H., & Jucker, M. 2006, "Koch's postulates and infectious proteins", *Acta Neuropathol.(Berl)*, vol. 112, no. 1, pp. 1-4.
400. Walter, E. D., Chattopadhyay, M., & Millhauser, G. L. 2006a, "The affinity of copper binding to the prion protein octarepeat domain: evidence for negative cooperativity", *Biochemistry*, vol. 45, no. 43, pp. 13083-13092.
401. Walter, E. D., Chattopadhyay, M., & Millhauser, G. L. 2006b, "The affinity of copper binding to the prion protein octarepeat domain: evidence for negative cooperativity", *Biochemistry*, vol. 45, no. 43, pp. 13083-13092.
402. Wang, D. Y., Pomfrett, C. J., & Healy, T. E. 1993, "Respiratory sinus arrhythmia: a new, objective sedation score", *British Journal of Anaesthesia*, vol. 71, no. 3, pp. 354-358.
403. Wang, F., Wang, X., Yuan, C. G., & Ma, J. 2010, "Generating a Prion with Bacterially Expressed Recombinant Prion Protein", *Science*, vol. 327, no. 5969, pp. 1132-1135.
404. Wang, J., Irnaten, M., & Mendelowitz, D. 2001, "Characteristics of spontaneous and evoked GABAergic synaptic currents in cardiac vagal neurons in rats", *Brain Res.*, vol. 889, no. 1-2, pp. 78-83.
405. Wang, Y., Jones, J. F., Jeggo, R. D., de Burgh, D. M., Jordan, D., & Ramage, A. G. 2000, "Effect of pulmonary C-fibre afferent stimulation on cardiac vagal neurones in the nucleus ambiguus in anaesthetized cats", *J Physiol*, vol. 526 Pt 1, pp. 157-165.
406. Wang, Y., Jordan, D., & Ramage, A. G. 2010, "Both GABAA and GABAB receptors mediate vagal inhibition in nucleus tractus solitarii neurones in anaesthetized rats", *Auton.Neurosci*, vol. 152, no. 1-2, pp. 75-83.
407. Weber, E. J., Molenaar, P. C., & van der Molen, M. W. 1992, "A nonstationarity test for the spectral analysis of physiological time series with an application to respiratory sinus arrhythmia", *Psychophysiology*, vol. 29, no. 1, pp. 55-65.
408. Weinberg, A., Klonsky, E. D., & Hajcak, G. 2009, "Autonomic impairment in borderline personality disorder: a laboratory investigation", *Brain Cogn*, vol. 71, no. 3, pp. 279-286.
409. Weise, F. & Heydenreich, F. 1991, "Age-related changes of heart rate power spectra in a diabetic man during orthostasis", *Diabetes Res Clin.Pract.*, vol. 11, no. 1, pp. 23-32.
410. Weissmann, C. 1999, "Molecular genetics of transmissible spongiform encephalopathies", *Journal of Biological Chemistry*, vol. 274, no. 1, pp. 3-6.
411. Wells, G. A., Hancock, R. D., Cooley, W. A., Richards, M. S., Higgins, R. J., & David, G. P. 1989, "Bovine spongiform encephalopathy: diagnostic significance of vacuolar changes in selected nuclei of the medulla oblongata", *Vet.Rec.*, vol. 125, no. 21, pp. 521-524.
412. Wells, G. A., Spencer, Y. I., & Haritani, M. 1994, "Configurations and topographic distribution of PrP in the central nervous system in bovine spongiform

encephalopathy: an immunohistochemical study", *Ann.N.Y.Acad.Sci.*, vol. 724, pp. 350-352.
413. Wells, G. A. H., Konold, T., Arnold, M. E., Austin, A. R., Hawkins, S. A. C., Stack, M., Simmons, M. M., Lee, Y. H., Gavier-Widen, D., Dawson, M., & Wilesmith, J. W. 2007, "Bovine spongiform encephalopathy: the effect of oral exposure dose on attack rate and incubation period in cattle", *Journal of General Virology*, vol. 88, no. 4, pp. 1363-1373.
414. Wieling, W., van Brederode, J. F., de Rijk, L. G., Borst, C., & Dunning, A. J. 1982, "Reflex control of heart rate in normal subjects in relation to age: a data base for cardiac vagal neuropathy", *Diabetologia*, vol. 22, no. 3, pp. 163-166.
415. Will, B. 2010, "Variant CJD: where has it gone, or has it?", *Practical Neurology*, vol. 10, no. 5, pp. 250-251.
416. Williams, P. L. & Warwick, R. 1980, *Gray's Anatomy*, 36th edition edn.
417. Woolfson, L. A. M., Glover, D. G., Pollard, B. J., & Pomfrett, C. J. "Symptomatic vCJD alters heart rate variability", in *Proceedings of the Physiological Society, Trinity College, Dublin: Communications J Physiol 551P, C47*.
418. Woolley, D. C., McWilliam, P. N., Ford, T. W., & Clarke, R. W. 1987b, "The effect of selective electrical stimulation of non-myelinated vagal fibres on heart rate in the rabbit", *J.Auton.Nerv.Syst.*, vol. 21, no. 2-3, pp. 215-221.
419. Woolley, D. C., McWilliam, P. N., Ford, T. W., & Clarke, R. W. 1987a, "The effect of selective electrical stimulation of non-myelinated vagal fibres on heart rate in the rabbit", *J Auton Nerv Syst*, vol. 21, no. 2-3, pp. 215-221.
420. Wroe, S. J., Pal, S., Siddique, D., Hyare, H., Macfarlane, R., Joiner, S., Linehan, J. M., Brandner, S., Wadsworth, J. D., Hewitt, P., & Collinge, J. 2006, "Clinical presentation and pre-mortem diagnosis of variant Creutzfeldt-Jakob disease associated with blood transfusion: a case report", *Lancet*, vol. 368, no. 9552, pp. 2061-2067.
421. Wuthrich, K. 2003, "Species Variation of the 3D Structure of the Cellular Prion Protein", in *Molecular Aspects of Transmissible Spongiform Encephalopathies*.
422. Yokoyama, K., Jennings, R., Ackles, P., Hood, P., & Boller, F. 1987, "Lack of heart rate changes during an attention-demanding task after right hemisphere lesions", *Neurology*, vol. 37, no. 4, pp. 624-630.
423. Yoshifumi Iwamaru, Yuka Okubo, Tamako Ikeda, Hiroko Hayashi, Mori-kazu Imamura, Takashi Yokoyama, & Morikazu Shinagawa 2005, *PRIONS, Food and Drug Safety* Springer.
424. Yuan, J., Xiao, X., McGeehan, J., Dong, Z., Cali, I., Fujioka, H., Kong, Q., Kneale, G., Gambetti, P., & Zou, W. Q. 2006, "Insoluble Aggregates and Protease-resistant Conformers of Prion Protein in Uninfected Human Brains", *J Biol.Chem*, vol. 281, no. 46, pp. 34848-34858.
425. Zanata, S. M., Lopes, M. H., Mercadante, A. F., Hajj, G. N., Chiarini, L. B., Nomizo, R., Freitas, A. R., Cabral, A. L., Lee, K. S., Juliano, M. A., de, O. E., Jachieri, S. G., Burlingame, A., Huang, L., Linden, R., Brentani, R. R., & Martins, V. R. 2002, "Stress-inducible protein 1 is a cell surface ligand for cellular prion that triggers neuroprotection", *EMBO J.*, vol. 21, no. 13, pp. 3307-3316.
426. Zhang, W., Lin, T. R., Hu, Y., Fan, Y., Zhao, L., Stuenkel, E. L., & Mulholland, M. W. 2004, "Ghrelin stimulates neurogenesis in the dorsal motor nucleus of the vagus", *J.Physiol*, vol. 559, no. Pt 3, pp. 729-737.
427. Zhong, Y., Bai, Y., Yang, B., Ju, K., Shin, K. S., Lee, M. H., Jan, K. M., & Chon, K. H. 2007, "Autonomic Nervous Nonlinear Interactions Lead to Frequency Modulation between Low- and High-Frequency Bands of the Heart Rate Variability Spectrum", *AJP - Regulatory, Integrative and Comparative Physiology* p. 00362.
428. Zigman, J. M., Jones, J. E., Lee, C. E., Saper, C. B., & Elmquist, J. K. 2006, "Expression of ghrelin receptor mRNA in the rat and the mouse brain", *J Comp Neurol.*, vol. 494, no. 3, pp. 528-548.

Appendix

Appendix 1.1 Batch output from written software to automatically calculate RMSSD

Lists of variables in relation to file for Tag b1205

Intervals	differences between intervals	Interval Differences squared
0.336		
0.348	0.012	0.000144
0.338	-0.01	1E-04
0.324	-0.014	0.000196
0.326	0.002	4E-06
0.3552	0.0292	0.00085264
0.3228	-0.0324	0.00104976
0.332	0.0092	8.464E-05
0.34	0.008	6.4E-05
0.332	-0.008	6.4E-05
0.334	0.002	4E-06
0.332	-0.002	4E-06
0.328	-0.004	1.6E-05
0.336	0.008	6.4E-05
0.346	0.01	0.0001
0.352	0.006	3.6E-05
0.372	0.02	0.0004
0.446	0.074	0.005476
0.422	-0.024	0.000576
0.284	0.006	3.6E-05
0.275	-0.009	8.1E-05
0.28	0.005	2.5E-05
0.286	0.006	3.6E-05
0.272	-0.014	0.000196
0.284	0.012	0.000144
0.286	0.002	4E-06
0.282	-0.004	1.6E-05
0.29	0.008	6.4E-05
0.296	0.006	3.6E-05
0.294	-0.002	4E-06
0.304	0.01	1E-04
0.308	0.004	1.6E-05
0.304	-0.004	1.6E-05
mean of differences squared =		0.001253838

Directory	F:\LASSWADE SHEEP DATA
File	RMSSD
tag b 1200	0.018337
tag b 1204	0.151865
tag b 1205	**0.0354**
tag b 1206	0.040319
tag b 1211 a	0.054277
tag b 1211 b	0.174725
tag b 1212	0.056394
tag b 1214	0.109737
tag b 1215	0.054594
tag b 1225	0.044366

tag b 1205	
RMSSD =	**0.0354**

Appendix Table 1 To show an example of manual calculation of RMSSD and agreement to the coded algorithm.

Appendix 1.2 Power spectral values from sheep and simulator

Appendix Table 2 Table to show "Heartsim200" power spectral values compared to those from sheep.

Note all values tend towards zero.

File	Grp	AUC 0-0.05Hz	AUC 0.05-1Hz	AUC 0.032-0.138Hz	AUC 0.15-0.5Hz
tag j 132	1	0.000014372	0.000027307	0.00003066	1.06565E-07
tag j 151	1	0.000165896	0.000069661	0.000129345	1.20146E-06
tag j 443	1	0.000038715	0.000006006	0.000010134	2.45499E-07
Tag j 090cut	2	0.000169519	0.000084101	0.000132198	1.06785E-06
tag j 121	2	0.000033219	0.000027831	0.000248802	9.07089E-06
tag j 352	2	0.000055161	0.000053519	0.000085513	3.90647E-07
tag j 357	2	0.000068168	0.000033185	0.00002035	1.68579E-07
tag j 168	3	0.000138621	0.000012143	0.000019771	5.09779E-07
tag j 189	3	0.000004145	0.000002512	0.00000325	3.37719E-08
tag j 354	3	0.000015974	0.000008855	0.000013003	1.2673E-07
tag j 377	3	0.000025556	0.000006344	0.000010578	1.98889E-07
tag j 388	3	0.000098928	0.000017359	0.000027247	6.73125E-07
tag j 423	3	0.000015226	0.000012297	0.000012367	2.3024E-07
tag j 370	4	0.000033093	0.000013301	0.000228224	1.42306E-05
tag b 1200	5	0.000055147	0.00005421	0.000065392	2.98618E-07
tag b 1204	5	0.000101672	0.000030259	0.000083812	2.30361E-06
tag b 1205	5	0.000031105	0.000055326	0.000365892	2.17247E-05
tag b 1206	5	0.000100862	0.000100556	0.000146455	1.50155E-06
tag b 1211 b	5	0.000091867	0.0000446	0.000060521	3.60068E-06
tag b 1212	5	0.000585721	0.000030446	0.00005841	4.98098E-07
tag b 1214	5	0.000177237	0.000025296	0.000093102	1.15668E-06
tag b 1215	5	0.000038134	0.000025189	0.000074162	2.42854E-06
tag b 1225	5	0.000037459	0.000008333	0.000018523	1.33434E-07
tag 141 a	6	0.000067291	0.0000336	0.000042535	5.39674E-07
tag 88 a	6	0.000026606	0.000008553	0.000012363	8.992E-08
tag 96 a	6	0.00014511	0.000017236	0.000053155	6.55319E-07
heartsim200di		**0**	**0.000000005**	**0.000000025**	**1.12686E-10**

Appendix 1.3 Differences in windowing functions in power estimates

To illustrate the difference in power estimation for HLF (top) and HHF (lower) using different windows for the FFT

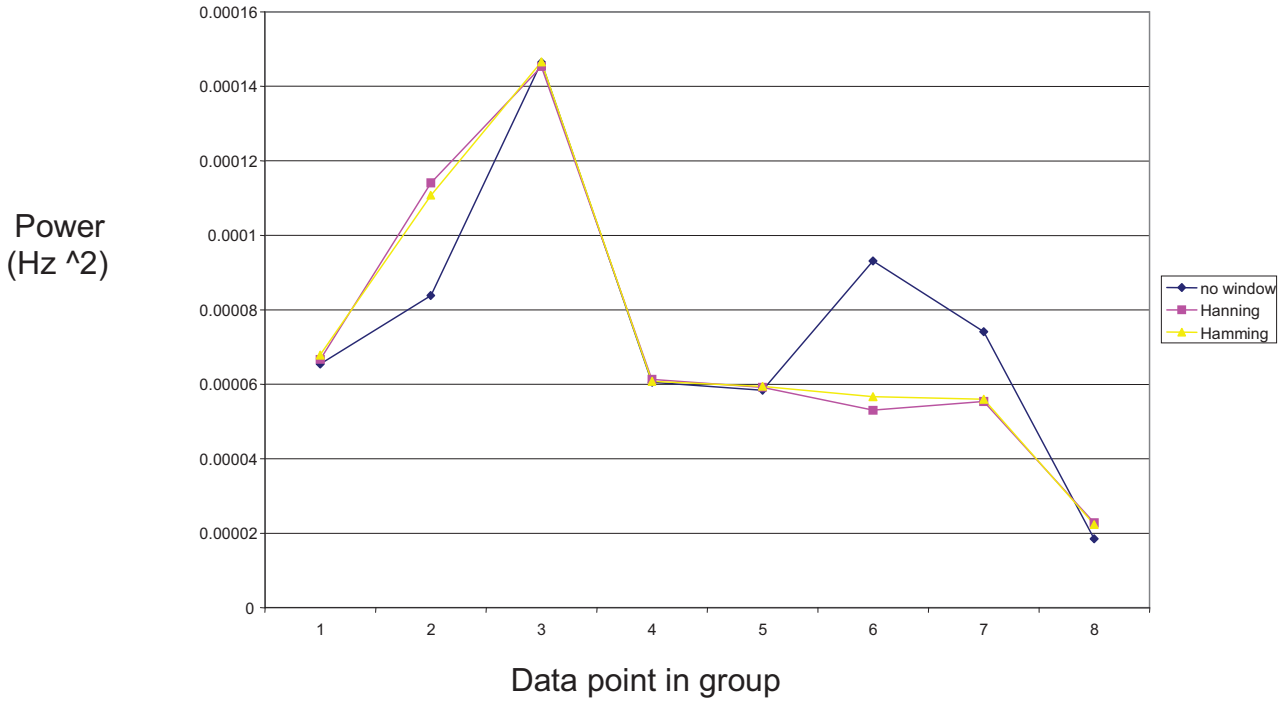

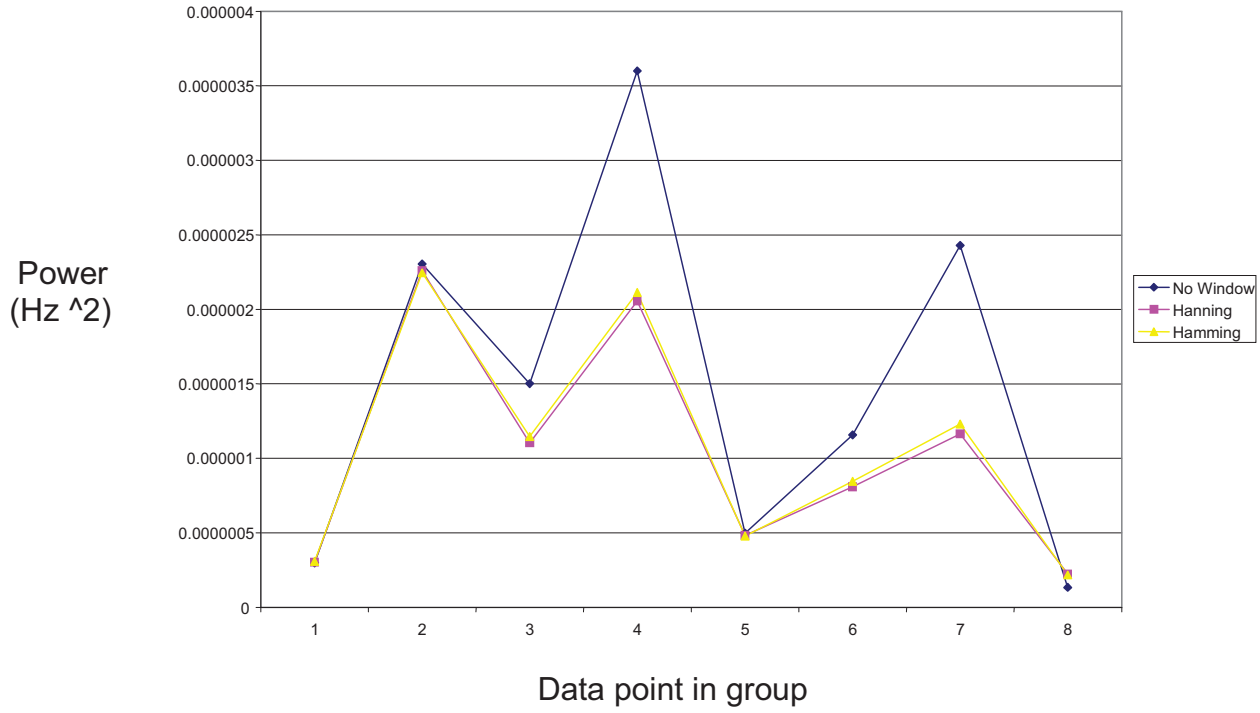

Appendix 1.4 Bland Altman method of measuring agreement between measured and estimated breaths

From 904 comparisons between measured and estimated breaths the mean difference ($\bar{d}$) was found to be **-0.51727** with a standard deviation of **1.56574.**

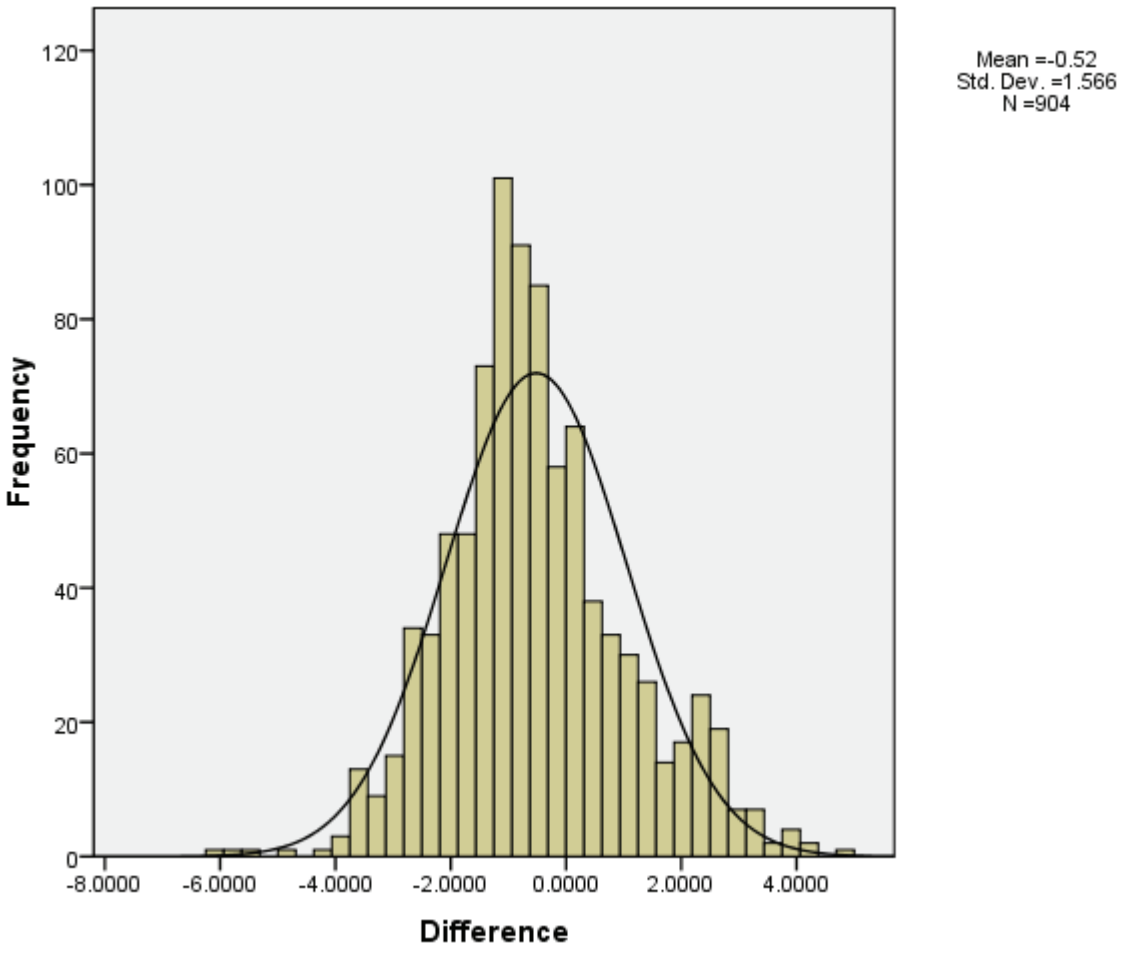

The differences were normally distributed as shown above

The standard error of $\bar{d}$ is given by $\sqrt{\frac{s^2}{n}}$,

where *n* is the sample size,

For the Breath estimate data *s* = 1.56574.

The standard error of $\bar{d}$ is thus **0.0521** , given by $\bar{d} = \sqrt{\frac{(1.56574)^2}{904}}$

There are 903 (n-1) degrees of freedom and *t* = 1.960 from tables of the t distribution with *n* -1 degrees of freedom.

The 95% confidence interval for the mean is given by the observed value minus t standard errors to the observed value plus t standard errors,

Hence;

-0.51727 - (1.960 * 0.0521) to -0.51727 + (1.960 * 0.0521) giving

-0.51727-0.1021 to -0.51727+0.1021

-0.61937 seconds to -0.41517 seconds

Therefore, the mean difference is **- 0.51723** with 95% confidence interval of **- 0.61937** seconds to **- 0.41517** seconds

The limits of agreement (from Bland and Altman (Bland & Altman.1986)) are given by

$\bar{d} - 2s$ = -0.51723 - 1.96(1.56574) = -3.64875

$\bar{d} + 2s$ = -0.51723 + 1.96(1.56574) = 2.614206

where s is standard deviation of differences. s= 1.56574.

These are illustrated in figure 4.6 of chapter 4

Appendix 1.5 Program listing, used to calculate circular statistics

```
'Automated script written by D.G.Glover to estimate breath events
from ECG trace using three parameters, finding the average and
smoothing estimates to make estimates physiologically relevant.
Then the script uses derived breath estimates and puts the time of
these events into an array along with the times of the R-waves
within the breath epoch (Breath to Breath time).  It then
calculates mean vector length and angle for certain groups of
breaths

var   v10%;
var v30%;
v30%:=FileOpen("",0,3);
ViewStandard();
FrontView();
var datafile$;
var Tag$;

'-----------------------------------------------------------

'This creates a memory channel representing the change in
amplitude of the ECG channel
'due to the change in impedance as the thorax moves towards and
way from the signal
 generator of the heart

XRange(0, MaxTime());
XRange(0,888.211);
Optimise(5);
ChanSelect(1,1);
ChanProcessAdd(1,2); 'Add DC Remove to channel 1
YRange(1,-0.0132233,0.66737);
Optimise(1);
MeasureX(102,1,"Cursor(0)","0",0);
MeasureY(101,1,"Cursor(0)","0",2);
MeasureToChan(0,"Channel 1",7,5,1,1,".01",3,1);
Process(0.0, 888.211, 0, 1, 401);
XRange(49.9314,532.196);
Optimise(401);
ChanSelect(401,1);
MeasureX(102,1,"Cursor(0)","0",0);
MeasureY(101,1,"Cursor(0)","0",0);
MeasureToChan(0,"ECGAMPR",3,4,401,5,"0.0",0,1);
Process(0.0, 482, 0, 1, 402);


ChanSelect(401,0);
ChanDelete(401,0);      'make second item non zero, say 1, if you
want confirm delete
ChanSelect(402,1);
ChanSave(402,15);       'Save to unused channel
ChanDelete(402,0);
Chanshow(15);


'-----------------------------------------------------------
```

```
'This creates an EDR (ECG Derived Respiration) channel, BrCubSpli
on chan 16
'that is a cubic spline interpretation of chan 3 the R-wave event
chan as per Yeon-Sik Noh

ChanShow(VirtualChan(0, "")); 'Created new virtual channel 0
VirtualChan(701, "IFc(3,0)", 0, 0.01, 0); 'Edit virtual channel
making cupic spline
interpretation of RR time series
Optimise(701);
XRange(36.1044,374.69);
Optimise(701);
Draw(8.81288,338.585);
MeasureX(102,1,"Cursor(0)","0",0);
MeasureY(100,1,"Cursor(0)","0",0);
MeasureToChan(0,"BrCubSpli",3,5,701,5,"0.01",0,1); '4 peak, 5
trough

Process(0.0, 512, 0, 1, 401);
ChanSelect(401,1);
ChanSave(401,16); 'Save to unused channel
ChanSelect(701,1);
ChanDelete(701,0);
ChanSelect(401,1);
ChanDelete(401,0);
Chanshow(16);

'-------------------------------------------------------
'This uses channel 14 to detect breath events and outputs them on
chan 17

ChanSelect(14,1);
MeasureX(102,1,"Cursor(0)","0",0);
MeasureY(100,14,"Cursor(0)","0",0);
MeasureToChan(0,"Channel 1",3,5,14,5,"0.001",0,1); '4 peak, 5
trough
Process(0.0, 482, 0, 1, 401);
ChanSelect(14,0);
ChanSelect(401,1);
ChanSave(401,17); 'Save to unused channel
ChanDelete(401,0);
Chanshow(17);

'-------------------------------------------------------


'this bit tidies the cursors up to equate to section that the FFT
was performed on

CursorSet(0);
DrawMode(12,5,1,1);
CursorNew();
CursorSet(1,0);

CursorSearch(1);
Cursor(1,(cursor(1)+10));
CursorNew();
```

```
Cursor(2,(cursor(1)+300)); 'Fetch the cursor

'To look at RR intervals within each breath epoch and look at how
they vary.
'could look at sd and if rr int varies by say 5ms or 10ms like
pn50 in Task force ie pnn5 or
pnn10


var data%;
var chan%;
var trig%:=408;
var size%;
var time:=-1;
var mem%;
var ct%;
var vh%;
var path$;
var name$;

path$:=FilePath$();
name$:=FileName$(0); '0-5 options depending on which parts of the
name you want.
PrintLog("\n");
Printlog(" the file is ",name$);
Data%:=FrontView();
Chan%:=MemChan(2); ' create memory event (2) channel ALL
ChanShow(Chan%);
ChanTitle$(Chan%,"All"); ' create mem chan called all with events
from 15, 16, 17
MemImport(Chan%,15,0,maxtime());
MemImport(Chan%,16,0,maxtime());
MemImport(Chan%,17,0,maxtime());
Mem%:=MemChan(2); ' create memory event (2) channel AVG

ChanShow(mem%);
ChanTitle$(Mem%,"Avg");
CursorActive(0,14, chan%, 4.01, "", "", 1); 'Data points given by
14, from chan%, ALL

MeasureX(102,1,"Cursor(0)","0",0); ' measure 102 means Time, 1 is
chan number for
measurement

MeasureY(100,1,"Cursor(0)","0",0); ' measure 100 means Value, 1 is
chan number for
measurement, both have no effect until measuretochan used

trig%:=MeasureToChan(0,"Channel 1",3,14,Chan%,4.012,1,0,1);
Process(0.0, View(data%).MaxTime(), 0, 1, Trig%);

repeat
Time:=NextTime(Trig%,Time);

If time>-1 then
ct%:=Count(Chan%,Time-2, Time+2);
Cursor(1,Time-2);
Cursor(2,Time+2);
Avg%();
Endif
```

```
Until

Time=-1;

Func avg%();
var Arr[ct%];
var Mean,SD;

ChanData(Chan%, arr[],Time-2, Time+2);
ArrSum(Arr[],Mean,SD);
MemSetItem(mem%,0,Mean);
return 1
end

' smoothing the AVG channel

var filtAVG%;
var SmoothAvg%;
filtAVG%:=MemChan(2); ' create memory event (2) channel filtAVG
ChanTitle$(filtAVG%,"FiltAVG"); ' create mem
ChanShow(filtAVG%);
CursorActive(0,14, mem%, 2.01, "", "", 1); 'Data points given by
14, from mem%, AVG
MeasureX(102,1,"Cursor(0)","0",0);
MeasureY(100,1,"Cursor(0)","0",0);
SmoothAvg%:=MeasureToChan(0,"smooth",3,14,Chan%,4,1,0,1); '
measuretochan 0 means
add new channel

Process(0.0, View(data%).MaxTime(), 0, 1, SmoothAvg%);



' need to get cursors to scan each event in FiltAvg, put time in
array, then run through array to get mean of intervals

var ArrSmooth[101];
var ArrInt[101];
var i%;
var coeff [5]; ' 5 point smoothing
var BigDaddy%;
var BreathEst%;
var trig2%;

ChanData(mem%, ArrSmooth[],0, MaxTime()); ' trying to write event
times from AVG channel into array

coeff[0]:=0.2;
coeff[1]:=0.2;
coeff[2]:=0.2;
coeff[3]:=0.2;
coeff[4]:=0.2;

ArrFilt(ArrSmooth[], coeff[]); ' five point smoothing of whole
array

for i%:= 0 to 98 do

    If ArrSmooth[i%+1]-ArrSmooth[i%]>3 then; ' only put breath
events back on the
channel if they are 3 secs apart...physiologically valid?
```

```
MemSetItem(filtAVG%,0,ArrSmooth[i%]);

endif

next
'-------------------------------------------------------
'This bit to amalgamate the Filtered AVG (FiltAVG) channel and the
Smooth Channel
(SmoothAVG%)

BigDaddy%:=MemChan(2); ' create memory event (2) channel BreathEST
ChanShow(BigDaddy%);
ChanTitle$(BigDaddy%,"SmoothFiltAvg"); ' create mem chan called
BigDaddy% with events
from 404 405 chan no 406


MemImport(BigDaddy%,404,0,maxtime());
MemImport(BigDaddy%,405,0,maxtime());

CursorActive(0,14, BigDaddy%, 4.01, "", "", 1); 'Data points given
by 14, from chan%, ALL

MeasureX(102,1,"Cursor(0)","0",0); ' measure 102 means Time, 1 is
chan number for

measurement

MeasureY(100,1,"Cursor(0)","0",0); ' measure 100 means Value, 1 is
chan number for

measurement, both have no effect until measuretochan used

trig2%:=MeasureToChan(0,"Channel 1",3,14,BigDaddy%,4.012,1,0,1);
Process(0.0, View(data%).MaxTime(), 0, 1, Trig2%);

BreathEst%:=MemChan(2); ' create memory event (2) channel
BreathEst
ChanShow(BreathEst%);
ChanTitle$(BreathEst%,"BreathEst");

repeat

Time:=NextTime(Trig2%,Time);

If time>-1 then
ct%:=Count(BigDaddy%,Time-2, Time+2);
Cursor(1,Time-2);
Cursor(2,Time+2);
Avg2%();

endif
Until
Time=-1;
Func Avg2%();
var Arr2[ct%];
var Mean2,SD2;

ChanData(BigDaddy%, arr2[],Time-2, Time+2);
ArrSum(Arr2[],Mean2,SD2);
```

```
MemSetItem(BreathEst%,0,Mean2);
return 1

end

MemSave(408,19,3,1);
Chanshow(19);

'-------------------------------------------------------------
' this bit tidys the cursors up to equate to section that the FFT
was performed on
CursorSet(0);
Cursor(0,0);
DrawMode(12,5,1,1);
CursorNew();
CursorSet(1,0);
CursorActive(1,4, 12, "Cursor(0)", "MaxTime()", "", "0.0", 0, 0);
'Peak find
CursorSearch(1);
Cursor(1,(cursor(1)+10));
CursorNew();
Cursor(2,(cursor(1)+300)); 'Fetch the cursor

'--------------------------------- to do the PSTH from which times
are put in arrays

var v12%;
var v17%;

var j%;
var k%;
var eT%;
var sweeptimes[12];
var sweep%;
var ST;
var chandata%;
var a%;
var SweepCount%;
var BreathTime [500];
var R-waveTime [500][500];
var RstDev;
var R-waveSorted[1000];
var R-wavecount%;
var R-waveflag%;
var breathno%;
var breathcount%;
var av;
var SD;

var breathepoch;
var R-waveangle[700][700];
var couplingangle[700][700];
var cosrangle[700][700];
var sinrangle[700][700];
var cosranglec[700][700];
var sinranglec[700][700];
var Xstd[50];
var Ystd[50];
var rvector;
var rvectorc;
var meanangle;
```

```
var meananglec;
var costotal;
var sintotal;
var costotalc;
var sintotalc;
var Xmean;
var Ymean;
var Xmeanc;
var Ymeanc;

var BrEpochCnt10%;
var totalintcountbe10%;
var totalintcountrp10%;
var intcountbe10%;
var intcountrp10%;
var sdcountbe%;
var sdcountrp%;
var simplicity%;
var z%;
var Rzero;
var Rfifth;
var Rthird;
var Rtwo;
var Rratio02;
var Rratio35;



'*********************************************************



v17%:=SetPsth(3,80,0.1,0,408,2,3,0,10); ' trigger channel changed
from 402 to 404,
now to 408 equates to AVG to Filt AVG to BreathEst *************

WindowVisible(0);
Process(View(-1).Cursor(1), View(-1).Cursor(2), 1, 1, 0, 408, 1.5,
0); ' trigger channel
changed from 402 to 404, now to 408 equates to AVG to Filt AVG to
BreathEst *************

ChanSelect(801,1);
DrawMode(801,9,2,16,1);
DrawMode(801,9,2,16,1);

'_____________________________________________________________


'To get output of PSTH and calculate RSA like Hand calc of RSA
excel spread sheet

'this section reads breath and R-wave event times and puts them
into arrays.

SweepCount%:=RasterGet(sweep%);
PrintLog (SweepCount%);
z%:= SweepCount%/10;
PrintLog (z%);
PrintLog("\n");
PrintLog("Tag","\t","File","\t","Breath Epoch","\t","Mean Vector
```

```
L","\t","Mean Vector Angle",
"\t","R-waveCount");

for i%:=0 to (SweepCount%-1) do 'reading values into arrays: i% is
breath epoch, a% is
R-wave within breath epoch

For a%:=0 to 10 do 'to look for first 11 (0-10) R-waves in each
breath cycle '

Problem with "10", if less than then 10 get repeats and over
run!!!!!!!!!!!!!!!!!!
'Read all into array then later filter array for Duplicates, only
using this filtered array for the calc of SD

chandata%:=RasterGet(801,sweep%,ST,sweeptimes[]);
BreathTime[i%]:=ST-BinToX(0); ' this is the breath time,
corresponding to this
sweep...breath epoch.... in which the relevant R-waves are
collected

R-waveTime[i%][a%]:=sweeptimes[a%];

next

sweep%:=sweep%+1;

    next
    ' results in 2 arrays, one holding time of breath epoch and
    the other holding the time of the R-wave in that epoch

'-------------------------------------------------------------




sorting since they may be read in a non ascending order as per
text output
'-------------------------------------------------------------


ArrSort(BreathTime[:SweepCount%]
      sorting Breath time array


limiting the sort function to the points of
interest else fills the first lots of array with zeros
'since it is in ascending order. Alternative was to declare
function (see 10a) so you can have dynamic array sizes depending
on SweepCount%. This is better!



j%:=0;

for i%:=0 to (SweepCount%-1) do ' Sorting R-wave array out and
filtering for duplicate values caused by reading overrun above

'j%:=0;

For a%:=0 to 10 do
```

```
'j%:=j%+1;

if R-waveTime[i%][a%]>0 then

 R-waveSorted[j%]:=R-waveTime[i%][a%]; 'convert 2D array into one
                          for sorting

j%:=j%+1;

endif

next

next

ArrSort(R-waveSorted[:j%]);

'j%:=0;
'-----------------------------------------------------------

'getting Breathepoch and converting R-wave events into angles,
where breath epoch i%+1 -
Breath epoch i% = 360 degrees

For i%:=0 to (SweepCount%-1) do '
For a%:=0 to j% do
if R-waveSorted[a%]>BreathTime[i%] and R-
waveSorted[a%]<BreathTime[i%+1] and
R-waveSorted[a%]<>R-waveSorted[a%+1]then ' need to change if since
a i swapped

breathepoch:= BreathTime[i%+1]-BreathTime[i%]; ' calculating
breath
epoch and R-wave event as angle

R-waveangle[i%][R-wavecount%]:=(R-waveSorted[a%]-
BreathTime[i%])/(breathepoch/360);




 'assign to R-wavecount% not j% since we want the breath and R-wave
                   tied not the jth iteration

couplingangle[i%][R-wavecount%]:=R-waveangle[i%][R-wavecount%]; '
put this value into a place that does not get zeroed!**use of R-
wavecount% not a% since latter related
to j% an iterative marker**

cosrangle[i%][a%]:=cos (R-waveangle[i%][R-
wavecount%]*(4.0*ATan(1.0)/180));

'in radians therefore *(4.0*ATan(1.0)/180)is equal to pi/180

sinrangle[i%][a%]:=sin (R-waveangle[i%][R-
wavecount%]*(4.0*ATan(1.0)/180));

'a i switched since arrays are rows by cols, arrsum gives means
for cols, ie want i to
```

```
be the columns

            R-wavecount%:=R-wavecount%+1; ' put flag here so it
assigns element at 0

            costotal:=costotal+cosrangle[i%][a%];

sintotal:=sintotal+sinrangle[i%][a%];

endif

   'simply add up each cosrangle and sinrangle and divide by R-
                              wavecount

    next


if R-wavecount%>0 then
Xmean:=(costotal/R-wavecount%);
Ymean:=(sintotal/R-wavecount%);

'NB if working out phi, (mean angle) then if xbar is less than 0
then
180+arctan (ybar/xbar)

rvector:= Sqrt((Xmean*Xmean)+(Ymean*Ymean));
meanangle:= atan (Ymean/Xmean); ' radians????? not degrees then
convert back?

meanangle:= meanangle*(180/(4.0*ATan(1.0)));
if Xmean<0 then
meanangle:=meanangle+180;

endif



if meanangle<0 then
meanangle:=meanangle+360; ' correction for all sinners take cocco,
positive angle direction anticlock quadrants

endif

datafile$:=Right$(name$,12);
datafile$:= Left$ (datafile$,8);
Tag$:=Right$(name$,16);
Tag$:=Left$ (tag$,3);

Printlog(Tag$,"\t",datafile$,"\t",BreathTime[i%],"\t",rvector,
"\t",meanangle,"\t",
R-wavecount%);

endif

R-wavecount%:=0;
Xmean:=0;
Ymean:=0;
costotal:=0;
sintotal:=0;

next
```

```
'-------------------------------------------------------


'Now to get the circle stats analysis of the a%th R-wave in each
breath epoch. To
investigate the pattern in intervals. Suspect the 5th and 6th R-
wave may show less
'association to the breath marker than the 0,1,2 etc of each
breath cycle.

Printlog ("\n");

Printlog ("R-wave No.","\t"," MVL","\t"," MVA","\t","R-wave
No.","\t","breaths");

For a%:=0 to 10 do

For i%:=0 to (SweepCount%-1) do

     if couplingangle[i%][a%] <> 0 then

            Printlog("breath event at ", "\t",BreathTime[i%],
"\t","R-wave angle is","\t",
couplingangle[i%][a%],"\t",R-waveangle[i%][a%],"\t","and a
is","\t",a%,"\t","and i is","\t",i%
);

            cosranglec[i%][a%]:=cos
(couplingangle[i%][a%]*(4.0*ATan(1.0)/180)); ' do
            these need to be in radians? Think so
*(4.0*ATan(1.0)/180)is equal to pi/180

            sinranglec[i%][a%]:=sin
(couplingangle[i%][a%]*(4.0*ATan(1.0)/180)); 'a i
            switched since arrays are rows by cols, arrsum gives
means for cols,i be columns

breathno%:=breathno%+1;
costotalc:=costotalc+cosranglec[i%][a%];
sintotalc:=sintotalc+sinranglec[i%][a%];

endif

next

R-wavecount%:=R-wavecount%+1;
if breathno%>0 then
Xmeanc:=(costotalc/breathno%);

    Ymeanc:=(sintotalc/breathno%);

                'NB if working out phi, (mean angle) then if xbar
is less than 0 then
                 180+arctan (ybar/xbar)

rvectorc:= Sqrt((Xmeanc*Xmeanc)+(Ymeanc*Ymeanc));
meananglec:= atan (Ymeanc/Xmeanc); ' radians????? not degrees then
convert back?
```

```
meananglec:= meananglec*(180/(4.0*ATan(1.0)));

if Xmeanc<0 then
meananglec:=meananglec+180;
endif


if meananglec<0 then
meananglec:=meananglec+360; ' correction for all sinners take
cocco, positive angle direction anticlockwise quadrants
      endif

      if a% = 0 then
      Rzero:=rvectorc;
      endif

      if a% = 5 then
      Rfifth:=rvectorc;
      endif




      if a% = 3 then
      Rthird:=rvectorc;
      endif

      if a% = 2 then
      Rtwo:=rvectorc;
      endif

Printlog( a%, "\t",rvectorc,"\t",meananglec,"\t",R-
wavecount%,"\t",breathno%);

endif

R-wavecount%:=0;
Xmeanc:=0;
Ymeanc:=0;
costotalc:=0;
sintotalc:=0;
breathno%:=0;

next

Rratio02:= Rzero/Rtwo;
Rratio35:= Rthird/Rfifth;
printlog ("\n");
Printlog (" 0:2ratio of first to third R-wave is","\t",Rratio02);
' add one for zero, ie a=0 is first

Printlog (" 3:5ratio of 4th to 6th R-wave is","\t",Rratio35);

'-------------------------------------------------------


' to get meanvector for 10 or so breaths---think about using ST as
no.breath epochs
and using this divided by 4,3,6 etc? use z
```

```
 ' first set of
 breaths.....................................................


For i%:=0 to (SweepCount%) do
 While i% >= 0 and i% < (z%) do 'try replacing for next i with

 i%:= i%+1;
 if i% < SweepCount% then

 'printlog (breathno%, "\t", SweepCount%, "\t",a%,"\t",i%);

 For a%:=0 to 10 do ' 10 R-waves


 if couplingangle[i%][a%] <> 0 then

 'Printlog("breath event at ", "\t",BreathTime[i%], "\t","R-wave
 angle
 is","\t",couplingangle[i%][a%],"\t",R-waveangle[i%][a%],"\t","and
 a is","\t",a%,"\t","and
 breath is","\t",i%);

 cosranglec[i%][a%]:=cos
 (couplingangle[i%][a%]*(4.0*ATan(1.0)/180)); ' do

 these need to be in radians? Think so *(4.0*ATan(1.0)/180)is equal
 to pi/180

 sinranglec[i%][a%]:=sin
 (couplingangle[i%][a%]*(4.0*ATan(1.0)/180)); 'a i

 switched since arrays are rows by cols, arrsum gives means for
 cols, ie want i to be columns

 R-wavecount%:=R-wavecount%+1;

 costotalc:=costotalc+cosranglec[i%][a%];
 sintotalc:=sintotalc+sinranglec[i%][a%];

 endif

 next;

 breathno%:=breathno%+1;

 endif

 'next

 wend;
 next

 'Halt;

 if breathno%>0 then
 Xmeanc:=(costotalc/R-wavecount%);
 Ymeanc:=(sintotalc/R-wavecount%);

 'NB if working out phi, (mean angle) then if xbar is less than 0
```

```
then 180+arctan (ybar/xbar)

rvectorc:= Sqrt((Xmeanc*Xmeanc)+(Ymeanc*Ymeanc));

meananglec:= atan (Ymeanc/Xmeanc); ' radians????? not degrees then
convert back?

meananglec:= meananglec*(180/(4.0*ATan(1.0)));
if Xmeanc<0 then
meananglec:=meananglec+180;

endif

if meananglec<0 then

meananglec:=meananglec+360; ' correction for all sinners take
cocco,
positive angle direction anticlock quadrants
endif
printlog ("\n");

Printlog("number of breaths used ","\t", breathno%,"\t","Length of
mean vector is ",
"\t",rvectorc, "\t","mean vector angle
is","\t",meananglec,"\t","and R-wavecount","\t",
R-wavecount%,"\t");

endif

R-wavecount%:=0;
Xmeanc:=0;
Ymeanc:=0;
costotalc:=0;
sintotalc:=0;
breathno%:=0;


' second set of
breaths.....................................................
.....................

For i%:=0 to (SweepCount%) do

While i% >= z% and i%<(2*z%) do 'try replacing for next i with

while**************************************
'For i%:=0 to (SweepCount%) do ' first 10 breaths
' need a check in here to see if i% is greater than sweep count or
do until loop

 i%:= i%+1;
if i% < SweepCount% then

'printlog (breathno%, "\t", SweepCount%, "\t",a%,"\t",i%);

For a%:=0 to 10 do ' 10 R-waves

'endif

if couplingangle[i%][a%] <> 0 then
```

```
            'Printlog("breath event at ", "\t",BreathTime[i%],
"\t","R-wave angle
is","\t",couplingangle[i%][a%],"\t",R-waveangle[i%][a%],"\t","and
a is","\t",a%,"\t","and
breath is","\t",i%);

cosranglec[i%][a%]:=cos
(couplingangle[i%][a%]*(4.0*ATan(1.0)/180)); ' do

these need to be in radians? Think so *(4.0*ATan(1.0)/180)is equal
to pi/180

sinranglec[i%][a%]:=sin
(couplingangle[i%][a%]*(4.0*ATan(1.0)/180)); 'a i

switched since arrays are rows by cols, arrsum gives means for
cols, ie want i to be columns

R-wavecount%:=R-wavecount%+1;

costotalc:=costotalc+cosranglec[i%][a%];
sintotalc:=sintotalc+sinranglec[i%][a%];

endif

next;
breathno%:=breathno%+1;

endif

'next

wend;
next

if breathno%>0 then
Xmeanc:=(costotalc/R-wavecount%);
Ymeanc:=(sintotalc/R-wavecount%);

               'NB if working out phi, (mean angle) then if xbar
is less than 0 then
180+arctan (ybar/xbar)

rvectorc:= Sqrt((Xmeanc*Xmeanc)+(Ymeanc*Ymeanc));
meananglec:= atan (Ymeanc/Xmeanc); ' radians????? not degrees then
convert back?

meananglec:= meananglec*(180/(4.0*ATan(1.0)));
if Xmeanc<0 then
meananglec:=meananglec+180;

endif

if meananglec<0 then
meananglec:=meananglec+360; ' correction for all sinners take
cocco,
positive angle direction anticlock quadrants

endif

printlog ("\n");
```

```
Printlog("number of breaths used ","\t", breathno%,"\t","Length of
mean vector is ",
"\t",rvectorc, "\t","mean vector angle
is","\t",meananglec,"\t","and R-wavecount","\t",
R-wavecount%,"\t");

    endif


R-wavecount%:=0;
Xmeanc:=0;
Ymeanc:=0;
costotalc:=0;
sintotalc:=0;
breathno%:=0;


'third set of
breaths.....................................................

For i%:=0 to (SweepCount%) do
While i% >= 2*z% and i%<(3*z%) do 'try replacing for next i with

while****************************************
'For i%:=0 to (SweepCount%) do ' first 10 breaths
' need a check in here to see if i% is greater than sweep count or
do until loop

 i%:= i%+1;
if i% < SweepCount% then

'printlog (breathno%, "\t", SweepCount%, "\t",a%,"\t",i%);

For a%:=0 to 10 do ' 10 R-waves

'endif

if couplingangle[i%][a%] <> 0 then

            'Printlog("breath event at ", "\t",BreathTime[i%],
"\t","R-wave angle
is","\t",couplingangle[i%][a%],"\t",R-waveangle[i%][a%],"\t","and
a is","\t",a%,"\t","and
breath is","\t",i%);

cosranglec[i%][a%]:=cos
(couplingangle[i%][a%]*(4.0*ATan(1.0)/180)); ' do

these need to be in radians? Think so *(4.0*ATan(1.0)/180)is equal
to pi/180

sinranglec[i%][a%]:=sin
(couplingangle[i%][a%]*(4.0*ATan(1.0)/180)); 'a i

switched since arrays are rows by cols, arrsum gives means for
cols, ie want i to be columns

R-wavecount%:=R-wavecount%+1;

costotalc:=costotalc+cosranglec[i%][a%];
```

```
sintotalc:=sintotalc+sinranglec[i%][a%];

endif

next;
breathno%:=breathno%+1;

endif

    'next

    wend;
next

'Halt;

if breathno%>0 then
Xmeanc:=(costotalc/R-wavecount%);
Ymeanc:=(sintotalc/R-wavecount%);

'NB if working out phi, (mean angle) then if xbar is less than 0
then 180+arctan (ybar/xbar)

rvectorc:= Sqrt((Xmeanc*Xmeanc)+(Ymeanc*Ymeanc));
meananglec:= atan (Ymeanc/Xmeanc); ' radians????? not degrees then
convert back?

meananglec:= meananglec*(180/(4.0*ATan(1.0)));
if Xmeanc<0 then
meananglec:=meananglec+180;

endif

if meananglec<0 then
meananglec:=meananglec+360; ' correction for all sinners take
cocco,
positive angle direction anticlock quadrants

    endif

printlog ("\n");

        Printlog("number of breaths used ","\t",
breathno%,"\t","Length of mean vector is ",
"\t",rvectorc, "\t","mean vector angle
is","\t",meananglec,"\t","and R-wavecount","\t",
R-wavecount%,"\t");

    endif

'wend

R-wavecount%:=0;
Xmeanc:=0;
Ymeanc:=0;

costotalc:=0;
sintotalc:=0;
breathno%:=0;
```

```
' fourth set of breaths

For i%:=0 to (SweepCount%) do
While i% >= 3*z% and i%<(4*z%) do 'try replacing for next i with

while**************************************
'For i%:=0 to (SweepCount%) do ' first 10 breaths
' need a check in here to see if i% is greater than sweep count or
do until loop

 i%:= i%+1;
if i% < SweepCount% then

'printlog (breathno%, "\t", SweepCount%, "\t",a%,"\t",i%);

For a%:=0 to 10 do ' 10 R-waves

'endif

if couplingangle[i%][a%] <> 0 then

            'Printlog("breath event at ", "\t",BreathTime[i%],
"\t","R-wave angle
is","\t",couplingangle[i%][a%],"\t",R-waveangle[i%][a%],"\t","and
a is","\t",a%,"\t","and
breath is","\t",i%);

cosranglec[i%][a%]:=cos
(couplingangle[i%][a%]*(4.0*ATan(1.0)/180)); ' do

these need to be in radians? Think so *(4.0*ATan(1.0)/180)is equal
to pi/180

sinranglec[i%][a%]:=sin
(couplingangle[i%][a%]*(4.0*ATan(1.0)/180)); 'a i

switched since arrays are rows by cols, arrsum gives means for
cols, ie want i to be columns

R-wavecount%:=R-wavecount%+1;

costotalc:=costotalc+cosranglec[i%][a%];
sintotalc:=sintotalc+sinranglec[i%][a%];

endif

next;
breathno%:=breathno%+1;

endif

'next

    wend;
next

'Halt;

if breathno%>0 then
Xmeanc:=(costotalc/R-wavecount%);
```

```
Ymeanc:=(sintotalc/R-wavecount%);

                'NB if working out phi, (mean angle) then if xbar
is less than 0 then
180+arctan (ybar/xbar)

rvectorc:= Sqrt((Xmeanc*Xmeanc)+(Ymeanc*Ymeanc));
meananglec:= atan (Ymeanc/Xmeanc); ' radians????? not degrees then
convert back?

meananglec:= meananglec*(180/(4.0*ATan(1.0)));
if Xmeanc<0 then
meananglec:=meananglec+180;

endif

if meananglec<0 then
meananglec:=meananglec+360; ' correction for all sinners take
cocco,
positive angle direction anticlock quadrants

    endif

printlog ("\n");

        Printlog("number of breaths used ","\t",
breathno%,"\t","Length of mean vector is ",
"\t",rvectorc, "\t","mean vector angle
is","\t",meananglec,"\t","and R-wavecount","\t",
R-wavecount%,"\t");

    endif



R-wavecount%:=0;

Xmeanc:=0;
Ymeanc:=0;
costotalc:=0;
sintotalc:=0;

breathno%:=0;


' fifth set of breaths

For i%:=0 to (SweepCount%) do
While i% >= 4*z% and i%<(5*z%) do 'try replacing for next i with

while**************************************
'For i%:=0 to (SweepCount%) do ' first 10 breaths
' need a check in here to see if i% is greater than sweep count or
do until loop

 i%:= i%+1;
if i% < SweepCount% then

'printlog (breathno%, "\t", SweepCount%, "\t",a%,"\t",i%);

For a%:=0 to 10 do ' 10 R-waves
```

```
'endif

if couplingangle[i%][a%] <> 0 then

            'Printlog("breath event at ", "\t",BreathTime[i%],
"\t","R-wave angle
is","\t",couplingangle[i%][a%],"\t",R-waveangle[i%][a%],"\t","and
a is","\t",a%,"\t","and
breath is","\t",i%);

cosranglec[i%][a%]:=cos
(couplingangle[i%][a%]*(4.0*ATan(1.0)/180)); ' do

these need to be in radians? Think so *(4.0*ATan(1.0)/180)is equal
to pi/180

sinranglec[i%][a%]:=sin
(couplingangle[i%][a%]*(4.0*ATan(1.0)/180)); 'a i

switched since arrays are rows by cols, arrsum gives means for
cols, ie want i to be columns

R-wavecount%:=R-wavecount%+1;

costotalc:=costotalc+cosranglec[i%][a%];
sintotalc:=sintotalc+sinranglec[i%][a%];

endif

next;
breathno%:=breathno%+1;

endif

'next

    wend;
next

'Halt;

if breathno%>0 then
Xmeanc:=(costotalc/R-wavecount%);
Ymeanc:=(sintotalc/R-wavecount%);

                'NB if working out phi, (mean angle) then if xbar
is less than 0 then
180+arctan (ybar/xbar)

rvectorc:= Sqrt((Xmeanc*Xmeanc)+(Ymeanc*Ymeanc));
meananglec:= atan (Ymeanc/Xmeanc); ' radians????? not degrees then
convert back?

meananglec:= meananglec*(180/(4.0*ATan(1.0)));
if Xmeanc<0 then
meananglec:=meananglec+180;

endif

if meananglec<0 then
```

```
meananglec:=meananglec+360; ' correction for all sinners take
cocco,
positive angle direction anticlock quadrants

    endif

printlog ("\n");

        Printlog("number of breaths used ","\t",
breathno%,"\t","Length of mean vector is ",
"\t",rvectorc, "\t","mean vector angle
is","\t",meananglec,"\t","and R-wavecount","\t",
R-wavecount%,"\t");

endif

'wend

R-wavecount%:=0;
Xmeanc:=0;
Ymeanc:=0;
costotalc:=0;
sintotalc:=0;
breathno%:=0;


' sixth set of breaths

For i%:=0 to (SweepCount%) do
While i% >= 5*z% and i%<(6*z%) do 'try replacing for next i with

while**************************************
'For i%:=0 to (SweepCount%) do ' first 10 breaths
' need a check in here to see if i% is greater than sweep count or
do until loop

 i%:= i%+1;
if i% < SweepCount% then

'printlog (breathno%, "\t", SweepCount%, "\t",a%,"\t",i%);

For a%:=0 to 10 do ' 10 R-waves

'endif

if couplingangle[i%][a%] <> 0 then

            'Printlog("breath event at ", "\t",BreathTime[i%],
"\t","R-wave angle
is","\t",couplingangle[i%][a%],"\t",R-waveangle[i%][a%],"\t","and
a is","\t",a%,"\t","and
breath is","\t",i%);

cosranglec[i%][a%]:=cos
(couplingangle[i%][a%]*(4.0*ATan(1.0)/180)); ' do

these need to be in radians? Think so *(4.0*ATan(1.0)/180)is equal
to pi/180

sinranglec[i%][a%]:=sin
(couplingangle[i%][a%]*(4.0*ATan(1.0)/180)); 'a i
```

```
switched since arrays are rows by cols, arrsum gives means for
cols, ie want i to be columns

R-wavecount%:=R-wavecount%+1;

costotalc:=costotalc+cosranglec[i%][a%];
sintotalc:=sintotalc+sinranglec[i%][a%];

endif

next;

breathno%:=breathno%+1;

endif

    'next

    wend;
next

'Halt;

if breathno%>0 then
Xmeanc:=(costotalc/R-wavecount%);
Ymeanc:=(sintotalc/R-wavecount%);

                'NB if working out phi, (mean angle) then if xbar
is less than 0 then
180+arctan (ybar/xbar)

rvectorc:= Sqrt((Xmeanc*Xmeanc)+(Ymeanc*Ymeanc));
meananglec:= atan (Ymeanc/Xmeanc); ' radians????? not degrees then
convert back?

meananglec:= meananglec*(180/(4.0*ATan(1.0)));
if Xmeanc<0 then
meananglec:=meananglec+180;

endif

if meananglec<0 then
meananglec:=meananglec+360; ' correction for all sinners take
cocco,
positive angle direction anticlock quadrants

    endif

printlog ("\n");

        Printlog("number of breaths used ","\t",
breathno%,"\t","Length of mean vector is ",
"\t",rvectorc, "\t","mean vector angle
is","\t",meananglec,"\t","and R-wavecount","\t",
R-wavecount%,"\t");

    endif

'wend
```

```
R-wavecount%:=0;
Xmeanc:=0;
Ymeanc:=0;
costotalc:=0;
sintotalc:=0;
breathno%:=0;



'seventh set of breaths

For i%:=0 to (SweepCount%) do
While i% >= 6*z% and i%<(7*z%) do 'try replacing for next i with

while**************************************
'For i%:=0 to (SweepCount%) do ' first 10 breaths
' need a check in here to see if i% is greater than sweep count or
do until loop

 i%:= i%+1;
if i% < SweepCount% then

'printlog (breathno%, "\t", SweepCount%, "\t",a%,"\t",i%);

For a%:=0 to 10 do ' 10 R-waves

'endif

if couplingangle[i%][a%] <> 0 then

            'Printlog("breath event at ", "\t",BreathTime[i%],
"\t","R-wave angle
is","\t",couplingangle[i%][a%],"\t",R-waveangle[i%][a%],"\t","and
a is","\t",a%,"\t","and
breath is","\t",i%);

cosranglec[i%][a%]:=cos
(couplingangle[i%][a%]*(4.0*ATan(1.0)/180)); ' do

these need to be in radians? Think so *(4.0*ATan(1.0)/180)is equal
to pi/180

sinranglec[i%][a%]:=sin
(couplingangle[i%][a%]*(4.0*ATan(1.0)/180)); 'a i

switched since arrays are rows by cols, arrsum gives means for
cols, ie want i to be columns

R-wavecount%:=R-wavecount%+1;

costotalc:=costotalc+cosranglec[i%][a%];
sintotalc:=sintotalc+sinranglec[i%][a%];

endif

next;
breathno%:=breathno%+1;

endif
```

```
'next

    wend;
next

'Halt;

if breathno%>0 then
Xmeanc:=(costotalc/R-wavecount%);
Ymeanc:=(sintotalc/R-wavecount%);

                'NB if working out phi, (mean angle) then if xbar
is less than 0 then
180+arctan (ybar/xbar)

rvectorc:= Sqrt((Xmeanc*Xmeanc)+(Ymeanc*Ymeanc));
meananglec:= atan (Ymeanc/Xmeanc); ' radians????? not degrees then
convert back?

meananglec:= meananglec*(180/(4.0*ATan(1.0)));
if Xmeanc<0 then
meananglec:=meananglec+180;

endif

if meananglec<0 then
meananglec:=meananglec+360; ' correction for all sinners take
cocco,

positive angle direction anticlock quadrants

endif

printlog ("\n");

        Printlog("number of breaths used ","\t",
breathno%,"\t","Length of mean vector is ",
"\t",rvectorc, "\t","mean vector angle
is","\t",meananglec,"\t","and R-wavecount","\t",
R-wavecount%,"\t");

    endif

'wend

R-wavecount%:=0;
Xmeanc:=0;
Ymeanc:=0;
costotalc:=0;
sintotalc:=0;
breathno%:=0;


'eigth set of breaths

For i%:=0 to (SweepCount%) do
While i% >= 7*z% and i%<(8*z%) do 'try replacing for next i with

while**************************************
'For i%:=0 to (SweepCount%) do ' first 10 breaths
' need a check in here to see if i% is greater than sweep count or
```

```
do until loop

 i%:= i%+1;
if i% < SweepCount% then

'printlog (breathno%, "\t", SweepCount%, "\t",a%,"\t",i%);

For a%:=0 to 10 do ' 10 R-waves

'endif

if couplingangle[i%][a%] <> 0 then

            'Printlog("breath event at ", "\t",BreathTime[i%],
"\t","R-wave angle
is","\t",couplingangle[i%][a%],"\t",R-waveangle[i%][a%],"\t","and
a is","\t",a%,"\t","and
breath is","\t",i%);

cosranglec[i%][a%]:=cos
(couplingangle[i%][a%]*(4.0*ATan(1.0)/180)); ' do

these need to be in radians? Think so *(4.0*ATan(1.0)/180)is equal
to pi/180

sinranglec[i%][a%]:=sin
(couplingangle[i%][a%]*(4.0*ATan(1.0)/180)); 'a i

switched since arrays are rows by cols, arrsum gives means for
cols, ie want i to be columns

R-wavecount%:=R-wavecount%+1;

costotalc:=costotalc+cosranglec[i%][a%];
sintotalc:=sintotalc+sinranglec[i%][a%];

endif

next;
breathno%:=breathno%+1;

endif

'next

    wend;
next

'Halt;

if breathno%>0 then
Xmeanc:=(costotalc/R-wavecount%);
Ymeanc:=(sintotalc/R-wavecount%);

                'NB if working out phi, (mean angle) then if xbar
is less than 0 then
180+arctan (ybar/xbar)

rvectorc:= Sqrt((Xmeanc*Xmeanc)+(Ymeanc*Ymeanc));
meananglec:= atan (Ymeanc/Xmeanc); ' radians????? not degrees then
convert back?
```

```
meananglec:= meananglec*(180/(4.0*ATan(1.0)));
if Xmeanc<0 then
meananglec:=meananglec+180;

endif

if meananglec<0 then
meananglec:=meananglec+360; ' correction for all sinners take
cocco,
positive angle direction anticlock quadrants

    endif

printlog ("\n");

        Printlog("number of breaths used ","\t",
breathno%,"\t","Length of mean vector is ",
"\t",rvectorc, "\t","mean vector angle
is","\t",meananglec,"\t","and R-wavecount","\t",
R-wavecount%,"\t");

    endif

'wend

R-wavecount%:=0;
Xmeanc:=0;
Ymeanc:=0;
costotalc:=0;
sintotalc:=0;
breathno%:=0;



'ninth set of breaths

For i%:=0 to (SweepCount%) do
While i% >= 8*z% and i%<(9*z%) do 'try replacing for next i with

while**************************************
'For i%:=0 to (SweepCount%) do ' first 10 breaths
' need a check in here to see if i% is greater than sweep count or
do until loop

 i%:= i%+1;
if i% < SweepCount% then

'printlog (breathno%, "\t", SweepCount%, "\t",a%,"\t",i%);

For a%:=0 to 10 do ' 10 R-waves

'endif

if couplingangle[i%][a%] <> 0 then

            'Printlog("breath event at ", "\t",BreathTime[i%],
"\t","R-wave angle
is","\t",couplingangle[i%][a%],"\t",R-waveangle[i%][a%],"\t","and
a is","\t",a%,"\t","and
breath is","\t",i%);
```

```
cosranglec[i%][a%]:=cos
(couplingangle[i%][a%]*(4.0*ATan(1.0)/180)); ' do

these need to be in radians? Think so *(4.0*ATan(1.0)/180)is equal
to pi/180

sinranglec[i%][a%]:=sin
(couplingangle[i%][a%]*(4.0*ATan(1.0)/180)); 'a i

switched since arrays are rows by cols, arrsum gives means for
cols, ie want i to be columns

R-wavecount%:=R-wavecount%+1;

costotalc:=costotalc+cosranglec[i%][a%];
sintotalc:=sintotalc+sinranglec[i%][a%];

endif

next;
breathno%:=breathno%+1;

endif

'next

    wend;
next

'Halt;

if breathno%>0 then
Xmeanc:=(costotalc/R-wavecount%);
Ymeanc:=(sintotalc/R-wavecount%);

'NB if working out phi, (mean angle) then if xbar is less than 0
then

180+arctan (ybar/xbar)

rvectorc:= Sqrt((Xmeanc*Xmeanc)+(Ymeanc*Ymeanc));
meananglec:= atan (Ymeanc/Xmeanc); ' radians????? not degrees then
convert back?

meananglec:= meananglec*(180/(4.0*ATan(1.0)));
if Xmeanc<0 then
meananglec:=meananglec+180;

endif

if meananglec<0 then
meananglec:=meananglec+360; ' correction for all sinners take
cocco,
positive angle direction anticlock quadrants

    endif

        printlog ("\n");

        Printlog("number of breaths used ","\t",
```

```
breathno%,"\t","Length of mean vector is ",
"\t",rvectorc, "\t","mean vector angle
is","\t",meananglec,"\t","and R-wavecount","\t",
R-wavecount%,"\t");

    endif

'wend

R-wavecount%:=0;
Xmeanc:=0;
Ymeanc:=0;
costotalc:=0;
sintotalc:=0;
breathno%:=0;

'tenth set of breaths

For i%:=0 to (SweepCount%) do
While i% >= 9*z% and i%<(10*z%) do 'try replacing for next i with

while****************************************
'For i%:=0 to (SweepCount%) do ' first 10 breaths
' need a check in here to see if i% is greater than sweep count or
do until loop

 i%:= i%+1;
if i% < SweepCount% then

'printlog (breathno%, "\t", SweepCount%, "\t",a%,"\t",i%);

For a%:=0 to 10 do ' 10 R-waves

'endif

if couplingangle[i%][a%] <> 0 then

            'Printlog("breath event at ", "\t",BreathTime[i%],
"\t","R-wave angle
is","\t",couplingangle[i%][a%],"\t",R-waveangle[i%][a%],"\t","and
a is","\t",a%,"\t","and
breath is","\t",i%);

cosranglec[i%][a%]:=cos
(couplingangle[i%][a%]*(4.0*ATan(1.0)/180)); ' do

these need to be in radians? Think so *(4.0*ATan(1.0)/180)is equal
to pi/180

sinranglec[i%][a%]:=sin
(couplingangle[i%][a%]*(4.0*ATan(1.0)/180)); 'a i

switched since arrays are rows by cols, arrsum gives means for
cols, ie want i to be columns

R-wavecount%:=R-wavecount%+1;

costotalc:=costotalc+cosranglec[i%][a%];
sintotalc:=sintotalc+sinranglec[i%][a%];

endif
```

```
next;
breathno%:=breathno%+1;

endif

'next

    wend;
next

'Halt;

if breathno%>0 then
Xmeanc:=(costotalc/R-wavecount%);

Ymeanc:=(sintotalc/R-wavecount%);

                'NB if working out phi, (mean angle) then if xbar
is less than 0 then
180+arctan (ybar/xbar)

rvectorc:= Sqrt((Xmeanc*Xmeanc)+(Ymeanc*Ymeanc));
meananglec:= atan (Ymeanc/Xmeanc); ' radians????? not degrees then
convert back?

meananglec:= meananglec*(180/(4.0*ATan(1.0)));
if Xmeanc<0 then
meananglec:=meananglec+180;

endif

if meananglec<0 then
meananglec:=meananglec+360; ' correction for all sinners take
cocco,
positive angle direction anticlock quadrants

    endif

printlog ("\n");

        Printlog("number of breaths used ","\t",
breathno%,"\t","Length of mean vector is ",
"\t",rvectorc, "\t","mean vector angle
is","\t",meananglec,"\t","and R-wavecount","\t",
R-wavecount%,"\t");

    endif

'wend

R-wavecount%:=0;
Xmeanc:=0;
Ymeanc:=0;
costotalc:=0;
sintotalc:=0;
breathno%:=0;
```

```
'-------------------------------------------------------------


      'Finally do the r vector length for all breaths in file

      For i%:=0 to (SweepCount%) do ' for all breaths

      For a%:=0 to 10 do ' 10 R-waves

      if couplingangle[i%][a%] <> 0 then

          'Printlog("breath event at ", "\t",BreathTime[i%], "\t","R-
      wave angle
      is","\t",couplingangle[i%][a%],"\t",R-waveangle[i%][a%],"\t","and
      a is","\t",a%,"\t","and
      breath is","\t",i%);

      cosranglec[i%][a%]:=cos
      (couplingangle[i%][a%]*(4.0*ATan(1.0)/180)); '
      these need to be in radians, so *(4.0*ATan(1.0)/180)is equal to
      pi/180

      sinranglec[i%][a%]:=sin
      (couplingangle[i%][a%]*(4.0*ATan(1.0)/180)); 'a i switched since
      arrays are rows by cols, arrsum gives means for cols, ie want i to
      be columns

      R-wavecount%:=R-wavecount%+1;

      costotalc:=costotalc+cosranglec[i%][a%];
      sintotalc:=sintotalc+sinranglec[i%][a%];

      endif
      next
      breathno%:=breathno%+1;
      next

      if breathno%>0 then
      Xmeanc:=(costotalc/R-wavecount%);
      Ymeanc:=(sintotalc/R-wavecount%);

        'NB if working out phi, (mean angle) then if xbar is less than 0
                          then 180+arctan (ybar/xbar)

      rvectorc:= Sqrt((Xmeanc*Xmeanc)+(Ymeanc*Ymeanc));
      meananglec:= atan (Ymeanc/Xmeanc); ' radians????? not degrees then
      convert back

      meananglec:= meananglec*(180/(4.0*ATan(1.0)));
      if Xmeanc<0 then
      meananglec:=meananglec+180;
      endif

      if meananglec<0 then
      meananglec:=meananglec+360; ' correction for all sinners take
      cocco, positive angle direction anticlockwise quadrants

          endif

              printlog ("\n");
```

```
        Printlog("For all breaths in file","\t","\t","Length of
mean vector is ", "\t",
rvectorc, "\t","mean vector angle all
breaths","\t",meananglec,"\t","and R-wavecount","\t",
R-wavecount%,"\t","and breath count is","\t",breathno%);

endif

R-wavecount%:=0;
Xmeanc:=0;
Ymeanc:=0;
costotalc:=0;
sintotalc:=0;
breathno%:=0;
```

Appendix 1.6 Frequency response of 5 point filter of Methods section of chapter 5

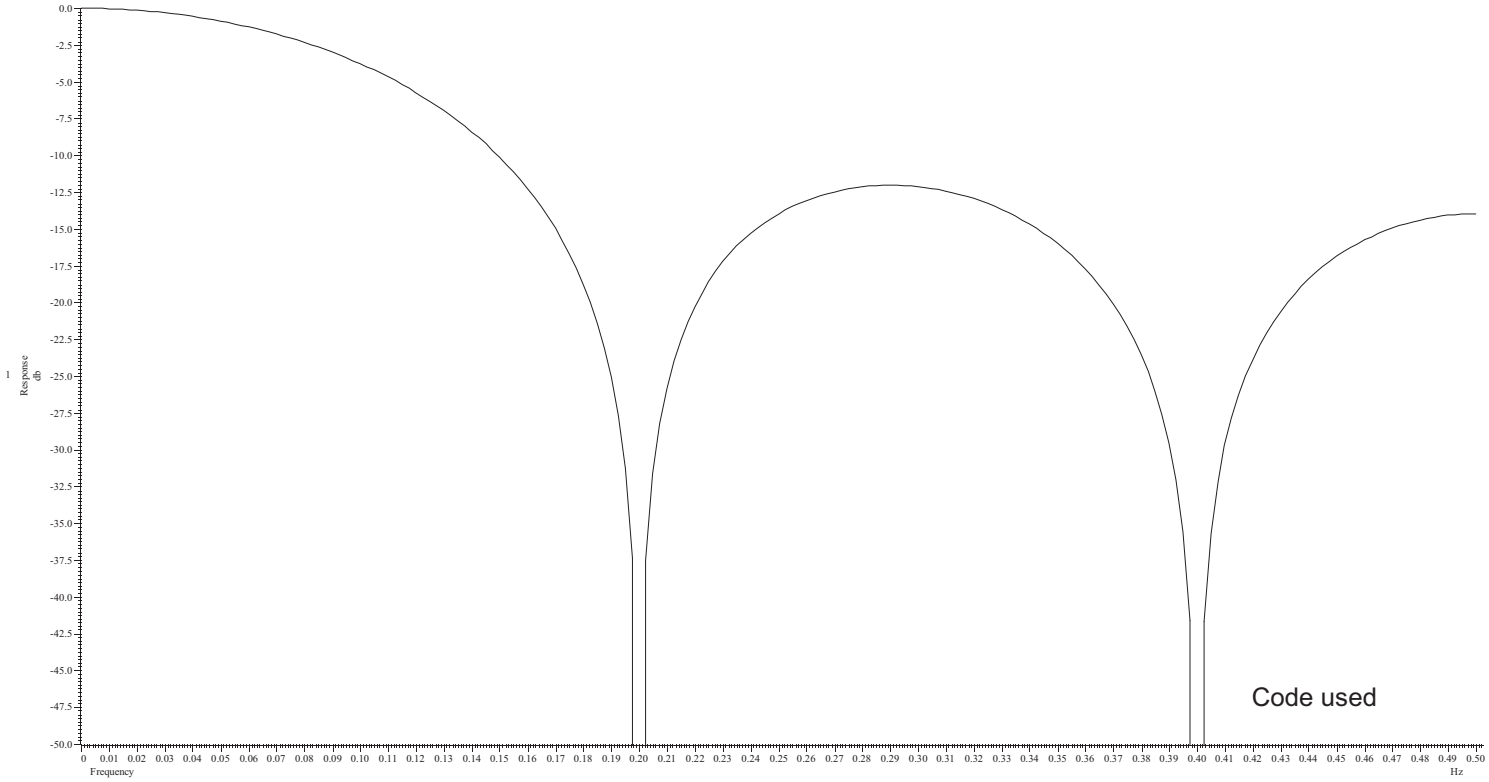

to visualise the frequency response of the 5 point FIR filter used:

```
'$FiltResp|Five point smoothing filter response
const nr% := 201;
const sampleRate := 1;    ' sample rate ,in Hz
var c[5], r[nr%], rv%;
ArrConst(c, 0.2);
FIRResponse(r, c, 0);       'calc in dB (use 1 for linear)
rv% := SetResult(nr%, 0.5*sampleRate/(nr%-1), 0, "Five point smooth; response", "Hz", "db",
"Frequency", "Response");
ArrConst([], r);
YRange(1, -50, 0);          ' show from 0 to -50 dB
'XAxisAttrib(1);             ' log x axis
DrawMode(1, 2);              ' draw as lines
WindowVisible(1);
```

This filter was applied to an array holding the breath event times and not a waveform.

Appendix 1.7. Typical output from the program of appendix 1.5

the file is F:\HRV PhD\Chapter 4 Breath to breath HRV\Chapter 4 Breath files\Human\IPEM2005 Data\8sepha.smr
48
4

Tag	File	Breath Epoch	Mean Vector L	Mean Vector Angle	R-waveCount
	a\8sepha	12.1301	0.0284924	75.3434	6
	a\8sepha	17.9314	0.040115	29.437 7	
	a\8sepha	23.6141	0.046812	269.244	7
	a\8sepha	29.7239	0.0221929	4.87478	7
	a\8sepha	35.9993	0.165211	185.922	6
	a\8sepha	42.1202	0.0760197	300.025	7
	a\8sepha	48.1829	0.0900342	213.06 6	
	a\8sepha	54.631	0.0617061	313.936	9
	a\8sepha	62.9264	0.0286147	178.665	7
	a\8sepha	69.5369	0.0576897	202.806	9
	a\8sepha	77.7709	0.0520453	292.591	8
	a\8sepha	84.2949	0.0421581	175.196	8
	a\8sepha	91.5581	0.0293583	5.47823	10
	a\8sepha	99.7776	0.0356867	359.521	9
	a\8sepha	106.746	0.0185659	194.539	8
	a\8sepha	113.343	0.0633714	172.28 8	
	a\8sepha	120.28	0.0426859	235.124	7
	a\8sepha	125.879	0.0397911	165.013	7
	a\8sepha	131.841	0.0464012	17.1697	6
	a\8sepha	136.734	0.0865041	163.685	6
	a\8sepha	142.17	0.0578009	321.279	8
	a\8sepha	148.017	0.0686742	18.0934	7
	a\8sepha	153.713	0.0105351	218.542	7
	a\8sepha	160.388	0.0370761	221.241	8
	a\8sepha	167.841	0.0326369	76.5668	6
	a\8sepha	173.508	0.0504545	186.996	7
	a\8sepha	180.533	0.0543148	191.06 6	
	a\8sepha	186.337	0.0971209	10.3465	6
	a\8sepha	191.562	0.105765	195.106	6
	a\8sepha	197.806	0.0457473	7.64085	7
	a\8sepha	204.194	0.0452931	303.313	7
	a\8sepha	210.721	0.0232243	178.374	6
	a\8sepha	216.619	0.111569	154.533	5
	a\8sepha	221.692	0.0260952	275.928	7
	a\8sepha	228.021	0.0196621	132.577	6
	a\8sepha	233.392	0.0317281	313.656	8
	a\8sepha	240.78	0.0271502	295.223	7
	a\8sepha	247.22	0.0640824	1.66014	7
	a\8sepha	253.491	0.067634	185.146	6
	a\8sepha	259.459	0.0688713	350.858	8
	a\8sepha	266.241	0.00288451	263.071	8
	a\8sepha	273.203	0.0513336	204.502	7
	a\8sepha	280.226	0.0159257	174.383	7
	a\8sepha	286.724	0.0952894	147.078	5
	a\8sepha	291.918	0.354072	114.345	9
	a\8sepha	303.55	0.0368578	207.285	7

breath event at	12.1301	R-wave angle is	13.0247	13.0247	R-Wave position is	0	Breath number is 0
breath event at	17.9314	R-wave angle is	4.66132	4.66132	R-Wave position is	0	Breath number is 1
breath event at	23.6141	R-wave angle is	39.0594	39.0594	R-Wave position is	0	Breath number is 2
breath event at	29.7239	R-wave angle is	39.9347	39.9347	R-Wave position is	0	Breath number is 3
breath event at	35.9993	R-wave angle is	53.622	53.622	R-Wave position is	0	Breath number is 4
breath event at	42.1202	R-wave angle is	14.9518	14.9518	R-Wave position is	0	Breath number is 5
breath event at	48.1829	R-wave angle is	25.6875	25.6875	R-Wave position is	0	Breath number is 6
breath event at	54.631	R-wave angle is	0.563303	0.563303	R-Wave position is	0	Breath number is 7
breath event at	62.9264	R-wave angle is	29.7138	29.7138	R-Wave position is	0	Breath number is 8
breath event at	69.5369	R-wave angle is	25.2324	25.2324	R-Wave position is	0	Breath number is 9
breath event at	77.7709	R-wave angle is	10.2161	10.2161	R-Wave position is	0	Breath number is 10
breath event at	84.2949	R-wave angle is	27.7604	27.7604	R-Wave position is	0	Breath number is 11
breath event at	91.5581	R-wave angle is	7.13513	7.13513	R-Wave position is	0	Breath number is 12
breath event at	99.7776	R-wave angle is	19.0303	19.0303	R-Wave position is	0	Breath number is 13
breath event at	106.746	R-wave angle is	40.2833	40.2833	R-Wave position is	0	Breath number is 14
breath event at	113.343	R-wave angle is	31.8713	31.8713	R-Wave position is	0	Breath number is 15
breath event at	120.28	R-wave angle is	13.5382	13.5382	R-Wave position is	0	Breath number is 16
breath event at	125.879	R-wave angle is	12.7245	12.7245	R-Wave position is	0	Breath number is 17
breath event at	131.841	R-wave angle is	13.5411	13.5411	R-Wave position is	0	Breath number is 18
breath event at	136.734	R-wave angle is	37.8285	37.8285	R-Wave position is	0	Breath number is 19
breath event at	142.17	R-wave angle is	20.7606	20.7606	R-Wave position is	0	Breath number is 20
breath event at	148.017	R-wave angle is	37.4658	37.4658	R-Wave position is	0	Breath number is 21
breath event at	153.713	R-wave angle is	43.9944	43.9944	R-Wave position is	0	Breath number is 22
breath event at	160.388	R-wave angle is	34.3572	34.3572	R-Wave position is	0	Breath number is 23
breath event at	167.841	R-wave angle is	36.4986	36.4986	R-Wave position is	0	Breath number is 24
breath event at	173.508	R-wave angle is	35.7589	35.7589	R-Wave position is	0	Breath number is 25
breath event at	180.533	R-wave angle is	22.1709	22.1709	R-Wave position is	0	Breath number is 26
breath event at	186.337	R-wave angle is	22.1181	22.1181	R-Wave position is	0	Breath number is 27
breath event at	191.562	R-wave angle is	49.506	49.506	R-Wave position is	0	Breath number is 28
breath event at	197.806	R-wave angle is	17.3752	17.3752	R-Wave position is	0	Breath number is 29
breath event at	204.194	R-wave angle is	34.9856	34.9856	R-Wave position is	0	Breath number is 30
breath event at	210.721	R-wave angle is	39.4709	39.4709	R-Wave position is	0	Breath number is 31
breath event at	216.619	R-wave angle is	37.8061	37.8061	R-Wave position is	0	Breath number is 32
breath event at	221.692	R-wave angle is	0.0290101	0.0290101	R-Wave position is	0	Breath number is 34
breath event at	228.021	R-wave angle is	8.42505	8.42505	R-Wave position is	0	Breath number is 35
breath event at	233.392	R-wave angle is	6.57817	6.57817	R-Wave position is	0	Breath number is 36
breath event at	240.78	R-wave angle is	15.2287	15.2287	R-Wave position is	0	Breath number is 37
breath event at	247.22	R-wave angle is	17.8915	17.8915	R-Wave position is	0	Breath number is 38
breath event at	253.491	R-wave angle is	37.1003	37.1003	R-Wave position is	0	Breath number is 39
breath event at	259.459	R-wave angle is	17.1525	17.1525	R-Wave position is	0	Breath number is 40
breath event at	266.241	R-wave angle is	38.6871	38.6871	R-Wave position is	0	Breath number is 41
breath event at	273.203	R-wave angle is	43.0483	43.0483	R-Wave position is	0	Breath number is 42
breath event at	280.226	R-wave angle is	27.2805	27.2805	R-Wave position is	0	Breath number is 43

breath event at	286.724	R-wave angle is	32.9154	32.9154	R-Wave position is	0	Breath number is	44
breath event at	291.918	R-wave angle is	1.9949	1.9949	R-Wave position is	0	Breath number is	45
breath event at	303.55	R-wave angle is	27.0432	27.0432	R-Wave position is	0	Breath number is	46
0	0.97155	25.3597	1	46				
breath event at	12.1301	R-wave angle is	64.5303	64.5303	R-Wave position is	1	Breath number is	0
breath event at	17.9314	R-wave angle is	61.2966	61.2966	R-Wave position is	1	Breath number is	1
breath event at	23.6141	R-wave angle is	96.3316	96.3316	R-Wave position is	1	Breath number is	2
breath event at	29.7239	R-wave angle is	94.7198	94.7198	R-Wave position is	1	Breath number is	3
breath event at	35.9993	R-wave angle is	107.261	107.261	R-Wave position is	1	Breath number is	4
breath event at	42.1202	R-wave angle is	75.1626	75.1626	R-Wave position is	1	Breath number is	5
breath event at	48.1829	R-wave angle is	92.3488	92.3488	R-Wave position is	1	Breath number is	6
breath event at	54.631	R-wave angle is	44.1346	44.1346	R-Wave position is	1	Breath number is	7
breath event at	62.9264	R-wave angle is	83.9548	83.9548	R-Wave position is	1	Breath number is	8
breath event at	69.5369	R-wave angle is	66.5053	66.5053	R-Wave position is	1	Breath number is	9
breath event at	77.7709	R-wave angle is	65.1206	65.1206	R-Wave position is	1	Breath number is	10
breath event at	84.2949	R-wave angle is	69.3456	69.3456	R-Wave position is	1	Breath number is	11
breath event at	91.5581	R-wave angle is	45.0204	45.0204	R-Wave position is	1	Breath number is	12
breath event at	99.7776	R-wave angle is	61.6527	61.6527	R-Wave position is	1	Breath number is	13
breath event at	106.746	R-wave angle is	84.0487	84.0487	R-Wave position is	1	Breath number is	14
breath event at	113.343	R-wave angle is	74.3699	74.3699	R-Wave position is	1	Breath number is	15
breath event at	120.28	R-wave angle is	66.3921	66.3921	R-Wave position is	1	Breath number is	16
breath event at	125.879	R-wave angle is	65.5619	65.5619	R-Wave position is	1	Breath number is	17
breath event at	131.841	R-wave angle is	77.7739	77.7739	R-Wave position is	1	Breath number is	18
breath event at	136.734	R-wave angle is	95.9742	95.9742	R-Wave position is	1	Breath number is	19
breath event at	142.17	R-wave angle is	72.4759	72.4759	R-Wave position is	1	Breath number is	20
breath event at	148.017	R-wave angle is	85.6245	85.6245	R-Wave position is	1	Breath number is	21
breath event at	153.713	R-wave angle is	90.0039	90.0039	R-Wave position is	1	Breath number is	22
breath event at	160.388	R-wave angle is	76.8588	76.8588	R-Wave position is	1	Breath number is	23
breath event at	167.841	R-wave angle is	96.85	96.85	R-Wave position is	1	Breath number is	24
breath event at	173.508	R-wave angle is	82.9611	82.9611	R-Wave position is	1	Breath number is	25
breath event at	180.533	R-wave angle is	85.1849	85.1849	R-Wave position is	1	Breath number is	26
breath event at	186.337	R-wave angle is	89.9776	89.9776	R-Wave position is	1	Breath number is	27
breath event at	191.562	R-wave angle is	104.228	104.228	R-Wave position is	1	Breath number is	28
breath event at	197.806	R-wave angle is	74.126	74.126	R-Wave position is	1	Breath number is	29
breath event at	204.194	R-wave angle is	88.2048	88.2048	R-Wave position is	1	Breath number is	30
breath event at	210.721	R-wave angle is	100.449	100.449	R-Wave position is	1	Breath number is	31
breath event at	216.619	R-wave angle is	99.3286	99.3286	R-Wave position is	1	Breath number is	32
breath event at	221.692	R-wave angle is	50.8821	50.8821	R-Wave position is	1	Breath number is	34
breath event at	228.021	R-wave angle is	71.6347	71.6347	R-Wave position is	1	Breath number is	35
breath event at	233.392	R-wave angle is	49.9973	49.9973	R-Wave position is	1	Breath number is	36
breath event at	240.78	R-wave angle is	65.9242	65.9242	R-Wave position is	1	Breath number is	37
breath event at	247.22	R-wave angle is	68.3555	68.3555	R-Wave position is	1	Breath number is	38
breath event at	253.491	R-wave angle is	97.3627	97.3627	R-Wave position is	1	Breath number is	39
breath event at	259.459	R-wave angle is	65.0328	65.0328	R-Wave position is	1	Breath number is	40
breath event at	266.241	R-wave angle is	82.8436	82.8436	R-Wave position is	1	Breath number is	41
breath event at	273.203	R-wave angle is	88.5721	88.5721	R-Wave position is	1	Breath number is	42
breath event at	280.226	R-wave angle is	76.1955	76.1955	R-Wave position is	1	Breath number is	43
breath event at	286.724	R-wave angle is	97.5901	97.5901	R-Wave position is	1	Breath number is	44
breath event at	291.918	R-wave angle is	29.3219	29.3219	R-Wave position is	1	Breath number is	45
breath event at	303.55	R-wave angle is	75.37	75.37	R-Wave position is	1	Breath number is	46
1	0.956232		77.4528	1 46				
breath event at	12.1301	R-wave angle is	123.172	123.172	R-Wave position is	2	Breath number is	0
breath event at	17.9314	R-wave angle is	114.638	114.638	R-Wave position is	2	Breath number is	1
breath event at	23.6141	R-wave angle is	151.306	151.306	R-Wave position is	2	Breath number is	2
breath event at	29.7239	R-wave angle is	148.759	148.759	R-Wave position is	2	Breath number is	3
breath event at	35.9993	R-wave angle is	160.077	160.077	R-Wave position is	2	Breath number is	4
breath event at	42.1202	R-wave angle is	133.473	133.473	R-Wave position is	2	Breath number is	5
breath event at	48.1829	R-wave angle is	151.529	151.529	R-Wave position is	2	Breath number is	6
breath event at	54.631	R-wave angle is	88.6607	88.6607	R-Wave position is	2	Breath number is	7
breath event at	62.9264	R-wave angle is	135.309	135.309	R-Wave position is	2	Breath number is	8
breath event at	69.5369	R-wave angle is	104.805	104.805	R-Wave position is	2	Breath number is	9
breath event at	77.7709	R-wave angle is	116.99	116.99	R-Wave position is	2	Breath number is	10
breath event at	84.2949	R-wave angle is	110.435	110.435	R-Wave position is	2	Breath number is	11
breath event at	91.5581	R-wave angle is	80.6719	80.6719	R-Wave position is	2	Breath number is	12
breath event at	99.7776	R-wave angle is	103.81	103.81	R-Wave position is	2	Breath number is	13
breath event at	106.746	R-wave angle is	127.105	127.105	R-Wave position is	2	Breath number is	14
breath event at	113.343	R-wave angle is	115.415	115.415	R-Wave position is	2	Breath number is	15
breath event at	120.28	R-wave angle is	122.268	122.268	R-Wave position is	2	Breath number is	16
breath event at	125.879	R-wave angle is	116.105	116.105	R-Wave position is	2	Breath number is	17
breath event at	131.841	R-wave angle is	138.401	138.401	R-Wave position is	2	Breath number is	18
breath event at	136.734	R-wave angle is	149.153	149.153	R-Wave position is	2	Breath number is	19
breath event at	142.17	R-wave angle is	123.883	123.883	R-Wave position is	2	Breath number is	20
breath event at	148.017	R-wave angle is	139.724	139.724	R-Wave position is	2	Breath number is	21
breath event at	153.713	R-wave angle is	149.93	149.93	R-Wave position is	2	Breath number is	22
breath event at	160.388	R-wave angle is	122.307	122.307	R-Wave position is	2	Breath number is	23
breath event at	167.841	R-wave angle is	154.089	154.089	R-Wave position is	2	Breath number is	24
breath event at	173.508	R-wave angle is	132.06	132.06	R-Wave position is	2	Breath number is	25
breath event at	180.533	R-wave angle is	144.416	144.416	R-Wave position is	2	Breath number is	26
breath event at	186.337	R-wave angle is	154.806	154.806	R-Wave position is	2	Breath number is	27
breath event at	191.562	R-wave angle is	161.025	161.025	R-Wave position is	2	Breath number is	28
breath event at	197.806	R-wave angle is	127.89	127.89	R-Wave position is	2	Breath number is	29
breath event at	204.194	R-wave angle is	143.961	143.961	R-Wave position is	2	Breath number is	30
breath event at	210.721	R-wave angle is	159.168	159.168	R-Wave position is	2	Breath number is	31
breath event at	216.619	R-wave angle is	161.915	161.915	R-Wave position is	2	Breath number is	32
breath event at	221.692	R-wave angle is	107.367	107.367	R-Wave position is	2	Breath number is	34
breath event at	228.021	R-wave angle is	128.61	128.61	R-Wave position is	2	Breath number is	35
breath event at	233.392	R-wave angle is	98.728	98.728	R-Wave position is	2	Breath number is	36
breath event at	240.78	R-wave angle is	119.861	119.861	R-Wave position is	2	Breath number is	37
breath event at	247.22	R-wave angle is	119.968	119.968	R-Wave position is	2	Breath number is	38
breath event at	253.491	R-wave angle is	154.911	154.911	R-Wave position is	2	Breath number is	39
breath event at	259.459	R-wave angle is	116.045	116.045	R-Wave position is	2	Breath number is	40
breath event at	266.241	R-wave angle is	131.292	131.292	R-Wave position is	2	Breath number is	41
breath event at	273.203	R-wave angle is	140.197	140.197	R-Wave position is	2	Breath number is	42
breath event at	280.226	R-wave angle is	126.329	126.329	R-Wave position is	2	Breath number is	43
breath event at	286.724	R-wave angle is	159.839	159.839	R-Wave position is	2	Breath number is	44
breath event at	291.918	R-wave angle is	57.732	57.732	R-Wave position is	2	Breath number is	45
breath event at	303.55	R-wave angle is	126.63	126.63	R-Wave position is	2	Breath number is	46
2	0.926806		129.886	1 46				
breath event at	12.1301	R-wave angle is	184.979	184.979	R-Wave position is	3	Breath number is	0
breath event at	17.9314	R-wave angle is	165.761	165.761	R-Wave position is	3	Breath number is	1
breath event at	23.6141	R-wave angle is	202.745	202.745	R-Wave position is	3	Breath number is	2

breath event at 29.7239 R-wave angle is 199.988 199.988 R-Wave position is 3 Breath number is 3
breath event at 35.9993 R-wave angle is 210.069 210.069 R-Wave position is 3 Breath number is 4
breath event at 42.1202 R-wave angle is 189.29 189.29 R-Wave position is 3 Breath number is 5
breath event at 48.1829 R-wave angle is 206.857 206.857 R-Wave position is 3 Breath number is 6
breath event at 54.631 R-wave angle is 133.751 133.751 R-Wave position is 3 Breath number is 7
breath event at 62.9264 R-wave angle is 183.451 183.451 R-Wave position is 3 Breath number is 8
breath event at 69.5369 R-wave angle is 142.711 142.711 R-Wave position is 3 Breath number is 9
breath event at 77.7709 R-wave angle is 164.335 164.335 R-Wave position is 3 Breath number is 10
breath event at 84.2949 R-wave angle is 153.408 153.408 R-Wave position is 3 Breath number is 11
breath event at 91.5581 R-wave angle is 115.885 115.885 R-Wave position is 3 Breath number is 12
breath event at 99.7776 R-wave angle is 145.864 145.864 R-Wave position is 3 Breath number is 13
breath event at 106.746 R-wave angle is 171.361 171.361 R-Wave position is 3 Breath number is 14
breath event at 113.343 R-wave angle is 156.513 156.513 R-Wave position is 3 Breath number is 15
breath event at 120.28 R-wave angle is 174.093 174.093 R-Wave position is 3 Breath number is 16
breath event at 125.879 R-wave angle is 164.232 164.232 R-Wave position is 3 Breath number is 17
breath event at 131.841 R-wave angle is 199.765 199.765 R-Wave position is 3 Breath number is 18
breath event at 136.734 R-wave angle is 202.067 202.067 R-Wave position is 3 Breath number is 19
breath event at 142.17 R-wave angle is 172.52 172.52 R-Wave position is 3 Breath number is 20
breath event at 148.017 R-wave angle is 197.236 197.236 R-Wave position is 3 Breath number is 21
breath event at 153.713 R-wave angle is 195.885 195.885 R-Wave position is 3 Breath number is 22
breath event at 160.388 R-wave angle is 168.72 168.72 R-Wave position is 3 Breath number is 23
breath event at 167.841 R-wave angle is 213.741 213.741 R-Wave position is 3 Breath number is 24
breath event at 173.508 R-wave angle is 182.696 182.696 R-Wave position is 3 Breath number is 25
breath event at 180.533 R-wave angle is 199.739 199.739 R-Wave position is 3 Breath number is 26
breath event at 186.337 R-wave angle is 220.943 220.943 R-Wave position is 3 Breath number is 27
breath event at 191.562 R-wave angle is 215.977 215.977 R-Wave position is 3 Breath number is 28
breath event at 197.806 R-wave angle is 179.569 179.569 R-Wave position is 3 Breath number is 29
breath event at 204.194 R-wave angle is 198.559 198.559 R-Wave position is 3 Breath number is 30
breath event at 210.721 R-wave angle is 215.812 215.812 R-Wave position is 3 Breath number is 31
breath event at 216.619 R-wave angle is 230.96 230.96 R-Wave position is 3 Breath number is 32
breath event at 221.692 R-wave angle is 160.836 160.836 R-Wave position is 3 Breath number is 34
breath event at 228.021 R-wave angle is 186.123 186.123 R-Wave position is 3 Breath number is 35
breath event at 233.392 R-wave angle is 147.946 147.946 R-Wave position is 3 Breath number is 36
breath event at 240.78 R-wave angle is 175.475 175.475 R-Wave position is 3 Breath number is 37
breath event at 247.22 R-wave angle is 177.206 177.206 R-Wave position is 3 Breath number is 38
breath event at 253.491 R-wave angle is 208.296 208.296 R-Wave position is 3 Breath number is 39
breath event at 259.459 R-wave angle is 167.535 167.535 R-Wave position is 3 Breath number is 40
breath event at 266.241 R-wave angle is 176.999 176.999 R-Wave position is 3 Breath number is 41
breath event at 273.203 R-wave angle is 192.334 192.334 R-Wave position is 3 Breath number is 42
breath event at 280.226 R-wave angle is 178.291 178.291 R-Wave position is 3 Breath number is 43
breath event at 286.724 R-wave angle is 228.603 228.603 R-Wave position is 3 Breath number is 44
breath event at 291.918 R-wave angle is 87.1324 87.1324 R-Wave position is 3 Breath number is 45
breath event at 303.55 R-wave angle is 180.505 180.505 R-Wave position is 3 Breath number is 46
3 0.886365 181.964 1 46
breath event at 12.1301 R-wave angle is 245.545 245.545 R-Wave position is 4 Breath number is 0
breath event at 17.9314 R-wave angle is 216.252 216.252 R-Wave position is 4 Breath number is 1
breath event at 23.6141 R-wave angle is 251.297 251.297 R-Wave position is 4 Breath number is 2
breath event at 29.7239 R-wave angle is 252.134 252.134 R-Wave position is 4 Breath number is 3
breath event at 35.9993 R-wave angle is 260.003 260.003 R-Wave position is 4 Breath number is 4
breath event at 42.1202 R-wave angle is 240.534 240.534 R-Wave position is 4 Breath number is 5
breath event at 48.1829 R-wave angle is 259.56 259.56 R-Wave position is 4 Breath number is 6
breath event at 54.631 R-wave angle is 177.409 177.409 R-Wave position is 4 Breath number is 7
breath event at 62.9264 R-wave angle is 231.266 231.266 R-Wave position is 4 Breath number is 8
breath event at 69.5369 R-wave angle is 182.454 182.454 R-Wave position is 4 Breath number is 9
breath event at 77.7709 R-wave angle is 208.038 208.038 R-Wave position is 4 Breath number is 10
breath event at 84.2949 R-wave angle is 199.355 199.355 R-Wave position is 4 Breath number is 11
breath event at 91.5581 R-wave angle is 151.975 151.975 R-Wave position is 4 Breath number is 12
breath event at 99.7776 R-wave angle is 187.608 187.608 R-Wave position is 4 Breath number is 13
breath event at 106.746 R-wave angle is 217.146 217.146 R-Wave position is 4 Breath number is 14
breath event at 113.343 R-wave angle is 199.115 199.115 R-Wave position is 4 Breath number is 15
breath event at 120.28 R-wave angle is 222.189 222.189 R-Wave position is 4 Breath number is 16
breath event at 125.879 R-wave angle is 212.42 212.42 R-Wave position is 4 Breath number is 17
breath event at 131.841 R-wave angle is 263.335 263.335 R-Wave position is 4 Breath number is 18
breath event at 136.734 R-wave angle is 259.285 259.285 R-Wave position is 4 Breath number is 19
breath event at 142.17 R-wave angle is 218.51 218.51 R-Wave position is 4 Breath number is 20
breath event at 148.017 R-wave angle is 253.611 253.611 R-Wave position is 4 Breath number is 21
breath event at 153.713 R-wave angle is 245.616 245.616 R-Wave position is 4 Breath number is 22
breath event at 160.388 R-wave angle is 213.154 213.154 R-Wave position is 4 Breath number is 23
breath event at 167.841 R-wave angle is 277.714 277.714 R-Wave position is 4 Breath number is 24
breath event at 173.508 R-wave angle is 231.999 231.999 R-Wave position is 4 Breath number is 25
breath event at 180.533 R-wave angle is 254.256 254.256 R-Wave position is 4 Breath number is 26
breath event at 186.337 R-wave angle is 288.114 288.114 R-Wave position is 4 Breath number is 27
breath event at 191.562 R-wave angle is 267.989 267.989 R-Wave position is 4 Breath number is 28
breath event at 197.806 R-wave angle is 233.163 233.163 R-Wave position is 4 Breath number is 29
breath event at 204.194 R-wave angle is 250.123 250.123 R-Wave position is 4 Breath number is 30
breath event at 210.721 R-wave angle is 275.448 275.448 R-Wave position is 4 Breath number is 31
breath event at 216.619 R-wave angle is 296.669 296.669 R-Wave position is 4 Breath number is 32
breath event at 221.692 R-wave angle is 210.722 210.722 R-Wave position is 4 Breath number is 34
breath event at 228.021 R-wave angle is 246.115 246.115 R-Wave position is 4 Breath number is 35
breath event at 233.392 R-wave angle is 193.412 193.412 R-Wave position is 4 Breath number is 36
breath event at 240.78 R-wave angle is 226.115 226.115 R-Wave position is 4 Breath number is 37
breath event at 247.22 R-wave angle is 234.387 234.387 R-Wave position is 4 Breath number is 38
breath event at 253.491 R-wave angle is 264.396 264.396 R-Wave position is 4 Breath number is 39
breath event at 259.459 R-wave angle is 213.557 213.557 R-Wave position is 4 Breath number is 40
breath event at 266.241 R-wave angle is 220.225 220.225 R-Wave position is 4 Breath number is 41
breath event at 273.203 R-wave angle is 239.498 239.498 R-Wave position is 4 Breath number is 42
breath event at 280.226 R-wave angle is 229.754 229.754 R-Wave position is 4 Breath number is 43
breath event at 286.724 R-wave angle is 299.516 299.516 R-Wave position is 4 Breath number is 44
breath event at 291.918 R-wave angle is 115.604 115.604 R-Wave position is 4 Breath number is 45
breath event at 303.55 R-wave angle is 228.085 228.085 R-Wave position is 4 Breath number is 46
4 0.83099 233.377 1 46
breath event at 12.1301 R-wave angle is 306.607 306.607 R-Wave position is 5 Breath number is 0
breath event at 17.9314 R-wave angle is 272.127 272.127 R-Wave position is 5 Breath number is 1
breath event at 23.6141 R-wave angle is 298.257 298.257 R-Wave position is 5 Breath number is 2
breath event at 29.7239 R-wave angle is 304.911 304.911 R-Wave position is 5 Breath number is 3
breath event at 35.9993 R-wave angle is 314.172 314.172 R-Wave position is 5 Breath number is 4
breath event at 42.1202 R-wave angle is 287.86 287.86 R-Wave position is 5 Breath number is 5
breath event at 48.1829 R-wave angle is 309.752 309.752 R-Wave position is 5 Breath number is 6
breath event at 54.631 R-wave angle is 218.203 218.203 R-Wave position is 5 Breath number is 7
breath event at 62.9264 R-wave angle is 283.546 283.546 R-Wave position is 5 Breath number is 8
breath event at 69.5369 R-wave angle is 220.754 220.754 R-Wave position is 5 Breath number is 9

breath event at	77.7709	R-wave angle is	251.409	251.409	R-Wave position is	5	Breath number is	10
breath event at	84.2949	R-wave angle is	242.774	242.774	R-Wave position is	5	Breath number is	11
breath event at	91.5581	R-wave angle is	191.262	191.262	R-Wave position is	5	Breath number is	12
breath event at	99.7776	R-wave angle is	228.423	228.423	R-Wave position is	5	Breath number is	13
breath event at	106.746	R-wave angle is	260.911	260.911	R-Wave position is	5	Breath number is	14
breath event at	113.343	R-wave angle is	243.43	243.43	R-Wave position is	5	Breath number is	15
breath event at	120.28	R-wave angle is	269.192	269.192	R-Wave position is	5	Breath number is	16
breath event at	125.879	R-wave angle is	262.781	262.781	R-Wave position is	5	Breath number is	17
breath event at	131.841	R-wave angle is	332.498	332.498	R-Wave position is	5	Breath number is	18
breath event at	136.734	R-wave angle is	321.934	321.934	R-Wave position is	5	Breath number is	19
breath event at	142.17	R-wave angle is	262.468	262.468	R-Wave position is	5	Breath number is	20
breath event at	148.017	R-wave angle is	306.004	306.004	R-Wave position is	5	Breath number is	21
breath event at	153.713	R-wave angle is	298.638	298.638	R-Wave position is	5	Breath number is	22
breath event at	160.388	R-wave angle is	254.206	254.206	R-Wave position is	5	Breath number is	23
breath event at	167.841	R-wave angle is	343.274	343.274	R-Wave position is	5	Breath number is	24
breath event at	173.508	R-wave angle is	279.099	279.099	R-Wave position is	5	Breath number is	25
breath event at	180.533	R-wave angle is	314.107	314.107	R-Wave position is	5	Breath number is	26
breath event at	186.337	R-wave angle is	354.733	354.733	R-Wave position is	5	Breath number is	27
breath event at	191.562	R-wave angle is	320.692	320.692	R-Wave position is	5	Breath number is	28
breath event at	197.806	R-wave angle is	289.971	289.971	R-Wave position is	5	Breath number is	29
breath event at	204.194	R-wave angle is	297.386	297.386	R-Wave position is	5	Breath number is	30
breath event at	210.721	R-wave angle is	337.036	337.036	R-Wave position is	5	Breath number is	31
breath event at	221.692	R-wave angle is	259.869	259.869	R-Wave position is	5	Breath number is	34
breath event at	228.021	R-wave angle is	309.727	309.727	R-Wave position is	5	Breath number is	35
breath event at	233.392	R-wave angle is	237.123	237.123	R-Wave position is	5	Breath number is	36
breath event at	240.78	R-wave angle is	274.519	274.519	R-Wave position is	5	Breath number is	37
breath event at	247.22	R-wave angle is	286.114	286.114	R-Wave position is	5	Breath number is	38
breath event at	253.491	R-wave angle is	324.116	324.116	R-Wave position is	5	Breath number is	39
breath event at	259.459	R-wave angle is	259.155	259.155	R-Wave position is	5	Breath number is	40
breath event at	266.241	R-wave angle is	262.934	262.934	R-Wave position is	5	Breath number is	41
breath event at	273.203	R-wave angle is	285.586	285.586	R-Wave position is	5	Breath number is	42
breath event at	280.226	R-wave angle is	277.672	277.672	R-Wave position is	5	Breath number is	43
breath event at	291.918	R-wave angle is	142.56	142.56	R-Wave position is	5	Breath number is	45
breath event at	303.55	R-wave angle is	275.024	275.024	R-Wave position is	5	Breath number is	46
5	0.78759	281.587	1	44				
breath event at	17.9314	R-wave angle is	337.378	337.378	R-Wave position is	6	Breath number is	1
breath event at	23.6141	R-wave angle is	347.457	347.457	R-Wave position is	6	Breath number is	2
breath event at	29.7239	R-wave angle is	358.262	358.262	R-Wave position is	6	Breath number is	3
breath event at	42.1202	R-wave angle is	334.71	334.71	R-Wave position is	6	Breath number is	5
breath event at	54.631	R-wave angle is	256.784	256.784	R-Wave position is	6	Breath number is	7
breath event at	62.9264	R-wave angle is	337.896	337.896	R-Wave position is	6	Breath number is	8
breath event at	69.5369	R-wave angle is	257.611	257.611	R-Wave position is	6	Breath number is	9
breath event at	77.7709	R-wave angle is	294.892	294.892	R-Wave position is	6	Breath number is	10
breath event at	84.2949	R-wave angle is	284.359	284.359	R-Wave position is	6	Breath number is	11
breath event at	91.5581	R-wave angle is	229.147	229.147	R-Wave position is	6	Breath number is	12
breath event at	99.7776	R-wave angle is	268.72	268.72	R-Wave position is	6	Breath number is	13
breath event at	106.746	R-wave angle is	303.913	303.913	R-Wave position is	6	Breath number is	14
breath event at	113.343	R-wave angle is	286.084	286.084	R-Wave position is	6	Breath number is	15
breath event at	120.28	R-wave angle is	317.737	317.737	R-Wave position is	6	Breath number is	16
breath event at	125.879	R-wave angle is	315.559	315.559	R-Wave position is	6	Breath number is	17
breath event at	142.17	R-wave angle is	306.672	306.672	R-Wave position is	6	Breath number is	20
breath event at	148.017	R-wave angle is	357.828	357.828	R-Wave position is	6	Breath number is	21
breath event at	153.713	R-wave angle is	349.664	349.664	R-Wave position is	6	Breath number is	22
breath event at	160.388	R-wave angle is	294.438	294.438	R-Wave position is	6	Breath number is	23
breath event at	173.508	R-wave angle is	327.326	327.326	R-Wave position is	6	Breath number is	25
breath event at	197.806	R-wave angle is	344.073	344.073	R-Wave position is	6	Breath number is	29
breath event at	204.194	R-wave angle is	343.767	343.767	R-Wave position is	6	Breath number is	30
breath event at	221.692	R-wave angle is	311.803	311.803	R-Wave position is	6	Breath number is	34
breath event at	233.392	R-wave angle is	282.004	282.004	R-Wave position is	6	Breath number is	36
breath event at	240.78	R-wave angle is	324.823	324.823	R-Wave position is	6	Breath number is	37
breath event at	247.22	R-wave angle is	338.588	338.588	R-Wave position is	6	Breath number is	38
breath event at	259.459	R-wave angle is	307.301	307.301	R-Wave position is	6	Breath number is	40
breath event at	266.241	R-wave angle is	309.624	309.624	R-Wave position is	6	Breath number is	41
breath event at	273.203	R-wave angle is	334.34	334.34	R-Wave position is	6	Breath number is	42
breath event at	280.226	R-wave angle is	330.022	330.022	R-Wave position is	6	Breath number is	43
breath event at	291.918	R-wave angle is	170.537	170.537	R-Wave position is	6	Breath number is	45
breath event at	303.55	R-wave angle is	323.565	323.565	R-Wave position is	6	Breath number is	46
6	0.808519		313.402	1 32				
breath event at	54.631	R-wave angle is	294.974	294.974	R-Wave position is	7	Breath number is	7
breath event at	69.5369	R-wave angle is	292.85	292.85	R-Wave position is	7	Breath number is	9
breath event at	77.7709	R-wave angle is	342.236	342.236	R-Wave position is	7	Breath number is	10
breath event at	84.2949	R-wave angle is	325.35	325.35	R-Wave position is	7	Breath number is	11
breath event at	91.5581	R-wave angle is	265.543	265.543	R-Wave position is	7	Breath number is	12
breath event at	99.7776	R-wave angle is	310.516	310.516	R-Wave position is	7	Breath number is	13
breath event at	106.746	R-wave angle is	348.169	348.169	R-Wave position is	7	Breath number is	14
breath event at	113.343	R-wave angle is	327.182	327.182	R-Wave position is	7	Breath number is	15
breath event at	142.17	R-wave angle is	351.862	351.862	R-Wave position is	7	Breath number is	20
breath event at	160.388	R-wave angle is	339.209	339.209	R-Wave position is	7	Breath number is	23
breath event at	233.392	R-wave angle is	327.763	327.763	R-Wave position is	7	Breath number is	36
breath event at	259.459	R-wave angle is	355.818	355.818	R-Wave position is	7	Breath number is	40
breath event at	266.241	R-wave angle is	357.968	357.968	R-Wave position is	7	Breath number is	41
breath event at	291.918	R-wave angle is	200.897	200.897	R-Wave position is	7	Breath number is	45
7	0.790612		322.743	1 14				
breath event at	54.631	R-wave angle is	337.981	337.981	R-Wave position is	8	Breath number is	7
breath event at	69.5369	R-wave angle is	328.439	328.439	R-Wave position is	8	Breath number is	9
breath event at	91.5581	R-wave angle is	302.114	302.114	R-Wave position is	8	Breath number is	12
breath event at	99.7776	R-wave angle is	354.223	354.223	R-Wave position is	8	Breath number is	13
breath event at	291.918	R-wave angle is	231.535	231.535	R-Wave position is	8	Breath number is	45
8	0.751353		315.59	1 5				
breath event at	91.5581	R-wave angle is	338.642	338.642	R-Wave position is	9	Breath number is	12
9	1	338.642	1	1				

0:2ratio of first to third R-wave is	1.04828
3:5ratio of 4th to 6th R-wave is	1.12541

number of breaths used	4	Length of mean vector is	0.0241996	mean vector angle is	205.251	and R-wavecount	27
number of breaths used	4	Length of mean vector is	0.0396785	mean vector angle is	269.931	and R-wavecount	29
number of breaths used	4	Length of mean vector is	0.0183318	mean vector angle is	235.598	and R-wavecount	35

number of breaths used	4	Length of mean vector is	0.0169137	mean vector angle is	203.637	and R-wavecount	32
number of breaths used	4	Length of mean vector is	0.00521598	mean vector angle is	175.616	and R-wavecount	27
number of breaths used	4	Length of mean vector is	0.00866175	mean vector angle is	23.9051	and R-wavecount	28
number of breaths used	4	Length of mean vector is	0.0291604	mean vector angle is	193.183	and R-wavecount	25
number of breaths used	4	Length of mean vector is	0.00611701	mean vector angle is	171.938	and R-wavecount	25
number of breaths used	4	Length of mean vector is	0.0143331	mean vector angle is	292.311	and R-wavecount	21
number of breaths used	4	Length of mean vector is	0.0259469	mean vector angle is	337.085	and R-wavecount	28
For all breaths in file	Length of mean vector is 326and breath count is	0.0116486 49	mean vector angle all breaths		175.84	and R-wavecount	

Appendix 1.8 Illustration of the changes in HRV over time in a vCJD patient.

Chapters 5 and 6 of this thesis demonstrated that people incubating vCJD displayed a change in HRV per breath compared to controls and indicated a variable but increasing MVL over time suggesting less variability in the R-waves within each breath compared to controls, as time progressed . This see-saw nature compares with the trend in different metrics of HRV seen in pre-clinical cattle (figures 4.13, 4.14).

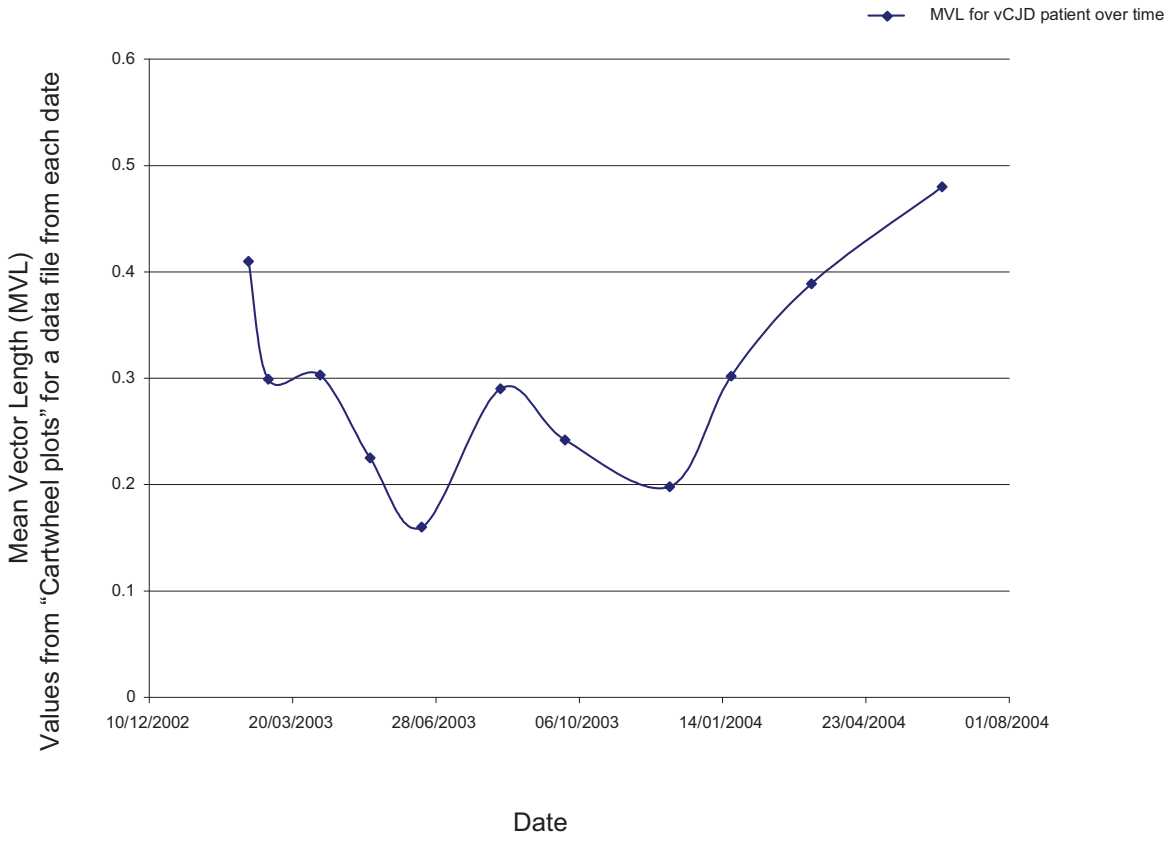

Changing MVL of vCJD patient over time.
The value of MVL for the heart simulator was 0.454. There was a significant difference ($p<0.05$) between the measurements taken in March 2003 and March 2004 (tested using a Mardia-Watson-Wheeler test).

Appendix 1.9 Difference in mean vector length when using corrected breath estimates versus uncorrected estimate.

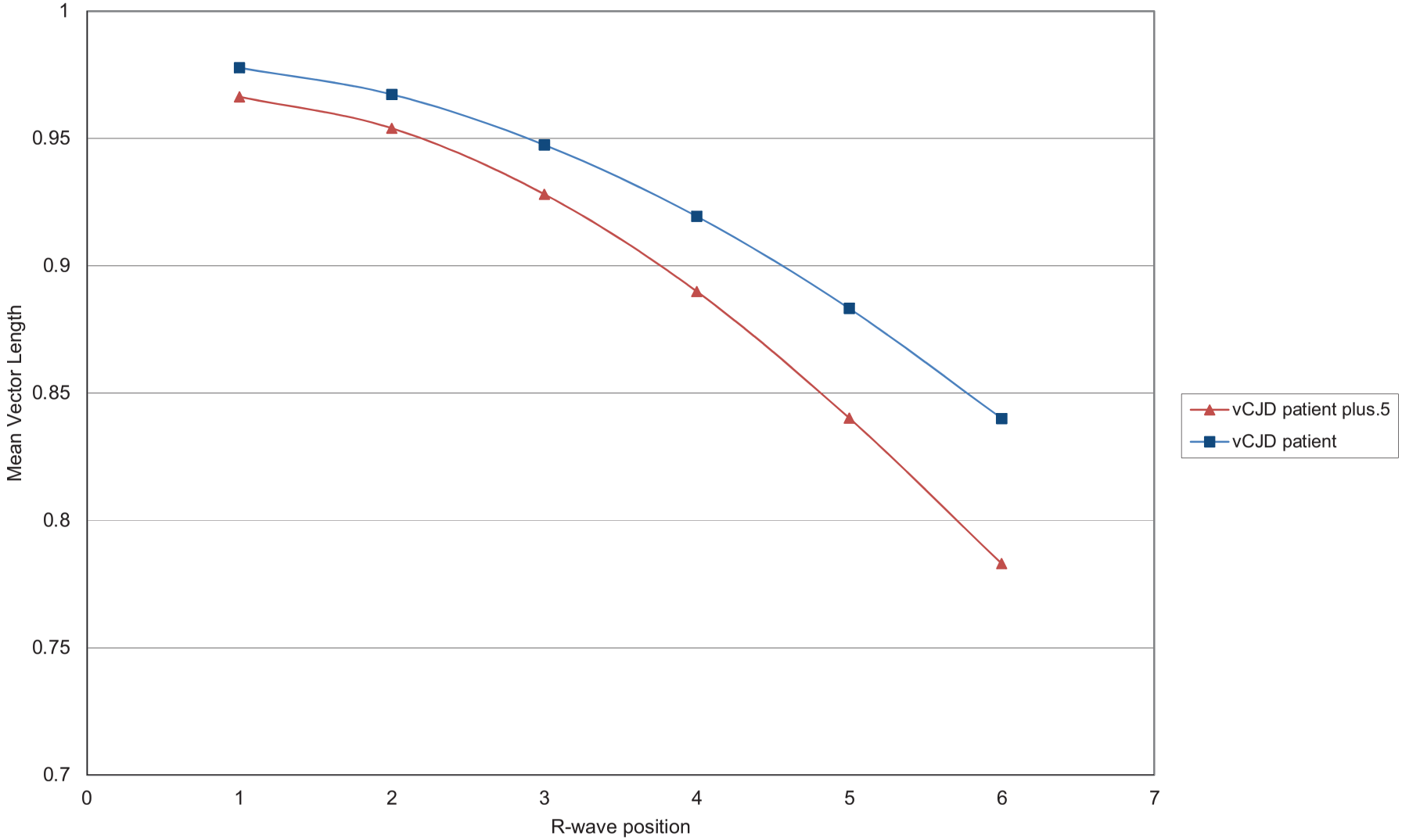

Mardia-Watson-Wheeler test indicates significant difference between the 4th, 5th and 6th R-waves ($p<0.05$).

Appendix 1.10 Figure to accompany figure 4.4

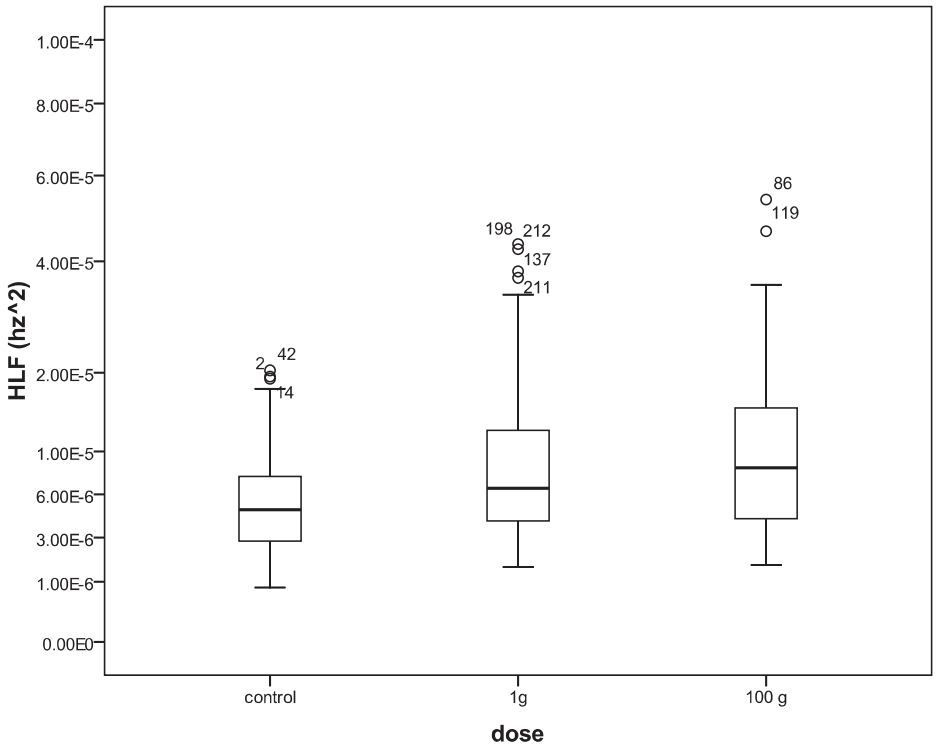

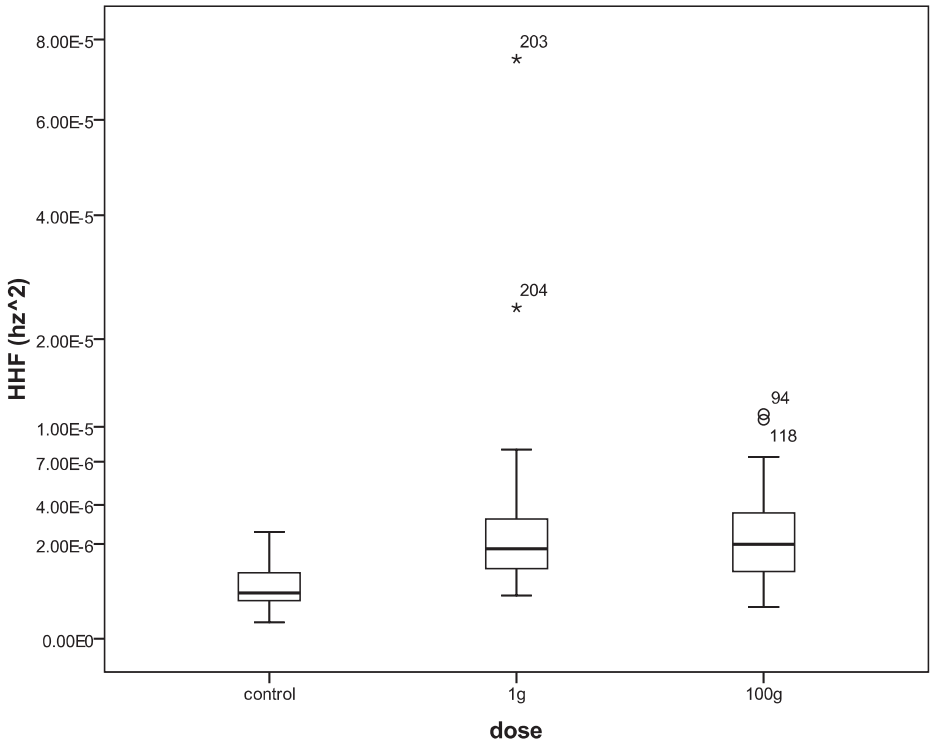

The y axis scale has been transposed in SPSS v 16 using the “power” exponent transform scale using the default 0.5 exponent. This represents the square root of the data and is performed to better show the ranges of measures for the left hand panel of figure 4.

Appendix 1.11 95% Confidence Intervals (CI) for the constituent mean vectors for the MVL data points of figures 5.9, 6.10 and 6.11.

95% Confidence intervals relating to data of Figure 5.19

Variable	control	control	control	control	control	control
R-Wave position	0	1	2	3	4	5
Mean Vector (μ) (degs)	26.744	81.944	137.164	191.807	246.013	282.692
Length of Mean Vector (r)	0.959	0.932	0.876	0.798	0.69	0.726
95% CI (-) for μ (degs)	24.011	78.399	132.316	185.516	237.847	274.328
95% CI (+) for μ (degs)	29.477	85.489	142.013	198.097	254.179	291.057
Variable	Patient	Patient	Patient	Patient	Patient	Patient
R-Wave position	0	1	2	3	4	5
Mean Vector (μ) (degs)	21.12	61.663	102.196	142.774	183.283	223.233
Length of Mean Vector (r)	0.978	0.964	0.934	0.892	0.838	0.788
95% CI (-) for μ (degs)	19.159	59.125	98.75	138.304	177.761	216.82
95% CI (+) for μ (degs)	23.082	64.202	105.643	147.243	188.805	229.646
Variable	Simulator	Simulator	Simulator	Simulator	Simulator	Simulator
R-Wave position	0	1	2	3	4	5
Mean Vector (μ) (degs)	17.958	57.443	96.399	134.796	172.724	211.43
Length of Mean Vector (r)	0.97	0.946	0.914	0.88	0.846	0.857
95% CI (-) for μ (degs)	16.902	51.615	88.985	125.935	162.639	201.614
95% CI (+) for μ (degs)	21.081	63.271	103.814	143.656	182.809	221.246

95% Confidence intervals relating to data of Figure 6.11 and 6.10

Variable	Before	Before	Before	Before	Before	Before
R-wave position	0	1	2	3	4	5
Mean Vector (μ) (degs)	20.464	58.355	97.324	137.447	170.511	199.973
Length of Mean Vector (r)	0.969	0.91	0.859	0.775	0.702	0.758
95% CI (-) for μ (degs)	18.501	54.977	93.041	131.939	163.905	193.87
95% CI (+) for μ (degs)	22.427	61.733	101.608	142.955	177.116	206.077
Variable	During	During	During	During	During	During
R-wave position	0	1	2	3	4	5
Mean Vector (μ) (degs)	25.674	77.591	129.649	181.87	233.624	278.249
Length of Mean Vector (r)	0.964	0.929	0.859	0.764	0.673	0.626
95% CI (-) for μ (degs)	23.556	74.596	125.367	176.2	226.57	270.035
95% CI (+) for μ (degs)	27.793	80.585	133.931	187.54	240.677	286.463
Variable	Sedation	Sedation	Sedation	Sedation	Sedation	Sedation
R-wave position	0	1	2	3	4	5
Mean Vector (μ) (degs)	19.614	56.745	93.818	130.612	168.046	204.909
Length of Mean Vector (r)	0.985	0.976	0.958	0.931	0.898	0.859
95% CI (-) for μ (degs)	16.845	53.244	89.237	124.662	160.775	196.277
95% CI (+) for μ (degs)	22.384	60.246	98.399	136.562	175.317	213.541
Variable	vCJD	vCJD	vCJD	vCJD	vCJD	vCJD
R-wave position	0	1	2	3	4	5
Mean Vector (μ) (degs)	21.26	65.499	109.557	153.516	197.342	240.661
Length of Mean Vector (r)	0.971	0.946	0.9	0.836	0.766	0.694
95% CI (-) for μ (degs)	20.342	64.238	107.811	151.258	194.589	237.389
95% CI (+) for μ (degs)	22.178	66.76	111.304	155.774	200.095	243.934

Appendix 1.12 Tables of significance testing for figure 6.11

*** in the tables indicates a significant difference following Bonferroni correction**

Sedation versus Anaesthesia

R-wave position	W statistic	p value	
R1	15.139	5.16E-4	*
R2	38.802	3.75E-8	*
R3	58.047	0	*
R4	62.734	0	*
R5	64.414	0	*
R6	58.782	0	*

Sedation versus vCJD patient

R-wave position	W statistic	p value	
R1	6.896	0.002	
R2	4.652	0.098	
R3	13.262	0.001	*
R4	18.623	9.04E-5	*
R5	22.867	1.08E-5	*
R6	24.998	3.73E-6	*

Sedation versus Patients Before Anaesthesia

R-wave position	W statistic	p value	
R1	7.096	0.029	
R2	8.106	0.017	
R3	15.010	5.50E-4	*
R4	13.450	0.001	*
R5	11.430	0.003	*
R6	2.086	0.352	

Appendix 1.13 Published work related to this thesis

All enclosed PDF versions of the listed papers relating to the subject of this thesis have been reproduced with permission from the publishers of the relevant journals.

Description of enclosed reprint material

Glover, D. G., Pollard, B. J., Gonzalez, L., Siso, S., Kennedy, D., & Jeffrey, M. 2007, "A non-invasive screen for infectivity in transmissible spongiform encephalopathies", Gut, vol. 56, no. 9, pp. 1329-1331. page 349

This publication suggests that changes in heart rate variability in sheep incubating scrapie may be an early feature of this disease.

Pomfrett, C. J., Glover, D. G., Bollen, B. G., & Pollard, B. J. 2004, "Perturbation of heart rate variability in cattle fed BSE-infected material", Vet.Rec., vol. 154, no. 22, pp. 687-691. page 352

A similar perturbation in heart rate variability in cows with BSE is observed to that observed in scrapie infected sheep. This may suggest that changes in HRV may be a common and early feature of transmissible spongiform encephalopathies.

Woolfson, L. A. M., Glover, D. G., Pollard, B. J., & Pomfrett, C. J. "Symptomatic vCJD alters heart rate variability", in Proceedings of the Physiological Society, Trinity College, Dublin: Communications J Physiol 551P, C47. page 357

Further study of changes in heart rate variability in human subjects incubating vCJD also illustrate a difference when compared to healthy control subjects.

Pomfrett, C. J., Glover, D. G., & Pollard, B. J. 2007, "The vagus nerve as a conduit for neuroinvasion, a diagnostic tool, and a therapeutic pathway for transmissible spongiform encephalopathies, including variant Creutzfeld Jacob disease", Med Hypotheses, vol. 68, no. 6, pp. 1252-1257. page 359

This paper postulates that the vagus nerve may provide a route of infection for prion diseases and underlines the involvement of a potential change in the function of the vagus nerve in prion diseases.

Pomfrett, C. J., Dolling, S., Anders, N. R., Glover, D. G., Bryan, A., & Pollard, B. J. 2009, "Delta sleep-inducing peptide alters bispectral index, the electroencephalogram and heart rate variability when used as an adjunct to isoflurane anaesthesia", Eur J Anaesthesiol., vol. 26, no. 2, pp. 128-134. page 365

This publication illustrates the diverse use of heart rate variability analysis and its use in investigating efficacy of novel interventions in routine anaeasthesia

Rockliff, H., Gilbert, P., McEwan, K., Lightman, S., & Glover, D. 2008, "A pilot exploration of heart rate variability and salivary cortisol responses to compassion-focused imagery", Clinical Neuropsychiatry, vol. 5, no. 3, pp. 132-139. page 372

Heart rate variability studies may also be effective in assessing psychopathology and changes in associated physiological variables such as cortisol levels.

A non-invasive screen for infectivity in transmissible spongiform encephalopathies

D G Glover, B J Pollard, L González, S Sisó, D Kennedy and M Jeffrey

Gut 2007;56;1329-1331
doi:10.1136/gut.2007.123141

patient groups with respect to their ratio of hGRα to hGRβ mRNA levels. Unfortunately, among the 12 patients evaluated prospectively, only one turned out to be steroid dependent and one steroid resistant in a two year follow up, allowing no statistical analysis. However, these two prospectively evaluated patients with impaired steroid response did not differ in their hGRβ mRNA expression from the steroid responders.

Our findings do not exclude the possibility that hGR protein levels may differ in the respective groups as a result of post-transcriptional regulation. However, quantification of hGR protein levels is difficult and does not provide evidence for the amount of ''free'' receptor with the ability to bind steroids. Nevertheless, our data indicate that the ratio of PBMC hGRα to hGRβ mRNA expression is not correlated with effective glucocorticoid treatment in IBD. Therefore, we conclude—in contrast to Honda and coworkers—that hGRβ expression has no predictive value for the efficacy of steroid treatment.

Acknowledgements

We thank Sabine Fink for technical assistance.

M Hausmann, H Herfarth, J Schölmerich, G Rogler

Correspondence to: Dr Gerhard Rogler, Clinic of Gastroenterology and Hepatology, Department of Internal Medicine, University Hospital of Zürich, 8091 Zürich, Switzerland; gerhard.rogler@usz.ch

doi: 10.1136/gut.2006.108035

Conflict of interest: None declared.

References

1 **Sandborn WJ**. Steroid-dependent Crohn's disease. *Can J Gastroenterol* 2000;**14**(suppl C):17–22C.
2 **Hollenberg SM**, Weinberger C, Ong ES, *et al*. Primary structure and expression of a functional human glucocorticoid receptor cDNA. *Nature* 1985;**318**:635–41.
3 **Bamberger CM**, Bamberger AM, de Castro M, *et al*. Glucocorticoid receptor beta, a potential endogenous inhibitor of glucocorticoid action in humans. *J Clin Invest* 1995;**95**:2435–41.
4 **Honda M**, Orii F, Ayabe T, *et al*. Expression of glucocorticoid receptor beta in lymphocytes of patients with glucocorticoid-resistant ulcerative colitis. *Gastroenterology* 2000;**118**:859–66.
5 **Rogler G**, Meinel A, Lingauer A, *et al*. Glucocorticoid receptors are down-regulated in inflamed colonic mucosa but not in peripheral blood mononuclear cells from patients with inflammatory bowel disease. *Eur J Clin Invest* 1999;**29**:330–6.

A non-invasive screen for infectivity in transmissible spongiform encephalopathies

The risk of transmissible spongiform encephalopathy (TSE) infection from endoscopic procedures has been discussed recently in this journal.[1 2] Subclinical carriers of variant Creutzfeldt–Jakob disease (vCJD), the numbers of whom are unknown, may present a risk of iatrogenic infection to susceptible patients participating in endoscopy. We report a pilot study, undertaken here on sheep, describing a non-invasive assessment of autonomic function based on heart rate variability (HRV) which may provide a useful screening method for subclinical carriers of certain TSE diseases.

Detection of disease associated prion protein (PrP^d) in the brain stem is used in confirmatory postmortem tests for bovine spongiform encephalopathy (BSE) and sheep scrapie; this protein is also present in humans with vCJD.[3–5] In scrapie, the timing of PrP^d accumulation in the dorsal motor nucleus of the vagus nerve (DMNX) indicates that this is a likely site of initial neuroinvasion.[4] Non-myelinated vagal fibres from the DMNX and faster myelinated vagal fibres from the nucleus ambiguus are involved in the control of HRV, which is the millisecond beat to beat change that is distinct from the heart rate. Cardiac vagal tone may be considered to be the sum of low frequency (LF) variation in HRV influenced by vagal efferents from the DMNX, plus high frequency (HF) variations, influenced by the respiratory frequency, resulting from the efferent output from the nucleus ambiguus.[6] The DMNX contains parasympathetic neurones whose axons communicate directly with the gut, heart, and other viscera and can be implicated in the transport and initial site of infection and subsequent infection in the nucleus tractus solitarius and the nucleus ambiguus.[4] Thus analysis of HRV may provide an index of vagal

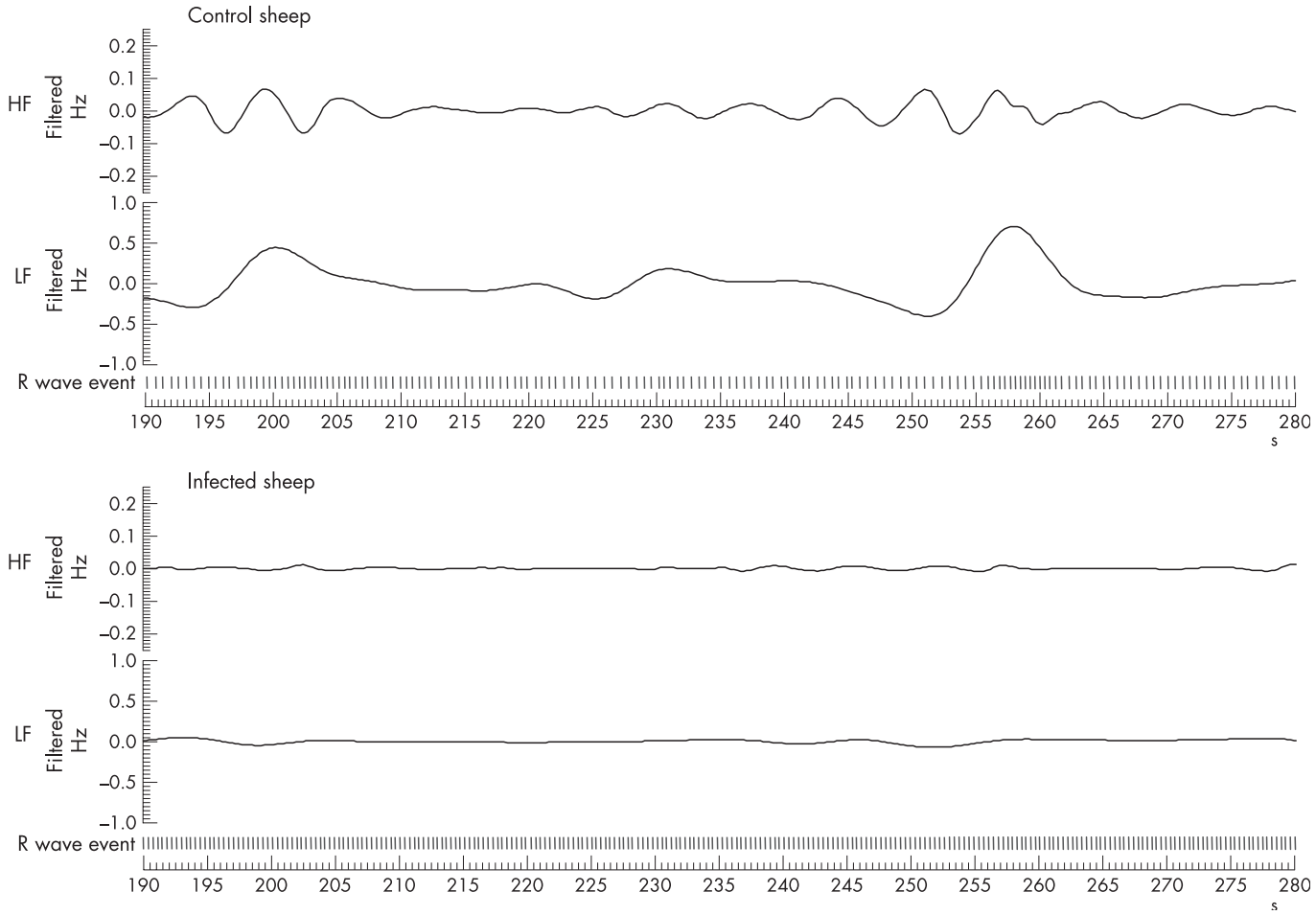

Figure 1 Typical high frequency (HF) and low frequency (LF) filtered tachygrams on which a fast Fourier transformation is done to give estimates of heart rate variability (HRV) in different frequency bands. The reduced HRV is indicated by the flatter lines in the infected sheep.

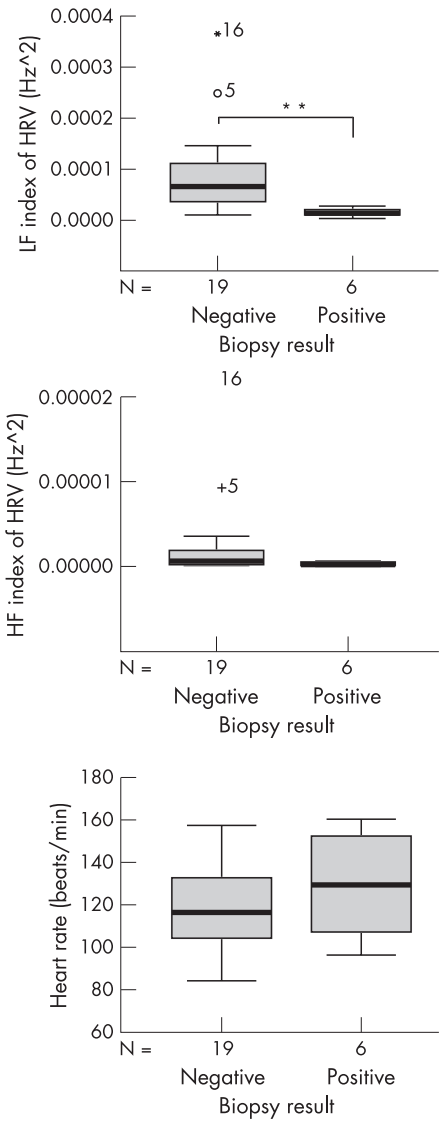

Figure 2 Box plots (median, upper and lower quartiles, and range) showing heart rate variability (HRV) measures, demonstrating a significant difference (**$p<0.005$) between biopsy positive and biopsy negative animals (Mann–Whitney test following a Kolmogorov–Smirnov test with Lilliefors significance correction to test for a normal distribution). There is no significant difference in the heart rates of the animals or in the high frequency range of HRV. Within the negative biopsy group, there was no difference in either low frequency or high frequency between the orally challenged and non-infected animals.

dysfunction caused by the presence of PrP^d in brain stem regions before clinical signs become noticeable.

PrP^d has been detected in vCJD rectal samples and implications for potential iatrogenic infection to humans of susceptible genotypes have been drawn.[1 2] Large scale studies of sheep scrapie show that PrP^d aggregates are consistently present in the recto-anal-mucosa-associated lymphoid tissue (RAMALT) of preclinically and clinically infected sheep.[7 8] This pilot study investigated the possibility that HRV might also recognise TSE infection in clinically normal sheep, positive for PrP^d in RAMALT biopsies.

Table 1 Summary of the genotypes of the sheep involved in the study

	Negative biopsy	Positive biopsy
Unexposed	2 ARQ/ARQ 1 VRQ/VRQ	–
Oral exposure	4 ARQ/ARQ	3 ARQ/ARQ 3 VRQ/VRQ
Natural exposure	9 ARR/ARR 2 ARQ/ARR 1 ARQ/ARQ	–

ARR/ARR and ARQ/ARR are resistant genotypes.

We recorded HRV data from 25 sheep. Six were clinically normal but PrP^d positive in RAMALT biopsies, and 19 were clinically normal and PrP^d negative in RAMALT biopsies. Among the latter, three were unchallenged controls, 11 were naturally exposed to scrapie infection and of resistant PrP genotypes, one was naturally exposed to scrapie and of susceptible genotype, and four were orally dosed and of susceptible genotypes. Experimentally infected sheep had been dosed with 5 g of a 10% homogenate of a pool from scrapie affected sheep brains.

ECG samples (300 s) were collected and digitised using a commercially available monitor (VariaCardio). ECG R wave timings were obtained to determine variability in the R–R intervals, and an instantaneous tachygram was constructed (fig 1) from which power spectra were calculated.

Power spectral analysis in the 0.032 to 0.138 Hz band (LF), but not the 0.15 to 0.5 Hz band (HF) showed significant differences (LF, $p<0.005$) between RAMALT biopsy negative and biopsy positive sheep (fig 2). As all positive sheep were asymptomatic, HRV assessment may be a useful preclinical test for TSE infection. This HRV index on its own, used once, may not distinguish between individual rectal biopsy positive animals and controls, as ranges overlapped. However, the negative and positive biopsy groups contained animals of different provenance—the negative biopsy group contained sheep of resistant genotypes, unexposed sheep, and sheep of uncertain infection status; the positive group contained infected sheep at approximately 40–90% of the incubation period. Owing to the small number of sheep investigated here, further large scale studies are needed to refine the methods and aid the interpretation of the results; however, being a live non-invasive screen for TSE infection it has the advantage that repeated measures over time may be taken to strengthen confidence in the interpretation.

We have previously demonstrated a similar reduction in HRV in BSE infected cattle[9] and in humans incubating vCJD[10] compared with controls. We herewith show that changes in HRV may be a common and early feature of TSE infections. Improved preclinical testing for TSEs using specific signature changes in HRV with respect to time could help minimise the risk of iatrogenic infection from endoscopy and other invasive procedures, and also provide an objective measure of the pathogenesis of the disease.

D G Glover, B J Pollard
Division of Cardiovascular and Endocrine Sciences, The University of Manchester, Department of Anaesthesia, Manchester Royal Infirmary, Manchester, UK

L González, S Sisó
Veterinary Laboratories Agency (VLA-Lasswade), Pentlands Science Park, Bush Loan, Midlothian, UK

D Kennedy
Moredun Research Institute, Pentlands Science Park, Bush Loan, Penicuik, Midlothian, UK

M Jeffrey
Veterinary Laboratories Agency (VLA-Lasswade), Pentlands Science Park, Bush Loan, Midlothian, UK

Correspondence to: D G Glover, Division of Cardiovascular and Endocrine Sciences, The University of Manchester, Department of Anaesthesia, Manchester Royal Infirmary, Oxford Road, Manchester M13 9WL, UK; david.glover@manchester.ac.uk

doi: 10.1136/gut.2007.123141

Conflict of interest: None declared.

References

1 **Wadsworth JDF**, Joiner S, Fox K, *et al*. Prion infectivity in variant Creutzfeldt-Jakob disease rectum. *Gut* 2007;**56**:90–4.
2 **Head MW**, Ironside JW. vCJD and the gut: implications for endoscopy. *Gut* 2007;**56**:9–11.
3 **Wells GA**, Spencer YI, Haritani M. Configurations and topographic distribution of PrP in the central nervous system in bovine spongiform encephalopathy: an immunohistochemical study. *Ann NY Acad Sci* 1994;**724**:350–2.
4 **van Keulen LJ**, Schreuder BE, Vromans ME, *et al*. Pathogenesis of natural scrapie in sheep. *Arch Virol Suppl* 2000;**16**:57–71.
5 **Will RG**, Ironside JW, Zeidler M, *et al*. A new variant of Creutzfeldt-Jakob disease in the UK. *Lancet* 1996;**347**:921–5.
6 **Porges SW**. The polyvagal perspective. *Biol Psychol* 2007;**74**:116–43.
7 **Gonzalez L**, Dagleish MP, Bellworthy SJ, *et al*. Postmortem diagnosis of preclinical and clinical scrapie in sheep by the detection of disease-associated PrP in their rectal mucosa. *Vet Rec* 2006;**158**:325–31.
8 **Gonzalez L**, Jeffrey M, Siso S, *et al*. Diagnosis of preclinical scrapie in samples of rectal mucosa. *Vet Rec* 2005;**156**:846–7.
9 **Pomfrett CJ**, Glover DG, Bollen BG, *et al*. Perturbation of heart rate variability in cattle fed BSE-infected material. *Vet Rec* 2004;**154**:687–91.
10 **Woolfson LAM**, Glover DG, Pollard BJ, *et al*. Symptomatic vCJD alters heart rate variability. *J Physiol (Lond)* 2003;**551P**:C47.

Transient elastography in patients with non-alcoholic fatty liver disease (NAFLD)

Non-alcoholic fatty liver disease (NAFLD) is one of the most common causes of chronic liver injury in many countries around the world.[1] NAFLD covers a wide spectrum, ranging from simple steatosis—which is generally non-progressive—to non-alcoholic steatohepatitis (NASH). There are no established non-invasive methods of evaluation for patients with NASH, and until recently liver biopsy was the only method for evaluating liver fibrosis. Transient elastography is a new technique that allows rapid, non-invasive measurement of mean tissue stiffness, which has been shown to be useful for accurate estimation of hepatic fibrosis in patients with chronic hepatitis C.[2]

We carried out a study to determine the value of liver stiffness measurement with the new medical device called the Fibroscan (EchoSens, Paris, France), based on ultrasound transient elastography, in patients with NAFLD. We carried out liver stiffness measurements in 67 NAFLD patients (mean (SD) age, 50.4 (3.3) years) in whom the diagnosis had

of *Mycoplasma mycoides* from milk goats in South Germany. In Agriculture: Contagious Agalactia and Other Mycoplasmal Diseases of Small Ruminants. Ed G. E. Jones. EUR 10984. Brussels, Commission of the European Communities. pp 51-57
KIRCHHOFF, H. & ROSENGARTEN, R. (1984) Isolation of a motile mycoplasma from fish. *Journal of General Microbiology* **130,** 2439-2445
LAMBERT, M. (1985) Application d'une technique ELISA informatisée au serodiagnostic de l'agalaxie contagieuse des petits ruminants. *Revue de la Médicine Vétèrinaire* **134,** 303-306
LAMBERT, M. (1987) Contagious agalactia of sheep and goats. In Mycoplasmoses of ruminants. *Revue Scientifique et Technique – Office International des Epizooties* **6,** 699-711
LAMBERT, M., CALMEL, M., DUFOUT, P., CABASSE, E., VITU, C. & PEPIN, M. (1998) Detection of false-positive sera in contagious agalactia with a multiantigen ELISA and their elimination with a protein G conjugate. *Journal of Veterinary Diagnostic Investigation* **10,** 236-330
LEFEVRE, P. C., JONES, G. E. & OJO, M. O. (1987) Pulmonary mycoplasmosis of small ruminants. *Revue Scientifique et Technique – Office International des Epizooties* **6,** 759-799
LE GOFF, C. & PERREAU, P. (1984) Possibilities and limitations of serological diagnosis in contagious agalactia of small ruminants. In Les Maladies de la Chèvre. Eds P. Yvore, G. Perrin. Niort, France, Les Colloques de l'Insitut National de la Rechercher Agronomique, Paris. pp 271-278
LEÓN VIZCAÍNO, L., GARRIDO ABELLÁN, F., CUBERO PABLO M. J. & PERALES, A. (1995) Immunoprophylaxis of caprine contagious agalactia due to *Mycoplasma agalactiae* with an inactivated vaccine. *Veterinary Record* **137,** 266-269
LEVISOHN, S., DAVIDSON, I. & CARO VERGARA, M-R. (1991) Use of an ELISA for differential diagnosis of *Mycoplasma agalactiae* and *Mycoplasma mycoides* subsp *mycoides* (LC) in naturally infected goat herds. *Research in Veterinary Science* **51,** 66-71
MADANAT, A., ZENDULKOVÁ, D. & POSPÍŠIL, Z. (2001) Contagious agalactiae of sheep and goats. A review. *Acta Veterinaria Brno* **70,** 403-412
NICHOLAS R. (1995) Contagious agalactia. *State Veterinary Journal* **5,** 13-15
NICHOLAS, R. (1996) Contagious agalactia: an update. In Mycoplasmas of Ruminants: Pathogenicity, Diagnostics, Epidemiology and Molecular Biology. Eds J. Frey, K. Sarris. EUR 16934. Brussels, European Commission. pp 60-62
NICHOLAS, R. (1998) Mycoplasma of small ruminants and their relevance to Macedonia. *Macedonian Veterinary Review* **27,** 35-39
NICOLET, J. & PAROZ, P. (1980) Tween 20 soluble proteins of *Mycoplasma hyopneumoniae* as antigen for an enzyme-linked immunosorbent assay. *Research in Veterinary Science* **29,** 305-309
RAZIN, S., YOGEV, D. & NAOT, Y. (1998) Molecular biology and pathogenicity of mycoplasmas. *Microbiology and Molecular Biology Reviews* **62,** 1094-1156
REAL, F., DÉNIZ, S., ACOSTA, B., FERRER, O. & POVEDA, J. B. (1994) Caprine contagious agalactia caused by *M agalactiae* in the Canary Islands. *Veterinary Record* **135,** 15-16
ROMANO, R., BUONAVOGLIA, D., MONTAGNA, C. O., TEMPERTA, M. & BUONAVOGLIA, C. (1995) Impiego di un test ELISA per la ricerca di anticorpi verso *M agalactiae* nei sieri ovini. *Acta Medica Veterinaria* **41,** 75-80
ROSENGARTEN, R., CITTI, C. & YOGEV, D. (1998) Consequences of surface antigenic variation in Mycoplasma diagnostics. In Mycoplasma of Ruminants: Pathogenicity, Diagnostics, Epidemiology and Molecular Genetics. Eds G Leori, F. Santini, E. Scanziani, J. Frey. EUR 18018. Brussels, European Commission. pp 54-57
SARRIS, K. (1996) Contagious agalactia. In Mycoplasma of Ruminants: Pathogenicity, Diagnostics, Epidemiology and Molecular Genetics. Eds J. Frey, K. Sarris. EUR 16934. Brussels, European Commission. pp 12-15
SCHAEREN, W. & NICOLET, J. (1982) Micro-ELISA for detecting contagious agalactia in goats. *Schweizer Archiv für Tierheilkunde* **124,** 163-177
TOLA, S., MANUNTA, D., ROCCA, S., ROCCHIGIANI, A. M., IDINI, G., ANGIOI, P. P. & LEORI, G. (1999) Experimental vaccination against *Mycoplasma agalactiae* using different inactivated vaccines. *Vaccine* **17,** 2764-2768
TSAKNAKES, S., KONTOS, P., MPOUPTZE, E., MEGA, A., SARRES, K., TSANAKIS, I. & SARRIS, K. (1992) Epidemiological studies on contagious agalactia in sheep and goats in Chalkidiki, northern Greece. *Bulletin of the Hellenic Veterinary Medical Society* **43,** 250-254
VILLALBA, E. J., POVEDA, J. B., FERNÁNDEZ, A., RODRíGUEZ, J. L., GUTIÉRREZ, C. & GÓMEZ-VILLAMANDOS, J. (1992) An outbreak caused by *Mycoplasma mycoides* species in goats in the Canary Islands. *Veterinary Record* **130,** 330-331

Perturbation of heart rate variability in cattle fed BSE-infected material

Veterinary Record (2004) **154,** 687-691

C. J. D. POMFRETT, D. G. GLOVER, B. G. BOLLEN, B. J. POLLARD

C. J. D. Pomfrett, BSc, PhD,
B. J. Pollard, MD, FRCA, Anaesthesia Research Group, University of Manchester, Manchester Royal Infirmary, Oxford Road, Manchester M13 9WL
D. G. Glover, BSc, Department of Anaesthesia, Central Manchester and Manchester Children's University Hospitals NHS Trust, Oxford Road, Manchester M13 9WL
B. G. Bollen, CChem, MRSC, Department of Chemistry, University of Reading, PO Box 224, Whiteknights, Reading RG6 6AD

The brainstem is the region of the brain of cattle with the highest concentration of the abnormal prion protein associated with bovine spongiform encephalopathy (BSE), and specific nuclei in the medulla oblongata of the brainstem, which exhibit changes as a result of the disease, are involved in the modulation of heart rate variability (HRV). The low- and high-frequency components of the HRV of 48 control cattle, 43 cattle fed 1 g of brain homogenate from BSE field cases and 42 cattle fed 100 g of brain homogenate from BSE field cases were analysed repeatedly for a year. There was a significant difference (P<0·001) between the level of high-frequency HRV observed in the control cattle and in both groups of cattle exposed to BSE. There was also a significant difference (P<0·01) between the low-frequency HRV of the cattle given the high dose and the other two groups.

AN important site for the autonomic control of heart rate is the medulla oblongata of the brainstem (Porges 1995, Austin and others 1997). Two anatomically distinct structures within the medulla, the dorsal vagal motor nucleus (DMNX) and the nucleus ambiguus, are the origin of parasympathetic neurons that form part of the vagus nerve (cranial nerve X) and modulate heart rate. Neurons from the DMNX also extensively innervate other organs connected to the parasympathetic nervous system, including the gut, and thereby provide a potential route for the transmission of neural diseases. The activity of the DMNX and nucleus ambiguus is modulated by a number of brain regions, including another structure of the medulla, the nucleus of the solitary tract (NTS), which receives sensory input from a wide range of locations, including stretch receptor input from the lungs, and has direct links to the limbic system of the higher brain. The limbic system, the NTS and the DMNX have abnormal prion immunoreactivity during the development of infectious transmissible spongiform encephalopathies (TSEs), including variant Creutzfeldt-Jacob disease (vCJD), believed to be the human analogue of

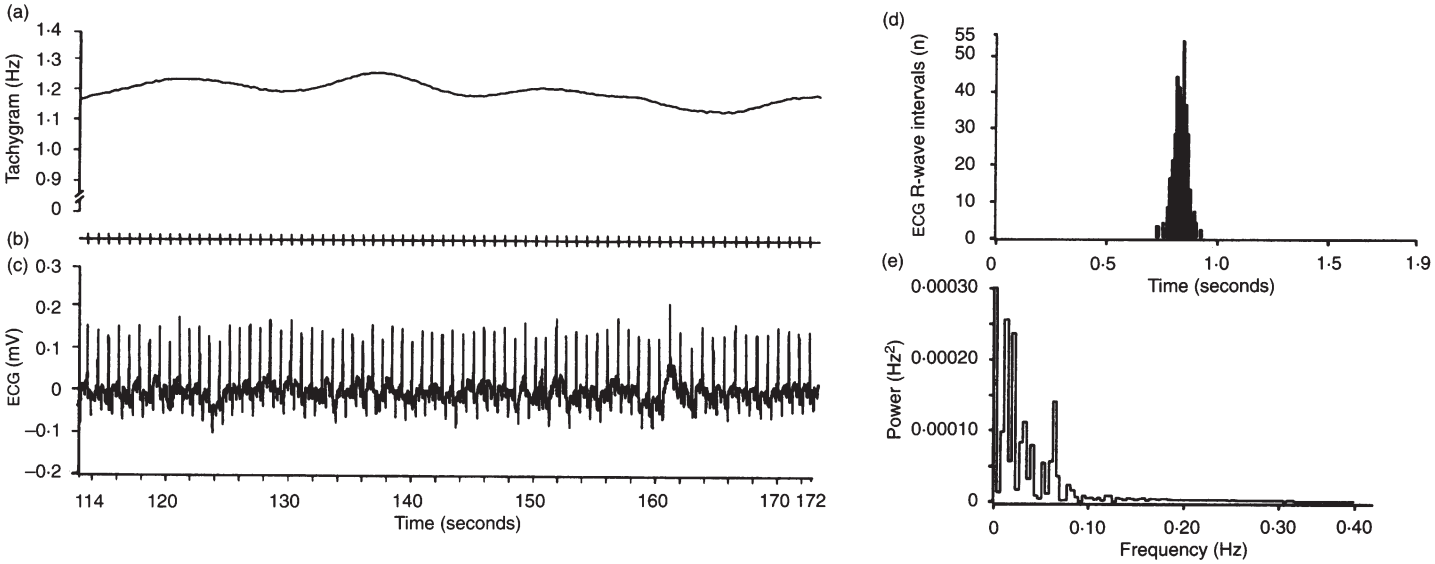

FIG 1: Analysis of data from a control animal, three years after challenge with normal feed, with a mean (sd) heart rate of 72·2 (2·6) bpm. (a) Tachygram of instantaneous frequency derived from the electrocardiogram (ECG) R-wave timings, (b) ECG R-wave timings, obtained by means of a robust peak detection algorithm (Wolfson Imaging Unit, University of Manchester) after a review of the raw data and the offline rejection of artefacts, (c) 100 seconds of the raw ECGs, (d) interval histograms showing the distribution of ECG R-wave intervals for five minutes of data, and (e) power spectra derived from five-minute epochs of tachygram data by using the fast Fourier transform (1024 points, Bsensor v5 script; CED)

bovine spongiform encephalopathy (BSE), but the distribution of abnormal prion immunoreactivity between these regions differs with the disease (Ironside 2000). For scrapie, a long-established TSE of sheep, a hamster model has shown that the central nervous system is initially invaded after an oral challenge with scrapie-infected feed via the vagus nerve (Beekes and others 1998, Groschup and others 1999, Beekes and McBride 2000). Beekes and others (1998) observed that the DMNX was infected first, followed by the NTS, and they suggested that the infectious material initially spread by retrograde transport within peripheral neurons of the vagus nerve. Another study has demonstrated immunohistochemical staining indicating abnormal prion protein in the vagus nerve and DMNX of deer showing signs of chronic wasting disease, an economically important TSE in Canada and the USA (Sigurdson and others 2001).

The functional status of the brainstem and vagus nerve has been measured extensively in human and animal subjects by measuring heart rate variability (HRV). Low-frequency modulation of HRV is believed to occur as a result of the activity of both sympathetic and parasympathetic neurons modulated at the NTS, the parasympathetic component of which originates at the DMNX (Porges 1995). High-frequency modulation of HRV at the respiratory frequency, that is, the modulation of heart rate due to breathing, is known as respiratory sinus arrhythmia (RSA). The neural (rather than mechanical) component of RSA is thought to be predominantly parasympathetic in origin and controlled by neurons originating at the nucleus ambiguus (Porges 1995). Functional imaging during pharmacological interventions, such as anaesthesia, shows that a reduction in the level of RSA is associated with the modulation of activity in identified nuclei of the brainstem, including the NTS (Pomfrett and Alkire 1999).

The normal heart rate and HRV in cattle have been described by Austin and others (1997) and Minero and others (2001). Cattle in the late stages of BSE occasionally develop bradycardia, which has been temporarily reversed by the administration of atropine sulphate, which is widely acknowledged to eliminate vagal parasympathetic activity (Austin and others 1997). This observation was clear evidence for some disruption of the parasympathetic nervous system during the terminal stages of BSE, together with the outwardly observable clinical signs. A subsequent study demonstrated that HRV was disrupted in one animal with terminal signs of BSE (Pomfrett and Austin 1997), but the specific components of HRV affected were not identified. A commercial product (Neuroscope; Pontoppidan) has been used to identify profound bradycardia in one animal with clinical signs of BSE, and it was concluded that BSE caused an increase in the level of parasympathetic tone which may be due to its effect on vagal nuclei (Little and others 1996).

The specific aims of this project were to determine whether feeding BSE-infected material caused any change in the HRV of cattle and to determine the time course of any such changes in readily identifiable components of HRV.

MATERIALS AND METHODS

Measurements were made during the course of a study of three herds of cattle kept separately under laboratory conditions; they consisted of 48 unchallenged control animals, 43 that had been challenged orally in August 1998 with 1 g brain homogenate made from confirmed field cases of BSE, and 42 that had been challenged at the same time with 100 g of the same material. The measurements started in January 2001, that is, 29 months after the challenge, when none of them was showing any clinical signs of BSE and none had been diagnosed with BSE by statutory pathological examination. The measurements ceased in December 2001, by which time two animals had developed various clinical and behavioural signs of BSE, and had been culled and confirmed pathologically as having the disease.

At least five minutes (usually five minutes and 30 seconds) of electrocardiogram (ECG) was collected from each animal by using a physiological amplifier (Model 1902; CED). Data were collected for considerably longer than five minutes when it was suspected that excessive movement of the ECG leads could have caused electrical noise in the recorded trace. The ECG was digitised (DAP 800 PC card, 12 bit, 1 KHz resolution) and archived by using a standard file format (SON data library; CED). The data were analysed offline at the University of Manchester. The ECG files were initially examined by eye to ensure the accurate registration of R-wave timings. When

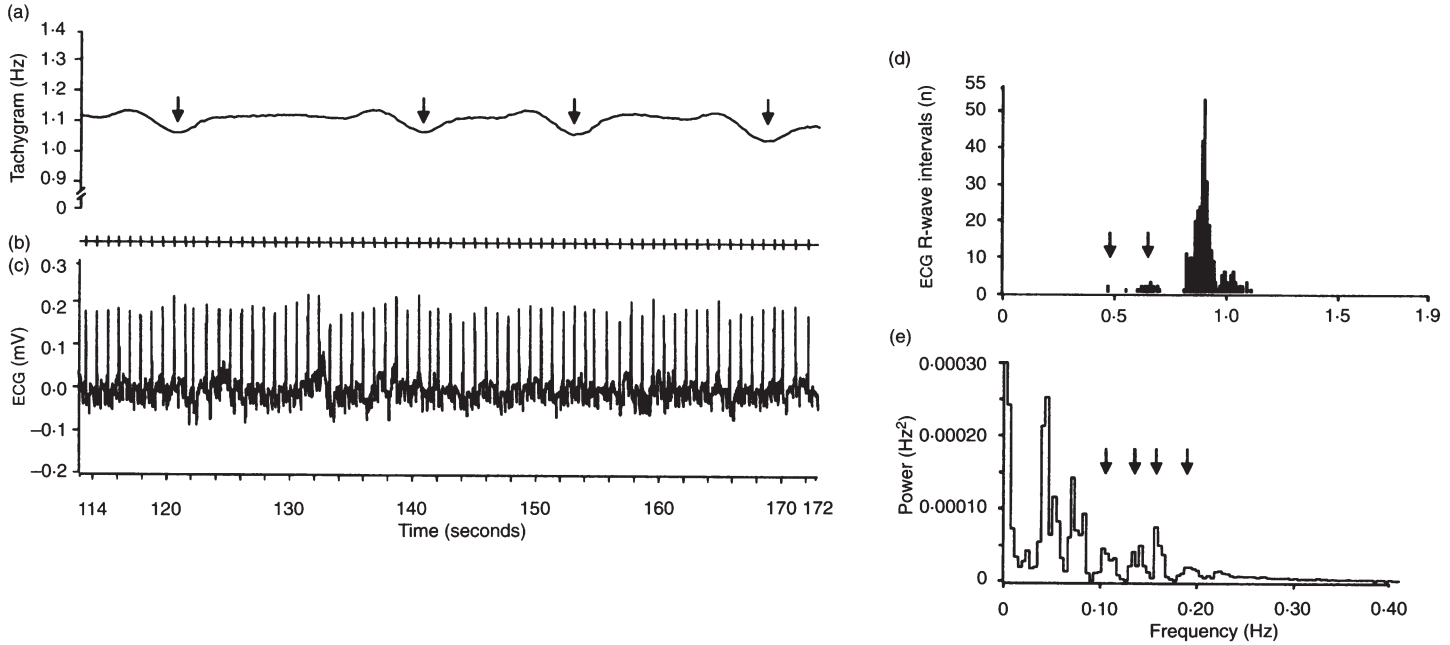

FIG 2: Analysis of data from an animal three years after challenge with 100 g of brain homogenate from bovine spongiform encephalopathy (BSE) field cases, which showed clinical signs of BSE confirmed postmortem, with a mean heart rate of 67·1 (2·7) bpm. (a) Tachygram of instantaneous frequency derived from the electrocardiogram (ECG) R-wave timings, (b) ECG R-wave timings, obtained by means of a robust peak detection algorithm (Wolfson Imaging Unit, University of Manchester) after a review of the raw data and the offline rejection of artefacts, (c) 100 seconds of the raw ECGs, (d) interval histograms showing the distribution of ECG R-wave intervals for five minutes of data, and (e) power spectra derived from five-minute epochs of tachygram data by using the fast Fourier transform (1024 points, Bsensor v5 script; CED). Arrows indicate regions where the high frequency component of heart rate variability has increased

movement artefacts had meant that R-waves were visible but not automatically detected (in around 4 per cent of files), the timings of these R-waves were inserted manually by using on-screen cursors in standard software (Spike2 version 4.02a; CED). Copies of data before and after such processing were archived for audit purposes. Occasional bursts of tachycardia, as described by Austin and others (1997), were not grounds for the rejection of files. Files were rejected only if the 300 seconds of R-wave timings required for automated analysis were not available (<1 per cent of files). Using batch processing of a whole directory of the scrutinised files, 300-second epochs of ECG were selected objectively and processed automatically under software control, with no user intervention (BSEnsor script version 5; TSEnse) to yield tachygrams of instantaneous frequency, to which fast Fourier transforms were applied with subsequent spectral analysis. Low-frequency (filter 0·0 to 0·05 Hz, transition gap 0·042 Hz) and high-frequency (filter 0·05 to 1 Hz, transition gap 0·04 Hz) descriptors of the power spectra were determined, and the data were output automatically as a summary table for further statistical analysis. Statistical comparisons were made between groups of normally distributed data by using Student's *t* test. Non-parametric data were compared by using the Mann-Whitney test (SPSS v10.1). Differences were significant at $P<0·05$.

RESULTS

The two cattle that developed clinical signs of BSE showed marked perturbations in HRV, but did not have bradycardia. Both of them had low levels of low-frequency HRV and high levels of high-frequency HRV in comparison with control animals examined at the same time. The unprocessed ECG strip from the animals with BSE was clearly abnormal, showing strong bursts of arrhythmic activity (Figs 1, 2). These were so marked that the authors could provisionally screen abnormal HRV in an animal in the late stages of BSE purely from its raw, visual ECG record, although quantitative analysis was necessary to define the extent of the change from the control cattle objectively.

A detailed examination of the time course of the HRV indices from the same two cattle, using repeated measures, showed that they had a characteristic profile of change in HRV in the high-frequency region, which initially increased in comparison with the controls and then decreased until just before the classical clinical signs of BSE developed, when the high-frequency HRV increased again markedly. Low-frequency HRV decreased progressively with time in these animals. This 'see-saw' effect, switching between low and high spectral frequencies during the incubation of BSE, was quite characteristic and not like the changes in HRV described after brainstem stroke, which induces a reduction in all components of HRV (Meglic and others 2001).

The pooled data for high-frequency HRV collated for the whole 12-month period (Fig 3) showed that there was a statistically significant difference between the mean values of the control animals and the animals challenged orally with BSE-infected material ($P<0·001$). Earlier studies by the Central Veterinary Laboratory suggested that not all animals will have demonstrable anatomical lesions in the brainstem at this stage in the incubation of BSE (T. Konold, personal communication); however, it is possible that some functional change has occurred in these regions of the brainstem, even in the absence of structural lesions, which may lead to a disruption in HRV.

There was a significant difference between the low-frequency HRV of the high- and low-dose groups ($P<0·01$), and between the high-dose group and the controls ($P<0·001$), but not between the low-dose group and the controls, suggesting that the extent of the perturbation of the low-frequency HRV was dose related.

The level of high-frequency HRV increased as a significant 'spike' in all the animals exposed to BSE-infected material (Fig 4), possibly indicating when the DMNX of the brainstem was

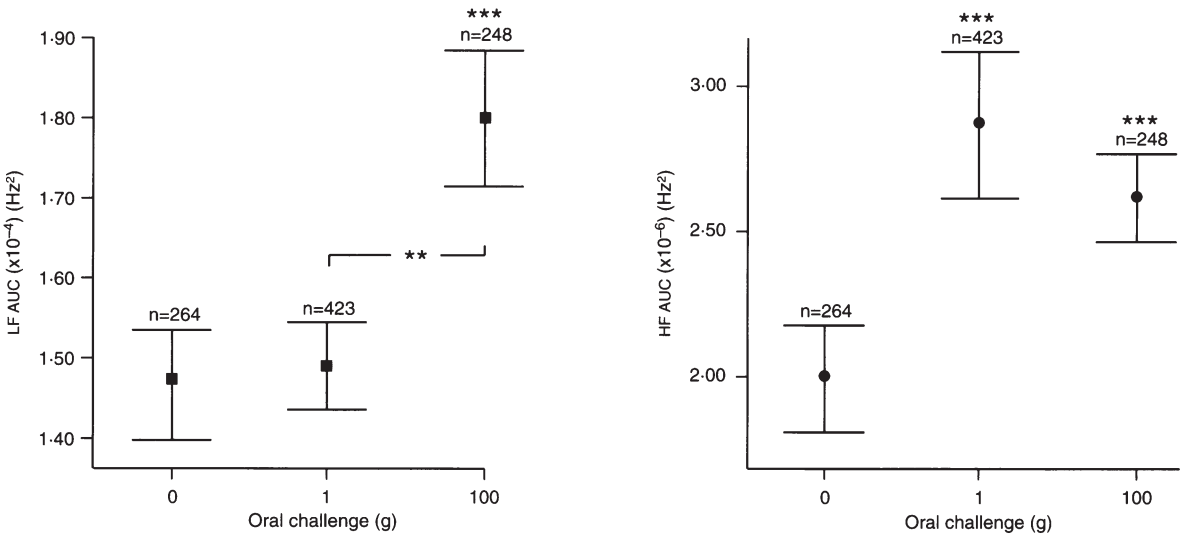

FIG 3: Areas under the curve (AUC) of the low-frequency (LF) and high-frequency (HF) power spectra of five-minute tachygrams of electrocardiogram (ECG) R-wave intervals of 48 control cattle, 43 cattle that received an oral dose of 1 g of brain homogenate from bovine spongiform encephalopathy (BSE) field cases and 42 cattle that received an oral dose of 100 g of brain homogenate from BSE field cases. The BSE-infected material had a significant effect on two indices of heart rate variability, but not on heart rate (data not shown). Each group is divided by the doses of BSE-infected material fed 29 to 42 months before the data were collected. The data were not normally distributed and significant differences were determined by using the Mann-Whitney test (SPSS v10.1). **P<0·01, ***P<0·001. n Number of measurements in each group

invaded. In contrast, there were no significant time-related changes in low-frequency HRV, suggesting that the effect on low-frequency HRV occurred over a different time scale. There was a significant change in the pooled high-frequency HRV data from the two challenged groups of cattle at least nine months before most of them showed any clinical signs of BSE. This change was still significant when the two cattle that did develop clinical signs of BSE were excluded from the analysis.

DISCUSSION

These results provide further evidence that HRV changes significantly in cattle showing the clinical signs of BSE, and they suggest that these changes may be detectable several months before the clinical signs develop. Specific changes in identified components of HRV that appear to change differentially during the incubation of the disease have also been measured. In addition, by examining a large group of animals challenged at the same time under controlled experimental conditions, it is possible to suggest that the relatively large 100 g dose of BSE material had a different effect on HRV, but during the same time course, than the smaller 1 g dose. Studies with rodent models of TSE infection with shorter incubation periods should make it possible to biopsy at the point of HRV change, to identify anatomical and pathological changes associated with specific antemortem indices of HRV. In light of the finding that an oral challenge can result in rapid neuroinvasion via the tongue and hypoglossal nerve (cranial nerve XII) (Bartz and others 2003), and that this route, as well as the vagal route, also results in abnormal prion deposits in the DMNX, HRV should be investigated as a potential tool for characterising the neural pathway of infection.

There was a dose-related difference in the low-frequency and high-frequency HRV when comparing the control cattle and the challenged cattle, suggesting that the DMNX-NTS pathway may have been disrupted only when the concentrations of abnormal prion material had increased sufficiently to leave the DMNX, and that this occurred at different times in different animals. In mice infected with scrapie, it has been shown that peripheral neuroinvasion is dependent on the concentration of abnormal prion protein present, and that the rate of axonal transport was around 0·7 mm per day (Glatzel and Aguzzi 2000). It would be interesting to investigate other factors which may affect the incubation time of BSE in cattle; for example, the shorter vagus nerve of younger animals would be expected to allow the brainstem to be invaded more rapidly.

The progressive reduction in low-frequency HRV during the incubation of BSE in the two clinically affected animals is interesting in relation to the fact that, in mice, more unmyelinated vagal fibres express normal prion than myeli-

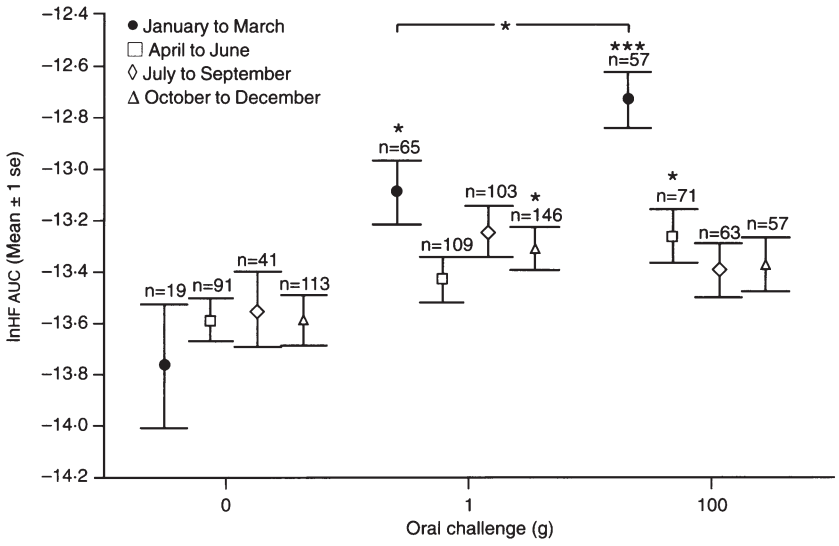

FIG 4: Changes in a component of heart rate variability with repeated measures for the pooled data. The control group did not change significantly during the study. There were significant changes during the first quarter of 2001 in the groups that received 1 or 100 g of bovine spongiform encephalopathy-infected material. The area under the curve (AUC) of the high frequency (HF) component of the power spectrum was normally distributed after a natural log transformation (lnHF AUC). *P<0·05, ***P<0·001 (Student's *t* test). n Number of measurements in each group

nated fibres (Ford and others 2002). It has been suggested that the unmyelinated vagal fibres encode low-frequency HRV and the myelinated vagal fibres encode high-frequency HRV (Porges 1995). If normal prion protein is recruited by abnormal prion protein in the axons of these fibres, and if the abnormal prion disrupts neuronal function, these changes in low-frequency HRV may be a functional correlate of this process.

HRV offers several advantages as a tool for the investigation of TSEs: experiments can be conducted on live suspects, both under controlled laboratory conditions and in the field; the data from five minutes of ECG recording can be analysed rapidly, and a single operator could collect data from many suspects per day; there are no costly reagents; and being computerised, the data can be collated as repeated measures and kept as a progressive measurement alongside the experimental subject's record. These advantages contrast with antemortem invasive brain biopsies or postmortem sections of the brainstem that are used only once and usually show a 'yes/no' condition, as does any blood or urine test indicating the presence or absence, but not the dose-related titre, of infectious prion protein. Furthermore, neuroinvasion via the vagus nerve does not require bloodborne transport of infectious agents, and so an experimental subject could potentially be incubating BSE via vagal transmission but no blood test, no matter how sensitive, could detect an early stage in the incubation of a TSE that has already affected the brainstem.

A rapid, non-invasive diagnostic test is essential, not only to confirm the diagnosis of BSE in cattle with the characteristic clinical signs, in order to exclude them from the human food chain, but also to identify subclinically affected animals and people incubating any TSE. Such a test would facilitate the control of TSEs and expedite the identification of infected subjects. Changes in HRV may provide a tool to develop such a test and could form a component of such a test (Pomfrett 2001), and they may also be useful as a non-invasive monitor of brainstem function during tests of putative treatments for TSEs.

References

AUSTIN, A. R., PAWSON, L., MEEK, S. & WEBSTER, S. (1997) Abnormalities of heart rate and rhythm in bovine spongiform encephalopathy. *Veterinary Record* **141,** 352-357

BARTZ, J. C., KINCAID, A. E. & BESSEN, R. A. (2003) Rapid prion neuroinvasion following tongue infection. *Journal of Virology* **77,** 583-591

BEEKES, M. & MCBRIDE, P. A. (2000) Early accumulation of pathological PrP in the enteric nervous system and gut-associated lymphoid tissue of hamsters orally infected with scrapie. *Neuroscience Letters* **278,** 181-184

BEEKES, M., MCBRIDE, P. A. & BALDAUF, E. (1998) Cerebral targeting indicates vagal spread of infection in hamsters fed with scrapie. *Journal of General Virology* **79,** 601-607

FORD, M. J., BURTON, L. J., MORRIS, R. J. & HALL, S. M. (2002) Selective expression of prion protein in peripheral tissues of the adult mouse. *Neuroscience* **113,** 177-192

GLATZEL, M. & AGUZZI, A. (2000) PrP(C) expression in the peripheral nervous system is a determinant of prion neuroinvasion. *Journal of General Virology* **81,** 2813-2821

GROSCHUP, M. H., BEEKES, M., MCBRIDE, P. A., HARDT, M., HAINFELLNER, J. A. & BUDKA, H. (1999) Deposition of disease-associated prion protein involves the peripheral nervous system in experimental scrapie. *Acta Neuropathologica* **98,** 453-457

IRONSIDE, J. W. (2000) Pathology of variant Creutzfeldt-Jakob disease. In Prion Diseases: Diagnosis and Pathogenesis. Eds M. H. Groschup, H. A. Kretzschmar. Vienna, Springer-Verlag. pp 143-151

LITTLE, C. J., JULU, P. O., HANSEN, S., MELLOR, D. J., MILNE, M. H. & BARRETT, D. C. (1996) Measurement of cardiac vagal tone in cattle: a possible aid to the diagnosis of BSE. *Veterinary Record* **139,** 527-528

MEGLIC, B., KOBAL, J., OSREDKAR, J. & POGACNIK, T. (2001) Autonomic nervous system function in patients with acute brainstem stroke. *Cerebrovascular Diseases* **11,** 2-8

MINERO, M., CANALI, E., FERRANTE, V. & CARENZI, C. (2001) Measurement and time domain analysis of heart rate variability in dairy cattle. *Veterinary Record* **149,** 772-774

POMFRETT, C. J. D. (2001) Analysis for the presence of degenerative brain disease. US Patent 6217521

POMFRETT, C. J. D. & ALKIRE, M. T. (1999) Respiratory sinus arrhythmia as an index of anaesthetic depth: evidence from functional imaging studies. *Journal of Physiology* **518** (Suppl P), 180

POMFRETT, C. J. D. & AUSTIN, A. R. (1997) Bovine spongiform encephalopathy (BSE) disrupts heart rate variability (HRV). *Journal of Physiology* **501** (Suppl P), 69

PORGES, S. W. (1995) Orienting in a defensive world: mammalian modifications of our evolutionary heritage. A polyvagal theory. *Psychophysiology* **32,** 301-318

SIGURDSON, C. J., SPRAKER, T. R., MILLER, M. W., OESCH, B. & HOOVER, E. A. (2001) PrP^{CWD} in the myenteric plexus, vagosympathetic trunk and endocrine glands of deer with chronic wasting disease. *Journal of General Virology* **82,** 2327-2334

ABSTRACTS

Safety of copper heptonate for the parenteral treatment of sheep

GROUPS of 12 Merino wethers, approximately nine months old, were treated intramuscularly with either 1 or 2 mg copper/kg bodyweight as copper heptonate or with an equivalent volume of saline. Muscle and liver biopsies showed that the copper had left the injection site within seven days and that most of it had been transferred to the liver. Although the liver copper concentrations of the sheep treated with 2 mg copper/kg had been increased to levels above those associated with copper toxicity, no signs of toxicity were observed. There were transient increases in the activity of the liver enzyme glutamate dehydrogenase, but no histological evidence of liver necrosis seven days after the treatment. There was no significant necrosis at the site of the injections.

JUDSON, G. J. & BABIDGE, P. J. (2004) An assessment of the safety of copper heptonate for parenteral therapy in sheep. *Australian Veterinary Journal* **82,** 75-78

Serum IgG_1 concentrations in atopic and non-atopic dogs

THE serum immunoglobulin G_1 (IgG_1) concentrations of 41 atopic dogs and 37 non-atopic dogs, of various breeds, which were receiving different levels of parasite control were compared. The non-atopic dogs receiving stringent parasite control had significantly lower total IgG_1 concentrations than either the atopic or non-atopic dogs receiving less stringent parasite control. After six months of treatment with allergen-specific immunotherapy, the concentration of IgG_1 in the atopic dogs had increased significantly. It is suggested that the serum concentration of IgG_1 is affected by parasitism, atopic dermatitis and allergen-specific immunotherapy.

FRASER, M. A., MCNEIL, P. E. & GETTINBY, G. (2004) Examination of serum total IgG_1 concentration in atopic and non-atopic dogs. *Journal of Small Animal Practice* **45,** 186-190

Trinity College Dublin (2003) **J Physiol 551P, C47**

Communications

Symptomatic vCJD alters heart rate variability

L.A.M. Woolfson*, D.G. Glover†, B.J. Pollard*† and Chris J.D. Pomfrett*

University Department of Anaesthesia, * University of Manchester, † Manchester Royal Infirmary, Oxford Road, Manchester M13 9WL, UK

Ante-mortem diagnosis of variant Creutzfeld Jacob disease (vCJD) is based on the subjective assessment of clinical signs, sometimes combined with invasive biopsy for the presence of infectious prion protein (PrPsc) in the tonsils. *Post mortem* diagnosis of transmissible spongiform encephalopathies in animals routinely depends on the microscopic immunohistochemical identification of PrPsc in the medulla oblongata of the brainstem (Wells *et al.* 1989), and in particular the nucleus tractus solitarii (NTS) and the dorsal vagal nucleus (DVN), the vagus nerve being a suspected route of infection in some species (Beekes *et al.* 1998). It has already been suggested that symptomatic bovine spongiform encephalopathy is associated with disturbance in heart rate variability (HRV) (Pomfrett & Austin, 1997), possibly occurring as a result of functional changes in NTS and DVN in the presence of PrPsc, and we sought to determine whether this is also the case in humans exhibiting symptoms of vCJD.

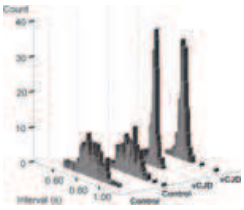

[High resolution image version]

Data were collected in accordance with a protocol approved by the North West Multi Centre Research Ethics Committee, including written, informed consent. Three-hundred-second samples of electrocardiogram (ECG) were collected at repeated intervals during a 3-month period from two subjects exhibiting definite clinical signs of vCJD, and who had also been confirmed as carrying PrPsc by tonsil biopsy. Control data were collected from seven healthy volunteers of comparable age not taking medication and with no relevant medical history. The ECG was digitised using a portable monitor (Fathom, Amtec Medical) at 1 kHz frequency and 12 bit resolution. Data were transferred to a PC, translated and analysed using standard software (CED Spike2 v4.02). The ECG waveform was reviewed by eye and artefacts rejected. Tachygrams of instantaneous ECG R-wave frequency were obtained in order to determine power spectra. Interval histograms of the R-R wave intervals were also plotted (see Fig.1). Non-parametric statistics were applied (SPSS v10.1).

We observed that symptomatic vCJD disturbed HRV. There was a significant difference in the variances of ECG R wave intervals between controls and vCJD suspects (Kruskal-Wallis H test, $P < 0.001$). Frequency histograms obtained from controls described normal distributions (Kolmogorov-Smirnov test, $P < 0.05$) whereas some frequency histograms of vCJD suspects demonstrated high levels of kurtosis, with significantly greater numbers of ECG R wave intervals in a narrow band between 0.9 and 0.98 s (Kruskal-Wallis test, $P < 0.05$). There was no significant difference between the mean heart rates of the two groups. Power spectral analysis revealed a significant increase in low frequency HRV (0-0.05 Hz) between the vCJD suspects and controls (Mann-Whitney U test, $P < 0.05$).

Further work is needed with a much larger sample size. However, this study allows us to suggest that measurement of HRV has potential as a non-invasive aid to the diagnosis of vCJD.

This study was funded by the Department of Health.

Beekes M *et al.* (1998). *J Gen Virol* **79**, 601-607.

Pomfrett CJD & Austin AR (1997). *J Physiol* **501.P**, 69*P*.

Wells GA *et al.* (1989). *Vet Rec* **125**, 521-524.

Where applicable, experiments conform with Society ethical requirements

Medical Hypotheses (2007) **68,** 1252—1257

ELSEVIER

medical hypotheses

http://intl.elsevierhealth.com/journals/mehy

The vagus nerve as a conduit for neuroinvasion, a diagnostic tool, and a therapeutic pathway for transmissible spongiform encephalopathies, including variant Creutzfeld Jacob disease

Chris J.D. Pomfrett *, David G. Glover, Brian J. Pollard

Division of Cardiovascular and Endocrine Sciences, The University of Manchester, Department of Anaesthesia, Manchester Royal Infirmary, Oxford Road, Manchester M13 9WL, UK

Received 17 October 2006; accepted 19 October 2006

Summary It is hypothesised that the vagus nerve (cranial nerve X) is an important conduit for infective neuroinvasion during the incubation of certain transmissible spongiform encephalopathies (TSEs) including scrapie in sheep, variant Creutzfeld Jacob disease in humans, chronic wasting disease in deer, and bovine spongiform encephalopathy in cattle. Presence of infection in the brainstem will disrupt normal function of this important region responsible for autonomic control of visceral function via the vagus nerve. It is proposed that physiological study of disrupted vagal function using techniques such as heart rate variability will indicate early, and ongoing, functional signs of infection even before levels of abnormal prion protein reach the thresholds currently used in tests for the presence of TSEs. It is further suggested that repeated measures of vagal function during treatment with experimental therapies will give a non-invasive, repeated measures index of drug efficacy. In addition, pharmaceutical interventions directed via the vagus nerve will bypass the blood brain barrier and take an anatomical route appropriate to the treatment of TSEs.

Introduction

Transmissible spongiform encephalopathies (TSEs) are contagious diseases of the nervous system associated with the accumulation of abnormal prion proteins. PrP^{d} will be used in this article as a label for disease-associated abnormal prion. Other reports freely interchange other labels, e.g. PrP^{Sc}, denoting the pathological isoform, and PrP^{res}, which indicates abnormal prion partially-resistant to digestion by the enzyme proteinase-K, an essential step in many biochemical tests for prion disease. Normal prion proteins (PrP^{c}) appear to have a role in neuronal copper transport [1,2] and are necessary for the propagation of TSEs. PrP^{c} is altered into PrP^{d}, which accumulates and is associated with pathological damage to neurones; the presence of PrP^{d} is both a symptom of and a biochemical marker for, TSEs. TSEs include bovine

* Corresponding author. Tel.: +44 161 276 8582; fax: +44 161 273 5685.
E-mail address: chris.pomfrett@manchester.ac.uk (C.J.D. Pomfrett).

0306-9877/$ - see front matter © 2006 Elsevier Ltd. All rights reserved.
doi:10.1016/j.mehy.2006.10.047

spongiform encephalopathy (widely known as mad cow disease or BSE), scrapie (sheep), chronic wasting disease (CWD in deer and other Cervidae), and variant Creutzfeld Jacob disease (vCJD in man). vCJD is of particular healthcare relevance, since cross infection has been demonstrated between vCJD infected humans receiving blood from asymptomatic vCJD donors, and between BSE-infected sheep by blood transfusion [3—5]. *Post-mortem* testing of prion disease in animals, for the purposes of disease surveillance and public food screening, is performed by biochemical detection of the presence of PrP^d in an obex section through the brainstem. The dorsal vagal motor nucleus (DMNX, after dorsal motor nucleus of cranial nerve X, the vagus) is located within the medulla oblongata of the brainstem, and has a high concentration of PrP^d in all animals orally challenged with TSE-infected brainstem, and symptomatic field cases of BSE. Concentration of PrP^d around neurones of DMNX has also been noted in humans with vCJD [6]. *Ante-mortem* live testing is performed on human subjects, and depends on the detection of PrP^d in biopsy samples of appendix, tonsil or brain tissue. No routine blood test has been implemented to date. Anatomical surrogate markers have also been reported in the brains of victims of vCJD, including the presence of changes in the pulvinar region of the thalamus observed by magnetic resonance imaging, and florid amyloid plaques observed *post-mortem* [6].

Hypotheses

The vagus nerve as an infectious conduit

It is proposed that the vagus nerve (cranial nerve X) is an important pathway for the neuroinvasion of infectious agent after oral challenge in all mammals susceptible to transmissible spongiform encephalopathies (TSEs), and not just scrapie (sheep and rodents) and chronic wasting disease (deer) where this has already been suggested [7—9]. The vagus will act as both a centripetal conduit, conveying infection from the gut to the central nervous system, and as a centrifugal pathway, spreading infection to viscera from the brainstem. This hypothesis is independent of prion protein only hypotheses for infection [10], and would be equally valid if some other infectious co-factor were discovered in addition to the PrP^d which is a widely accepted marker for TSEs. The proposed vagal route is not the sole pathway of neuroinvasion, and will operate in parallel with other routes of entry for TSE-associated pathogens entering the central nervous system e.g. other cranial nerves, the sympathetic nervous system, spinal cord etc. It should be considered that the vagus nerve has unique anatomy facilitating a fast track for neuroinvasion of the brainstem that bypasses the blood brain barrier. Early neuroinvasion via the vagus nerve may prime the brainstem to the presence of the disease, and hence predispose the mammal to succumb on challenge via the other, slower, routes delivering their pathogenic agents to the central nervous system later in the course of incubation. The short length of vagal nerves in young mammals e.g. beef calves, and small mammals e.g. rodents, may be a factor in the shorter incubation times observed in younger and smaller mammals, which would support this hypothesis. The medulla oblongata is widely accepted as a diagnostic region of choice for a number of TSEs [10], and the entry of the vagus at the medulla oblongata may explain the high concentration of abnormal prion in the brainstem at diagnostic, and frequently overtly symptomatic, stages of TSEs. Experimental lesion of the vagus nerve, either by physically cutting the nerve or by pharmacological intervention, will test this hypothesis.

Vagus nerve activity as a diagnostic tool

Monitoring vagally-mediated physiological activity (e.g. heart rate variability) gives an indirect index of brainstem function at the sites of neuroinvasion of infectious agents and replication of PrP^d, and so may be used as both a diagnostic screen, and as a repeated measures index of disease progression. Such a tool would be especially useful as an indirect indication of neurophysiological recovery during trials of putative therapies for TSEs. Repeated measures of heart rate variability after inoculation will test this hypothesis.

The vagus as a therapeutic pathway from the gut and lungs to the brainstem

It is suggested that the vagus nerve is a potential therapeutic route for the administration of drugs for the treatment of TSEs, permitting such drugs to enter identified regions of the brainstem with the highest concentrations of prion infection whilst bypassing the blood-brain barrier. Inoculation of a labelled virus known to use the gut to vagus nerve axis as a conduit (e.g. pseudorabies virus) in animals already incubating a TSE, and measuring any co-localisation of label with abnormal prion protein, will test the potential for this hypothesis.

Discussion

There is ongoing debate regarding whether PrP^d is the sole infectious component of TSEs. Infection appears to have occurred with passage of brain tissue containing undetectable levels of PrP^d in a mouse model of the disease, suggesting that an additional component is necessary in order to cause infection [11]. In addition, infection of sheep with scrapie occurs even when digestion in the gut denatures all measurable PrP [12]. Whatever the eventual outcome of this debate, accumulation of PrP^d is a symptom of TSEs, as is progressive neurophysiological impairment. Other symptoms are behavioural and reflect advancing functional disruption of neuronal activity; behavioural symptoms include hallucination and ataxia in humans, and loss of motor control in cattle. Why does DMNX have such a high concentration of PrP^d after oral challenge? The vagal conduit hypothesis would suggest that transport of PrP^d is via the vagus nerve from infected regions of the gut directly to DMNX. Vagal neurones with cell bodies located in DMNX innervate the gut (and other organs such as the heart) via their axons within the vagus nerves. The function of these vagal motor fibres is to facilitate autonomic function such as gut motility, gastric secretion, and the control of heart rate. Such function is affected by pharmacological intervention at the synapse, as seen during surgical planes of anaesthesia, where functional imaging on human volunteers has confirmed that vagal brainstem functional control of heart rate variability is impaired in an anaesthetic dose- dependant relationship [13]. The synapses between these motor cell bodies, local interneurones within DMNX, and interneurones connecting DMNX to adjacent structures in the brainstem, such as the nucleus tractus solitarii, would be the first sites for replication and passage of infectious prion within the central nervous system. It is interesting that DMNX, as part of the brainstem, is a specified risk material in BSE and absolutely prohibited from entry into the human food chain, and yet axons within the vagus, that can be considered tubes of cytoplasm (arising from the cell bodies that comprise DMNX) located in the vagus nerve, are not specified risk material and will be eaten as mechanically recovered material from the carcass' of cattle, and from vagal axonal material released when the cattle are decapitated. The vagus of only one BSE-infected cow has been tested to date and that was shown to be positive for PrP^d [14].

Studies on the sub-cellular pathology of neurones from the DMNX during infection of sheep with scrapie have revealed characteristic structures e.g. coated pits and vesicles along with frequently herniated myelin sheaths around axons [15,16]. The coated pits and vesicles suggested increased levels of uptake of PrP^d from extracellular compartments. Disruption of myelin would hamper saltatory conduction, an important method by which myelinated neurones propagate action potentials rapidly along the axon. Both of these observations describe processes that could affect the ability of neurones to function efficiently, and would be expected to adversely affect the control of vagally modulated reflexes, e.g. heart rate variability (HRV, millisecond changes in heart rate varying breath by breath) at early stages of neuroinvasion. The neuroanatomy of synaptic connections between neurones has been studied in mice infected with scrapie [17]. The authors observed that there was a significant loss of synapses during incubation of scrapie, at stages well before subsequent neuronal death. It was suggested that progressive loss of synapses, and the consequent reduction in quantities of neurotransmitter received at post synaptic sites, could serve to facilitate subsequent neuronal death.

The vagal route of neuroinvasion has been demonstrated very clearly in deer suffering from CWD [8], a disease endemic in the natural deer and elk populations of North America. The vagus nerve has stained positive for the presence of PrP^d in one study of deer exhibiting symptoms of CWD [8]. In that study, a single anatomical section was prepared through the vagus nerve (near the brainstem) and through the medulla oblongata that clearly demonstrated the contiguous nature of the staining, with some (but notably not all) individual axons within the vagus nerve staining positive for PrP^d, as well as DMNX. A potential problem with such work is that the vagus is a long and extensively branched nerve, and studies need to be conducted on all branches of the vagus, and not just an unidentified sample from a sensory branch that connects to regions of the body that may not express PrP^c, such as the lungs. Should an infectious co-factor other than prion be involved with the initiation of PrP^d replication, e.g. as some form of catalyst, the vagus would be a possible route for its passage into the CNS, even if PrP^d takes a different and parallel route. If that was the case, PrP^d would not be measurable in the vagus, and yet the vagus could still be a potential source of infection if eaten.

The vagal route may be of therapeutic use as a fast track to the brainstem, by-passing the blood brain barrier and facilitating axonal transport of

vesicles (both natural and theoretically synthetic). Certain viruses are known to use the vagus nerves as a conduit for neuroinvasion (e.g. influenza A and pseudorabies). Perhaps this could be exploited by modifying such an existing, vagally-vectored, virus to act as a carrier for targeted anti-TSE therapeutics? Since such therapy will be following the same route as the original infection, this should facilitate treatment.

It has been demonstrated that heart rate variability (HRV), comprising perturbation in the millisecond timing of sequential heart beats, is modulated by vagal brainstem function. In cattle, after oral challenge with TSE infected material, the medulla oblongata of the brainstem reaches a stage whereby PrP^d is detectable using *post-mortem* tests. This presumably occurs *in vivo* some time before classical behavioural symptoms of disease e.g. staggering, since the medulla oblongata is not involved in dysfunction of voluntary motor control that would cause staggering. It has been demonstrated *in vitro* that TSE infection upsets electrical properties of living neuronal synapses in cell culture [18,19]; after hyperpolarisation was enhanced, making neurones more excitable, which would disrupt timings within neuronal networks *in vivo*. The brainstem includes such neural networks, the physiological role of which includes modulation of HRV. The most readily identified component of HRV is respiratory sinus arrhythmia (RSA), a parasympathetic, vagally-modulated reflex. Although also present in mature adults, RSA is most readily observed in the heart beat timing of children and young adults, where the electrocardiogram (ECG) P—P wave variability can exceed 10%; children and other immature mammals have

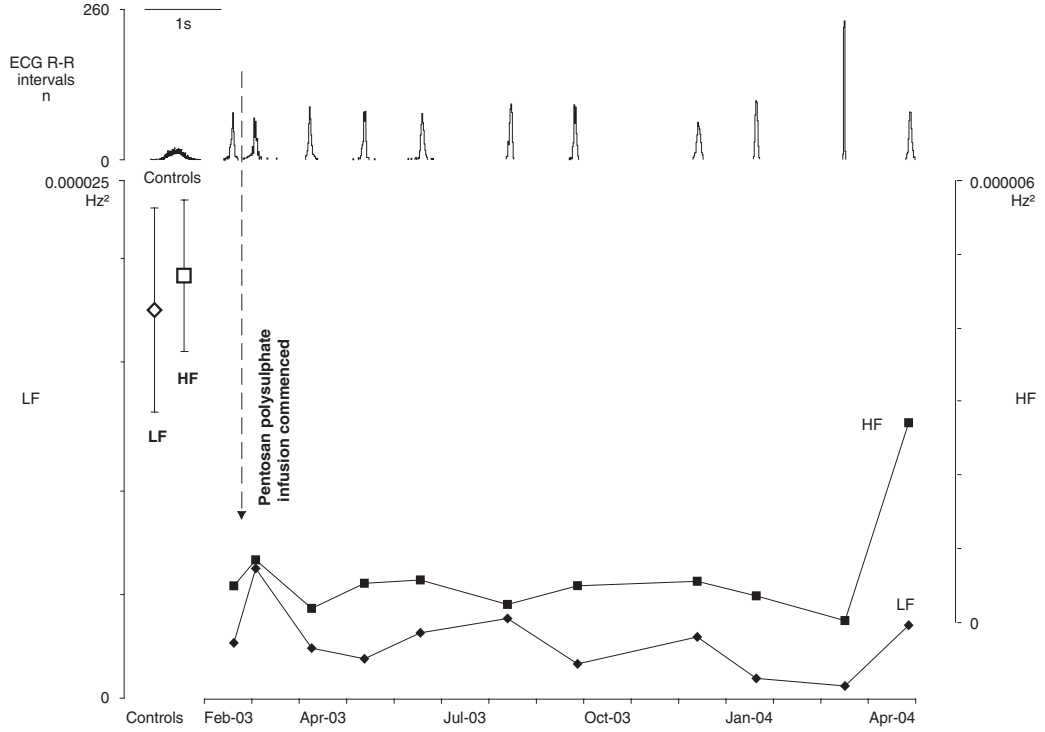

Figure 1 Repeated measurements of heart rate variability (HRV) in a patient exhibiting the symptoms of variant Creutzfeld Jacob disease (vCJD). Representative mean values of HRV (±1 standard error) are also shown for fifty healthy controls. The study was approved by the UK North West Multicentre Research Ethics Committee (study 01/8/92). The methodology was similar to that already used in cattle with BSE [20]. The measurements were: electrocardiogram R—R wave intervals presented as a histogram of numbers of intervals within 50 ms bins (upper trace); the power spectral derivatives low frequency area under the curve (LF; 0.032—0.138 Hz) and high frequency area under the curve (HF; 0.15—0.5 Hz). Wider ECG R—R wave histograms indicate greater heart rate variability whereas narrower histograms indicate less variability. The lowest level of HRV (narrowest histogram) was seen in March 2003. HF HRV is solely mediated by activity in the vagus nerve, LF HRV and ECG R—R interval histograms contain components of vagal (parasympathetic autonomic nervous system), as well as a sympathetic autonomic nervous system origin. The patient started receiving a putative therapeutic (pentosan polysulphate) by intraventricular cerebral infusion after the first measurement of HRV was made. All values were below those observed for controls, suggesting that vagal control of HRV has been impaired. The patient is still alive (October 2006), some five years after the onset of symptoms.

a high vagal tone. RSA results in the speeding up of heart rate during inspiration whilst lying down, as a result of a cyclic reduction in vagal tone. The presence of PrP^d in those centres of the brainstem responsible for controlling cardiac timing, upsetting neuronal timing as it does *in vitro*, would be expected to alter such HRV, including RSA, *in vivo*.

Significant perturbation of HRV in cattle incubating BSE after experimental oral challenge has been reported [20]. In that study, cattle had been fed 100 g, 1 g or no homogenised brainstem from symptomatic, BSE-infected cattle. Repeated measures data obtained from those cattle indicated that, while pre-symptomatic, there were significant differences in HRV between the high, low and control groups, indicating that the presence of infection disrupted brainstem function in a dose-dependant manner before other clinical signs were apparent. The changes in HRV were observed as a sustained increase in low frequency HRV compared with controls (indicative of increased activity at DMNX) and ''spikes'' in high frequency HRV. This suggested an alteration in vagal balance during the incubation of TSEs.

A more pronounced disruption in the HRV of patients exhibiting classical clinical signs of vCJD has been demonstrated [21]. Human subjects are examined at a much later state than cattle; animals in obvious signs of distress are euthanized, and are not allowed to live to the same stage as human patients receiving extensive palliative care. The human clinical profile of HRV is, therefore, further advanced than that observed in animals. In four human subjects with vCJD, severe reductions in HRV were observed. One subject is the longest survivor with vCJD (5 years post symptoms) and has been in receipt of experimental intraventricular infusion of pentosan polysulphate. The HRV of this patient was monitored repeatedly during the course of treatment (Fig. 1). Unfortunately, this is the only case in whom repeated physiological measures have been made during therapy, and then only from 2003 to 2004. One other subject showed progressive reduction in HRV up to death.

The vagus nerves are short in immature mammals, and lengthen during maturation. Young cattle and humans seem more susceptible to TSEs, with shorter incubation times. Could it be that the shorter vagus nerves result in more rapid neuroinvasion by the infectious agent? Young mammals have a greater resting level of HRV than adults, due in part to a higher level of activity in the vagus nerve. Does this higher activity equate to higher levels of PrP^c transferred between neurones as a result of copper transport. Might this result in an age-related effect on the passage of TSE- associated infectious agent?

The vagus nerve is an essential component of the normal inflammatory reflex [22]. TSEs are characterised by the lack of a classical immune reflex. However, spread of PrP^d has been shown to be increased in animals with an inflammatory reflex to other diseases [23]. Should this immune reflex to other pathogens be accompanied by increased vagal activity, this could facilitate vagal transport of the infectious agent for TSEs, and so indirectly affect neuroinvasion.

Conclusions

Current biochemical tests for PrP^d were validated by the European Union for use as tools for disease surveillance. As such, the priority was for high sensitivity in symptomatic animals, with high specificity i.e. no false positives. These tests were not validated for use on pre-symptomatic animals incubating BSE, and yet they are now being used, in conjunction with the removal of specified risk material known to be infectious, to protect the public from infection by BSE-infected, asymptomatic, animals, not just in the EU but world-wide. There is still a need for ante-mortem tests for infectivity, both for asymptomatic food animals and for human blood donors. HRV may form a component of such a live test.

There are potentially important consequences that arise should the vagus be a route for neuroinvasion in animals entering the human food chain. Vagus nerves, by their Latin name, wander, and are not the easiest of tissues to dissect in the laboratory. Consider the difficulty of removing vagus nerve from the carcass of slaughtered cattle on a production line. Vagus nerves are not classified as specified risk material and would not be removed from the carcass; we may be eating fragments of vagus nerves within processed meat products. It has been demonstrated, in one bovine with classical symptoms of BSE, that the vagus was indeed positive for PrP^d [14]. It is, therefore, possible that the human food chain is still being exposed to infectious material from asymptomatic cattle, at the early signs of infection, via the vagus nerve.

Acknowledgement

The authors acknowledge funding from the Department of Health (UK Government), grant M00051014 66, 2002—2004.

References

[1] Brown DR. Prion protein expression aids cellular uptake and veratridine-induced release of copper. J Neurosci Res 1999;58:717—25.

[2] Kretzschmar HA, Tings T, Madlung A, Giese A, Herms J. Function of PrP(C) as a copper-binding protein at the synapse. Arch Virol 2000;16(Suppl.):239—49.

[3] Houston F, Foster JD, Chong A, Hunter N, Bostock CJ. Transmission of BSE by blood transfusion in sheep. Lancet 2000;356:999—1000.

[4] Ironside JW, Bishop MT, Connolly K, et al. Variant Creutzfeldt-Jakob disease: prion protein genotype analysis of positive appendix tissue samples from a retrospective prevalence study. BMJ 2006;332:1186—8.

[5] Llewelyn CA, Hewitt PE, Knight RS, et al. Possible transmission of variant Creutzfeldt-Jakob disease by blood transfusion. Lancet 2004;363:417—21.

[6] Ironside JW. Pathology of variant Creutzfeldt-Jakob disease. Arch Virol 2000;16(Suppl.):143—51.

[7] Beekes M, McBride PA, Baldauf E. Cerebral targeting indicates vagal spread of infection in hamsters fed with scrapie. J Gen Virol 1998;79:601—7.

[8] Sigurdson CJ, Spraker TR, Miller MW, Oesch B, Hoover EA. PrPCWD in the myenteric plexus, vagosympathetic trunk and endocrine glands of deer with chronic wasting disease. J Gen Virol 2001;82:2327—34.

[9] van Keulen LJN, Schreuder BEC, Vromans MEW, et al. Pathogenesis of natural scrapie in sheep. In: Groschup MH, Kretzschmar HA, editors. Prion diseases: diagnosis and pathogenesis. New York: Springer-Verlag; 2000.

[10] Prusiner SB, Fuzi M, Scott M, et al. Immunologic and molecular biologic studies of prion proteins in bovine spongiform encephalopathy. J Infect Dis 1993;167:602—13.

[11] Lasmezas CI, Deslys JP, Robain O, et al. Transmission of the BSE agent to mice in the absence of detectable abnormal prion protein. Science 1997;275:402—5.

[12] Jeffrey M, Gonzalez L, Espenes A, et al. Transportation of prion protein across the intestinal mucosa of scrapie-susceptible and scrapie-resistant sheep. J Pathol 2006;209:4—14.

[13] Pomfrett CJD, Alkire MT. Respiratory sinus arrhythmia as an index of anaesthetic depth: evidence from functional imaging studies. J Physiol (Lond) 1999;518P:180.

[14] Iwamaru Y, Okubo Y, Ikeda T, et al. PrPSc distribution of a natural case of bovine spongiform encephalopathy. In: Prions: food and drug safety. Tokyo: Springer-Verlag; 2005.

[15] Ersdal C, Simmons MM, Goodsir C, Martin S, Jeffrey M. Subcellular pathology of scrapie: coated pits are increased in PrP codon 136 alanine homozygous scrapie-affected sheep. Acta Neuropathol (Berl) 2003;106:17—28.

[16] Ersdal C, Simmons MM, Gonzalez L, Goodsir CM, Martin S, Jeffrey M. Relationships between ultrastructural scrapie pathology and patterns of abnormal prion protein accumulation. Acta Neuropathol (Berl) 2004;107:428—38.

[17] Jeffrey M, Halliday WG, Bell J, et al. Synapse loss associated with abnormal PrP precedes neuronal degeneration in the scrapie-infected murine hippocampus. Neuropathol Appl Neurobiol 2000;26:41—54.

[18] Barrow PA, Holmgren CD, Tapper AJ, Jefferys JG. Intrinsic physiological and morphological properties of principal cells of the hippocampus and neocortex in hamsters infected with scrapie. Neurobiol Dis 1999;6:406—23.

[19] Johnston AR, Black C, Fraser J, MacLeod N. Scrapie infection alters the membrane and synaptic properties of mouse hippocampal CA1 pyramidal neurones. J Physiol 1997;500(Pt 1):1—15.

[20] Pomfrett CJD, Glover DG, Bollen BG, Pollard BJ. Pertubation of heart rate variability in cattle fed BSE-infected material. Vet Rec 2004;154:687—91.

[21] Woolfson LAM, Glover DG, Pollard BJ, Pomfrett CJD. Symptomatic vCJD alters heart rate variability. J Physiol (Lond) 2003;551P:C47.

[22] Tracey KJ. The inflammatory reflex. Nature 2002;420:853—9.

[23] Heikenwalder M, Zeller N, Seeger H, et al. Chronic lymphocytic inflammation specifies the organ tropism of prions. Science 2005;307:1107—10.

Delta sleep-inducing peptide alters bispectral index, the electroencephalogram and heart rate variability when used as an adjunct to isoflurane anaesthesia

Chris J.D. Pomfrett[a], Stuart Dolling[b], Nicola R.K. Anders[c], David G. Glover[c], Angella Bryan[c] and Brian J. Pollard[d]

Background and objective **Delta sleep-inducing peptide (DSIP) is an endogenous peptide that crosses the blood–brain barrier, named after its association with natural sleep and enhanced electroencephalogram (EEG) delta rhythm. The objective of this study was to determine whether DSIP could be used as an adjunct to volatile anaesthesia in humans, our hypothesis being that DSIP is a natural hypnotic that would increase anaesthetic depth. The aims were to assess depth of anaesthesia using bispectral index (BIS), the EEG and heart rate variability (HRV), and to determine whether DSIP altered the symmetry of EEG between the left and right cerebral hemispheres.**

Methods **Twenty-four female ASA I or II patients gave written, informed consent to a protocol approved by our local research ethics committee. Twelve were randomly assigned as controls to receive saline. The other 12 were randomly allocated to receive one of three intravenous bolus doses of DSIP (Clinalfa) at 25, 50 or 100 nmol kg^{-1}. The first administration of DSIP was while awake and the second after induction of anaesthesia with propofol and maintenance with isoflurane. BIS and EEG parameters were measured continuously using a bilateral electrode montage.**

Results **DSIP significantly increased heart rate, decreased HRV and, paradoxically, significantly reduced delta rhythm along with reducing burst suppression and increasing BIS at 25 nmol kg^{-1} during isoflurane anaesthesia. DSIP also significantly altered bilateral symmetry of EEG.**

Conclusion **DSIP probably reduced parasympathetic tone and decreased (lightened) the depth of anaesthesia measured using BIS. *Eur J Anaesthesiol* 26:128–134**

European Journal of Anaesthesiology 2009, **26**:128–134

Keywords: anaesthesia, electrocardiograph: analysis, electroencephalography: delta rhythm, inhalation: pharmacology

[a]Research School of Clinical & Laboratory Sciences, The University of Manchester, [b]Hope Hospital, Salford Royal NHS Foundation Trust, [c]Manchester Royal Infirmary, Central Manchester and Manchester Children's Hospital NHS Trust and [d]School of Medicine, The University of Manchester, Manchester, UK

Correspondence to Chris J.D. Pomfrett, PhD, Lecturer in Neurophysiology Applied to Anaesthesia, Department of Anaesthesia, Manchester Royal Infirmary, The University of Manchester, Oxford Road, Manchester M13 9WL, UK
Tel: +44 161 276 8582; e-mail: chris.pomfrett@manchester.ac.uk

Accepted 24 September 2008

Introduction

Delta sleep-inducing peptide (DSIP) is an endogenous sleep-associated hormone, first characterized in 1977 [1–3], that enhances delta wave activity in the electroencephalogram (EEG). DSIP is present in blood, crosses the blood–brain barrier, and has been used therapeutically in the treatment of insomnia [4,5].

Direct administration of DSIP to the brainstem of anaesthetized cats was reported to modulate heart rate variability (HRV) [6]. This was likely to be a direct effect on the dorsal vagal nucleus, nucleus ambiguus and/or the nucleus tractus solitarius, which together constitute the vagal complex of the medulla oblongata and are responsible for the control of HRV. It is known from a functional imaging study (positron emission tomography) that volatile anaesthesia affects glucose metabolism in this vagal complex of the brainstem in humans in an asymmetric (right side of the brainstem), dose-dependent manner [7] when vagal tone was assessed using HRV.

Bispectral index (BIS) is a proprietary, weighted composite of processed EEG derivatives presented as a number from 0 to 100 [8], widely used to indicate the depth of anaesthesia. Certain multichannel BIS monitors enable the recording of bilateral EEG derivatives, in addition to BIS.

Based on the literature, we considered that DSIP was a putative natural hypnotic. The principal objective of our studies was to determine whether DSIP has a therapeutic role as an adjunct to hypnotic anaesthesia. Our hypothesis was that DSIP would increase the overall depth of anaesthesia as measured using BIS and HRV. We are not aware of any prior literature by other groups reporting the effects on EEG or HRV of co-administration of DSIP with a volatile anaesthetic in humans.

0265-0215 © 2009 Copyright European Society of Anaesthesiology DOI:10.1097/EJA.0b013e32831c8644

Methods

The design of this study was a randomized, controlled pilot to characterize the effect of DSIP on bilateral components of the EEG and HRV in patients undergoing routine elective surgery. No power calculations were possible, as DSIP has been given in conjunction with anaesthesia in neither animals nor humans. Twenty-four ASA I or II, right-handed female patients scheduled for minor elective surgery gave written, informed consent to a protocol approved by the Central Manchester local research ethics committee, which entailed contact and distribution of information sheets at least 24 h before surgery. Patients were tested and had to be negative to a screen for drugs.

Clinical anaesthesia was standardized to propofol induction and isoflurane maintenance. Two anaesthetists attended. One anaesthetist made up the independently randomized test pack of DSIP (Clinalfa) provided by our hospital pharmacy, and administered the agent. The other anaesthetist administered a routine propofol induction/isoflurane maintenance surgical anaesthetic and was blinded to whether the agent was active or placebo.

The experimental procedure is shown in Fig. 1. Doses were chosen on the basis of prior therapeutic administration of DSIP reported in the literature for the treatment of insomnia [5]. One of three doses of DSIP ($25\,nmol\,kg^{-1} = 21.2\,\mu g\,kg^{-1}$; $50\,nmol\,kg^{-1} = 42.4\,\mu g\,kg^{-1}$ or $100\,nmol\,kg^{-1} = 84.8\,\mu g\,kg^{-1}$) was randomly administered intravenously to each patient in the active group using the contralateral arm to that used for injection of anaesthetic agents. The same dose of DSIP was administered once while awake and once during isoflurane anaesthesia. The control group received an equivalent volume of saline. In order to screen for adverse events, the first administration of DSIP after a 10 min baseline was in the form of a tolerance test, and was conducted while the patient was lying awake in the reception area of the operating rooms and monitored with standard ECG and noninvasive blood pressure equipment. A delay of at least 30 min allowed for washout of DSIP after the awake tolerance test, and before induction of anaesthesia.

In addition to standard monitoring (SpO_2, noninvasive blood pressure, and ECG), a series of independent monitors were attached to the patient for continuous, automated high-resolution logging to a PC. These comprised EEG (Aspect Medical Systems A-1000 with BIS v3.3, bilateral two-channel referential montage 10/20 locations Fp1–F7, Fp2–F8 with ZipPrep electrodes and matched impedances, updating every 15 s); ECG at 1 kHz (CED 1401 with Digitimer Neurolog amplifier); and end-tidal and inspired gas concentrations (Datex Ultima-1). Bilateral EEG electrode-derived data included the following parameters (as described by the manual for the A-1000 monitor): unfiltered BIS; absolute delta power (0.5–3.75 Hz measured in decibel with respect to $0.001\,\mu V^2$); relative delta power (% of delta power within the total power); total power (0.5–30.0 Hz measured in decibel with respect to $0.001\,\mu V^2$); electromyogram (EMG) band (70–110 Hz measured in decibel with respect to $0.001\,\mu V^2$); burst suppression (percentage of epochs in the past 63 s in which the EEG signal is suppressed, i.e. free of any waveform [8]); signal quality index (percentage of artefact-free epochs in the last minute that could be used for BIS calculations); spectral edge frequency (SEF; the frequency derived from spectral analysis of the EEG waveform below which 95% of the power is present); median frequency [the frequency derived from spectral analysis of the EEG waveform that is at the median (50%) of the power distribution]. Ten-minute epochs of EEG, HRV and gas data were identified after administration of DSIP or saline. Data were analysed off-line using standard software (CED Spike2 version 4.0 and Microsoft Excel). Tachygrams of instantaneous ECG frequency were calculated from *R–R* wave intervals resampled at 4 Hz. A 1024-point fast Fourier transform-based power spectral analysis was performed on these tachygrams in order to determine low-frequency (LF; 0.032–0.138 Hz; sympathetic and parasympathetic activity) and high-frequency (0.15–0.5 Hz; predominately vagal parasympathetic activity) HRV from 5 min

Fig. 1

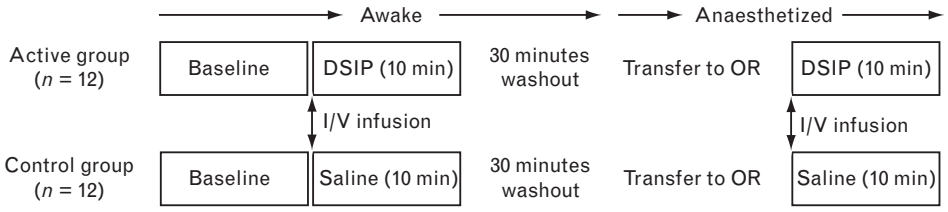

Diagram of the experimental procedure showing two parallel and randomly selected groups of 12 patients receiving either intravenous (I/V) saline (control) or intravenous delta sleep-inducing peptide in one of three doses (25, 50 or 100 nmol kg^{-1}) before and during isoflurane anaesthesia. Boxes denote data collection epochs. DSIP, delta sleep-inducing peptide.

epochs of ECG, as previously described [9]. Data were statistically analysed using standard software (SPSS version 15). All EEG data were marked as 'missing' when the signal quality index was less that 95.

Normality of data was rejected using the Kolmogorov–Smirnov test, and the Mann–Whitney *U* nonparametric test was subsequently used to compare the randomized active (DSIP) versus control (saline) groups. The effect of DSIP in the awake patients was assessed by calculating in each patient the difference between BIS before and after DSIP administration. Coincident measurements of paired, processed bilateral unsmoothed raw EEG (Aspect A-1000) collected in the same patients every 15 s were studied using a Wilcoxon signed ranked test. Statistical significance was assigned with P less than 0.001 for EEG data and P less than 0.05 for HRV data.

Results

Awake

DSIP was well tolerated in participants while awake; there were no adverse reactions. There was no significant change in heart rate (HR) or HRV when DSIP was administered to patients while awake (data not shown). The Wilcoxon signed rank test showed that asymmetry in left and right paired BIS values was significant with 25 nmol kg^{-1} and 100 nmol kg^{-1} DSIP (Fig. 2). This asymmetry was confirmed when changes in BIS relative to pre-DSIP baseline were calculated (Fig. 3) in the same patients. The relative BIS changes observed while awake were significantly different between 50 and 100 nmol kg^{-1} DSIP (Fig. 3).

Fig. 2

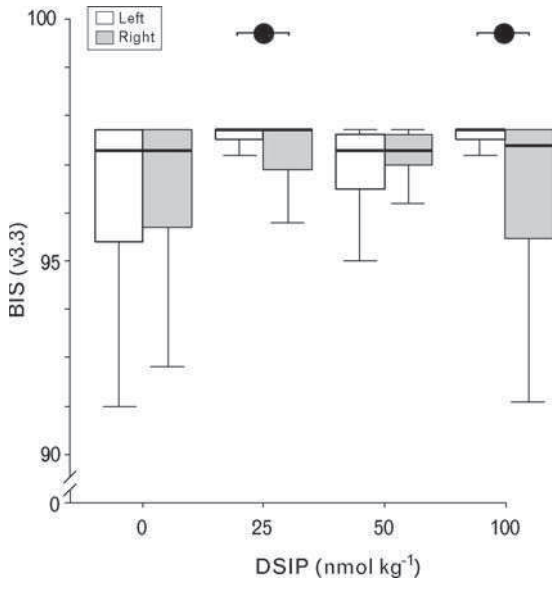

Graph showing absolute levels of bispectral index while awake. This and subsequent graphs show median (bold line), quartiles (boxes) and ranges including extreme and outlier values (whiskers). Unshaded bars indicate activity from the left side of the head and shaded bars the activity from the right side. Closed circles in this and subsequent figures denote significant difference between paired sides of EEG data (same patients, $P < 0.001$, Wilcoxon signed rank test).

Fig. 3

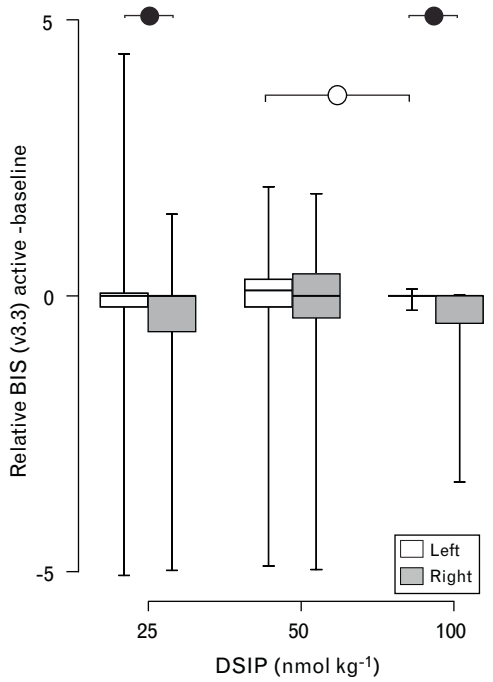

Graph showing relative changes in bispectral index after administration of delta sleep-inducing peptide in 12 awake participants, calculated by subtracting each 15 second BIS value from the corresponding paired value in the baseline, pre-delta sleep-inducing peptide epoch obtained from the same patient and then performing paired statistics between pre-delta sleep-inducing peptide and post-delta sleep-inducing peptide values. The open circle denotes a significant difference between 50 and 100 nmol kg^{-1} delta sleep-inducing peptide groups ($P < 0.001$).

Anaesthetized

There was no significant difference in the level of end-tidal isoflurane administered between each of the experimental or control groups (data not shown). When anaesthetized, administration of 25 nmol kg^{-1} DSIP resulted in a significant increase in mean HR (from 73.6 to 92.4 beats min^{-1}; $P < 0.05$), whereas HRV significantly decreased; the low-frequency area under the curve (LFAUC) fell significantly from 1.4×10^{-6} to 2.6×10^{-7} Hz^2 ($P < 0.05$) and the high-frequency area under the curve (HFAUC) fell significantly from 3.010^{-8} to 4.7×10^{-9} Hz^2 ($P < 0.05$). No significant changes were observed in HR or HRV at the other DSIP doses (50 nmol kg^{-1} DSIP: mean HR 62.8 beats min^{-1}, LFAUC 7.2×10^{-7} Hz^2, HFAUC 5.71×10^{-9} Hz^2; 100 nmol kg^{-1} DSIP: mean HR 65.4 beats min^{-1}, LFAUC 1.3×10^{-6} Hz^2, HFAUC 2.2×10^{-8} Hz^2).

Fig. 4

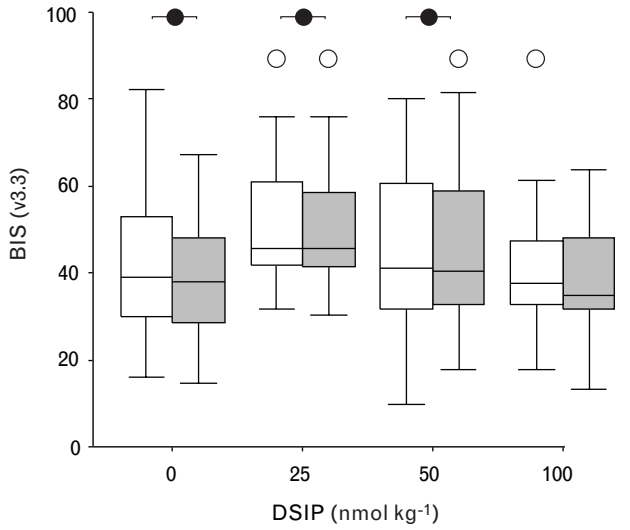

Graph showing absolute levels of bispectral index in patients anaesthetized with isoflurane. The open circles in this and subsequent figures denote significant differences between the delta sleep-inducing peptide-treated patients and different control patients ($P < 0.001$ Mann–Whitney *U*-test).

Figure 4 shows the significant increase in bilateral BIS observed with 25 nmol kg^{-1} DSIP. Most notable was that no BIS values below 30 were recorded when 25 nmol kg^{-1} DSIP was administered, suggesting that a component of processed EEG within the BIS algorithm, and essential for coding deep anaesthesia, had been attenuated. No BIS level above 65 was observed when 100 nmol kg^{-1} DSIP was administered, at which level the significant asymmetry in BIS values observed at lower levels of DSIP was lost.

Figure 5 shows that total power of the EEG was significantly reduced with 25 and 100 nmol kg^{-1} DSIP compared with saline controls during isoflurane anaesthesia. Significant asymmetry in total power was observed at 0, 25 and 50 nmol kg^{-1} DSIP.

Figure 6 demonstrates that a significant reduction in the right relative delta rhythm was observed with 25 and 100 nmol kg^{-1} DSIP administered during isoflurane anaesthesia. Significant asymmetry in relative delta rhythm observed in the control groups was not seen on administration of DSIP.

Figure 7 demonstrates that the low levels of burst suppression (<2%) encountered during isoflurane anaesthesia were significantly reduced on the left side of the head with 25 nmol kg^{-1} DSIP, and eliminated with 50 nmol kg^{-1} DSIP. At 100 nmol kg^{-1} DSIP, bilateral levels of burst suppression significantly increased compared with saline controls.

Fig. 5

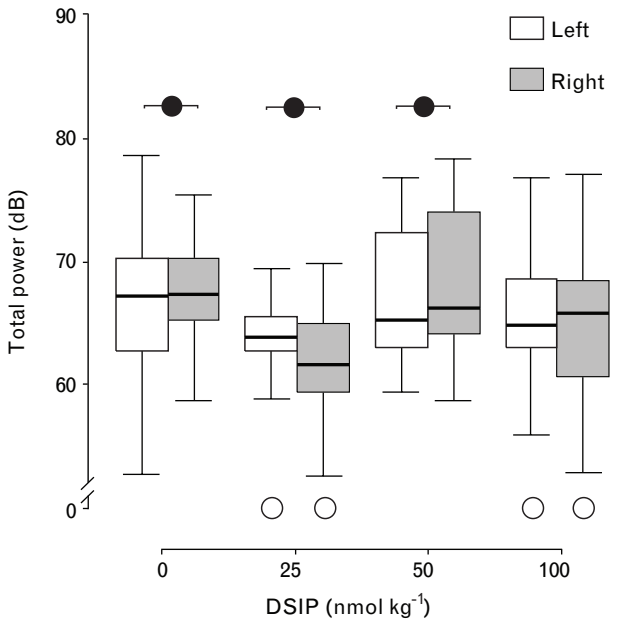

Graph showing the total power of the EEG (0.5–30 Hz) at different levels of delta sleep-inducing peptide during anaesthesia with isoflurane.

Figure 8 demonstrates that significant asymmetry in the EMG frequency band (70–110 Hz) was present during anaesthesia. The magnitude of EMG asymmetry was most pronounced in non-DSIP controls and smallest with

Fig. 6

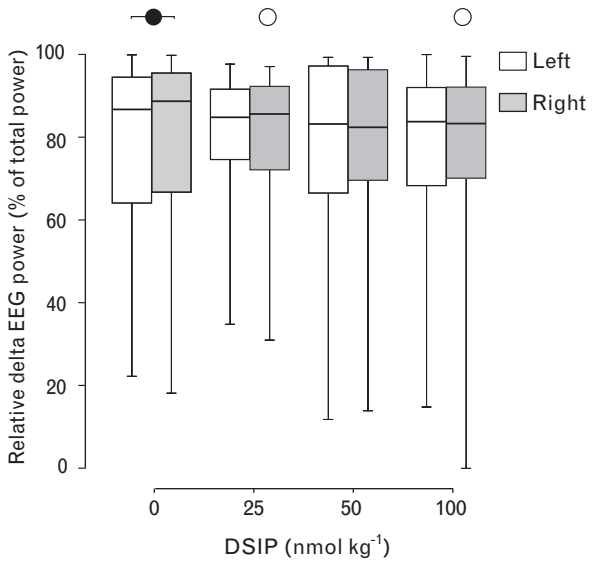

Graph showing the percentage of delta rhythm comprising the total power of the EEG at different levels of delta sleep-inducing peptide during anaesthesia with isoflurane. Open circles denote significant differences between right relative delta power and controls with 25 and 100 nmol kg^{-1} delta sleep-inducing peptide.

Fig. 7

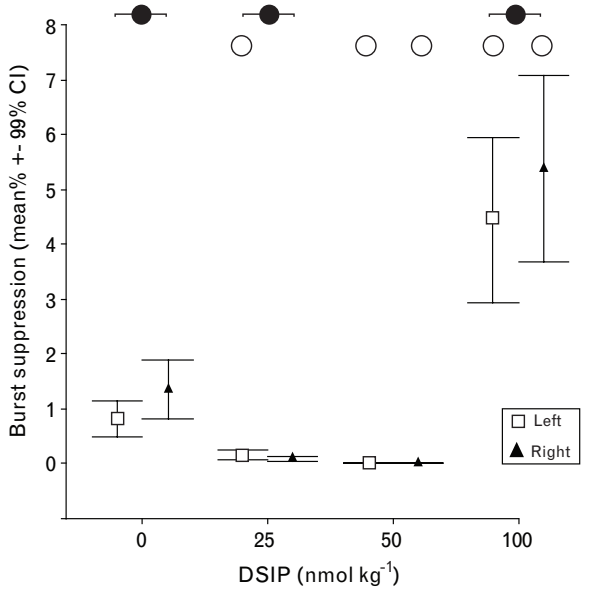

Graph showing the level of burst suppression of the EEG at different levels of delta sleep-inducing peptide during anaesthesia with isoflurane. Data are shown as means (%) ±99% confidence interval for the mean.

100 nmol kg^{-1} DSIP. Significant increases in EMG power were observed with 25 nmol kg^{-1} DSIP compared with controls, with significant decreases in EMG power at 50 and 100 nmol kg^{-1} DSIP.

Fig. 8

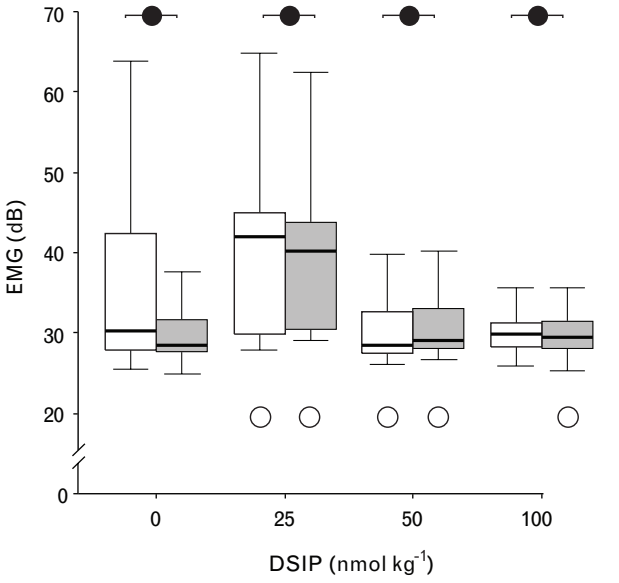

Graph showing the absolute level of frontalis electromyogram activity at different levels of delta sleep-inducing peptide during anaesthesia with isoflurane.

Fig. 9

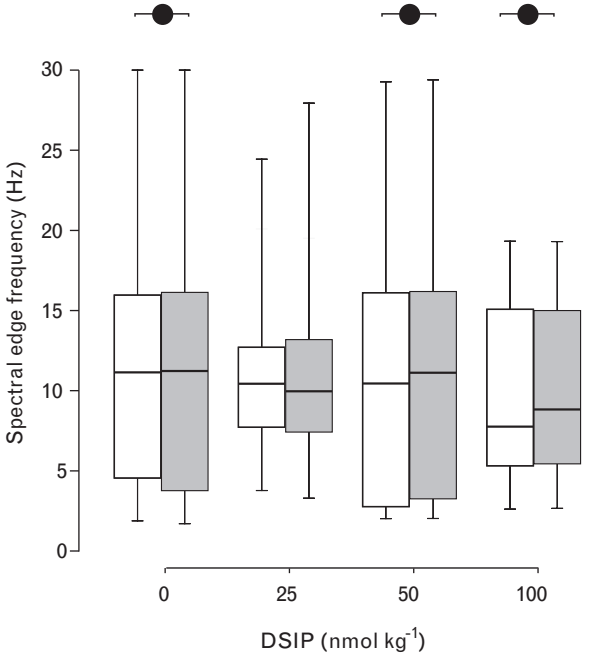

Graph showing the spectral edge frequency at different levels of delta sleep-inducing peptide during anaesthesia with isoflurane.

Figure 9 demonstrates that the unilateral level of SEF was not significantly altered by DSIP. Significant bilateral asymmetry of SEF was observed in anaesthetized controls and with 50 and 100 nmol kg^{-1} DSIP.

Median frequency was significantly reduced compared with controls in the left EEG montage during administration of 25 nmol kg^{-1} DSIP (Fig. 10). Paired analysis suggested significant asymmetry in median frequency in controls and those treated with 50 nmol kg^{-1} DSIP. The range of median frequency values was notably large in control and 50 nmol kg^{-1} DSIP groups.

Discussion

DSIP did not induce hypnotic anaesthesia when administered as the sole agent. Our hypothesis was that DSIP could act as a hypnotic adjunct to isoflurane. Although we did observe some significant changes in HR, HRV, BIS and components of the EEG, these effects were relatively small and so the original hypothesis was not supported. It is possible that DSIP will have more clinically relevant synergistic actions with anaesthetic agents other than isoflurane. After data collection was completed, and initial analysis was performed, we were advised that a crossover rather than randomized, controlled experimental design would have been more appropriate for looking at the small changes in EEG we observed in this study. Such a design would have no controls, and analysis would be based on a comparison of EEG in each participant before and after intervention with DSIP. Although such

Fig. 10

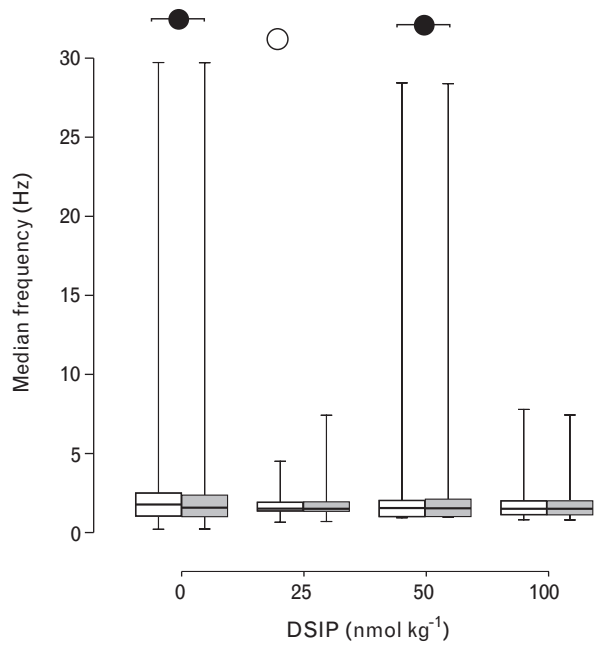

Graph showing the median frequency at different levels of delta sleep-inducing peptide during anaesthesia with isoflurane.

retrospective analysis was possible on data collected from awake participants in this study (Fig. 3), the drawback with such a crossover design would have been an additional delay in surgery of 10 min while baseline EEG data were collected before administration of DSIP, which was impossible for most of the cases we studied (and not in the approved experimental protocol). Ideally, future research into DSIP should consider such a crossover design.

DSIP (25 nmol kg^{-1}) rapidly, and significantly, reduced both LFAUC and HFAUC components of HRV in patients already anaesthetized with isoflurane, accompanied by a significant increase in HR. HFAUC is believed to be mostly parasympathetic in origin, whereas LFAUC is reported to be a combination of sympathetic and parasympathetic tone [9]. A reduction in parasympathetic tone would be expected to increase HR, whereas an equal reduction in parasympathetic and sympathetic tone may not alter HR. Therefore, our results suggest that DSIP is effecting a small reduction in parasympathetic tone.

DSIP (25 nmol kg^{-1}) caused a small, but statistically significant, rise in BIS during anaesthesia (Fig. 4). BIS is a complex analysis incorporating several different signal analyses of the EEG waveform, including several others apparently influenced by DSIP in this study, such as delta rhythm, burst suppression, SEF and median frequency; any combination of which may have been influenced by DSIP. The version of BIS studied here was 3.3, the most recent available for the A-1000 monitor. The A-1000 was used, rather than a more recent BIS monitor, as it had the capability to record asymmetry in BIS values during anaesthesia, and because the A-1000 is compatible with ZipPrep electrodes needed for a bilateral electrode montage, rather than BIS sensors designed for application to one side of the head. We noted a wide range of median frequency values in 0 and 50 nmol kg^{-1} groups that may be indicative of artefacts present within the median frequency data even with a signal quality index greater than 95, which was used as our automatic screen for artefacts.

The site(s) of action for the DSIP administered in this study is unknown. It is known that DSIP crosses the blood–brain barrier [1]. DSIP is reported to increase (gamma-aminobutyric acid) $GABA_A$-activated currents, and to inhibit *N*-methyl-D-aspartic acid activated currents [10,11] *in vitro* (cultured cerebellar and hippocampal neurones). Considering the small effect on parasympathetic tone that we have described and the effect of DSIP reported when administered directly to the brainstem of the cat [6], a putative site for such a central effect *in vivo* would be the vagal complex of the medulla oblongata, especially the dorsal vagal nucleus and nucleus ambiguus.

We were surprised by the degree of asymmetry in BIS observed in this study, even with no DSIP. This asymmetry in BIS was accompanied by asymmetry in the facial EMG and was also present in multiple EEG parameters. The magnitude of EMG asymmetry was most pronounced in the absence of DSIP, but the greatest EMG activity was observed with 25 nmol kg^{-1} DSIP. Facial EMG originates neurally in the brainstem [12]. This supports the suggestion that DSIP has a direct effect on this region of the brainstem. Future studies using functional imaging (e.g. positron emission tomography) of the brainstem during anaesthesia in volunteers treated with DSIP may help to locate the sites of action for this agent.

Whether DSIP has any clinical utility during anaesthesia, rather than just insomnia, remains to be demonstrated. We found some evidence that DSIP at 25 and 50 nmol kg^{-1}significantly reduced burst suppression of the EEG, i.e. periods of isoelectric EEG during deepening depths of anaesthesia. Burst suppression constitutes a large part of the BIS algorithm when BIS is less than 40 [13], which is the region of BIS implicated in cumulative deep hypnotic time (BIS < 45) as described by Monk *et al.* [14]. Reducing the level of anaesthetic agent would be the first course of action to reduce the amount of burst suppression, but perhaps DSIP or an agent with a similar profile could serve some role in moderating the level of burst suppression in a preventive manner.

We found that DSIP appeared to asymmetrically influence the level of EMG activity (Fig. 8). BIS changed in a similar way (Fig. 4), especially when asymmetry was taken into account. It has already been suggested that the EMG affects BIS levels when ZipPrep electrodes are used with an A-1000 monitor in a bipolar frontal montage [15] and the A-2000 monitor using a four-electrode Quattro Sensor [16]. It would be of interest to study bilateral responses from the EMG, especially with respect to their influence on BIS and other EEG-derived indices. Should EMG demonstrate measurable asymmetry, this may provide additional methods to extract it from the EEG signal.

Synthetic DSIP is currently prohibitively expensive for all but research use, although a more potent derivative of DSIP is commercially available in some countries (Deltaran). We observed a reduction in parasympathetic HRV that may be of interest in certain specialties, such as cardiac anaesthesia and intensive care medicine. The apparent lack of side-effects and rapid breakdown of DSIP make it suitable for further study.

References

1 Monnier M, Dudler L, Gachter R, Schoenenberger GA. Transport of the synthetic peptide DSIP through the blood-brain barrier in rabbit. *Experientia* 1977; **33**:1609–1610.

2 Monnier M, Dudler L, Gachter R, *et al.* The delta sleep inducing peptide (DSIP). Comparative properties of the original and synthetic nonapeptide. *Experientia* 1977; **33**:548–552.

3 Schoenenberger GA, Monnier M. Characterization of a delta-electroencephalogram (-sleep)-inducing peptide. *Proc Natl Acad Sci U S A* 1977; **74**:1282–1286.

4 Pollard BJ, Pomfrett CJD. Delta sleep-inducing peptide. *Eur J Anaesthesiol* 2001; **18**:419–422.

5 Schneider-Helmert D, Graf M, Schoenenberger GA. Synthetic delta-sleep-inducing peptide improves sleep in insomniacs. *Lancet* 1981; **1**:1256–1257.

6 Pokrovsky VM, Osadchiy OE. Regulatory peptides as modulators of vagal influence on cardiac rhythm. *Can J Physiol Pharmacol* 1995; **73**:1235–1245.

7 Pomfrett CJD, Alkire MT. Respiratory sinus arrhythmia as an index of anaesthetic depth: evidence from functional imaging studies. *J Physiol (Lond)* 1999; **518P**:180.

8 Rampil IJ. A primer for EEG signal processing in anesthesia. *Anesthesiology* 1998; **89**:980–1002.

9 Pomfrett CJD. R-R intervals and the depth of anaesthesia. In: Adams AP, Cashman JN, editors. *Recent advances in anaesthesia and analgesia*. Edinburgh: Churchill Livingstone; 1995. pp. 89–105.

10 Grigorev VV, Ivanova TA, Kustova EA, *et al.* Effects of delta sleep-inducing peptide on pre and postsynaptic glutamate and postsynaptic GABA receptors in neurons of the cortex, hippocampus, and cerebellum in rats. *Bull Exp Biol Med* 2006; **142**:186–188.

11 Sudakov KV, Umriukhin PE, Rayevsky KS. Delta-sleep inducing peptide and neuronal activity after glutamate microiontophoresis: the role of NMDA-receptors. *Pathophysiology* 2004; **11**:81–86.

12 Sethi NK, Sethi PK, Torgovnick J, *et al.* EMG artifact in brain death electroencephalogram, is it a cry of 'medullary death'? *Clinic Neurol Neurosurg* 2008; **110**:729–731.

13 Morimoto Y, Hagihira S, Koizumi Y, *et al.* The relationship between bispectral index and electroencephalographic parameters during isoflurane anesthesia. *Anesth Analg* 2004; **98**:1336–1340.

14 Monk TG, Saini V, Weldon BC, Sigl JC. Anesthetic management and one-year mortality after noncardiac surgery. *Anesth Analg* 2005; **100**:4–10.

15 Bruhn J, Boullon TW, Shafer SL. Electromyographic activity falsely elevates the bispectral index. *Anesthesiology* 2000; **92**:1485–1487.

16 Liu N, Chazot T, Huybrechts I, *et al.* The influence of a muscle relaxant bolus on bispectral and Datex-Ohmeda entropy values during propofol-remifentanyl induced loss of consciousness. *Anesth Analg* 2005; **101**:1713–1718.

A PILOT EXPLORATION OF HEART RATE VARIABILITY AND SALIVARY CORTISOL RESPONSES TO COMPASSION-FOCUSED IMAGERY

Helen Rockliff, Paul Gilbert, Kirsten McEwan, Stafford Lightman and David Glover

Abstract

This study measured heart-rate variability and cortisol to explore whether Compassion-Focused Imagery (CFI) could stimulate a soothing affect system. We also explored individual differences (self-reported self-criticism, attachment style and psychopathology) to CFI. Participants were given a relaxation, compassion-focused and control imagery task. While some individuals showed an increase in heart rate variability during CFI, others had a decrease. There was some indication that this was related to peoples self-reports of self-criticism, and attachment style. Those with an increase in heart rate variability also showed a significant cortisol decrease. Hence, CFI can stimulate a soothing affect system and attenuate hypothalamic-pituitary-adrenal axis activity in some individuals but those who are more self-critical, with an insecure attachment style may require therapeutic interventions to benefit from CFI.

Key Words: Compassion – Cortisol – Depression – Imagery – Heart Rate Variability – Self-Criticism

Declaration of Interest: None

Helen Rockliff, Paul Gilbert, Kirsten McEwan, Mental Health Research Unit, Kingsway Hospital, Derby, UK DE22 3LZ
Professor Stafford Lightman, Henry Wellcome Laboratories for Integrative Neurosciences & Endocrinology, Bristol, UK
David Glover, Manchester Royal Infirmary, Manchester, UK

Corresponding Author
Professor Paul Gilbert, Mental Health Research Unit, Kingsway Hospital, Derby, UK DE22 3LZ
Email: p.gilbert@derby.ac.uk – Fax: 01332 624576

Self-criticism is a major vulnerability factor to psychopathology (Gilbert & Procter 2006, Whelton & Greenberg 2005, Zuroff et al. 2005). In addition, it can undermine the success of traditional psychotherapies such as Cognitive Behavioural therapy (Rector et al. 2000). Recent research has explored the use of compassion-focused imagery (CFI) as part of a therapeutic process to help people who are highly self-critical (Gilbert 2000; Gilbert & Irons 2004, 2005; Wheatley et al. 2007)

For thousands of years imagination has been used to stimulate various physiological states (Frederick & McNeal 1999, Leighton 2003). Sexual, anxious, excited and calm feelings, along with self-confidence and preparation for tasks, can be stimulated via the imagination (Singer 2006). Mental imagery has also been used as a therapeutic aid to help desensitisation to aversive stimuli, coping with stress, and for the promotion of positive states of mind (Arbuthnott et al. 2001, Hall et al. 2006, Holmes et al. 2007, Singer 2006). Recent research and clinical work has focused on the value of helping patients develop self-compassion via various means including imagery (Gilbert 2007; Gilbert & Irons 2004, Gilbert et al. 2006).

Compassion evolved with the attachment system, such that signals of care, support and kindness, help to calm and sooth distressed individuals (Bowlby 1969). The soothing/calming that results from receiving kindness and support from others has been linked to a specific oxytocin-opiate 'affiliative' type of positive affect regulation system (Carter 1998, Depue & Morrone-Strupinsky 2005, Wang 2005) and reduces sensitivity in the amygdala, especially to socially threatening stimuli (Kirsch et al. 2005). This can be contrasted with an 'agentic' positive affect regulation system associated with drive and excitement (Depue & Morrone-Strupinsky 2005). Imagery and fantasising are believed to access these different systems – much as other forms of imagery stimulate other affect systems (e.g., anxious or sexual).

Porges's Polyvagal theory (2003, 2007) details how the evolution of the myelinated vagus nerve has supported interpersonal approach behaviours that enable social affiliations, caring and sharing. The myelinated vagus nerve evolved with attachment and the ability for infants to be calmed by parental caring behaviours (Depue & Morrone-Strupinsky 2005). This addition to the autonomic nervous system can inhibit sympathetically driven threat-defensive behaviours (e.g. fight/flight) and hypothalamic-pituitary adrenal (HPA) axis activity, and promote a calm physiological state, conducive to interpersonal approach and social

Submitted April 2008, Accepted June 2008

affiliation. In general, the safer people feel, the more open and flexible they can be in response to their environment (Gilbert 1993). This is reflected in the dynamic balancing of the sympathetic and parasympathetic nervous systems that give rise to the variability in heart rate (Porges 2007). Hence, feeling safe is linked to HRV, and higher HRV is linked to a greater ability to *self*-sooth when stressed (Porges 2007).

In contrast, when individuals feel unsafe, they will tend to rely on more threat focused and stereotyped defensive behaviours (Dickerson & Kemeny 2004, Gilbert 1993) characterised by a less flexible balance of the sympathetic and parasympathetic nervous systems, with lower tone in the myelinated vagus nerve (Porges 2007). This relative inflexibility and unbalance of the autonomic nervous system, associated with lower measures of HRV, has been associated with both mental and physical ill health (Appelhans & Luecken 2006; Thayer & Lane 2007).

This study is a pilot exploration of both the impact of baseline HRV measures on individual experiences of CFI, and the acute effects of CFI on HRV and cortisol. Imagery conditions were designed to stimulate two *different* types of positive affect. One type focused on being the *recipient* of compassion, while the control imagery focused on anticipation of reward (making one's ideal sandwich). Having two types of imagery targeted to stimulate the two different positive affects enables exploration of the specificity effects of positive affect on HRV.

We also explored the influence of self-reported self-criticism, self-compassion, attachment style, ease of feeling socially safe and stress, anxiety and depression on HRV responses to the CFI. We hypethesised whether self-criticism was associated with people finding CFI difficult and if this would be reflected in HRV and cortisol measures.

Method

Participants

Participants were recruited from the University of Derby (n =184) and completed a self-report screening questionnaire. Inclusion criteria were: aged between 18 and 35 years; BMI between 19 and 28; non-smoker; not-currently using medication (except contraception) or illicit drugs; consuming under 30 units alcohol per week; not working night shifts; no history of cardiovascular problems; and no major mental health problems (47 met these criteria). The final analyses consisted of 22 participants, exclusions included: A heart arrhythmia, being unable to sit still and concentrate, falling asleep, and imagining pity rather than compassion.

Procedures

All experimental sessions commenced at 14:00 (to allow consistent recording of cortisol levels) in the psychology department at the University of Derby. Participants were welcomed by the researcher and seated in a relaxed but upright position with arm and head supports for the duration of the study. Figure 1 outlines the procedure.

Imagery

Imagery was verbally guided by the researcher. Each condition (relaxation/baseline, compassion and control) lasted five and a half minutes. This was to ensure that 300 seconds of artefact-free ECG data was available for calculation of HRV metrics (Task Force 1996). During 'relaxation' participants were asked to 'allow the tension to drain from each of their muscles in turn'. Previous studies have used a variety of different instructions for obtaining baseline measures, including continuous counting, instructions to 'relax' (Osumi et al. 2006) and no baseline but inclusion of a control condition (Takahashi et al. 2005).

CFI

The CFI imagery asked participants to imagine compassion for them coming from an external source. The researcher suggested that some people find it

Figure 1. *Procedure*

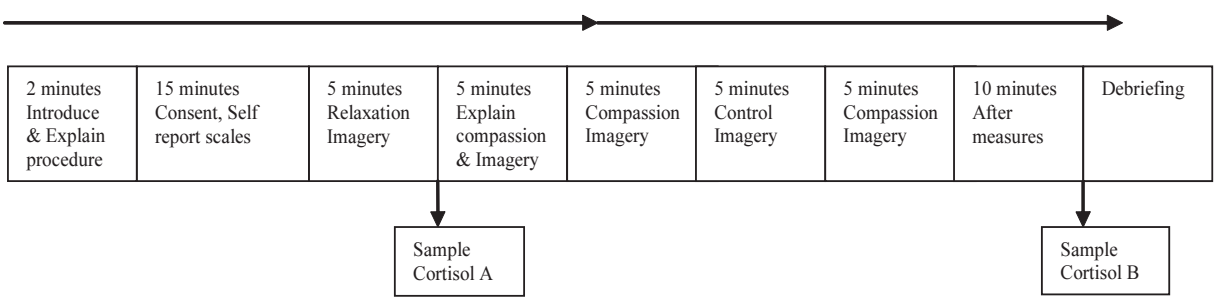

helpful to create a mental picture of this compassionate other (human or non-human). It was stressed that the image was to help them *feel* they were the recipient of compassion, and it was *feeling* that compassion that the research was exploring.

Participants were verbally prompted every 60 seconds by the researcher with various statements such as: "Allow yourself to feel that you are the recipient of great compassion; allow yourself to feel the loving-kindness that is there for you".

Control Imagery

As noted, the positive affect system underpinning appetitive and resource acquiring activity is different to the soothing/contentment system (Depue & Morrone-Strupinsky 2005). Therefore to compare different types of positive affect inducing imagery, our control imagery focused on preparing one's favourite sandwich. Participants were prompted every 60 seconds with statements like 'Imagine entering the shop of your choice and taking some time to browse and look around at the selection of food before you' and 'Imagine preparing your bread and beginning to build your sandwich.' The full script is available on request.

Measures

Laboratory Measures

A three lead ECG was recorded using Ag-AgCl disposable electrodes with Biopac PRO Lab software version 3.6.7 and MP30 Hardware (Linton Instrumentation). Data was sampled at 1Khz to ensure millisecond accuracy of the Inter-Beat Intervals (IBIs). IBIs were determined off line using the Biopac R-wave detection algorithm for 3 x 300 second periods corresponding to baseline and each imagery condition. All IBIs were manually checked by a researcher to ensure their accuracy, and to correct missed and ectopic beats due to the reported effects from such errors (Berntson et al. 2005). Artefacts were corrected according to the Task Force (1996) recommendations.

Heart Rate Variability Metrics

Using the artefact corrected ECG data, inter-beat intervals were measured and from these heart rate was calculated. CMetx software (Allen et al. 2007) was used to calculate the SDNN, the standard deviation of inter-beat intervals, a measure recommended by the Task Force (1996). This is a global measure of HRV, reflecting the sum of all of cyclic components contributing to the variation of inter-beat intervals. This was chosen as an appropriate measure for pilot work, which would give good indication as to the likely merit of further exploration using other measures of HRV.

To obtain measures of HRV reactivity to CFI the raw HRV metrics corresponding to each condition (baseline, compassion and control) were used to calculate participants' *change* in HRV values. These change values were calculated by subtracting each participant's control imagery HRV value from their CFI HRV value. (The control imagery HRV value was used as it attempts to keep constant the possible effects of mental effort and visualisation on HRV). Since HRV shows less acute reactivity in individuals with low HRV (Porges 2007), we adjusted the raw HRV change values in proportion to the participants baseline value by expressing HRV *change* values as a percentage of the baseline HRV value. These variables, which we will refer to as *HRV change,* make the magnitude of HRV response to imagery comparable between individuals.

Cortisol

Saliva samples were collected using salivettes (Sarstedt Ltd). The final cortisol sample was optimally timed to allow for a delay in possible HPA axis response to CFI (Dickerson & Kemeny 2004). All samples were frozen before being assayed for cortisol by Obsidian Research Ltd (Port Talbot, UK) using an Enzyme-Linked ImmunoSorbent Assay (ELISA).

Self-Report Measures

Participants completed a demographics form, the following self-report scales and additional questions.

Forms of Self-Criticism/Self-Reassuring Scale (FSCRS) (Gilbert et al. 2004).

This 22-item scale assesses participant's thoughts and feelings about themselves during a perceived failure. Two subscales measure forms of self-criticising, *(inadequate self* and *hated self)* and one subscale measures tendencies to be reassuring to the self *(reassured Self*). Participants respond on a Likert scale 0 – 4. The scale has good reliability with Cronbach's alphas of .90 for inadequate self, .86 for hated self, and .86 for reassured self (Gilbert et al. 2004).

Self-Compassion Scale (SCS) (Neff 2003)

This 26-item scale assesses levels of self-compassion. There are three factors of *positive* self-compassion: *self-kindness, common humanity* and *mindfulness,* and three factors that focused on a *lack* of self-compassion: *self-judgement, isolation* and *over-identification.* Participants indicate how often they engage in these ways of self-relating on a Likert scale 1 – 5. The scale has good reliability (Cronbach's alphas ranging from .75 to .81).

Adult Attachment Scale (Collins & Read 1990)

This 18-item scale measures three attachment dimensions. *Depend* measures abilities to depend on others, *anxious* measures degree of worry about abandonment and *close* measures ease of getting close to others. Respondents are asked to rate on a Likert scale 1 – 5 how characteristic each statement is of them.

The Cronbach's alphas were 0.75 for depend, 0.72 for anxiety and 0.69 for close.

Social Safeness Scale (Gilbert et al. submitted)

This 11-item scale was developed to measure the extent to which people experience their social world as safe, warm and soothing, and their ability to enjoy feelings of closeness with others. Each item is scored on a Likert scale 0 – 4. This scale had a Cronbach's alpha of .82.

Depression, Anxiety and Stress Scale (DASS-21) (Lovibond & Lovibond 1995)

This 21-item shortened version of the DASS-42 consists of three subscales measuring *depression*, *anxiety* and *stress*. Participants are asked to rate how much each statement applied to them over the past week, on a Likert scale 0 – 4. The DASS-21 subscales have Cronbach's alphas of .94 for Depression, .87 for Anxiety and .91 for Stress (Antony et al. 1998).

Results

Analysis was conducted using SPSS version 14. The data were screened for normality of distribution and for outliers.

Table 1. *Means and standard deviations of SDNN across conditions for both groups*

Condition	SDNN	
	Group1M(SD)	Group2M(SD)
Baseline (Relaxation)	55.28 (17.74)	64.06 (23.35)
Compassion imagery	44.61 (17.09)	60.05 (16.44)
Control imagery	53.85 (15.25)	51.51 (18.87)

Participants' reported 'boredom' and fatigue during the second CFI (C2) and therefore we removed this data as it was unreliable.

Heart *rate* changes and HRV changes are related but distinctly different measures. We therefore performed an ANOVA to determine whether there were any differences in heart rate between the three experimental conditions, or between groups. There were no significant differences, indicating that any changes in HRV found were not merely a product of changes in heart rate. Physical demands were kept constant throughout the study to ensure that any changes in the measures taken could be attributed to thought induced alterations of metabolic demand.

Heart Rate Variability

The HRV data showed two opposing responses to CFI. Some people showed a reduction in HRV (measured by SDNN) in response to compassion, while others showed an increase. We felt these were important differences and therefore split participants into two groups. Group 1 contains 11 individuals who showed a reduction in SDNN value from control to CFI (called 'Group $1^{SDNNdowns}$'), while Group 2 contains 11 individuals who showed an increase in SDNN value during the CFI (called 'Group $2^{SDNNups}$'). This equal number arose by chance.

Means and standard deviations for each condition and group are reported in Table 1. In addition, the mean SDNN for each group during each condition are depicted in Diagram 1.

The SDNN was analysed using repeated measures ANOVAs to explore the effects of imagery condition (relaxation, control and compassion) and group (i.e. whether participants decreased or increased in SDNN in response to CFI). The SDNN value calculated for each imagery condition was used as within-subjects variable, and group was used as a between-subjects variable. Post hoc t-tests were performed to explore where any significant differences lay between different imagery tasks.

The ANOVA showed both a significant main effect of imagery condition ($F(1.15, 23.00) = 4.41$, $p = .042$) and interaction effects with group ($F(1.15, 23.00) = 5.18$, $p = .028$). The difference in mean SDNN value between Group $1^{SDNNdowns}$ and Group $2^{SDNNups}$ is apparent at relaxation and is accentuated during the CFI. However, the groups are very similar in SDNN during the control imagery. The implications of this are that for some positive imagery tasks (e.g. making a sandwich), there are no discriminatory effects on HRV. However, for positive imagery associated with affiliative interpersonal affects (warmth, kindness and social connectedness) certain individuals responded with a decrease in HRV whilst others had an increase in HRV. The post hoc t-test revealed a significant difference between groups during the CFI ($t(20) = -2.20$ $p = .043$). This is visually represented in Diagram 1.

Cortisol

Cortisol values after relaxation and before CFI (Cortisol A), and after CFI (Cortisol B) were analysed using a repeated measures ANOVA, with group as a between-subjects variable. There was a significant main effect of imagery on cortisol value ($F = 4.54$, ($df = 1, 19$) $p = .046$) but no significant interaction of group. Post-hoc t-tests revealed a non-significant difference between the two groups cortisol A values (Group $1^{SDNNdowns}$ = 5.80ng/ml, Group $2^{SDNNups}$ = 5.40ng/ml). Both groups showed a mean cortisol value decrease after CFI (Group $1^{SDNNdowns}$ = 5.70ng/ml; Group $2^{SDNNups}$ = 4.92ng/ml). However, for Group $2^{SDNNups}$ this decrease in cortisol was significant, while for Group $1^{SDNNdowns}$ the decrease was non-significant. This greater decrease in Group $2^{SDNNups}$ resulted in a significant difference between the group means for cortisol B ($t = 2.50$, $p = .022$) and can be seen clearly in Diagram 2. Cortisol A correlated negatively with change in cortisol meaning that the lower a participant's initial cortisol value was,

Diagram 1

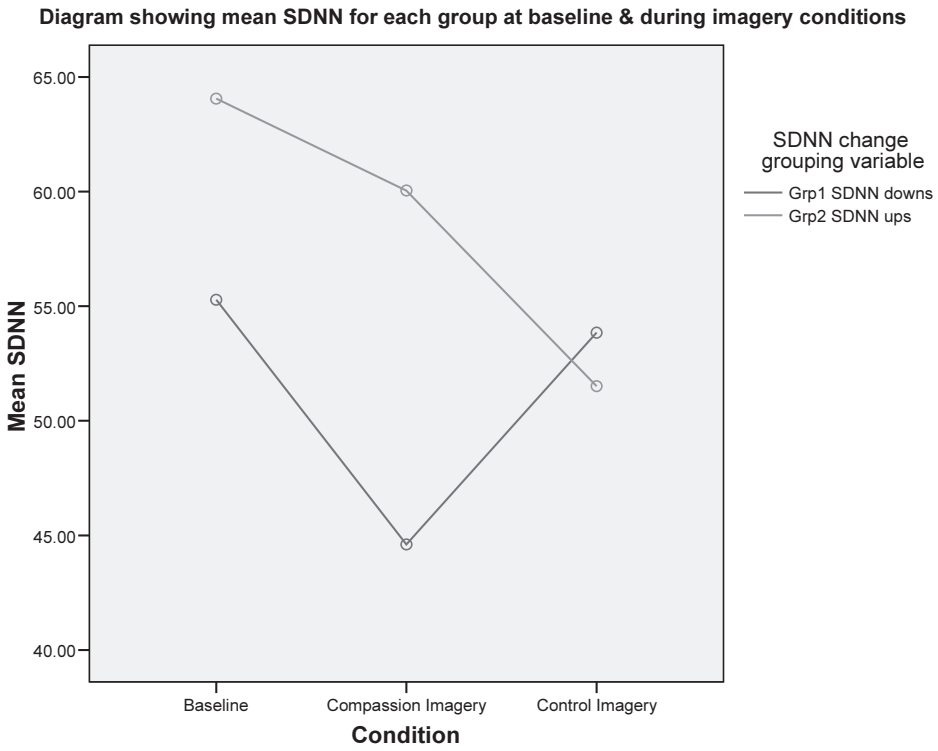

Diagram 2

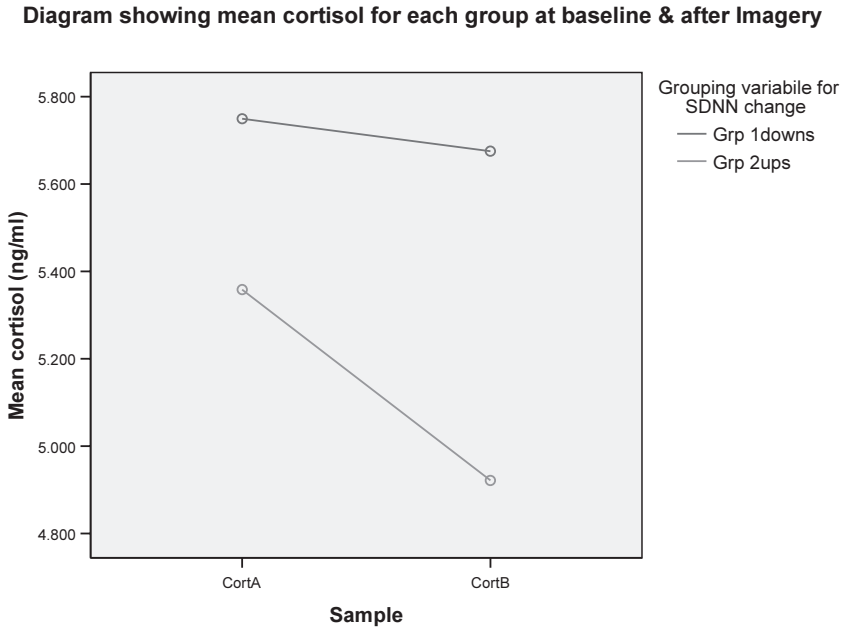

Table 2. *Correlations between change in HRV measures and self-report scales*

Self report measure		Inadequate self	Reassured self	Self Compassion	Self Coldness	Depend Attachment	Anxious Attachment	Close Attachment	Social Safeness	Depression DASS	Anxiety DASS	Stress DASS
SDNN (% Change)	*r* (*p*)	-.54* (.010)	.36 (.098)	.33 (.130)	-.30 (.169)	.52* (.014)	-.48* (.025)	.18 (.424)	.57** (.006)	-.22 (.328)	-.37 (.088)	-.19 (.403)

* $p < .05$
** $p < .01$

Note for readers interested in the results of other HRV metrics: 'RMSSD change' also showed a correlation with the 'Depend' attachment subscale (r = .44, p =.043), 'Toichi's Cardiac Vagal Index change' also showed positive correlations with the 'Depend' attachment subscale (r = .45, p =.034), Toichi's Cardiac Sympathetic Index also showed a significant correlation with the social safeness and pleasure scale (r = .45, p =.035)

the bigger their decrease in cortisol during compassion also was. These results show that for people who had an increase in HRV during CFI there was a significant decrease in cortisol. While for those who had a decrease in HRV during CFI, there was a minimal non-significant decrease, as would be expected from diurnal rhythm alone.

Mauchly's test indicated that the assumption of sphericity was violated for SDNN. Therefore, Greenhouse-Geisser estimates of sphericity were used to correct the degrees of freedom. Calculations of effect size (indicated by partial eta squared) revealed that effect sizes associated with cortisol measures were higher (i.e. ω^2>.08). than for SDNN (ω^2= <.08).

Self-Report Scales

Data were screened for normality of distributions, skewness values ranged from 0.09 to 1.43 and Kurtosis values from -0.23 to 1.42. The 'hated self' subscale derived from the forms of self-criticism and reassurance scale was skewed and kurtotic. This is not surprising to find in a non-clinical population due to a floor effect, and we chose to remove this subscale from further analyses. T-tests were conducted to examine differences in self-report scores between groups $1^{SDNNdowns}$ and $2^{SDNNups}$. A significant difference was found between social safeness scores (t=0.03), with Group $1^{SDNNdowns}$ having a lower mean score (38.00) than Group $2^{SDNNups}$ (44.64). We also noted that the group differences on the other self-report variables are all in the predicted directions, however statistical significance was not reached, possibly a limitation of the small numbers.

Correlation Analysis

Pearson's correlation coefficients for self-report scales, cortisol measures, baseline HRV and HRV change data are given in Table 2.

Change in SDNN was positively correlated with ability to depend on others (adult attachment scale), and with the social safeness and pleasure scale (r = .52, .014 and r = .57, p = .006 respectively). In other words, HRV response to CFI is linked to people's current experiences of themselves in social relationships. This is further indicated with the contrasting result that anxious attachment was negatively correlated with *change* in SDNN (r = -.48, p = .025). We also found self-criticism that focuses on feelings of self-inadequacy was negatively associated with reduced HRV when trying to engage in CFI (r=-.54). In addition, although not significant, the ability to be self-reassuring (r=.36) and self-compassionate (r=.33) were positively correlated with SDNN change.

Discussion

This study aimed to explore the impact of CFI on two different physiological measures (HRV and cortisol) we also explored individual differences informed by clinical observations that some people find CFI difficult or threatening (Gilbert 2007). Our data indicates two key processes. First, CFI does impact on HRV. Some people show a clear increase in HRV, whereas others show a more threat-like response with a reduction in HRV. We also found that those individuals who showed elevated HRV to compassionate imagery experienced a drop in cortisol, indicative of a soothing effect on the HPA axis. In contrast, those who showed a reduction in HRV experienced a non-significant cortisol change. There is research suggesting that some individuals with secure attachments, typically engage in soothing images and memories of feeling cared for and these can aid emotional regulation (Baldwin 2005, Mikulincer & Shaver 2007). Buddhism also specifically focuses on training people in CFI (Leighton 2003).

It appears that different people have different physiological responses to CFI. So the question is to try to identify the sources of these differences. Why do some people benefit from CFI and experience it as soothing while others appear threatened? We explored this with self-report measures. The self-report data suggests that people's experiences of CFI are related to current experiences of social safeness; Group $2^{SDNNups}$ had higher mean scores of social safeness. Although other self-report measures did not show significant differences between the two groups, all differences showed trends in the expected directions (e.g. Group $1^{SDNNdowns}$ had higher mean scores of self-criticism, self-coldness, anxious attachment and psychopathologies; whilst Group $2^{SDNNups}$ had higher mean scores of self-compassion, self-reassurance and ability to depend on

others and experience close relationships). This would fit with Gilbert's (1989) concepts of a safeness system and Porges' (2003, 2007) view that higher HRV is linked to interpersonal approach and socially adaptive behaviours.

Further evidence for this link was revealed in the pattern of correlations. A significant positive correlation was found between change in SDNN during CFI and social safeness and ability to depend on others. In contrast, anxious attachment was negatively associated with SDNN change; in other words, anxious attachers may find CFI more threatening. The data raises important implications for psychotherapy (Gilbert & Irons 2005; Gilbert & Procter 2006). The differences in HRV response seen between participants reflect clinical observations; that for some people (particularly self-critics and those scoring low in social safeness), focusing on compassion can at first be unfamiliar, threatening and feel unsafe (Gilbert 2007; Gilbert & Irons 2005; Gilbert et al. 2006). Self-critics often report feeling reluctant to 'let go' of their self-criticism for fear of their 'standards slipping'; that they might become selfish or arrogant, or that it constitutes a change to self-identity. They can also 'fear' compassion because they feel they do not deserve compassion or because it is unfamiliar, triggers sadness, or it is frightening to let others (even imagined ones) get close (Gilbert & Procter 2006).

It is unclear which aspects of compassion are particularly threatening because our CFI involved experiencing acceptance, loving kindness, warmth, and compassion. Clinically, people often experience sadness and grief when their attachment systems are activated (Bowlby 1969, 1980). Compassionate imagery involves activating these systems and drawing on emotional memories of attachment (Gilbert 2007). The finding that self-criticism was linked to an SDNN decrease when engaging in CFI provides further support that self-critics may find CFI difficult at first, this could also be related to a lack of compassionate memories on which to draw. This difficulty, and/or negative response to feeling compassion for the self, can be a barrier to the development of self-compassion, and could also be a cause of the HRV decrease seen in Group $1^{SDNNdowns}$. This suggestion fits with data by Segerstrom and Solberg Nes (2007) who found HRV decreases to be associated with self-regulatory processes, such as inhibition of emotion.

A number of authors have noted that self-criticism is a major vulnerability factor for low mood and psychopathologies (Whelton & Greenburg 2005). Both criticism from others (Dickerson & Kemeny 2004) and self-criticism is linked to HPA axis arousal and cortisol release (Mason et al. 2001). Gilbert (2007) suggests that chronic self-criticism continually stimulates the threat system thus having a detrimental impact on positive affect.

We concentrated on reporting the SDNN as recommended by the global HRV metric Task Force, (1996). However, there are other methods for exploring the periodic processes involved in HRV, which may shed more light on the relationships indicated by this study. Second, we did not measure respiration or muscle tension, and consequently the HRV changes could be attributable to changes in breathing rate/depth, or muscle tension. However, physical demands were kept constant throughout the study making this unlikely.

Yet to be explored is whether training and working through the fears and blocks to self-compassion, will impact on HRV and other neurophysiological processes linked to social soothing, and if this methodology could be adapted for evaluating psychotherapies. Given the increasing interest in compassion as a therapeutic aid, further research into the neurophysiological mediators and effects of compassion, may indicate ways of developing psychotherapeutic techniques (Gilbert & Irons 2005).

Acknowledgments

The authors would like to thank Linton Instrumentation (Diss, Suffolk) for their facilitative attitude and help with using Biopac software. This work was undertaken by the Mental Health Research Unit who received a proportion of its funding from the Department of Health. The views expressed in this publication are those of the authors and not necessarily those of the Department of Health.

References

Appelhans BM & Luecken LJ (2006). Heart rate variability as an index of regulated emotional responding. *Review of General Psychology* 10, 229-240.

Allen JJB, Chambers AS & Towers DN (2007). The many metrics of cardiac chronotropy: A pragmatic primer and brief comparison of metrics. *Biological Psychology* 74, 243-262.

Antony MM, Bieling PJ, Cox BJ, Enns MW & Swinson RE (1998). Psychometric properties of the 42-item and 21-item versions of the depression anxiety stress scales in clinical groups and a community sample. *Psychological Assessment* 10, 176-181.

Arbuthnott KD, Arbuthnott DW & Rossiter L (2001). Guided imagery and memory: Implications for psychotherapies. *Journal of Counselling Psychology* 48, 123-132.

Baldwin MW (Ed) (2005). *Interpersonal Cognition.* Guilford, New York.

Berntson GG, Lozano DL & Chen YJ (2005). Filter properties of root mean square successive difference (RMSSD) for heart rate. *Psychophysiology* 42, 246-252.

Bowlby J (1969). *Attachment and Loss: Attachment*, vol. 3. Basic Books, New York.

Bowlby J (1980). *Loss: Sadness and Depression. Attachment and Loss,* Vol. 3. Hogarth Press, London.

Carter CS (1998). Neuroendocrine perspectives on social attachment and love. *Psychoneuroendorinlogy* 23, 779-818.

Collins NL & Read SJ (1990). Adult attachment, working models and relationship quality in dating couples. *Journal of Personality and Social Psychology* 58, 644-663.

Depue RA & Morrone-Strupinsky JV (2005). A neurobehavioral model of affiliative bonding: Implications for conceptualizing a human trait of affiliation. *Behavioural and Brain Sciences* 28, 313-350.

Dickerson SS & Kemeny ME (2004). Acute stressors and cortisol response: A theoretical integration and synthesis of laboratory research. *Psychological Bulletin* 130, 335-39.

Frederick C & McNeal S (1999). *Inner Strengths: Contemporary Psychotherapy and Hypnosis for Ego Strengthening*. Lawrence Erlbaum Associates, Mahwah, NJ.

Gilbert P (1989). *Human Nature and Suffering.* Lawrence Erlbaum Associates, London.

Gilbert P (1993). Defence and safety: Their function in social behaviour and psychopathology. *British Journal of Clinical Psychology* 32, 131-153.

Gilbert P (2000). Social mentalities: Internal 'social' conflicts and the role of inner wamth and compassion in cognitive therapy In Gilbert P, Baily KG (Eds). *Genes on the Couch: Explorations in Evolutionary Psychotherapy*. Brunner-Routledge, Hove, pp.118-50.

Gilbert P (2007). *Psychotherapy and Counseling for Depression*. Sage, London.

Gilbert P & Irons C (2004). A pilot exploration of the use of compassionate images in a group of self-critical people. *Memory* 12, 507-516.

Gilbert P & Irons C (2005). Focused therapies and compassionate mind training for shame and self-attacking **I**n Gilbert P (Ed) *Compassion: Conceptualisations, Research and Use in Psychotherapy*. Routledge, London, pp. 263-325.

Gilbert P & Procter S (2006). Compassionate mind training for people with high shame and self criticism: Pilot study of a group therapy approach. *Clinical Psychology and Psychotherapy* 13, 353-379.

Gilbert P, Clarke M, Hempel S, Miles JNV & Irons C (2004). Criticizing and reassuring oneself: An exploration of forms style and reasons in female students. *British Journal of Clinical Psychology* 43, 31-50.

Gilbert P, Baldwin M, Irons C, Baccus J & Palmer M (2006). Self-criticism and self-warmth: An imagery study exploring their relation to depression. *Journal of Cognitive Psychotherapy: An International Quarterly* 20, 183-200.

Gilbert P, McEwan K, Mitra R, Mills A, Bellew R, Irons C, Gale C & Legg L (submitted). Safeness and two types of positive affect. *Cognition and Emotion.*

Hall E, Hall C, Stradling P & Young D (2006). *Guided Imagery: Creative Interventions in Counselling and Psychotherapy.* Sage, London.

Holmes E, Arntz A & Smucker M (2007). Imagery rescripting in cognitive behaviour therapy: Images, treatment techniques and outcomes. *Journal of Behavior Therapy and Experimental Psychiatry* 38, 297-305.

Kirsch P, Esslinger C, Chen Q et al. (2005). Oxytocin modulates neural circuitry for social cognition and fear in humans. *The Journal of Neuroscience* 25, 11489-11493.

Lovibond SH & Lovibond PF (1995). *Manual for the Depression Anxiety Stress Scales*, 2nd Ed. Sidney Psychology Foundation.

Leighton TD (2003*). Faces of Compassion: Classic Bodhisattva Archetypes and their Modern Expression*. Boston, Wisdom Publications.

Mason JW, Wang S, Yehuda R, Riney S, Charney DS & Southwick SM (2001). Psychogenic lowering of urinary cortisol levels linked to increased emotional numbing and a shame-depressive syndrome in combat-related posttraumatic stress disorder. *Psychosomatic Medicine* 63, 387-401.

Mikulincer M & Shaver PR (2007). *Attachment in Adulthood: Structure, Dynamics, and Change*. Guilford, New York.

Neff K (2003). Self-compassion: An alternative conceptualization of a healthy attitude toward oneself. *Self and Identity* 2, 85-102.

Osumi T, Shimazaki H, Imai A, Sugiura Y, Ohira H (2006). Psychopathic traits and cardiovascular responses to emotional stimuli. *Personality and Individual Differences* 42, 1391-1402.

Porges S (2003). The Polyvagal theory: phylogenetic contributions to social behaviour. *Physiology & Behavior* 79, 503-513.

Porges SW (2007). The polyvagal perspective. *Biological Psychology* 74, 116-143.

Rector NA, Bagby RM, Segal ZV, Joffe RT & Levitt A (2000). Self-criticism and dependency in depressed patients treated with cognitive therapy or pharmacotherapy. *Cognitive Therapy & Research* 24, 571-584.

Segerstrom SC & Solberg Nes L (2007). Heart rate variability reflects self- regulatory strength, effort, and fatigue. *Psychological Science* 18, 275-281.

Singer JL (2006). *Imagery in Psychotherapy.* American Psychological Press, Washington DC.

Takahashi T, Murata T, Hamada T, Omori M, Kosaka H, Kikuchi M, Yoshida H & Wada H (2005). Changes in EEG and autonomic nervous activity during meditation and their association with personality traits. *International Journal of Psychophysiology* 55, 199-207.

Task Force of the European Society of Cardiology and the North American Society of Pacing and Electrophysiology (1996). Heart rate variability: Standards of measurement, physiological interpretation, and clinical use. *Circulation* 93, 1043-1065.

Thayer J & Lane RD (2007). The role of vagal function in the risk for cardiovascular disease and mortality. *Biological Psychology* 74, 224-242.

Wang S (2005). A conceptual framework for integrating research related to the physiology of compassion and the wisdom of Buddhist teachings. In Gilbert P (Ed) *Compassion: Conceptualisations, Research and Use in Psychotherapy.* London, Routledge, pp. 75-120.

Wheatley J, Brewin CR, Patel T, Hackmann A, Wells A, Fischer P & Myers S (2007). "I'll believe it when I see it": Imagery re-scripting of intrusive sensory memories. *Journal of Behaviour Therapy and Experimental Psychiatry* 39, 371-385.

Whelton WJ & Greenberg LS (2005). Emotion in self-criticism. *Personality and Individual Differences* 38, 1583-1595.

Zuroff DC, Santor D & Mongrain M (2005). Dependency, self-criticism, and maladjustment. In Auerbach JS, Levy KN, Schaffer CE (Eds) *Relatedness, self-Definition and Mental Representation: Essays in Honour of Sidney J. Blatt*. London, Routledge, pp.75-90.